An Investigation Into the Passive Intermodulation Properties of Space Qualified Materials

Stuart David Mitchell

B.Eng., Ph.D.

This thesis is submitted to fulfil the requirements of the Degree of Doctor of Philosophy in Electronic Engineering

from the University of Kent at Canterbury

1997

Abstract

Intermodulation products are spurious frequency components which are produced when two or more signals mix in nonlinear components and devices. Particularly in multi-signal environments like those encountered on satellites, the spurious frequency components may severely degrade system performance through interference.

Nonlinearities are commonly known to exist in the active devices associated with components in transmitters and receivers. However, nonlinearities are also found in passive components and give rise to a phenomenon known as passive intermodulation interference.

This thesis describes the work undertaken during a study of passive intermodulation (PIM). The project was directed towards the characterisation of PIM in materials which are commonly used in spaceborne RF hardware. Satellite systems are particularly vulnerable to interference from passive non-linearities and little information is available to help engineers avoid the problem.

The work described includes the development of a highly sensitive PIM detection system. This involved the design and development of several custom components including connectors, band-stop filters and two different 3 dB couplers. The system was used to perform an investigation into the parameters which affect the generation of PIM signals in aerospace materials. Results are presented for measurements carried out at L-band frequencies.

An extensive review of previous studies on passive intermodulation is presented including descriptions of the nonlinear mechanisms which are most likely to occur in passive structures. The experimental results are then used to propose the mechanisms which are likely to dominate the levels of passive intermodulation in the samples tested.

The measurement system was also used to carry out measurements for the European Space Agency at the European Space Research and Technology Centre. The tests involved the detection and measurement of PIM sources in a test chamber used for characterising satellite payloads.

Acknowledgements

I would like to take this opportunity to thank the following people who helped in the completion of this project.

First I would like to thank my supervisor, Mr. Adrian Rawlins, for giving me the opportunity to carry out this work. Thanks are also due for his advice and guidance throughout the project and for establishing a good working environment.

I would also like to thank Mr. John Petit of the Noise Measurements Group at UKC for his help and for allowing me to tap into his wealth of experience every now and again.

Many thanks to Mr. Alan Woode of ESTEC for his help and guidance during my many visits to Noordwijk. And also for arranging funding for the project without which it would have been impossible to complete this work.

Thanks are also due to Dr. Tony Foord for his advice and support at the beginning of this project and for helping me to settle quickly into postgraduate study.

I would like to thank the technical staff at the electronics laboratories for their constant help throughout this project. Without their help it would not have been possible to design and build many of the system components as successfully as we did. Particular thanks are due to Mr. Dave Smith, Mr. Alan Hollands, Mr. Terry Rockhill and Mr. Simon Jakes.

I have also consulted with many other people both at the University of Kent and elsewhere, and for their help I am most grateful.

I must also mention my friends for their part in helping me to complete this project. Without their constant encouragement and advice I would never have made it to the end. I owe Barnaby Wallace particular thanks for helping me to put this thesis together.

Finally I'd like to thank my family, particularly mum and dad, for their constant and enduring support throughout all of my studies - I couldn't have done it without you.

CONTENTS

CHAPTER 4:

Measurement System Development

Glossary of Terms

ARTEMIS ..... Advanced Relay and Technology Mission

BSF ..... Bandstop Filter

CASE ..... Collaborative Awards in Science and Engineering

CPTR ..... Compact Payload Test Range

CSJ ..... Coaxial Sample Jig

DUT ..... Device Under Test

EMC ..... Electromagnetic Compatibility

EMI ..... Electromagnetic Interference

EPSRC ..... Engineering and Physical Sciences Research Council

ESA ..... European Space Agency

ESJ ..... Engineering Sample Jig

ESTEC ..... European Space Research And Technology Centre

HFSS ..... High Frequency Structure Simulator

IM ..... Intermodulation

IMD ..... Intermodulation Distortion

IMI ..... Intermodulation Interference

IMP ..... Intermodulation Product

INSPEC ..... Information Service for Physics, Electronics, and Computing

LNA ..... Low Noise Amplifier

MARECS ..... Maritime European Communications Satellite

MDS ..... Microwave Development Software

MIM ..... Metal-Insulator-Metal

PIM ..... Passive Intermodulation

PIMI ..... Passive Intermodulation Interference

PIMP ..... Passive Intermodulation Product

PLO ..... Phase Locked Oscillator

PTFE ..... Polytetrafluoroethylene

RF ..... Radio Frequency

SGSJ ..... Small Geometry Sample Jig

SSA ..... Solid Sate Amplifier

CHAPTER 1

Introduction

This chapter serves to outline the work which is presented within this thesis. An introduction to the subject of Passive Intermodulation Interference is followed by a breakdown of the project objectives and a description of the project management strategy. The chapter concludes with a discussion on the organisation of the thesis.

1.1 An Introduction to Passive Intermodulation Interference (PIM)

Passive intermodulation interference is an electromagnetic compatibility (EMC) problem which can interfere with the correct operation of sensitive communications-electronic (CE) equipment.

Problems associated with PIM have long been recognised and date back to the early days of radio communications. PIM is intermodulation interference (IMI) from passive components (e.g. coaxial cables, connectors, waveguide flanges) and is typically caused by the presence of weak non-linearities in high-power, multi-frequency circuits; particularly where high-power transmitters are in close proximity to sensitive receivers.

Examples of passive non-linearities are the hysteresis effect which is observed in ferromagnetic materials and ferrites, and the rectification of current flow at loose or corroded metal junctions.

The effect of PIM is to generate a series of discrete signals which can interfere with, and seriously impair communications channels. In extreme cases the channel may even be rendered useless.

Shipboard communications systems have traditionally been cited as highly vulnerable to the effects of PIM and the term "rusty-bolt phenomenon" was often used to describe its effects. This stems from early work in the field where the problem could often be traced

to corrosion at structural metallic joints. Shipboard systems require to transmit signals at high power due to the long distances over which communication takes place. Transmitters and receivers are in close proximity due to the limited size of the vessel and the salt water environment leads to increased rates of corrosion.

The latest systems to lend themselves susceptible to interference from PIM are satellites. In the space environment, communication takes place over extremely long distances (circa 30,000 Km), hence, due to losses, transmitted signals are at very high power levels, whilst received signals are at extremely low power levels. Satellites are also very small, therefore, transmitters and receivers are usually spaced no more than a few metres apart. These characteristics contrive to make satellite communications systems highly vulnerable to PIM.

Recent work in the field of PIM has identified many potential mechanisms that could be responsible for PIM generation [1]. These relate to the properties of materials used in the construction of communications hardware and the techniques used in the manufacturing processes.

In the past it has usually been possible to provide a simple engineering solution to the problem such as a change of frequency or the repositioning of equipment. However, the application of such straightforward measures is now much less feasible owing mainly to the following reasons:

(i) Increasing use of the electromagnetic spectrum limits the availability of alternative frequencies.

(ii) Increased system vulnerability due to greater complexity, higher signal powers, and more sensitive detectors.

(iii) The drive for reduced size and weight makes the repositioning of equipment more difficult.

(iv) Complex equipments need solutions to be incorporated at the design stage in order to avoid expensive modification later.

Nowhere are these factors more restrictive than in the design of satellite systems. State-of-the-art mobile communications satellites are being developed that are breaking new ground in all areas of design. The current drive is for more channels, higher transmission powers and more sensitive receivers. When this is coupled with the fact that the space environment is already extremely hostile in terms of the physical conditions that equipment has to endure, it is evident that there is a high probability of incurring problems due to PIM.

Due to the isolation of satellites in orbit, they do not readily lend themselves to 'ad hoc' remedial measures. This means that the payload must be fully functional before launch and so requires extremely rigorous testing. It is in the nature of PIM problems that they are usually detected at the latter stages of integration and if problems are discovered at this stage, remedial work can be a lengthy and costly process.

Examples of the problems which can occur are found in reference [2]. In the paper the authors cite four communications satellites, launched between 1975 and 1985, which have been adversely affected by PIM, namely FLTSATCOM, MARISAT, MARECS and INTELSAT V MCS. Take, for example, the MARECS satellite which was launched in 1981. This satellite had to have its entire transmit chain re-designed in order to eliminate an interfering, 43rd order, PIM signal.

Consequently there has been increasing emphasis on the provision of preventative measures that can be applied from the very start of the design stage in order to avoid PIM. However before this approach can be adopted a much better understanding of the fundamental mechanisms which give rise to PIM is required.

The current state of understanding of PIM phenomena is poor. Researchers have tended to concentrate on testing the PIM levels generated by commonly used system components. Only a few people have addressed the issue of the mechanisms which cause PIM, and even so there has been disagreement over the findings. Much of the work has concentrated on a few basic mechanisms without the consideration of other, less obvious, sources of non-linearity. The adopted approach has been to demonstrate the presence of non-linearities in carefully prepared scientific samples. However, there is no evidence to suggest that these are the effects which occur in everyday engineering situations.

Currently there exists no unequivocal data on the mechanisms which cause PIM. There has been no attempt to establish a hierarchy of dominant mechanisms in terms of the levels of PIM which they produce. Additionally, there is very little data of use to engineers concerned with the design of systems, vulnerable to PIM, regarding materials and practices. In short there are no areas on the subject of PIM that would not benefit from further work.

Primarily, what is required is a better understanding of the non-linear effects which dominate PIM levels in engineering environments. This will provide engineers with more reliable information with which to develop low-PIM systems of the future. In order to achieve this, measurements have to be carried out on commonly used engineering materials and in a format that allows engineering type finishes and structures to be tested.

Standardised measurement techniques are also required in order that the characteristics of the materials and samples may be measured and compared in a reliable and consistent manner. This will deliver greater confidence in the results and conclusions.

1.2 Background

The Noise Measurements Group of at the University of Kent (UKC) has over 10 years experience of PIM and PIM research stemming originally from a government sponsored contract on the characterisation of shipboard RF interference. A significant portion of work has been carried out on land-mobile radio communications sites at VHF frequencies [3-7] and was mainly diagnostic in nature. This experience was instrumental in the European Space Agency (ESA) awarding the university a contract of work to carry out more fundamental research.

The European Space Agency (ESA) was formed in 1973 and comprises 14 member states who between them have stipulated that the role of ESA is:

> ***"to provide for and to promote, for exclusively peaceful purposes, cooperation among European states in space research and technology and their space applications, with a view to their being used for scientific purposes and operational space applications systems".***

In fulfilling this role, ESA has become one of the world's largest exponents of satellite technology and has managed and advised on, numerous satellite missions over its 23 year history.

ESA is keen to establish more about the intrinsic mechanisms of PIM due to the high vulnerability of satellite communications systems to this type of interference. In the past, ESA have performed some PIM tests themselves [8-11]. However these measurements have mainly been qualification tests, carried out on flight hardware in order to meet predefined specifications and say very little about the actual causes of PIM. With this in mind, ESA contracted the Noise Measurements Group to carry out an independent study into potential causative mechanisms of PIM in space communications hardware [1]. On the strength of the study, further contracts have been awarded to the group to set up a PIM measurement system and carry out an investigation of the PIM properties of space qualified materials.

The system developed at UKC has also been used to scan the Compact Payload Test Range (CPTR) at ESTEC for sources of PIM [12, 13]. ESTEC (the European Space Research and Technology Centre) is the headquarters of ESA's technical activities and the

CPTR is used to perform electromagnetic tests on satellite payloads. It is planned to use the range for future PIM tests hence the need to determine any background levels which the range generates itself.

The latest communications satellite under development by ESA has one of the most challenging specifications to date. The ARTEMIS satellite is designed to provide mobile communications across the whole of Europe and areas of North Africa. The payload has the capacity to handle over 900 voice channels operating at L-band frequencies. It has been recognised that problems arising due to PIM could seriously threaten the success of the ARTEMIS program and therefore the terms of the contract have specified that the results of the UKC PIM study should be directly applicable to the payload configuration of this satellite.

The work reported in this thesis is based upon the research carried out for ESA. The project was also supported by the Engineering and Physical Sciences Research Council (EPSRC) under the auspices of a CASE award (Cooperative Awards in Science and Engineering) in conjunction with ESA. As part of the CASE award, the author has spent approximately 3 months working at ESTEC, carrying out the CPTR test mentioned previously. This work will also be reported.

1.3 Project Objectives

As a result of the collaboration with ESA, the objectives of the project fall into two distinct areas. Firstly there are those objectives relating to the PIM diagnostic work based at the University and then there are those which are concerned with the body of work carried out at ESTEC in the Netherlands. Both are outlined below.

The work, undertaken at the University of Kent, takes the form of an experimental study into the specific area of passive intermodulation occurring in space qualified materials.

The objectives of the study were set out as follows:

- To design and build a highly sensitive but stable and consistent PIM measurement system.
- To propose a standard methodology to enable the PIM characteristics of materials to be measured and compared in a consistent manner.
- To produce a set of PIM measurements which describe the PIM characteristics of selected aerospace materials.
- To identify the dominant causative mechanisms of PIM behaviour in the materials tested.

At the start of the project the ARTEMIS satellite was under development by ESA and it was decided that the research should be directly applicable to this current project. The study was therefore carried out at L-band frequencies in order to coincide with the down-link (transmission) frequencies of ARTEMIS.

The objectives of the CPTR measurement campaign, at ESTEC, were defined as follows:

- To reconfigure the existing L-band measurement system at UKC to carry out PIM tests in the CPTR at ESTEC
- To locate and measure any sites of intermodulation generation in the CPTR
- To gauge the observed levels with respect to the threat they might pose to the sensitivity of PIM measurements on satellite payloads.

1.4 Resources

The facilities at the University of Kent and ESTEC which have been essential for a project of this nature are described below:

(i) Noise Measurements Group

The Noise Measurements Group at UKC comprises one laboratory in which the measurement system was assembled. Most of the equipment used in this study has been purchased specially and includes a Hewlett Packard (HP) 8561E spectrum analyser which is used to detect and measure the PIM signals.

The group is managed by Mr. A.D. Rawlins, a lecturer in the Electronics department at the university. Mr. Rawlins originally established the group and has over 10 years experience in PIM research.

The group also employs Mr. J.S. Petit as a research fellow on PIM. Mr. Petit has 8 years experience working in PIM and multipactor (another anomalous phenomenon found in satellite systems) which he gained by working for 9 years at ESTEC and 3 years at UKC.

(ii) Electronics Laboratories at UKC

Thorough use of the computing facilities at UKC has been made. These include a network of Sun Sparc Workstations which run the software packages which have been used. This includes the HPEEsof suite of programs (Academy, Libra, etc.) and Hewlett Packard's Microwave Development Software (MDS) (both

used for microwave network simulation). Extensive use was also made of HP's High Frequency Structure Simulator (HFSS) and Sonnet Software's E.M. simulation package which both deal with the electromagnetic modelling of physical structures.

The electronics laboratories at Kent includes a well equipped workshop facility. This provides equipment and staff for the manufacture of prototype components and equipment. This was used comprehensively in the development of custom components for the PIM measurement system.

A Wiltron 360 vector network analyser is also available at the university. This proved invaluable in the characterisation of the components which were used in the L-band measurement system.

(iii) European Space Research & Technology Centre (ESTEC)

The CPTR work at ESTEC made exclusive use of UKC equipment apart from three L-band waveguide horns which were purchased by ESTEC.

During the course of the project, the author was in close liaison with Mr. A. Woode of the XR division at ESTEC. Mr. Woode has been employed at ESTEC for over 15 years. He also has over 8 years experience of the PIM problem.

(iv) Library Search Facilities at UKC.

In the search for literature on previous PIM studies and component design, the search facilities of the library were thoroughly used. There are three means of sourcing journal papers and citations namely INSPEC, BIDS and CATS.

INSPEC is produced on CD-ROM by the IEE and covers the world's published literature on all aspects of physics, electronics, electrical engineering, computer science, control and information technology. The facility at UKC covers records from 1989 to date.

BIDS (or the Bath ISI Data Service) is an on-line search facility giving access to the citation indexes in Science, Social Science and Arts and Humanities. The indexes span the years from 1981 to the present.

CATS is a program used exclusively for searching the catalogue of literature available at the UKC library. The system does not list individual articles but can be used to determine whether a particular journal and volume is available. The library stores copies of the more popular periodicals in most subjects both past and present. Articles which are not available on campus may be obtained via the inter-library loan system.

Searches of the databases were carried out on the following areas:

- Passive intermodulation interference.
- Active Intermodulation interference.
- Non-linear physical mechanisms.
- Measurement techniques.
- High power filter design.
- Coupler design.
- CAD modelling techniques.

1.5 Organisation of Thesis

The work described in this thesis is arranged into eight chapters as follows:

CHAPTER 1: Introduction. The thesis begins with a simple introduction to the field of Passive Intermodulation Interference and its significance in satellite communication systems. There then follows a brief synopsis of the background and interests of the two bodies involved in this study, namely the University of Kent and the European Space Agency. The objectives of the project are then briefly outlined followed by a description of the resources available to the project. The chapter concludes with a discussion of the organisation of the thesis.

CHAPTER 2: Passive Intermodulation Interference in Multi-Frequency Systems, introduces the concept of non-linearity and discusses its relevance to the theory of intermodulation interference (IMI). This is followed by a discussion of the passive intermodulation (PIM) phenomenon. Some of the potential mechanisms thought to generate PIM are then presented. Next, there is a thorough review of previous research related to PIM in multi-frequency communications systems. The chapter concludes with a discussion of the refined project objectives and project approach.

CHAPTER 3: PIM Measurement System Design is concerned with the design and implementation of a PIM measurement system using commercially available components. A discussion of the particular design considerations which are pertinent to PIM measurement systems is presented, including a review of measurement systems used by researchers to date. This is followed by a description of a system which has been designed to measure 3rd order intermodulation products at L-band, and includes a description of the system hardware and the system performance. The implementation of techniques for improving the system are presented and the chapter ends on a discussion of the improved system performance.

CHAPTER 4: Measurement System Development describes the techniques and implementation of custom built system components which have been designed to generate very low levels of intrinsic PIM. Topics include low-PIM connection methods, low-PIM enclosures, band-stop filter design and 3 dB coupler design. There then follows a discussion on the improvement offered by these components and the chapter concludes with the design of special low-PIM test jigs for the investigation of PIM in aerospace materials.

CHAPTER 5: Measurement Programme describes the laboratory measurement of PIM. First, the revised measurement system configuration and performance are briefly discussed. Next, the types of test samples used, the various experimental procedures and the resulting PIM levels are presented. Observations were made at each stage in the measurements and these are also presented.

CHAPTER 6: Analysis Of Results presents an analysis of the experimental work discussed in Chapter 5. The analysis takes the form of a discussion of the possible mechanisms which are responsible for the levels of PIM observed during the measurements.

CHAPTER 7: PIM Characterisation of Compact Payload Test Range is concerned with the PIM characterisation of the ESTEC CPTR. There is a description of the measurement system which has been reconfigured to perform radiated tests. The measurements are then presented followed by an analysis of the results and a discussion of the conclusions.

CHAPTER 8: Conclusions and Recommendations concludes the main body of the thesis and summarises the work presented. Recommendations are made for the direction and nature of future work in the field.

1.6 Novel Aspects.

In order to fulfil the requirements for the degree of PhD, there is a need for the work which is carried out on this project to demonstrate a degree of novelty. In this section, the novel aspects of the work will be highlighted, these being expanded upon throughout the remainder of the thesis.

1. Fundamental transmission line technology has been novelly applied in the development of consistent, low-PIM, connection principles

2. These principles have been used to develop a new, low-PIM, connector design and a new, low-PIM, enclosure design. Both have been used extensively to implement couplers and test jigs having state-of-the-art PIM performance.

3. Further techniques have been developed in the design and implementation of low-PIM bandstop filters namely, a contactless resonator structure and a differential-pitch tuning mechanism.

4. The work to develop low-PIM components has culminated in the implementation of a state-of-the-art, L-band, coaxial PIM measurement system. The system displays a hitherto unheard of degree of sensitivity compared with previous work in the field. This equates to some 10dB better than other coaxial systems and a residual PIM variation of less than 1.0dB.

5. Novel sample jigs have been devised to carry out a series of experiments on conducting materials. Standard material sample formats have also been designed in order to maintain uniformity and consistency between tests and this too is a new concept in PIM testing.

6. The coaxial measurement system has been used to conduct an investigation into the PIM properties of aerospace materials. The approach taken towards the measurement campaign was also novel in that samples of an "engineering" nature were tested as these were more indicative of real world situations and therefore more relevant to system designers.

7. Several new results were obtained as a direct result of the measurement campaign:

   (i) Observation of non-linearity in so-called linear metals.

   (ii) Demonstrated a clear link between PIM performance and surface finish.

   (iii) Clearly demonstrated that plating can be effective in reducing PIM from intrinsically non-linear materials.

   (iv) Established that an Alochrom coating on aluminium can cause extremely high levels of PIM and should be avoided.

   (v) Observed an anomalous effect in solid copper under the influence of an external magnetic field.

   (vi) Showed that contrary to what one might expect, some varieties of stainless steel can be quite linear.

7. The system was also used to carry out a novel measurement campaign in an antenna test range. The objective of the campaign was to determine the usefulness of the chamber for carrying out radiated PIM tests. The results of the campaign indicated that the chamber itself generated unacceptably high levels of PIM and therefore could not be used in such a capacity. The sources of PIM could be pinpointed quite accurately and were easily identified.

CHAPTER 2

Passive Intermodulation Interference in Multi-Frequency Systems

This chapter presents a more detailed look at PIM in communications systems. The nature of PIM is developed from the fundamental concepts of non-linearity. This is followed by a summary of non-linear physical mechanisms that may contribute to PIM generation. Next there is a review of PIM research to date and the chapter concludes with the enlarged objectives of the project.

2.1 Intermodulation Interference in Telecommunications Systems

Our society relies on the ability to establish and maintain extensive reliable communications. Communications requirements have increased drastically as a result of the mobility of our society and our dependence on computers. The cellular telephone has significantly increased the capacity of our mobile communications and fixed point-to-point microwave and satellite communications systems provide an extensive data transmission network for computer systems.

One of the most important considerations in the design, installation and operation of a communicating electronic (CE) system is that of achieving and maintaining electromagnetic compatibility (EMC) between the system and other CE equipment in the vicinity. EMC is the ability of equipment and systems to function as intended without degradation or malfunction in their operational electromagnetic environment. The equipment should not adversely affect the operation of, or be adversely affected by, any other equipment or system.

Electromagnetic interference (EMI) is said to exist when undesirable voltages or currents are present to adversely influence the performance of a system or equipment. These voltages or currents may reach the victim device by conduction or by electromagnetic field radiation.

In a typical communications system, the receiver must be able to pick up its intended signal, which is probably relatively weak, while operating in the presence of a number of relatively strong potentially interfering signals from other communications or electronic systems operating in close proximity. Conversely, the transmitter must be able to transmit a relatively strong signal without causing interference to nearby sensitive receivers.

Intermodulation products are spurious signals which are generated by the mixing of signals in non-linear components or mechanisms [14]. In multi-frequency communications systems and environments, these signals can readily lend themselves to EMI problems. Such problems arise when the frequency band of an intermodulation product (IMP) occurs at or near, the fundamental pass-band of any near by receivers and when the level of the IMP is comparable to that of the desired incoming signal. The magnitude and frequency of the generated IMPs are directly related to the magnitude and frequency of the original mixing signals and to the transfer function of the non-linear component or mechanism.

2.2 Intermodulation Processes

2.2.1 Non-Linearity

In order to understand the basic theory of intermodulation signal generation, it is first necessary to define the concept of a non-linear system.

A linear system is one whose output is directly proportional to the input. The output and input are related by a constant of proportionality which can be any real or complex number but must be fixed over the range of operation of the system. A good example of linear behaviour is described by Ohm's law in metals which relates the current density, J, to the electric field, V, by a constant, σ, the conductivity:

$$J = \sigma \cdot V \qquad \text{Eq.2.1}$$

One important property of such systems is that when they are excited by a single frequency - a sinusoid - the response, although it may be altered in amplitude and phase, is at that frequency only. The response to multiple input frequencies is the sum of the response to each one individually i.e. superposition holds. Linearity is often a practical requirement, but nature is inherently non-linear, so that in engineering applications it is common to restrict the input to imperfectly linear systems to some range over which the deviations from linearity can be neglected.

For many, non-linear systems the response can be modelled as a power series. For example the non-linear transfer function of a component may be represented by an n^{th} order power series thus:

$$V_o = a_1 V_i + a_2 V_i^2 + a_3 V_i^3 + a_4 V_i^4 + \ldots + a_n V_i^n \qquad \text{Eq.2.2}$$

Where a_n, is the n^{th}coefficient of the relevant term. When excited by a single frequency, the output of this system not only contains that frequency, but multiples of it. This is described as harmonic distortion.

If such a system is excited by multiple input frequencies, the response consists of these frequencies, their harmonics, and new frequencies which are equal to the sums and differences of the input frequencies and of their harmonics, i.e. intermodulation products.

2.2.2 Product Generation

Consider the simplified case where the non-linear component described by Eq.2.2 is simultaneously excited by two equal amplitude, unmodulated signals, $Vcos(\omega_1 t)$ and $Vcos(\omega_2 t)$. The input to the system, V_i, is just the sum of the two signals:

$$V_i = V[cos(\omega_1 t) + cos(\omega_2 t)] \qquad \text{Eq.2.3}$$

Substituting Eq.2.3 into Eq.2.2 and using standard trigonometric formulae shows that the output of the system, V_O, may be written as:

$$\begin{aligned} V_O = {} & a_1 V(cos\omega_1 t + cos\omega_2 t) \\ & + a_2 V^2\left(1 + \frac{1}{2}cos2\omega_1 t + \frac{1}{2}cos2\omega_2 t + cos(\omega_1 + \omega_2)t + cos(\omega_1 - \omega_2)t\right) \\ & + a_3 V^3\left(\frac{1}{4}cos3\omega_1 t + \frac{1}{4}cos3\omega_2 t + \frac{3}{4}cos(2\omega_1 - \omega_2)t + \frac{3}{4}cos(2\omega_2 - \omega_1)t + \ldots\right) \\ & + a_4 V^4(\qquad) \\ & + a_n V^n \ldots \end{aligned} \qquad \text{Eq.2.4}$$

Thus, in general, distortion components at $n\omega 1 \pm m\omega 2$ appear at the output. The component at $n\omega 1 \pm m\omega 2$ is called the $(n+m)^{th}$ order intermodulation product. For example, the V_i^3 term produces third order harmonic components at $3\omega_1$ and $3\omega_2$ and third-order intermodulation products at $(2\omega_1-\omega_2)$ and $(2\omega_2-\omega_1)$. The whole frequency

spectrum of V_o therefore consists of the two excitation signals at ω_1 and ω_2, as well as many newly generated harmonic and intermodulation products and is illustrated in Fig.2.1. A linear system produces no such additional signals.

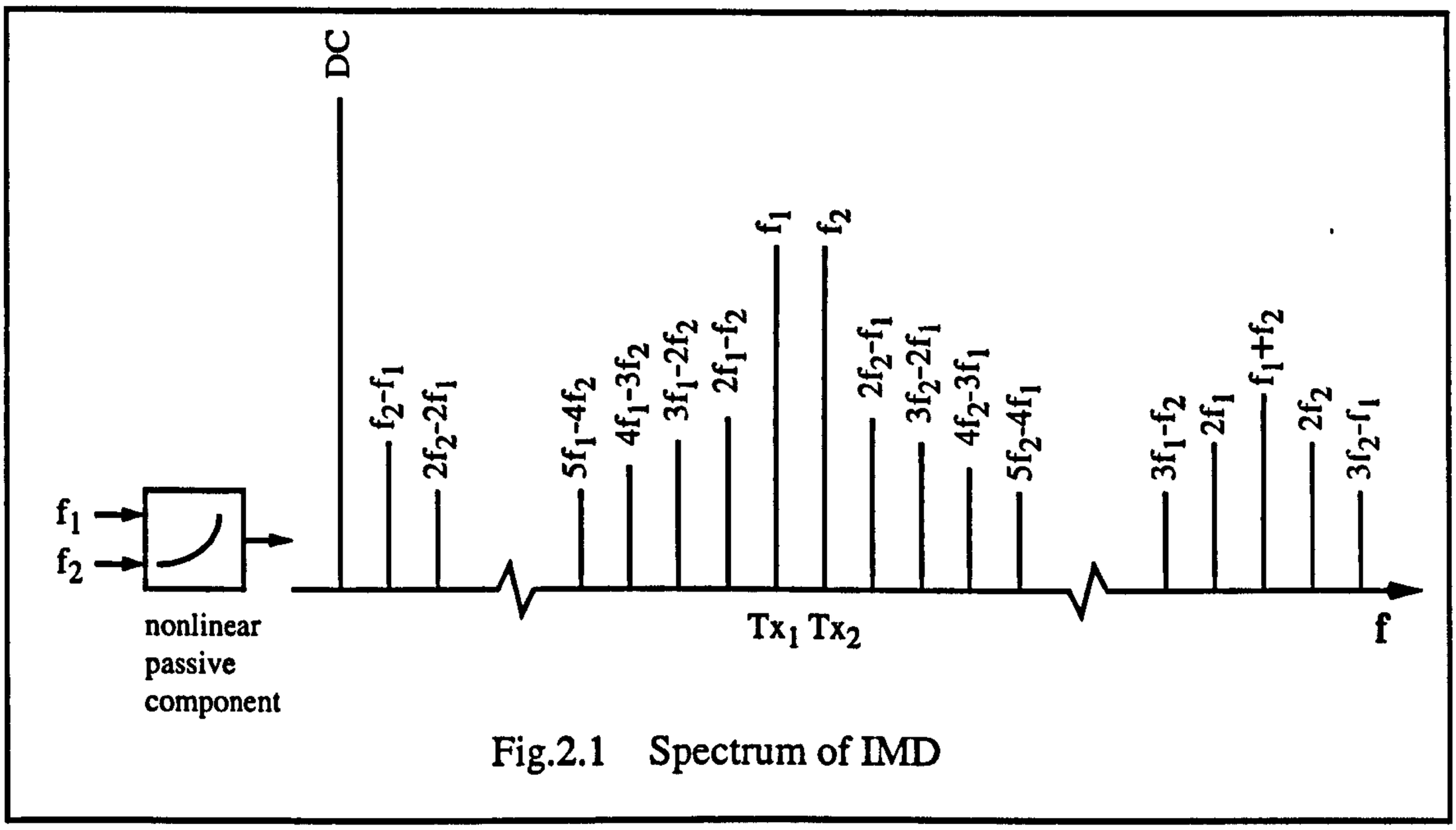

Fig.2.1 Spectrum of IMD

So far only a simple two-frequency case has been considered. In multi-frequency environments as would normally be encountered in practical situations, the problem becomes much more serious. For simplicity, consider that only one site or mechanism of non-linearity is operative, it has been shown that the total number of intermodulation products increases rapidly as the number of simultaneous broadcasting channels goes up [16, 17]. The rate of increase is indicated in Fig.2.2. If the addition of extra channels meant an increase in the number of points of non-linearity (this is a reasonable assumption given that circuit complexity will have to be increased for extra channels), then it is easy to see how IM signals could be combined and strengthened in a communications environment and cause serious EMI problems.

Interference from intermodulation products is normally limited to specific orders. For the weak non-linearities encountered in most practical situations, the coefficients, a_n, of Eq.2.2 get rapidly smaller as n increases. Accordingly, the power levels of the intermodulation products tend to diminish as the order of the product gets higher. This is significant as it means that interference is usually only caused by the lowest order product to fall into the receive band of the susceptible system, the third order intermodulation product generally being the worst. This isn't to say that higher orders are insignificant. In the MARECS satellite example of Chapter 1 it was the 43rd order intermodulation products which caused problems [2]. Additionally, in most cases it is the odd-order products which are problematic since these normally occur in the same band of frequencies as the fundamental excitation signals.

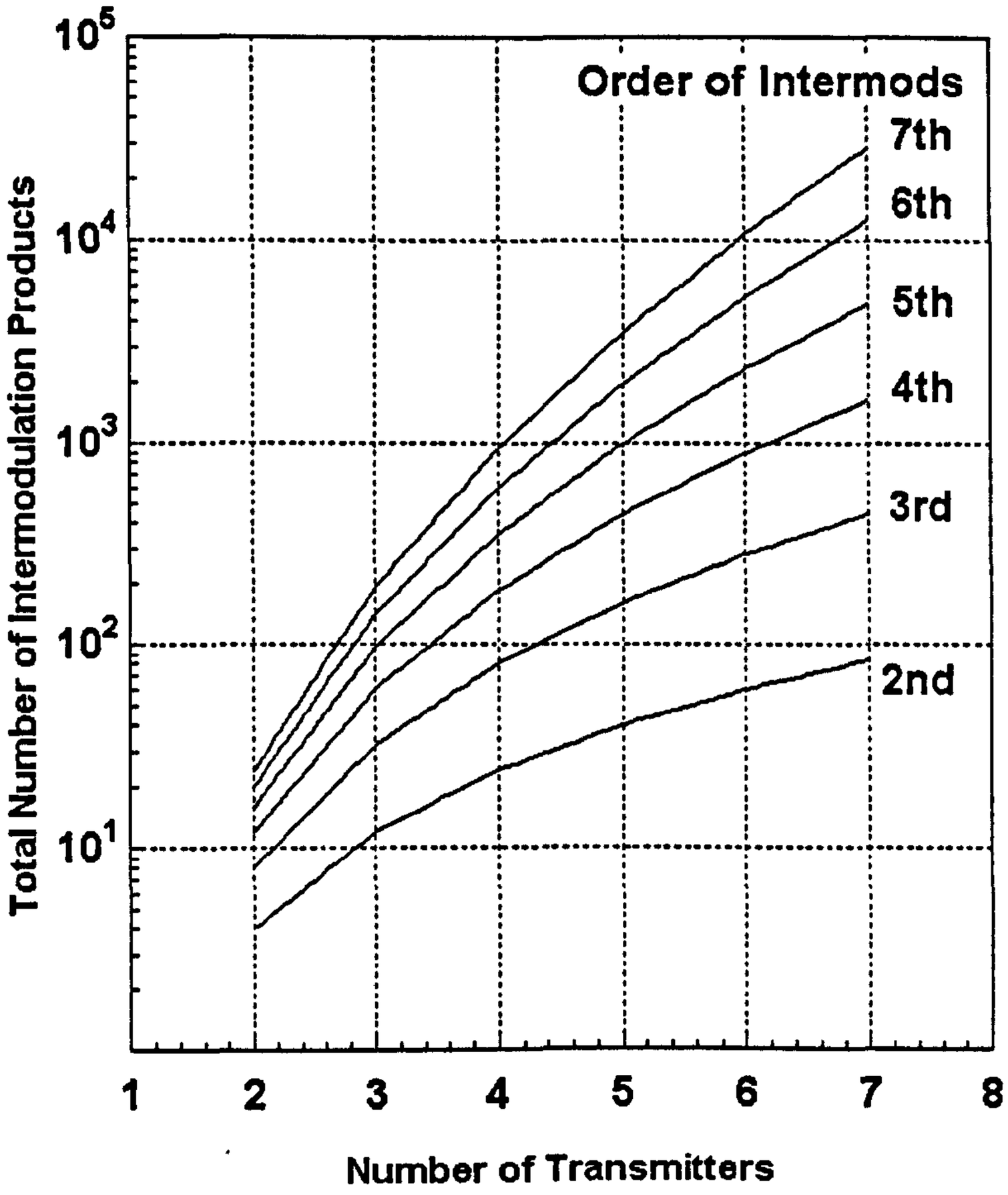

Fig.2.2 Increase in Intermodulation Products with No. of Channels

2.2.3 Power Relationships

The generation of intermodulation signals is widely recognised as the most sensitive test of linearity known. A deviation from linearity as little as 1 part in 10^6 will readily produce a detectable signal. Fig.2.3 on page 17. gives an indication of the extent to which such small deviations from linearity can give rise to significant levels of intermodulation.

The next point worth consideration is the relationship between the input power levels and the power level of a PIM product generated by *one* of the terms of Eq.2.4. Care must be taken at this point to distinguish between the *total* power level of an intermodulation product and the level of one of its constituent components. Individual intermodulation products will have contributions from many terms of Eq.2.4 and, although contributions from higher order terms are small, they can have a significant affect as will be discussed later.

First let us consider the third order intermodulation level at $\omega_{IMP} = (2\omega_2 - \omega_1)$, arising from the third term in Eq.2.4. Assuming now, that the two input or parent signals are not at the same amplitude, but are, $V_1 cos(\omega_1 t)$ and, $V_2 cos(\omega_2 t)$, then the contribution to

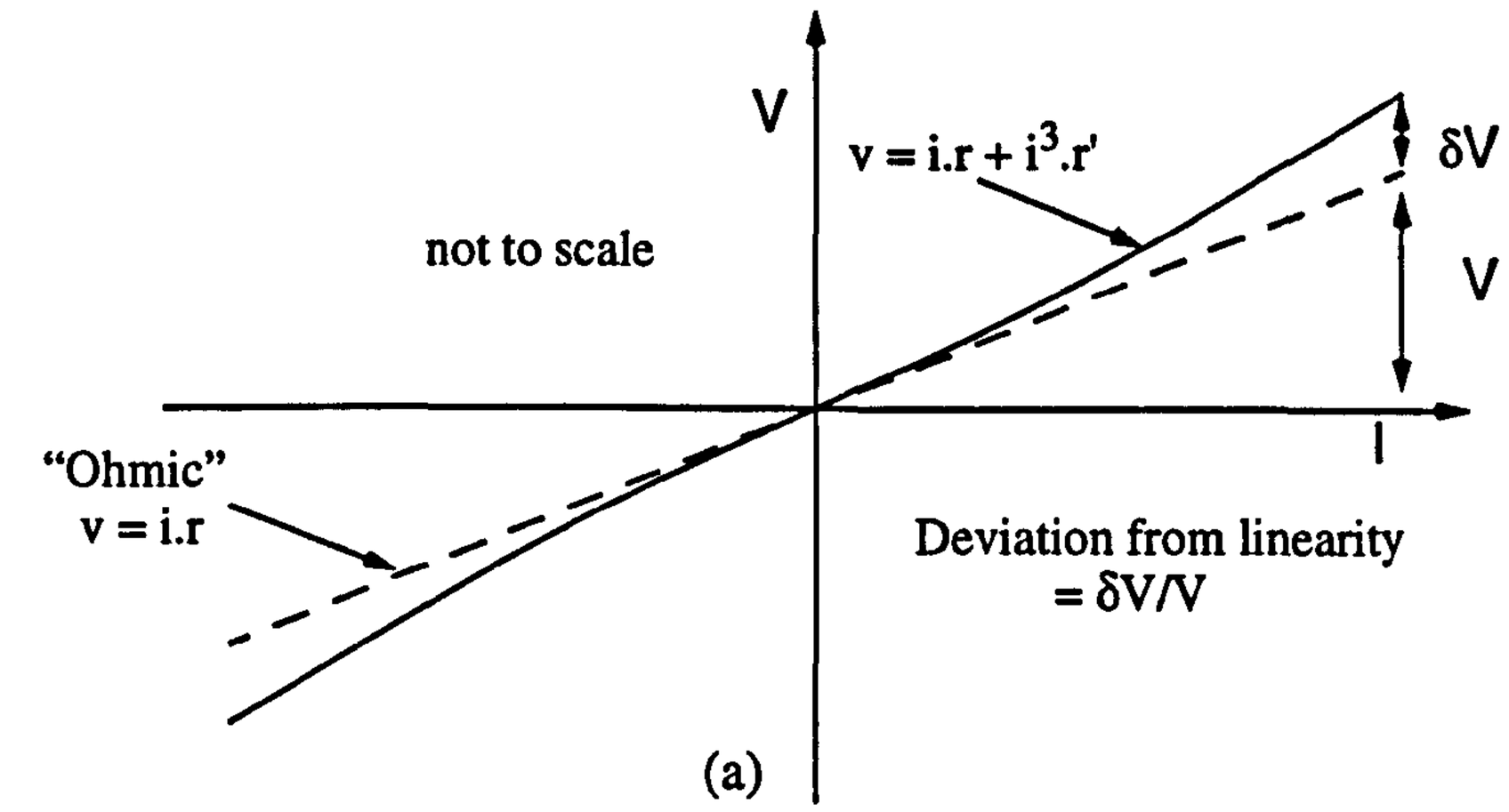

(a)

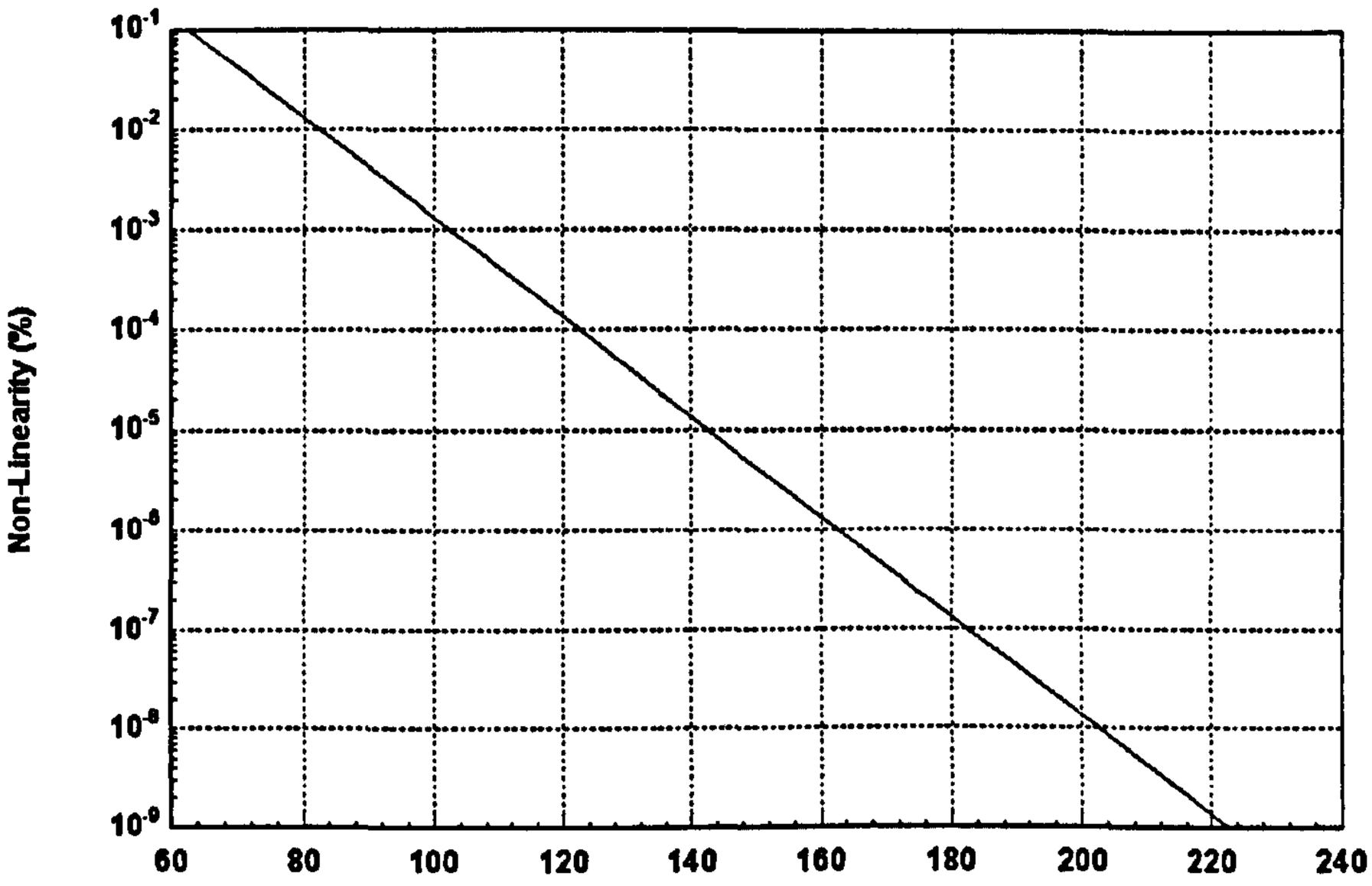

(b)

Fig.2.3 Sensitivity of Intermodulation Measurements to Non-linearity.

Graph (a) is the current-voltage characteristic for a hypothetical system which deviates slightly from Ohm's law (dotted line) so as to generate a third order product. For a given current the deviation may be defined as $\delta V/V$.

In (b), the minimum detectable deviation is plotted logarithmically as a function of measurement sensitivity. It is assumed that two carriers of 25 W (44 dBm) each are used, and the sensitivity is given in dB below this power level (dBc).

$$V_{IMP} = \frac{3}{4}[a_3 V_1 V_2^2]cos(2\omega_1 - \omega_2)t \qquad \text{Eq.2.5}$$

If P_1 and P_2 are the powers of the signals ω_1 and ω_2 respectively, and P_{IMP} is the contribution to ω_{IMP} from the third term of Eq.2.4,

$$\text{then} \qquad P_{IMP} \propto P_1 P_2^2 \qquad \text{Eq.2.6}$$

$$\text{If } P_1 = P_2 \text{ then } P_{IMP} \propto P_1^3 \text{ or } P_2^3 \qquad \text{Eq.2.7}$$

From these equations, the relationship between P_{IMP}, P_1 and P_2 can be summarised as follows:

(i) From Eq.2.6, P_{IMP} should vary as 1dB/dB with the input of P_1 when P_2 is held constant.

(ii) From Eq.2.6, P_{IMP} should vary as 2dB/dB with the input of P_2 when P_1 is held constant.

(iii) From Eq.2.7, P_{IMP} should vary as 3dB/dB with the combined input ($P_1 + P_2$) when P_1=P_2.

Similarly, the contribution from the *nth* order term of Eq.2.4 to the *nth* order PIM frequency should vary as n dB/dB with the combined input power ($P_1 + P_2$).

It is the experience of most other researchers and of the Noise Measurements Group at the University of Kent, that the rate of change in PIM signal with combined input power is always less than these figures suggest. Previously, there has been little in the way of explanation for this effect, and certainly none which is based on theory. Most people readily neglect the contributions to PIM signals from the higher order terms of Eq.2.4 by virtue of the fact that they are relatively small.

Consider once again, the two-tone combined input signal of Eq.2.3 which is repeated here:

$$V_i = V[cos(\omega_1 t) + cos(\omega_2 t)] \qquad \text{Eq.2.3}$$

Let us now consider the effect of expanding this function to the n^{th} degree, reducing the terms to single powers of cos(x). Expansion up to the fourth power follows:

$$(cos\alpha + cos\beta)^2 = \frac{1}{4}[4 + 2cos2\alpha + 4cos(\alpha - \beta) + 4cos(\alpha + \beta) + 2cos2\beta]$$

$$(cos\alpha + cos\beta)^3 = \frac{1}{8}[2cos3\alpha + 6cos(2\alpha - \beta) + 6cos(2\alpha + \beta) + 18cos\alpha$$
$$+ 2cos3\beta + 6cos(2\beta - \alpha) + 6cos(2\beta + \alpha) + 18cos\beta]$$

$$(cos\alpha + cos\beta)^4 = \frac{1}{16}[36 + 2cos4\alpha + 8cos(3\alpha - \beta) + 8cos(3\alpha + \beta)$$
$$+ 12cos(2\alpha - 2\beta) + 12cos(2\alpha + 2\beta) + 32cos2\alpha$$
$$+ 2cos4\beta + 8cos(\alpha - 3\beta) + 8cos(\alpha + 3\beta)$$
$$+ 48cos(\alpha - \beta) + 48cos(\alpha + \beta) + 32cos2\beta]$$

These expansions have been written in such a format to demonstrate how a further simplification of the expansion process may be made.

Careful inspection of the above expansions indicates that the coefficients of expansion may be mapped onto a two axis coordinate system such that,

$(\cos\alpha + \cos\beta)^2$ is given by

```
                β axis
                ^
                1
            2   0   2
        1   0   4   0   1   > α axis
            2   0   2
                1
```

with multiplying factor $(1/2)^2$.

$(\cos\alpha + \cos\beta)^3$ is given by

```
                    1
                3   0   3
            3   0   9   0   3
        1   0   9   0   9   0   1
            3   0   9   0   3
                3   0   3
                    1
```

with multiplying factor $(1/2)^3$.

$(\cos\alpha + \cos\beta)^4$ is given by

				1				
			4	0	4			
		6	0	16	0	6		
	4	0	24	0	24	0	4	
1	0	16	0	36	0	16	0	1
	4	0	24	0	24	0	4	
		6	0	16	0	6		
			4	0	4			
				1				

with multiplying factor $(1/2)^4$.

Inspection of the above mapping procedure reveals two simple rules of transformation when progressing from any power to the next higher power:

the overall multiplying factor for a given power, n, is $(1/2)^n$

the value of a coefficient for power n is the sum of the nearest orthogonal coefficients for the power $(n\text{-}1)$ expansion table.

Hence, when transforming from $n = 3$ to $n = 4$;

the D.C. term $(\alpha = 0, \beta = 0)$ becomes $9 + 9 + 9 + 9 = 36$

the term $\alpha = 1, \beta = 1$ becomes $9 + 9 + 3 + 3 = 24$

the term $\alpha = 2, \beta = 1$ becomes $0 + 0 + 0 + 0 = 0$

Examination of the expansion tables shows that for a given PIM frequency in a table (of odd or even power) there will be additional contributions from all greater tables (those of greater powers of n) where their power is odd or even, respectively. An example is used to elucidate this.

Consider a third order PIM signal with frequency given by $(2\alpha + \beta)$. The expansion table with $n = 3$ gives an expansion coefficient of 6. (The $(-2\alpha - \beta)$ term is the same as the $(2\alpha + \beta)$ term thus we have $3 + 3$ in total). The table with $n = 5$ however, also contains terms associated with $(2\alpha + \beta)$ (value = 50 + 50) and likewise with all of the following tables with odd powers. If one considers contributions up to the power of $n = 7$, the output voltage for that frequency alone can be written as,

$$V_{out} = a_3\left(\frac{V}{2}\right)^3 6\cos(2\alpha+\beta) + a_5\left(\frac{V}{2}\right)^5 100\cos(2\alpha+\beta) + a_7\left(\frac{V}{2}\right)^7 1470\cos(2\alpha+\beta) \qquad \text{Eq.2.8}$$

The variation of power for V_{out} versus V for the above expression has been plotted for different values of power law coefficients, refer to Fig.2.4. A pure third order expression which demonstrates the expected 3 dB per dB power variation has also been plotted for comparison. It is very interesting to note that the above expression only follows the 3 dB per dB relation when the higher order coefficients are very small compared to the fundamental coefficient (a_3). When these higher order coefficients become larger the power law actually shows a gradient much greater than 3 dB per dB. The only case so far investigated which produces a gradient less than 3 dB per dB is when one coefficient changes sign. However, the lower gradient only persists for a limited range in voltage, see Fig.2.4, until a dip is observed followed by a very steep increase in output power.

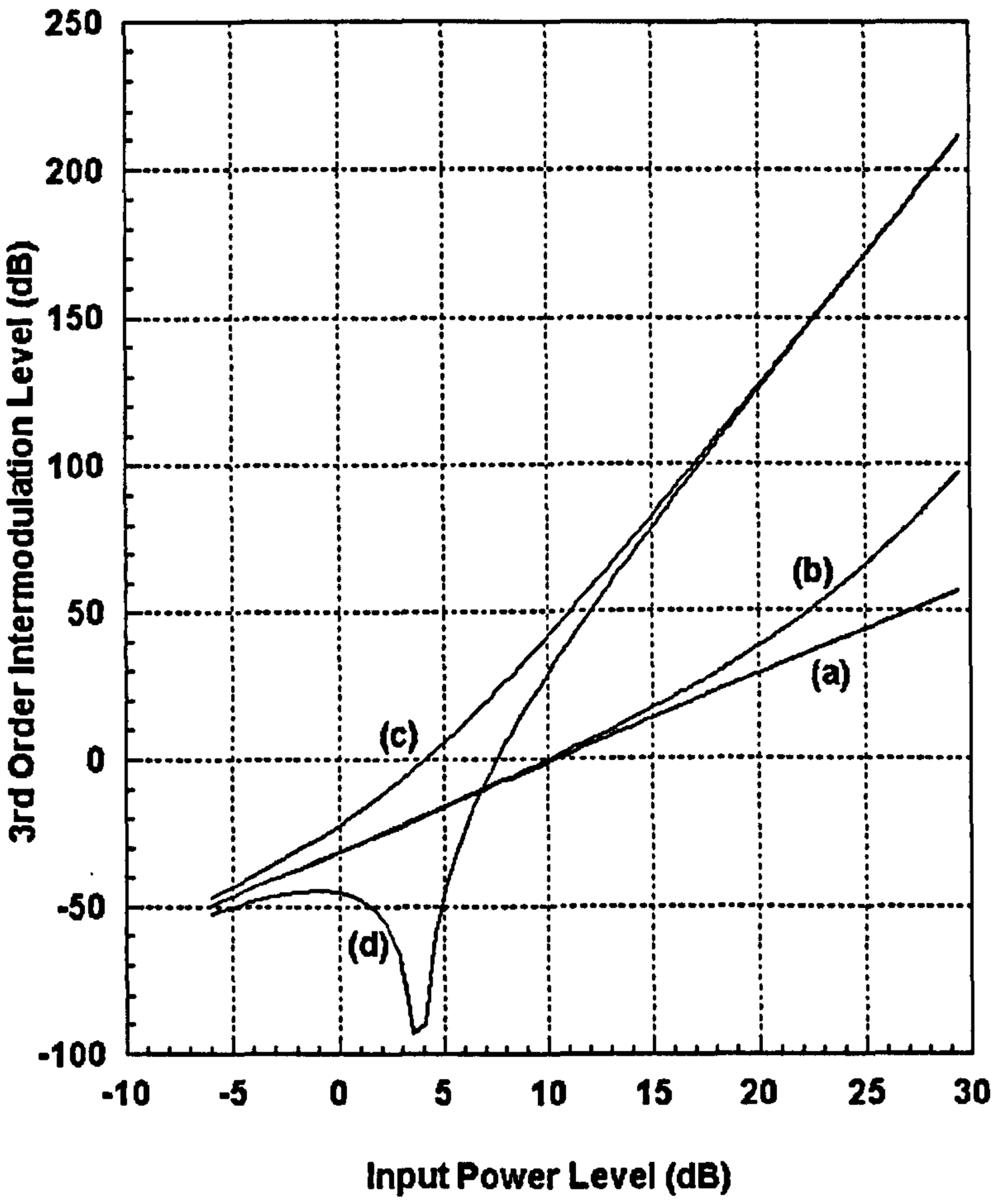

(a) Pure 3 dB/dB relationship.

(b) $a_3 = \frac{1}{10}$; $a_5 = \frac{1}{100^2}$; $a_7 = \frac{1}{1470^4}$

(c) $a_3 = \frac{1}{10}$; $a_5 = \frac{1}{100}$; $a_7 = \frac{1}{1470^4}$

(d) $a_3 = \frac{1}{10}$; $a_5 = -\frac{1}{100}$; $a_7 = \frac{1}{1470^4}$

Fig.2.4 3rd Order PIM Variation with Input Power

Theoretical considerations of the power variation of PIM signal versus stimulus signals therefore shows that the traditionally expected power gradient (3 dB per dB for a third order effect) only holds true when the higher order power law coefficients are several orders of magnitude lower than the fundamental one. (The fundamental coefficient is the first one appearing in the polynomial series for the PIM frequency of interest). The model which did show such a variation used power law coefficients with a difference of 20 dB in voltage terms.

In practice the rate of change of PIM signal with input power is always less than the traditionally expected one. This is not readily predicted by fundamental theory when the power law coefficients are only considered as constants. Indeed, it forces one to consider that these power law coefficients could, themselves, be functions of the stimulus voltage. Alternatively, it may be that the nature of the practical non-linearity changes with the level of the impressed signal. The significance of this analysis is in the modelling of PIM. It is plain that the problem is complex and requires more theoretical analysis than has been afforded in the past.

2.3 Active Intermodulation Interference

The generation of intermodulation products is normally associated with active devices (e.g. transistors, travelling wave tubes etc.) and is referred to as *active intermodulation*. There are generally two cases which lead to the generation of active intermodulation products. Firstly, some active devices are just inherently non-linear. Alternatively, other active devices have transfer functions which are approximately linear over some range, outside of which, the response deviates increasingly from a straight-line relationship. At some point, however, these devices will saturate causing extremely non-linear behaviour. These effects are minimised by careful design and by restricting the input levels applied to a system.

Intrinsically non-linear devices are most frequently found in high-power amplifiers where maximum output is promoted at the expense of linearity resulting in the devices being operated close to saturation. For example, the power amplifiers used in transmitter systems are usually operated in the class-C mode and are inherently non-linear. Now when transmitters are located in close proximity, there is a strong chance that an amount of energy at a given frequency from one transmitter, will be coupled into the circuitry of another operating close-by. The coupling mechanism may take several forms, the most common being mutual coupling between transmit antennas, coupling between antenna feed lines, or direct coupling between co-located transmitter CE equipment. In any case, given more than one signal passing through one or more stages of amplification, intermodulation generation is unavoidable. As a result, mixing occurs between the different signals

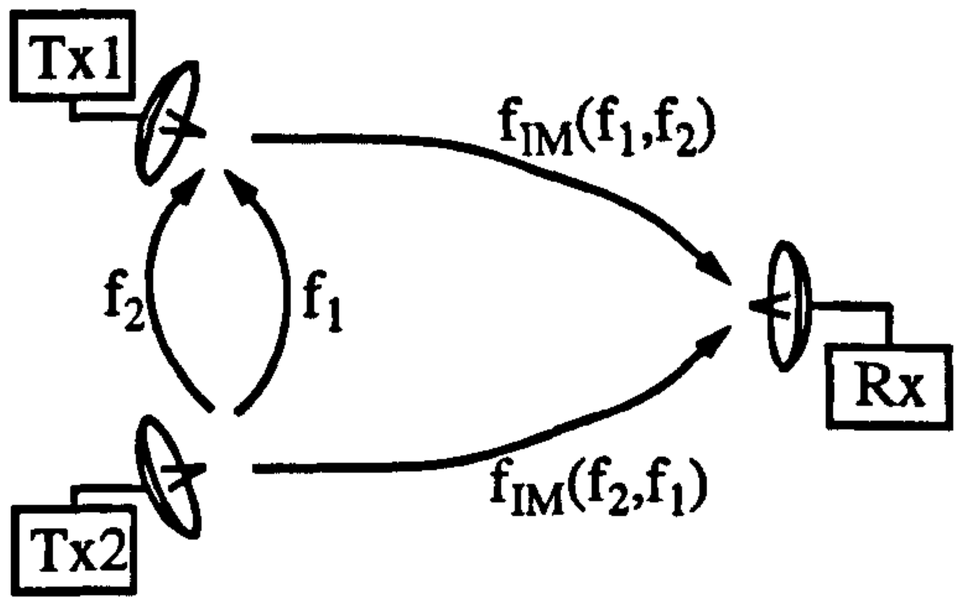

Fig.2.5 Transmitter Intermodulation Distortion

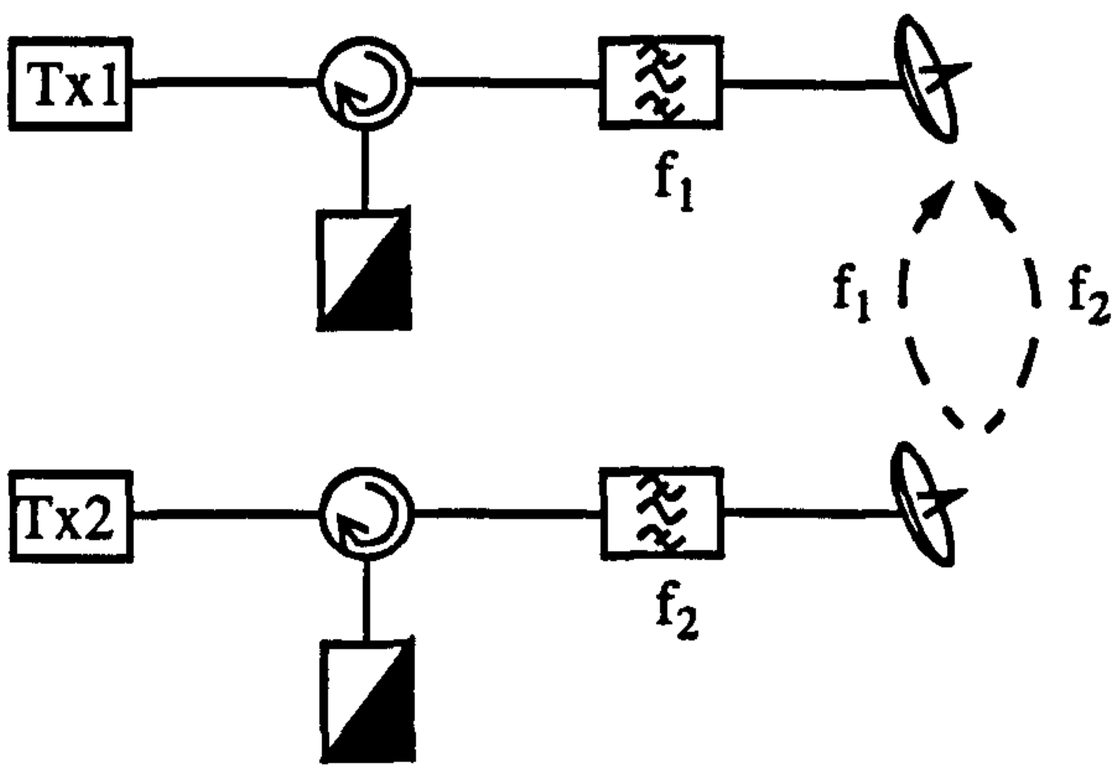

Fig.2.6 Transmitter IM Countermeasures

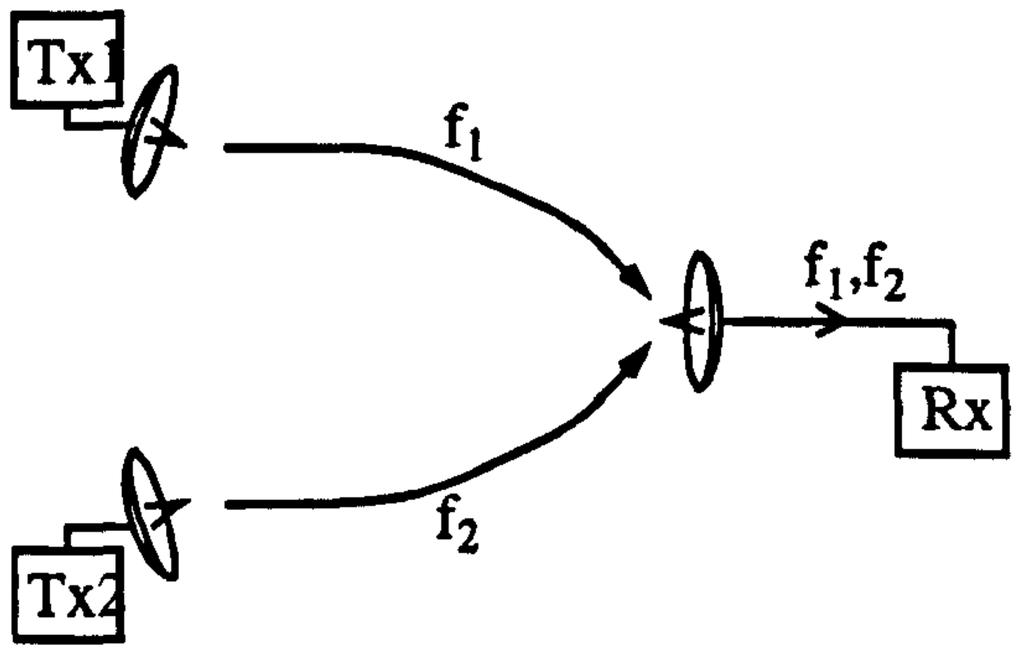

Fig.2.7 Receiver Intermodulation Distortion

and intermodulation products and harmonics are produced. These new products along with the fundamental carrier signals are re-radiated and can cause interference to nearby systems. The transmitter intermodulation problem is illustrated in Fig.2.5.

Several steps may be taken in order to counter the generation of transmitter IM, the most obvious being to physically separate the interfering sources. Alternatively, the two sources may be isolated electrically by using isolators and filters as in Fig.2.6. The filters prevent transmission of signals other than those in the frequency band of the transmitter. The circulators serve to redirect signals, travelling back towards the power amplifier, into

a load. This not only prevents intermodulation generation but also guards the amplifier output stages against overload. These unwanted signals may have been generated by the transmitter and reflected by the filter or picked up by the antenna from external sources.

The second type of active intermodulation is more commonly found in receiver systems. The problem occurs when two or more strong signals fall into the pass-band of an operating receiver as shown in Fig.2.7 on page 23. These signals can drive the input stages of the receiver into non-linear modes of operation and generate intermodulation products which can directly interfere with the intended receive signals.

The way to eliminate IMI of this kind is to reduce the level of any signals which are likely to cause receiver intermodulation before they reach the non-linear elements of the circuit. This is best achieved using high Q filters. Such filters offer a high degree of roll-off and hence significant rejection, even at frequencies a few MHz from the desired signal.

Other ways to minimise receiver vulnerability are to plan the local frequency regime to avoid IMI or to physically separate the sensitive receivers from any signals which pose a threat to their normal operation.

In general, the active intermodulation interference problem is well understood and can be taken into account in the design of systems where problems are likely. However, active intermodulation problems can still arise due to factors such as antenna damage, feeder damage, component malfunction or simply from poor design and installation.

Active intermodulation is also significant in the design of passive intermodulation measurement systems. Such systems contain power amplifiers, low-noise amplifiers and other active devices. As the two effects produce signals at the same frequencies, extreme care must be taken to ensure that active intermodulation products generated by the system do not interfere with measurements of passive intermodulation.

2.4 Passive Intermodulation

Passive intermodulation (PIM), is the generic term used to describe any intermodulation signals in communications systems which have been generated by passive non-linearities in a system or its surrounding environment. Signals may, by whatever means, be coupled into such non-linearities then re-transmitted along with PIM signals which can then be captured by sensitive receiver systems and cause interference.

2.4.1 Sources, Levels and Effects

In contrast to intermodulation generated by non-linear active devices, passive components such as resistors, capacitors, cables, connectors, filters etc. are widely considered to be linear. Exceptions to this are ferromagnetic cores where non-linear behaviour is familiar. In fact, some degree of non-linearity is observed in all of these items and the consequences are described as passive intermodulation. In the past this has appeared as less of a problem than intermodulation in active devices because the deviation from linearity is (usually) smaller. However, it is components such as cables, waveguide, connectors and antenna systems that are required to handle multiple signals in multiplexed systems, and passive intermodulation is an increasing problem as system requirements become more stringent. The RF industry has been slow to pick up on the PIM phenomenon and the problems associated with it. Accordingly, the PIM performance of commercial components is never specified which makes the design of low-PIM systems all the more difficult.

PIM is a highly unpredictable and erratic phenomenon and the level of transmitted PIM signals depends upon several factors; the level of the incident transmitter signals, the degree of coupling into the non-linear mechanism, the characteristics of the non-linearity and the ability of the non-linear mechanism to re-transmit the generated signals. Particularly high levels of PIM are associated with simple contacts between metal surfaces. Fig.2.3 on page 17 has already been seen to demonstrate the extent to which even very small deviations from linearity can give rise to significant levels of intermodulation.

Generally speaking, since passive non-linearities are relatively weak, PIM signal levels are small; often more than 100 dB below the parent signal power. However, in certain cases, the levels can be much higher. A typical example is given in [46] where waveguide joints were observed to generate PIM levels as great as -25 dBm when using two 30 dBm transmitters.

2.4.2 Potential Mechanisms.

The complex mechanisms responsible for the non-linear effects in passive components are little understood. A recent report [1] highlighted over 22 individual mechanisms which are likely, given the correct conditions, to exhibit non-linear characteristics. This is a large number of candidate mechanisms in itself (and certainly more than had previously been considered by researchers in the field), but in general, several of these effects may be operative at any one time. Many potential causes of PIM can arise from the interaction of two or more effects and this results in a bewildering number of possible combinations. While some effects seem likely to be of much greater consequence than others, there is a

lack of experimental evidence to support any organisation in order of relative significance. Most of the published studies of the various effects relate to D.C. or low frequency currents. It is not readily apparent how applicable the conclusions are at microwave frequencies, although previous work on PIM has often relied on theories developed for low frequencies.

It is important to note that in conventional studies of electrical conduction it is often possible to identify one or two dominant mechanisms and then to neglect other combinations. However, such simplification is not valid when considering sources of PIM. A mechanism may be responsible for only a small fraction of the total current flow yet be the major cause of a PIM product if it contains the appropriate non-linear term.

Essentially there are two main types of passive non-linearity; those associated with disruption to the RF current flow in conductors at metallic contacts or cracks for example, and non-linearities associated with the intrinsic, bulk, physical properties of materials, e.g. ferromagnetism. It has been suggested that many phenomena of both types exist and a thorough review has been given in the literature [1]. Rather than repeat this body of data, there follows a brief summary of some of the more commonly cited sources of PIM encountered in the literature review.

First, however, with respect to contact phenomena, the relationship between junction pressure and PIM level is introduced, irrespective of which non-linear mechanism is at work.

2.4.2.1 Junction Phenomena

In a report for the Philco-Ford Corporation, Rootsey, et al. [19] proposed a model for any current dependant non-linearities at waveguide flanges or similar junctions. Their theory states that regardless of the mechanism responsible, if a major non-linearity exists at such junctions, and if the contact model is correct, then a well defined behaviour should be evident. The principle is depicted in Fig.2.8 which illustrates the current flow across a metallic interface as the pressure, forcing the contact together, is increased. The model is based upon non-linear effects which are current dependant: That is to say, if the current density is increased or decreased, the PIM level will change accordingly. Considering Fig.2.8(a), if the two sides of the junction are lightly touching, there will be few points of physical contact (commonly called 'asperities' or 'a-spots') and the current density through these points will be high. As the pressure on the junction is increased, the number of a-spots is increased and the current is distributed more. The PIM level, in theory, can therefore be altered by changing the contact pressure.

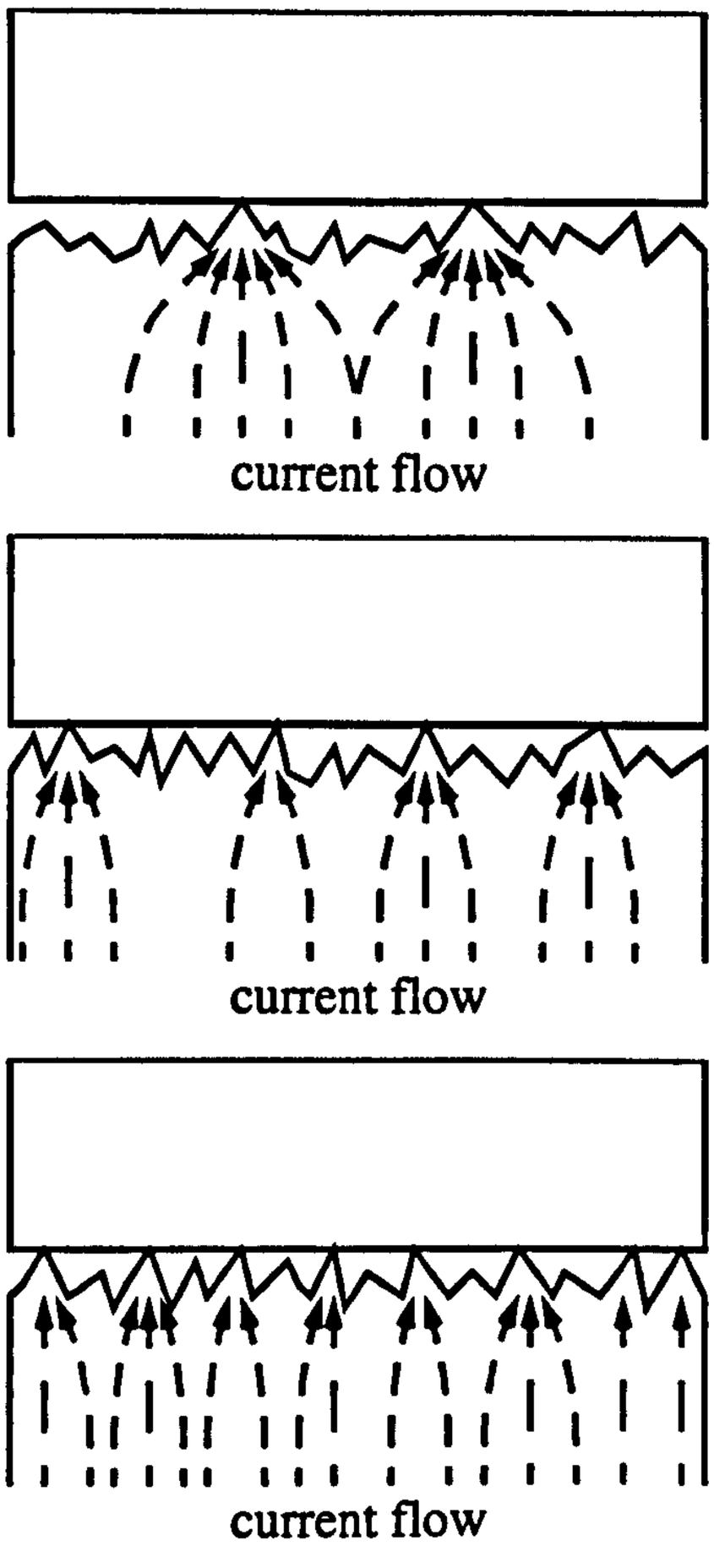

Fig.2.8 Contact model

The researchers went on to try the model by performing experiments on waveguide flanges. A wide range of junctions were prepared by varying the junction parameters such as surface finish, contact pressure etc. Results showed that for a given contact pressure, the coarser joints produce more PIM due to their being less points of contact at the flange interface. In all cases, when the joints were tightened, the PIM level dropped as more points of contact came into being. In the final report, however, the actual contact pressures used are unclear and conservative estimates of 60MPa. are stated for the recommended pressure. It is also stated that their measurement system was unstable and inconsistent therefore the results may not be totally reliable. The researchers also ignored other effects such as those due to temperature and therefore the validity of the results must be questioned.

In any case, the contact model does not explain the actual mechanisms which cause PIM in the first place. Two of the most commonly cited junction effects will be considered next; electron tunnelling and thermionic emission.

2.4.2.2 Electron Tunnelling

Electron tunnelling through dielectric films is an effect which occurs at the junction between two metals. All metals will readily react in air to produce a thin layer of the metal oxide on its surface. Generally these oxides are insulating but they can also be semi-conducting. When two pieces of oxidised metal are brought into contact, a complex sandwich of metal-oxide-oxide-metal is formed. The oxide layers normally act as a barrier to the flow of electrons from one metal to the other. However, if the barrier is sufficiently thin (less than 10 Å or 20Å, where $1Å=1x10^{-10}m$) there is a significant probability that an electron which impinges on the barrier will pass from one metal to the other; this is known as tunnelling. The current across the barrier is heavily dependant on oxide thickness and has a non-linear relationship to the voltage across the barrier. The effect is generally well understood for certain junctions and has been exploited in devices such as the tunnel diode [20].

The effect of tunnelling has been used by several researchers to explain the generation of PIM at oxidised aluminium contacts [22, 23]. However, researchers have disagreed as to the correct from of the tunnelling equations used [24]. Other research has indicated PIM levels to be independent of oxide thickness, and more recent studies have concluded that tunnelling theory, as it stands, is insufficient to explain the non-linear effects observed at metal-metal junctions [25]. The reasoning given is as follows:

(i) Much research has been done in this area of work but with disagreement as to the correct form of the tunnelling equations.

(ii) Current state-of-the-art tunnelling theory can only predict current-voltage relationships at d.c. with no frequency dependence.

(iii) Measured current-voltage curves on carefully controlled, idealised oxidised contacts, even at d.c., are not accurately represented by modern electron tunnelling models.

(iv) The oxidised contacts that occur in real engineering situations are much more complex than those fabricated in the laboratory and are unlikely to behave according to the electron tunnelling models.

It can be seen therefore that although the tunnelling effect is one of the most commonly cited mechanisms thought to be responsible for PIM, there is little hard evidence to support it. The electron tunnelling mechanism may be able to explain PIM generation at specially fabricated junctions, however, in normal engineering situations, it is likely to be only one of a number of different effects in operation.

2.4.2.3 Thermionic Emission

If we again consider the barrier system of metal-insulator-insulator-metal for two oxidised pieces of metal brought into contact, another means of electron transport across the barrier is explained by thermionic emission. This is also known as the 'semiconductor' or 'Schottky' effect. This relates to the possibility that the statistical distribution of thermal energy across the junction will enable some electrons to pass *over* the potential barrier between the two conductors [26, 27, 28]. Clearly, the probability of crossing a barrier, and hence the maximum current density, increases with temperature. The application of an external electric field across the barrier can distort the built-in potential, lowering the potential barrier for one polarity and increasing it for the other. A lower potential barrier increases the probability of electrons having sufficient thermal energy to surmount it and this is described as enhanced thermionic emission. The effect favours current flow in one direction over the other and so is distinctly non-linear. In much of the published literature concerning PIM, metallic contacts are assumed to behave like metal-oxide-metal semiconductor junctions. However, a previous study [19] of non-linear mechanisms has pointed out that unless the following characteristics are experimentally evident, the semiconductor mechanism does not provide an adequate description:

(i) The non-linearity should be independent of atmospheric pressure.

(ii) The PIM level should be somewhat dependent on d.c. bias level for high impedance contact.

(iii) The PIM level should be relatively independent of oxide layer thickness after a certain threshold thickness is established.

Various contact non-linearity tests [19] have shown that conditions (i) and (iii) could be satisfied but not (ii). Thus, it was concluded by the authors that the classical semiconductor theory of thermionic emission does not entirely explain the non-linear effect at metallic contacts. However, theory also predicts a rapid variation in current density with temperature and this could provide a method of distinguishing between thermionic emission and tunnelling.

The thermal dependency of thermionic emission means that at low temperatures the current due to this effect will be small. Tunnelling is comparatively independent of temperature and therefore tends to dominate at low temperatures. At higher temperatures the current due to thermionic emission increases to levels well above the current due to tunnelling and dominates the current flow across the junction [28]. An example of this is shown in Fig.2.9 on page 30. This dependence on temperature was not considered by the researchers at Philco-Ford [19] and this must cast some doubt on their conclusions.

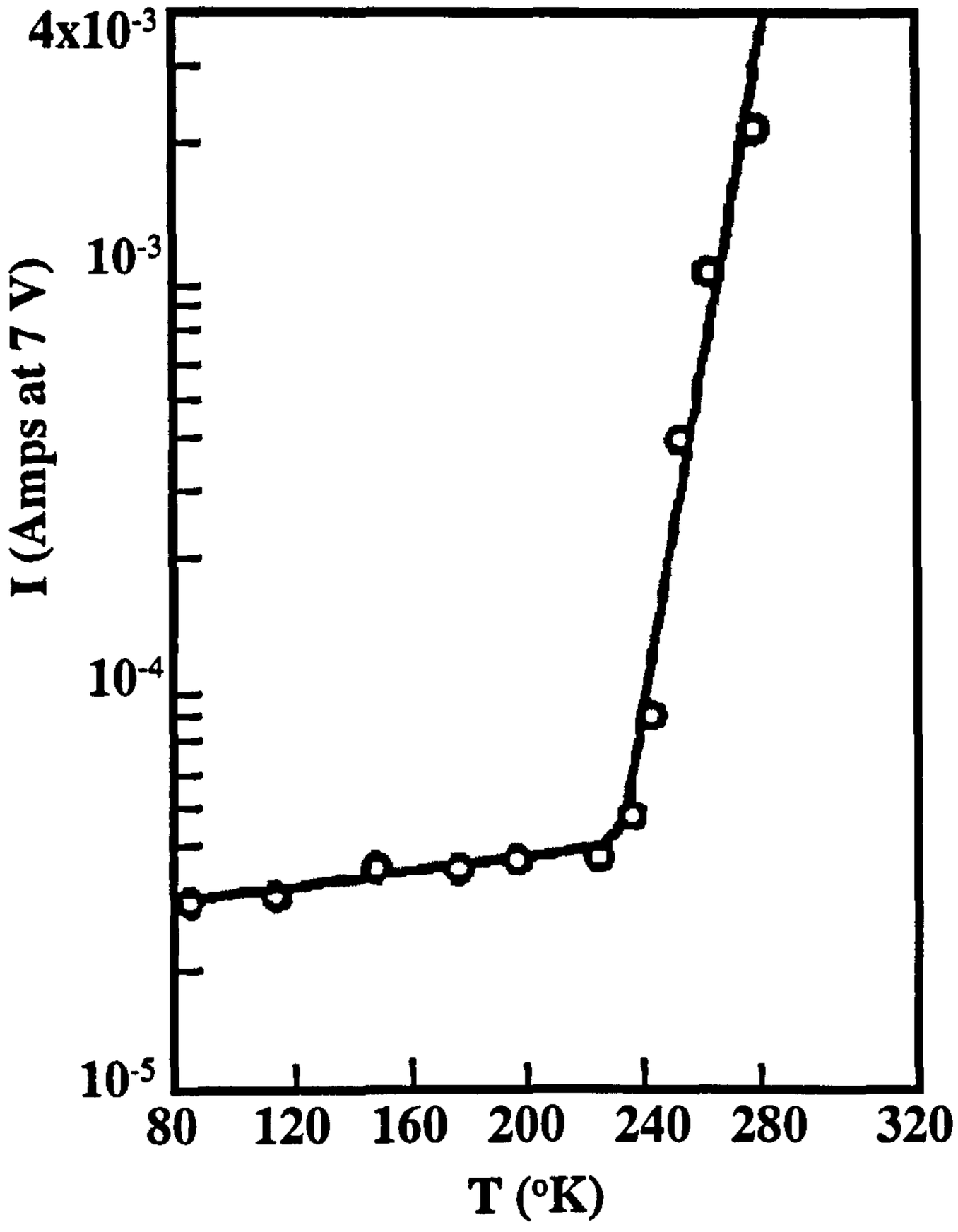

Fig.2.9 Current as a function of temperature for an aluminium oxide film with lead electrodes. At low temperatures, the small temperature coefficient indicates a tunnelling mechanism. Schottky emission becomes dominant at higher temperatures as demonstrated by the greatly increased temperature coefficient. From reference [28].

2.4.2.4 Ferromagnetic Effects

In a ferromagnetic material, atomic magnetic dipoles tend to align parallel to each other [29]. This alignment extends over small regions known as magnetic domains which, in an unmagnetised sample, are randomly orientated. The application of an increasing external magnetic field can cause rotation of the atomic dipoles and the growth of some domains at the expense of others, thus progressively magnetising the sample. As a result, ferromagnetic materials have large permeabilities (at least for low frequencies). The permeability varies non-linearly with the magnetic field up to some field strength at which the process saturates and becomes linear. Plotting magnetic flux density (B) against magnetic field (H) produces the familiar hysteresis curve of Fig.2.10 as the domains tend to retain their previous orientation.

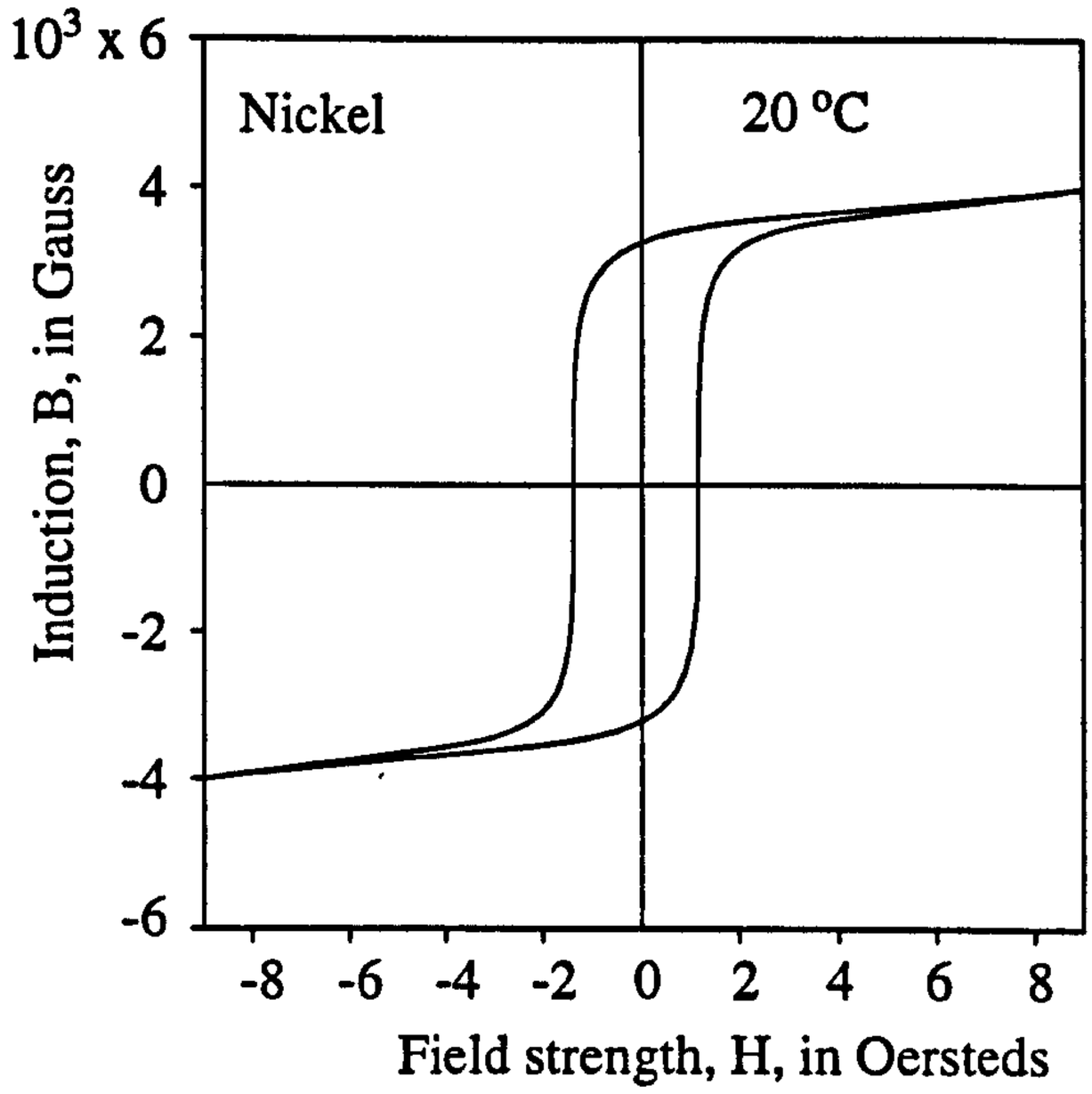

Fig.2.10 Non-linear ferromagnetic hysteresis

Non-linear variation in the permeability ferromagnetic materials with applied field has been attributed to PIM generation by causing variation in the current density through the surface layer at high frequencies [30]. The skin effect limits high frequency current flow in conductors to a surface layer only a few microns deep. This skin depth is defined by the equation:

$$\delta_s = \frac{1}{\sqrt{(\pi \cdot f \cdot \sigma \cdot \mu)}} \qquad \text{Eq.2.9}$$

Where σ is the conductivity and μ is the permeability of the material. It is therefore evident that variation in μ with applied field will vary the skin depth, and hence the current density through the material, in a non-linear fashion. Since the passage of an alternating electric current creates a fluctuating magnetic field which, in turn, induces an alternating electric current, the non-linear behaviour of the permeability is said to act as a source of PIM.

Ferromagnetic materials are known to be responsible for very high levels of intermodulation in some circumstances, and this is a view shared by almost all PIM researchers over the years. Bailey and Ehrlich investigated this mechanism in nickel samples by measuring intermodulation at VHF as a function of a static magnetic bias field and obtained results which confirmed the presence of a magnetic effect [35, 30]. Fig.2.11 shows a typical example.

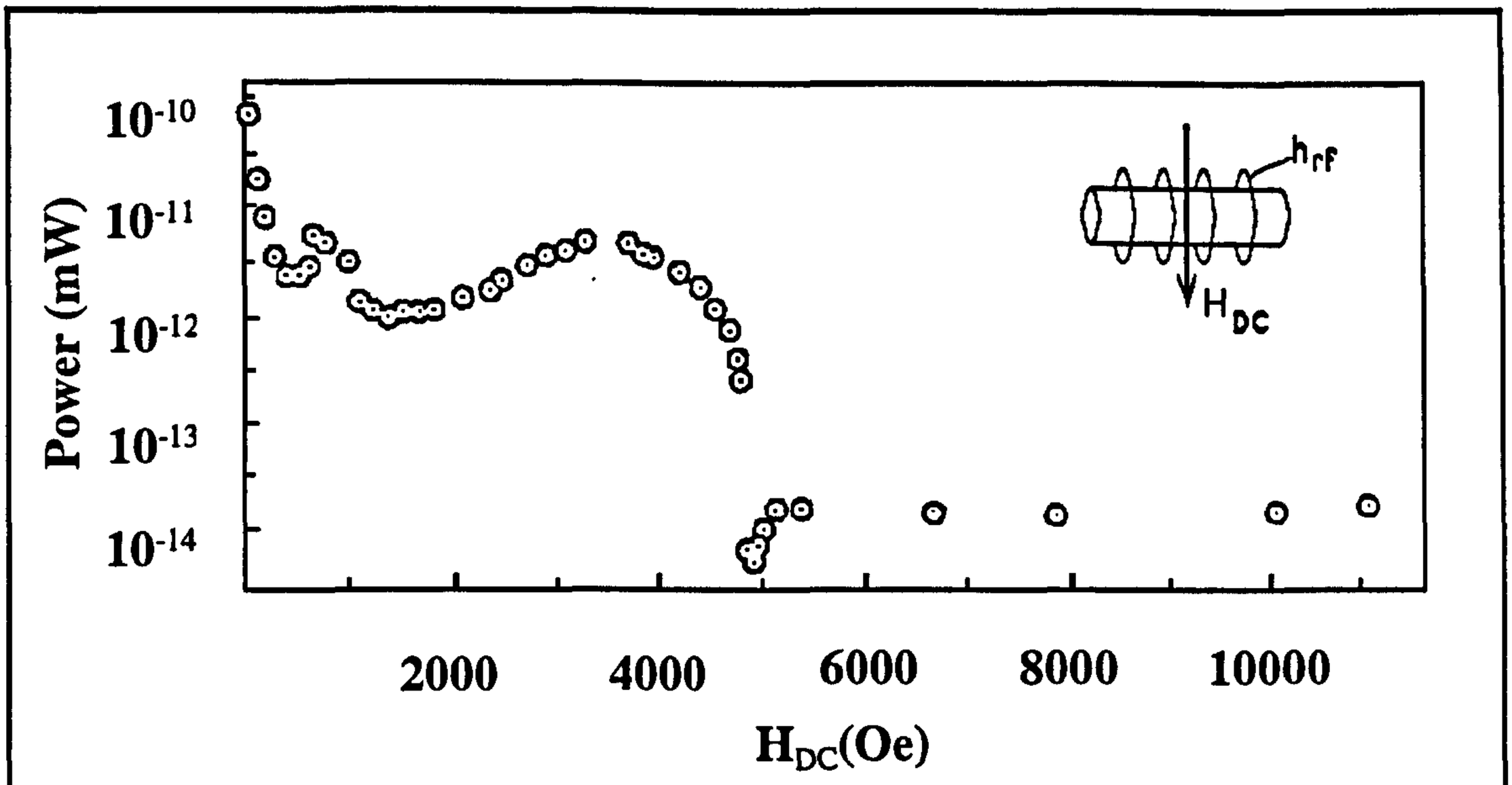

Fig.2.11 Intermodulation levels generated by a nickel-plated copper wire as a function of applied DC field. From Ref. [35].

Measurements on various nickel-plated RF connectors at VHF/UHF were undertaken by Young, who also obtained positive results [30, 36, 37] whilst Lee [38] obtained the highest level of PIM for cold rolled steel at UHF. However, Arazm and Benson did not observe any intermodulation in mild steel or nickel samples in their test arrangement at L-band [39].

2.4.2.5 Non-linear Effects in Dielectrics

PIM generation is not solely attributed to non-linear mechanisms in conductors. Very little work has been carried out on contributions to PIM interference from effects in dielectrics but theory predicts a few ways as to how this may come about, by non-linear permittivity for example.

The linear relationship between polarisation P, and electric field strength, E, in dielectrics (expressed by $P = \varepsilon_o \cdot \chi \cdot E$, where χ is susceptibility and ε_o is the permittivity of free space) is a consequence of the small mean displacement of bound charges and ceases to apply at high fields [40, 41, 42, 43]. In reference [42], a value for the field at which deviation from linearity becomes apparent is given as around 1000 V/mm. This implies high, but not unreasonable, current densities in the dielectric at microwave frequencies. For example, at 1.5 GHz and for a relative permittivity of 2.1 (typical of teflon and similar materials) this field strength corresponds to a displacement current density of 17 A/cm^2.

The non-linear polarisation may be modelled as a power series of susceptibility terms. Only odd powers will be present for dielectrics which do not exhibit spontaneous polarisation, since a polarity reversal in the electric field reverses the direction of polarisation but does not alter its intensity. The first non-linear term to become significant is cubic in the electric field:

$$P = \varepsilon_o \cdot (\chi \cdot E + \zeta \cdot E^3) \qquad \text{Eq.2.10}$$

Where ζ is the third-order susceptibility coefficient. This gives rise to a current term which is also proportional to the cube of the electric field and so third order intermodulation products will be generated.

Stauss et al. [30] dismiss non-linear permittivity as a source of PIM in dielectrics on the grounds that it is less significant than the indirect modulation of permittivity by means of electrostriction. It should be noted however, that the examples given in the reference are good non-polar dielectrics such as teflon which are selected for their desirable properties as insulators at radio frequencies and are of a high purity. Thus only electronic polarisation contributes to the relative permittivity and these materials are not representative of dielectrics in general.

Electrostriction refers to dimensional changes produced by electric fields [32], [33]. It is more common to consider only the change in volume as this is more simply derived although, in general, there will also be a change of shape.

In dielectrics, the volume change depends on the square of the electric field and may be positive or negative depending on the material. This occurs in all dielectrics and is not related to piezoelectricity. Kumar [34] attributes PIM generation in coaxial cables to electrostriction in the PTFE dielectric. A theoretical treatment of this is given in [30]. There is an associated thermal effect so that the volume change can also result in a temperature variation.

Recently, more conclusive work has been carried out at UKC [44] into the generation of third order harmonic signals due to the non-linearity in commonly used dielectrics. High levels of third harmonic signal have been observed for Nylon-66, Polythene and cross-linked Polystyrene which have been directly attributed to electrostriction. However no effect was observed in PTFE or alumina.

2.4.3 Avoidance Measures

Thus far we have considered the theory behind PIM generation and examined some of the mechanisms which may be responsible. The question now arises as to how to avoid PIM problems in the design of electronic components and systems. Many researchers have published guidelines for minimising passive intermodulation product generation which should be followed in order to reduce the likelihood of generating PIM [2, 7, 53, 76, 89]. These are summarised as follows:

A) The most effective way to reduce PIM interference is to isolate the low-level receive signals from the high power transmit signals. If the two signals can be run through separate signal paths, separate components and separate antennas, then there will be less chance of PIM products becoming a problem.

B) If a common path for low and high power signals cannot be avoided, then proper selection of transmit and receive frequencies is the starting point for PIM reduction. The PIM product power decreases as the PIM product order increases although not always in a directly calculable way. Thus the transmit and receive bands should be as widely separated as possible in the frequency regime so avoiding the stronger low-order products and hence lowering the risk of PIM products causing interference.

C) In the detailed design of a multichannel communications there are a number of guidelines to be used in the selection of system components:

(i) No ferromagnetic materials should be used in the system or in the vicinity of the system where they could be exposed to the transmitted signals. This includes connectors, cables, waveguide and structural components. Materials that should be avoided include steel, nickel and stainless steel. If, for some reason these materials have to be included in the system, they should be coated or plated in a highly conductive linear material such as gold or copper.

(ii) Careful attention should be paid to the reduction of the current density in the conductors of the system. regions of high current density should be reduced by increasing the dimensions of the RF components.

(iii) Tuning screws should not be used in the system because these can easily become loose or pick up dirt and then generate high levels of PIM products.

(iv) Where connections are required, these should be kept to an absolute minimum. At these interfaces, MIM junctions can form and generate high levels of PIM interference. Where possible, contact should be made at points of low current density.

(v) When coaxial cables are used, solid shield cables are the preferred type. When braided cables are used, the braid should not be made out of a ferromagnetic material. Cable lengths in general should be minimised, especially where flexible waveguides or cables are being used.

(vi) Contacts, connectors and components in general should be cleaned thoroughly at all stages of assembly. This is essential in order to prevent dirt from causing poor contacts and PIM.

D) The following mechanical design considerations should also be considered:

(i) Sharp edges should be avoided as these can act to concentrate the current flowing through the conductors.

(ii) Mechanical contacts and especially moving contacts should be avoided as much as possible.

(iii) Joints should be welded if possible as a properly welded joint generates very little noise.

(iv) All junctions should be rigidly mounted to minimise the possibility of vibration which can agitate PIM sources and cause interference.

(v) Good workmanship must be demanded during all operations. It is expensive and time consuming to locate and replace a component which is generating PIM products, only to find that the problem could have been avoided through better workmanship. However, as a precautionary measure, all equipment, components and assemblies should be tested before final integration.

These rules have been derived from the measurements carried out by researchers thus far. However, they cannot be guaranteed to provide a totally PIM free system and a better understanding of the causative mechanisms of PIM is required before more accurate recommendations can be defined.

2.5 Current Interest

The list of mechanisms which were presented are those more commonly put forward by researchers as being responsible for the generation passive intermodulation interference. Even so, it is evident that there is a great deal of disagreement and contradiction in the interpretation of the experimental data which exists.

Additionally, the recommendations for PIM avoidance, which are only basic "rules-of-thumb", are based upon the doctrine that if something poses even a small threat of PIM generation then it should be avoided completely.

In both cases there is little evidence to suggest the validity of the claims that are made or the confidence with which the results may be used. Also, there is extremely little information indicating which effects or countermeasures are most influential or more dominant. This presents a great deal of inadequate information to communication systems design engineers making it extremely difficult for them to adopt low-PIM techniques and practices in which they can be confident.

Clearly, there is a need for clarification of the present data and a requirement for greater understanding of the phenomena responsible for PIM product generation. Presently, there is no area in which unquestionable results exist and which would not benefit from further scrutiny. Hence, in order to provide a sound scientific basis for the design of low-PIM systems, much more experimental work is required.

The need for additional data on the nature of PIM signals implies that some sort of measurement capability is required. Initially, the necessary data will be identified by the needs of engineers and should therefore apply directly to practical situations and problems. Analysis of this data should then define those areas which will provide useful and interesting results in the investigation of the fundamental physical mechanisms of PIM generation. The understanding developed from a study of this type should, in turn lead to much better guidelines for improving hardware design and system performance.

2.6 Expanded Objectives

In Chapter 1, the objectives of the UKC PIM study were set out. In this section these will be expanded in order to justify the work carried out on this project.

- Design and build a highly sensitive but stable and consistent PIM measurement system.

The need to build a PIM measurement system was defined in the last section. The system must be dedicated solely to PIM measurements due to the significant time and effort required to optimise the performance of such a system.

The system must also be highly sensitive to PIM signals generated in a given test sample in order to indicate the smallest fluctuations due to changes in test parameters. This will obtain the maximum amount of information from the measurements but requires maximum suppression of the residual intermodulation levels generated by the system itself.

The level of system residual PIM must also be stable and consistent. This ensures that the measurements will be repeatable and not influenced by variation in the system performance. Thus, comparisons between measurement results will be valid and will reflect the different characteristics between samples or test parameters.

- Propose a standard methodology to enable the PIM characteristics of materials to be measured and compared in a consistent manner.

In keeping with the repeatable performance of the measurement system, the measurement techniques and sample configuration must also be consistent from test to test. This is the only way to minimise errors and allows direct comparisons to be drawn between different parameters. The samples should be able to be formed from a wide range of materials so that they may be directly compared. The sample format must remain flexible enough to incorporate new features and allow any interesting results to be developed further. It should also be possible to vary the parameters of the samples in order to gauge their significance on PIM generation.

- Produce a set of PIM measurements which describe the PIM characteristics of selected space qualified materials.

As the information on PIM mechanisms to date is scant and unreliable, the approach taken was to initially acquire data of immediate use to engineers. This would take the form of measurements on particular materials and the effects of standard engineering practices on these materials. From the data obtained it is possible to highlight areas that will benefit from more detailed study and the process of investigating the operation of particular mechanisms can begin. This is in contrast to previous programmes where, in some cases, particular mechanisms are targeted and investigated but with no substantiated evidence that they predominate in real-life situations.

- To identify the dominant causative mechanisms of PIM behaviour in the materials tested.

Due to the weakness of existing knowledge, and in view of the wide range of materials and possible mechanisms, only the initial phases of an experimental programme can be considered. The direction taken will depend on the outcome of the work on the engineering data.

(vi) Analysis.

If the mechanisms responsible for PIM generation are little understood then the modelling of these mechanisms is even more ambiguous. It is expected that to accurately model the behaviour of PIM mechanisms will be difficult and will call upon many of the more subtle aspects of solid-state physics and electromagnetic theory. It is therefore not envisaged that exact models will be derived for specific mechanisms. It is intended more to establish what would be required of the measurement system and experimental data in order to make progress in this area.

2.7 Review of Previous PIM Research.

Over the past fifty years, there have been many investigations of passive intermodulation in multi-frequency radio environments. To appreciate the scope of previous studies and the significance of the present project, a brief review of previous investigations is presented in the following sections.

Copies of approximately 88 scientific papers and reports relating directly to PIM were obtained. They cover the period from 1937[45] to the present day. It is believed that this represents a very nearly comprehensive collection of the publicly available reports and scientific literature published in Western Europe and the United States. There is a considerable degree of overlap between the publications as they represent the work of comparatively few organisations and individuals. Thus it is believed that any literature as yet uncovered would not contribute much new information.

Of the literature collected, around 27 references address the question of fundamental causative mechanisms, either theoretically or experimentally. The remainder are concerned with measurement techniques for different situations or with tests on particular systems. Most investigators have concentrated on one or two mechanisms and this has sometimes resulted in the neglect of necessary experimental controls and procedures. Due to the many different test samples used, the various techniques for exciting these samples and for collecting any intermodulation products, and the wide range of frequencies employed, it is impossible to sensibly compare results. This problem is aggravated in many cases by insufficient data on the material samples tested.

The following review is divided into seven sections which deal with either specific communications environments or passive components. It mainly covers the experimental aspects of PIM research.

2.7.1 Waveguide Components and Reflector Antennas

Microwave engineers often overlook the fact that many passive components can generate significant levels of PIMI. One of the papers paying a great deal of attention to this matter was published by Cox [46]. In this paper he describes a measurement circuit to measure the *3rd*, *5th* and *7th* order intermodulation signals generated in the waveguide components of a 6 GHz communications system. Tests were conducted on waveguide joints, flexible waveguide, isolators and circulators. The measurements revealed that loose waveguide joints and waveguide tuning screws can generate *3rd* order PIM levels as great as -25 dBm when using two 30 dBm transmitters. The sources of mixing products in the flexible waveguide were found to be mainly in the transitions between the flanged joints and flexible waveguide. In all cases observed, loose metallic joints were found to generate erratic and high levels of intermodulation signals.

Detailed investigations of the generation of PIM in antenna feeds, filters and microwave components used in a multi-carrier system with high-power transmitters and low-noise receivers have been reported by Chapman et al.[47] and Rootsey et al.[19]. They developed a measurement setup capable of delivering microwave power up to 10 kW and detecting intermodulation signals down to -140 dBm in the 8GHz band. The PIM levels were measured as functions of total input power, proportional power between carriers and waveguide current densities. The specific problems encountered in fabricating waveguide components and their relationships to intermodulation generation were studied. Specific emphasis was given to the study of waveguide flanges, tuning devices, seams, materials and the degeneration of these components with time. They also studied the physical mechanisms responsible for PIM generation at metallic contacts. The measurements revealed no correlation between the PIM levels and materials used in antenna feeds. However, the PIM levels were related directly to how the metals were joined together, the quality of the mating surface finish, the pressure of the junction contact, and the quality and cleanliness of the brazing or soldering process. A simple non-linear model was derived and compared with experimental results. Guidelines for designing low PIMP microwave systems were also suggested.

Nuding [48] investigated the non-linearities of flange transitions in standard waveguide transmission lines carrying high RF power. a test facility was developed to test flanges up to 1 kW in the 2 GHz band. Measurements revealed that with input power up to 500 W, the amplitudes of the 3rd order PIM products vary according to the third power of the applied signal level. Above 500 W, the relationship between the input signals and the intermodulation products does not follow the same relationship. No explanation was given for this effect.

In the 70's, Matos [49] published a short review paper on PIM generation in waveguide joints, coaxial cables and circulators. Mato's paper summarises the investigations carried out by Young [36], Cox [46], Rootsey et al.[19], Bayrak and Benson [50], and Betts and Ebenezer [71].

Large reflector antennas are usually fabricated by assembling a large number of small aluminium panels onto a large structure according to a paper by Higa [22]. In NASA Deep Space Network antennas, the difference between the transmit and receive signal levels can be as large as 250 dB. Under such conditions, the intermodulation signals generated by aluminium joints can cause serious PIM. Higa investigated this problem and gave a detailed discussion of the mechanisms proposed as responsible for the PIM generation. He developed a model based on the electron-tunnelling theory and performed laboratory experiments at around 2 GHz to support his model. His paper also describes the electron-tunnelling phenomenon in terms of an antenna structure and analyses the antenna as a non-linear circuit element.

Guenzer [24] was critical of both the analysis and the interpretation of Higa's experimental results. Bond, Guenzer and Carosella [23, 30] later published measurements of intermodulation levels (attributed to tunnelling), I-V characteristics, and capacitances for specially fabricated aluminium-oxide-aluminium junctions. A test facility was developed to measure the *3rd* order (290 MHz) intermodulation signal. The PIM levels were correlated with the junction parameters and tunnelling theory. Measurements revealed that oxide surfaces with implanted metallic ions are more conductive and linear than ordinary oxide surfaces.

Kellar [51] made similar measurements on contacts between two pieces of aluminium and observed that the junction effect was reduced after a DC potential had been applied across the junction. greater contact force was also observed to reduce intermodulation.

Shands and Woody [25] measured PIM (also attributed to tunnelling) generated by different forms of riveted joint, for various alloys and surface treatments. they concluded that present theories of tunnelling are not adequate to model real junctions at radio frequencies.

The non-linearity of carbon fibre has been studied theoretically by Ghione and Orefice [52]. In the 80's Lee [38, 53] developed a VHF measurement system to characterise carbon fibre and other non-linear materials. A half-wavelength long coaxial line was designed to accommodate a test sample which forms the inner conductor of the coaxial line. he concluded that carbon fibre generates high levels of intermodulation signals. Around the same time, Watson [73, 74] of Plessey also investigated the non-linearity of

carbon fibre composite (CFC). He used an experimental set-up which is different from Lee's system and showed that jointless CFC materials are linear, but jointed CFC panels generate discernable harmonic products.

2.7.2 Coaxial Cables, Connectors and RF Components

In the 60's researchers at IIT Research Institute in Chicago studied the non-linearities of cables, connectors, dummy loads and metals [54, 55]. They discovered that ferromagnetic materials such as nickel and stainless steels generate harmonic and intermodulation products, and the product levels increase as a function of current density. Distributed loads such as long lengths of coaxial cable were found to be more linear than lumped loads.

In the 70's several researchers studied the non-linear effects of cables, connectors and metals in the microwave bands [39,50, 58-62]. First Bayrak and Benson [50] made a detailed experimental study of the non-linear effects at contacts between similar and dissimilar metals. An S-band experimental set-up was designed to measure the *3rd* and *5th* order intermodulation signals. Contact materials of commercial copper, brass, mild steel, aluminium alloy, stainless steel, nickel and electroplated brass contacts of gold, silver, copper and tin, were studied under various test conditions. Test samples were fabricated in three different forms; surface, spherical and point contacts, with different contact areas. they also carried out preliminary measurements on coaxial cables with different types of construction and a variety of coaxial and waveguide components. Bayrak's work was later continued by Sanli [58]. Sanli improved Bayrak's experimental set-up and tested samples with mechanically polished, electropolished and oxidised surfaces. Arazm's work [39] is similar to that carried out by Bayrak. He tested a variety of metals including some home-made steels at frequencies around 1.5 GHz. The *3rd* and 5th order intermodulation signals were measured as functions of the types of metal, input power levels and axial force applied to the metallic contacts. Arazm's work was later extended by Sanli [59].

Amin and Benson [60, 61] measured the odd order PIM product levels of commercially available and specially constructed cables at L-, S- and C-band frequencies. The parameters studied include composition of braid materials, lengths of cable, types of inner conductor and braid construction, number of braids, braid filling factor, discontinuities and corrosion in the braids, fundamental frequencies and ambient temperature. They observed that the ambient temperature in the case of polythene dielectric cables and oxides on copper-wire braids considerably affects the generation of PIM in a coaxial cable. It was concluded that the composition of the braid materials is by far the most important parameter in PIM generation.

Martin of ERA [62] studied the PIMP generation in bulk materials, cables and connectors in the HF and UHF bands. He developed a simple test bench and investigated the effects of surface films, RF power levels, contact pressure, effect of frequency and ageing on PIM generation. Problems in cables, connectors and structures were outlined and some suggestions were made as to how best to reduce them. Many of the conclusions drawn by Martin are similar to those reported by researchers at the University of Sheffield [39,50, 58-61].

Young's investigation [36] concentrates on the non-linear effect of ferromagnetic materials adaptors and connectors. He developed a low-noise VHF test set to characterise a large number of commercially available RF components. The non-linear effects of stainless steel, nickel plating, and hermetic sealing were studied. He also measured the PIM levels as functions of the magnetic field strength, RF power and types of metals.

In 1970, Von Heinz Neubauer at Rhode and Schwartz investigated connections between the outer braid of flexible coaxial cable and various connectors [63]. Only badly corroded assemblies displayed a distinctive PIM signal.

In the 80's, the PIM problem in cables and connectors was again addressed. Shands, Denny and Woody of Georgia Tech [64, 65] tested 83 samples made from various coaxial cables, connectors and cable-connector combinations. Samples were measured at frequencies from 22 MHz to 450 MHz and at power levels up to 126 W. Empirical models were developed as functions of various test parameters and then verified by characterising new samples.

A recent paper by Kellar [51] describes the measurement system, experiments and test results of corroded and loose connectors used in cable television systems. The results obtained are similar to those reported by Bayrak and Benson [50].

The investigations described so far have concentrated on coaxial cables, connectors and waveguide components. Gardiner et al. [66] investigated the IM generation in typical multicoupler components. Two areas have been identified as possible sources of PIMI: (i) the aluminium interfaces at cavity walls. (ii) The bi-metallic interfaces such as the centre conductor to cavity wall connection, connectors to outer case, copper sheet to cavity walls etc. A VHF measurement system was developed to compare PIM levels generated by specially made reference components and standard components. Measurements revealed that the standard components generate stronger intermodulation signals and could be the potential PIM sources at radio sites.

The latest paper to be published on PIM in connectors is by King [67]. The paper highlights the increasing problem of PIM in coaxial connectors. The advent of the global system for mobile communications (GSM), digital communications systems (DCS) and personal communications services (PCS), has resulted in increased power requirements. This leads to an increased vulnerability to PIM generation. The author highlights the lack of standard approaches to PIM characterisation and recommends measures for minimising PIM in connector design. No experimental data is presented.

2.7.3 Shipboard Communications Systems

One of the earliest papers on PIMI in a ship environment was published by Blake [68]. He conducted field experiments in the VHF band on a wooden test tower and a naval vessel. Results revealed that the interference signals were generated at the tie plates and bolts of the wooden tower. these signals could also be reproduced by touching together any two pieces of corroded metal. The effect was found to be very strong if the length of metal was approximately a multiple of one half-wavelength. During field trials, the footropes, pulley shackles and a loose aerial rod aboard the vessel were identified as principal interference sources.

Mason's paper [69] describes a method for measuring the spurious signals generated by a multi-channel HF system radiating from a common antenna aboard a ship. He observed that the residual PIM level changed considerably from day to day. He associated these variations with the changes in atmospheric conditions and the unstable properties of non-linear contacts.

A large scale project which involved laboratory and field experiments and the development of PIM detection techniques on naval vessels was carried out by the US Navy in the late 60's [56, 57, 70]. It was concerned with the narrowband multiple-transmission communications system. Research efforts were directed towards an assessment of the relative intermodulation contribution of the two non-linear mechanisms. results revealed that using the PIM level to input power relationship is not a reliable way to separate the contact non-linearity from the ferromagnetic non-linearity. Laboratory experiments showed that loose contacts generate much stronger and less stable PIM signals than those generated by steel. Field trials indicated that ferromagnetic non-linearity probably accounts for a significant proportion of the residual PIM level associated with the clean ship. In all cases observed, the most significant PIM sources located are the loose and/or corroded metallic joints [57, 70].

Papers by Betts and Ebenezer [71, 72] describe the set-up and results of a laboratory investigation in which steel samples were tested in the HF band with known field strength and orientation. Attention has been given to the PIM level dependence upon surface preparation, which includes machined and polished, electro-deposited cadmium, cold sprayed zinc finishes, corroded and clean surfaces. A comparison of PIM levels for various types of steel was made. the main purpose of the field trials was to determine whether the ship structure is a significant interference source, and the possibility of separating it from the contact non-linearity.

The work of Watson [73, 74] concentrates on the measurement of harmonic and intermodulation products generated by metallic and carbon fibre junctions in structures. His papers describe a 100 MHz to 8 GHz harmonic backscatter free space measurement system and an HF intermodulation detection system to characterise passive non-linearities. He also developed a laboratory waveguide test jig to measure the properties of non-linear junctions and materials. Measurements revealed that joined metallic objects such as lengths of rigging including shackles and eyebolts generate significant harmonic products, but the bulk and jointless materials generate no measurable harmonic products.

2.7.4 Aircraft Communications Systems

The PIM generated by aircraft passive components and structures have been operationally and experimentally shown to be large enough to degrade system performance. In a surveillance aircraft where high-power transmitters and sensitive receivers are co-located, the problem can be very serious [75, 76]. Shands and Woody have investigated the non-linearities of coaxial cables and connectors used on aircraft [64, 65]. Recently they have investigated the PIM generated by aircraft structures [25]. Test samples which closely resemble the actual aircraft panel joints were constructed. The 3rd order intermodulation signals were measured from 20 MHz to 1100 MHz with typical input power of 44dBm. The relationships between the PIM levels and various parameters such as vibration, temperature, pressure, input power, frequency, types of joint and metal, chemical treatments and sealants were studied. A model based upon the experimental data was built to describe the PIM behaviour as a function of some of these parameters.

2.7.5 Terrestrial Radio Sites

PIM problems at land-based radio sites is very well known and have been widely reported [3-7], [14-88]. In the mid 70's, Betts [84] explained the significance of PIM in mobile radio communications systems. A few years later, Betts and Debney [85] measured PIM levels at three VHF land mobile radio sites. Their measurements revealed that

with a typical transmitter level of 32 W per channel, the intermodulation signals generated due to antennas, tower structures and surrounding metalwork are negligible. However, at higher transmitter power, 500 W, PIM signals were measurable up to the 11th order product.

At Bradford University, Mawjoud and Gardiner [81] measured the DC I-V characteristics of corroded metallic joints and modelled them as two back-to-back diodes and without added resistance. They also carried out field measurements of a simulated corroded joint and the results agree to those reported by Sturton [82] and Shepherd [83].

The recent work at City University [86] concentrates on the development of chemical compounds to suppress PIM. A VHF laboratory measurement system and a remote control field data acquisition system have been developed to evaluate the performance of the chemical compounds. Samples such as gold, platinum, copper, steel and corroded steel were fabricated in the form of a small tube for laboratory test.

The UK Home Office [87, 88] also conducted laboratory and field investigations of the 'rusty bolt' effect at land mobile radio sites. the field measurement [87] studied the relationships between the PIM levels and the polarisation, transmitter configuration and audio impairment caused by PIM. In all the laboratory measurements, tests were conducted without using any real samples, the passive non-linearity of the measurement system was used to simulate the 'rusty bolt' effect.

More recently, Lui and Rawlins [3-7] at the University of Kent carried out investigations into PIM generation by structural components at terrestrial mobile radio sites operated by the Home Office. The studies involved both laboratory and field investigations at high band VHF. Using a laboratory set-up the relationships between PIM level, input power, types of metals and joints, joint pressure, effects of vibration and moisture were all studied. The field measurements were conducted under operating conditions similar to those experienced at a normal radio site, the aim being to study relationships between PIM levels, transmitter output power and weather conditions. From the laboratory experiments it was established that mild steel produced the most significant levels of PIM but that these levels could be reduced considerably by applying a galvanised zinc coating to British Standard BS 729. It was found that badly rusted joints proved to be a serious problem only if the joints were loose or the area of contact was relatively small. No firm conclusions could be drawn from the field experiments however. Additionally, an attempt was made to explain the non-linearities in terms of physical mechanisms but again no firm conclusions were reached.

2.7.6 Spaceborne Satellite Payloads

The recent work of Kumar [34] concentrates on the passive IMI problems in high-power satellite systems. Kumar's paper describes the causes of PIM and summarises the design guidelines for minimising the generation of PIM in RF components and systems. A similar paper by Hoeber et al.[2] also considers the problem in satellite systems but goes further and gives a detailed review of the PIM problems encountered on the FLTSATCOM, MARISAT, MARECS and INTELSAT V payloads. As a result of the review, detailed design considerations are given for the avoidance of PIM and a summary of PIM generation theory is provided with a review of previous work. The conclusion is that PIM signals appear unpredictable under different test conditions and levels are highest for third order. Further conclusions are given on the reasons for PIM problems.

A great deal of experimental work has been carried out by workers in the satellite industry. Staff at the technical centre of the European Space Agency, ESTEC (European Space Research and Technology Centre) have carried out numerous tests on antennas at L-band, solar arrays at C-band and waveguide components and flanges at Ku-band [8-11]. However much of the work has been concerned with the qualification of actual space flight hardware. Accordingly, tests have only been carried out at frequencies where potential problems exist. These tend to involve the higher-order intermodulation products which are generally accepted to be weaker than low-order PIM signals and as such no PIM signals were observed during any of the tests. This is typical of most of the work carried out in the satellite industry to date although MBB of Munich [108] have investigated the use of bar-line technology for low-PIM, low volume, high power components. this issue has also been covered by A.Mok [109].

The latest research to be carried out with respect to satellite systems also has implications throughout the field of PIM. At the University of Kent, Khattab and Rawlins [44] have conducted preliminary studies into the generation of third harmonic signals by dielectric materials which are commonly used in communications systems, satellites in particular. By using the high field strength in a coaxial cavity of high Q, they were able to demonstrate that samples of Nylon-66, Polystyrene and Polythene all exhibit an obvious non-linear relationship, whilst harmonics generated by samples of PTFE and Alumina (Al_2O_3) were not discernible from the background levels in the system. A theoretical analysis was carried out and several likely mechanisms were proposed to be responsible for the observations with electrostriction being the most viable.

2.8 Summary

It is evident from the literature review that much of the work carried out to date has been centred around the testing of system components. This serves to gauge their suitability for use in a PIM sensitive environment, but without much consideration as to the mechanisms behind their behaviour.

In fact PIM literature contributes little to the identification of basic mechanisms, apart from the observations that high PIM levels are generated at metal-metal contacts and that this occurs for a wide range of metals. There are a number of reasons for this lack: Only a small proportion of the work was undertaken for the express purpose of determining PIM generation mechanisms. Many of the papers consider only one or two of the possible causes and, as a result, experimental controls to distinguish between other effects are absent. Effort and expertise have been directed at the RF measurement problems and the vital, and complex, materials and solid-state physics aspects have largely been neglected or oversimplified.

There are two types of IM in multi-carrier communications environments and systems. Active IMI is known to be a more serious problem but can be minimised by well developed techniques. However, the equally well known passive IMI problem cannot be minimised by the same techniques. From the recent published literature, it can be concluded that there is no evidence that this problem is well understood or anywhere near to being solved.

CHAPTER 3

PIM Measurement System Design

This chapter deals with the theory and techniques employed in designing PIM measurement systems. The chapter includes a description of the initial experimental set-up at the University of Kent and an analysis of its performance. The chapter concludes by considering those areas of the system where changes could be made in order to improve the performance.

3.1 Introduction to PIM Measurements

One of the first articles to report on the phenomenon of PIM was published in 1937 [45]. Since then many researchers have endeavoured to measure and quantify the effect and descriptions of approximately 44 systems for measuring low levels of non-linear behaviour at radio frequencies were obtained from the literature.

The performance of early PIM measurement systems was relatively poor. However they were effective at the time for studying PIM in areas like shipboard [56, 57, 68-74], and aircraft [25,64, 65, 75, 76] communications. The specifications of these systems, in terms of intrinsic PIM levels, were far less demanding than those of today's high performance communications satellites. It is not uncommon for satellite systems to operate with a dynamic range of over 200 dB between the levels of transmit and receive signals [47]. It is evident therefore that any measurement system used in the qualification of spacecraft materials and equipment should be able to demonstrate the absence of PIM over such a range.

Generally, PIM measurement systems can be classified as either conductive or radiative.These are indicated in Fig.3.1 and Fig.3.2. Conducting systems are suitable for testing items such as non-linear materials, connectors, cables, filters and waveguide components. They are normally housed in a laboratory environment, are terminated in a matched load

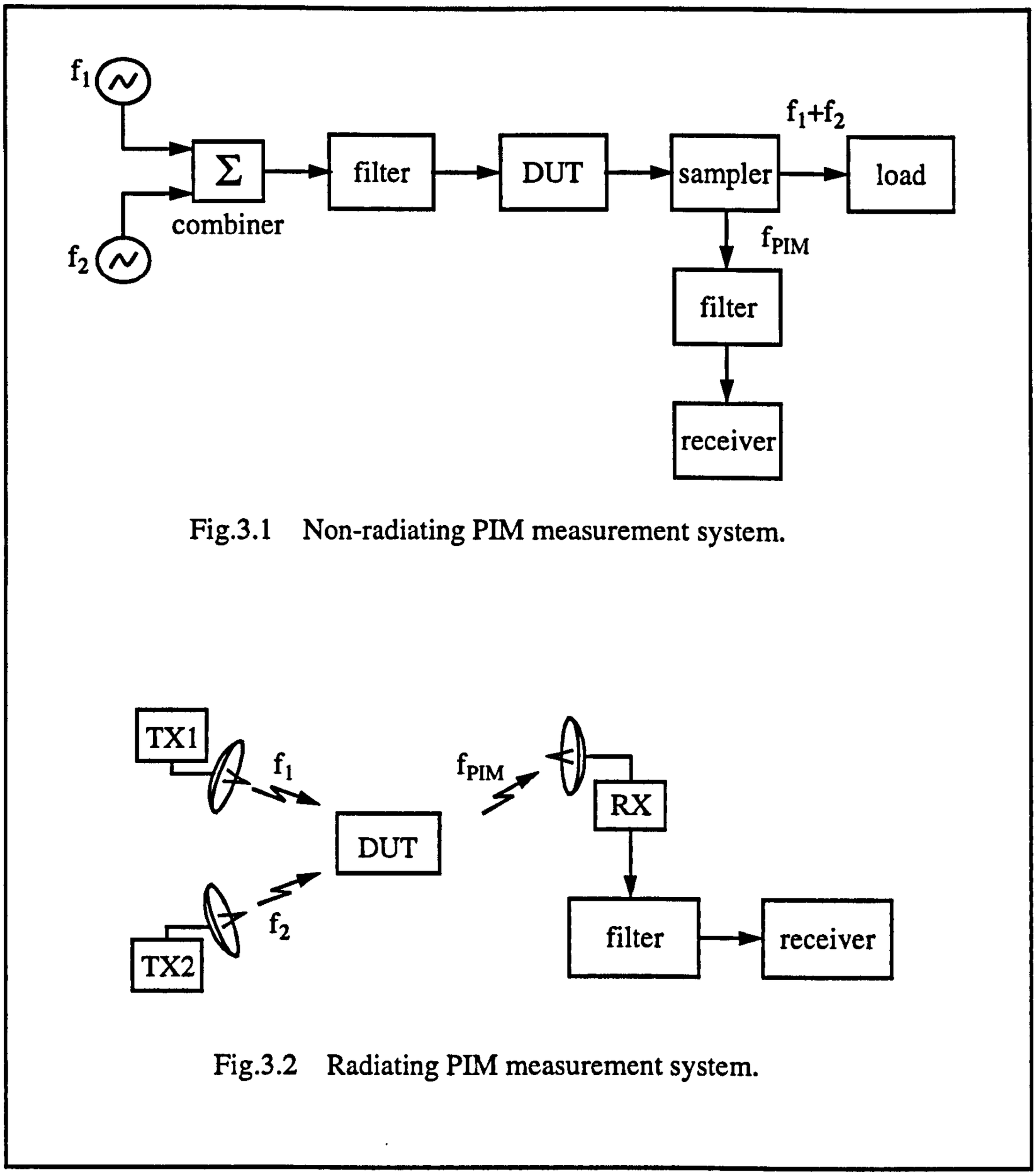

Fig.3.1 Non-radiating PIM measurement system.

Fig.3.2 Radiating PIM measurement system.

and ideally, no energy is radiated. Radiative systems are used for investigating components associated with radiating structures. These include; antennas, feeds and large structural components. Radiative systems are normally used in association with anechoic chambers. The conducting system is more widely used because the user has better control over the test parameters and the test environment. However, the radiative system is essential for certain tests, although it can be adversely affected by the local signal environment.

In either case, the technique which has been most commonly employed in the study of IMD is the use of dual-frequency, equal power signals. The dual frequencies are used to excite the sample and any intermodulation signals generated are filtered and measured. Equal power levels are used in order to simplify the analysis of the results.

The principle problem in assembling a PIM measurement system is that the measurement system itself is vulnerable to intermodulation generation. This system IMD or "residual intermodulation" must be eliminated as far as possible otherwise the sensitivity of the system will be poor.

An essential feature of PIM measurement systems is that the level of any residual PIM should be as stable and repeatable as possible. This is so that measurements are consistent and not dominated by system variability.

This chapter deals with the design of PIM measurement systems. It includes discussions on system requirements, design considerations, system hardware, implementation and performance. The concluding part of the chapter deals with techniques for locating sources of residual PIM and improving the system performance.

3.2 System Requirements

The function of a PIM measurement system is to accurately measure and quantify PIM generation from a particular source. The source may be any DUT including passive RF and microwave components. These are usually tested to determine their suitability for use in PIM sensitive systems.

For diagnostic research work, the system should also provide for the study of various parameters which affect PIM generation in the DUT under a controlled environment. By studying these parameters it should be possible to characterise the behaviour of the nonlinearity and isolate the physical mechanisms responsible. In order to set up such a system several key requirements were identified:

(i) The system should have the capability to excite the nonlinearity in test samples and to detect the resulting low level intermodulation signals.

(ii) The system should have a high degree of linearity and hence a low residual intermodulation level.

(iii) Any residual intermodulation signals should be extremely stable.

(iv) The system should be flexible enough to carry out a wide variety of tests.

(v) It should be possible to easily change the test samples without adversely affecting the system performance.

(vi) The system should have a configuration that can be set up using standard equipment.

From these general system requirements we can begin to build up an idea of how the system should function and we can start to develop the system specification. Consider Fig.3.1, firstly it is essential that we have two independent signal sources at the desired test frequencies. These signals will then have to be amplified to the high levels required to produce a detectable PIM signal. Next, the two signals will have to be combined into a transmission medium common to the device or sample that is to be excited. During these stages it is likely that IMD will be generated due to both active and passive non-linearities. This will have to be suppressed before the excitation signal passes through the DUT otherwise the level of PIM due solely to the DUT will be obscured.

Next, the excitation signal must be transmitted to the DUT where it can excite a PIM signal. The PIM signal will then have to be isolated from the excitation signals and measured. Due to the high power of the excitation signals, they must be heavily attenuated before reaching the detection circuit. If not, there will be significant intermodulation produced in the active devices, or even irreparable damage, such is the sensitivity of this part of the system. The next section considers some of the different aspects to the design of such a system

3.3 Design Considerations

On closer examination of the system requirements it is evident that there are a number of considerations which are particular to the design of a PIM measurement system. One of the most important of these is that PIM specifications are not presently published for standard components and typical levels are usually too high for measurement applications. System design work relies on past experience and the avoidance of certain constructional techniques and materials which were outlined in Section 2.4.3. Where this is not possible with commercial components, custom components must be specially made for the system. However, during the initial stages of system development, extensive use of commercial components must be made so that a process of refinement can commence. In general it has been found that good PIM performance is only achieved by the modification and adjustment of existing system components.

3.3.1 Propagation Direction

One choice that has to be made is whether to measure forward PIM (i.e. propagating in the same direction as the carriers), reverse PIM, or both. Sometimes this is determined by the test requirement, for example in the feed to a common transmit/receive antenna it is probably the reverse PIM specification that is of interest.

Dimensionally small PIM sources, would typically be expected to produce more or less equal PIM levels in both directions and the more convenient one may be monitored. Distributed sources such as cables which are longer than a fraction of a wavelength and have significant attenuation, produce PIM levels which vary with the length and are dependent on direction.

In the case of multiple or distributed sources of PIM, the implications of the choice of direction are very significant. Where the non-linear properties of a sample are being considered with respect to PIM generation, let us assume that these properties are manifest in a stable and consistent manner. When the sample acts as a conducting medium for an electromagnetic wave, it can be reasonably assumed that the majority of non-linear sites will produce intermodulation signals which are phase correlated to the stimulus signals. Consequently, all PIM sources which have the same fundamental mechanism will also be phase correlated. These PIM sites can be regarded as a large number of distributed sources which can be summed together to produce a resultant PIM signal.

Consider the PIM voltage contribution of several elements, dz, along a material with its axis in the z direction as depicted in Fig.3.3. Assume that each element in the material generates PIM with the same magnitude, V_p in each direction.

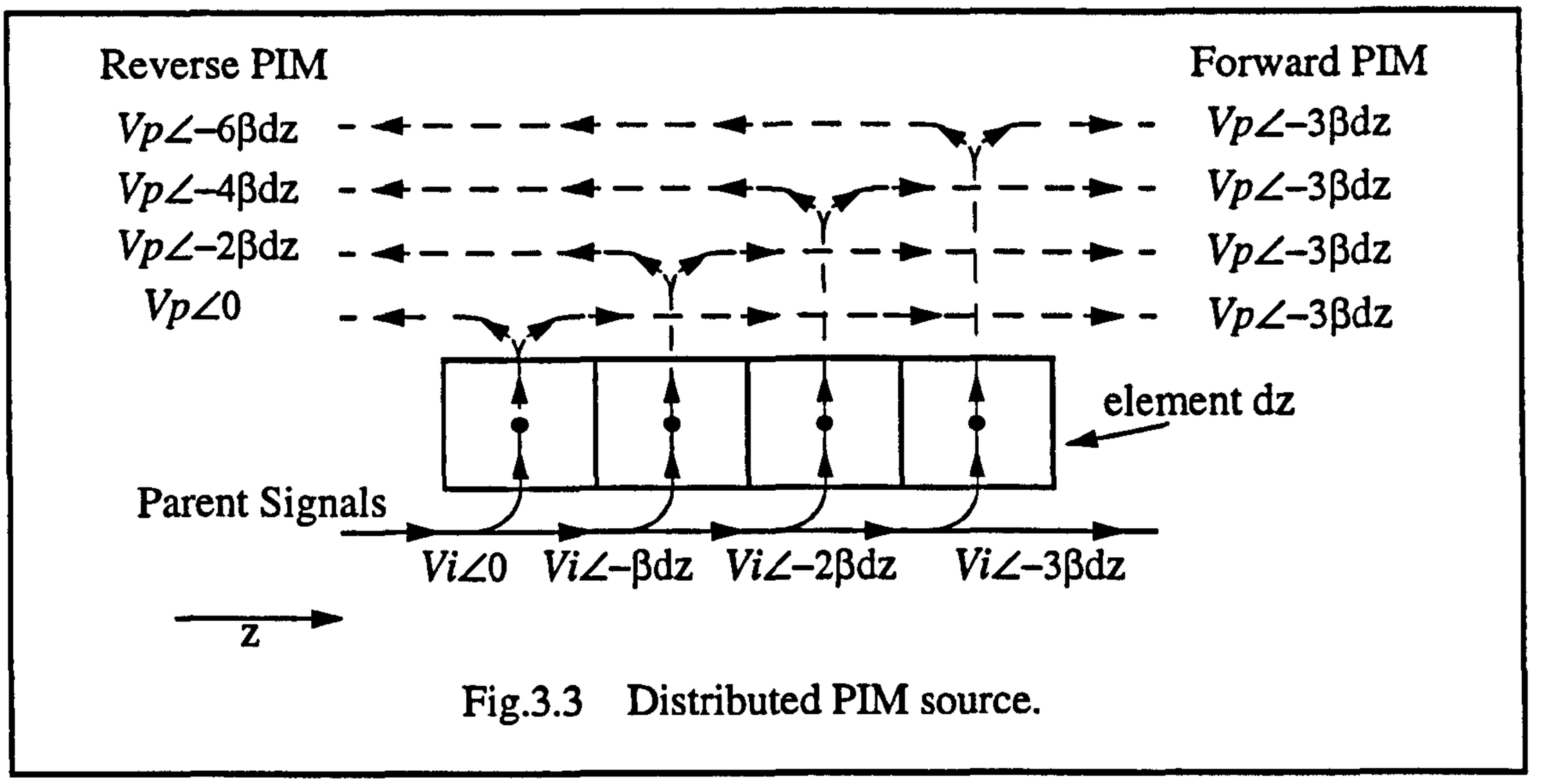

Fig.3.3 Distributed PIM source.

Ignoring attenuation, as the parent signals propagate along the sample, at any instant in time, they are phase-delayed by βdz at subsequent elements. In the forward direction, all of the PIM signals will be in phase and the overall PIM signal will, therefore, have an amplitude equal to the sum of the amplitudes of the individual elements dz. The forward PIM level will therefore increase as the length of the distributed source increases.

In the reverse direction, the relationship is not so straight forward. Since the parent signals and PIM signals are travelling in opposite directions, the delay between subsequent PIM signals will add to the delay of the parent signals and the phase shift will be doubled. The reverse PIM level will therefore be related to the phasor-sum of the individual PIM signals from elements *dz*, and hence, to the length of the source.

Consider two PIM sources at points P_1 and P_2, separated by a distance *l*. At time *t*, the reverse travelling PIM signal from P_1 may be described by:

$$V_p cos(\omega t + \phi_p) \qquad \text{Eq.3.1}$$

ϕ_p is an arbitrary constant phase term to account for any phase offset at time, t=0.

The signal from P_2 will then be described by:

$$V_p cos(\omega t + \phi_p - 2\theta_l) \qquad \text{Eq.3.2}$$

Where $\theta_l = \frac{\omega l}{c}$ and *c* is the speed of light.

Then, for a distributed source of length *l*, the signal at P_1 will be given by:

$$\int_0^{\theta_l} V_p cos(\omega t + \phi_p - 2\theta) d\theta \qquad \text{Eq.3.3}$$

Eq.3.3 simplifies to:

$$V_p sin(\theta_l) \cdot cos(\omega t + \phi_p - \theta_l) \qquad \text{Eq.3.4}$$

Eq.3.4 clearly comprises an amplitude term $V_p sin(\theta_l)$ and a phase term $cos(\omega t + \phi_p - \theta_l)$. Therefore, the amplitude of the reverse travelling PIM signal is a function of *l*. The spatial variation of Eq.3.4 is plotted in Fig.3.4 as a normalised power function indicating the variation of total PIM power as a function of the electrical length of material.

The implication of Eq.3.4 is that when a distributed PIM sample is being investigated it is important to choose the correct electrical length. If the sample is chosen to be an integer number of half wavelengths long then the resultant PIM signal will be a minimum, therefore, little or no contribution from the sample to the PIM level would be observed. If the sample is an odd number of quarter wavelengths then a maximum PIM signal will be achieved. These maxima and minima will only be observed if the PIM contribution from the sample is significantly above that of the system residual.

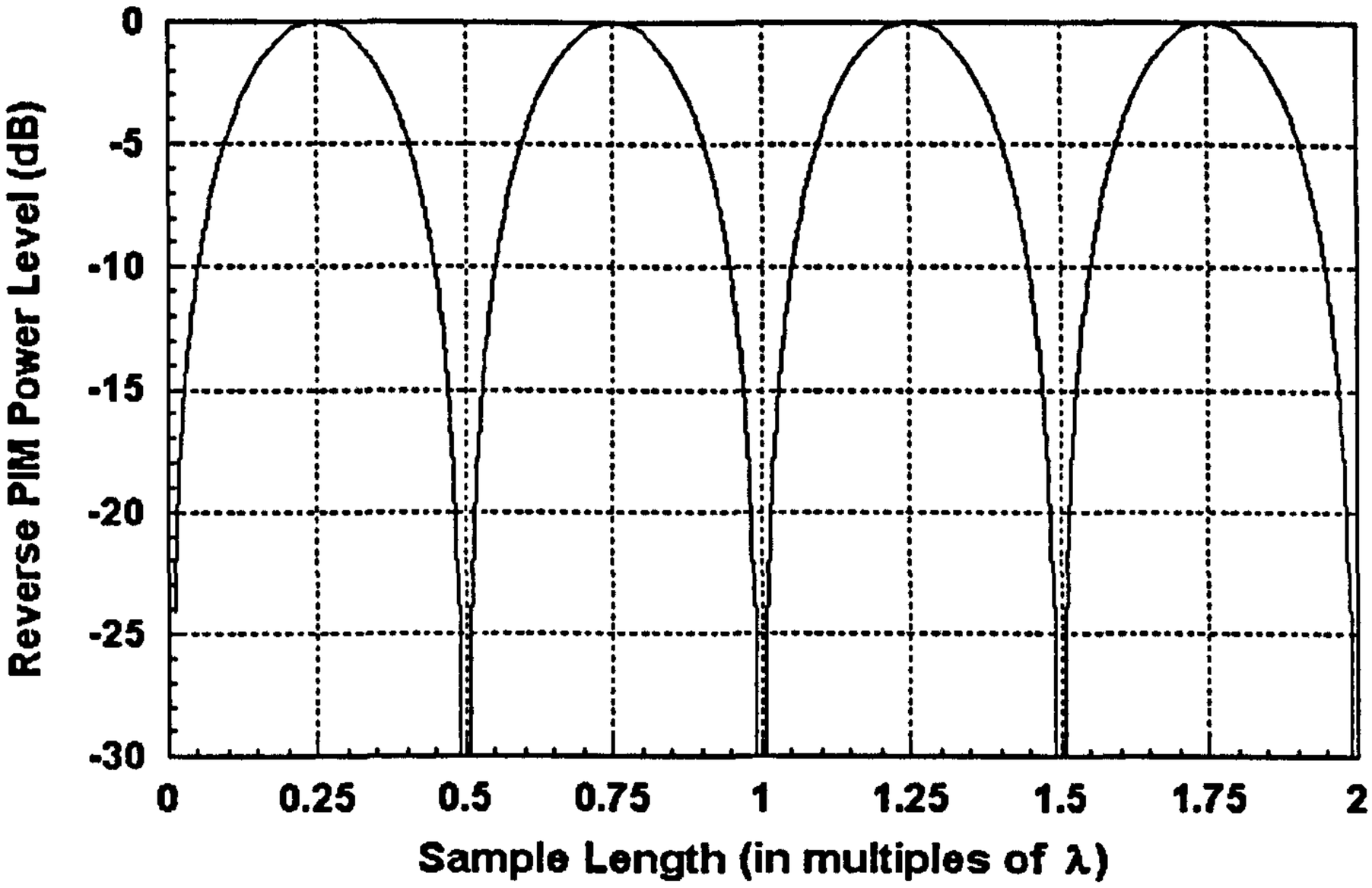

Fig.3.4 Amplitude variation of reverse PIM.

3.3.2 PIM Product Selection

The sensitivity of a PIM measurement system will generally be limited by one of two factors, either the thermal noise floor or residual intermodulation within the system. Typically, which of these is the limiting factor will depend on the intermodulation order being measured. Intermodulation power normally falls off rapidly with increasing order (as in Section 2.2.2), so for higher orders the system sensitivity will be limited by thermal noise while at lower orders it is determined by the residual intermodulation.

Usually, the intermodulation product to be measured is determined by the lowest PIM order of significance in the system frequency plan. If PIM performance is a major concern, measurements are likely to involve higher order products as the operational frequencies will have been chosen to avoid low order products. Under these circumstances very high sensitivities, limited only by system thermal noise, can be achieved. This does not, however, correspond to a sensitive technique for detecting intermodulation for just as intermodulation in the measurement system is reduced at higher orders, so too is that from the device or system under test. For scientific investigation of PIM behaviour, the selection of a low order product offers certain advantages. One of these is that less carrier power is needed to excite a detectable PIM signal.

3.3.3 Excitation Method

Another consideration is whether to excite the test sample by radiation or conduction, as in Fig.3.1 and Fig.3.2. The choice depends mainly on the nature of the sample to be tested. Coupling the excitation signals to the DUT by radiation is usually employed where PIM data is required for a large structure or object such as a radio tower or antenna dish. The nature of such measurements is that antennas are required to transmit the excitation signals and also to detect the PIM which is radiated from the sample. Radiation in free space can involve substantial losses and generally requires high power to excite a large test sample. Another problem is that the introduction of a large test sample in the excitation field can change the field pattern and this can complicate the system design.

For diagnostic work and measurements on system components the more common conducted setup of Fig.3.1 is employed. Here the samples can be kept small and well defined which aids analysis and makes it far easier to control the environment in which the tests are taking place. Excitation and detection of PIM signals is achieved by straightforward line connections to the DUT resulting in low transmission loss. This in turn means that a lower excitation power is required to generate current densities of the same order as those in a radiated setup.

3.3.4 Choice of Transmission Line

Choice of transmission line type is another important factor in system design. Even radiative systems require conductors to transfer power to and from the transmit and receive antennas respectively. The choice is directly between coaxial conductors or waveguide.

The benefits of waveguide are its low loss characteristics at high frequency and its high power handling capability. The structure is quite simple and connections are made via flanges on the end of the guide which can be made to deliver very low return loss figures. Waveguide does suffer some serious drawbacks. Probably the most important of these is that transmission is band-limited to a fixed range of frequencies. This means that if we want to look at a broad range of PIM orders or PIM from excitation signals which are considerably spaced in the spectrum, the waveguide may not be able to cope. Waveguide is also inherently bulky. At lower frequencies. the size of the waveguide section gets very large. This not only makes the waveguide and components very expensive but also means that waveguide systems can become prohibitively large. The final limitation is that almost all instrumentation is designed for coaxial systems and some sort of adaptor is invariably required between the two media.

Seven systems constructed in waveguide are described in the literature [11, 19, 46,48,95,96,97,]. The performance of these systems is broadly equivalent to that achieved by coaxial systems but the application areas are somewhat different. Waveguide based systems are, naturally, intended for tests on waveguide components or devices such as antennas which have waveguide feeds. In terms of PIM, most problems with waveguide occur at the flange connections.

The alternative to waveguide is a coaxial system. Coaxial cables are much smaller than waveguide and the resulting systems and components are more compact. The cables can be shaped to alter the physical path of transmission making layout of the system relatively straightforward. Connection is made by means of connectors which can be mounted and de-mounted quickly to allow simple reconfiguration of a given system. Although return loss from the connectors is not generally as good as that of waveguide flanges, the performance is more than adequate over a very wide range of frequencies.

However, there are some drawbacks. The power handling of coaxial line is lower than that of waveguide simply due to the smaller dimensional clearances which create higher field strengths for the same transmitted voltages. Secondly, the losses on coaxial line become appreciable as the frequency is increased. This is mainly due to the skin effect which effectively increases the resistivity of the conductors at microwave frequencies. In terms of PIM, coaxial cables have the potential to create many problems. Metal contacts abound in the braided outer conductors of many flexible cables. Crimped and clamp-on connectors also result in poor metal contacts whilst the small geometries of the connector centre pins lead to high current densities and high PIM levels.

Sixteen coaxial systems have been described in the literature and these are summarised in Table 3.1 on page 58 for comparison. HF is taken to mean roughly 3-30 MHz, VHF 30-300 MHz and UHF 300-3000 MHz. Column 3 gives the frequency separation of the carriers and the third order PIM signal as a percentage of the centre frequency. In the last two columns, "diplexer" denotes an unspecified type of directional filter.

Coaxial line is effective over a very wide band of frequencies and is limited at the upper end by increasing loss, the effective bandwidth of the connectors and higher-order mode propagation. The principal mode of propagation in a coaxial line is the TEM mode. Most coaxial components (amplifiers, filters, couplers, etc.) are designed on the basis that the input signal will be in the TEM mode. There are, however, other ways in which electromagnetic energy can propagate along coaxial lines and these are called higher-order propagation modes. These higher modes can only propagate when the signal exceeds a certain frequency known as the cutoff frequency of the mode. Higher modes draw their energy from the fundamental TEM mode and can cause system malfunction.

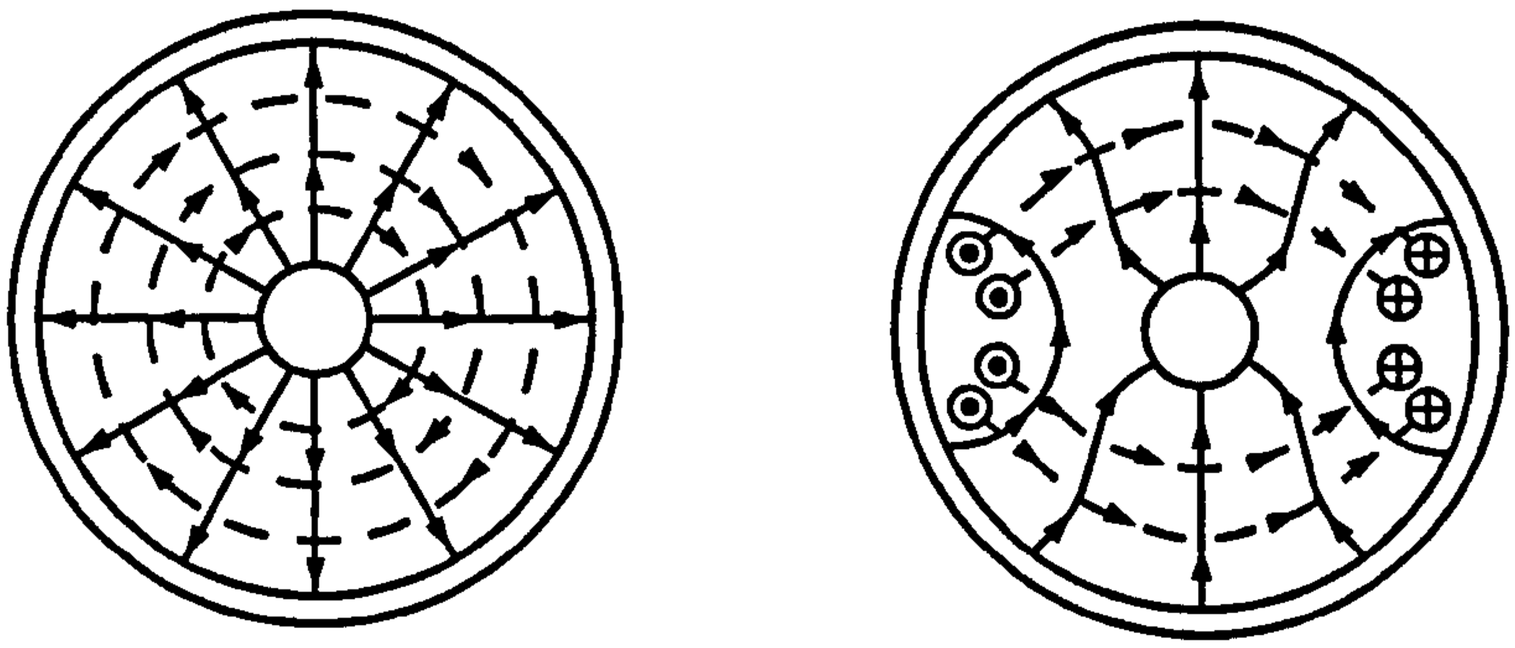

(a) TEM Mode (b) TE_{11} Mode

Fig.3.5 Transmission modes of coaxial lines

The field patterns and cutoff frequencies of these modes can be obtained by solving Maxwell's equations and applying the boundary conditions associated with the coaxial structure. The mode with the lowest cutoff frequency is called the TE-11 mode and it is this mode that invariably limits the bandwidth of the transmission line. The field patterns of both modes are shown in Fig.3.5. and an approximate expression for the cutoff wavelength in terms of the coaxial line dimensions is given below:

$$f_c = \frac{c}{\pi(a+b)\sqrt{\mu_R \varepsilon_R}} \qquad \text{Eq.3.5}$$

Where a, is the radius of the inner conductor and b, is the inner radius of the outer conductor. For UT-250 semi-rigid cable, with a=0.815mm, b=2.675mm and ε_r=2.1, the cutoff frequency of the TE_{11} mode is around 18.9GHz.

3.3.5 Parent Signal Combination

Further consideration in the design of a PIM measurement system should be given to the method by which the two excitation or parent signals will be combined. Most researchers have chosen one of three methods.

The carriers may be simply combined using a T-junction and phasing cables as indicated in Fig.3.6 [35, 36, 60, 85]. However, the T-junction is inherently badly matched and offers poor isolation between the ports so the performance of the filters is of utmost importance to prevent intermodulation generation in the amplifiers.

Ref.	Band	ΔF %	Power W	Power Combination	PIM Separation	Sensitivity dBm/dBc
62	HF	12	30	X-piece & filters	X-piece & filters	-88 -133
64	HF	10	13	lumped filters & pi matching net-works	20 dB coupler	-88 -129
85	VHF	2	15.5	T-piece & cavity filters	T-piece & cavity filters	-70 -112
36	VHF	8	50	T-piece & cavity filters	Interdigital filter diplexer	-140 -187
35	VHF	1	5	T-piece & cavity filters	T-piece & cavity filters	-145 -182
38	VHF	9	25	90° hybrids & b/pass filters	Diplexer	-120 -164
76	VHF	9	25	90° hybrids & b/pass filters	Diplexer	-120 -164
6	VHF	3	25	90° hybrid	20 dB coupler	-110 -154
50	S	13	3	Stripline ratrace hybrid	Stripline ratrace hybrid	-90 -125
62	UHF	3	30	X-piece & filters	X-piece & filters	-95 -140
60	L	27	20	T-piece & interdigital filters	Coupler	-87 -130
60	S	13	13	T-piece & interdigital filters	Coupler	-85 -126
60	C	20	20	T-piece & interdigital filters	Coupler	-87 -130
39	L	2	2	Stripline ratrace hybrid	Stripline ratrace hybrid	-106 -139
64	UHF	13	13	Stripline hybrid	20 dB coupler	-104 -145
98	UHF	10	10	T-piece & cavity filters	T-piece & cavity filters	-73 -113

Table 3.1 Summary of coaxial measurement systems

Alternatively, a 3dB, 90° hybrid coupler may be used as illustrated in Fig.3.7 [6, 64]. This can offer additional isolation between the high power amplifiers and their associated filters or isolators and so make up for deficiencies in the intermodulation performance of these components. Unfortunately, this technique is inefficient and results in the loss of half the carrier power at the unused hybrid port.

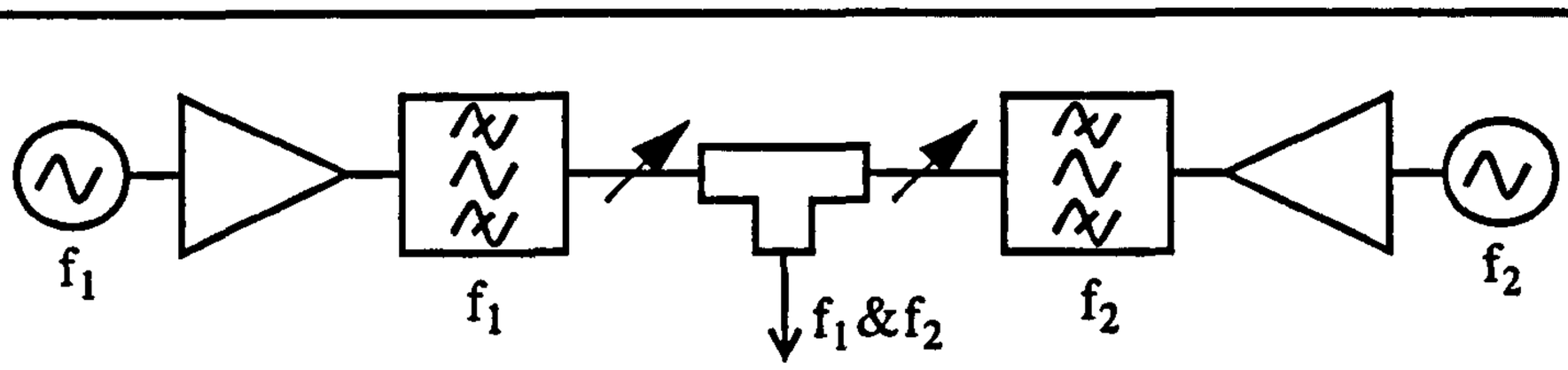

Fig.3.6 Carrier combination using t-piece, filters and phasing cables

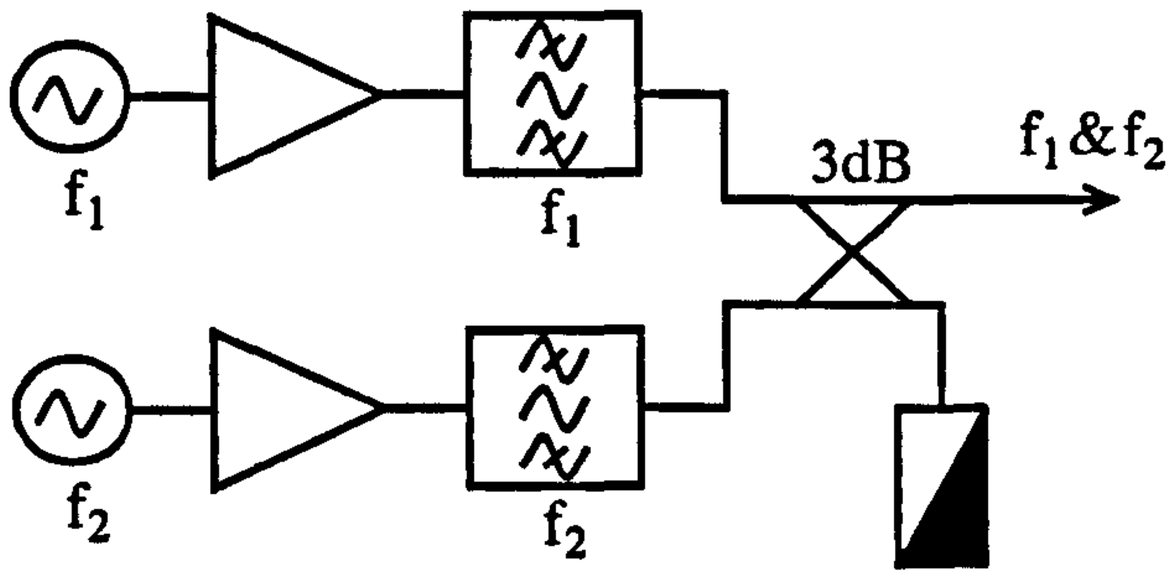

Fig.3.7 Carrier combination using one hybrid

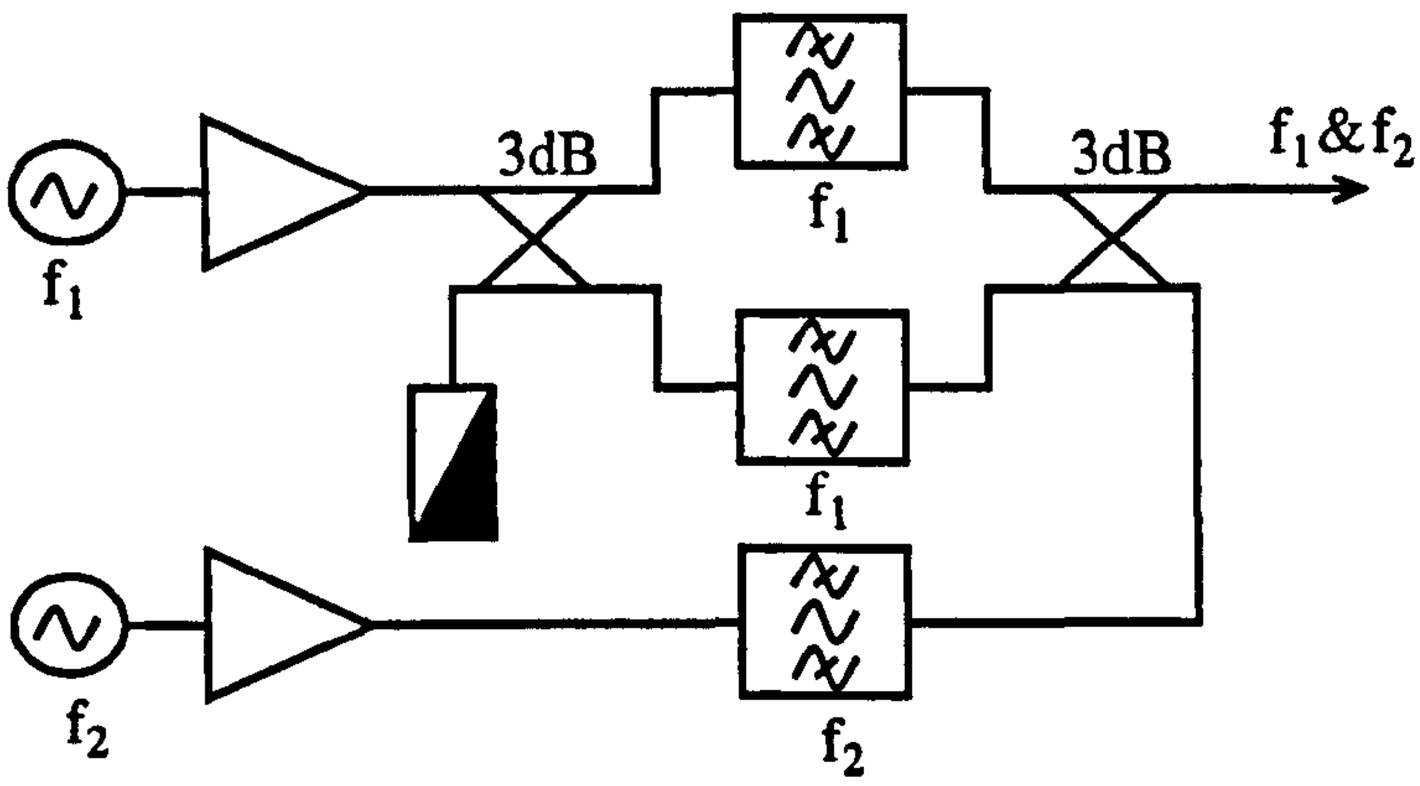

Fig.3.8 Directional filter made with reflective filters and hybrids

In terms of good match and minimum power loss, the optimum method for combining the two parent signals is shown in Fig.3.8. The circuit is a form of directional filter and offers excellent isolation between the two feed chains and the only loss in power is due to the insertion losses of the constituent components [38, 76]. If the bandpass filters are very narrowband, the circuit also prevents the propagation of any spurious signals from the amplifiers.

3.3.6 PIM Signal Extraction

Similar consideration should be given to the separation of the desired (low power) PIM signal from the (high power) carriers used to excite the DUT. This is necessary to prevent intermodulation or damage occurring in the active devices of the detection apparatus. One approach is to sample a fraction of the power using a directional coupler and to pass it through filters to give the necessary carrier rejection as in Fig.3.9 [60, 64]. This greatly reduces the intermodulation performance required of the filters by reducing the carrier powers to which they are exposed, but also reduces the level of the desired PIM signal. Unfortunately, if the PIM signal is not sufficiently high enough above the noise floor, the sensitivity of the system will be reduced. Again, the best way to tackle the problem is to use a directional filter type arrangement and isolate the PIM signal from the carriers as in Fig.3.10. Note, this set-up can also be implemented using band-stop filters to redirect the PIM signal to the isolated port of the first hybrid where it can be detected.

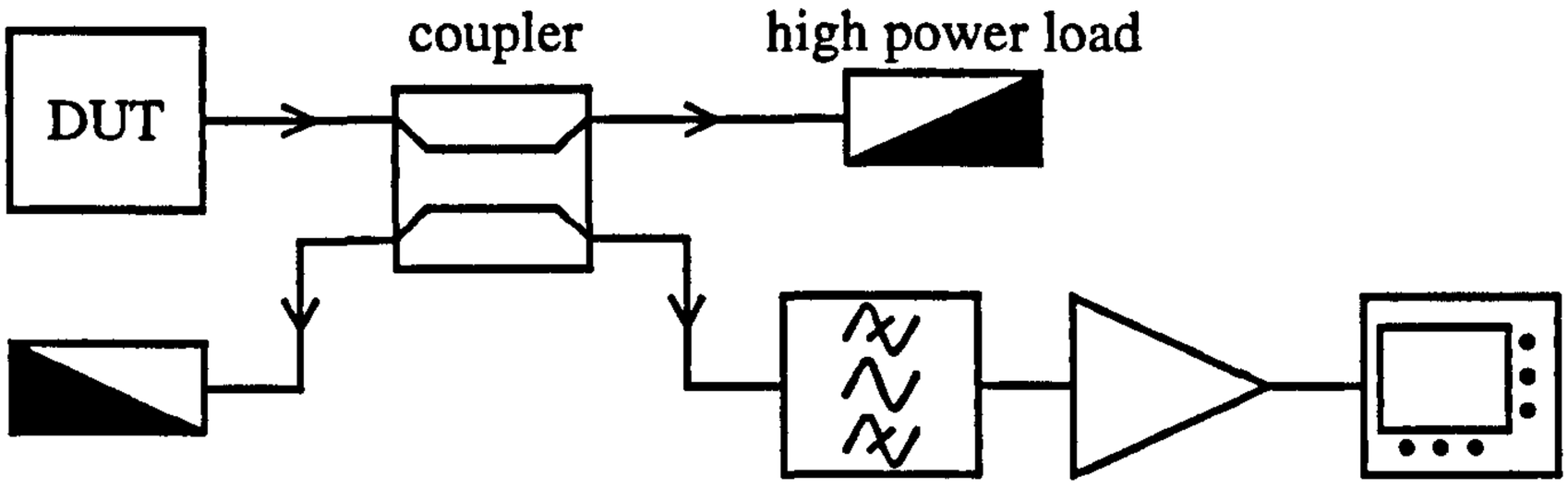

Fig.3.9 PIM sampling using a directional coupler

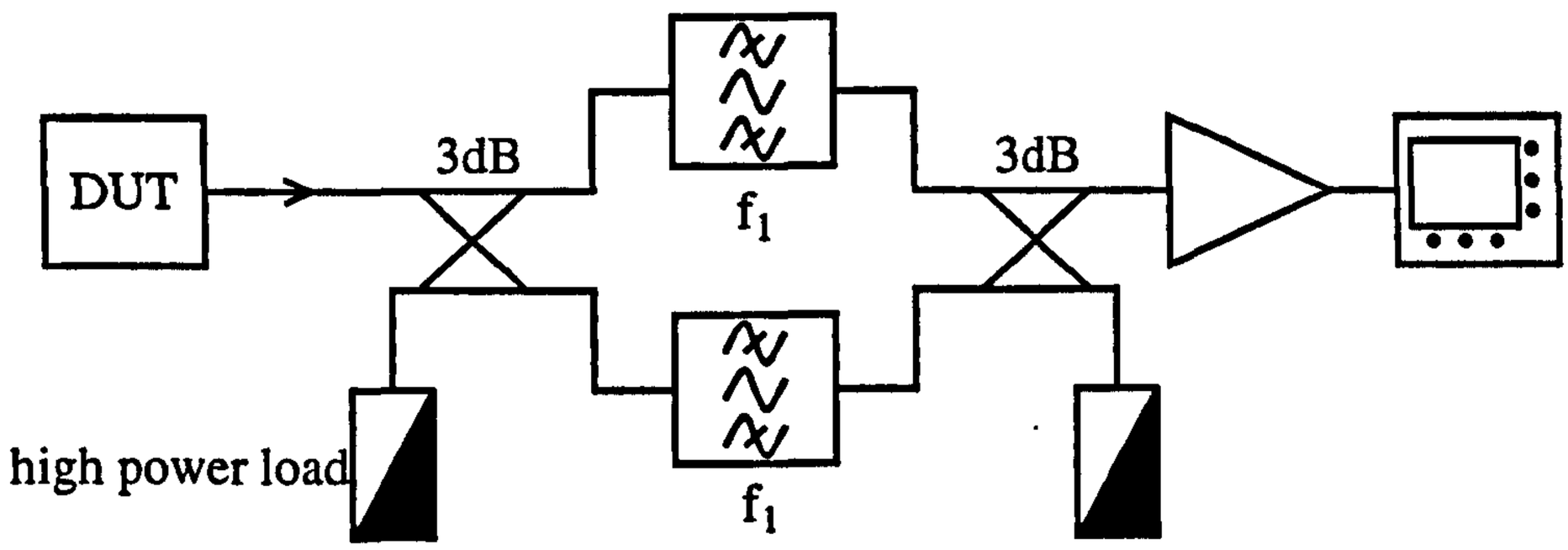

Fig.3.10 PIM extraction using a directional filter

3.4 Initial UKC L-Band System

3.4.1 Design Strategy

System configuration depends on the test requirements and which of the design considerations are deemed applicable to the particular measurement situation. Most of the measurement systems developed by other researchers have suffered limitations in terms of measurement flexibility, sensitivity, residual PIM stability and the ability to handle various types of test sample. It was the objective of the author at the outset to design a system in which those limitations were minimal and which would still meet the requirements stated in Section 3.2.

For the study of PIM mechanisms at UKC, the system was set up to monitor PIM at L-band. This is in line with ESA requirements for the Artemis satellite. The detection of 3rd order intermodulation products was initially selected as this offers the most sensitive means of measuring non-linearity.

Most DUTs require a conductive setup to provide satisfactory excitation and detection of PIM signals, hence, a conductive set-up was chosen. This also makes it easier to control the test environment and avoids the inefficient space losses associated with radiative setups. The author has also carried out radiative tests whilst working at ESA. This work is described in Appendix A.

At L-band the physical size of waveguide starts to get very large (a cross section of 165.1 x 82.55 mm for 1.14-1.73 GHz) and therefore, expensive. To this end it was decided to use coaxial lines in the system. It was also decided to employ a directional filter of the type shown in Fig.3.8 to combine the parent signals and make the maximum signal power available at the DUT. A directional filter was also used to extract the PIM signal, maximising the PIM power to the detector and optimising the sensitivity.

Initially, the system was configured using commercially sourced equipment of standard specification. It was not expected that this would deliver the level of performance sought, hence, it was not intended to carry out any sample measurements using this system. Commercial low-PIM components are not readily available therefore the performance of the initial system could not be guaranteed. The purpose of this exercise was to provide a starting point for the development of a highly-sensitive, low-PIM, measurement system. Previous research in the field of PIM measurements has shown that considerable time and effort is necessary to reduce residual intermodulation. Accordingly, it was decided that custom low-PIM components and techniques would be developed as and when the need arose.

3.4.2 System Design

A block diagram of the initial system configuration is shown in Fig.3.11. As far as possible, the number of different components in the PIM critical areas of the system has been kept to a minimum. This reduces problems of identifying and eliminating sources of intermodulation in the system itself. PIM critical areas are identified as those parts of the system where both parent signals share the same transmission path at high-power levels and where any resulting PIM signals can be directly channelled to the detector.

The system generates two carrier signals at frequencies of 1530 MHz and 1560 MHz (chosen for compatibility of measurements with the Artemis transmit band of 1530 - 1559 MHz) and monitors the upper 3rd order intermodulation product at 1590 MHz. Such close signal spacing (approx. 2% of centre frequency) allows narrow band components to be used and tested but places stringent demands on filter performance.

The parent signals are generated by two separate phase locked oscillators (PLO's) and then amplified by two medium power, solid-state amplifiers (SSA's) to provide the drive levels to two high power, linear-valve amplifiers.

The high power carriers are combined using a directional filter assembly consisting of two 90 degree, 3dB hybrid couplers and three reflective bandpass filters, each consisting of six resonant cavities. Two of the filters are tuned to 1530 MHz and the other to 1560 MHz. This type of directional filter is tolerant of small differences in filter characteristics and coupling factors and so allows good performance using standard components with no need for tuning. Bandpass filters were specified as they were the only commercially available filter design offering sufficiently rapid roll-off so as to isolate the carriers from each other in the high-power amplifier output stages, thereby avoiding active intermodulation generation. The directivity of the hybrids provides additional isolation between the feed chains.

The carrier signals are combined as follows; The 1530MHz signal is divided by hybrid No.1 into two half power components with a phase difference of 90 degrees. These components then pass through the 1530MHz filters and recombine at one output of hybrid No.2 whilst cancelling at the port connected to the 1560MHz filter. Meanwhile, the 1560MHz carrier passes through the 1560MHz filter and into the isolated port of hybrid. No.2. Here it is also divided into two half power components with a 90 degree phase difference. These are reflected from the 1530MHz filters and then recombine in phase at the output of hybrid. No.2. Now we have both signals available on a common path at the output of the directional filter and free of any spurious harmonics or active intermodulation products.

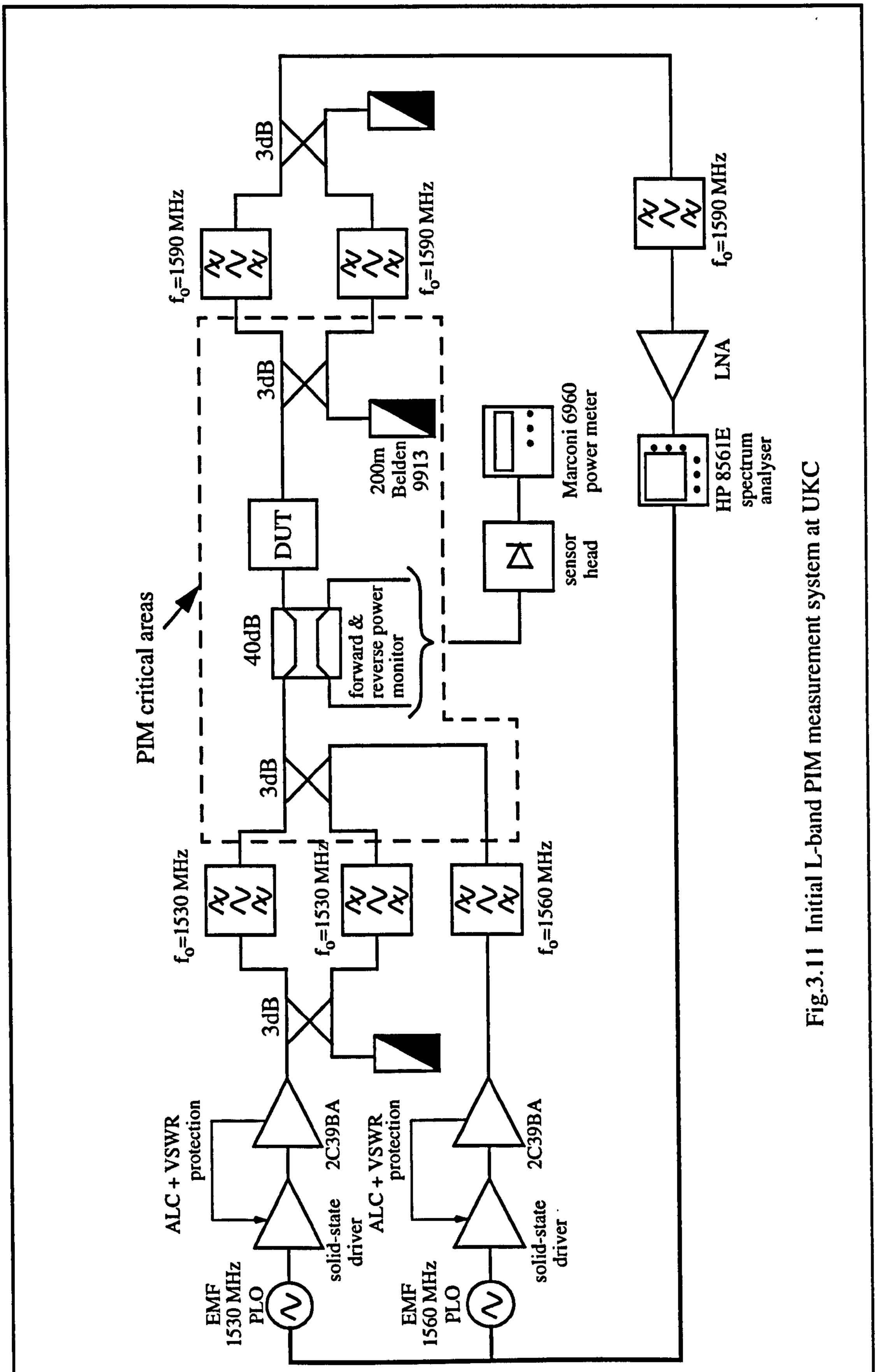

Fig.3.11 Initial L-band PIM measurement system at UKC

The combiner load is provided by a 50 metre reel of URM43, lossy coaxial cable terminated in a 1 Watt load. Under normal operating conditions this load will not be subjected to high power, however, should a system malfunction occur it is able to dissipate the maximum input power of the system. URM43 also provides a good match ensuring optimum performance of the directional filter assembly.

The total forward and reverse power are monitored via the 40dB sampling coupler and power meter. Reverse power is monitored as a check of correct system operation since any malfunction will generally result in a significant mis-match and an increase in reflected power levels.

PIM signals generated at the DUT and propagating in the forward direction are separated from the carriers by a second directional filter assembly operating in a similar manner to the power combiner. In this case the two parent signals are diverted to an isolated port and dissipated in a 250metre length of Belden 9913 coaxial cable. Meanwhile, the PIM signal is passed through another high Q bandpass filter to further reduce the carrier levels and prevent the generation of active intermodulation products in the LNA's and spectrum analyser.

For PIM signal detection, an HP 8561E spectrum analyser was used which offered excellent sensitivity, selectivity and dynamic range. Spectrum analysers are frequently used for intermodulation measurements as described in the literature [99-101].

The majority of cables used to connect the system components were made from Belden 9913, a flexible cable with an inner screen of immunised plastic and an outer braided conductor. All cables and components were fitted with silver plated, brass, N-type connectors. The number of connections was kept to a minimum to reduce the generation of PIM signals. Care has been taken to ensure that all current paths are clean and free of ferromagnetic materials since dirty contacts and ferromagnetic materials can produce strong intermodulation signals.

3.5 System Hardware

The following sections provide more detailed descriptions of the more critical components used for setting up the L-band PIM measurement system at UKC.

3.5.1 Signal Sources and Amplification

Two crystal controlled, phase locked oscillators (PLO's) manufactured by EMF Systems Inc. were used to generate the parent signals. These are fixed frequency devices and, when locked to a common reference derived from the spectrum analyser, they offer

excellent stability with very little frequency drift. This permits the use of very narrow detection bandwidths resulting in a low level of thermal noise. Which in turn allows the maximum dynamic range of the spectrum analyser to be applied and maximises the sensitivity of the measurements.

The outputs of the oscillators are 100 mW (30 dBm) each. These levels are increased to approximately 10 Watts (40 dBm) by two solid-state power amplifiers (SSPAs). These were manufactured by Mutek Ltd. and are modified versions of units produced for amateur radio applications and were therefore low in cost. The SSPAs are used to provide sufficient drive power for two 100 Watt (50 dBm) linear power amplifiers (also by Mutek Ltd.) which are based on 2C39BA thermionic valves. The output stages of the 100 Watt amplifiers have in-built forward and reverse power monitors and these are connected to automatic level control inputs on the 10 Watt SSPAs. This serves to maintain stable output power levels and to provide protection against high reverse power levels resulting from any impedance mis-match. The frequency response of the HPA's is flat from 1.5 to 1.6 GHz and the nominal gain is 10 dB. In practice, the gain is found to be around 9 dB giving a maximum recorded output power of around 80 Watts per channel. The insertion loss between the high-power output and the test position is 4.3 dB at 1530 MHz and 4.6 dB at 1560 MHz, therefore the maximum power into the sample was limited to equal signals of around 30 Watts (44.7 dBm) per channel. Throughout the laboratory measurements, the two signals were used in the continuous wave (C.W.) mode

3.5.2 Frequency Combiners

As mentioned in section 3.3., there are several ways of combining and sampling R.F. signals. Ideally a signal combiner or sampler used in a PIM system should satisfy the following requirements:

(i) Low insertion loss (less than 0.5dB is good).

(ii) High isolation between ports (greater than 20dB)

(iii) Low VSWR (or high return loss) e.g. less than 1.25 (>25dB)

(iv) Good linearity

(v) Sufficient bandwidth to cover the frequencies of interest.

(vi) High power rating.

(vii) Low cost.

In practice however, there are always trade-offs between these factors.

3.5.2.1 Filters

The directional filter set-up used in the UKC system was required to combine two signals which are very closely spaced in the frequency spectrum, therefore some very narrowband filters were required to obtain a sufficient degree of isolation between each feed chain. Practically, this was achieved using commercially available, high-Q, reflective band-pass filters each of which consists of six resonant cavities. Band-pass filters were specified as they are the only standard filter design to offer sufficiently rapid roll-off thus avoiding the situation of having both carriers present at high power levels in the same component. The filters, supplied by Trilithic®, use quarter-wavelength resonant structures. Each unit is housed in an aluminium case with silver-plated cavities to reduce losses and achieve high Q. The cavities are iris coupled and are shielded to minimise R.F. leakage. This is important in order to minimise the amount of R.F. energy which is picked up by the spectrum analyser due to radiation. If this is too high, intermodulation may be generated in the active components of the analyser obscuring the PIM signals which are being measured.

In the combiner, two filters are tuned to have their centre frequencies at 1530 MHz and one at 1560 MHz. The rejection provided by these filters at the adjacent parent signal frequency, 30 MHz from mid-band, is around 70 dB. The insertion loss at mid-band of around 3 dB and is poor. However, the choice of filter was constrained by funds and these are the best that could be obtained. The power handling of the filters is around 1200 Watts C.W. and is well within the specification of the system. The only deviation from the standard specification of the filters was the request that the Nickel plated N-type connectors be replaced by non-ferrous, silver-plated ones. Nickel is ferromagnetic material, therefore its use should be avoided [37], as stated in Section 2.4.2.4.

3.5.2.2 Hybrid Couplers

The other components that go to make the directional filter assembly are the3dB, quadrature, hybrid couplers. Again, these are standard specification, commercially available units manufactured by Radiall Microwave Components Ltd. For the best possible performance of the directional filter, the couplers should have a flat 3dB coupling across the band, ensuring an even split of power at all frequencies. There should also be a constant 90^{o} phase difference at the output coupled ports of the device to ensure the optimum phase relationships in the completed assembly. To this end, it is essential that all of the connecting cables used in the directional filter are the same length to avoid introducing additional phase changes. The directivity of the couplers is also important as this determines the isolation provided by the device between the input port and the uncoupled

port. The units have a bandwidth of 1-2GHz over which the directivity is greater than 25 dB. The return loss over the same range is also greater than 25 dB and the coupling is 3 dB ±0.3 dBm. The couplers are of a quarter-wavelength, overlay coupled stripline design and have a C.W. power rating of 200 Watts.

3.5.2.3 Directional Filter Assemblies

In the complete directional filter assembly, isolation of the parent signals is provided for by the out-of-band rejection of the filters plus the directivity of the couplers. This equates to over 90 dB isolation between the parent signals in each feed chain. The reduction of these signals by such a degree means that the level of any IM which is generated in the high-power amplifiers will be extremely low and pose no threat to the sensitivity of the system or to the correct operation of the amplifiers.

A similar directional filter assembly was used to isolate the PIM signal for amplification and detection. The circuit prevents the two high-power parent signals from causing damage to the highly sensitive detection circuitry by greatly reducing their power in this part of the circuit. This directional filter should meet the same fundamental requirements of the combiner as listed in Section 3.5.2. Isolation of the PIM signal from the parent signals is once again provided for by the out-of-band rejection of the band-pass filters and the directivity of the hybrid couplers. An additional filter is added at the output of the directional filter to further increase the parent signal rejection (as indicated in Fig.3.11). With the filters tuned to pass the 3rd order PIM signal at 1590 MHz, the rejection at 1560 MHz is around 75dB and at 1530 MHz is about 90 dB. In conjunction with the 25 dB directivity of the hybrids, the isolation of the PIM signal is over 155 dB at 1560 MHz and 195 dB at 1530 MHz. The high insertion loss of the circuit of 6.7 dB is again governed by the insertion loss of the filters. This can potentially affect the sensitivity of the measurement system particularly if the residual PIM is at or near the thermal noise floor.

3.5.3 Dummy Loads

In non-radiating PIM measurement systems, dummy loads are used to absorb the transmitted carrier power. It is very important that these loads should generate no significant amount of PIM. Commercially available dummy loads which are adequate for most applications, are not normally designed to achieve the high degree of linearity required by a PIM measurement system. Research on dummy loads has indicated that distributed loads are generally more linear than lumped element loads[54]. Distributed loads take the form of a long length of lossy coaxial cable. For a long, lossy, open-ended line, the voltage

of the wave reflected from the open circuit and measured at the input, will be small compared to the voltage of the incident wave. This is due to the fact that the incident wave will have been attenuated over twice the length of the line.

Factors which govern the selection of a distributed load are its linearity, characteristic impedance, power handling capability, attenuation per unit length and cost. The characteristic impedance of the load determines the match of the load to the system and in this case should be 50 Ω. A high attenuation constant will result in a shorter length of cable for a given amount of attenuation but this will cause the cable to heat up more as the energy is dissipated. This in turn can limit the power handling capability of the line and so a trade-off must be made to obtain the optimum performance for a given situation. The linearity of RF cable is never specified and cannot be guaranteed, hence, extreme care should be taken when choosing a suitable cable for the job. Large cross sectional dimensions are preferred in order to keep current densities low. Certain materials should be avoided such as copperweld steel (where the centre conductor is made of copper supported on a steel core) or ferromagnetic Nichrome. Care should also be taken to avoid cables which have metallic contacts exposed to high current flow such as the outer copper braid or the multi-core centre conductor used in many cables.

In the UKC L-band setup, only one load is required to dissipate the energy in the carrier signals. Other loads are required on the isolated ports of the directional filter assemblies to provide a good match. In general, however, these loads are exposed to signals which have been heavily attenuated and are less likely to generate PIM. Based upon the considerations discussed, the high power load was implemented using a 250m length of Belden 9913 coaxial cable. This is a flexible cable with an outer conductor comprising of an inner screen of aluminised plastic and a double braided, silver plated, outer shield. The dielectric is formed from foamed polythene and supports a large, silver plated, solid copper centre conductor. This cable attenuates the parent signals by approximately 2 dB per 10 metres thus providing a total attenuation of 100 dB at the input to the load. This level of attenuation results in a reflected wave which is far smaller than the reflected wave caused by the finite return loss of the load connector which is typically about 25dB down on the incident level. Therefore, the attenuated signal should cause no problems in the system.

3.5.4 Cables and Connectors

Research work has shown that connectors are very often the major source of PIM in cable-connector combinations [30, 36, 37, 50, 63, 65]. Any connectors with mechanical imperfection (such as slightly bent centre pins), or a ferromagnetic material content may

generate high levels of intermodulation. The method of construction employed in joining the cables to the connectors and the cleanliness of all the surfaces are also very critical. Studies concerning the generation of PIM in coaxial cables and connectors have been conducted [65] and indicate that it is essential to choose the correct type of cable and connector.

The cables used for connecting the system together were made from Belden 9913 cable for the same fundamental reasons that this cable was chosen as the dummy load. The selection criteria and cable properties are described in the previous section.

All of the instruments and components used in the system were specified with N-type connectors. These offer a good performance up to microwave frequencies in terms of insertion loss (<0.05dB at 1.6GHz) and return loss (>35dB up to 5GHz). They also have a high power handling capability and therefore make a natural choice for the PIM measurement system. The connectors were specified to have no ferromagnetic components since nickel is commonly used as a plating material. It was also decided that the centre pins be soldered to the centre conductor rather than crimped so that a sound mechanical and electrical connection would be achieved. Care has been taken to ensure the cable-connector combinations were properly constructed and all the contacts were tight and free of visible oxides and dirt. Prior to assembly, all connectors and cable ends were ultra-sonically cleaned in isopropyl alcohol (IPA) to ensure the removal of even the smallest particles.

3.5.5 Low Noise Amplifiers and Spectrum Analyser

The spectrum analyser is an instrument commonly used for Intermodulation measurement [99-101]. However in order to detect signals which are close to the thermal noise floor of the measurement system, a degree of signal enhancement is necessary. The spectrum analyser which was procured for the system was a Hewlett Packard HP 8561E unit. The instrument was chosen due to its excellent dynamic range and sensitivity. In a resolution bandwidth of 10Hz, the analyser can measure signals less than -135dBm in amplitude [105]. Such low levels of detection are essential to get the maximum possible sensitivity from the measurement system. Even at these low levels however, the sensitivity can be considerably improved by pre-amplifying the PIM signal with a low-noise amplifier. For the UKC set-up a Miteq Inc. AMF-4A-1020-N(F/M) amplifier was chosen with a gain of 43.3 dB and noise figure of 1.76 dB at 1600 MHz. The gain must be sufficient to amplify the signal from near the absolute thermal noise floor of the system to within the detection range of the analyser. The noise figure is a measure of the degradation in signal-to-noise ratio as contributed by the amplifier and this should be as small as possible.

3.6 Theoretical System Limits

The absolute performance of the system is gauged in terms of the smallest PIM signal that can be detected and attributed to a particular source or location. The smaller the signal that can be detected, the more sensitive the system will be to deviations in linearity.

In practice, the limitations of the measurement can be governed by three separate effects:

(i) The thermal noise floor of the system.

(ii) Generation of Active Intermodulation in the detector.

(iii) Passive Intermodulation produced by the system itself (Residual PIM).

(i) and (ii) can be analysed theoretically[103, 104], however, the amount of residual PIM in the system can only be measured directly and is more of an unknown quantity. Obviously, in the design of a good PIM measurement system, all three of these effects must be suppressed as far as possible.

3.6.1 Thermal Noise Limit of Sensitivity

The maximum sensitivity that can be obtained in the measurement system is fundamentally limited by the thermal noise of the system. Thermal noise arises from the thermally induced motion of electrons in conductive media and increases with temperature. The noise power, N, from a given conductor at temperature T_o (K) is obtained from a standard formula:

$$N = k \cdot T_o \cdot B \quad \text{Watts} \qquad \text{Eq.3.6}$$

Where k = Boltzmann's Constant (1.38×10^{-23} J/K) and B is the bandwidth (in Hz) over which the noise is measured.

At 290K (room temperature) this equates to a thermal noise level of -174dBm/Hz. The thermal noise floor of the HP 8561E spectrum analyser, however, was measured at -141dBm over a 10Hz resolution bandwidth and is limited by the amount of thermal noise which it produces itself [105]. It is obvious that in order to improve the sensitivity of the detector and measure extremely weak signals, some amplification will be required. Unfortunately, not only do amplifiers amplify the signal and noise levels, but they also add to the noise power as well degrading the signal to noise ratio (SNR).

The noise figure of an amplifier is a commonly specified parameter and is a measure of the degradation of the SNR after amplification. In modern state-of-the-art low noise amplifiers this can be specified to be very low and given a suitably high gain, a substantial improvement in sensitivity can be obtained. We can express the noise figure as:

$$F = \frac{(S_i/N_i)}{(S_o/N_o)}$$

where F = noise figure as a power ratio,
S_i = input signal power
N_i = true input noise power,
S_o = output signal power,
N_o = output noise power. Eq.3.7

The detection circuitry is shown in Fig.3.12. To determine the sensitivity of the system, the first step is to calculate the noise figure of the spectrum analyser. If we examine Eq.3.7, we can simplify it for the spectrum analyser. First of all, the output signal is the input signal times the gain of the amplifier. Second, the gain of the analyser is unity because the signal level at the output (indicated on the display) is the same as the level at the input connector[101]. So, substituting in Eq.3.7 and rearranging we get:

$$F = \frac{N_o}{N_i} \qquad \text{Eq.3.8}$$

This expression means that all that is required to determine the noise figure is to compare the noise level as read on the display to the true noise level at the input connector. Noise figure is usually expressed in terms of dB, or:

$$NF(\text{dB}) = 10log(F) = 10log(N_o) - 10log(N_i) \qquad \text{Eq.3.9}$$

For the HP 8561E, the average noise power over a 10Hz bandwidth was measured at -141dBm. In the same bandwidth the true noise at the input connector is -164dBm. This gives a noise figure of NF_{SA}=23 dB (199.5 linear).

Now given that the noise figure of the low noise amplifier is F_{LNA}=1.76 dB (1.5 linear) and the gain is G_{LNA}=43.3 dB (21379.6 linear), the overall noise figure for the detection circuit is found from:

$$\begin{aligned} NF_T\ (\text{dB}) &= 10log\left(F_{LNA} + \left(\frac{F_{SA}-1}{G_{LNA}}\right)\right) \\ &= 10log\left(1.5 + \frac{199.5}{21379.6}\right) \\ &= 1.76\ \text{dB} \end{aligned} \qquad \text{Eq.3.10}$$

The sensitivity at the input to the LNA can now be determined by knowing that the noise figure of the system is the amount of additional noise contributed by the amplifiers and the spectrum analyser:

$$\begin{aligned} S_{LNA} &= N\,(\text{dBm}) + F_T\,(\text{dB}) \\ &= -164 + 1.76 \\ &= -162.24\ \text{dBm} \end{aligned} \qquad \text{Eq.3.11}$$

Where S_{LNA} is the smallest signal at the input to the LNA which can be detected above the noise on the trace of the spectrum analyser. Therefore, the minimum detectable signal referred to the spectrum analyser input (for this particular setup) is simply S_{LNA} dBm plus the gain of the LNA in dB, i.e.:

$$\begin{aligned} S_{analyzer} &= -162.2\ \text{dBm} + 43.3\ \text{dB} \\ &= -118.9\ \text{dBm} \end{aligned} \qquad \text{Eq.3.12}$$

In order to determine the smallest signal which can be detected at the DUT, we have to take into account the losses between the DUT and the LNA due to the cables, connectors and directional filter isolation assembly. These have been measured at 6.7dB therefore the signal, S_{DUT}, must be 6.7dB above the noise floor at the DUT:

$$\begin{aligned} S_{DUT} &= -162.2\ \text{dBm} + 6.7\ \text{dB} \\ &= -155.5\ \text{dBm} \end{aligned} \qquad \text{Eq.3.13}$$

Hence the minimum detectable signal levels at each point in the detector circuit can now be determined and are shown in Fig.3.12.

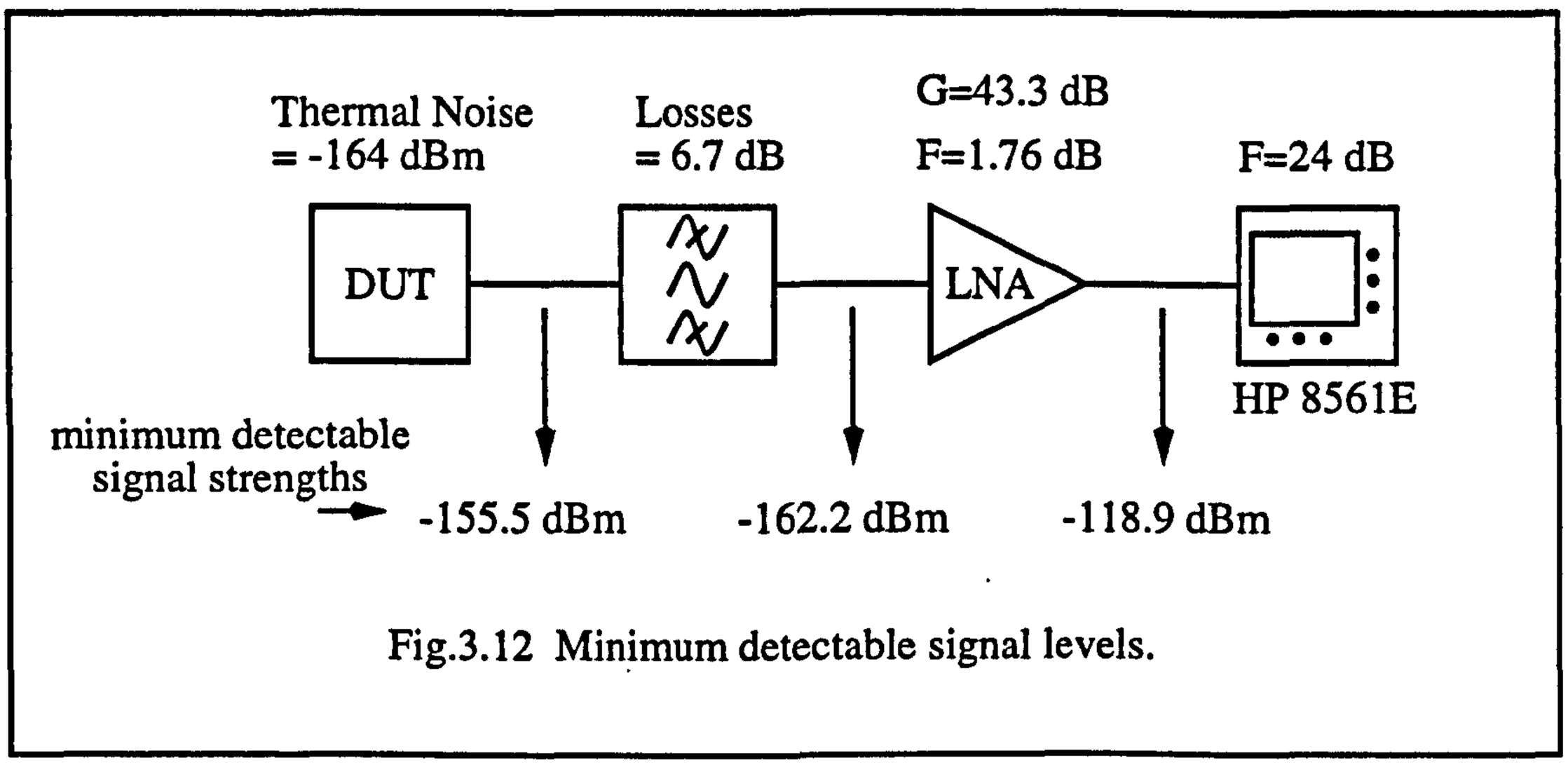

Fig.3.12 Minimum detectable signal levels.

3.6.2 Active IMD Contribution

In addition to passive intermodulation products generated by the DUT in which we are solely interested, additional IM products can arise due to non-linearities within the components of the detector circuitry. The sources of these non-linearities are the active devices that constitute the low-noise preamplifier and the spectrum analyser. These components can be subjected to the same excitation signals as the DUT. Although the carrier signals are heavily attenuated before the detection circuit, radiation and reflection (return loss) can create sufficient signal strength to cause problems. Active nonlinearities are generally much stronger than those due to passive mechanisms and as such will produce similar levels of intermodulation at much lower levels of excitation. The active IMPs naturally occur at the same frequencies of PIMPs therefore, in order for the measurement system to provide a true indication of the level of *passive* intermodulation, these undesired signals must be minimised. Reducing the effects of active IMD is achieved by minimising the level of the carrier signals that impinge upon the active components. The degree to which this is necessary can be calculated by a knowledge of the thermal noise floor of the system and of the IMD contribution of each component. Since IMD is intrinsic to active devices and 3rd order IMD is usually the strongest, most non-linear devices are supplied with their 3rd order IMD response as part of the specification.

3.6.2.1 Spectrum Analyser

For the particular spectrum analyser used in the UKC L-band experimental setup, the 3rd order IMD is specified as follows: 'If two equal strength signals of -30 dBm and spaced greater than 1 kHz apart are applied at the input mixer of the analyser (after the input attenuator) then the level of 3rd order intermodulation products produced will be less than 78 dB below the level of excitation i.e. -78 dBc or -108 dBm. [105].

Active IMD is generally much more well behaved than PIM and lends itself to approximate modelling in that for every 1 dB change in the level of the excitation signals, there will be an n dB change in the level of the IMD, where n is the order of the intermodulation product. A plot of third order IMD against carrier power will therefore have a slope of 3:1. It is more common however to express IMD in terms of dynamic range, i.e. the difference in dB between the maximum and minimum signal levels. For 3rd order IMD, the dynamic range vs the carrier level varies 2 dB for every 1 dB change in carrier power [103].

The well defined relationship between 3rd order IMD and excitation level when used in conjunction with the specification of the device allows us to plot the 3rd order IMD characteristic of the unit over a wider range of carrier levels (as in Fig.3.13). Note that for a spectrum analyser, there is no gain so the output or displayed carrier level is the same as the input.

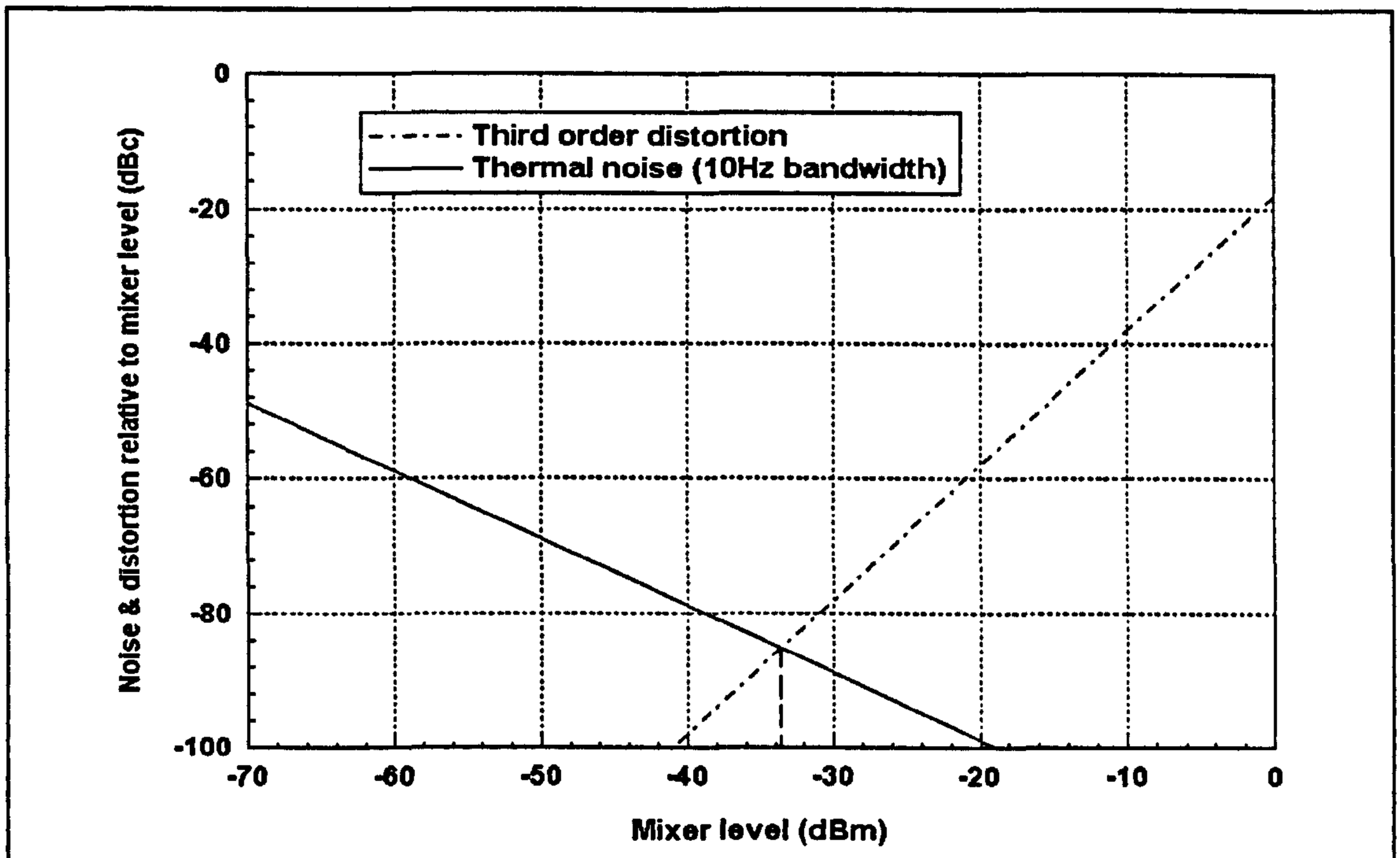

Fig.3.13 HP 8561E spectrum analyser - third order distortion

The minimum detectable signal at the analyser was calculated in Section 3.6.1 to be -118.9 dBm and remains constant in a fixed measurement bandwidth, independent of the power applied to the input. If this is illustrated on the same plot as the IMD figures (as in Fig.3.13) then the area above the two lines represents the useful measurement range of the instrument. The point where the two graphs cross represents the point at which the carrier levels at the input mixer are strong enough to produce a 3rd order IM product which is just discernable from the thermal noise floor of the system. If the excitation level is increased the active IMD will be clearly visible on the analyser and limit the sensitivity of measure-ments at this frequency. Therefore in order to limit the sensitivity of the system to the thermal noise floor, the carrier signal levels at the input mixer of the analyser should be kept below the level at which the two graphs cross. For this particular analyser this occurs at a level of around -34 dBm. Referred back to the input of the LNA this gives a maximum allowable carrier level of -34 - 43.3 = -77.3 dBm.

3.6.2.2 Low Noise Amplifier

For the low-noise preamplifier, the third order IMD level is expressed in a slightly different manner. Specifying IM distortion products by suppression, in dB, from the excitation level has a major problem in that different manufacturers will specify IMD wrt different carrier levels and this makes figures difficult to compare. An accepted method to normalise these differences is to specify "third-order intercept points". Intercept points are theoretical points at which the excitation signals and the IM products have equal amplitude. These points are only ever theoretical because saturation in amplifiers ultimately limits the output power to less than the intercept point. Intercept calculation is only valid when extrapolated from the linear operation range of the device. Again, due to the well defined behaviour of IMD in active circuits the intercept point can be used to plot the IMD performance of the device over a wider range of excitation levels which allows us to determine the maximum dynamic range of the system.

The particular LNA used in the L-band set-up is specified as having a third order intercept point approximately 10 dB greater than the 1 dB compression point. This is the point where the device begins to saturate and occurs when the output power is exactly 1 dB less than the input power plus the gain (in dB). For this device, the 1 dB compression point is at +16 dBm at 1.6 GHz, hence the third-order intercept point occurs at +26 dBm. The performance of the device is depicted in Fig.3.14. Again, the thermal noise floor of the system is also plotted, referred to the output of the LNA. The crossover point indicates that the maximum level of carrier signal which the LNA can bear before affecting the sensitivity of the system is -66 dBm at the input of the LNA. Comparing this with the performance of the analyser it is clear that the spectrum analyser dictates the maximum allowable carrier signal which is allowed to impinge upon the detection circuitry. Accordingly, the maximum allowable parent signal levels at the input to the LNA are -77.3 dBm per carrier and the maximum level displayed on the analyser should be -34 dBm.

The next step is to measure the level of each carrier signal using the spectrum analyser and establish if there is a threat to system sensitivity from third order intermodulation generation by the detection circuitry.

3.6.3 Breakthrough

Breakthrough is the term used to describe the level of each carrier signal which manages to get into the detection circuitry. As mentioned previously this can be as a result of the pick-up of radiated emissions or due to insufficient rejection from the system itself.

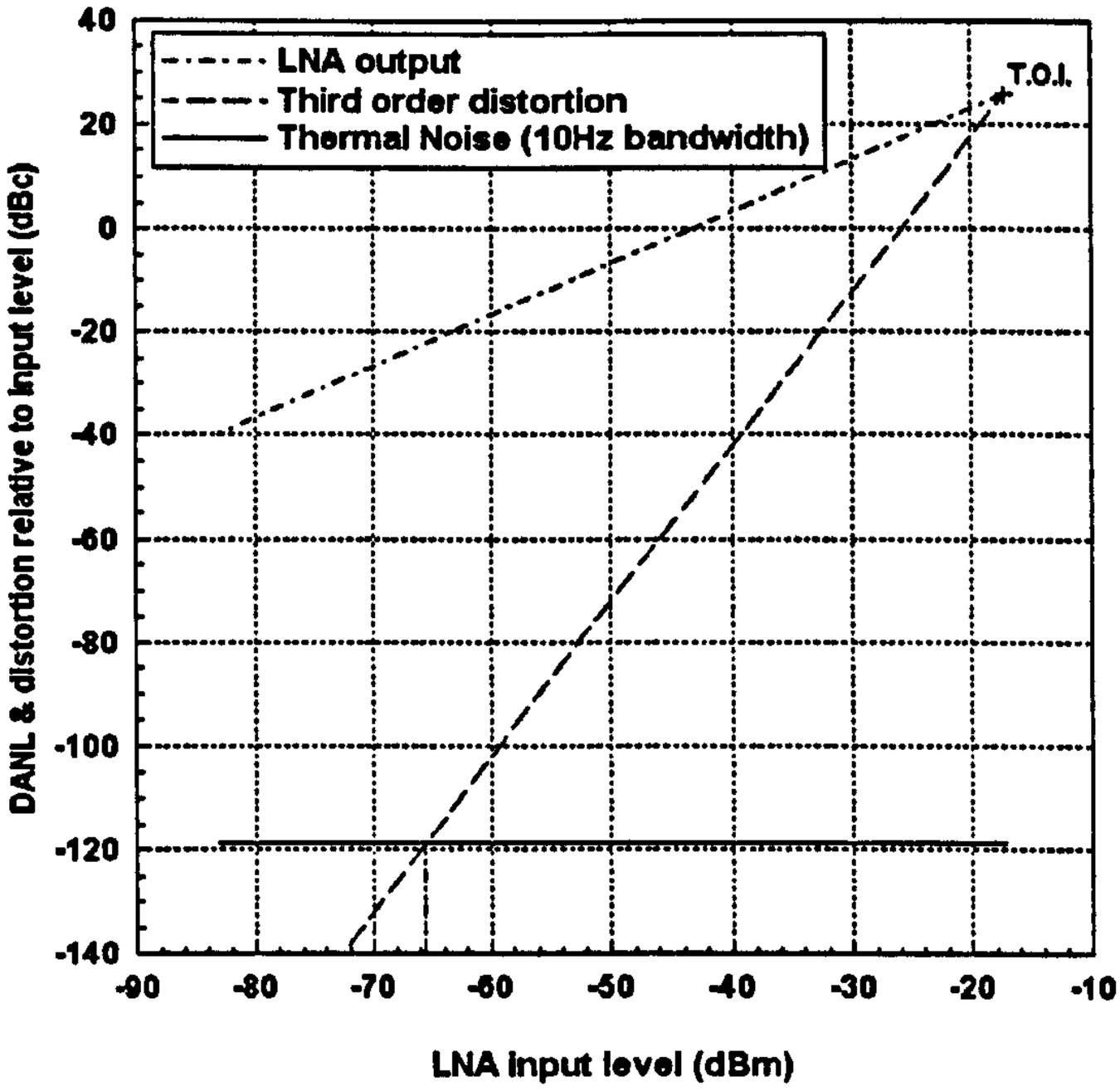

Fig.3.14 Miteq LNA - third order distortion

The levels are measured directly from the spectrum analyser when the system is operating as it would, at high power, during any PIM test. For this initial set-up the levels of break-through observed for 25 Watts of applied carrier power (per channel) were as follows:

1530 MHz: -33 dBm 1560 MHz: -32 dBm

These levels when compared with the theoretical limits of active Intermodulation generation were clearly too high.

The breakthrough of the carrier signals was traced to pick-up of radiated emissions by the LNA since they were observed to decrease on turning the LNA off. The emissions were located using a small dipole antenna connected to a crystal detector and thence to an oscilloscope. Variations in the level of signal picked up by the antenna could be observed as fluctuations in the displayed voltage. This allowed the radiated emissions to be traced and it was found that they were largely associated with radiation from the outer surface of the flexible coaxial cable located in the high power sections of the system. Radiation was also evident from the high-power valve amplifiers. It was obvious, therefore, that in order to minimise the possibility of active intermodulation interfering with PIM measurements that the pick-up of these radiated emissions had to be suppressed.

3.7 System Performance

Since the system consists of connectors, cables, filters, couplers and instruments, there are inevitably a number of metallic contacts which arise from connecting the system together. Even with the careful choice of system components and thorough cleansing of components during assembly, some of these contacts and components may generate intermodulation signals. The residual PIM of the system and must be extremely low in order to make maximum use of the available sensitivity.

In order to asses the system performance and residual PIM levels, a straightforward test was carried out. The transmit section of the measurement system is connected directly to the detection circuit with no sample or test chamber in place. Any PIM which is recorded will be entirely generated by the system. Although the basic system described was constructed from good quality commercial parts and carefully assembled, a residual PIM level of approximately -60dBm at the DUT for carrier powers of 20Watts each, was recorded. In comparison with the desired degree of sensitivity of around -150 dBm, this was extremely poor.

Generally, PIM levels associated with contact phenomena are fairly inconsistent and somewhat random in nature [19, 37]. However, in this case the high level of residual intermodulation was observed to be very stable. Such consistency may be expected from distributed PIM sources like ferromagnetic materials but since there are no such materials in the system, this cannot be the case. One might also expect to see a consistently high level of IMD due to nonlinearities in active devices, however, the recorded levels of carrier breakthrough would result in much lower levels of intermodulation suggesting that this isn't the cause. A reasonable explanation could be that there are a large number of contacts which are producing PIM and are distributed through the system such that statistically, they tend to average out at a high level. In order to find out more it was decided to embark upon a measurement programme to locate the source(s) of the residual intermodulation and remove it.

3.8 System Component Tests

In order to identify those parts of the system which contributed to the level of residual intermodulation, it was decided to perform PIM tests on the various components that go to make up the system. However, the performance of most of these components can only be investigated at their design frequency and, in the absence of a separate low-PIM L-band test facility, this presented a problem. Any measured PIM in the system could be influenced by several components making it difficult to attribute PIM generation to any one device.

The difficulty with trying to eliminate sources of PIM is that the level is usually dominated by one particular mechanism or component. Changes can be made that reduce PIM from other mechanisms or components, however, no improvement will be evident until the dominant source is removed. It is also worth noting that if changes have been made prior to the eradication of the dominant source of PIM, then the improvement which is observed may not be entirely due to the removal of that source.

In the event, a lengthy series of tests was undertaken on different combinations of components in order to try and establish those which dominate the residual PIM. The results indicated problems in 4 principal areas, namely, couplers, filters, cables and connectors. The findings are discussed next.

3.8.1 3dB Hybrid Couplers

One of the coupler units was disassembled in order to examine the construction of the device. On closer inspection it was discovered that there were several features in the construction of the coupler which could be susceptible to PIM generation. The most obvious of these was the female, N-type, panel mount connectors. There are four of these on each device and each one is fixed to the coupler body using only 2 small diameter screw fasteners. This is not generally considered sufficient to provide the high contact pressures required to reduce PIM at metal interfaces. Similarly, the enclosure which houses the coupler is of a box and lid arrangement, the lid being fixed by eight small diameter screws which are also considered to be inappropriate for a low-PIM device.

Inside the device it was found that the coupling mechanism is facilitated by overlay coupled strip transmission lines which had been etched onto either side of an unknown substrate material. This too gave cause for concern as it was difficult to determine the nature of the materials used in the construction of the unit. The materials used in the coupling section will be exposed to the full excitation power of the system during normal operation and so should not generate a significant amount of PIM. It is known that Chromium is often used in the microstrip industry as a base material to provide superior adhesion to substrate materials. The chromium is then plated to the desired thickness using copper or gold. Chromium however, is a known ferromagnetic material hence its presence is highly undesirable in any low-PIM assembly. The substrate material too is an unknown quantity. Little research has been conducted to determine the PIM performance of dielectrics or substrate materials, and as a rule, their use should be limited to situations where they are exposed to low field strengths.

The transitions between the N-type connectors and the strip-line sections were made by soldering the centre-pins of the connectors directly to the copper track. Upon opening the device it was discovered that one of the transitions had been poorly soldered and the two conductors had become detached. The joint had been maintained only by the pressure fit of the enclosure and was very unlikely to deliver low PIM operation.

The hybrids were tested by applying both carriers to one port at a nominal power level of 2Watts per carrier, and then measuring the PIM level at one of the coupled ports. Both of the unused ports were terminated with reels of UR M43 cable to act as 50 Ohm loads. However, in all cases, no increase in the residual intermodulation level of the test setup was observed. This is likely to be due to the presence of more dominant sources of PIM, from the filters for example.

3.8.2 Filters

The Trilithic® filters which were used in the system were opened up and examined thoroughly. Fig.3.15 shows the internal construction of one filter. From inspection it appeared that these filters would be more likely to be a cause of high residual PIM levels. The body is manufactured from silver plated aluminium but consists of many individual

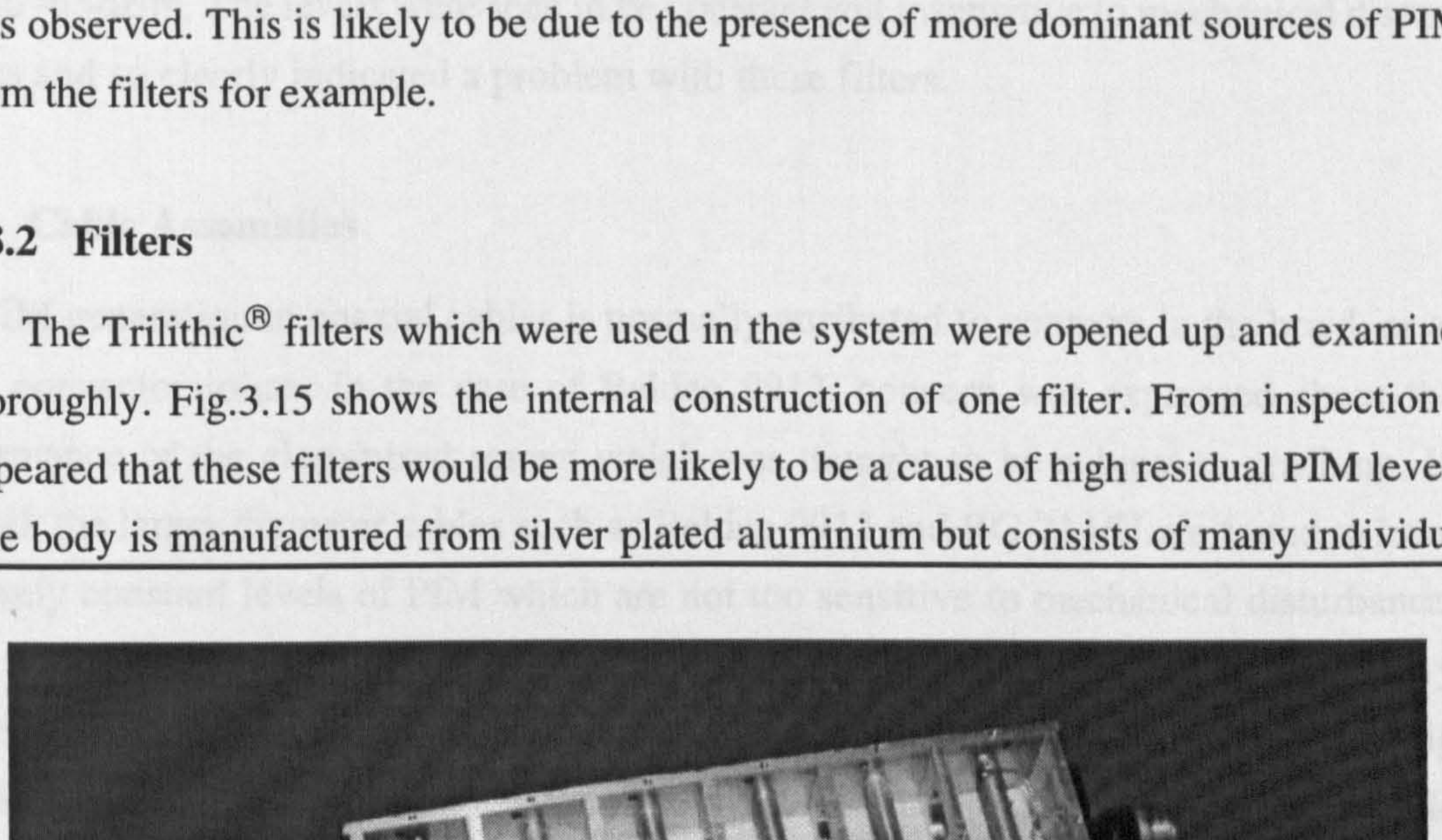

Fig.3.15 Trilithic® filter - internal construction

pieces held together with small screws. The top plate, bottom plate, and internal cavity dividers are all separate. The resonant elements are also attached to the body at one end

by screws and there are many threaded tuning adjustments. Any PIM problems arising from the many areas of metal to metal contact will be exacerbated by the fact that the cavities are of very high Q in order to give the narrow bandwidth required. Therefore, in the combiner section, one carrier in each chain will be present at very high power densities leading to high voltage and current intensity at localised points.

The filters had to be tested in different ways due to their different resonant frequencies. It would be unwise to test the forward PIM levels of the 1560MHz filter for example because the filter would tend to reflect any PIM signals which it generated. Measurements revealed that for carrier levels of 1 Watt per channel, all of the filters generated PIM levels around -65 dBm. The levels were seen to be constant and insensitive to mechanical disturbances and so clearly indicated a problem with these filters.

3.8.3 Cable Assemblies

PIM generation in coaxial cables is normally attributed to contacts in the braid, or at cable connector joints. In the case of Belden 9913, concern was expressed about the performance of the aluminised screen which was thought to be subject to cracking. In general, the larger diameter cables such as Belden 9913 and RG 214/U are found to have relatively constant levels of PIM which are not too sensitive to mechanical disturbance, while smaller cables such as UR M43 and RG 58C/U can give low PIM levels but are very sensitive to disturbances where the cable enters the connector, commonly causing increases of 10dB to 30dB. An exception to this is RG 213, a 10.3 mm diameter cable similar to UR M67, which was sensitive to handling along its length.

The results of the cable tests are summarised in Table 3.2. All the cables tested were representative of normal laboratory cables in that all were at least a few months old but none had been subjected to mechanical damage or exposed to harsh environments. Silver-plated, brass, N-type connectors by Greenpar Ltd., were used on all the flexible cable assemblies. Connection to the braid is by a clamp-type arrangement whilst the centre pins are soldered. The connectors were thoroughly cleaned with IPA before the tests.

The best results that could be obtained are given and, particularly in the case of the small diameter cables and RG 213/U, much worse results were more common. All the tests were performed with 2 Watt carriers. PIM levels in the region of better than -100dBm should be taken as representing the limitations of the test system; higher levels are indicative of PIM generation in the test cable and are more precise.

PIM levels in cables are known to be a function of length. In the table, S, M, and L denote short medium and long cables respectively. The actual lengths depend on the attenuation for each cable type. Short cables are typically 15 cm to 50 cm long, such as would be used for interconnections between system components, and where the PIM level is likely to be largely determined by the cable-connector interface. Medium cables are around 10 metres in length for the lower loss cable, with an attenuation of between 1 dB and 3 dB to allow detection of forward PIM generation in the cables themselves. Finally long cables are 50 metres or more for the smaller diameter cables, and 250 metres in the case of Belden 9913, so that essentially all the carrier power is absorbed and the reverse PIM level is representative of that expected for use as a dummy load.

Cable Type	Length	Forward PIM dBm/dBc	Reverse PIM dBm/dBc
Belden 9913	S	-100 -133	-100 -133
Belden 9913	M	-93 -126	-87 -120
Belden 9913	L	N/A	-62 -95
Belden 9914	M	-95 -128	-95 -128
RG 213/U	M	-100 -133	-100 -133
RG 214/U	M	-103 -136	-93 -126
UR M43	S	N/A	-105 -138
RG 58C/U	S	N/A	-90 -123

Table 3.2 PIM generation in coaxial cables

3.9 Conclusions

Tests on the individual system components have established that the main contributors to the residual intermodulation are the Trilithic® filters and the reel of Belden 9913 cable used for the dummy load (any PIM generation in the short lengths of 9913 used for the interconnections is insignificant in comparison). Although no residual PIM was attributed to the hybrid couplers at the modest power levels tested, there was concern over the way in which the hybrids were packaged and in particular, the mounting of the N-type connectors. The connectors themselves must also come under further scrutiny. One area for concern is where the outer conductor braid of the cable is fixed to the connector body. Clamping seems to produce mechanically sensitive joints which are not conducive to obtaining a repeatable and stable level of residual PIM. The centre pins having small geometries are subject to high current densities and these too could prove problematic in the quest for a highly sensitive and stable measurement system.

3.10 Initial Improvements

Several steps were taken towards improving the PIM measurement system. These short-term actions were carried out in order to reduce the level of system residual PIM and the breakthrough of the high power source signals to the detector.

3.10.1 Shielding

The breakthrough levels recorded in Section 3.6.3 are potentially threatening to the sensitivity of PIM measurements using the system. As previously mentioned the level of breakthrough was largely associated with the pick-up of radiated emissions from flexible coaxial cables and from the high-power valve amplifiers. To control the level of breakthrough it was deemed necessary to provide electromagnetic shielding between the high power part of the system and the detection circuitry.

Due to impending tests at ESA's site in the Netherlands [13] (described in Appendix A) it was felt that the portability of the system should not be compromised. It was therefore decided to integrate each of the two parent signal sources, with attendant preamplifiers and D.C. supplies, in two separate 19 inch racking units, with the combiner circuit in a third. These were than mounted in a 19 inch wheeled trolley frame, with the high-power linear valve amplifiers mounted below. Additional shielding was added to the rear of the high power amplifier unit in order to curb the signal leakage problem that was found there. The result was a highly mobile and robust assembly that is laboratory mobile and could be readily transported, with minimal disruption, in a small van.

Fabricated in heavy duty aluminium sheet, the racking units help to reduce emissions from coaxial cables and discrete components. Suitably connected, the units also provide a sound grounding system on which to mount components, ensuring adequate earth continuity throughout the system. The units are shown in Fig.3.16.

In addition to preventing radiated emissions from reaching the sensitive detector, it was also decided to reduce the susceptibility of the LNA by placing it inside a galvanised metal box. The D.C. supply lines were fitted with capacitive feed-throughs to attenuate signals entering the box via the leads by over 70 dB. R.F. bulkhead connectors were also employed for the same reason.

The effect of the above measures was to reduce the breakthrough of the high power source signals to the levels indicated below:

1530 MHz: -85 dBm 1560 MHz: -80 dBm

Fig.3.16 19-inch rack assembly

Although the levels have not been completely suppressed, any active IM produced by the LNA or the spectrum analyser will be well below the thermal noise limitations of the system and will pose no threat to the sensitivity of PIM measurements.

3.10.2 Recabling

As indicated in Section 3.8.3, the flexible cable assemblies in the system which were subjected to the high-power source signals, were found to be a dominant source of residual PIM as well as providing a significant level of radiated emissions. In order to cure

the problems associated with this type of cable construction, the flexible cable assemblies were replaced with semi-rigid media. The solid outer conductor used in semi-rigid cable gives improved shielding and PIM performance over the braid or foil shields used in flexible cable. This is primarily due to the absence of metal junctions and more consistent dimensional characteristics. This is particularly evident at bends in the cable where the field patterns can become distorted, which, in braided cable can cause current to appear on the outside of the outer conductor.

Cables and connections in the PIM critical areas of the system, i.e. where both parent signals exist at high power, were replaced with industry standard UT 250-A semi-rigid cable. This is a 0.25 inch diameter cable with a seamless solid copper outer conductor, solid PTFE dielectric and a silver plated, solid copper inner conductor. This size of cable has greater conductor dimensions than the more commonly used UT 141 (0.141 inch outer conductor) and therefore delivers lower associated current densities and consequently a reduced propensity to generate residual PIM. In areas where PIM generation was not considered to be a problem (e.g. in the isolated feed chains) but radiated leakage was still a possibility, the cables were replaced by the UT 141-A cable which offers the same shielding qualities but is less costly and easier to work with.

In addition to the recabling, the test bed was covered by a large section of aluminium sheet which was earthed at several points along its length. The purpose of the sheet is to provide sound earth continuity for the components of the system, which rest on top. The components, which largely make up the PIM sensitive areas of the system, were arranged to have bare metal contact with the ground plane which involved the removal of paint and coatings where necessary. This type of ground plane, referred to as a multi-point grounding system, is one where each ground connection is made directly to the ground plane at the closest possible point to it, thus minimising ground connection path lengths [15]. This provides a multiplicity of different paths and avoids the resonance problems that can arise in single point earthing. The ground plane is necessary to provide a well defined ground reference for the system and to aid in the reduction of EMI in the system due to the pick-up of signals from other equipments.

In addition to reducing emissions, complete semi-rigid cable-connector assemblies have a much better overall PIM performance than those using flexible cables. Flexible cable is far more susceptible to PIM where it is joined to a connector because the braid or foil of the outer conductor is merely clamped into the connector. This results in multiple metal-metal junctions, having a loose structure and therefore an unpredictable PIM behav-

iour. On the other hand, semi-rigid cables tend to be soldered into the connector providing a far more consistent connection and a more continuous current path. This leads to lower levels of PIM which are far more stable and consistent.

3.10.3 Improvement of High Power Load

The high power load, used to dissipate the parent signals, has been shown to be a significant source of residual PIM. Any non-linearity associated with the load will generate PIM signals which will propagate back into the detector circuit thus raising the level of system residual PIM. The best loads, in terms of linearity, have been found to be long lengths of coaxial cable.

Previously, in the UKC system, a long length of Belden 9913 flexible coaxial cable was used for this purpose. However, as discussed, this type of cable has been found to be a major source of residual PIM and was therefore replaced by two coils of UT .141 semi-rigid cable, each 20 metres long plus an additional 45 metre length of UT .250. The UT .250 has higher power handling capability but lower attenuation, and is used to reduce the parent signal levels before they reach the UT .141 cable.

As has been discussed, semi-rigid is less prone to PIM production than flexible cable. This load provides approximately 70 dB attenuation of the parent signals, and further attenuation may be achieved by adding a length of flexible coaxial cable to the end. Any PIM produced in the flexible cable will not be of a significant level since the parent signals will have been attenuated by the previous length of semi-rigid cable and the PIM signal itself will be similarly attenuated on the return journey up the cable.

3.11 Improvement in PIM Performance

To verify the effectiveness of the system in the new configuration with new cables and shielding, tests were carried out to measure the residual PIM of the system in the configuration of Fig.3.11. Results for two 25Watt carriers indicated that the Trilithic® filters, in use throughout the system, remained the dominant source of PIM in the system; hence, there are no figures for improvement in this area. However, the residual PIM level was observed to be far more consistent than before, in that it was no longer observed to fluctuate in relation to cable movement. Thus, it is reasonable to suppose that PIM sources associated with the cables and connectors are now greatly reduced, although the filters remain the principal residual sources.

As a result of the experimental findings, and upon closer scrutiny of the system components, it was evident that the performance of several of the system components was unsatisfactory. Improvement of the system shown in Fig.3.11 was required in the PIM

critical areas of power combination and PIM signal isolation. The specific components targeted for development were connectors, hybrids and filters. Experience with commercially manufactured components led to the decision to design and manufacture a range of purpose designed, low-PIM devices at UKC. The development of these components and the low-PIM techniques employed are the subject of the next chapter.

CHAPTER 4

Measurement System Development

This chapter describes the components which were designed to improve the performance of the PIM measurement system. This involved the modification of the system in 3 main areas namely, connectors, filters and hybrid couplers. Their development is reported along with the design and implementation of test enclosures for the proposed measurement program. The chapter concludes with a description of the improved system.

4.1 Introduction

The development of a passive intermodulation (PIM) measurement system using commercial components was described in Chapter 3. At present it is not possible to obtain commercial components which can be configured to deliver the very low levels of residual PIM required of modern measurement systems. This has been shown to be the case. However, the initial objective of building a working PIM measurement system has been achieved.

In general the residual PIM level of a system or device will be governed by one dominant mechanism at a time. This will tend to obscure the effects of other, less intense, sources of PIM. Accordingly, the only way to observe a reduction in the level of residual PIM in a system is to successively cancel the effects of the most dominant mechanism leaving the next dominant mechanism to dictate the performance. If measures are taken to improve the system which reduce the effect of sub-dominant mechanisms yet do not affect the dominant mechanism, little or no improvement will be recorded. This contrives to make the improvement of PIM systems a difficult task. It is also very difficult to give exact figures for the improvement in PIM system performance in response to specific counter-measures. Measures taken to reduce PIM may be seen to be ineffectual but the effects may

be masked by more dominant PIM sources. Hence, the development and improvement of PIM measurements involves a lot of cut and try experimentation in order to identify and minimise the dominant PIM mechanisms. Every PIM measurement system will inevitably require this process of development as it is extremely unlikely that a system will deliver state-of-the-art performance at the first time of asking.

One of the primary objectives of this project was to develop a stable and reliable PIM measurement system with a very low level of residual intermodulation. In the last chapter it was observed that this was far from being the case owing to PIM generation from most of the functional parts of the system i.e. cables, connectors, filters and couplers. Examination of these components indicated that each was likely to generate significant levels of intrinsic PIM. The next step was to consider each of these elements individually and, by applying the experience and knowledge gained, to develop custom low-PIM replacements.

This chapter deals with the developments which came about as a result of the effort to improve the L-band system. It has already been discussed that the flexible coaxial cables used in the critical parts of the system were replaced by semi-rigid media with promising results.

4.1.1 Change of PIM Product

As the principle sponsor of this project the European Space Agency has had a significant amount of input as to the direction of the project. It has been mentioned in Section 1.2 that the ARTEMIS communications satellite is currently giving cause for concern due to its high vulnerability to interference from PIM. In particular, it is the upper 7th order PIM product at 1650MHz which poses the greatest threat.

Due to the early difficulties which were initially encountered in trying to achieve a very low level of third order residual PIM, the system was reconfigured to enable measurements of 7th order products. This allowed a direct comparison to be made between the UKC system performance and that of other established systems operating at 7th order. The 7th order products are those which relate directly to the ARTEMIS program, therefore ESA contractors (Ericsson and Matra Marconi Space) working on ARTEMIS have developed PIM test beds for performing qualification tests on ARTEMIS sub-systems. Comparable performance by the UKC system with these systems was taken as an indication that satisfactory performance had also been achieved at 3rd order. The switch to 7th order also means that any measurement data produced by the system will be directly applicable to the ARTEMIS project without the need for extrapolation.

The principal effect of the change was that the custom low-PIM components described in this chapter should operate at the 7th order product frequency of 1650MHz. In practice the broadband components were designed to operate from the low carrier at 1530MHz to the upper 7th order product. This equates to a 7.5% bandwidth which should not present any difficulty. The narrowband components i.e. the filters, were designed to be tuneable over the same range.

4.2 Development Aids

During this phase of the project, several development tools were utilised to design and test the low-PIM components. These will be described first.

4.2.1 Software

Two different software packages were used in the development of the components described in this chapter. The packages are used to simulate different structures and circuits, allowing their operation to be verified and fine tuned before they are built.

4.2.1.1 High-Frequency Structure Simulator

The HP 85108A High-Frequency Structure Simulator (HFSS) from Hewlett Packard is a software package that analyses the electrodynamic behaviour of passive structures. It computes scattering parameter (S-parameter) responses and electromagnetic field distributions for passive, three-dimensional structures.

The package is used to draw the geometry of any multi-port, enclosed structure which is to be modelled. The simulator then uses Maxwell's equations to solve for the electromagnetic fields and calculates the S-parameters to user-specified accuracy. The system can handle unrestricted geometries that can contain an unlimited number of dielectrics and ports and is only limited by the computing power or hardware which is available.

The traditional, manual, process for solid modelling and analysis consists of two-dimensional paper drafting, submitting the design to a workshop for prototyping, building the structure, testing it and measuring its properties.

With HFSS, this 'cut and try' process is replaced by modelling and analysis at the computer workstation. The software allows the designer to draw and revise a model. A number of post-processing capabilities allow the designer to determine and observe the electromagnetic properties of the structure as field plots on the computer screen, thereby providing much more information about the structure than could ever be delivered using traditional methods.

4.2.1.2 Microwave Design System

Hewlett Packard also produce a large suite of software packages collectively known as the HP 85200A Microwave Design System (MDS). MDS is a fully integrated, computer-aided engineering environment which provides capabilities for taking designs from conception through physical representation, and production documentation.

The main function of MDS is to provide for complete network modelling and analysis. Circuit schematics are entered using extensive libraries of individual components, including transmission lines, capacitors, transistors etc. These components are connected together to form individual circuits. e.g. designs can be formed on multiple layers to allow for the design of complete systems.

The individual responses of the basic building-block components are described mathematically within the software, based on the most up-to-date models available. The parameters of each component (e.g. transmission line impedance, length, dielectric constant, loss etc.) are user-definable in order to customise circuits to correspond to the specific user application. It is also possible for users to define their own models, incorporate real measurement data from network analysers etc. and incorporate output data from packages such as HFSS.

Due to the mathematical representation of the components, simulation is very fast and efficient. Much larger circuits can be simulated than with HFSS. Once simulated, the circuits may be analysed in numerous different ways. Circuits may be fine-tuned and altered in order to gauge trade-offs between parameters and predict manufacturing sensitivities. The whole system is controlled via a completely integrated graphical user interface which makes for easy interpretation of results and general ease of use.

4.2.2 Network Analyser

The network analyser is a vital piece of equipment to any RF or microwave engineer. The instrument is used to provide data on the physical performance of both active and passive, high-frequency components. The Wiltron 360 vector network analyser used throughout this project provides both amplitude and phase information about the propagation of signals through a certain device.

Network analyser systems contain the following elements in one form or another:

(i) Signal source

(ii) Test Set

(iii) Network Analyser

The signal source provides the stimulus to the device under test. Frequency stability of the source is an important factor in the accuracy (especially the phase accuracy) of the network analyser. The test set is a two port instrument that samples the incident, reflected and transmitted signals. Finally, the network analyser analyses the I.F. signals from the test set for phase and magnitude data which is then presented on the display. The analyser also acts as the central controller for all of the individual components, synchronising their operation.

Measurements are made by comparing the relative magnitude and phase variations between the signal incident upon the device under test (DUT) and the reflected or transmitted signal from the DUT. Since the measurements are relative, they accurately define the response of the DUT only. Anomalies in the incident signals are removed by calibrating the system before performing any measurements.

4.3 Low - PIM Connection Principles.

4.3.1 Introduction

It is evident from previous studies of PIM and from initial work on the UKC L-band measurement system that points of direct metal-metal contact (and their associated mechanisms), are prominent sites of PIM generation. Points of contact are discrete, localised and easily identified. PIM generation at these points is, however, very difficult to control. Until now, the problem has been dealt with by simple brute force. Junctions are made at very high pressures (>60MPa [19])in order to force a large number of microscopic point contacts (or a-spots) to support current flow. The effect is merely to reduce the current density at any one point of contact which reduces the amount of overall PIM produced (as seen in Section 2.4.2.1). However the degree of improvement is not readily predictable and is likely to be highly variable. The resulting PIM levels are also liable to be unrepeatable as the microscopic properties of a junction under high pressure are prone to change over time or if subjected to even slight mechanical agitation.

The dominant factor at such junctions is the current density across the junction. In general, the effect of any non-linear behaviour in the conduction of current is reduced as the current density is reduced, resulting in lower levels of generated PIM. This is the logic behind the high pressure approach.

This section examines a novel approach to the problem and that is to use established transmission line techniques [110-113] to greatly reduce the flow of current across points of metal-metal contact. It will be seen that these techniques can be readily applied to the PIM measurement system situation in order to provide low-PIM connections in all of the

critical areas of the system. These techniques will also provide structures that improve the PIM performance of the discrete system components such as filters and couplers. It will also be seen that the methods minimise the high variability in PIM performance which has troubled most systems to date.

4.3.2 Series Connected, Branch-line Stub.

A single-stage, series connected, branch-line stub is depicted in Fig.4.1. When the length of the stub, l_s, is $\lambda/4$ long at the design frequency, ω_O, the open circuit terminating the stub is transformed, by the intrinsic nature of transmission lines, to a short circuit at the input of the stub at A-A′ as follows.

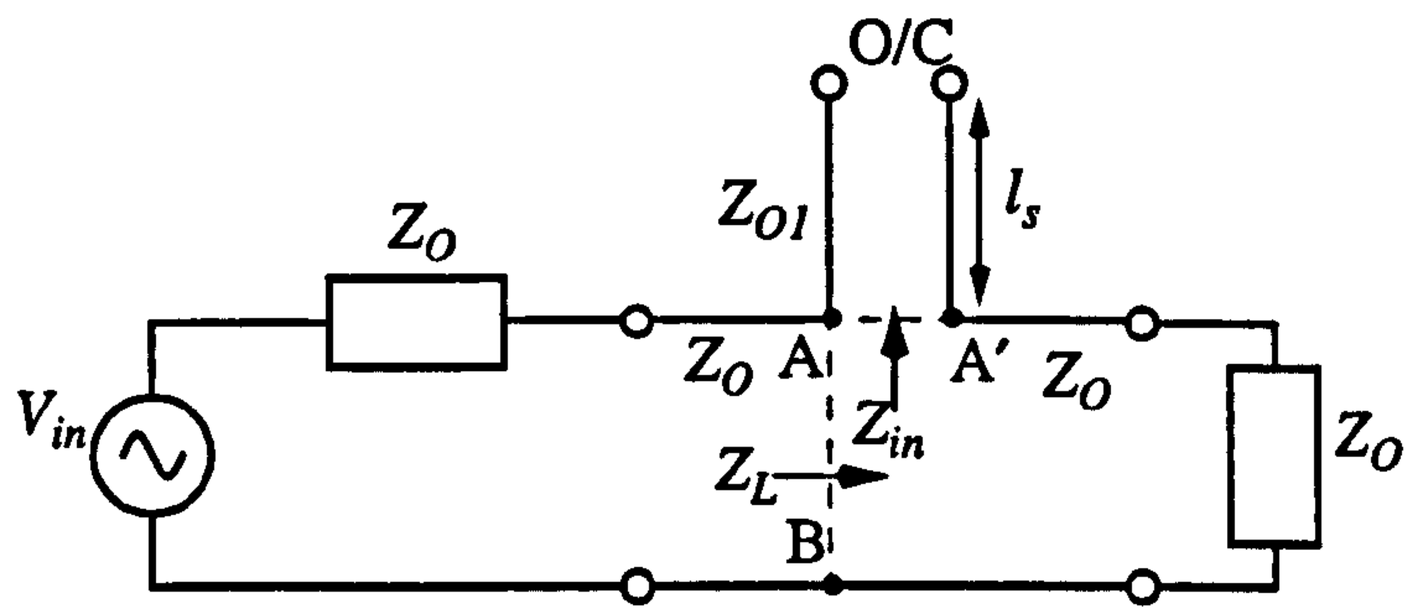

Fig.4.1 Single-Stage, Series Connected, Open Ended Stub.

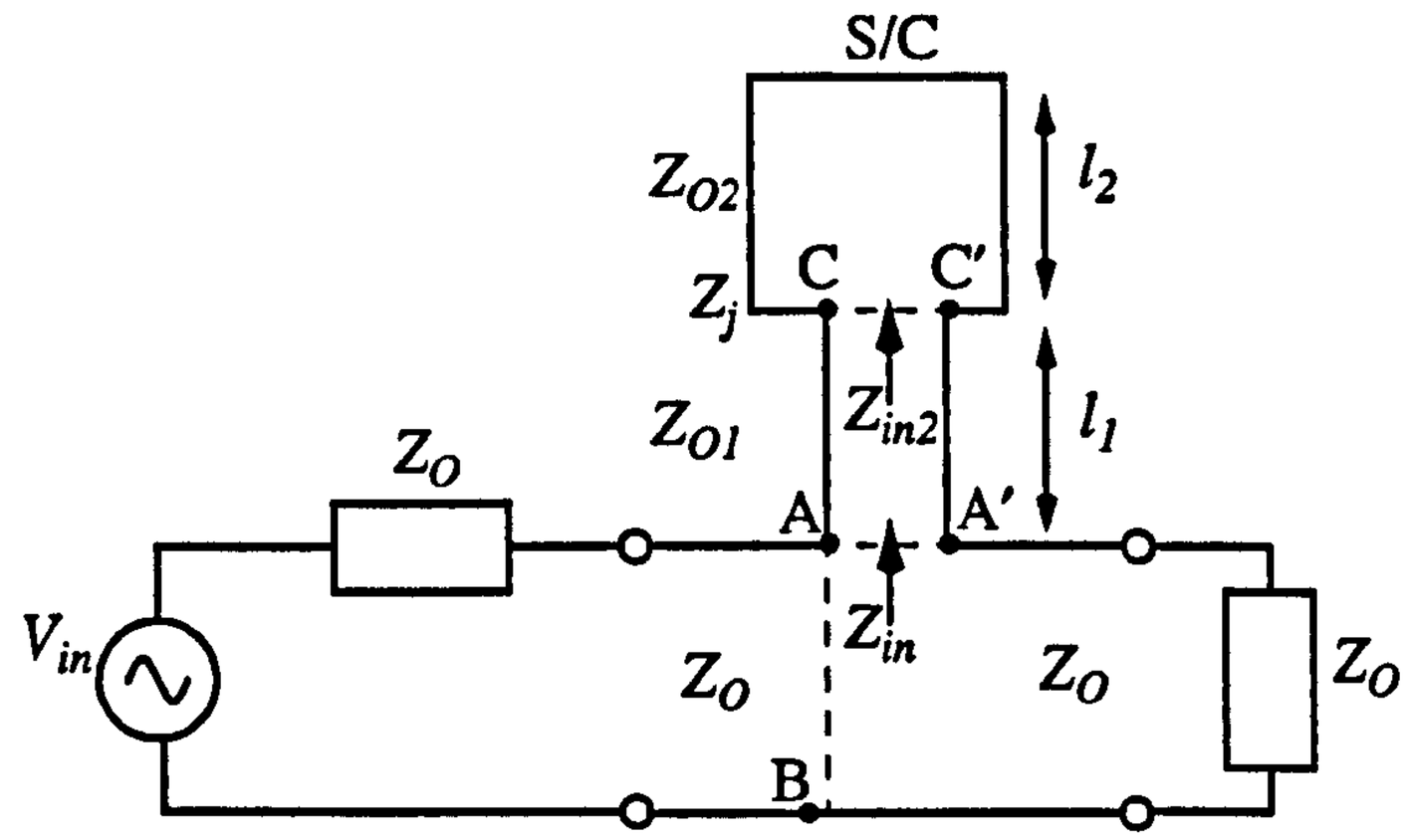

Fig.4.2 Two-Stage, Series Connected, Short Circuited Stub.

The input impedance to a length of line, l, of characteristic impedance, Z_O, and terminated in an impedance Z_L is defined as:

$$Z_{in} = Z_O \cdot \frac{Z_L + jZ_O \cdot tan\beta l}{Z_O + jZ_L \cdot tan\beta l} \qquad \text{Eq.4.1}$$

$\beta=\omega/v$, where ω is the frequency and v is the velocity of propagation. When $Z_L=\infty$ i.e. open circuit, and $l=\lambda/4$, i.e. $\beta l=90^o$ then Z_{in} equals zero.

At point A-B, the signal on the main, through, transmission line will see an impedance of $Z_L=Z_{in}$(stub)$+Z_O$(main line). At the design frequency Z_{in}(stub) is zero and the impedance seen by the main line is just Z_O. The junction is therefore perfectly matched and the RF signal in the main line passes unattenuated to the output port of the network. However current still flows in the branch line and a large standing wave ratio is present. Note, that there is no physical contact between one of the input conductors and the corresponding output conductor, therefore there will be no problems associated with PIM at points of contact.

In many practical cases, it is difficult to achieve an ideal open circuit termination. If the open circuit is coupled to free space, it will act, to a certain degree, as an antenna and will readily transmit and receive signals via the stub. In terms of EMC this is highly undesirable and therefore, an alternative must be found. The situation may be avoided by adding a second length of transmission line to the end of the stub which is terminated in a short circuit, as in Fig.4.2.

For the single stage stub it was found that an open circuit termination is transformed by a quarter wavelength section of transmission line to a short circuit. The converse is also true, that is, a quarter-wavelength section of transmission line terminated in a short circuit, will have an infinite input impedance, i.e. an open circuit.

The length of the additional second stage is made $\lambda/4$ long at the design frequency so that the short circuit is transformed to an open at C-C′ by Eq.4.1. This is further transformed to a short circuit at A-A′ as for the single stage stub, giving the desired, low reflection at the design frequency.

The current flowing in the branch is a maximum and the voltage across the branch is zero at the short circuit termination and at the input at A-A′. At C-C′, the 'effective' open circuit, the voltage is a maximum and the current is zero. Since the current is zero, the circuit may be broken there and the physical connection made between the two lines. At the mid band frequency, any junction impedance or discontinuity effects (represented by Z_j) will be in series with an open circuit, therefore no current flow will exist across the connection and once again, the amount of PIM generation associated with the junction will be greatly diminished.

Since both of these circuits use a resonant configuration, depending on the lengths, l_s, being $\lambda/4$ at the frequency of interest, the frequency sensitivity of the impedance at the junction must be taken into account in order to determine its useful operational band-

width. The useful bandwidth is the range of frequencies where the transmission of RF signals takes place with minimum attenuation or reflection. For most systems a return loss of greater than 25 dB is acceptable.

4.3.3 Analysis

To find a useful expression for the bandwidth of the circuit, it is necessary to obtain an expression for the return loss in terms of the only variable, frequency. All other parameters for a practical circuit will be constant. The two-stage stub is the more complex circuit, hence, only it's analysis will be covered in detail.

The equivalent circuit of Fig.4.2 is as shown in Fig.4.3:

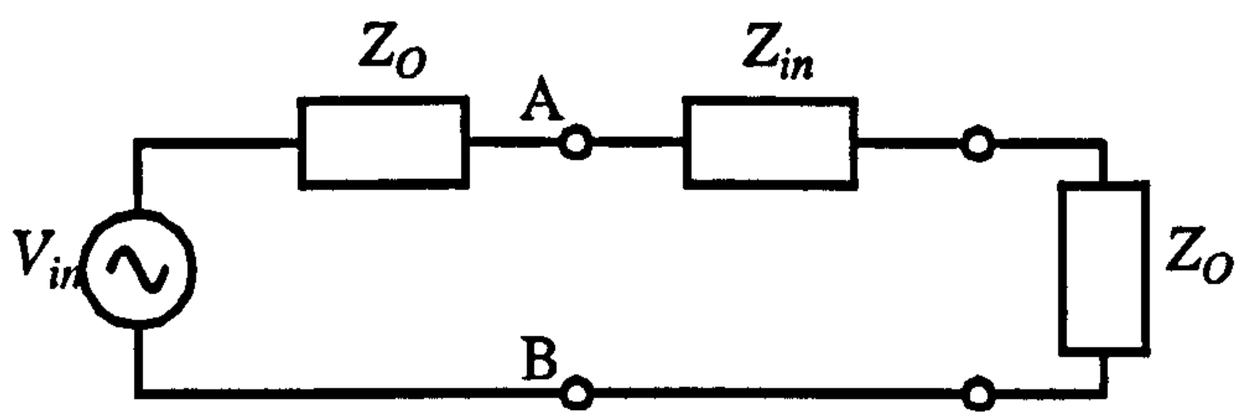

Fig.4.3 Equivalent Circuit of Fig.4.2

The reflection coefficient at A-B, seen by the generator is given by:

$$\Gamma = \frac{Z_L - Z_G}{Z_L + Z_G} = \frac{Z_{in}}{Z_{in} + 2Z_O} \qquad \text{Eq.4.2}$$

Consider Fig.4.2. Using the impedance transformation equation (Eq.4.1) and working back from the short-circuit termination (Z_L=0) we have:

$$Z_{in_2} = jZ_{O2} \cdot tan\beta l_2 \qquad \text{Eq.4.3}$$

Given that $l_2=\lambda_O/4$:

$$\beta l_2 = \left(\frac{\omega l_2}{v}\right) = \left(\frac{\pi}{2} \cdot \frac{\lambda_O}{\lambda}\right) = \left(\frac{\pi}{2} \cdot \frac{\omega}{\omega_O}\right) \qquad \text{Eq.4.4}$$

Near mid-band, $\omega \approx \omega_O$ and $tan\beta l_2$ will be very large, infinite at mid-band. If the junction impedance, Z_j (contact resistance and other discontinuity effects), is kept less than Z_{in2}, it may be neglected. This suggests the desirability of making Z_{O2} as large as possible, which as we shall see later, is desirable for other reasons as well.

Next we must take account of the second quarter wavelength section of transmission line of impedance Z_{O1}. Neglecting Z_j, the impedance terminating this section of line is just Z_{in2}. Once again, using the impedance transformation of Eq.4.1, this can be referred back to the plane of the junction, at A-A′ to get:

$$\begin{aligned} Z_{in} &= Z_{O1} \cdot \frac{Z_{in2} + jZ_{O1} tan\beta l_1}{Z_{O1} + jZ_{in2} tan\beta l_1} \\ &= jZ_{O1} \cdot \frac{Z_{O2} tan\beta l_2 + Z_{O1} tan\beta l_1}{Z_{O1} - Z_{O2} tan\beta l_1 tan\beta l_2} \\ &= -\frac{jZ_{O1}}{tan\beta l_1} \cdot \frac{1 + \dfrac{Z_{O1} tan\beta l_1}{Z_{O2} tan\beta l_2}}{1 - \left(\dfrac{Z_{O1}}{Z_{O2}} \cdot \dfrac{1}{tan\beta l_1 \cdot tan\beta l_2}\right)} \end{aligned} \qquad \text{Eq.4.5}$$

Additionally, given $l_1 = \lambda_O/4$, we may write after Eq.4.4:

$$\beta l_1 = \beta l_2 = \frac{\pi}{2} \cdot \frac{\omega}{\omega_O} \qquad \text{Eq.4.6}$$

Near mid-band $tan\beta l \approx \infty$ therefore we may neglect the term $\dfrac{Z_{O1}}{Z_{O2}} \cdot \dfrac{1}{tan\beta l_1 \cdot tan\beta l_2}$ in the denominator of Eq.4.5, hence:

$$Z_{in} \approx -jZ_{O1} \cdot \frac{1}{tan\left(\dfrac{\pi}{2} \cdot \dfrac{\omega}{\omega_O}\right)} \cdot \left(1 + \frac{Z_{O1}}{Z_{O2}}\right) \qquad \text{Eq.4.7}$$

Now ω can be expressed as $\omega_O - \Delta\omega$ where ω_O is the mid-band frequency at which $\beta l = \pi/2$ and $\Delta\omega$ is the difference between ω and ω_O, hence:

$$\begin{aligned} \frac{1}{tan\left(\dfrac{\pi}{2} \cdot \dfrac{\omega}{\omega_O}\right)} &= \frac{1}{tan\left(\dfrac{\pi}{2} \cdot \left(\dfrac{\omega_O - \Delta\omega}{\omega_O}\right)\right)} \\ &= \frac{1}{tan\left(\dfrac{\pi}{2} - \left(\dfrac{\pi}{2} \cdot \dfrac{\Delta\omega}{\omega_O}\right)\right)} \end{aligned} \qquad \text{Eq.4.8}$$

By trigonometric identity:

$$tan(\alpha-\beta) = \frac{tan\alpha - tan\beta}{1 + tan\alpha\, tan\beta} = \frac{1 - \frac{tan\beta}{tan\alpha}}{\frac{1}{tan\alpha} + tan\beta} \qquad \text{Eq.4.9}$$

With $\alpha=\pi/2$, $\tan\alpha=\infty$ and $\beta = \frac{\pi}{2}\cdot\frac{\Delta\omega}{\omega_O}$, Eq.4.8 becomes $tan\left(\frac{\pi}{2}\cdot\frac{\Delta\omega}{\omega_O}\right)$.

Near mid-band $\Delta\omega$ is small and for θ small, $tan\theta \approx \theta$, 1, therefore $tan\left(\frac{\pi}{2}\cdot\frac{\Delta\omega}{\omega_O}\right)$ is well approximated by $\left(\frac{\pi}{2}\cdot\frac{\Delta\omega}{\omega_O}\right)$ and Eq.4.7 may be written:

$$Z_{in} \approx -jZ_{O1}\cdot\left(\frac{\Delta\omega}{\omega_O}\cdot\frac{\pi}{2}\right)\cdot\left(1+\frac{Z_{O1}}{Z_{O2}}\right) \qquad \text{Eq.4.10}$$

Since losses have been neglected, the impedance Z_{in}, is naturally, purely reactive. The reflection coefficient may now be determined from Eq.4.2. Near mid-band, Z_{in} will be much less than $2Z_O$, hence:

$$\Gamma = \frac{Z_{in}}{Z_{in}+2Z_O} \approx \frac{Z_{in}}{2Z_O} = -j\cdot\frac{Zo_1}{2\cdot Zo}\cdot\left(\frac{\Delta\omega}{\omega_O}\cdot\frac{\pi}{2}\right)\cdot\left(1+\frac{Z_{O1}}{Z_{O2}}\right) \qquad \text{Eq.4.11}$$

$$\text{and } |\Gamma| = \frac{Zo_1}{2\cdot Zo}\cdot\left(\frac{\Delta\omega}{\omega_O}\cdot\frac{\pi}{2}\right)\cdot\left(1+\frac{Z_{O1}}{Z_{O2}}\right)$$

Rearranging to get $\frac{\Delta\omega}{\omega_O}$ gives us the desired expression in terms of frequency:

$$\frac{\Delta\omega}{\omega_O} = \frac{4\cdot Z_O\cdot|\Gamma|}{\pi\cdot Z_{O1}}\cdot\frac{1}{\left(1+\frac{Z_{O1}}{Z_{O2}}\right)} \qquad \text{Eq.4.12}$$

Now, $\Delta\omega/\omega_O$ is known as the half-fractional bandwidth and is representative of the separation from the mid-band frequency, ω_O, to the lower frequency at which the magnitude of the reflection coefficient is $|\Gamma|$. Due to the symmetry of the response about ω_o, the bandwidth between points of equal $|\Gamma|$ is simply twice $\Delta\omega$.

It will be noted that the bandwidth is proportional to: (a) Z_O/Z_{O1} and (b) $(1+Z_{O2}/Z_{O1})$. Therefore, to achieve the highest possible bandwidth for a given return loss, it is desirable, in view of (a), to make Z_{O1} as small as possible compared with Z_O. In view of (b) it is desirable to make Z_{O2} as large as possible compared with Z_{O1}; the desirability of making Z_{O2} large was pointed out in the discussion leading to Eq.4.5. However, the bandwidth will always be limited to $2\omega_O$ due to the resonant nature of the quarter wavelength sections.

Several plots of return loss against normalised frequency, ω/ω_O, are presented in Fig.4.4 to illustrate the relationships. The plots represent different values of Z_O/Z_{O1} and Z_{O1}/Z_{O2} and were obtained using Eq.4.5.

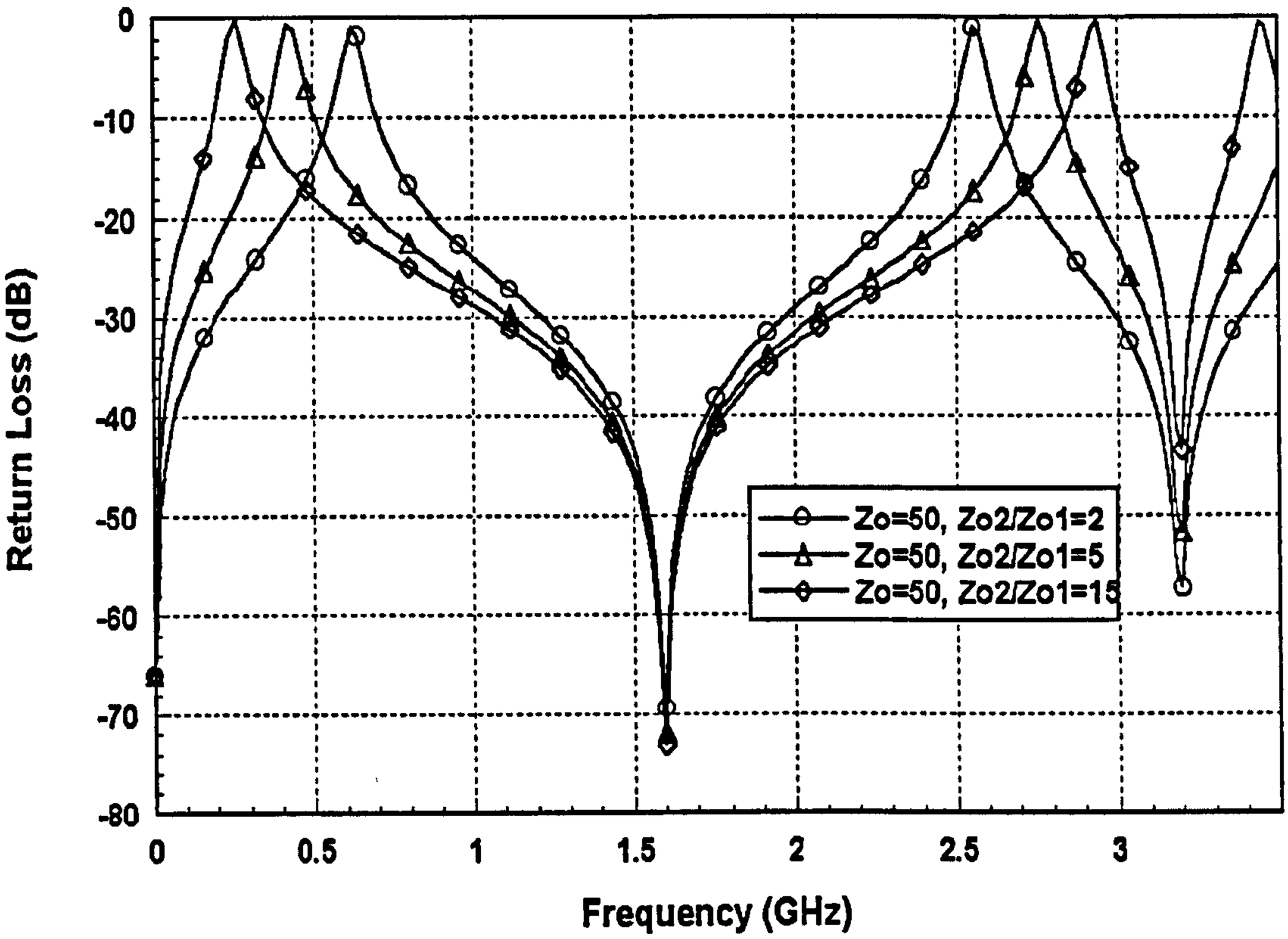

Fig.4.4 Return loss two stage stub

Recalling the single stage stub of Fig.4.1, a similar analysis yields:

$$\frac{\Delta\omega}{\omega_o} = \frac{2}{\pi} \cdot tan^{-1}\left(\frac{2 \cdot Z_O \cdot |\Gamma|}{Z_{O1}}\right) \qquad \text{Eq.4.13}$$

Which also indicates the need to keep $Z_O >> Z_{O1}$. These impedance relationships are important to bear in mind when implementing the circuits.

4.3.4 Implementation

There are several ways of physically implementing the circuits of Fig.4.1 and Fig.4.2. In this project, the transmission medium was coaxial line, hence, only coaxial versions of the circuits were considered. Fig.4.5 and Fig.4.6 illustrate cross sections of some of the possible configurations.

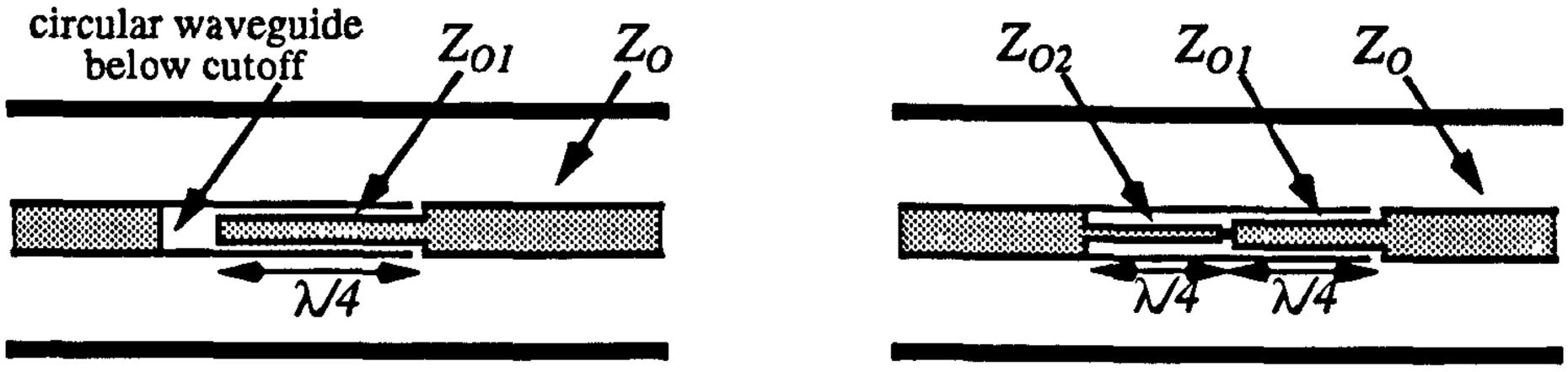

(a) Single Stage

(b) Two Stage

Fig.4.5 Inner Conductor Configurations

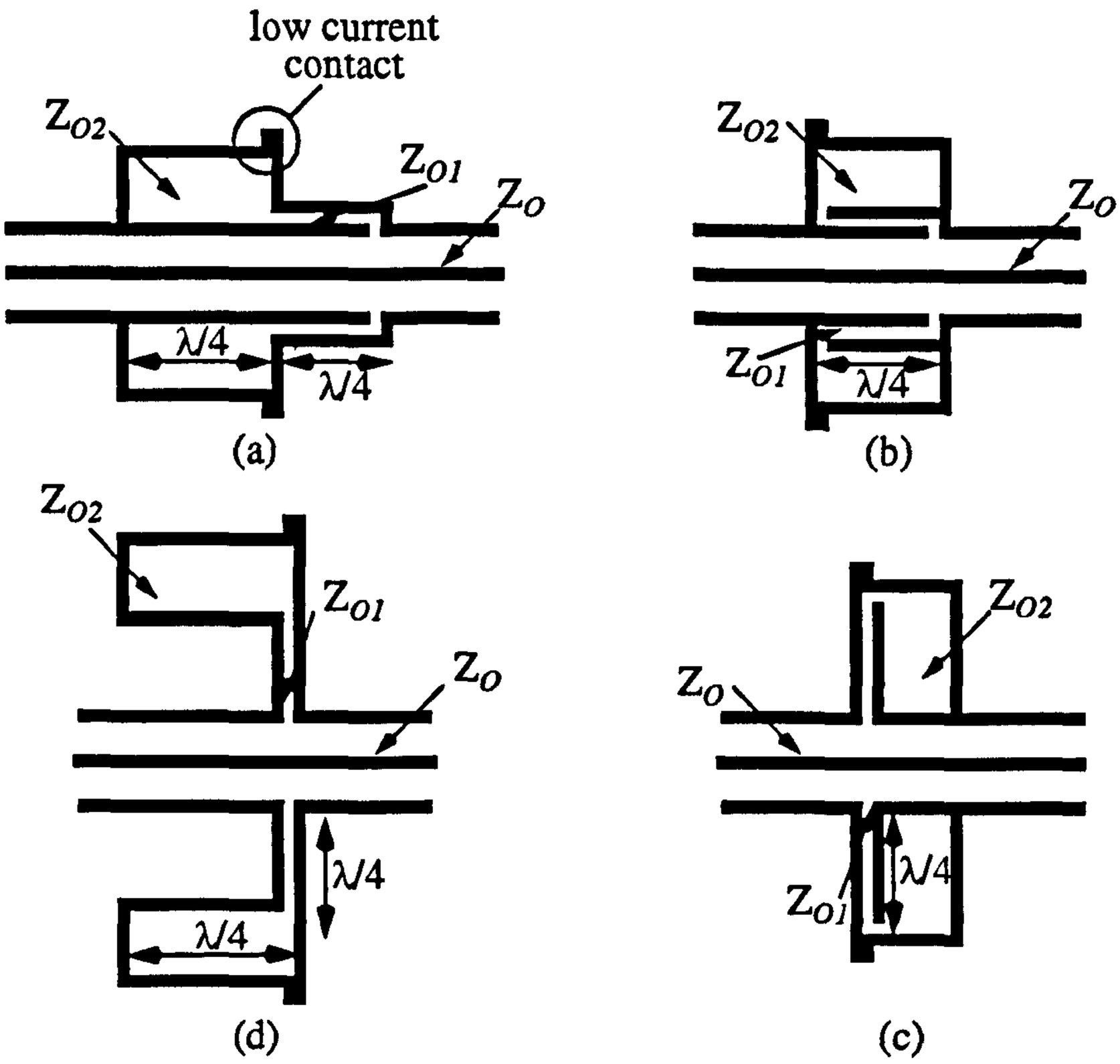

Fig.4.6 Two Stage Outer Conductor Configurations

The single stage series branch-line stub can be implemented quite readily in the centre conductor of a coaxial transmission line structure as illustrated in Fig.4.5 (a). Provided that the gap in the centre conductor of the through line is small compared with a wavelength (<0.1λ), the previous analyses will hold true.

The open circuit is formed at the end of the stub by making the receptor hole slightly longer than the stub. This leaves a short section of small diameter circular waveguide which will not support RF transmission of the coaxial TEM mode. The cutoff frequency, f_c, for the next higher mode is at a frequency whose wavelength is $1.706 \cdot r_s$, where r_s, is the radius of receptor hole. When r_s is small, say 3mm, f_c is greater than 50GHz therefore at lower frequencies the short section of waveguide acts as a very effective open circuit.

If enhanced performance is required then the configuration of Fig.4.5 (b) may be used. However, it is more difficult to implement since the centre conductor diameter of coaxial lines is usually of the order of a few millimetres, hence, the structure would be difficult to fabricate.

Fig.4.6 depicts cross sections through the outer conductor of the coaxial transmission line. A single stage stub in the outer conductor would be impractical since the open circuit termination would provide an electrical interface with the outside world, hence, only two stage stubs have been considered.

The branch impedances are formed by using the outer conductor of the main line as the inner conductor of the stub. For the connectors developed at UKC, subsequent discussions will be limited to the configurations of Fig.4.5 (a) and Fig.4.6(a).

4.4 UKC Low-PIM Coaxial Connector

The series branch-line stub techniques described above have been used to design and manufacture low-PIM connectors for:

(i) Mating together, two pieces of UT-.250 semi-rigid coaxial cable.

(ii) Mating UT-.250 coaxial cable to custom designed coaxial components in the UKC, L-band measurement system. The components consist of filters, couplers and test enclosures and will be discussed in subsequent sections.

To demonstrate the design principles, the UT-.250-UT-.250 connector assembly will be discussed in detail. A schematic of the assembly is illustrated in Fig.4.7. The design frequency of the device was chosen to be 1.56GHz, at the mid-band of the measurement system.

The series stub is formed in the centre conductor after the arrangement of Fig.4.5 (a). The centre conductor of UT-.250 cable is only 1.63mm in diameter, therefore it was not possible to machine the structure directly from the cable. Accordingly, special pins were fabricated from brass which were soldered directly onto the centre conductor of the UT-.250.

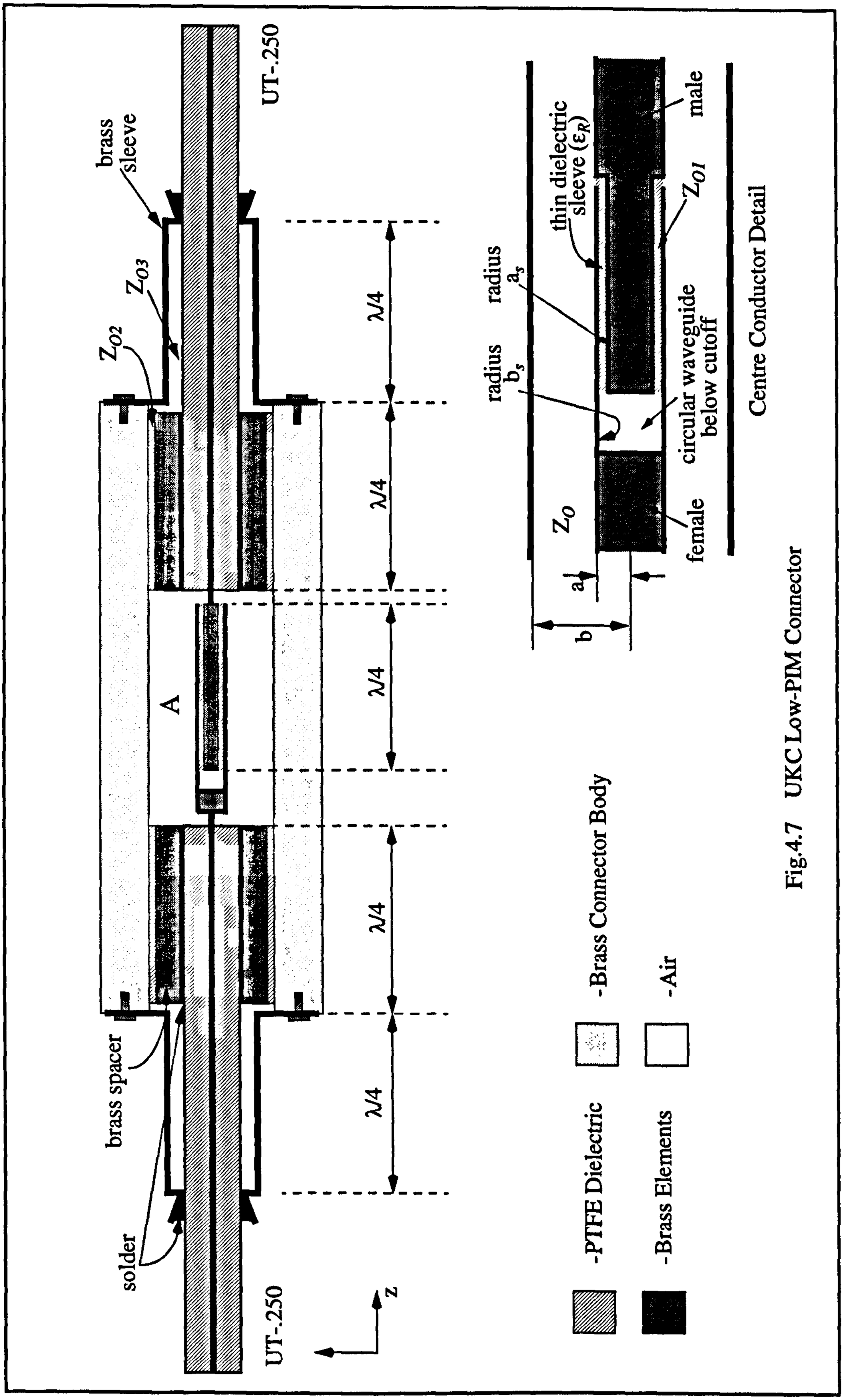

Fig.4.7 UKC Low-PIM Connector

The male pins were made to be a_s=3mm in diameter which was considered large enough to be easily machined and provide the desired mechanical rigidity; yet small enough so that the female section of the connector (or component) did not have to be excessively large to accommodate it. The pin is covered with a heat-shrinkable PTFE sleeving which forms a tight fit around the pin and prevents Ohmic contact between the two pins. On heating, the sleeving reduces to 0.15mm in thickness, increasing the effective diameter of the pin to 3.3mm. The male probe then slots into the hole in the female pin which has been drilled out to b_s=3.3mm. The internal assembly is shielded by the female pin and the concentric conductors serve to effect the impedance Z_{OI}.

The characteristic impedance of coaxial line is given as:

$$Z_O = \frac{138}{\sqrt{\varepsilon_r}} \cdot log\left(\frac{b}{a}\right) \qquad \text{Eq.4.14}$$

Where, *b*, is the inner diameter (i.d.) of the outer conductor and, *a*, is the outer diameter (o.d.) of the inner conductor. Hence, the value of Z_{OI} can be made small (as desired) by choosing ε_r as large as possible and by making the thickness of the sleeve, and hence *b/a*, as small as possible. In this case $Z_{OI}\approx 4\Omega$ and given that Z_O is 50Ω the criteria of $Z_{OI} << Z_O$, from Eq.4.12, is satisfied.

The fit of the connection must be close in order to minimise the effects of air-gaps. Air gaps reduce the effective dielectric constant of the section and increase the impedance. However, care must be taken to ensure that the inner surfaces of the female pin are smooth and free of burrs and sharp edges which can snag or tear the PTFE sleeve, fouling the connection.

Now, the o.d. of the female pin forms the inner conductor of the connector through line (section A of Fig.4.7). For a perfect match at mid-band, the impedance of this section should be 50Ω. Using Eq.4.14, the ratio of *b/a* in air to give an impedance of 50Ω was calculated to be ≈2.3. Accordingly, the through hole size was chosen to be 10.3mm, giving a female pin diameter of 4.4mm.

The outer conductor branch is formed in the manner of Fig.4.6(a), using a custom designed sleeve which fits over the outside of the UT-250 cable. The sleeve is designed to be a quarter wavelength long in air, internally, at the design frequency of 1.56 GHz. One end of the sleeve is soldered to the UT-.250 outer conductor to form the short circuit at the end of the stub. The gap between the internal surface of the sleeve and the external

surface of the UT-250 outer conductor serves to effect the high impedance second stage of the stub (Z_{O3} of Fig.4.7). The i.d. of the sleeve is 7.4mm and the o.d. of the UT-.250 is 6.35mm giving an impedance, Z_{O3}, of 9.2Ω, from Eq.4.14.

The low impedance first stage is formed by soldering the sleeve, such that a length of the UT-250, which is λ/4 long in PTFE, is exposed at the end as in Fig.4.8.

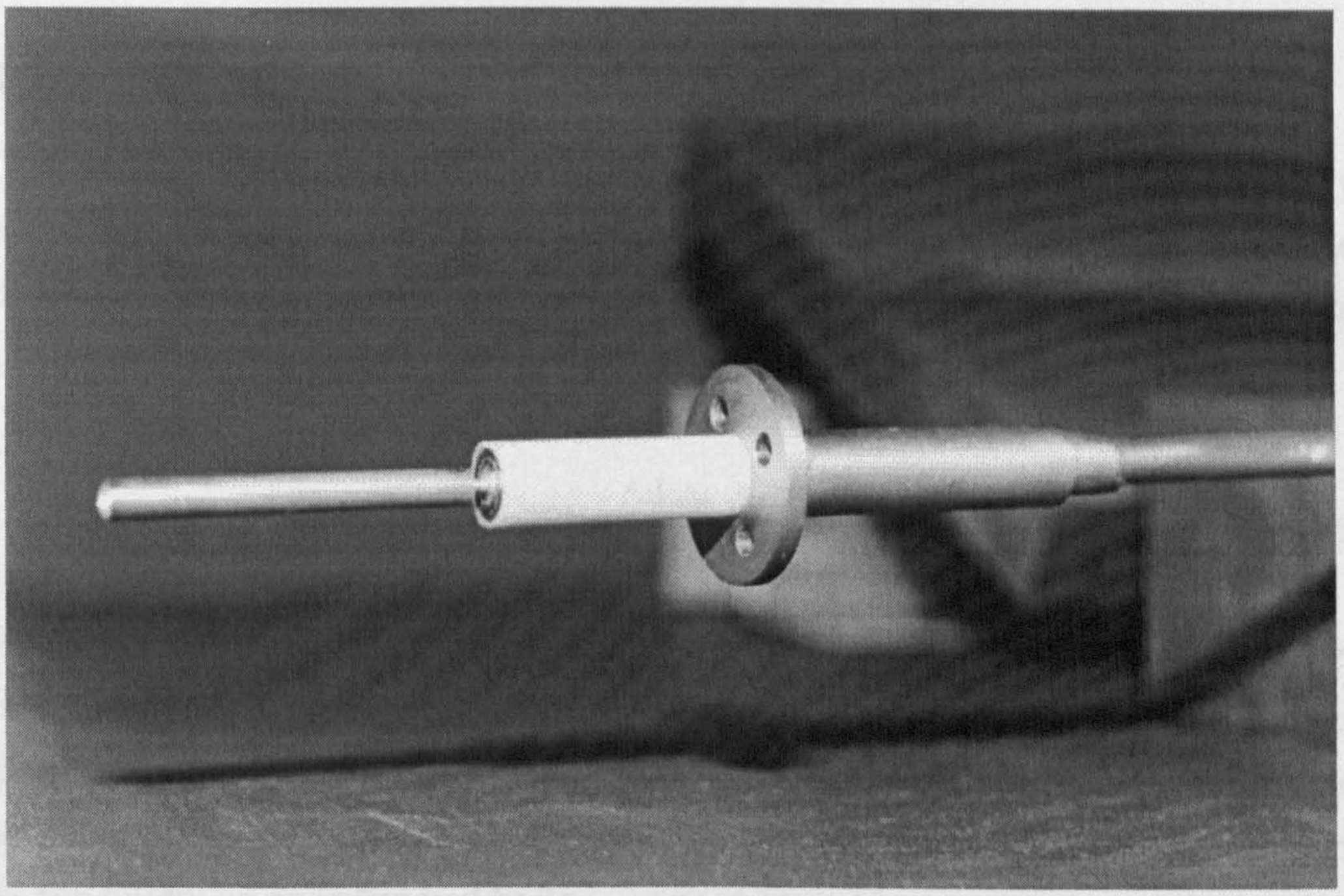

Fig.4.8 Photograph of UKC Low-PIM Connector

The outer diameter of UT-.250 cable is 6.35mm, and is obviously much smaller than the 10.3mm hole in the connector body. To make the gap between cable and connector smaller, and Z_{O2} smaller, a brass spacer was soldered to the UT-.250 as indicated in Fig.4.7. The diameter of the spacer was chosen so that when it is sheathed with PTFE tubing, it fits closely into the hole in the connector body and forms the low impedance first stage of the outer branch.

The spacer is 9.1mm in diameter and the hole is 10.3mm. Hence, by Eq.4.14, the low impedance section, Z_{O2}, is ≈5.2Ω. The ratio Z_{O3}/Z_{O2} is approximately 2. By Eq.4.12, this ratio should be as high as possible. In practice Z_{O3} was limited by the diameter of the sleeve. Making the diameter large to increase Z_{O3} would result in a much larger flange diameter, making the whole connector very bulky. However, from Fig.4.4 a ratio of 2 provides adequate performance over the frequency band of the UKC system.

The physical connection between the sleeve and the connector body is made at the low current point between the two sections as indicated in Fig.4.6 (a). The sleeve is screwed firmly to the body of the connector using M4 screws to give a strong connection which is mechanically sound and ensures a low series impedance across the joint. A good ohmic connection is still extremely important in order to produce a highly stable, low PIM signature from the joint.

4.4.1 Bandwidth Performance

The bandwidth of the individual stubs may be determined from the analyses of Section 4.3.3 using the impedance values established in the previous section. The bandwidth was calculated to determine the frequency range where the return loss is greater than or equal to 25dB. In terms of the reflection coefficient, the return loss is given as:

$$L_R = 20log\left(\frac{1}{|\Gamma|}\right)\text{dB} \qquad \text{Eq.4.15}$$

For L_R=25dB, Γ=0.056 and from Eq.4.12 the useful bandwidth ($2\cdot\Delta\omega$), of the outer, two-stage, branch lines was therefore calculated to be $0.88\cdot\omega_O$. And from Eq.4.13 the bandwidth, of the inner, single-stage branch line was calculated to be $1.21\cdot\omega_O$. The system bandwidth is (1590MHz-1530MHz)/1560MHz$\approx 0.04\cdot\omega_O$, hence, each stub will provide ample bandwidth on an individual basis.

The bandwidth of the complete assembly, however, must take into account the combined mis-match of all three stubs in the connector. At other than the design frequency, each stub causes a reflection because it presents a finite reactance in series with the main line.

Prior to building the connector, the whole circuit was simulated using the MDS package (described in Section 4.2.1.2) in order to more accurately determine the useable bandwidth of the device. Results are presented in Fig.4.9 and indicate that for a return loss of 25dB the bandwidth is around 950MHz centred on 1.56GHz or $0.61\cdot\omega_O$, which is more than adequate for the present system. However, additional degradation in the actual bandwidth may be incurred due to additional transition discontinuities in the connector.

4.4.2 Transition Discontinuities

In addition to reflections from the mis-match of the finite reactances of the out-of-band branch-lines, the actual transition between the UT-250 and the centre pins of the connector will also present a mis-match to R.F. signals. This is due to changes in the phys-

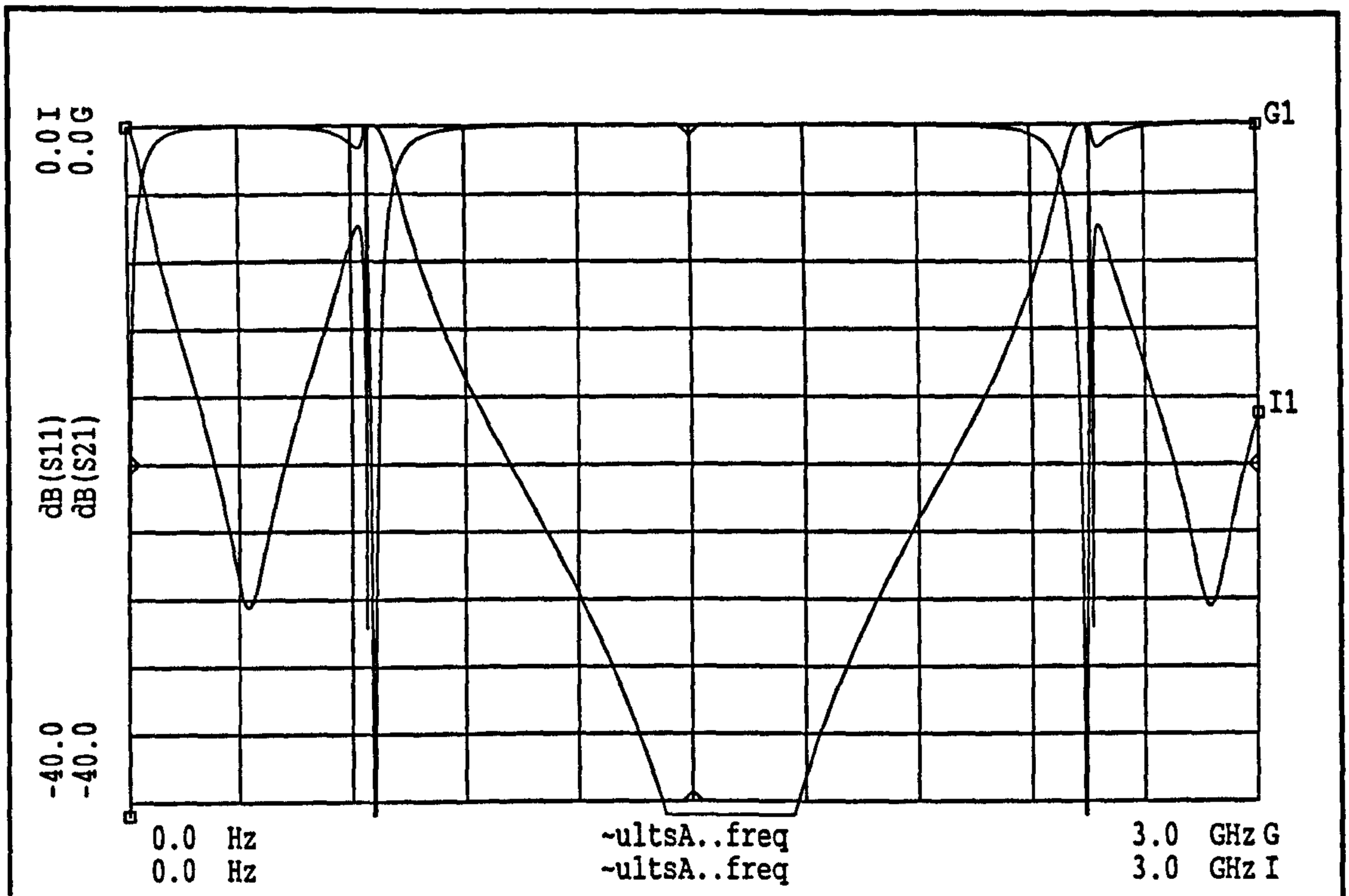

Fig.4.9 Simulated low-PIM connector performance

ical dimensions and changes of dielectric on the transmission line. An important design consideration for components in general is that reflections associated with transitions are minimised.

If the characteristic impedance of the two lines is equal on either side of the transition, one might conclude that no reflection occurs at the junction. This is not the case. The effect of the discontinuity is to distort the dominant TEM field in the vicinity of the transition. In the paper by Whinnery and Jamieson [114], it is stated that the localised distortion of the field pattern at the transition may be modelled by the superposition of 'higher-order' wave types or modes (of the type discussed in Section 3.3.4 on page 55) i.e. the transition is seen to generate modes other than the dominant TEM mode. Theory indicates that these wave types attenuate exponentially at an extremely rapid rate unless the transverse dimensions of the transmission line are of the order of $\lambda/2$ at the highest frequency of interest. The attenuation of these waves is reactive and the effect of the discontinuity may be modelled by a lumped discontinuity capacitance shunted between the lines at the junction, which causes a reflection.

The standard method of dealing with this situation is to extend a short section of the smaller inner conductor into the larger coaxial line as in Fig.4.10. This creates a high impedance line section due to the larger ratio between outer and inner conductor dimensions. If this high impedance section is kept short $l<<\lambda$, its behaviour approximates that of a series inductance.

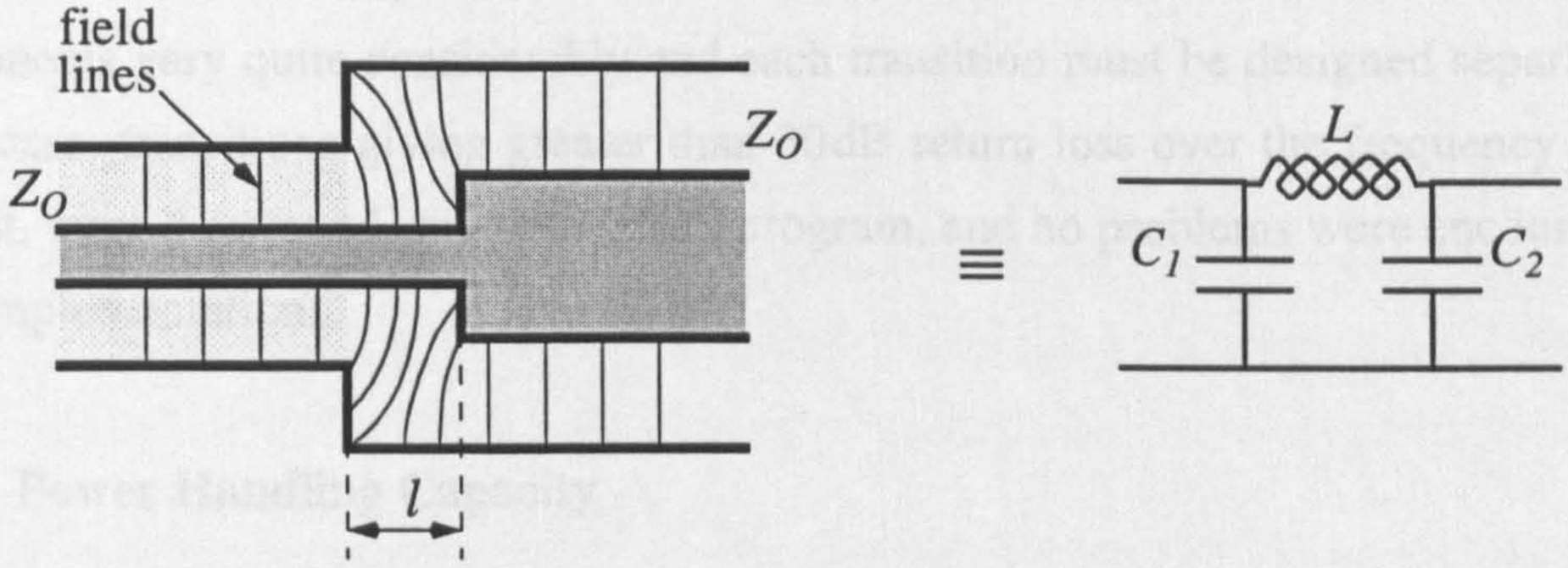

Fig.4.10 Transition Discontinuity

$$Z_{i1} = Z_O \cdot \frac{Z_L + jZ_O \cdot tan\beta l}{Z_O + jZ_L \cdot tan\beta}$$

$$\text{Given } \beta l \leq \frac{\pi}{6} \qquad Z_{i1} \approx Z_O \cdot \frac{Z_L + jZ_O \cdot \beta l_1}{Z_{O1} + jZ_L \cdot \beta l_1} \qquad \text{Eq.4.16}$$

$$\approx Z_L + jZ_O \cdot \beta l_1$$

$$\text{Given } Z_O \gg Z_L \qquad Z_{i1} \approx jZ_O \cdot \frac{\omega l}{v}$$

If C_1 and C_2 are the shunt capacitances due to the steps in the inner and outer conductors respectively, an approximate equivalent circuit for the transition is two shunt capacitors in series with an inductance (as in Fig.4.10). The voltage-standing-wave-ratio (VSWR) can be minimised by choosing the inductance L so that:

$$L = Z_{O1}^2 \cdot (C_1 + C_2) \qquad \text{Eq.4.17}$$

Where, Z_{O1} is the characteristic impedance of the short, high impedance section of line. C_1 and C_2 will vary from transition to transition depending upon transmission line dimensions and the types of dielectric used. For cylindrical coaxial systems the literature by Whinnery and Jamieson are an excellent source of data [114],[115]. However, most of the custom built components for the UKC PIM measurement system utilise a rectangular-bar coaxial system for which the data is inaccurate. Nevertheless, the data in the papers

can be used for a first approximation by considering a coaxial system with similar dimensions. The final transition is best modelled on a computer using electromagnetic analysis software such as HFSS (discussed in Section 4.2.1.1). This allows the transition to be tuned and optimised for the particular application.

For this project, numerous different transition configurations were required in the design of the new components. The transverse transmission line dimensions of the components vary quite considerably and each transition must be designed separately. In every case, transitions giving greater than 30dB return loss over the frequency band of interest, were developed using the HFSS program, and no problems were encountered in their implementation.

4.4.3 Power Handling Capacity

4.4.3.1 Dimensional Considerations

The final consideration that was given to the connector design was on the issue of the maximum power handling capability of the structure. One would expect that the small clearances and small diameters occurring in the branch lines might lead to a serious decrease in the power handling capacity of the low-PIM connector. On examination, it is found that the small diameters of the inner conductor branch do lead to such a reduction, but it is found that the small dimensions of the clearances do not lead to high electric fields, since the voltage across the gap goes down quickly as the gap is decreased.

For a certain voltage, V, on a coaxial transmission line, the electric field, E, at any point between the centre conductors is given by:

$$E = \frac{V}{r \cdot ln\left(\frac{b}{a}\right)} \qquad \text{Eq.4.18}$$

Where r is the radius to the particular point between the conductors so that $a \leq r \leq b$. E and V represent the rms values of the a.c. quantities.

From Eq.4.18, the largest value of electric field occurs at $r=a$, therefore, breakdown of the dielectric occurs, initially, near the surface of the inner conductor. To avoid this condition, its peak value, $\sqrt{2} \cdot E$, at $r=a$, must be less than the dielectric strength of the insulator, E_d. Thus the maximum allowable rms voltage across the coaxial line becomes:

$$V_{max} = \frac{a \cdot E_D}{\sqrt{2}} \cdot ln\left(\frac{b}{a}\right) \qquad \text{Eq.4.19}$$

Since standing waves are possible on the line, the maximum allowable voltage may be considerably less, namely, $V_{max} = \frac{V(E_D)}{1+|\Gamma|}$.

Consider now, the connector detail of Fig.4.11. The inner stub has the smallest diameter, a_1, and a reflection coefficient of $\Gamma = 1$ due to the open circuit termination. Therefore, by Eq.4.19, it is the inner stub which will dictate the maximum power rating of the connector.

The highest voltage in this branch occurs across the line at the open circuit where the stub changes from dielectric loaded coaxial line to air-spaced waveguide below cutoff (indicated as point 'x' in Fig.4.11). Generally, the breakdown strength of dielectrics is much higher than that of air, therefore, the worst case situation would be if the small gap at the end of the line was only filled with air.

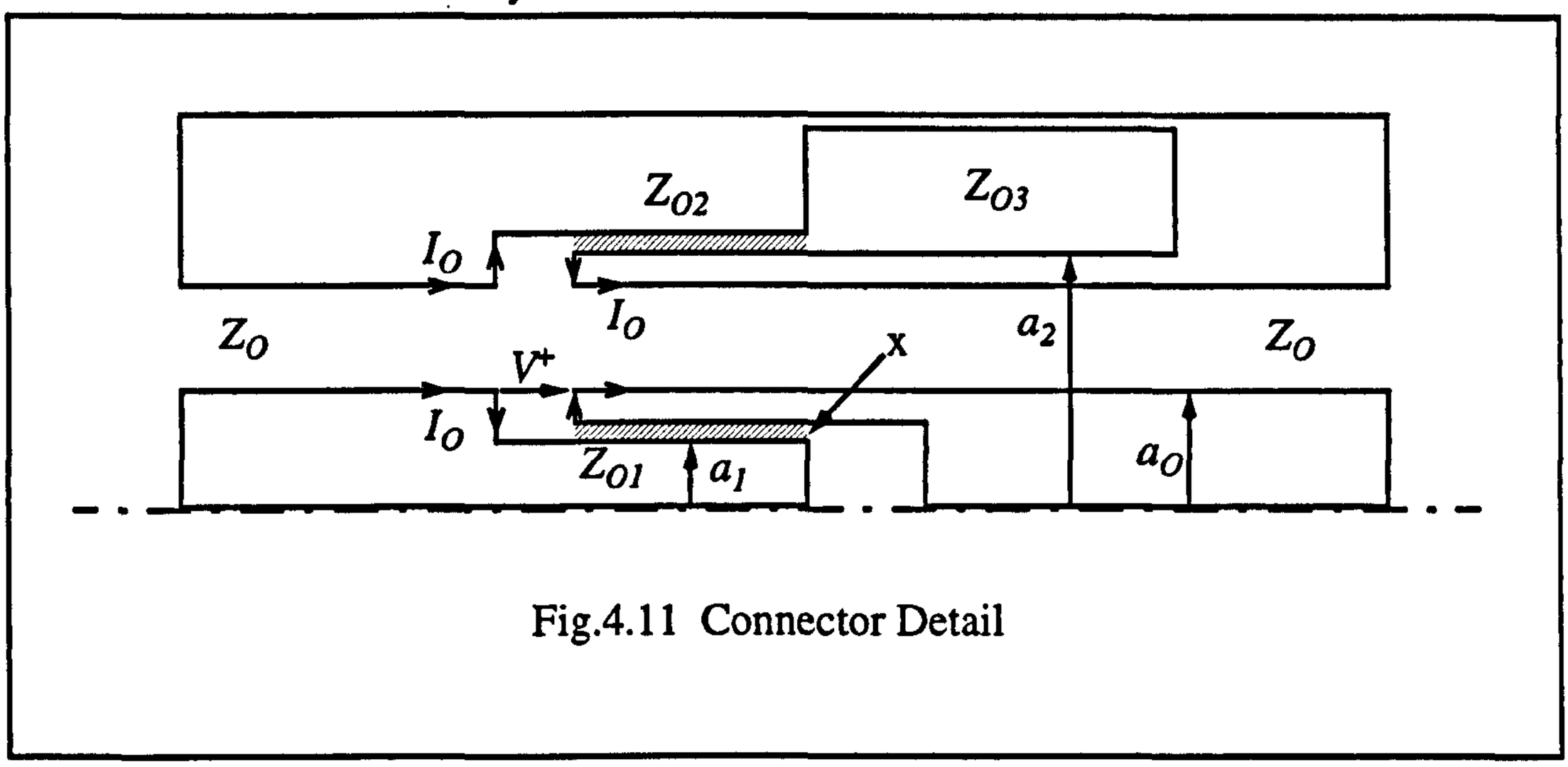

Fig.4.11 Connector Detail

The inner branch is excited by a current of amplitude I_O where it joins the main line. Consider the situation at mid-band where the line is exactly a quarter wavelength long. From Eq.4.19 the excitation voltage at the input to the line has the amplitude:

$$V_{rms} = \frac{I_O \cdot Z_{O1}}{\sqrt{2}} = \frac{60 \cdot I_O}{\sqrt{2} \cdot \sqrt{\varepsilon_r}} \cdot ln\left(\frac{b_1}{a_1}\right) \qquad \text{Eq.4.20}$$

The line is terminated in an open circuit ($Y_L = \infty$), therefore the reflection coefficient is, $\Gamma_L = \frac{Y_O - Y_L}{Y_O + Y_L} = 1$, and the rms voltage across the open circuit is:

$$\begin{aligned} V_{O/C} &= V_{rms}(1+\Gamma_L) \\ &= 2 \cdot V_{rms} \\ &= \frac{120 \cdot I_0}{\sqrt{2}} \cdot ln\left(\frac{b_1}{a_1}\right) \end{aligned} \qquad \text{Eq.4.21}$$

Equating this with the equation for the maximum allowable voltage on the line (Eq.4.19) we obtain:

$$V_{max} = \frac{a_1 \cdot E_D}{\sqrt{2}} \cdot ln\left(\frac{b_1}{a_1}\right) = \frac{120 \cdot I_0}{\sqrt{2}} \cdot ln\left(\frac{b_1}{a_1}\right) \qquad \text{Eq.4.22}$$

$$\therefore I_{Omax} = \frac{a_1 \cdot E_D}{120}$$

From Fig.4.11 it is clear that I_{Omax} will be the peak current delivered by the generator, hence the maximum average power will be given by:

$$\begin{aligned} P_{max} &= \left(\frac{I_{Omax}}{\sqrt{2}}\right)^2 \cdot Z_O \\ &= \left(\frac{a_1 \cdot E_D}{120}\right)^2 \cdot \frac{Z_O}{2} \end{aligned} \qquad \text{Eq.4.23}$$

Eq.4.23 is exact mathematically, however we have neglected the effect of the abrupt discontinuity at the end of the conductor in the stub. This will tend to concentrate the field at the end of the line. In order to avoid increased fields in this region, the centre conductor should be rounded at the end with a radius of curvature no less than its respective cylindrical radius. Similarly, although no difficulty from breakdown in the outer branch is to be expected, it is advisable to ensure that there are no sharp edges where lines Z_{O2} and Z_{O3} join.

At room temperature and a pressure of one atmosphere, $E_{Dair} \approx 3 \cdot 10^6$ V/m for air. However, this value can be considerably reduced in cases where air gaps are present in dielectric filled lines. This will be considered next.

4.4.3.2 Effect Of Air Gaps

Ideally, the dielectric sleeve in the contactless series stub is a perfect fit. However, in practical situations, this is very rarely the case, and very thin films of air are formed between the conductors and the close fitting dielectric (depicted in Fig.4.12). The air film is generally thin enough to cause a negligible deviation in line voltage, characteristic impedance and power transmission, but still so thick that it contains enough gas to give

breakdown trouble. Any thickness which is large compared with the mean distance through which an accelerated electron moves, between collisions with the molecules of the gas, would be sufficient to cause problems due to voltage breakdown. Since this mean distance is of the order of 10^{-5} cm for air at atmospheric pressure, it is clear that films of air, several orders of magnitude greater than this figure could easily occur.

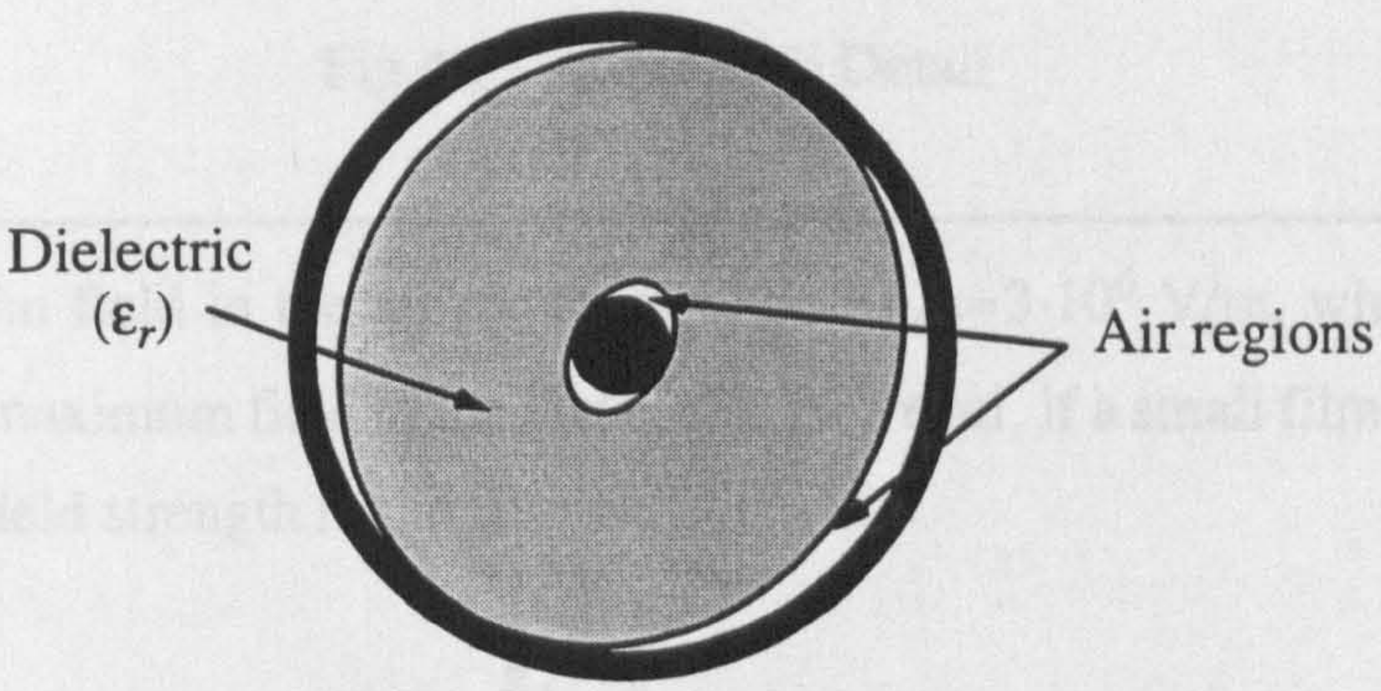

Fig.4.12 Air Gaps In Dielectric Loaded Coaxial Line

The breakdown strength of practically all dielectrics is known to exceed that of air by a large factor at RF frequencies. Hence, one does not expect any limitation on power due to breakdown in the body of the dielectric. Maximum field strengths occur at the inner conductors of coaxial lines, therefore, the effect of an air-gap at the outer conductor may be neglected. Consider the inner film of Fig.4.12. Gauss' Law leads to the boundary condition that the normal component of electric flux density **D** is continuous across a boundary between two dielectrics. In the case of a coaxial system operating in the TEM mode, all of the flux density is normal to the boundary between the air and the dielectric so that:

$$\begin{aligned} \boldsymbol{D}_{\text{material1}} &= \boldsymbol{D}_{\text{material2}} \\ \varepsilon_1 \cdot \bar{\boldsymbol{E}}_{\text{material1}} &= \varepsilon_2 \cdot \bar{\boldsymbol{E}}_{\text{material2}} \end{aligned} \qquad \text{Eq.4.24}$$

For very thin films, the electric field strength at the boundary is only very slightly less than that at the conductor therefore at $r=a$, we can write:

$$\varepsilon_1 \cdot \boldsymbol{E}_{\text{material1}} \approx \varepsilon_2 \cdot \boldsymbol{E}_{\text{material2}} \qquad \text{Eq.4.25}$$

Now, at the end of the series coaxial stub line, the total voltage across the dielectric filled section is the same as the voltage across the terminating air-gap (as indicated in Fig.4.13), and by Eq.4.18, the field in the dielectric will be almost identical with that in the air gap at any given radius.

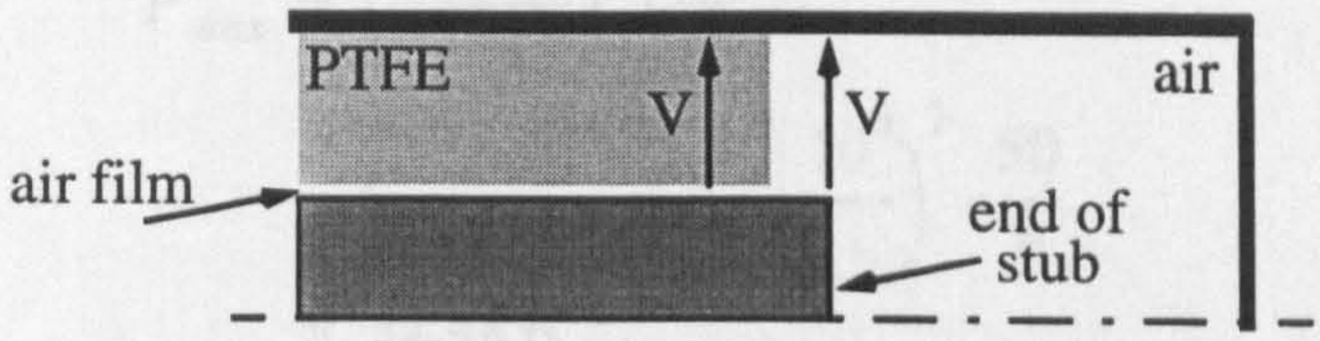

Fig.4.13 Inner Stub Detail

The maximum field in the air region will be $E_{Dair} \approx 3 \cdot 10^6$ V/m, which, by Fig.4.13 must also be the maximum field in the dielectric. However, if a small film of air is present, by Eq.4.25, the field strength in the film will be:

$$\bar{E}_{\text{air}} \approx \frac{\varepsilon_2}{\varepsilon_{\text{air}}} \cdot \bar{E}_{\text{dielectric}} \qquad \text{Eq.4.26}$$

For PTFE dielectric $\varepsilon_2=2.08$, while $\varepsilon_1=1$ for air, hence the field in the air film will be over twice that in the dielectric. To prevent breakdown in the air film, the voltage in the line must therefore be reduced by a factor of $\varepsilon_2/\varepsilon_1$, and the power must be reduced by a factor of $(\varepsilon_2/\varepsilon_1)^2$.

4.4.3.3 Maximum Power Handling

The maximum power handling of the series branchline has been considered in the previous sections, where it was indicated that the standing wave on the inner stub would be the limiting factor. The breakdown voltage of air at atmospheric pressure is given as $E_{Dair} \approx 3 \cdot 10^6$ V/m. However, due to the effect of air-gaps after Section 4.4.3.2 this must be reduced by a factor of $\varepsilon_2/\varepsilon_1$ where $\varepsilon_2=2.08$, the permittivity of the PTFE sleeve and $\varepsilon_1=1$, the permittivity of air. Hence the maximum electric field strength must be:

$$E_{s(max)} = \frac{E_{D(air)}}{\left(\frac{\varepsilon_2}{\varepsilon_1}\right)} \qquad \text{Eq.4.27}$$

$$= 1.44 \cdot 10^6 \text{ V/m}$$

This must be the maximum strength of the electric field which is allowed to exist on the centre conductor stub. Given an inner stub diameter of $a_1=3.0$mm and a characteristic impedance of 50Ω, by Eq.4.23 on page 108, the maximum power which can be delivered to the connector is given by:

$$P_{max} = \left(\frac{a_1 \cdot E_D}{120}\right)^2 \cdot \frac{Z_O}{2}$$
$$= \left(\frac{3 \times 10^{-3} \cdot 1.44 \cdot 10^6}{120}\right)^2 \cdot \frac{50}{2} \qquad \text{Eq.4.28}$$
$$= 32.4\text{kW}$$

This is well above the maximum CW power rating of UT-250 cable which is governed by thermal effects. It was not intended to operate the system above more than a hundred watts therefore there should be no risk of breakdown in the low-PIM connector.

4.4.4 Actual Performance

The finished connector was electrically tested on the Wiltron network analyser described in Section 4.2.1.2. The results are presented in Fig.4.14, and indicate a good agreement with the theoretical results from MDS. The return loss is slightly lower than 25dB across the band but was deemed acceptable. Invariably there will be additional reflections during testing caused by the test cables and connector adaptors and this will tend to raise the measured return loss.

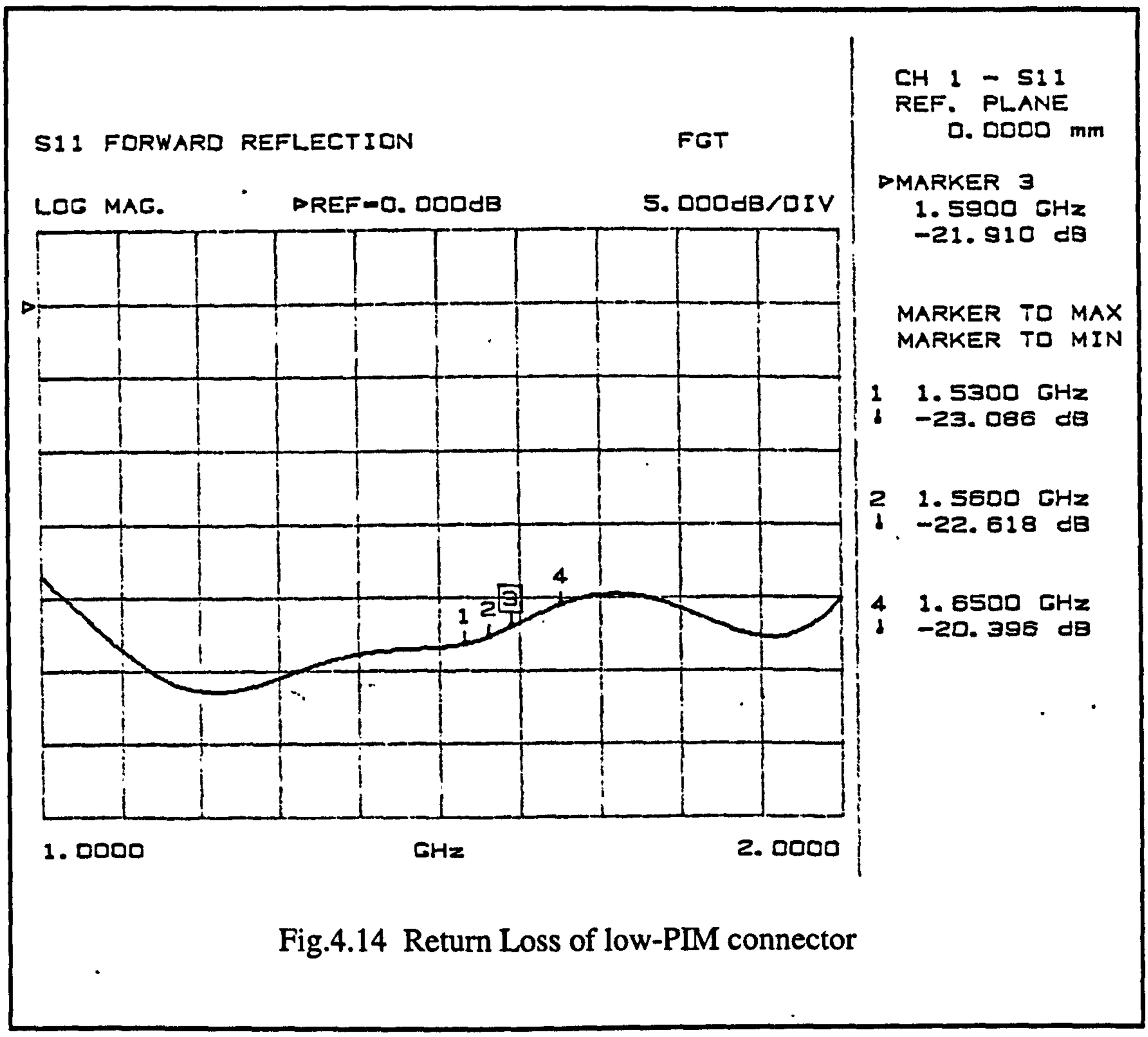

Fig.4.14 Return Loss of low-PIM connector

Initially, the low-PIM connector was used to connect the semi-rigid load to the system. However, due to the presence of the original filters and N-type connectors, no improvement in the system residual was observed.

The connector was significantly loosened to try and produce a visible degradation in residual PIM - none was observed. However, the same exercise on an N-type connector clearly produces a significant increase in the system residual. This suggested that the low-PIM connector was more robust than the N-type. The low-PIM performance and stability of the connector was verified as the new components were introduced incorporating low-PIM connections.

Low-PIM connections were provided on the new components using the same techniques described in this section. However, instead of having a female pin, the male probe slots directly into the centre conductor of the device as shown in Fig.4.15.

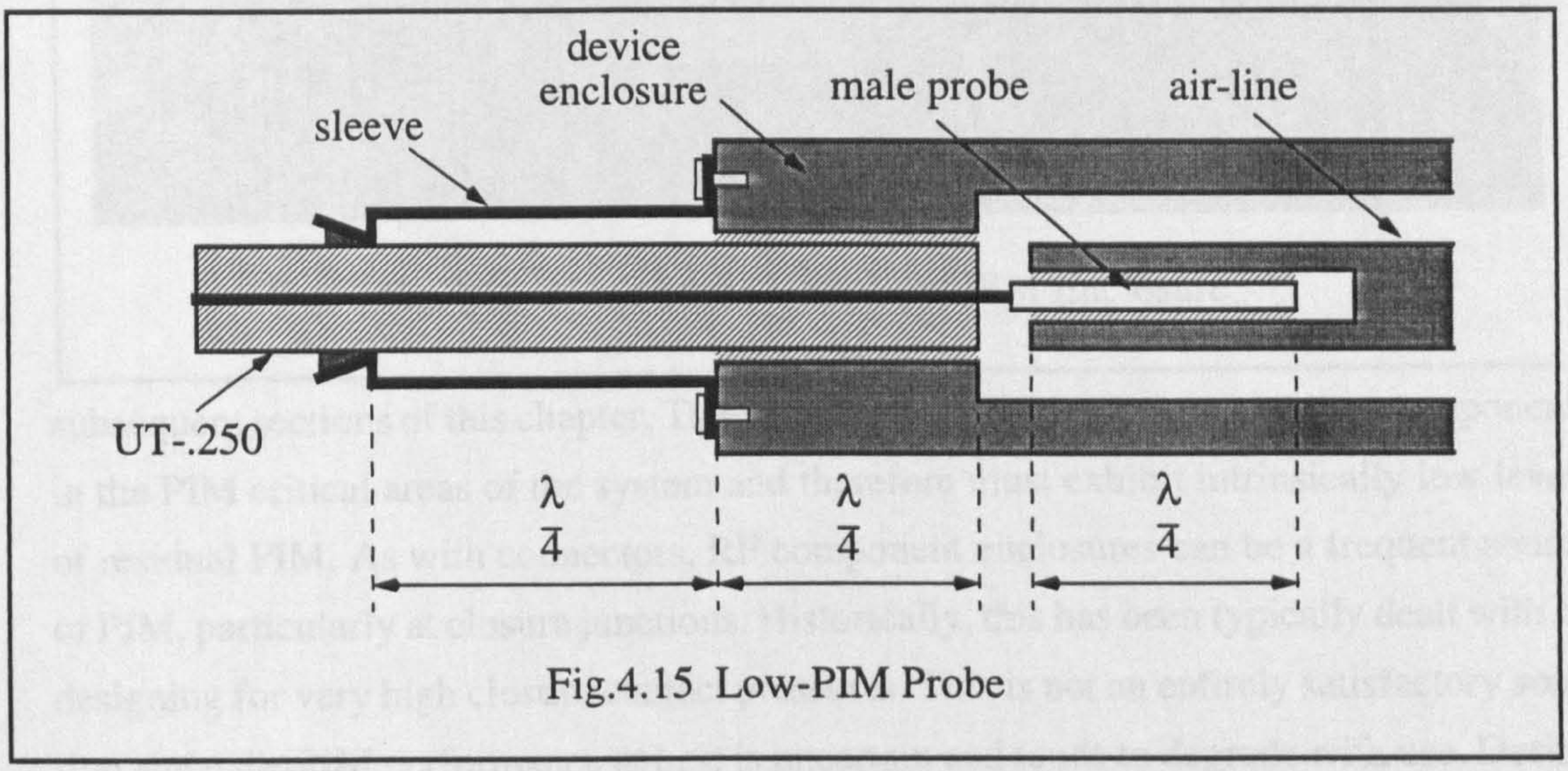

Fig.4.15 Low-PIM Probe

4.5 Low-PIM Enclosures

4.5.1 Theory

An elementary part of any R.F. component is the enclosure in which it is packaged. The enclosure is required to provide EMI shielding of the internal components and in most cases is essential to the operation of the device by acting as the ground plane for the R.F. signals. Design of the enclosure should form an integral part of the overall component design process and the degree of consideration given to the design of enclosures for low-PIM performance should be even greater.

The low current contact methods discussed in the previous sections have been taken a stage further and used to design a low-PIM enclosure. The enclosure is indicated in Fig.4.16 and was developed for use in housing the bar-line structures discussed in the

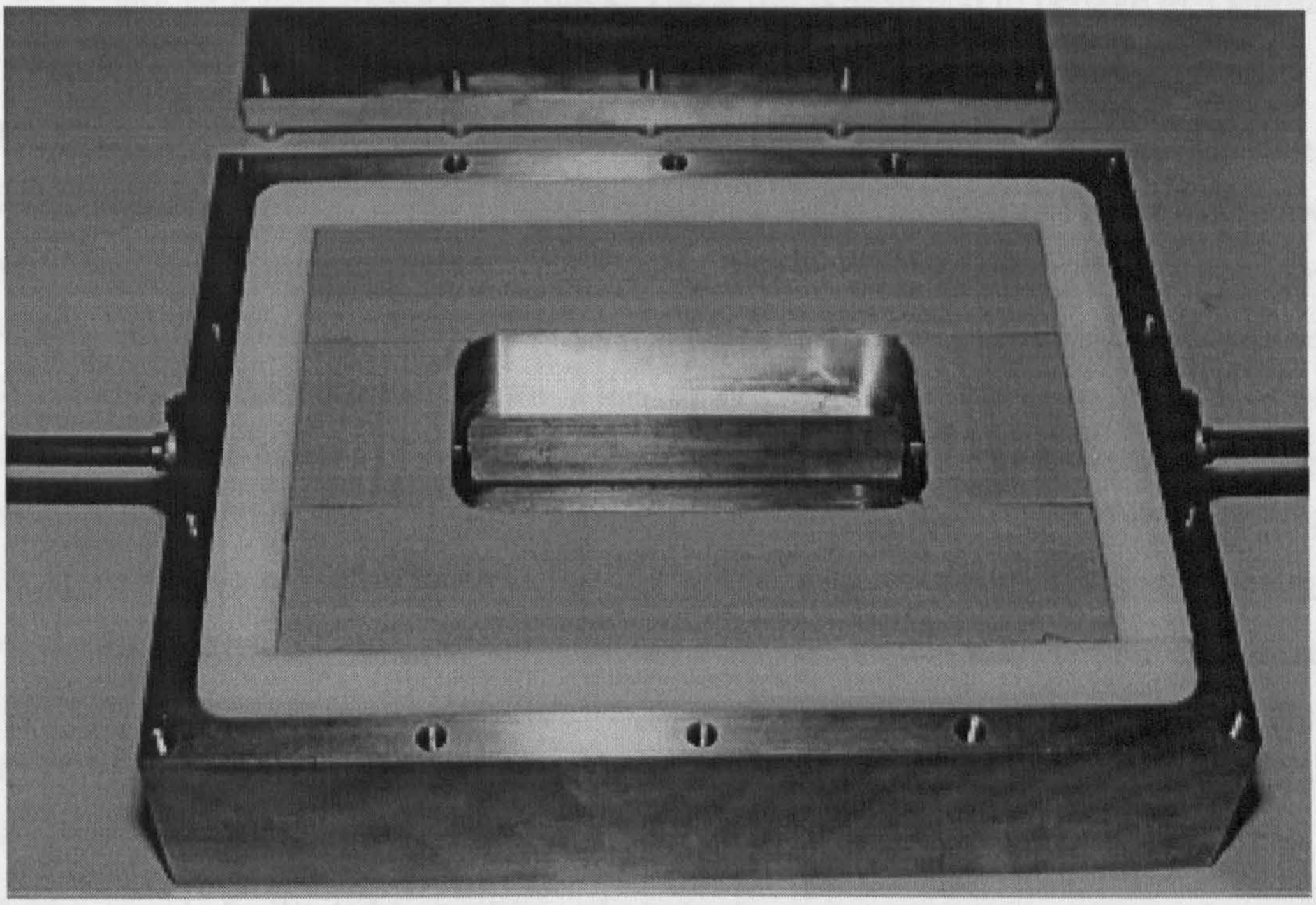

Fig.4.16 Photo of the UKC Low-PIM Enclosure

subsequent sections of this chapter. These structures were designed to replace components in the PIM critical areas of the system and therefore must exhibit intrinsically low levels of residual PIM. As with connectors, RF component enclosures can be a frequent source of PIM, particularly at closure junctions. Historically, this has been typically dealt with by designing for very high closure contact pressures. This is not an entirely satisfactory solution since the PIM performance at best is uncertain and tends to degrade with use. During the development of low-PIM system components it is desirable to have frequent access to the device internals for adjustment, and a repeatable PIM performance from a device using high contact pressures could not be guaranteed. Also, in the design of PIM test chambers, allowances should be made for the rapid and frequent change of test samples without compromising consistency in the PIM performance of the chamber itself.

The low-PIM box, when used in conjunction with the low-PIM cable entries described previously, offers a novel solution to the problem and minimises the dependency on contact pressures.

A schematic of the low-PIM enclosure is depicted in Fig.4.17 and consists of an internal box machined from solid material which is surrounded by a narrow trough which is a quarter wavelength deep at the design frequency. The trough, in turn, is bounded by

an outer wall which provides screening from the outside. The internal box is separated from the trough by a wall which is $\lambda/4$ thick. The setup is designed to behave in a similar fashion to the two-stage series branch line.

The dividing wall is slightly lower than the outer wall of the enclosure so that when the flat lid is fixed in place, a small gap is present. This gap is employed to provide a low impedance section of transmission line which couples to the $\lambda/4$ deep trough which in turn acts as a section of high-impedance line. The bottom of the trough acts as a short circuit which is transformed to an open circuit at the top of the trough. The connection between the lid and the box made at this open circuit point. The arrangement forces a current minimum at the point of contact so that the likelihood of significant PIM generation at this point is considerably reduced. The internal box bounded by the $\lambda/4$ wall is presented with a short circuit at the top of the internal wall and behaves as a normal shielded enclosure. The internal components of the low-PIM device such as a filter or coupler etc., may then be put inside. The enclosure will therefore further reduce the amount of PIM contributed by that particular component.

Cable entry is facilitated by making a hole in the end walls of the chamber, through the trough and $\lambda/4$ wall into the internal box. The hole is large enough to accommodate the UT-250 cable and PTFE sleeve. A collar is soldered to the cable at the appropriate distance from the cable end and this is bolted to the side of the box to hold the cable securely in place and provide a sound ohmic contact. The $\lambda/4$ wall again acts as an impedance transformer and provides a virtual short circuit between the cable and internal box to ensure a minimal mismatch.

4.5.2 Performance

A prototype low-PIM enclosure was designed and fabricated at UKC. The box was designed to accommodate a simple 50Ω bar-line to link the input and output ports. The design is shown in Fig.4.16.

The box was made from a solid aluminium alloy block. The troughs were filled with solid PTFE slab in order to exploit the size reduction offered by the higher dielectric constant than that of air. The final dimensions are indicated in Fig.4.17. The internal bar-line centre conductor was initially soldered onto the UT-250 feed lines. Contactless cable entry was avoided at this stage as we wanted to gauge the performance of the enclosure only and extra quarter wavelength lines may affect the bandwidth measurements.

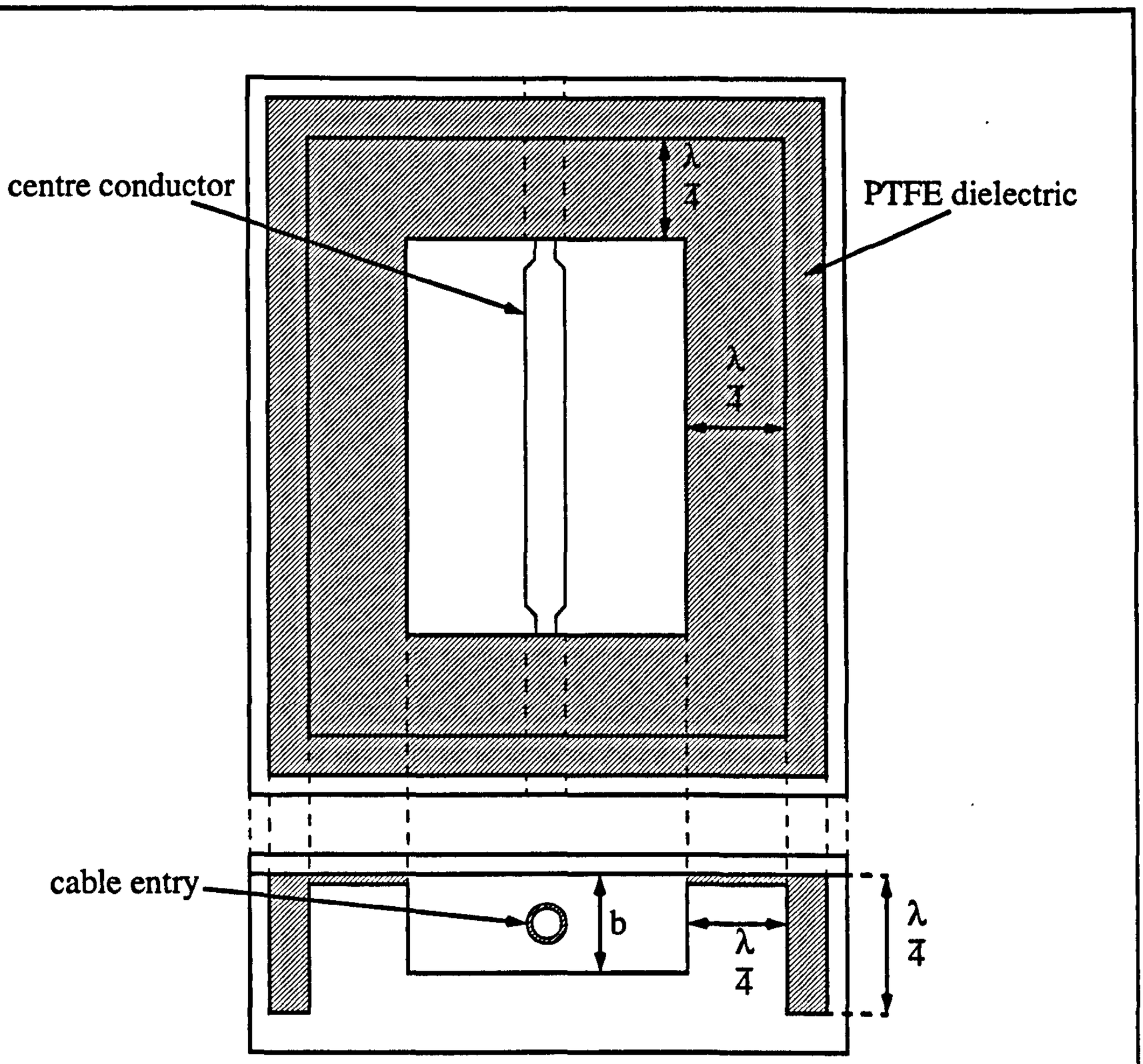

Fig.4.17 Schematic of Prototype Low-PIM Enclosure

The impedances of the quarter wavelength coupling sections were designed on the basis that the sections would approximate waveguide and that the ratio of their impedances was equivalent to the ratio of their heights. In this case the ratio of their heights was assumed to be Z_O=18.8mm Z_{O1}=15mm and Z_{O2}=1mm hence the bandwidth at 25 dB return loss was calculated from Eq.4.12 to be ≈2 GHz.

The box was electrically tested on the Wiltron 360, network analyser and a graph of the return loss is presented in Fig.4.18. The performance is seen once again to be adequate with a return loss of better than 23dB at the frequencies of interest. The bandwidth compares favourably with that calculated, any difference being attributed to the assumptions made about the impedance ratio.

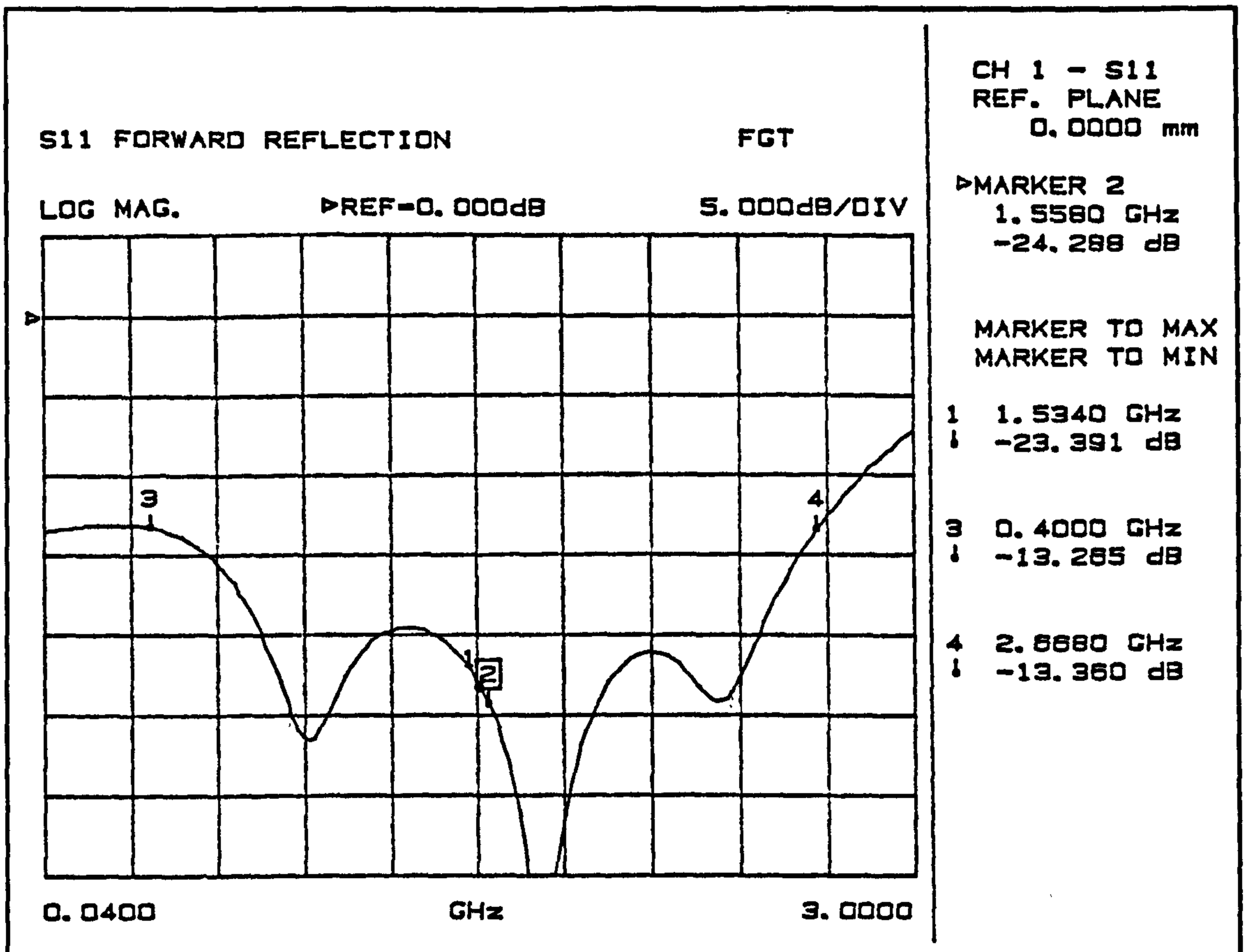

Fig.4.18 Return Loss of low-PIM enclosure

Once again, initial PIM tests were inconclusive due to the high residual levels. However, once the system had been improved, it was discovered that the PIM performance of the prototype was good and, at the time of testing, showed no degradation in the 7th order residual level of -140dBm for 2x20 Watt carriers.

4.6 Low-PIM Bandstop Filter Design and Implementation

4.6.1 Introduction

Experimental tests reported in Section 3.8 indicated that the original Trilithic® band-pass filters used in the system were responsible for generating very high levels of residual PIM. These filters use high Q (Quality factor), coaxial cavity resonators to couple a narrow band of frequencies from the input port to the output. The loaded Q of a resonator is a measure of the energy stored in the resonator compared with the energy dissipated in the rest of the network [112].

The high Q cavities used in the Trilithic® filter design suggests that the level of stored energy at the pass-band frequencies will be relatively high. The high level of energy is manifest by high levels of voltage and current within the resonator which will be many times greater than those of the 50Ω feed lines. In terms of PIM this is highly undesirable. Any points of non-linearity in the cavity construction will be subjected to extremely high current densities, much higher than those encountered in the rest of the system.

In the PIM system, only one carrier is resonant in a given filter. However, in cases where the filter is used to reflect the second carrier, it too will be present, albeit at lower energy levels. Nevertheless, the increased levels of the one, resonant carrier, will be sufficient to generate considerably higher levels of PIM than would otherwise be obtained.

It was not considered prudent to replace all of the bandpass filters in the system at once since there was no guarantee of improved performance and would be an expensive exercise, In order to improve the sensitivity of the system, it was decided to suppress the residual PIM signal before it reached the DUT position, by using additional filtering at the output of the combiner circuit. For the reasons given above, it was also decided that for consistent low-PIM performance, band-pass filters would be unsuitable for the task.

It was shown in Section 2.2.2 that the frequencies of PIM signals are well defined. It was therefore decided to use a highly selective band-stop filter to heavily attenuate the PIM signal. The band-stop filter uses high-Q resonant elements to reflect the resonant band of signals, back towards the input port, thus preventing transmission. Using a band-stop filter to reflect the PIM frequency means that it is the relatively low-level PIM signal which will be resonant, and, as a result, the stored energy in the resonator will also be relatively low. More importantly, the parent signals will not be resonant and hence will be at voltage and current levels no greater than those at other parts of the system.

The requirements of a band-stop filter for this application are as follows:

(i) The filter must exhibit a low level of intrinsic PIM. Although the parent signals will not be resonant, they will still have enough power to generate significant PIM levels.

(ii) The filter should be adaptable. It was decided during the development of the system to measure different orders of PIM. By making the filter tuneable over a reasonable bandwidth it should be possible to reject most of the odd-order products up to 7th order (at 1650 MHz in this case).

(iii) The filter must be highly selective; it must deliver significant attenuation at the PIM frequency but must also present little or no attenuation at the two parent frequencies. Third order PIM products are closest in frequency to the parent signals and therefore dictate the maximum stop-band bandwidth of the filter.

(iv) Finally, the filter should have as simple a structure as possible. The filter would be fabricated at the university using the mechanical workshop, therefore, the design must readily lend itself to manufacture in such an environment. Additionally, there should be no parts of the design which are highly sensitive to mechanical tolerances.

The remainder of this section is concerned with the design of a filter which meets all of the above requirements.

4.6.2 Bandstop Filter Design

A thorough search of the existing literature on filters was conducted in order to find a structure that could be adapted to satisfy the criteria defined in the previous section [123-134]. In the event, a band-stop filter using capacitively coupled, open-circuit, resonant elements was a natural choice. The structure and its equivalent circuit are illustrated in Fig.4.19. This structure is particularly suited to this application for several reasons:

(i) Theoretically, the structure can be configured to deliver any value of Q. As a result, the filter can be made very narrowband.

(ii) The non-contacting, capacitively coupled elements result in a very simple centre conductor pattern. The structure may be formed using any TEM mode transmission media and can be implemented easily.

(iii) Open-circuit terminations avoid the need for providing short-circuit metal to metal joints between the inner and outer conductors. Such joints can act as possible sources of PIM.

(iv) Tuning is achieved by adjusting the capacitance and element length thus removing the need for tuning screws, which again, can act as sources of PIM.

(a) Centre Conductor Pattern

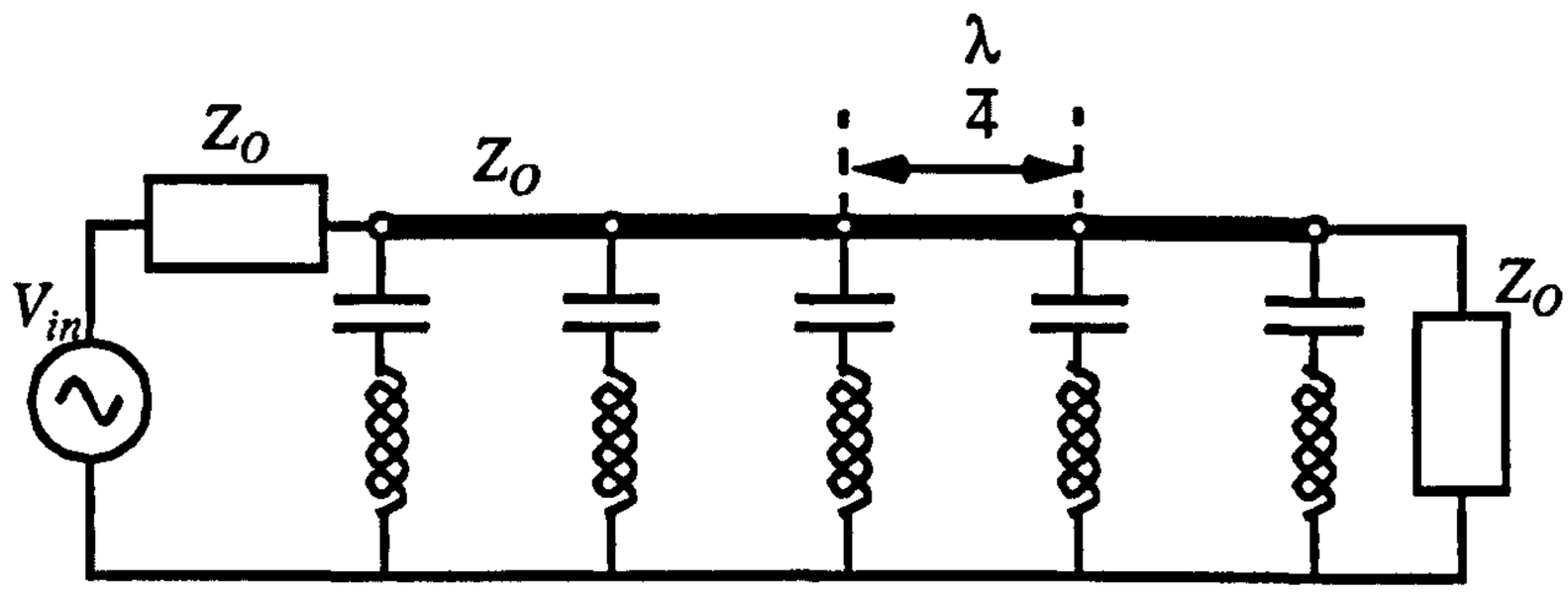

(b) Equivalent Circuit

Fig.4.19 Capacitively Coupled Band-stop Filter

4.6.2.1 External Q of Capacitively Coupled Resonator

Fig.4.20 shows an open ended line connected to a matched generator via a shunt connected series capacitance C. The following analysis shows that by suitable choice of C, one can realize almost any desired value of Q.

Since the open line and capacitance are connected in series, the total input reactance is:

$$X_{in} = -\frac{1}{\omega \cdot C} - Z_{O1} cot\beta l$$
$$= -X_C - Z_{O1} cot\frac{\omega l}{v} \qquad \text{Eq.4.29}$$

Series resonance occurs when $X_{in}=0$ and the resonant condition is given by rearranging Eq.4.29:

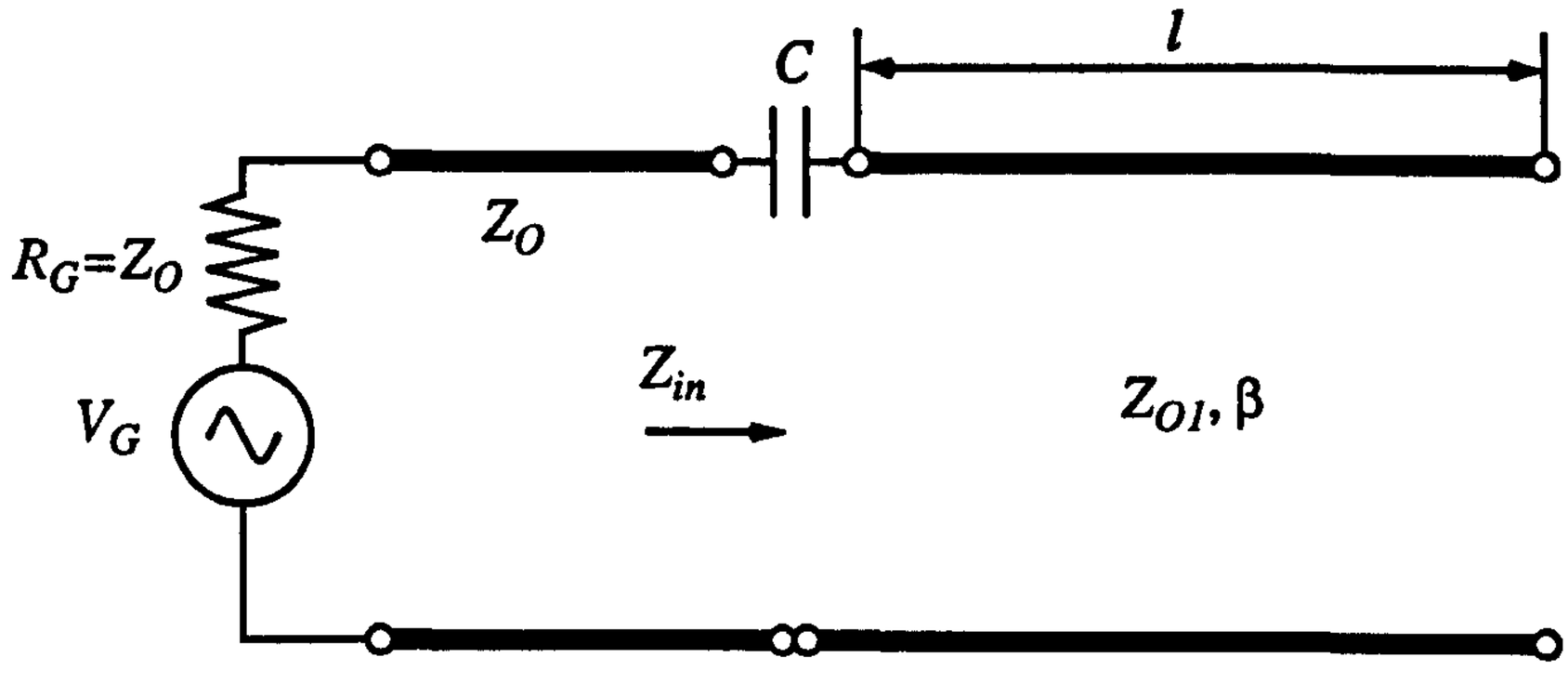

Fig.4.20 Capacitively Coupled Open-Circuited Resonator

$$\frac{\omega_O l}{v} = \phi_O = tan^{-1}\left(-\frac{1}{\bar{X}_{CR}}\right) = \pi - tan^{-1}\left(\frac{1}{\bar{X}_{CR}}\right) \qquad \text{Eq.4.30}$$

where $X_{CR}=1/(\omega_O C)$, $\bar{X}_{CR} = X_{CR}/Z_O$ and ω_O is the resonant frequency.

The external Q of a resonator is defined as:

$$\text{External } Q\text{: } Q_E \equiv \omega_R \frac{\text{Energy Stored in the Resonant Circuit}}{\text{Power Loss in the External Circuit}} \qquad \text{Eq.4.31}$$

For series resonance Q_E may be calculated as follows [112]:

$$Q_E = \frac{1}{2}\lim_{\Delta\omega \to 0}\left(\frac{\frac{\Delta X}{R_G}}{\frac{\Delta\omega}{\omega_O}}\right) = \frac{\omega_O}{2R_G}\frac{dX}{d\omega}\bigg|_{\omega = \omega_R} \qquad \text{Eq.4.32}$$

For a matched generator $R_G=Z_O$ therefore, substituting Eq.4.29 into Eq.4.32:

$$Q_E = \frac{Z_{O1}}{2Z_O} \cdot [\bar{X}_{CR} + \phi_R(1 + \bar{X}_{CR}^2)] \qquad \text{Eq.4.33}$$

From Eq.4.30, $\phi_R \approx \pi$ for high values of Q_E (i.e. $X_{CR} >> 1$). The capacitive value and hence X_{CR} may be chosen to obtain any desired value of Q_E.

4.6.3 A 1590 MHz Bandstop Filter Design

The design of transmission line band-stop filters is thoroughly covered in the literature [123,124,127,129] and only a brief synopsis of the theory will be presented here. The important aspect of the design is the way in which the filter was implemented and developed for a low-PIM application and this will be dealt with in subsequent sections.

First of all we need to know the desired specification of the filter. The first filter was developed before the change in PIM measurement order. Hence, initially, it was desired to heavily attenuate the 3rd order residual PIM signals at 1590MHz whilst leaving the excitation signals at 1530MHz and 1560MHz largely unaffected. The proximity of the upper parent frequency at 1560MHz and the PIM signal at 1590MHz requires that there is a high roll-off at the band-edge of the device and determines the stop band as being very narrow and the loaded Q as being very high. The filter was planned around a Tschebychev filter, since, from classical filter theory, Tschebychev filters deliver a higher degree of roll-off than their maximally-flat alternatives [124].

The stop-band bandwidth is defined as the frequency spacing between the equi-ripple points on a Tschebychev filter, ω_2-ω_1 in Fig.4.22. In this case, the bandwidth was chosen to be 40MHz, i.e. 20MHz either side of 1590MHz, to avoid attenuation of the 1560MHz signal.

The maximum rejection offered by any ideal bandstop filter is infinite at ω_O. The usual manner in which the attenuation is specified is to define a minimum attenuation over a certain bandwidth around ω_O (defined by ω_U-ω_L in Fig.4.22). In this instance, in order to significantly reduce the PIM signal, the minimum attenuation was specified as 80dB over a 10MHz bandwidth about ω_O, i.e. from ω_L=1585MHz to ω_U=1595MHz, the attenuation of the filter should be greater than 80dB. Not only does this place demands upon the rejection performance of the filter but it also reflects the accuracy to which the filter must be tuned. From curves in reference [124] it was established that at least 5 resonant elements would be required to deliver the desired performance.

Finally, the ripple, L_R, of the Tschebychev response was chosen to be 0.1dB to minimise the out-of-band insertion loss. The next step was to determine the parameters of the capacitively coupled resonators that would deliver the specified performance.

The first stage, using classical filter design theory, is to derive a lumped element, low-pass filter prototype circuit of the type shown in Fig.4.23. The normalised element values are obtained from the Tschebychev polynomial using, n=5 (the number of elements), and L_R (the ripple) =0.1dB, these are indicated in the figure.

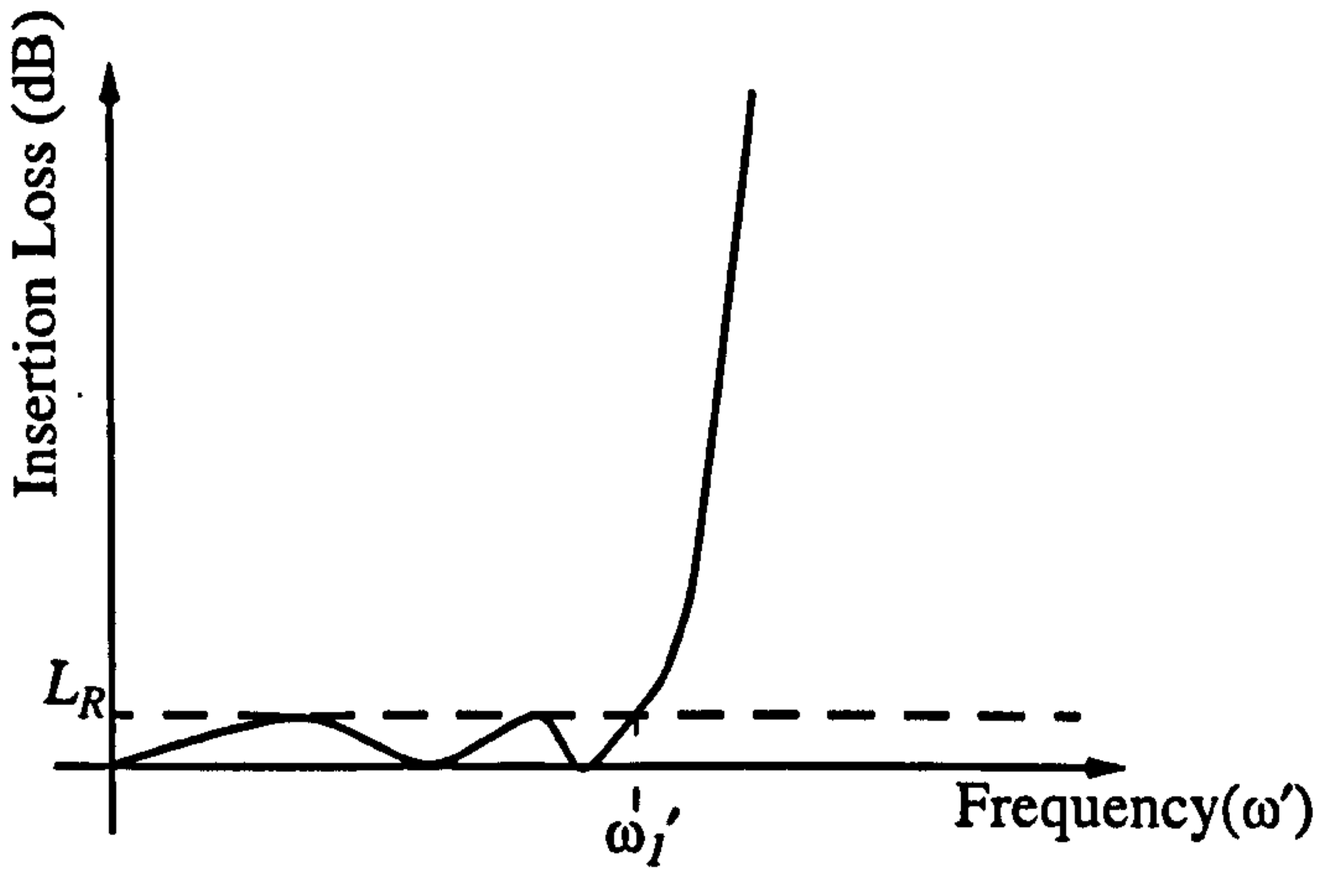

Fig.4.21 Tschebychev Low-Pass Filter Response

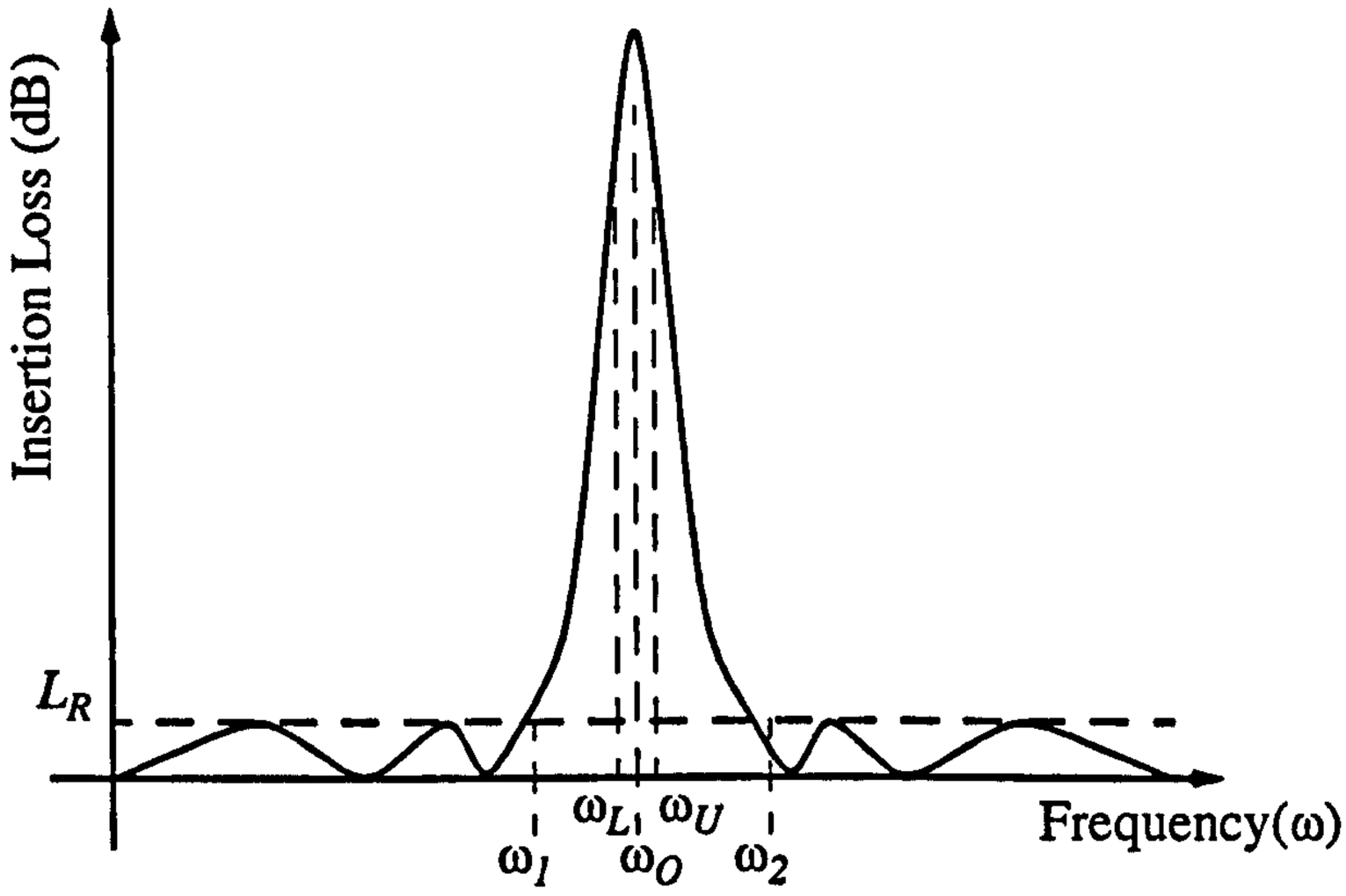

Fig.4.22 Tschebychev Band-Stop Filter Response

A low-pass filter prototype such as that in Fig.4.23 can be transformed, by a suitable frequency translation, into the band-stop configuration of Fig.4.24. The translation is given as:

$$\frac{1}{\omega'} = \frac{1}{w\omega_1'} \cdot \left(\frac{\omega}{\omega_O} - \frac{\omega_O}{\omega} \right) \qquad \text{Eq.4.34}$$

Where: $\omega_O = \sqrt{(\omega_1 \cdot \omega_2)}$ and: $w = \dfrac{\omega_2 - \omega_1}{\omega_O}$

Where ω_1' is the equi-ripple point of the low-pass prototype and ω' is the frequency variable (as defined in Fig.4.21). The terms on the right of the expression are defined in Fig.4.22.

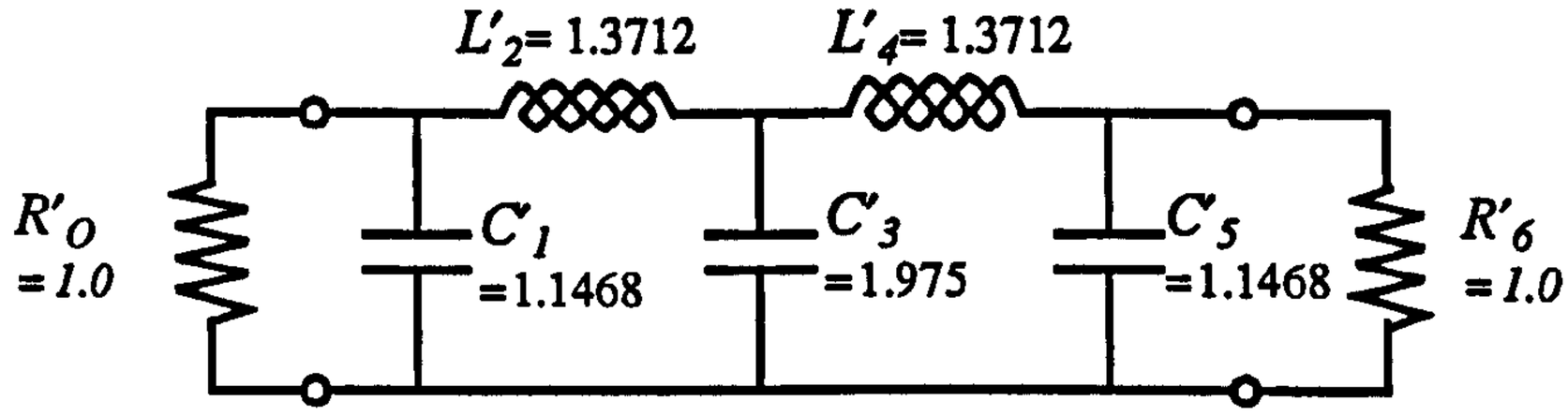

Fig.4.23 Tschebychev Low-Pass Prototype

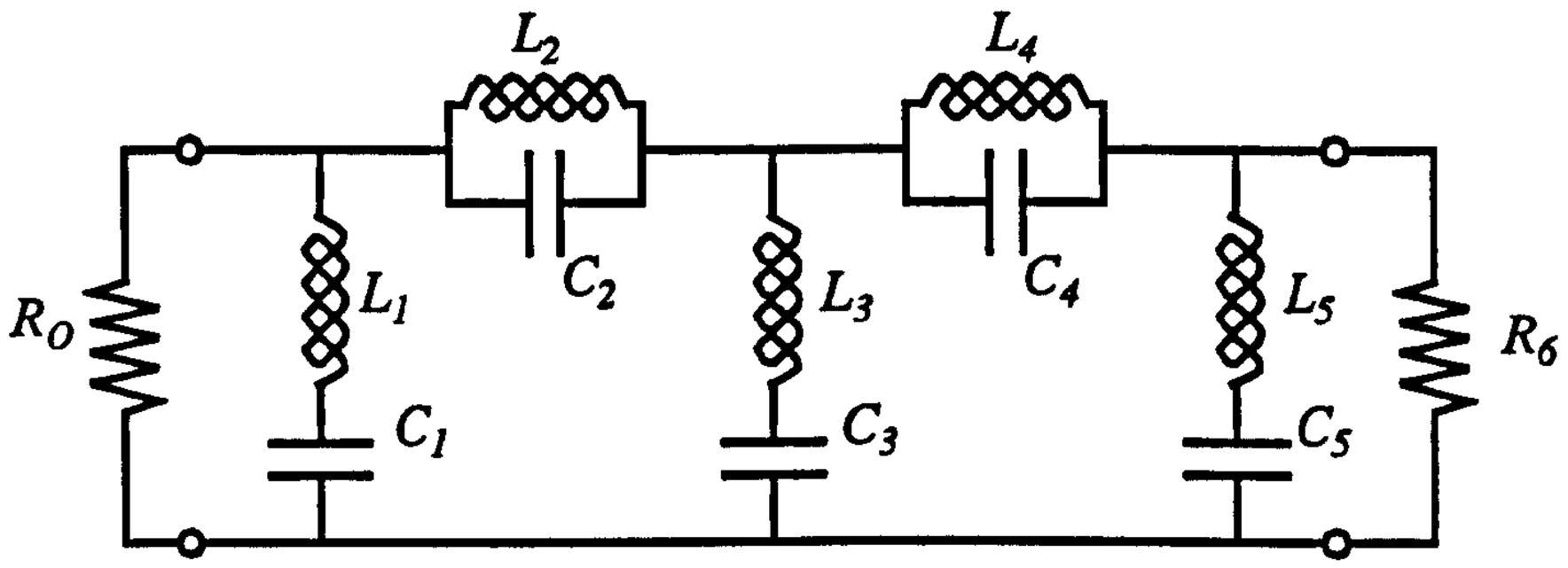

Fig.4.24 Tschebychev Band-Stop Prototype

Let the parallel lowpass prototype parameters of Fig.4.23 be denoted g_i, and the series parameters be denoted g_j. For shunt branches, in order to obtain the L_i and C_i of Fig.4.24 in terms of the g_i of Fig.4.23, we derive the circuit such that series impedances go to other series impedances and shunt admittances to other shunt admittances. Multiplying both sides of Eq.4.34 by 1/gi and equating reactances, one obtains the desired relations:

$$\omega L_i - \frac{1}{\omega C_i} = \frac{1}{g_i \omega'} = \frac{1}{w\omega_1' g_i}\left(\frac{\omega}{\omega_O} - \frac{\omega_O}{\omega}\right)$$

$$\text{at } \omega_O, \qquad \omega_O L_i - \frac{1}{\omega_O C_i} = 0 = \frac{1}{w\omega_1' g_i}\left(\frac{\omega}{\omega_O} - \frac{\omega_O}{\omega}\right) \qquad \text{Eq.4.35}$$

$$= \frac{1}{w\omega_1' g_i} - \frac{1}{w\omega_1' g_i}$$

$$\text{Equating terms gives} \qquad \omega_O L_i = \frac{1}{\omega_O C_i} = \frac{1}{w\omega_1' g_i}$$

Similarly, for series branches, equating suceptances we get:

$$\omega_O C_j = \frac{1}{\omega_O L_j} = \frac{1}{w\omega_1' g_j} \qquad \text{Eq.4.36}$$

This results in the parameters of Fig.4.24 having the same normalised impedance levels as the prototype. To change to another level (e.g. 50Ω), every R & L should be multiplied by the impedance scale factor, whilst every G & C should be divided by it.

The circuit of Fig.4.24 obviously contains both series and parallel resonant branches. In microwave band-stop filters it is difficult to realise both types simultaneously. Normally it is more convenient to use only shunt branches, or only series branches. For TEM transmission media, series branches of the type discussed in Section 4.6.2.1 are much more easily implemented. To convert the circuit of Fig.4.24 to one utilising all series branches, quarter-wavelength impedance inverters are used.

We have already seen in Section 4.4.1 that a quarter-wavelength section of line will transform an open-circuit termination to a short-circuit at the input. Using the impedance transformation equation, Eq.4.1, it can also be shown [124] that a quarter-wavelength section of line will also transform the properties of a series connected, parallel resonant circuit to those of a shunt connected, series resonant circuit, and vice versa. Hence, by placing a length of transmission line, $\lambda/4$ long at the resonant frequency, between the resonant branches, all of the parallel branches can be replaced with series branches without altering the electrical properties of the circuit. The circuit of Fig.4.24 then becomes that of Fig.4.19(b).

The next step is to implement the series resonant branches using capacitively-coupled, open-circuited resonators. As a basis for establishing the resonant properties of resonators regardless of their form it is convenient to specify their resonant frequency, ω_o, and their slope parameter, χ, where, for series resonance:

$$\chi = \frac{\omega_o}{2}\frac{dX}{d\omega}\bigg|_{\omega=\omega_o} \qquad \text{Eq.4.37}$$

The slope parameter defines the rate of change of the input reactance to the resonator and is closely linked to the Q of the resonator (compare with Eq.4.32).

Implementing the transmission line resonators to deliver the same performance as the lumped element equivalent requires that the reactance slope parameter of the different resonators is equated.

The slope parameter of a lumped element, series resonator, reactance $X = \omega L - \frac{1}{\omega C}$ is given by:

$$\chi = \frac{\omega_O}{2}\frac{dX}{d\omega}\bigg|_{\omega=\omega_o} = \frac{\omega_O}{2}\frac{d}{d\omega}\left(\omega L - \frac{1}{\omega C}\right)$$

$$= \frac{\omega_O}{2}\left(L + \frac{1}{\omega^2 C}\right) \qquad \text{Eq.4.38}$$

At $\omega = \omega_O$, $\omega_O L = \frac{1}{\omega_O C}$

$$\therefore \chi = \omega_O L_i = \frac{1}{\omega_O C_i} = \frac{1}{w\omega_1' g_i}$$

The input impedance to the capacitively coupled, open-ended, transmission line resonator of Fig.4.20 is given by Eq.4.29. At resonance, the reactance of the resonator should be zero, therefore, when $\omega = \omega_R$:

$$Z_{O1}\cot\beta l = \frac{1}{\omega_O \cdot C} \qquad \text{Eq.4.39}$$

and the reactance slope parameter is therefore:

$$\chi = \frac{\omega_O}{2}\frac{d}{d\omega}\left(Z_{O1}\cot\beta l - \frac{1}{\omega \cdot C}\right)\bigg|_{\omega=\omega_o}$$

$$= \frac{Z_{O1}}{2}(\theta_O \csc^2\theta_O - \cot\theta_O), \qquad \theta_O = \frac{\omega_O l}{v} \qquad \text{Eq.4.40}$$

$$= \frac{Z_{O1}}{2} \cdot F(\theta)$$

Where $F(\theta) = (\theta_O \csc^2\theta_O - \cot\theta_O)$. Given $F(\theta)$, θ is readily found by iterative computation on microcomputer. Equating Eq.4.38 and Eq.4.40:

$$\frac{1}{w\omega_1' g_i} = \frac{Z_{O1}}{2} \cdot F(\theta) \qquad \text{Eq.4.41}$$

To determine the three design parameters Z_{O1}, C and l, of the stub, one of them may be selected arbitrarily. In most cases it makes sense and is more practical to select a value for Z_{O1}. The slope parameter is determined from the lumped element lowpass prototype therefore θ and hence l can be determined from Eq.4.41. Finally, the value of C is found from Eq.4.39.

To aid in the tuning process, the theoretical 3dB bandwidth of each resonator was also calculated. The 3dB bandwidth of the resonator is the separation between the points where the insertion loss of the resonator is 3dB (i.e. the half-power points) and is given by [129]:

$$u_i = \frac{Z_O}{Z_{O1}} \cdot \frac{\omega_O}{F(\theta_i)} \qquad \text{Eq.4.42}$$

The design equations pertaining to a 5 element Tschebychev bandstop filter were programmed on a microcomputer using MathCAD 5.0, (a P.C. based mathematical development tool) which allowed us to quickly gauge the effects of any change to the filter specification and to provide a means of designing filters with alternative characteristics.

Given the same characteristic impedance, the properties of the resonators for a 5 element filter are symmetrical about the centre element. For the first bandstop filter, the element impedance was 68.6 Ω (see next section). Inserting the desired specification into the equations, the resonator parameters for the low-PIM filter were found to be:

Resonator Number	Coupling Capacitance (pF)	Electrical Length (radians)	3dB Bandwidth (MHz)
1&5	0.375	86.721	22.937
2&4	0.4125	86.002	27.424
3	0.5031	84.306	35.501

Table 4.1 Resonator Parameters

4.6.4 Prototype 3rd Order PIM Rejection Filter

A prototype bandstop filter was designed and built in order to verify the design equations and methodology as well as giving the chance to asses the practicalities of constructing such a device.

It was initially decided to manufacture the filter using thick stripline or bar-line technology [121]. The bar-line structure and field pattern of the dominant TEM mode are indicated in Fig.4.25. The main incentive for using bar-line technology was the ease with which structures can be manufactured in the average mechanical workshop. The geometries of the conductors are well defined therefore machining is straightforward. Bar-line is also very compact, low-loss and can support relatively high-power signals. Additionally, the mode of propagation is the TEM mode, hence, the low-PIM techniques developed at the beginning of the chapter can easily be implemented into the design.

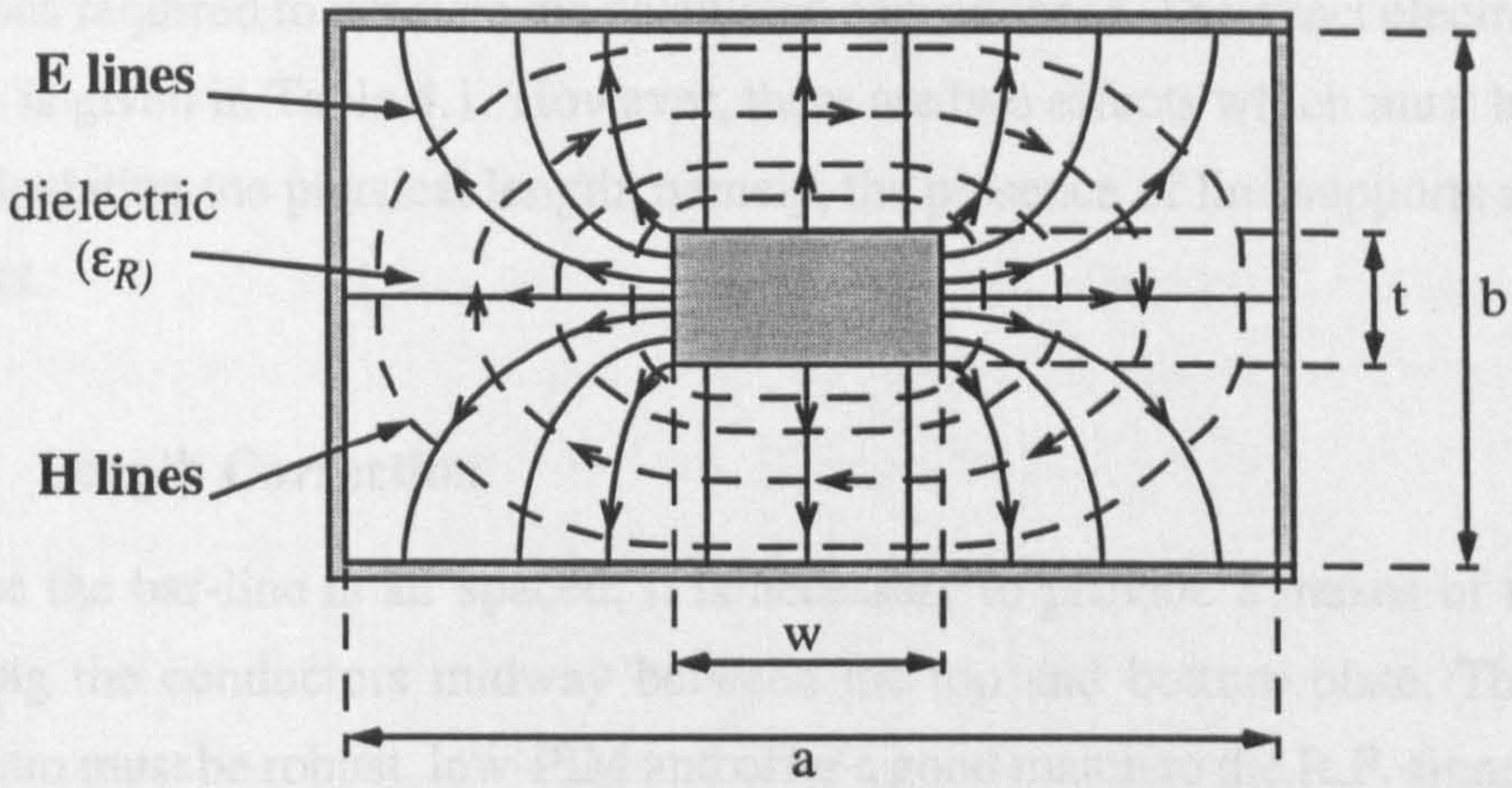

Fig.4.25 Bar-Line Transmission Medium

The cross sectional dimensions were chosen, based upon standard material sizes available from suppliers. The through line consisted of a solid brass conductor 12.7mm wide and 6.35mm high. This gives a good size material to work with and provides the thickness necessary to effect the capacitive coupling to the resonators. As the line gets thinner, the capacitive gap dimension must get smaller in order to maintain the correct capacitance in the gap. This quickly gets to the point where it is not possible to implement the desired capacitance.

Brass was chosen as the principle material in most of the custom made components for two main reasons. The first is that brass is very easy to machine using most standard workshop processes. The second is that brass has been found by previous researchers to deliver excellent PIM performance [38], [53].

The branch stubs were each made of square cross section, 6.35mm by 6.35mm. Although the choice of stub impedance is arbitrary, approximate calculations based upon the parallel capacitance between the main line and the stub indicated that these dimensions make for sensible capacitive gap spacings of the order of a couple of millimetres.

Using available design data [116] the centre line was made to be 50Ω using air dielectric and by setting the ground plane spacing, b, equal to 18.8mm. This gave the branch line impedances as Z_{O1}=68.6Ω. The impedances were checked using HFSS and were found to be in good agreement with the calculated value.

What remained to be established was the physical length of the stubs and the gap dimensions required to produce the calculated capacitances. The exact electrical length of the stubs is given in Table 4.1. However, there are two effects which must be considered when calculating the physical length, namely, the presence of line supports and the open-end effect.

4.6.4.1 Length Correction

Since the bar-line is air spaced, it is necessary to provide a means of mechanically supporting the conductors midway between the top and bottom plate. The supporting mechanism must be robust, low-PIM and offer a good match to the R.F. signals. Additionally, the supports must also serve to clamp the inner conductors firmly in place in order to maintain the capacitive gap spacings. Failure to provide for this could result in the final device becoming easily de-tuned.

The 'bead' support shown in Fig.4.26 is useful at frequencies below 3GHz [112]. To ensure low reflections, its length is typically $0.05 \cdot \lambda$ or less at the highest frequency of interest. The 'bead' represents a very short length of low impedance line, therefore,

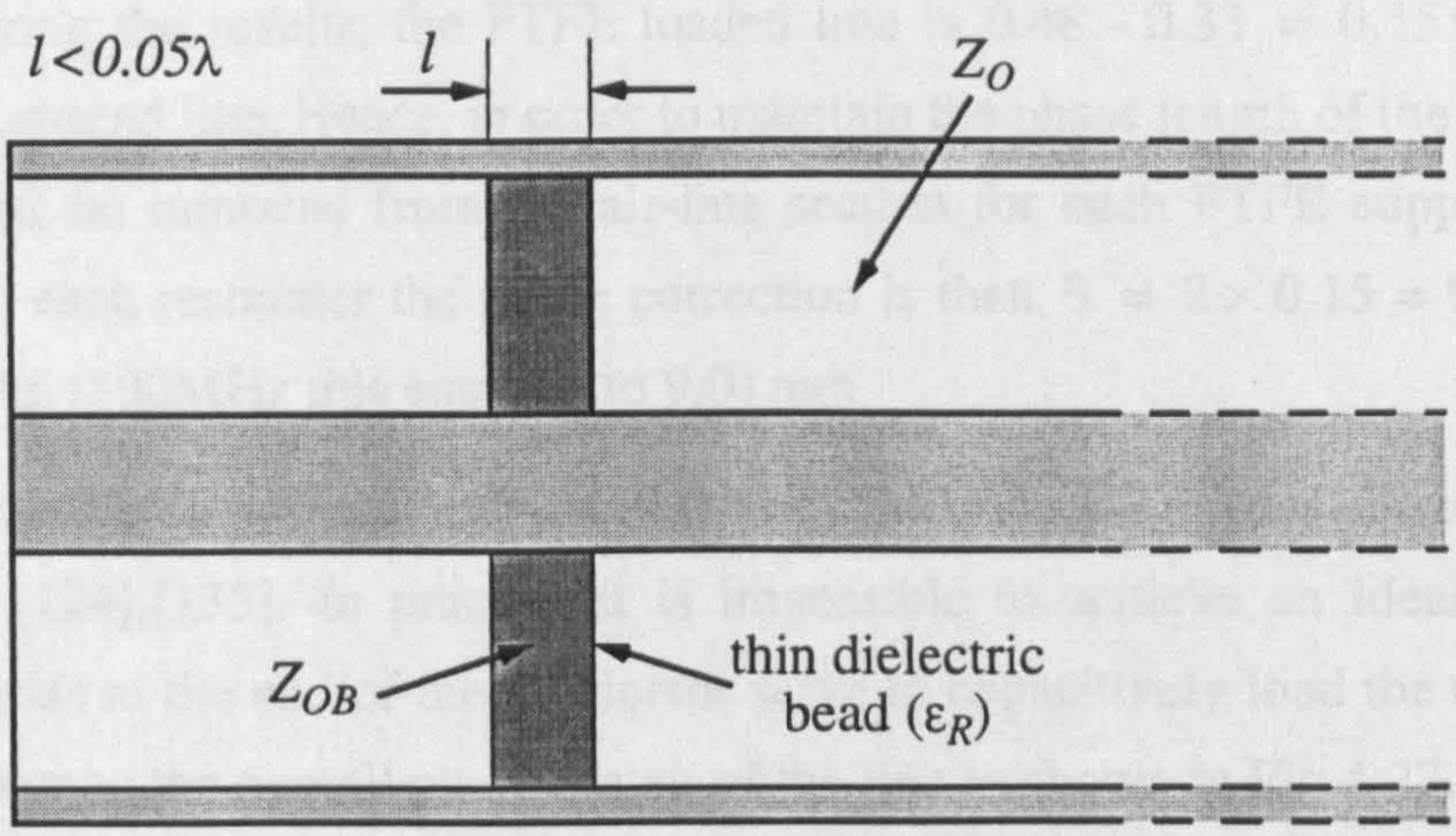

Fig.4.26 Coaxial Line Bead Support

by Eq.4.1, it is equivalent to a small shunt capacitance whose VSWR increases as the operating frequency is increased. Due to the electrical requirement that the bead be less than $0.05 \cdot \lambda$, a mechanically rigid support becomes difficult to achieve at the higher microwave frequencies.

For the low-PIM L-band filter, 10mm lengths of PTFE were used to implement line supports, one at each end of the main line and two to hold up each of the resonators (as indicated in Fig.4.32 on page 138). An important effect of the PTFE supports is that due to the higher dielectric constant of PTFE compared to air, (ε_R=2.08 for PTFE and 1 for air) a given physical length of transmission line will be electrically longer in PTFE than in air. Accordingly, the lengths of the supported resonant stubs must be compensated or they will resonate at the wrong frequency. The effect of adding two 10mm PTFE sections to each resonator can be calculated thus:

At 1590MHz, 10mm of air spaced transmission line = $\frac{\omega \cdot l}{c} = 0.33$ radians.

Now the speed of electromagnetic waves in dielectric media is lower than that for air by the factor $1/(\sqrt{\varepsilon_r})$ where ε_r is the relative permittivity of the media, therefore $v_{\text{dielectric}} = \frac{c}{\sqrt{\varepsilon_r}} = \frac{3 \cdot 10^8}{\sqrt{2.08}} = 2.08 \cdot 10^8 ms^{-1}$. Hence, at 1590MHz, 10mm of PTFE supported transmission line = $\frac{\omega \cdot l \cdot \sqrt{\varepsilon_r}}{c} = 0.48$ radians.

Comparing the results, the PTFE loaded line is $0.48 - 0.33 = 0.15$ radians longer than the air spaced line. Hence, in order to maintain the phase length of the resonator, this amount must be removed from the air-line section for each PTFE support. With two supports on each resonator the phase correction is then $\theta = 2 \times 0.15 = 0.3$ radians per resonator. At 1590MHz this equates, to 9.01 mm

The second effect which influences the physical length of the resonators is the open end effect [124],[135]. In practice it is impossible to achieve an ideal open circuit. Fringing fields at the end of the conductor serve to capacitively load the end of the line and contribute to the overall phase length of the line as shown in Fig.4.27.

Methods of determining Δl, the physical extension of the electrical open circuit at T' from T, the location of the physical end of the line, are considered in the literature [124],[135]. However, these methods are only valid for infinitely wide centre conductors (w=∞ in Fig.4.25) and at best can only give a good approximation to the real situation.

The HFSS computer program was employed to provide a better calculation of the end effect for the particular case in question. By comparing the phase of the reflected incident signal with that expected from an ideal termination we can calculate Δl. In this case the end effect was found to add an apparent 4.34mm to the physical end of the line.

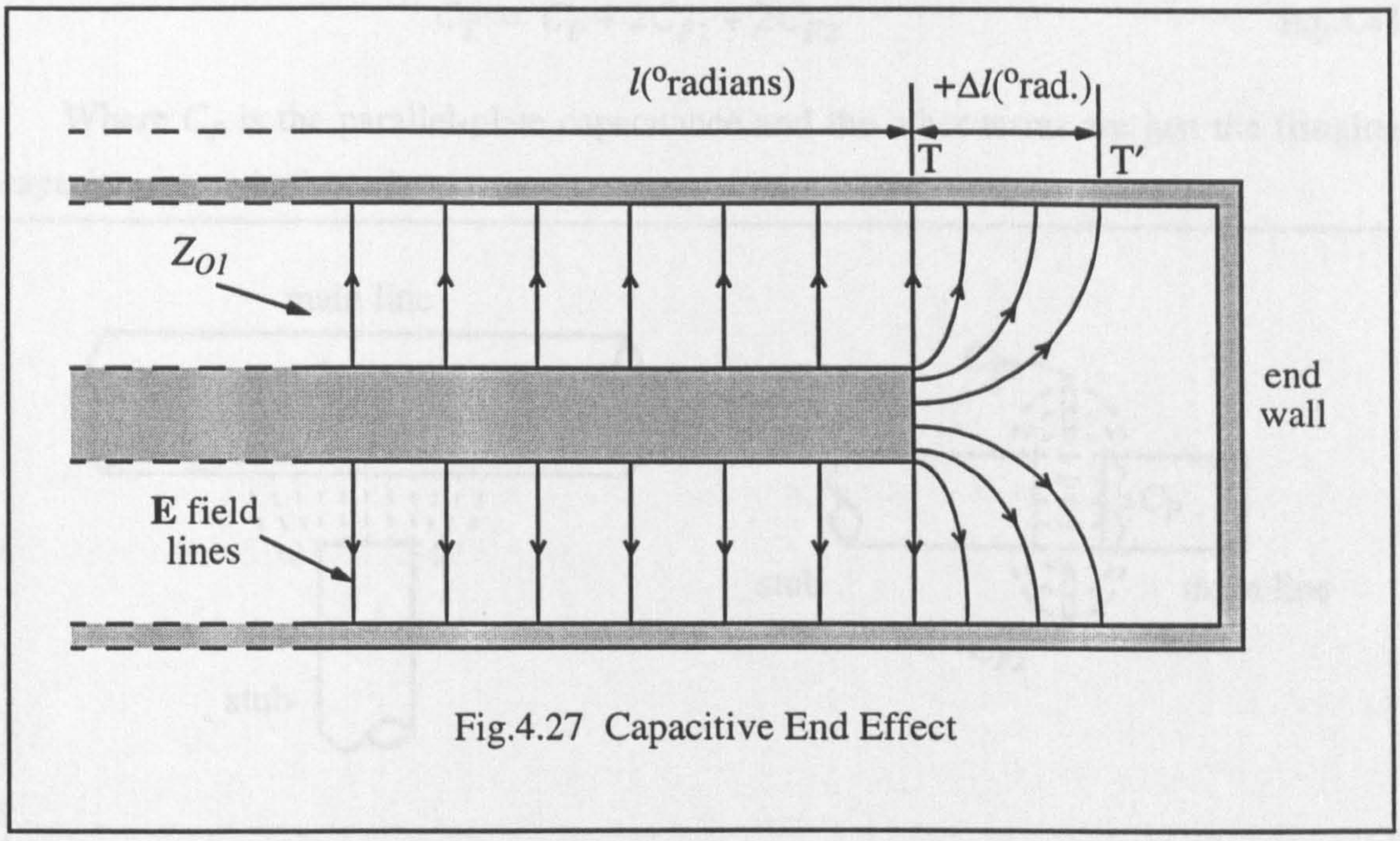

Fig.4.27 Capacitive End Effect

Taking account of the PTFE supports and the open-end capacitance, the physical lengths of the stubs were calculated to be:

Resonators 1&5 = 73.371mm; 2&4 = 72.652mm; 3 = 70.956mm

In practice, the stubs were made slightly oversize. This allows margins for errors in the calculations and for imperfections in setting up the filter. The lengths would be trimmed to their final values during the tuning process.

4.6.5 Capacitive Gap Implementation

4.6.5.1 Spacing

Thorough consideration must be given to the implementation of the coupling capacitance. The first thing is to establish that the conductor dimensions are chosen correctly in order to give a practical gap spacing. If the gap is too small, the capacitance will be difficult to realise; it will be highly sensitive to small dimensional changes; and can limit the power handling of the filter due to potential breakdown problems in the gap. If the gap is too large, the field lines from the main line will tend to couple with the ground plates and not the resonator. The capacitance between the centre conductors will not be effective so the filter will not function properly.

It is difficult to accurately calculate the capacitance due to the significant effect of fringing fields at the edges of the conductors. Consider the fields of Fig.4.28. It is clear that the total capacitance of the system will be given by:

$$C_T = C_P + 2C_{F1} + 2C_{F2} \qquad \text{Eq.4.43}$$

Where C_P is the parallel-plate capacitance and the other terms are just the fringing capacitances as indicated.

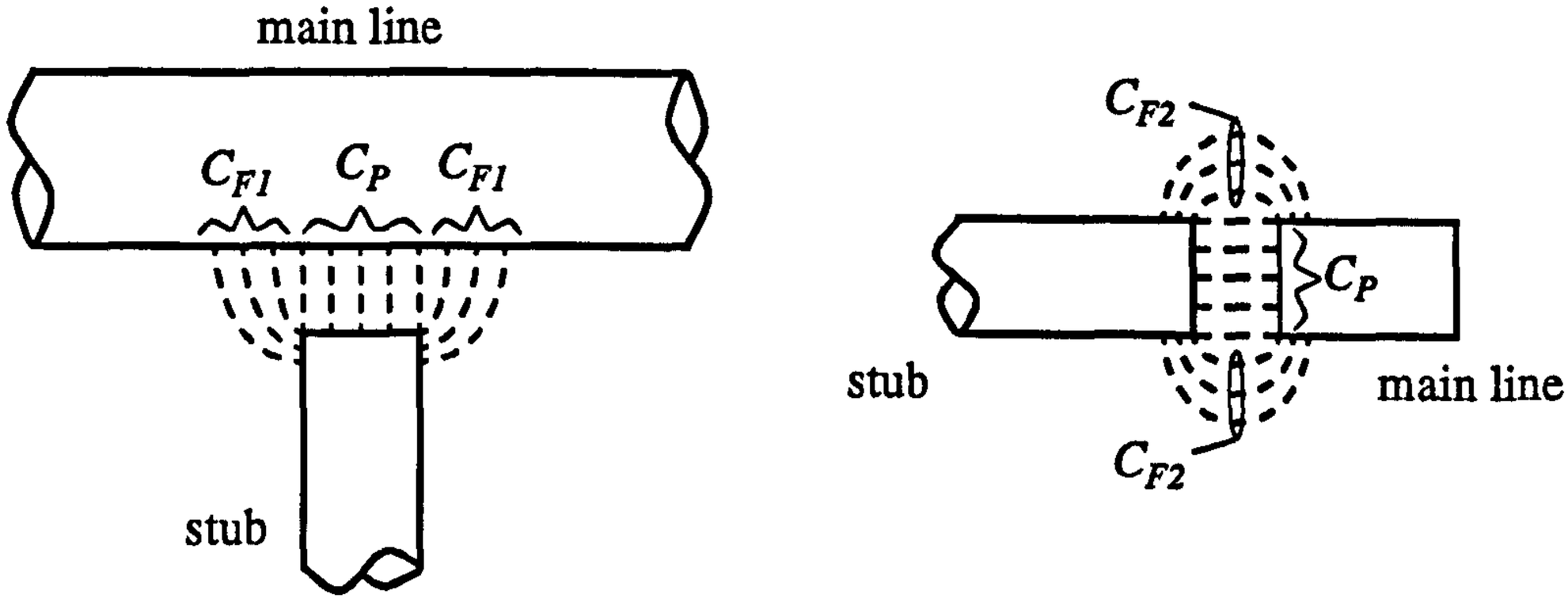

Fig.4.28 Fringing Capacitances

Based solely on the parallel plate capacitance, C_P, and given the stub area as 6.35mmx6.35mm, the capacitive gap is given by:

$$C_P = \frac{\varepsilon_O \varepsilon_R A}{d} \qquad \text{Eq.4.44}$$

For C_P=0.4pF, d, the gap spacing is around 1.0mm. However, in practice it was found that the fringing capacitance is approximately equal to C_P. Therefore, in order to give C_T=0.4pF, C_P must be halved. This resulted in gap spacings of the order of 2.0mm.

4.6.5.2 Sensitivity

The next factor to consider concerning the capacitive gap spacing is how changes in the gap dimension affect the tuning of the filter. Obviously, if the resonant frequency varies greatly with small variations in the gap spacing then the filter may become easily de-tuned from even the slightest knock. However, the gap should be sensitive enough to allow the filter to be easily tuned.

It is quite straightforward to calculate the sensitivity of one system parameter to another [136], [137]. In general we want to establish the percentage change in the result of a function due to a certain percentage change in one of its variables. The percentage change in some variable, say α, can be expressed as:

$$\frac{\Delta\alpha}{\alpha} \times 100\% \qquad \text{Eq.4.45}$$

The sensitivity of a function β to α is defined as follows:

$$S_{\beta}^{\alpha} = \frac{\left(\frac{\partial\alpha}{\alpha}\right)}{\left(\frac{\partial\beta}{\beta}\right)} = \frac{\beta}{\alpha}\cdot\frac{\partial\alpha}{\partial\beta} \qquad \text{Eq.4.46}$$

Where $\frac{d\alpha}{\alpha}$ is the limiting value of $\frac{\Delta\alpha}{\alpha}$ as $\Delta\alpha$ tends to zero. Similarly, the inverse sensitivity function can be expressed as:

$$\frac{1}{S_{\beta}^{\alpha}} = S_{\alpha}^{\beta} = \frac{\alpha}{\beta}\cdot\frac{\partial\beta}{\partial\alpha} \qquad \text{Eq.4.47}$$

We would like to determine the sensitivity of the resonant frequency to the capacitive gap spacing. Or $S_d^{\omega_o}$, where ω_o is the resonant frequency and d is the gap spacing. Now in Eq.4.39 and Eq.4.44 we have a set of equations relating the two variables. The overall sensitivity can be calculated in two stages using the capacitance, C, as a common variable. The sensitivity can be expressed as:

$$S_d^{\omega_o} = S_C^{\omega_o}\cdot S_d^C \qquad \text{Eq.4.48}$$

First let us determine the sensitivity of the capacitance, C_T, to the spacing, d. Consider Eq.4.43 for the total capacitance. In order to simplify the calculation we will say that over a small change in d, the change in the fringing capacitance will be negligible and the total fringing capacitance may be approximated by a constant, K. So that:

$$C_T = C_P + K \qquad \text{Eq.4.49}$$

From Eq.4.44, the sensitivity S_d^C is calculated as follows:

$$\begin{aligned} S_d^{C_T} &= \frac{d}{C_T}\cdot\frac{\partial C_T}{\partial d} \\ &= \frac{d^2}{\varepsilon_O\varepsilon_R A}\cdot\frac{\partial}{\partial d}\left(\frac{\varepsilon_O\varepsilon_R A}{d}+K\right) \\ &= \frac{d^2}{\varepsilon_O\varepsilon_R A}\cdot\varepsilon_O\varepsilon_R A\cdot\left(-\frac{1}{d^2}\right) \\ &= -1 \end{aligned} \qquad \text{Eq.4.50}$$

Which means that for every percentage *increase* in d there will be an equivalent percentage *decrease* in C and vice versa.

Now let us consider the sensitivity of frequency to changes in capacitance. Arranging Eq.4.39 gives:

$$C = -\frac{1}{\omega_O Z_{O1}} \cdot tan\frac{\omega_O l}{v} \qquad \text{Eq.4.51}$$

It is clear that to get ω_O in terms of C would be difficult. However we can make use of Eq.4.47 and obtain the sensitivity using Eq.4.51 as follows:

$$S_C^{\omega_o} = \frac{1}{\left[\frac{\omega_O}{C} \cdot \frac{dC}{d\omega_O}\right]} \qquad \text{Eq.4.52}$$

Let, $\theta_r = \frac{\omega_O l}{v}$, then using the product rule for differentiation:

$$\frac{dC}{d\omega} = -\frac{1}{Z_O}\left[-\frac{tan\theta_r}{\omega_O^2} + \frac{1}{\omega_O v} sec^2\theta_r\right]$$

$$= -\frac{1}{Z_O}\left[-\frac{tan\theta_r}{\omega_O^2} + \frac{1}{\omega_O v}(1 + tan^2\theta_r)\right] \qquad \text{Eq.4.53}$$

$$= -\frac{1}{Z_O}\left[\frac{1}{\omega_O v} tan^2\theta_r - \frac{1}{\omega_O^2} tan\theta_r + \frac{1}{\omega_O v}\right]$$

Substituting Eq.4.51 and Eq.4.53 into Eq.4.52 gives:

$$\frac{1}{S_C^{\omega_o}} = (-\omega_O^2 Z_O cot\theta_r) \cdot -\frac{1}{Z_O}\left(\frac{1}{\omega_O v} tan^2\theta_r - \frac{1}{\omega_O^2} tan\theta_r + \frac{1}{\omega_O v}\right)$$

$$= \frac{\omega_O}{tan\theta_r}\left(\frac{l}{v} tan^2\theta_r - \frac{1}{\omega_O} tan\theta_r + \frac{l}{v}\right) \qquad \text{Eq.4.54}$$

$$\therefore S_C^{\omega_o} = \frac{tan\theta_r}{\omega_O} \cdot \frac{1}{\left(\frac{l}{v} tan^2\theta_r - \frac{1}{\omega_O} tan\theta_r + \frac{l}{v}\right)}$$

Now the values of interest can be inserted into Eq.4.54 to obtain the sensitivity function. Given $\omega_O = 2 \cdot \pi \cdot 1590\text{MHz}$, $v = 3 \cdot 10^8\ \text{ms}^{-1}$ and $l = 87\text{mm}$, $S_C^{\omega_o} = -0.075$.

Given the result of Eq.4.50 the overall sensitivity of the resonant frequency to a small change in the capacitive gap is:

$$\begin{aligned} S_d^{\omega_o} &= S_C^{\omega_o} \cdot S_d^C \\ &= -0.075 \cdot -1 \\ &= 0.075 \end{aligned} \qquad \text{Eq.4.55}$$

Hence, for the system under consideration here, a change of 0.1 mm or 5% in the gap will produce a change of 0.375% or around 6 MHz in the resonant frequency. In practice, it is not expected that there will be as much as 0.1mm of 'play' in the resonator, hence, the filter should be reasonably resistant to de-tuning. However, it does mean that great care will be required when tuning the filter in the first place.

4.6.5.3 Power Handling

The close proximity of the resonator end to the main line also raises the question of the power handling capability of the filter [130]. At resonance, a large voltage will exist across the capacitive gap which must not be allowed to exceed the value at which electrical breakdown in the gap will occur. Only the first resonator will be exposed to the full power incident upon the filter therefore its limitation on power handling should be known.

The Thevenin equivalent circuit of a single resonator is indicated in Fig.4.29. At resonance Z_{in}=0. Assuming conductor losses to be negligible the resonant current is given simply by:

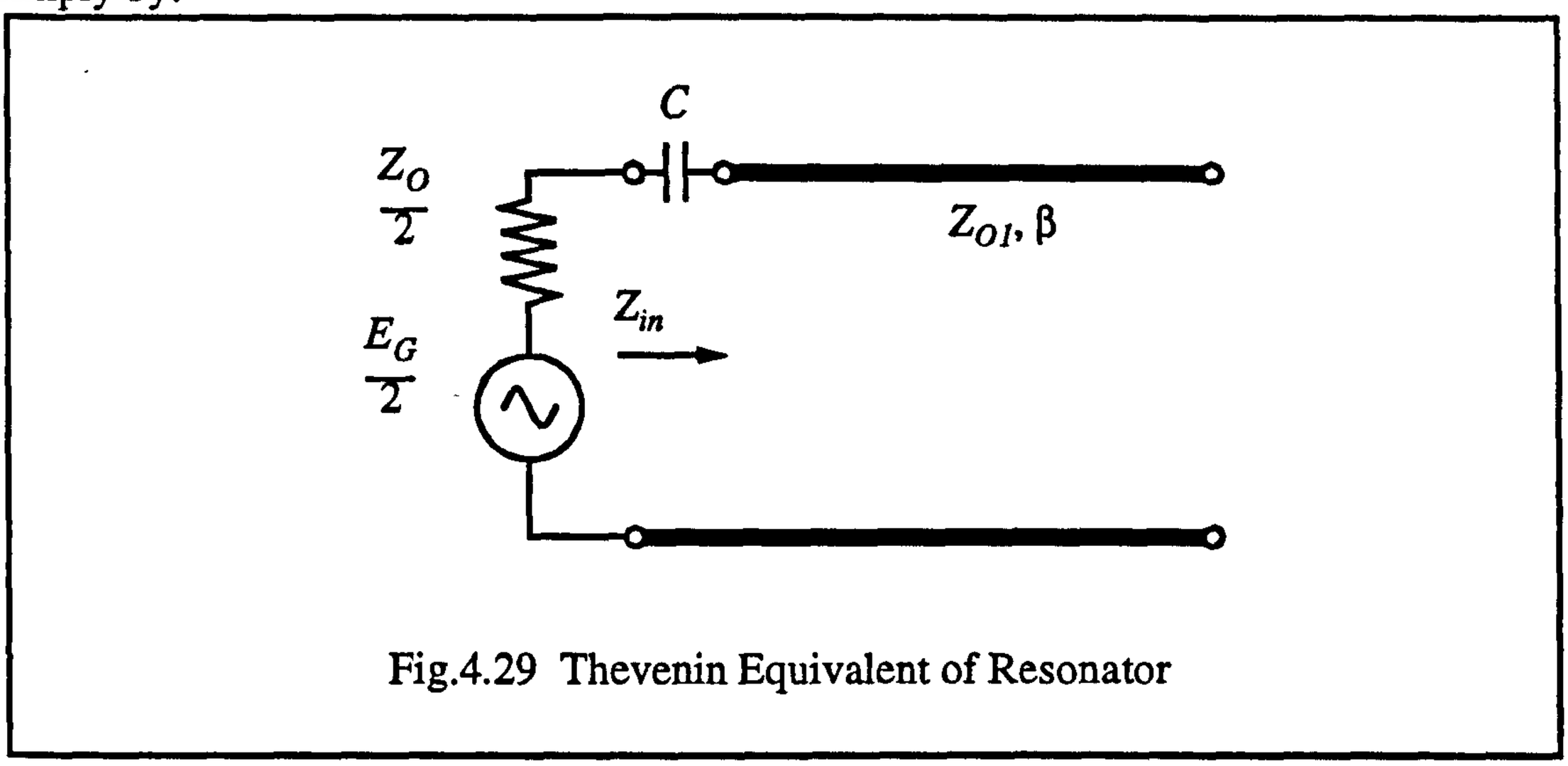

Fig.4.29 Thevenin Equivalent of Resonator

$$I_{Res} = \frac{E_G/2}{Z_O/2} = \frac{E_G}{Z_O} \qquad \text{Eq.4.56}$$

Now, the peak voltage across the capacitive part of the resonator, $\hat{E}_C$, is given by:

$$\hat{E}_C = \hat{I}_{Res} \cdot X_{CR} = \frac{\hat{E}_G}{Z_O} \cdot X_{CR} \qquad \text{Eq.4.57}$$

Where $\hat{E}_G$ is the peak generator voltage, X_{CR} is the reactance of the capacitor at resonance, and Z_O is the impedance of the main line.

$\hat{E}_G$ is related to the forward power delivered by the generator. On considering Fig.4.30, it is obvious that $\hat{E}_G$ is split equally between the generator impedance and the load impedance for a matched system.

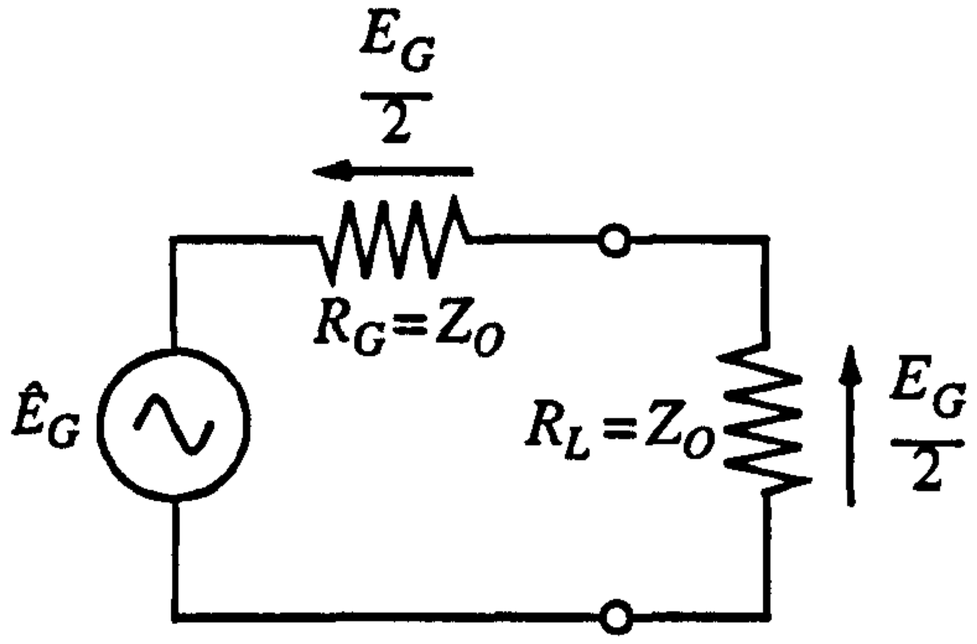

Fig.4.30 Power Distribution

The available power is given as:

$$P^+ = \frac{(E_G/2)^2}{Z_O} = \frac{E_G^2}{4Z_O} \qquad \text{Eq.4.58}$$

Where E_G is the rms value of the generator voltage. The peak voltage is given by $E_G = \sqrt{2}E_G$ hence;

$$P^+ = \frac{(\hat{E}_G/\sqrt{2})^2}{4Z_O} = \frac{\hat{E}_G^2}{8Z_O} \qquad \text{Eq.4.59}$$

Substituting Eq.4.59 in Eq.4.57 and rearranging gives the main line power for a given value of $\hat{E}_C$:

$$P^+ = \frac{\hat{E}_C^2 Z_O}{8X_{CR}^2} \qquad \text{Eq.4.60}$$

The value of X_{CR} is available from the design data for C_T. The breakdown field strength of air at atmospheric pressure is $3 \cdot 10^6$ V/m. Given that none of the capacitive gaps are smaller than 1 mm, Eq.4.60 gives the maximum value for $\hat{E}_C$ as $3 \cdot 10^3$ V. With Z_O equal to 50Ω and X_{CR} in the region of 300Ω the maximum forward power which the filter can safely withstand is 625 Watts which is well above the operating levels of the PIM measurement system.

4.6.5.4 Differential Pitch Tuning Screws

The tuning process involves adjusting the capacitive gap spacing and is quite sensitive to changes in gap dimensions as shown in Section 4.6.5.2. Some time was spent in consideration of the problem and an excellent solution was found in the differential pitch tuning rod.

Every screw, nut and bolt has a thread cut into it which provides a mechanism of converting rotational motion into axial motion allowing joints and fastenings to be tightened under axial pressure. The pitch of a thread is defined as the amount of linear movement for one complete, 360°, rotation of the thread about its longitudinal axis. For example, the thread of a standard M4 bolt (diameter 4mm) has a pitch of 0.8mm so if an M4 bolt is inserted into an M4 tapped hole, it will move 0.8mm into the hole for every complete rotation. The pitch of a thread tends to increase with thread diameter. For example, a 6mm diameter, M6 bolt has a pitch of 1.0mm. It is possible to exploit the differences in pitch to construct a tuner which gives a very fine and accurate degree of longitudinal adjustment.

Consider the system of Fig.4.31. A tuning screw was made by using a sharp tool to cut two different threads onto a single nylon rod, one M4 and the other M6. An M4 thread was then tapped into the end of the resonator and an M6 thread machined into the wall of

the filter enclosure. The system was then assembled as shown. If the screw is rotated once, it will move 1.0mm into the filter enclosure. As long as the resonator is prevented from rotating, the same rotation will cause the resonator to move towards the enclosure wall by 0.8mm. The net effect is that the resonator moves into the filter by 0.2mm. By this method a much more refined tuning mechanism is achieved.

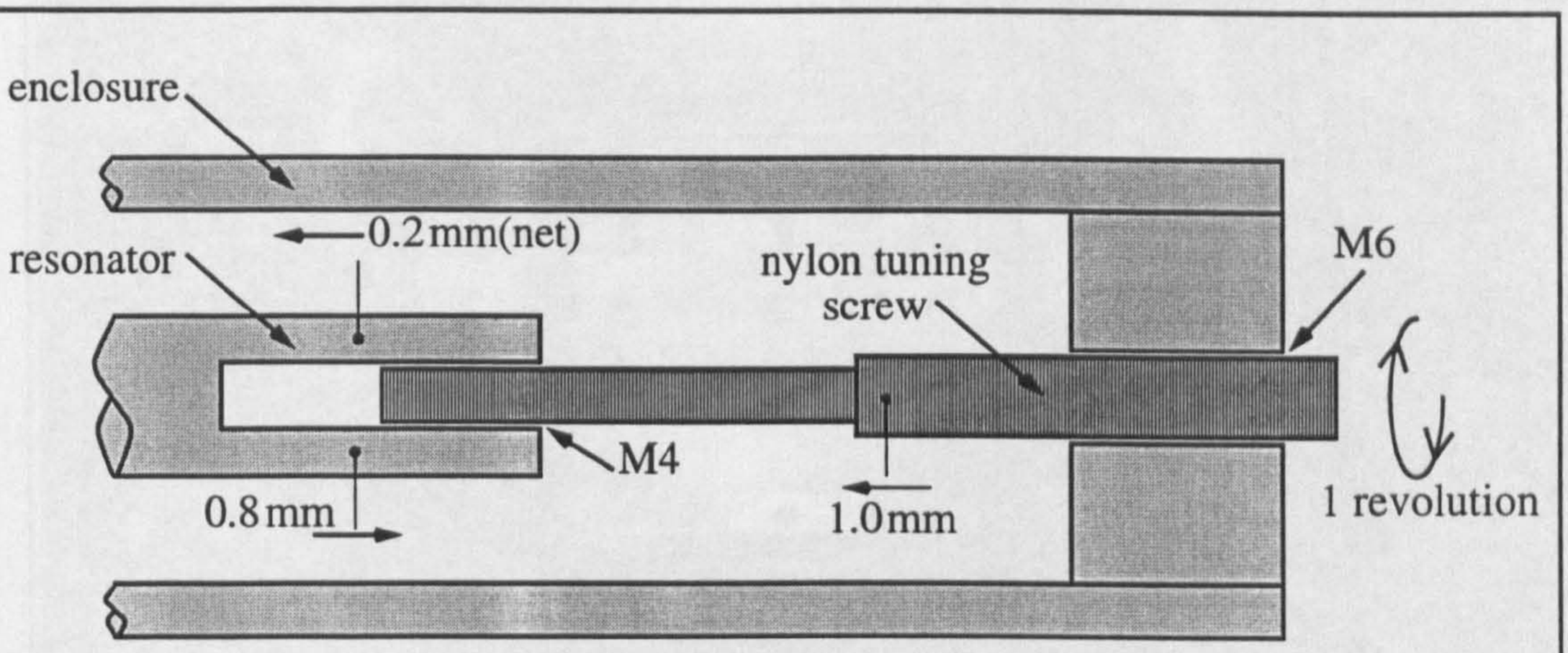

Fig.4.31 Differential Pitch Tuning

The screw is made from nylon in order to avoid the metal-metal contacts which readily cause PIM and to preserve the open circuit condition at the end of the resonator. The presence of the nylon has the effect of slightly increasing the capacitive end-effect of the resonator open circuit due to it's higher dielectric constant. This effectively increases the electrical length of the resonator and can be countered by slightly shortening the physical length.

4.6.6 Construction

The complete construction of the filter is illustrated in the photograph of Fig.4.32. The inner conductors as mentioned previously, were made from ex. stock brass bar. These were polished to remove surface oxides and contaminants. The sharp edges were slightly rounded using a fine grade emery paper to reduce the likelihood of breakdown due to field concentration at these points. The outer screened box is also made from brass. This first prototype filter was built before work on the low-PIM connectors and enclosures had been developed therefore a simple box was made consisting of four walls, a floor and a lid. The box is held together by over 50 M6 bolts which can sustain a high torque, necessary to give a high clamping force between the lid, floor and walls and thereby reduce the amount of PIM produced by the filter.

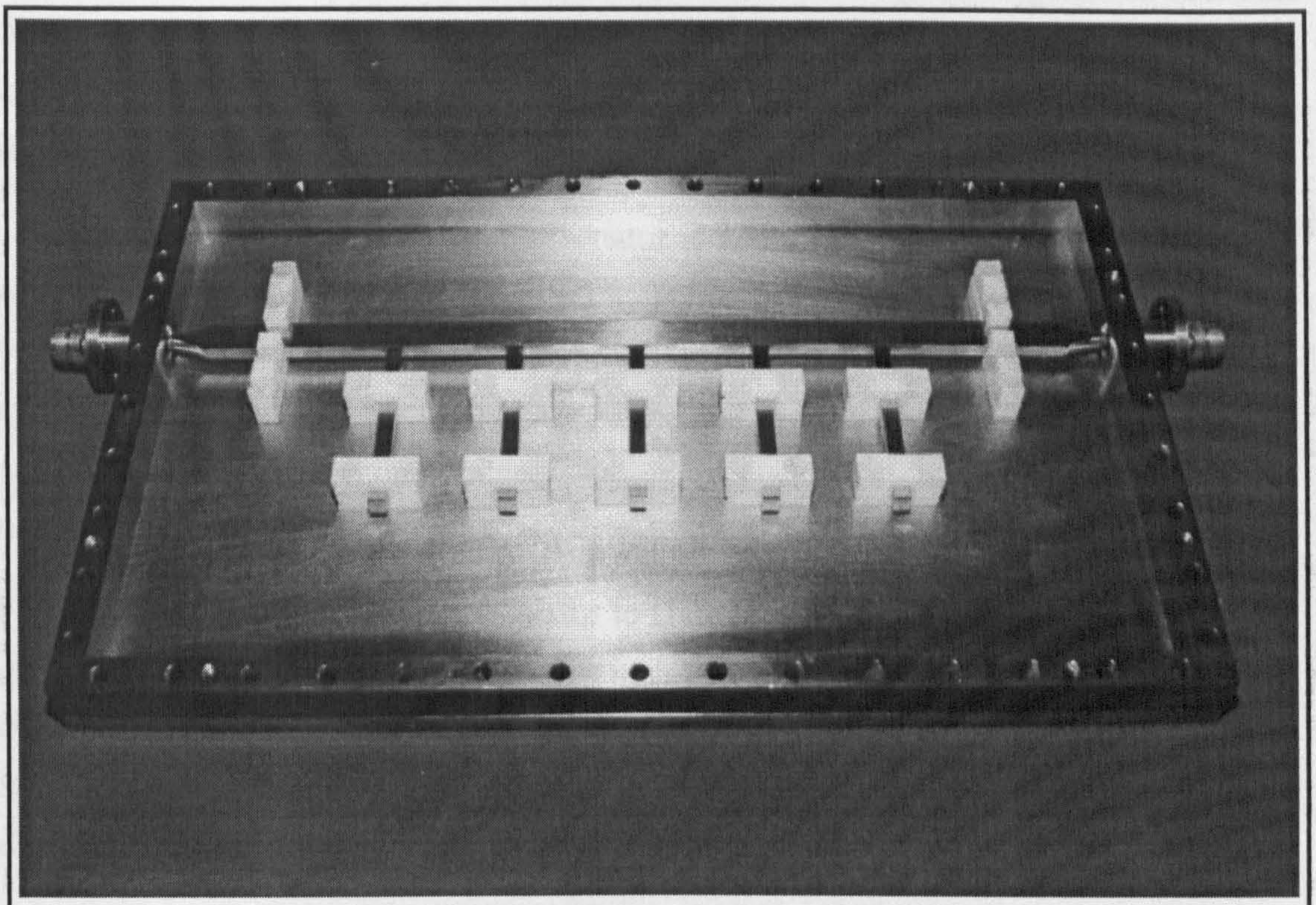

Fig.4.32 Band-stop Filter Construction

The PTFE supports were made in two halves which fit around the centre conductors. These are then fixed into the floor of the filter using nylon screws, one on either side of the conductor, then tightened to clamp the line firmly in place.

Transitions between the N-type connectors and bar-line centre conductor were designed using HFSS. The models delivered a return loss of over 30dB from 1-2GHz which was considered adequate for the application.

4.6.6.1 Setup And Tuning

With all details of the filter design finalised, the filter was constructed and assembled as in Fig.4.32. The next step was to finalise the resonator dimensions, tune the filter and test its electrical performance before inserting it into the PIM system. The filter was setup by monitoring the response using the Wiltron 360 vector network analyser described in Section 4.2.2.

The first task was to check the match of the transitions and 50Ω through-line of the filter. All resonators and associated PTFE supports were removed and the filter connected between the ports of the analyser. Measurements indicated a return loss of over 25dB from 1-2GHz verifying the design of the transitions and the 50Ω through-line dimensions.

Next, the resonant elements had to be set up to deliver the specified performance. This is indicated when the resonator delivers the correct 3dB bandwidth (as calculated in Section 4.6.3) at the desired resonant frequency. The resonators are tuned one at a time with the other resonators removed so that they do not influence the results.

The individual response of each resonator is wholly dependant upon the capacitive coupling gap spacing and the length of each resonator. It was mentioned in Section 4.6.5 that it is often difficult to compute the appropriate capacitive gap size with as much accuracy as desired. As such it is frequently easier and more convenient to experimentally adjust the coupling to its proper value.

Initially, the adjustments were made by slightly loosening the clamping pressure of the PTFE supports, allowing the resonator to slide in and out. Each resonator was tuned by extending the capacitive gap to over its nominal size. This decreases the capacitance, increases the resonant frequency and decreases the 3dB bandwidth for a given resonator length. The differential pitch tuning mechanism was used to progressively close the gap and gradually reduce the resonant frequency.

The capacitive gap of the stub was adjusted to give peak attenuation at the desired 1590 MHz then the 3dB bandwidths of the individual stubs were measured. The measured 3dB bandwidth for each stub was compared with the theoretical 3dB bandwidth. The resonators were originally made to be slightly over length (as described in Section 4.6.4.1).When the resonator is over length, the 3dB bandwidth is too narrow, therefore, the resonators were gradually shortened until the computed 3dB bandwidth was obtained at the desired resonant frequency.

Since the resonator configurations are symmetrical about the centre element, it is only necessary to tune half of the resonators. Once the proper element lengths have been obtained, they can simply be duplicated for the remaining resonators.

Once they were machined to their final lengths and their individual performance was re-checked, the five stubs were secured along the line as shown in Fig.4.32. They should be set $\lambda/4$ apart, between centres, at 1590MHz. However, due to the extremely narrow stop-band, the spacing is not overly critical, and they were simply placed 47mm apart and not further adjusted.

The next step was to tune all five resonators to the centre stop-band frequency. This is a more difficult task since, when one or two resonators have been tuned to the same resonant frequency, it becomes difficult to tell whether the resonant frequencies of additional elements coincide at exactly the same point. The null becomes less well defined.

The dynamic range of the network analyser is at best, 80dB, therefore, a stop-band null of around 80dB from the filter will not be readily observed as the thermal noise of the analyser becomes dominant.

The difficulty was overcome by providing a means to short each resonator to ground near the end which forms the capacitive gap. This greatly alters the electrical response of the individual resonator without altering its physical settings. The effect is to remove the resonant null of the element from the vicinity of the frequency to which the filter is being tuned. All of the resonators are inserted into the filter and roughly set up according to the data obtained during the individual tuning stage. All but one resonator is then shorted to ground to electrically 'remove' them. The remaining resonator is then tuned to the desired resonant frequency. The resonator supports are tightened to fix it in place, then it too is shorted out and the next resonator tuned. This process is continued until all of the resonators are set up correctly. The shorting mechanisms are then removed and all of the resonators are seen to be tuned at the correct frequency. The overall response of the filter can then be properly measured.

The shorting mechanism was facilitated by drilling small diameter holes in the lid of the filter, directly above the resonator positions. In order to short the resonators to the ground plate or lid, several stiff pieces of wire were inserted into the hole and lowered to make a light contact between the top of the resonator and the lid. This proved to be sufficient to disrupt the response of the resonator as desired.

4.6.7 Electrical Performance

Once all of the resonators had been tuned, the shorting wires were removed and the overall filter response was measured. Fig.4.33 indicates that far from achieving the desired symmetrical response of +80dB rejection over a 6% bandwidth, the filter delivered only around 50dB rejection. Additionally, the profile of the response was very irregular and non-symmetric. Further attempts to re-tune the filter proved fruitless with similar results being recorded each time.

It was subsequently discovered, however, that the internal dimensions of the filter enclosure were sufficient to support the next higher order mode of propagation of R.F. energy, the TE_{11} or waveguide mode.

Higher order modes of propagation have been mentioned in Section 3.3.4 and Section 4.4.2. A mode is a single discrete solution of Maxwell's equations to which the boundary conditions of the transmission line have been applied. The boundary conditions are defined by the physical dimensions of the line and each solution of Maxwell's equations

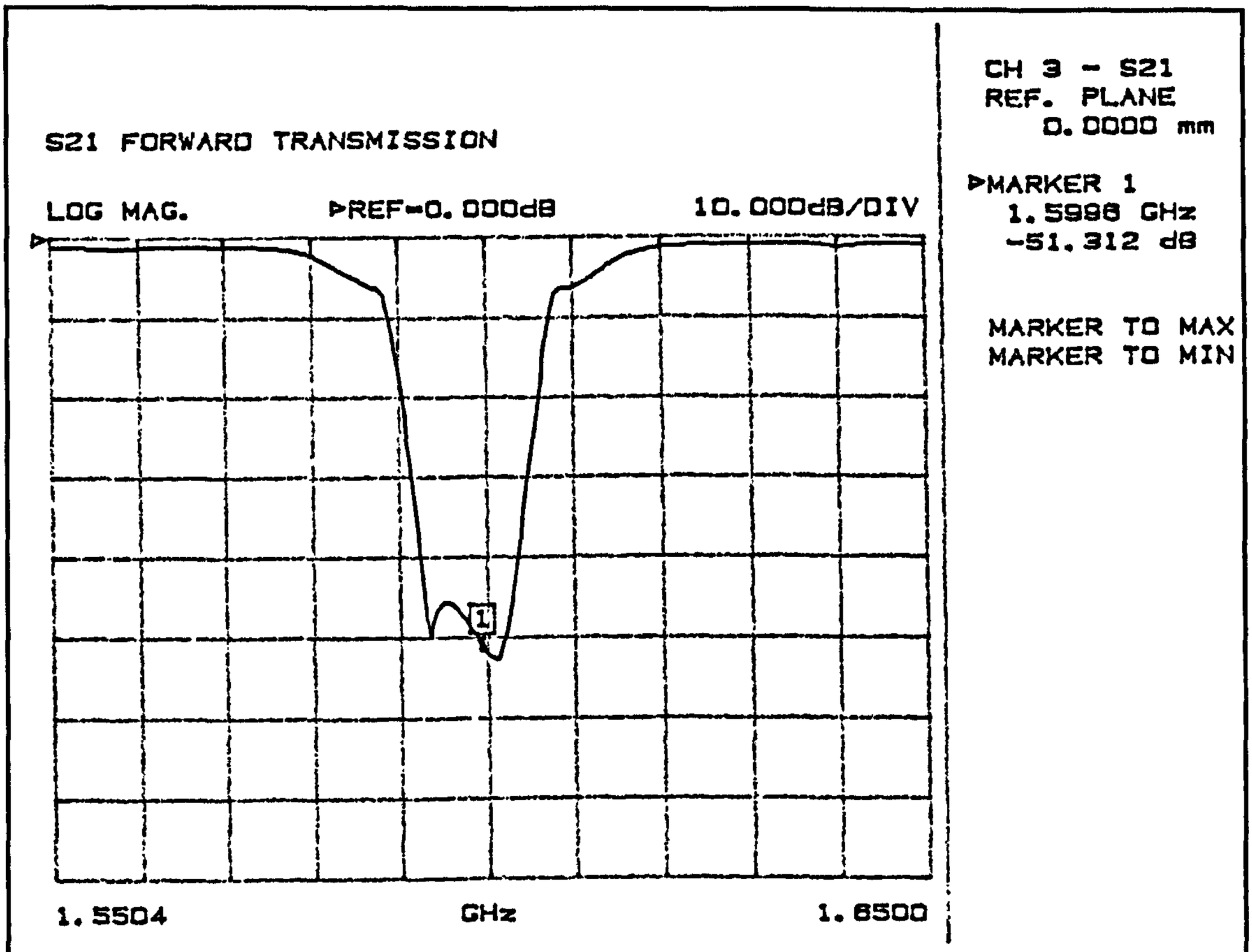

Fig.4.33 Prototype band-stop filter response.

must satisfy these conditions. It can be shown [43] that for a given transmission lines cross section, there exists an infinite number of solutions to Maxwell's equations and hence, an infinite number of modes.

A given mode, however, will propagate as a wave only if its frequency, f, is above a critical cut-off value, f_c. Below this frequency, the mode is not supported by the guide and is heavily attenuated in the direction of transmission. The mode that will propagate at the lowest frequency is called the dominant mode of the medium, other modes are called higher-order modes. Modes are characterised by their electromagnetic field patterns which differ from mode to mode and determine the propagation characteristics of the energy in a particular mode.

Consider a section of standard bar-line depicted in Fig.4.25. In order to ensure only TEM mode propagation in the frequency range of interest, the transverse dimensions of the line must be chosen so that the cut-off frequencies of the higher-order modes are greater than the highest frequency of interest. The two most problematic modes, since their cut-off frequencies are the lowest of the higher-order modes, are depicted in Fig.4.34. The mode of Fig.4.34(a) is known as the TE_{11} mode has as a cut-off frequency determined by Eq.4.61 [112]:

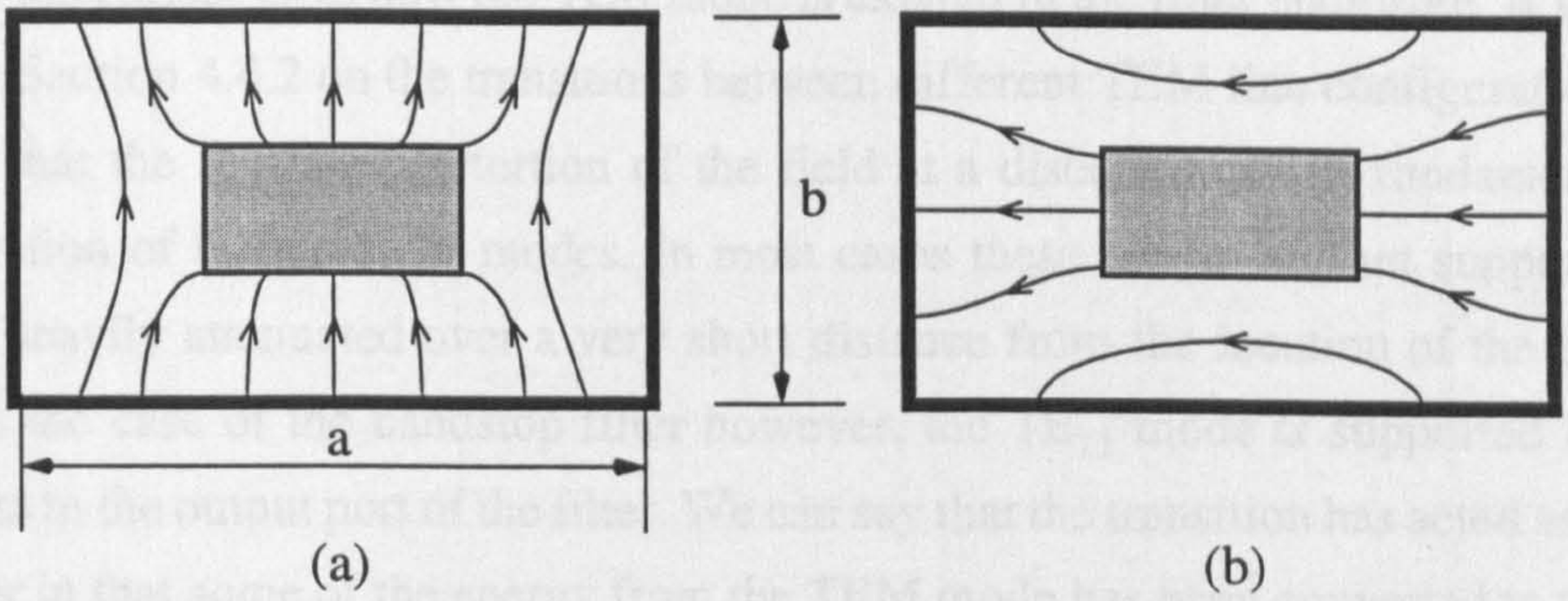

Fig.4.34 Higher Order Mode Patterns

$$f_{\max} = \frac{c}{2a\sqrt{\mu_r \varepsilon_r}} \qquad \text{Eq.4.61}$$

The cut-off frequency of the other mode in Fig.4.34(b) is given by:

$$f_{\max} = \frac{c}{4b\sqrt{\mu_r \varepsilon_r}} \qquad \text{Eq.4.62}$$

Propagation of both modes is obviously governed by the internal enclosure dimensions. From Eq.4.61, the maximum width, a_{max}, of the enclosure before TE_{11} mode propagation will be supported was calculated to be 93.44mm at f=1.6GHz. Similarly, $b_{\max}$, the maximum height of the enclosure governed by Eq.4.62 was found to be 46.88mm in air.

This effect was not considered when designing the filter and on examining the internal cross-sectional dimensions of the filter enclosure, it was seen that the a & b dimensions were 220mm & 18.8 mm respectively, therefore, the enclosure will readily support TE_{11} mode propagation.

Most components and devices are designed on the basis that the input signal will be in a particular mode. In most cases, this will be the dominant mode of the transmission structure, and indeed, the bandstop filter was designed for the TEM mode of propagation. If a mode other than the desired mode is allowed to propagate in the filter, the fields of this mode will not respond to the internal filter elements in the same manner as the dominant mode. Any signals in the TE_{11} mode will not be reflected by the resonators.

Given that the input signal on the coaxial line to the filter is in the TEM mode, the question then arises as to how the TE_{11} mode is excited in the filter enclosure. If we again consider Section 4.4.2 on the transitions between different TEM line configurations, it is recalled that the localised distortion of the field at a discontinuity is, fundamentally, a superposition of higher-order modes. In most cases these modes are not supported and become heavily attenuated over a very short distance from the location of the discontinuity. In the case of the bandstop filter however, the TE_{11} mode ***is*** supported and will propagate to the output port of the filter. We can say that the transition has acted as a mode converter in that some of the energy from the TEM mode has been converted to the TE_{11} mode.

The idea of mode conversion at the transitions would explain the spurious response observed for the bandstop filter. It is assumed that mode conversion at the transition is reciprocal (to a certain degree) so that energy in the TE_{11} mode will be readily converted back to the TEM mode at a transition. Therefore, at the output transition of the filter, an amount of the TE_{11} energy which has been transmitted through the filter, will be converted to the TEM mode and registered at the output of the device. The majority of the energy at the input of the device remains in the TEM mode but this is reflected by the action of the resonators. In this way, the filter appears to deliver less attenuation than expected, just as in Fig.4.33. Hence it can be said that the filter response has been impaired due to over-moding.

In order to verify that over-moding was indeed responsible for the poor electrical response of the filter, the two side-walls of the filter were replaced by adjustable copper walls. Each wall can slide into the filter enclosure and its position altered to vary the box width '*a*' as shown in Fig.4.35.

With the bandstop filter connected to the network analyser, the side walls were interactively adjusted to obtain the best response. It was observed that by sliding the walls closer together, the moding effect could be reduced by a significant amount, but not eliminated. However, as the walls began to approach the centre conductors the filter response was seen to degrade rapidly. On the one side, as the wall approaches the 50Ω through line, the electric field lines linking with the side wall are increased and the characteristic impedance of the line changes. The line is no longer properly matched and significant reflected waves are produced at all frequencies, thus degrading the response of the filter.

On the other side, as the wall approaches the end of the resonators, the field linkage to the wall is once again increased. This affects the behaviour of the open circuit and the electrical length of the resonator, which cause the filter to become de-tuned.

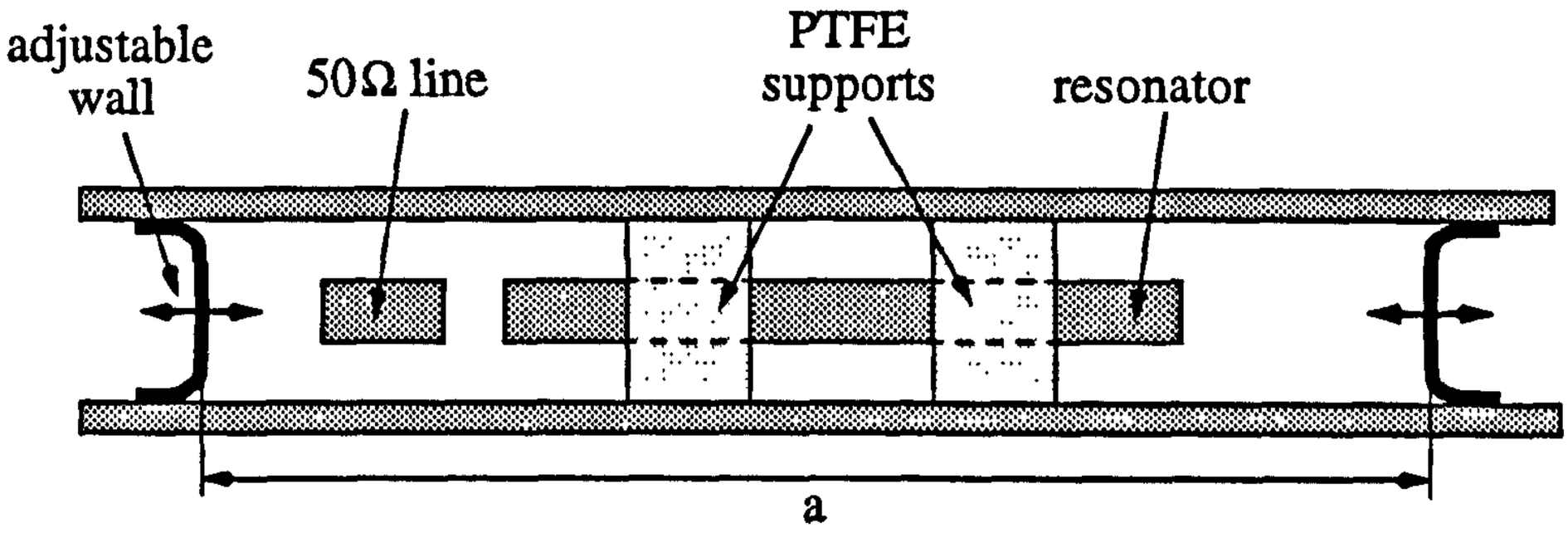

Fig.4.35 Adjustable Copper Side Walls

As a first step, it was decided that the original side plates be replaced in the filter but at the new position determined by the optimum position of the sliding copper walls. However, as the moding remained in evidence (albeit at a lower level) it was clear that further mode suppressing techniques had to be found. The main problem was that due to the physical length of the resonant elements it simply was not possible to reduce the width of the box to less than 93.44mm as determined by Eq.4.61 to prevent overmoding.

An alternative means of suppressing the TE_{11} mode is to short the top and bottom ground plates at discrete points along the longitudinal length of the filter at intervals of $\lambda/8$ at the highest frequency of interest[112]. The transverse separation between shorting points should be less than the a_{max} calculated from Eq.4.61. This technique suppresses the longitudinal or 'z' component of the TE_{11} magnetic field and hence prevents this mode from propagating.

On further consideration, however, it became apparent that higher order mode propagation will not be limited to the longitudinal axis of the filter. Since the resonators are orthogonal to the main line, the TEM fields on which they operate will also be orthogonal to the main line. From the point of view of the resonators, their transverse dimension, '*a*' of Fig.4.34, will be equal to the length of the filter and the TE_{11} mode will, again, be easily supported. It is therefore necessary to provide for additional mode suppression along the length of the resonators.

Unfortunately, due to the $\lambda/4$ spacing of the resonators, it is not possible to facilitate shorting points at intervals of $\lambda/8$ along the longitudinal axis without seriously disrupting the performance of the filter. It is only possible to create shorting points between the reso-

nators resulting in a $\lambda/4$ spacing. However, it was decided that it would be a worthwhile exercise to try $\lambda/4$ spaced points in order to establish whether any improvement was possible.

The next step was to consider the method by which the ground plates would be shorted together. Using metal posts, for example, to provide direct contact between the plates would defeat the principle objective of developing a low-PIM structure. Numerous metal-metal contacts would significantly increase the likelihood of PIM generation and are highly undesirable. Although this filter was a prototype model, it was intended to accommodate the device in a low-PIM enclosure of the type discussed in Section 4.5 and contacting posts would not be in keeping with a low-PIM design.

As a result, an alternative shorting mechanism was developed. Once again, the impedance transformation properties of transmission lines (Section 4.3.2) were exploited by using open-circuit terminated $\lambda/4$ sections to effect short-circuits between the ground plates. The principle can best be explained with reference to the diagram of Fig.4.36.

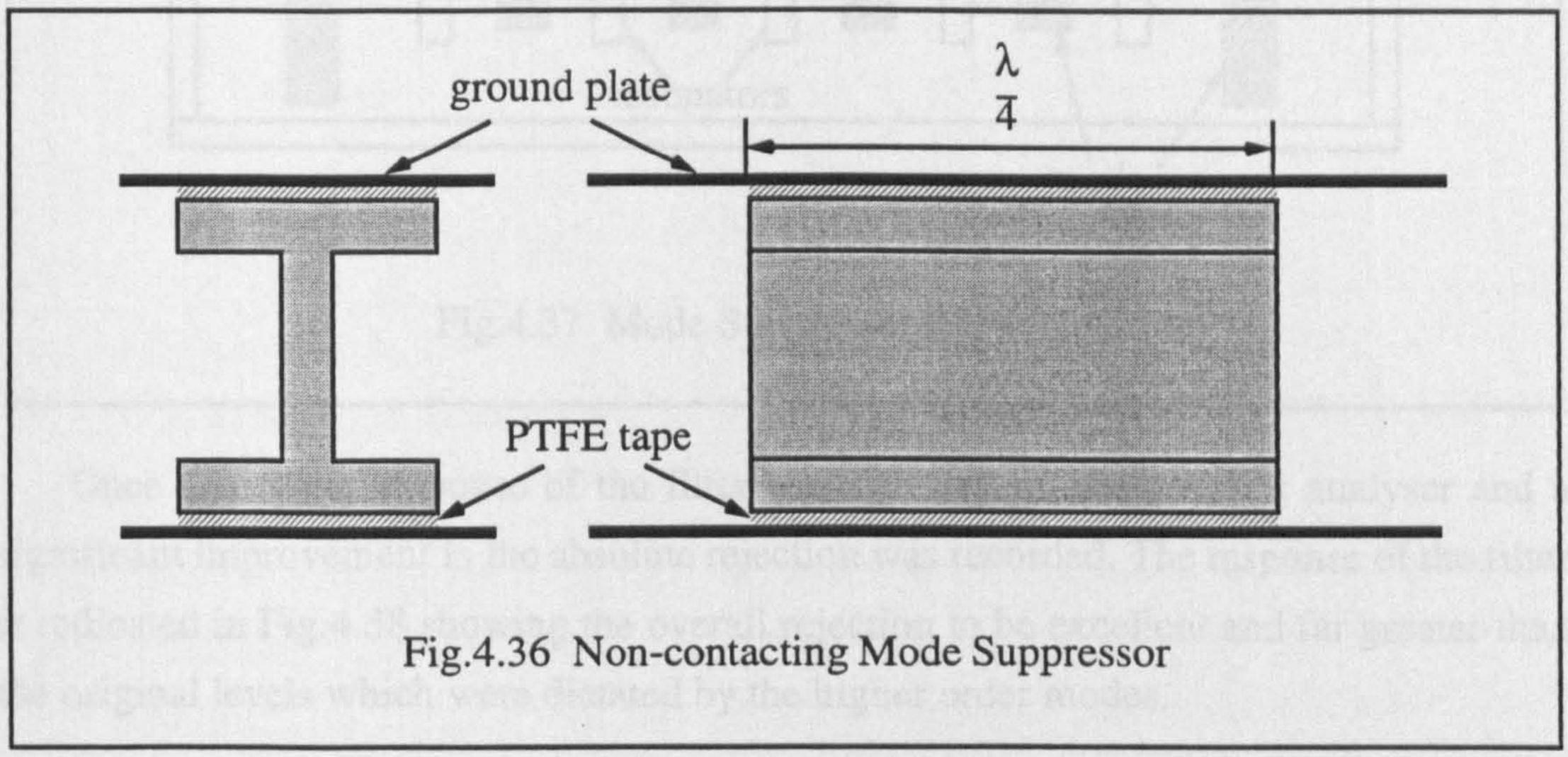

Fig.4.36 Non-contacting Mode Suppressor

The '**I**' shaped section is made from aluminium, the top and bottom have strips of PTFE tape applied to them and the whole unit is a tight fit between the two earth plates when the filter lid is in place. The section is $\lambda/4$ long (in PTFE) at the resonant frequency of the filter. It is placed in the filter, parallel with the direction of propagation of the mode which is to be suppressed. In the TE_{11} mode, impedances are directly related to the height between the two ground planes so that the small-clearance PTFE section has a much smaller characteristic impedance than that of the remainder of the enclosure. The section, therefore, acts as a quarter-wave transformer and by Eq.4.1 converts the relatively high impedance at one end of the section to a very low impedance at the other end. The

mismatch at the input to the mode-suppressor is virtually the same as would be offered by a short circuit. However, as opposed to short circuiting posts, there are is no mechanical contact and hence a much reduced probability that PIM will be generated.

Several '**I**' section mode suppressors were inserted in the main body of the filter. Many different configurations were tested. The setup giving the best performance is illustrated in Fig.4.37.

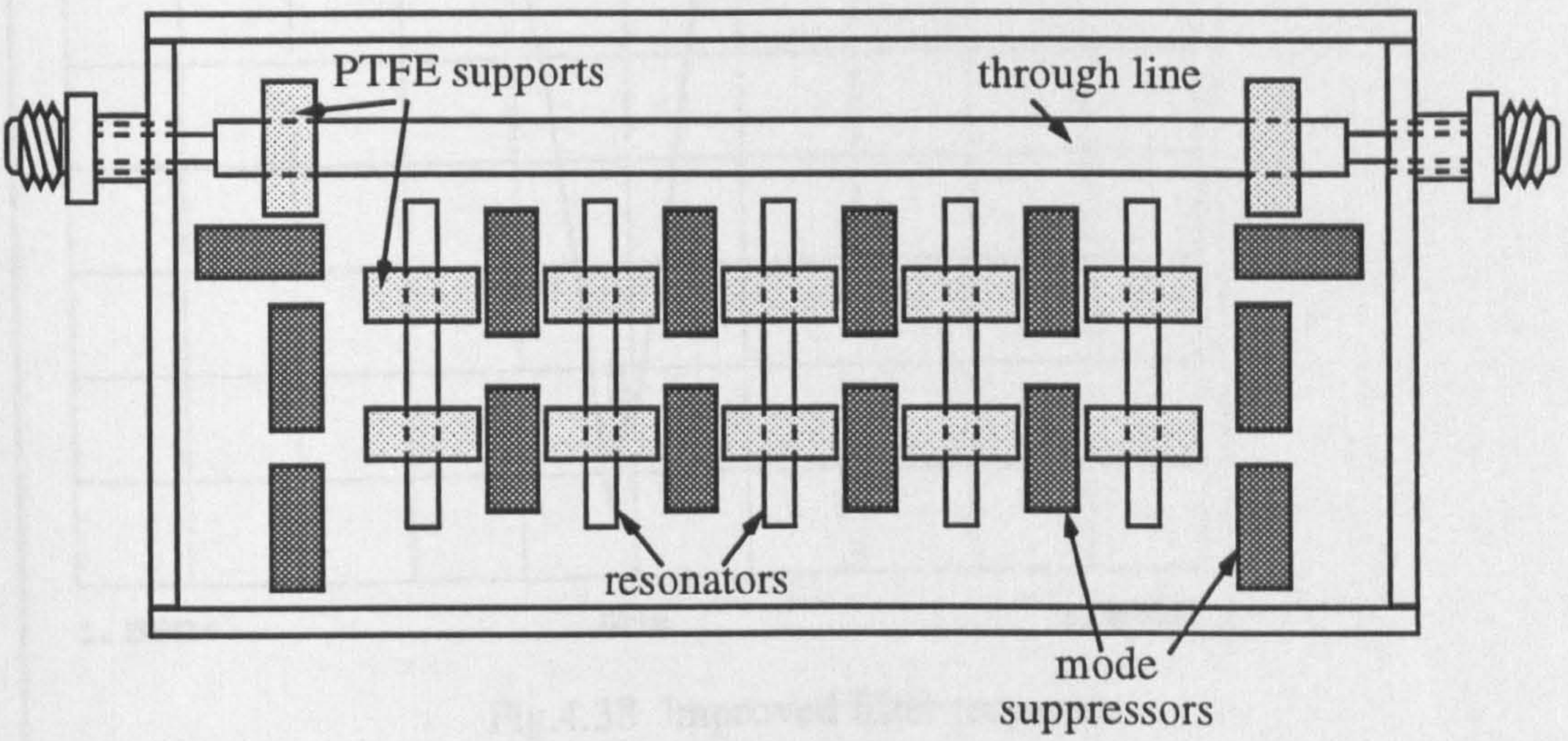

Fig.4.37 Mode Suppressor Locations

Once again, the response of the filter was checked on the network analyser and a significant improvement in the absolute rejection was recorded. The response of the filter is indicated in Fig.4.38 showing the overall rejection to be excellent and far greater than the original levels which were dictated by the higher order modes.

4.6.8 PIM Performance

The next step was to test the filter at high-power for PIM. The first stage was to dismantle the filter and thoroughly clean each of its constituent parts. Cleanliness is an essential part of a good PIM measurement system as even the smallest particles of dirt or dust can cause untold problems in trying to reduce the residual PIM of a system.

Next the filter was reassembled, tuned and the bolts which clamp the filter together were thoroughly torqued up.

The filter was then tested at high power, however, initial results were not promising. The transmitted PIM was checked using 20 Watts per channel. Prior to inserting the filter, the system indicated a residual PIM level of -105 dBm. After inserting the filter, the level

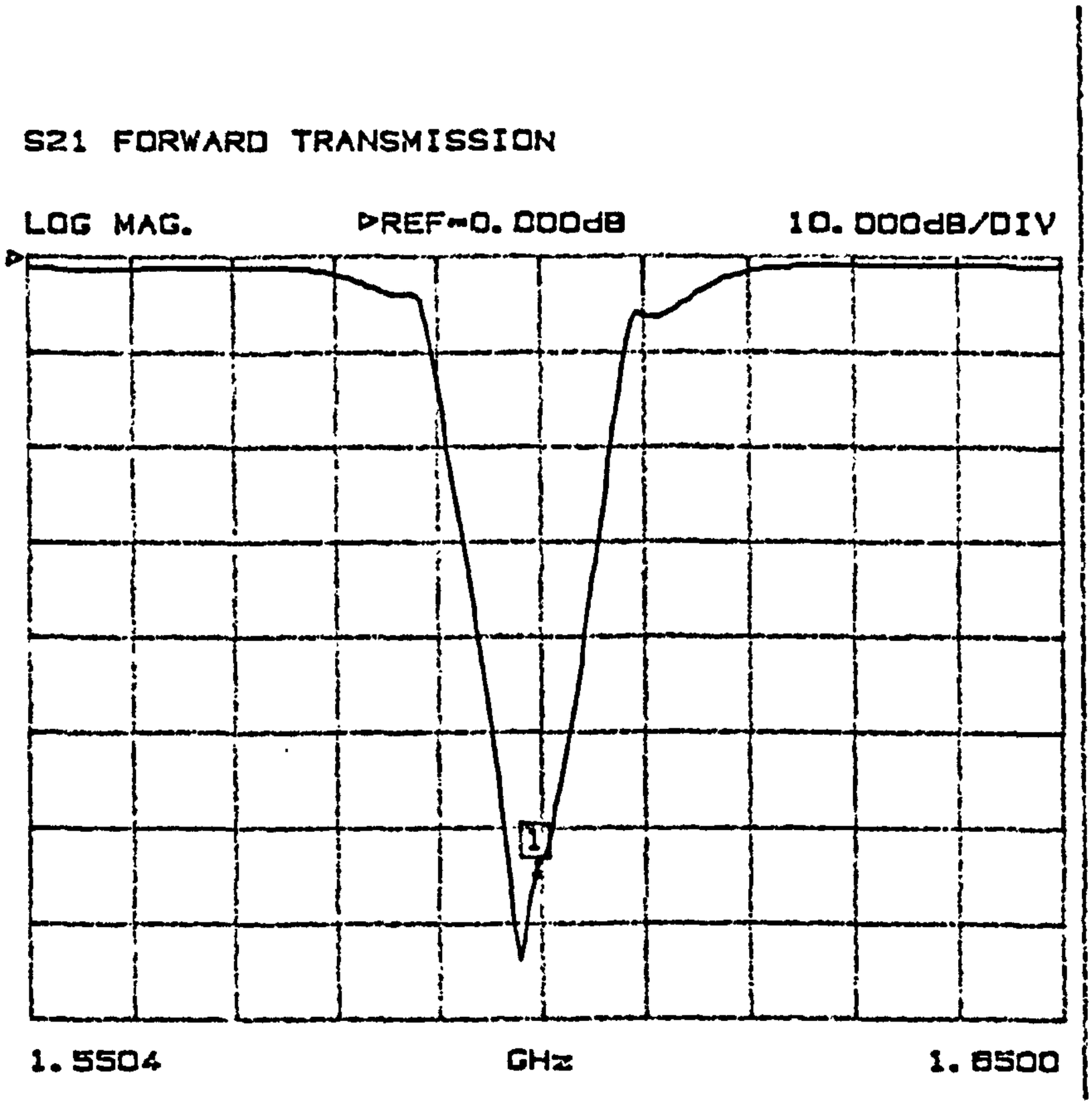

Fig.4.38 Improved filter response.

had only dropped to -117 dBm. Measurements of the reverse PIM actually indicated an increase in the PIM level. However, this could be a result of PIM signals from other components being reflected off the filter.

After the results were confirmed, the filters were dismantled. It was discovered that during the tests, the nylon tuning rod on the first resonator had overheated and melted at the end of the resonator. The first resonator is exposed to the highest levels of incident power and as such will develop the highest voltages at the open end. The loss tangent of Nylon is not insignificant and in conjunction with the high field strength was enough to cause overheating. It was thought that the failure of this mechanism had led to the filter becoming de-tuned and therefore the PIM which was observed was due to insufficient rejection of the residual PIM. The tuning elements were thus removed, the filter was cleaned once more, reassembled and tuned without the tuning elements. However on testing it was found that there was little improvement in the PIM performance. Subsequent tests revealed that a high degree of variability in the PIM level was evident from adjusting the clamping pressure of the lid (particularly near the cable entry points where the current density will be greatest) and by adjusting the mating torque of the connectors.

It was decided at this point to review the filter design and develop a second prototype for the following reasons:

- Likelihood of significant PIM generation from lid & N-type connectors.
- Failure of the tuning mechanism which clearly required further development.
- Undesirable presence of mode suppressors which were prone to becoming dislodged inside the enclosure.

4.7 Second Prototype Bandstop Filter

A second prototype bandstop filter was developed based on the original design described in the previous sections. Several changes were made to the original design and these are discussed in this section.

4.7.1 Contactless Filter Enclosure

The first major change was to design the new filter structure around the low-PIM enclosure techniques discussed in Section 4.5. This involved making a much larger box so that it could accommodate the internal components of the filter. The enclosure was made from solid aluminium alloy with no metal-metal contacts except at the forced low current points where the lid is attached.

Given that the enclosure was made from solid material, the mode suppressors were machined as part of the structure. The suppressors take the form of thin dividing walls between the resonators. The walls were again made to be a quarter wavelength long and topped with PTFE strips to prevent contact with the lid. The structure can clearly be seen in the photograph of Fig.4.39.

4.7.2 Self-Shorting Quarter Wavelength Resonator

The second major change was in the resonator configuration. It was adjudged that the original resonator configuration was not satisfactory. The resonator supports had to be loosened in order to tune the filter and on tightening could knock the filter out of tune. More significantly however, is that these same dielectric supports create discontinuities on the resonator (albeit relatively small), causing reflections which will serve to disrupt the wave patterns on the resonator and adversely affect the Q of the filter.

A more effective type of non-contacting resonator was developed to avoid having supports on the resonator at any point along its length. The design is illustrated in Fig.4.40 The new configuration comprises a cylindrical section resonant element ($\approx\lambda/4$) and a quarter wavelength shorting block. The resonator and block are fabricated in one piece.

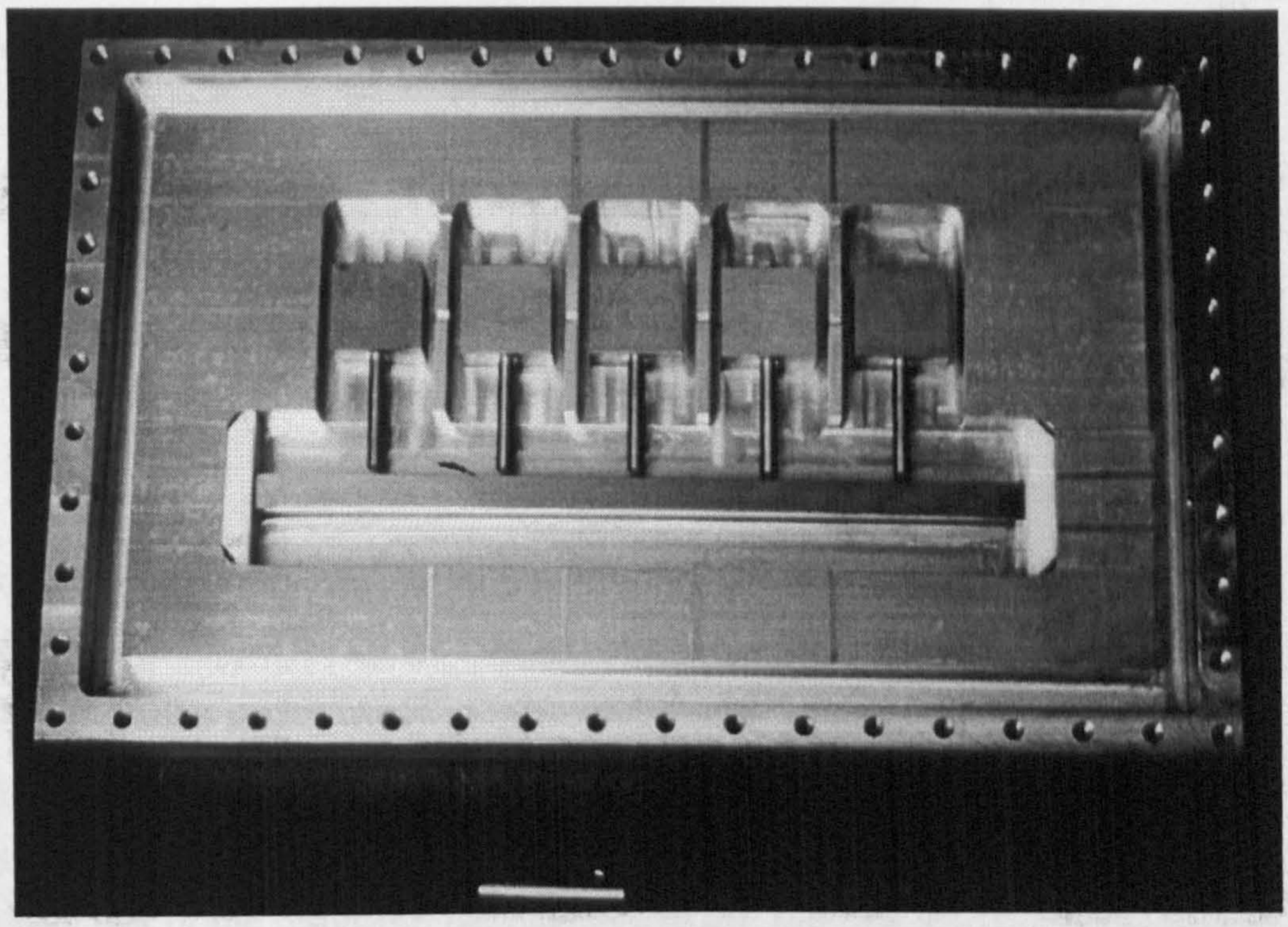

Fig.4.39 2nd prototype band-stop filter construction.

The resonator was given a circular cross section to make fabrication easier. The impedance of a circular section centre conductor between two ground planes is given in ref. [119]. as:

$$Z_O = \frac{138}{\sqrt{\varepsilon_R}} \cdot log\frac{4b}{\pi\phi} \qquad \text{Eq.4.63}$$

The cylindrical section behaves just as a capacitively coupled short-circuited resonator as described in ref. [124]. In reality there is little difference between this type of resonator and the open circuit resonator of the original design apart from a quarter wavelength difference in length, therefore, only a minor adjustment is required to be made to the design equations.

The short circuit is provided for by the quarter wavelength block on the end of the resonant element. This works on much the same principle to the mode suppressor except that in this case the mode in question is the dominant TEM mode. The block has PTFE tape applied to both top and bottom to prevent contact with the ground planes. The PTFE sections also act as lengths of low impedance line. The block is ended abruptly inside the enclosure at point 'B', so that the TEM mode will not be supported and will regard the block as being terminated in an open circuit. This will be transformed back to the front of

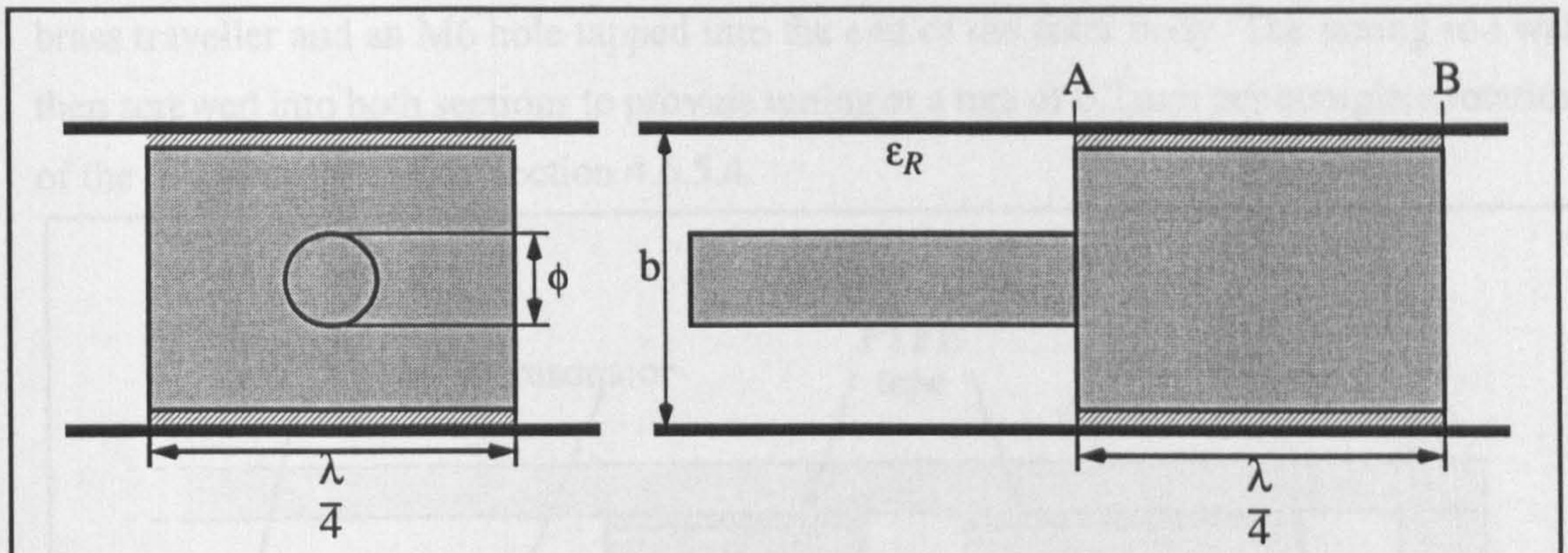

Fig.4.40 Self-Shorting Resonator

the block at point 'A', to give the desired short circuit termination to the resonant element. The resonator is supported by the shorting block and eliminates the need for dielectrics, resulting in a better performance.

The quality of the short circuit at 'A' is obviously frequency dependant. Recalling the analysis of Section 4.3.3 it is clear that as long as the impedance of the λ/4 section is much lower than that of the resonator, the effective bandwidth of the short circuit will be far greater than the bandwidth of the high-Q resonant element, hence this should not be a problem.

4.7.3 External Differential Pitch Tuner

The final change to be made for the new filter was the development of a new tuning mechanism. The previous mechanism utilised threaded sections of nylon dielectric rod to avoid forming metal to metal contacts in areas of significant current flow. It has been discussed how the rod failed due to losses. A new tuning device was developed based on the same differential pitch mechanism of Section 4.6.5.4 but located outside the filter enclosure. Hence, the components of the mechanism will not be exposed to RF fields and are not likely to generate PIM or yield to any other RF related anomaly.

The new tuning mechanism is illustrated in Fig.4.41. The resonator is connected through two narrow elongated holes in the floor of the filter enclosure to a brass traveller. It is fixed in place using specially manufactured cross-linked polystyrene screws. These have mechanical rigidity, a dielectric constant similar to PTFE and a low loss tangent. The brass traveller sits in a channel which has been machined into the base of the filter and is free to travel in the direction of the longitudinal axis of the resonator. A differential pitch tuning rod was made using M4 and M6 brass studding. An M4 thread was tapped into the

brass traveller and an M6 hole tapped into the end of the filter body. The tuning rod was then screwed into both sections to provide tuning at a rate of 0.2 mm per complete rotation of the rod as described in Section 4.6.5.4.

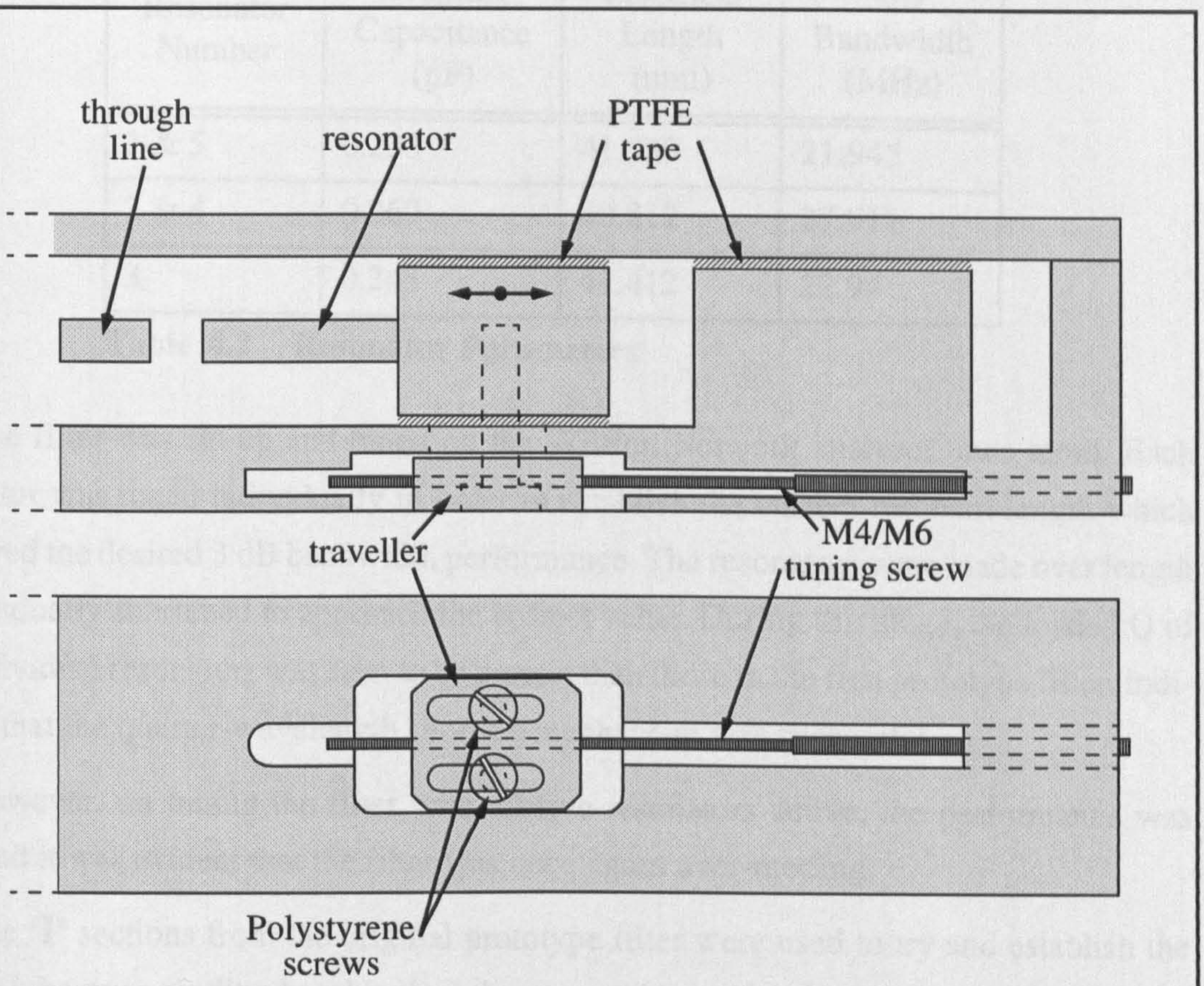

Fig.4.41 External Tuning Mechanism

4.7.4 Electrical Performance

The new filter was designed on the basis of capacitively coupled, shorted stubs to the same specification as that discussed in Section 4.6.3. The design parameters were calculated by slightly modifying the original computer program. The resonator cross section was given a diameter of 6.35 mm the same as the thickness of the bar-line used for the main conductor of the filter. This was to preserve the cross sectional area of the end of the resonator and deliver similar capacitive gap dimensions to the original prototype filter.

For b=18.8mm (to maintain the main line impedance as 50Ω), and ϕ=6.35mm, Z_O=79Ω. The remaining parameters are listed in Table 4.2.

Resonator Number	Coupling Capacitance (pF)	Electrical Length (mm)	3dB Bandwidth (MHz)
1 & 5	0.238	41.539	21.945
2 & 4	0.269	40.817	27.911
3	0.243	41.412	22.94

Table 4.2 Resonator Parameters

The filter was set up and tuned on the Wiltron Network analyser once more. Each resonator was tuned individually in order to establish the correct resonant length which delivered the desired 3 dB bandwidth performance. The resonators were made over length and gradually shortened to approach the correct value. During this stage, the loaded Q of the individual resonators was seen to be greater than those in the first prototype filter, indicating that the quarter-wavelength shorting mechanism was successful.

However, on tuning the filter with all five resonators active, the performance was poor and it was evident that the filter was once again over-moding.

The '**I**' sections from the original prototype filter were used to try and establish the cause of the over-moding but this time they were observed to have little effect no matter what their position inside the internal enclosure.

It was observed however that loosening the lid caused the moding problem to get much worse. Copper tape was used to try and improve the contact between the lid and the box but once again this had little effect.

The next step was to short the $\lambda/4$ dividing wall of the low-PIM enclosure to the lid. Narrow slits were cut in the PTFE tape on top of the quarter wavelength walls. This bared the metal underneath. Next a short length of soft solder wire was placed in the slit in contact with the wall. Initially this was performed at two points in the filter, one on either side of the of the broad wall as shown as points (a), in Fig.4.42. When the lid was tightened onto the filter enclosure it came into contact with the solder wire which deformed to give a good ohmic contact. Immediately, a significant drop in the level of over-moding was registered. Further pieces of solder were inserted at the points, (b), indicated in Fig.4.42, and the rejection of the filter became so great that it could not be measured due

to the finite dynamic range of the network analyser (i.e. rejection >90dB). The solder was removed and the moding problem returned. This suggested that energy was being coupled between the ports via the quarter wavelength dividing walls.

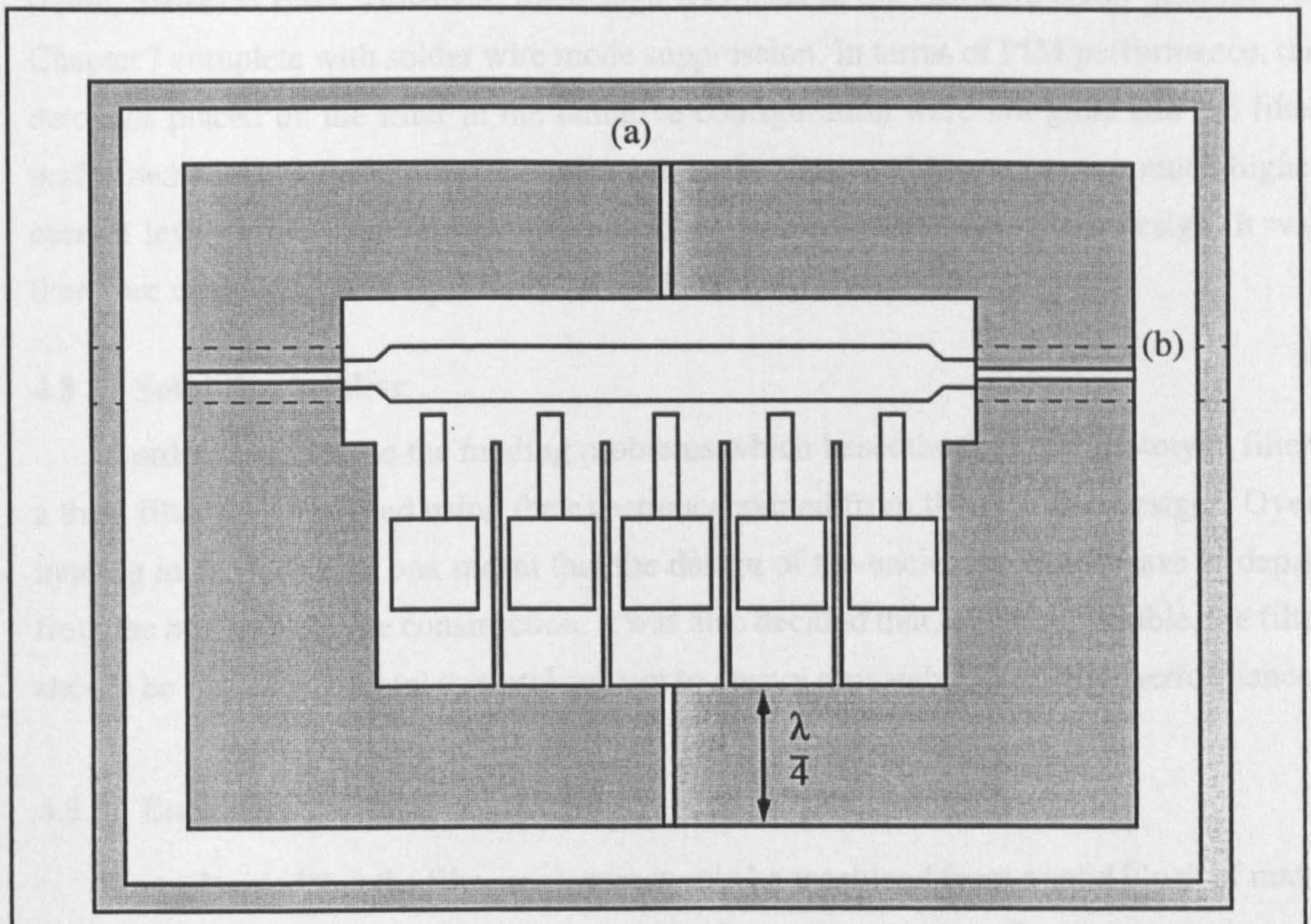

Fig.4.42 λ/4 Wall - shorting points

A cross section of the low-PIM enclosure was simulated using the HFSS package. An analysis was performed on the higher order modes supported by this structure which showed that an enclosure of this cross sectional configuration will readily support modes other than TEM, TE_{11} being of the highest intensity. Further simulation concluded that mode conversion readily takes place at the transitions and that the TE_{11} mode will be about 30dBm down on the TEM mode for each transition. This was consistent with the measured data which indicated the rejection of the filter to be no greater than about -60/-65dBm when the overmoding was present. i.e. Energy is converted to the TE_{11} mode at the input transition, it passes unattenuated to the output transition where some of it is converted back into the TEM mode. A drop of ≈30dB per transition equates to an insertion loss of ≈60dB for the whole filter.

To the TE_{11} mode, the λ/4 walls simply give the enclosure a much greater transverse width. By Eq.4.61 it is evident that for this configuration, the cut off frequency of the TE_{11} mode will be well below the operating frequency of the filter and so will not be attenuated.

It was considered at this point that the insertion of soft solder wire to form a connection between the lid and the filter body was not consistent with the goal of achieving a stable, low-PIM filter. However, the design was used in the radiative setup described in Chapter7 complete with solder wire mode suppression. In terms of PIM performance, the demands placed on the filter in the radiative configuration were not great and the filter performed adequately. In the conductive set up the filter will be exposed to much higher current levels and it was felt that there would be no benefit to using this design. It was therefore decided to develop a more robust band-stop filter.

4.8 Solid Block Filter

In order to overcome the moding problems which beset the first two prototype filters a third filter was designed using the experience gained from the first two designs. Over-moding in the low-PIM box meant that the design of the enclosure would have to depart from the box and lid type construction. It was also decided that, as far as possible, the filter should be free of any metal to metal contact to ensure repeatable, low-PIM performance.

4.8.1 Enclosure

It was decided that the filter enclosure would be machined from a solid block of material. Cylindrical holes were drilled in the block to accommodate the centre conductors. One hole, down the length of the block, forms the outer conductor of the main line. Five other holes were machined at right-angles to the main hole as shown in Fig.4.43 to take the resonators.

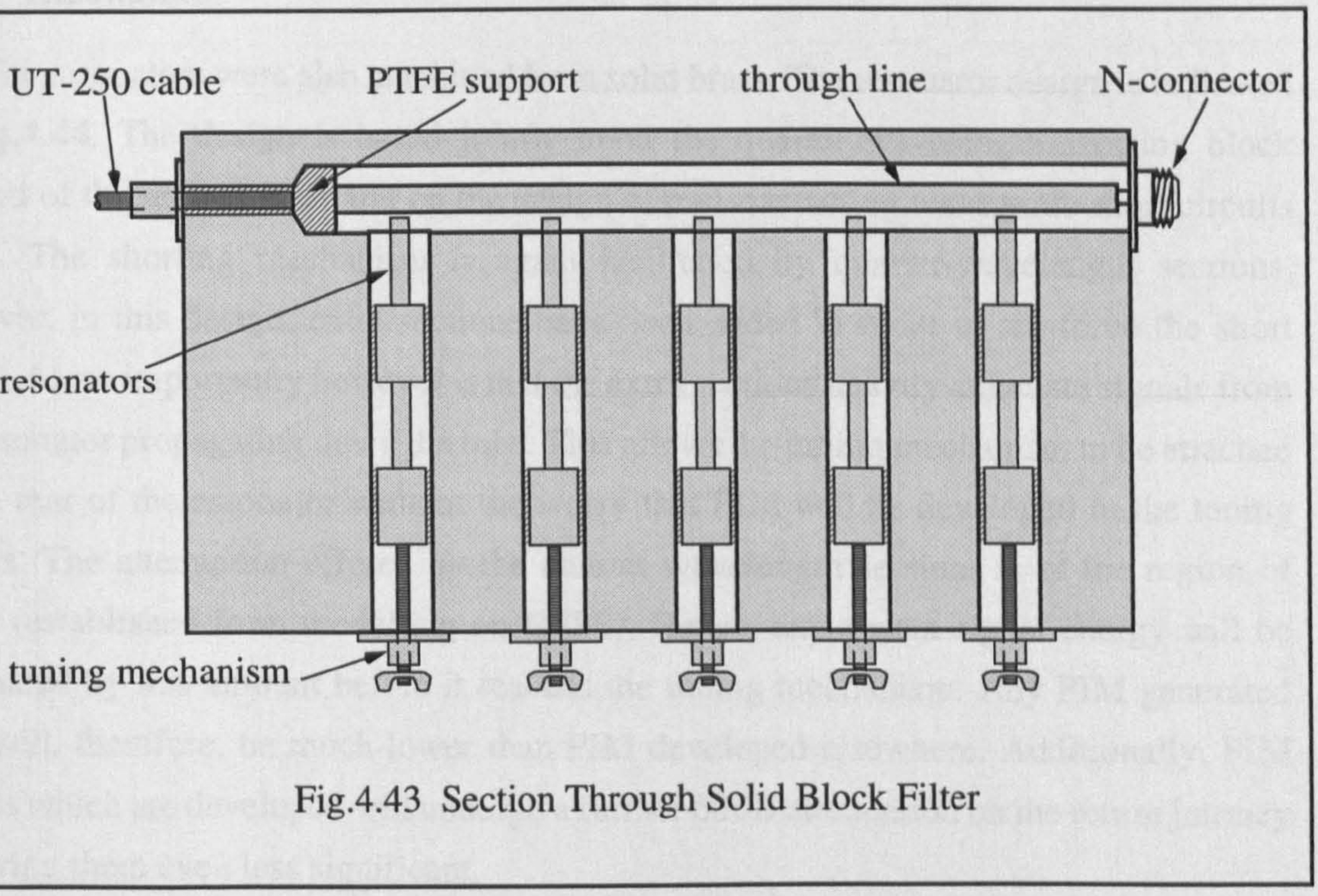

Fig.4.43 Section Through Solid Block Filter

The cylindrical holes meant that the new filter would depart from bar-line technology and use a coaxial system of conductors. This was not regarded as a disadvantage. In coaxial conductors, the currents and voltages are evenly spaced and symmetrical. In bar-line, the same fields tend to be concentrated at the corners resulting in slightly higher losses, less Q and less power handling capacity than a similar coaxial system [121],[124],[130]. The design of the coaxial lines was not a problem as the design formulae for coaxial transmission lines are well established.

The body of the filter was made from aluminium alloy. This was chosen principally because it is cheaper than the alternative of brass. It is also relatively lightweight and easy to machine. Additionally, there was no evidence to suggest that it's PIM performance was any worse than that of brass.

The through line was made of solid brass and designed to accept a low-PIM connector (see Section 4.3) at one end. A low-PIM connection was only deemed necessary at one end because the PIM rejection provided by the filter will heavily attenuate any PIM generated by the connector on the other end. It was also the case that it would have been difficult to implement a low-PIM connection at the other end due to the large diameter of the through hole. Instead, the other end of the line was fitted with a plain N-type connector. It should be emphasised that the filter must be connected in the correct manner with the low-PIM connector nearest to the test position. Otherwise, PIM generated by the N-type connector will interfere with measurements.

4.8.2 Resonators

The resonators were also machined from solid brass. The resonator design is indicated in Fig.4.44. The design is based jointly upon the quarter wavelength shorting block method of the second filter and on the design of non-contacting waveguide short circuits [110]. The shorting mechanism is again facilitated by quarter-wavelength sections, however, in this design, extra sections have been added in order to reinforce the short circuit. More importantly however is that the extra sections heavily attenuate signals from the resonator propagating down the tube. This allows the tuning mechanism to be attached to the rear of the resonator without the worry that PIM will be developed in the tuning screws. The attenuation offered by the quarter wavelength sections is of the region of 60dB (established from modelling on HFSS). Hence, any parent signal energy will be attenuated by this amount before it reaches the tuning mechanism. Any PIM generated here will, therefore, be much lower than PIM developed elsewhere. Additionally, PIM signals which are developed will undergo a further 60dB attenuation on the return journey rendering them even less significant.

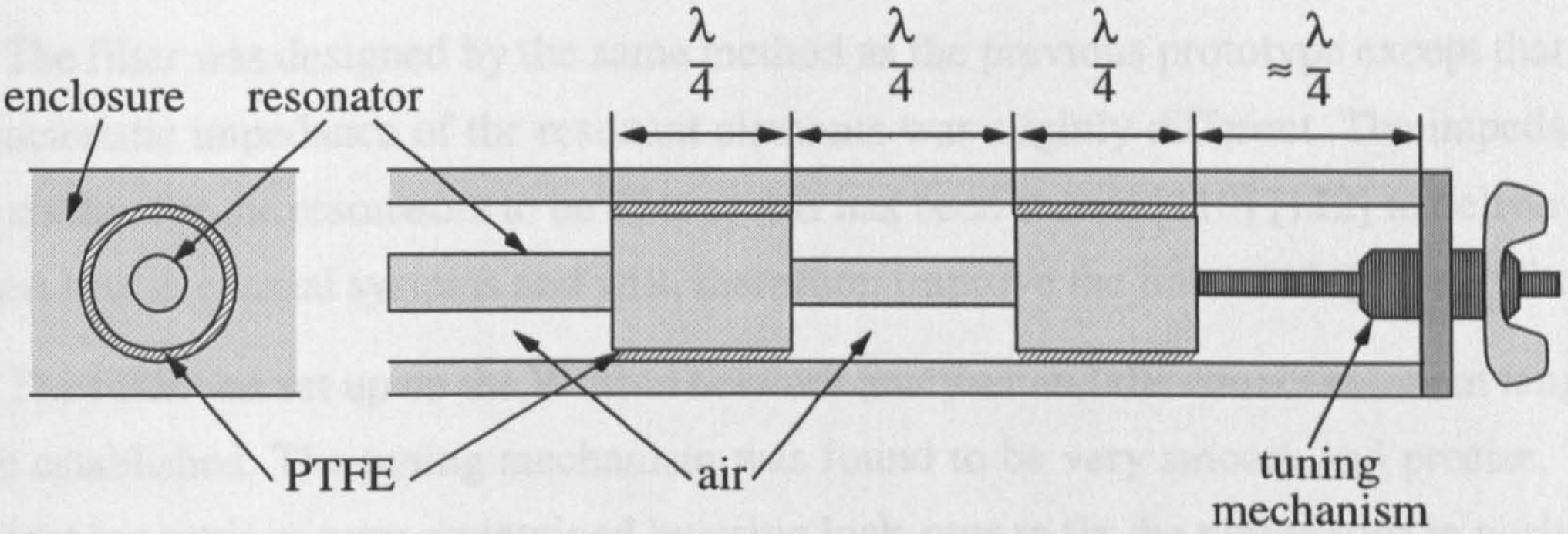

Fig.4.44 Two Stage Self-Shorting Resonator

4.8.3 Tuning Mechanism

Tuning is once again performed using the differential pitch tuning mechanism. The mechanism has been altered in this case and is indicated in Fig.4.45. A short length of M6 brass studding has an M4 hole cut straight through its centre. A length of M4 studding is screwed through the M6 studding and into the end of the resonator where it is fixed in place. A bush was made to fit over the hole on the side of the filter. The bush has an M6 threaded hole cut into it to take the section of M6 studding. The whole arrangement is fitted together as in the diagram. Two nuts are glued onto the exposed ends of the M4 and M6 sections. Fine linear tuning can now be effected by rotating the section of M6 studding inside the bush whilst holding the M4 studding to prevent the resonator from rotating.

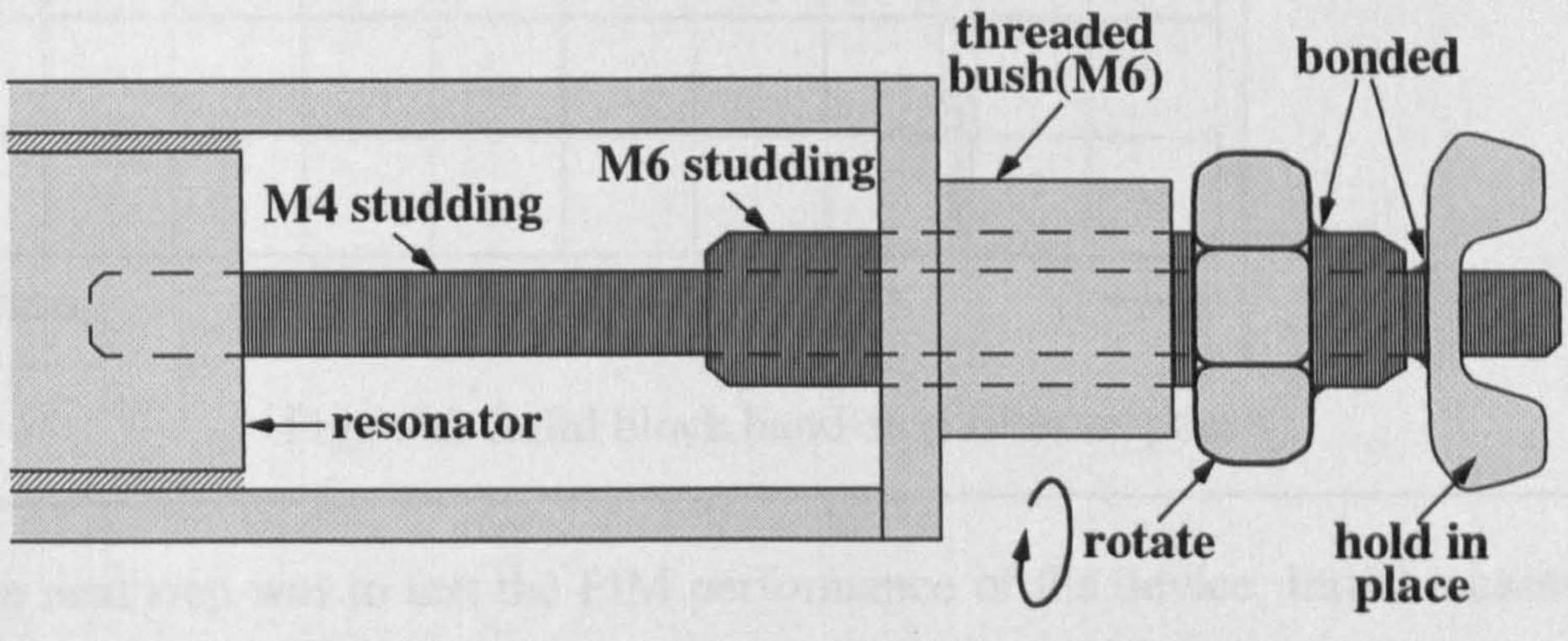

Fig.4.45 Tuning Mechanism

The system was designed so that the length of M4 studding inside the resonator was approximately λ/4 long at the resonant frequency. The studding acts like another section of high impedance transmission line and helps to reinforce the short circuit at the end of the resonator.

4.8.4 Performance

The filter was designed by the same method as the previous prototype except that the characteristic impedance of the resonant elements was slightly different. The impedance was chosen for the resonators to be 77Ω as this has been shown [110] [112] to deliver the lowest loss in coaxial systems and will, therefore, improve the unloaded Q of the filter.

The filter was set up on the Wiltron network analyser and the correct resonant lengths were established. The tuning mechanism was found to be very smooth and precise. The final tuning settings were maintained by using lock-nuts to fix the tuning rods in position. The overall electrical performance of the device was seen to be excellent. Fig.4.46 indicates the rejection offered by the device to be superior than any of the previous units.

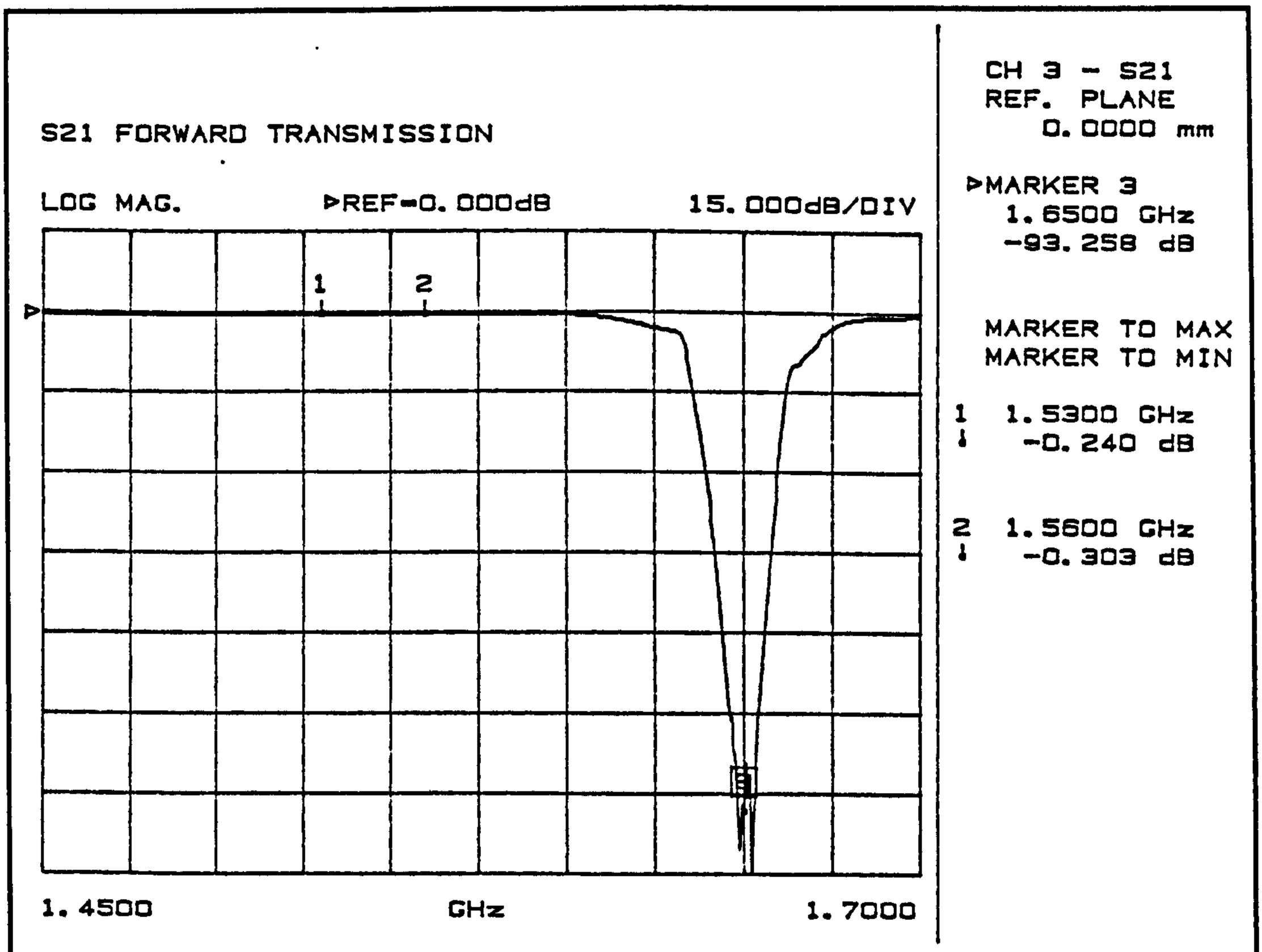

Fig.4.46 Solid block band-stop filter response.

The next step was to test the PIM performance of the device. Initial measurements indicated a decrease in the residual PIM of the system. However, the couplers used in the system began to dominate the PIM level and the true performance of the filter could not be determined. Eventually, however, when the final system was assembled, the filters were at least as good as the -154dBm residual level obtained for 2x25 Watt carriers.

4.9 Low PIM Coupler Implementation

4.9.1 Introduction

It has been mentioned in Section 3.5.2.2 that the commercial 3dB hybrid couplers used in the initial system configuration gave cause for concern over their PIM performance. Initial tests failed to indicate PIM generation from these devices, however, during the course of system development, the system sensitivity improved and the couplers were observed to increasingly dominate the levels of residual PIM.

Given the poor construction of the couplers in terms of PIM, it was decided to research alternative ways of implementing a low-PIM 3dB quadrature hybrid coupler. Like the filter, standard off-the-shelf components are not available with guaranteed low-PIM performance therefore the new couplers would have to be manufactured in-house.

4.9.1.1 Requirements of New Couplers

The requirements of any coupler employed in a PIM measurement system were identified and are listed below:

(i) The device should be low-PIM and not contribute significantly to the system residual level.

(ii) The coupler should have a well defined electrical response with minimal deviation from the nominal 3dB coupling and a 90° phase shift between output ports.

(iii) TEM line technology should be used in order to exploit the low-PIM techniques which have been developed.

(iv) The coupler must be capable of handling high power, at least 100Watts

(v) It must provide EMC integrity.

(vi) The design should be robust and be easily manufactured in a standard machine shop environment.

From a search of the literature, two very different structures were selected for investigation; the re-entrant cross section coupler and the branchline coupler [138 - 151]. Both couplers have a TEM mode structure and readily lend themselves to low-PIM implementation. Both are described in the following sections.

4.9.2 The Re-entrant, Broad Band, 3dB Coupler

4.9.2.1 Design

The re-entrant coupler uses a novel TEM-mode coupling cross section which has been patented by it's inventor, S.B Cohn [138]. A completely shielded version is shown in Fig.4.47.

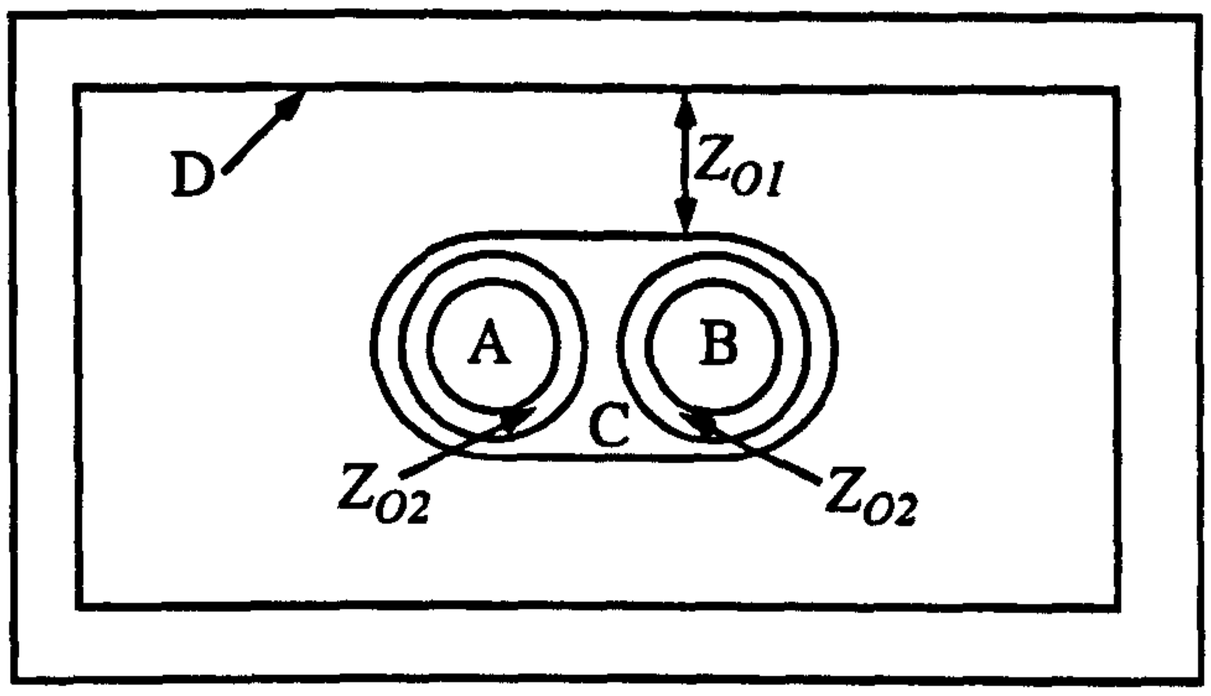

Fig.4.47 Re-entrant Coupled Cross Section

The attraction of the re-entrant coupling mechanism is that none of the inner conductors of the cross section are in contact with one another. This immediately rules out the likelihood of PIM problems due to junction phenomenon. The device also operates in the TEM mode and can be configured to take low-PIM connectors. Additionally, compared with other couplers, the structure is much more tolerant of manufacturing errors[138].

Consider two coaxial transmission lines placed side-by-side. Their inner conductors are entirely separate but their outer conductors touch and become conductor C. Conductor C is made a quarter-wavelength long and it's potential "floats" between that of the two conductors, A & B, and that of the metal case D. The characteristic impedance of C within D is denoted Z_{O1} and the two concentric lines within C each have the characteristic impedance Z_{O2}. An analysis by the classical even and odd-mode impedance method [139, 140] indicates that the coupling can be quite easily controlled by a judicious choice of Z_{O1} and Z_{O2}. The boundary conditions for the analysis are indicated in Fig.4.48.

For the odd mode, A & B, are at equal and opposite potentials and C, is at ground potential therefore the odd mode impedance, Z_{OO}, is:

$$Z_{OO} = Z_{O2} \qquad \text{Eq.4.64}$$

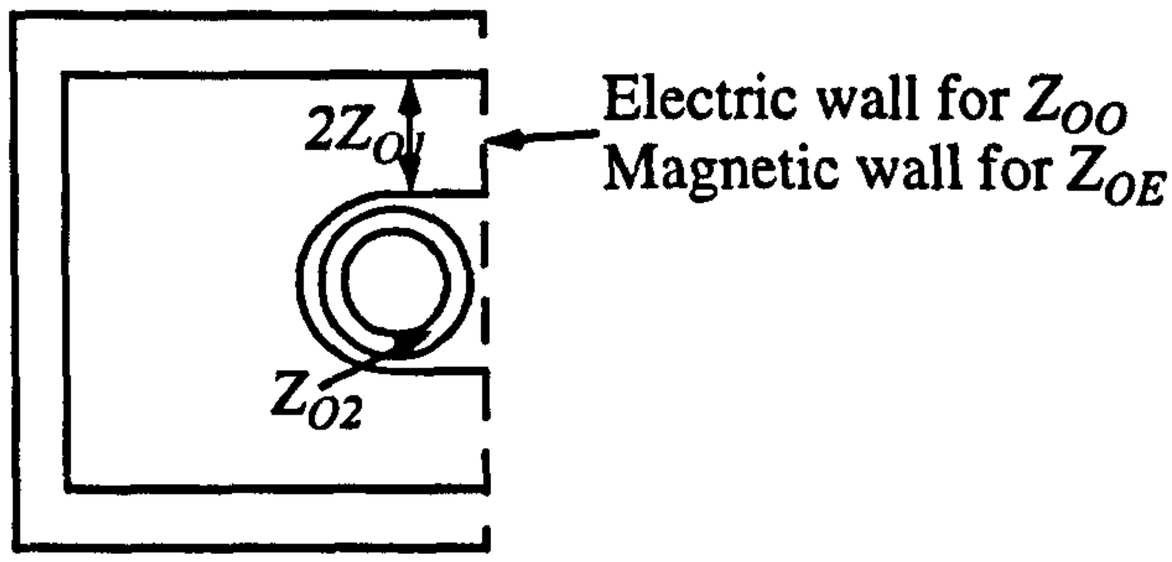

Fig.4.48 Boundary Conditions for Even- and Odd-modes

For the even mode, each inner coaxial line (A or B to C) is in series with half the outer line (C to D) because the floating conductor C, passes the currents flowing from its inner surface to its outer surface which is therefore in series with it hence:

$$Z_{OE} = Z_{O2} + 2Z_{O1} \qquad \text{Eq.4.65}$$

The coupling factor is given by the ratio of coupled voltage to incident voltage:

$$k = \frac{V_O}{V_i} = 10^{\left(\frac{\text{coupling in dB}}{20}\right)} \qquad \text{Eq.4.66}$$

For -3dB coupling Eq.4.66 gives k=0.708. Isolation and input match will be perfect when:

$$Z_O = \sqrt{Z_{OO} Z_{OE}} \qquad \text{Eq.4.67}$$

Where Z_O is the impedance of the terminating lines.

k is given as [138]:

$$k = \frac{Z_{OE} - Z_{OO}}{Z_{OE} + Z_{OO}} = \frac{Z_{O1}}{Z_{O1} + Z_{O2}} \qquad \text{Eq.4.68}$$

therefore, Z_{OE} and Z_{OO} may be determined by:

$$Z_{OE} = Z_O\sqrt{\frac{1+k}{1-k}} \qquad Z_{OO} = Z_O\sqrt{\frac{1-k}{1+k}} \qquad \text{Eq.4.69}$$

The necessary values of Z_{O1} and Z_{O2} are therefore:

$$Z_{O1} = \frac{1}{2}(Z_{Oe} - Z_{OO}) \qquad Z_{O2} = Z_{OO}$$
$$= Z_O\frac{k}{\sqrt{1-k^2}} \qquad = Z_O\sqrt{\frac{1-k}{1+k}} \qquad \text{Eq.4.70}$$

For the low-PIM coupler, a coupling factor of -2.8dB was specified to account for conductor losses so that k=0.724, Z_{O1}=52.545Ω and Z_{O2}=19.987Ω.

4.9.2.2 Implementation

A schematic of the final device is shown in Fig.4.49. The impedances Z_{O1} & Z_{O2} were calculated using standard formulae with air dielectric. The inner conductors were supported by thin (<0.1λ at f_{max}), close-fitting, PTFE beads (see Section 4.6.4.1). The conductors A & B were extended out from the ends of conductor C in order to accommodate λ/4, low-PIM, male connectors at either end. The extensions were designed to have an impedance of 50Ω in the PTFE dielectric and were also used to support the re-entrant section inside the cavity.

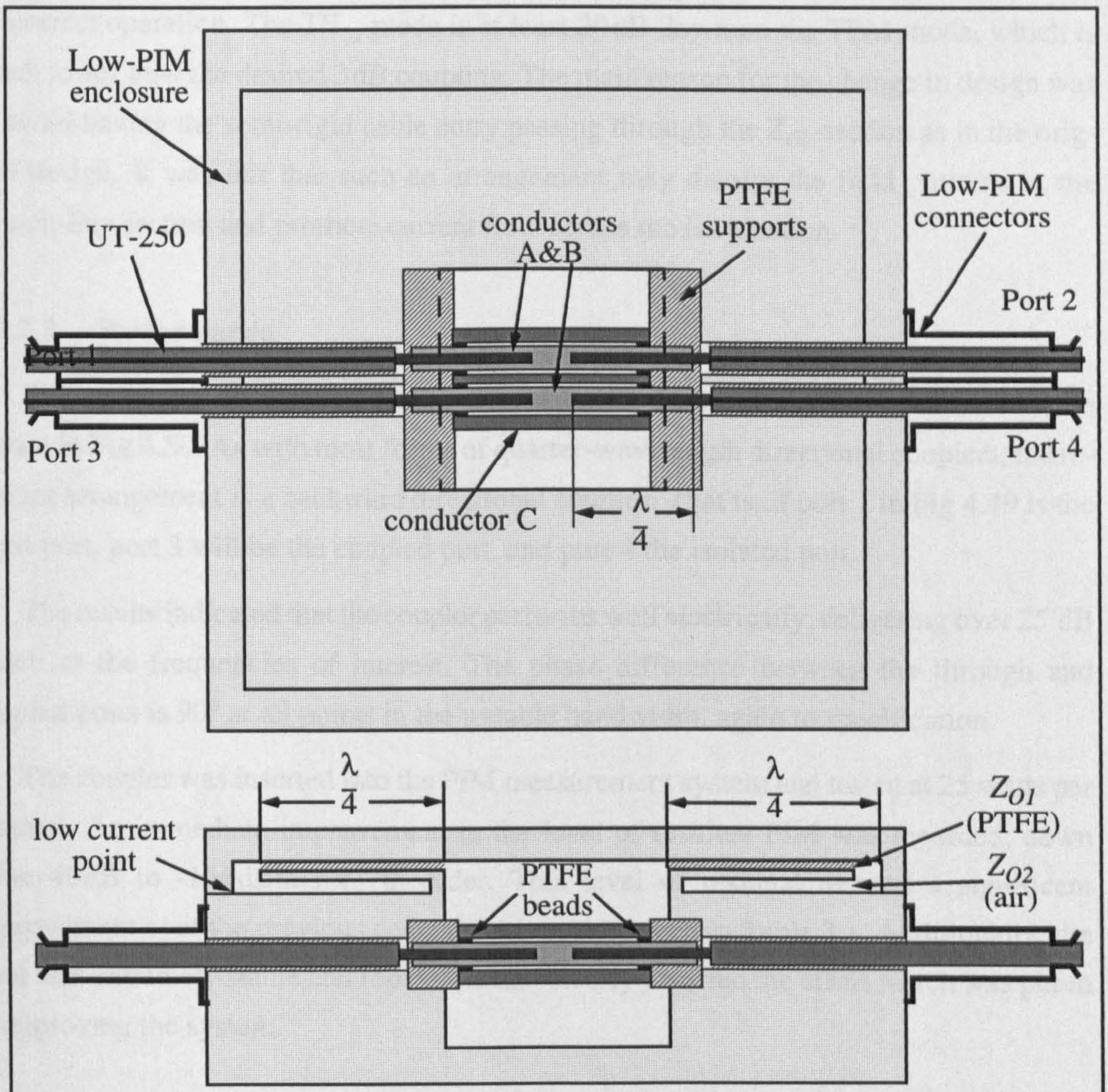

Fig.4.49 Re-entrant 3dB Coupler Implementation

Input and output lines were made low-PIM by using the connectors described in Section 4.3, and the whole device was housed in a low-PIM box to minimise PIM generation at the lid junction.

A slightly different approach was taken in implementing the contactless enclosure compared with that of the second band-stop filter prototype. Rather than have the channels arranged around the periphery of the enclosure, the double-choke section was folded back on itself as indicated in Fig.4.49 to effect the point of minimum current flow at the junction between the lid and the box. Impedance Z_{OI} is formed by applying PTFE tape to the top surface of the lid and forming a compression fit when the lid is tightened.

The configuration still remains vulnerable to over-moding, however, for the coupler, the levels of over-moding observed in the filter of Section 4.7.4 will pose little threat to its correct operation. The TE_{11} mode is at least 30dB down on the TEM mode, which is much lower than the desired 3dB coupling. The main reason for the change in design was to avoid having the semi-rigid cable entry passing through the Z_{O2} section as in the original design. It was felt that such an arrangement may disrupt the field patterns in the branch-line section and promote current flow across the lid junction.

4.9.2.3 Performance

The re-entrant coupler was characterised on the network analyser. The results are shown in Fig.4.50. As with most forms of quarter-wavelength directional couplers, the re-entrant arrangement is a backward directional coupler. That is, if port 1 in Fig.4.49 is the input port, port 3 will be the coupled port, and port 4 the isolated port.

The results indicated that the coupler performs well electrically, delivering over 25 dB match at the frequencies of interest. The phase difference between the through and coupled ports is 90° at all points in the useable bandwidth, again to specification.

The coupler was inserted into the PIM measurement system and tested at 25 watts per channel. An immediate improvement in the level of residual PIM was recorded, down some 40dB to -154dBm for 7th order. This level of residual marked a significant improvement over the previous coaxial systems described in Table 3.1. Additionally, the level was extremely stable and repeatable and clearly justified the effort which was put in to improving the system.

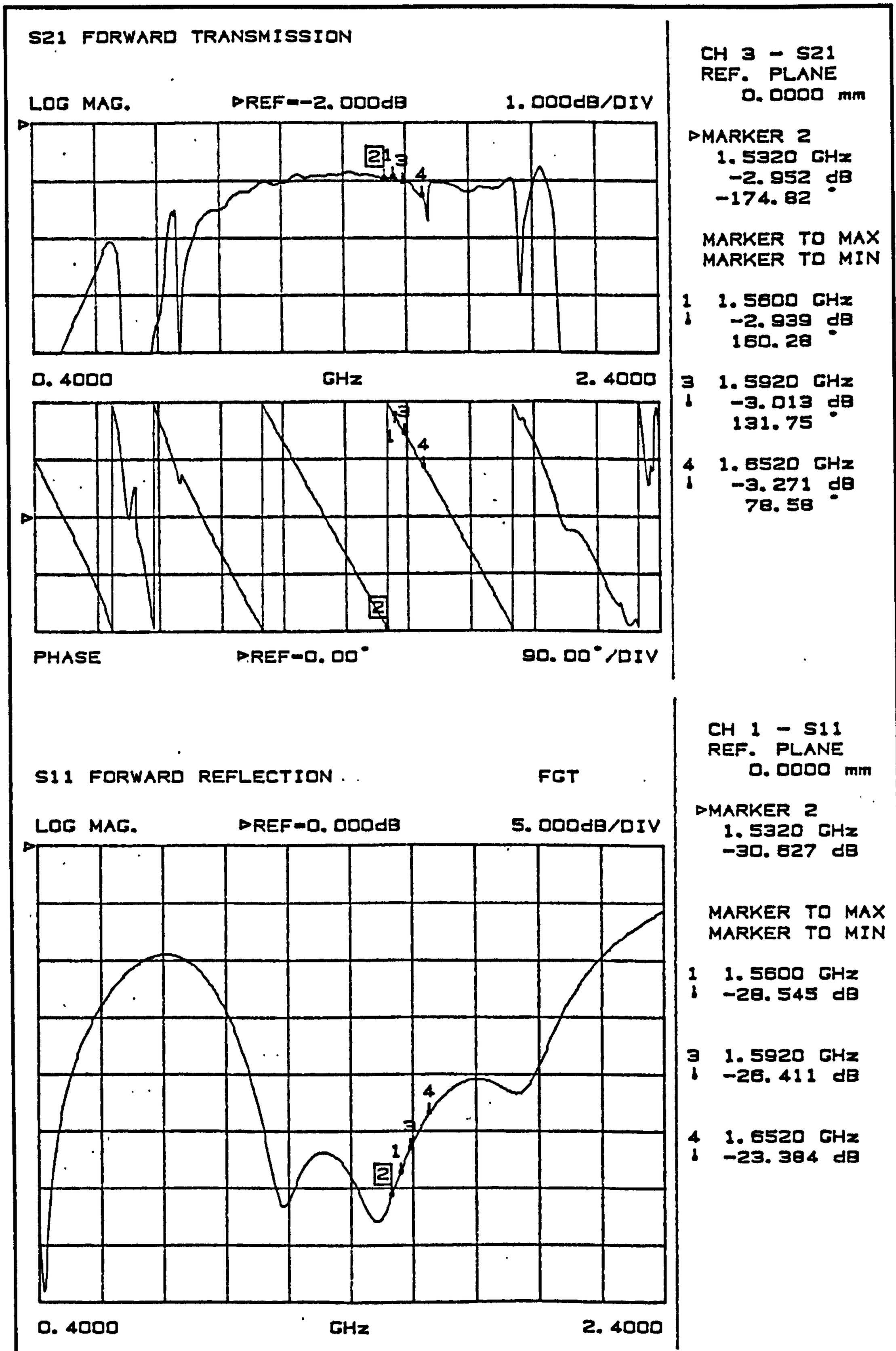

Fig.4.50 Re-entrant low-PIM coupler performance

4.9.3 The Branch-Line Hybrid Coupler

Whilst the design of the re-entrant coupler was in progress, a parallel study was made of the branchline coupler structure illustrated in Fig.4.51.

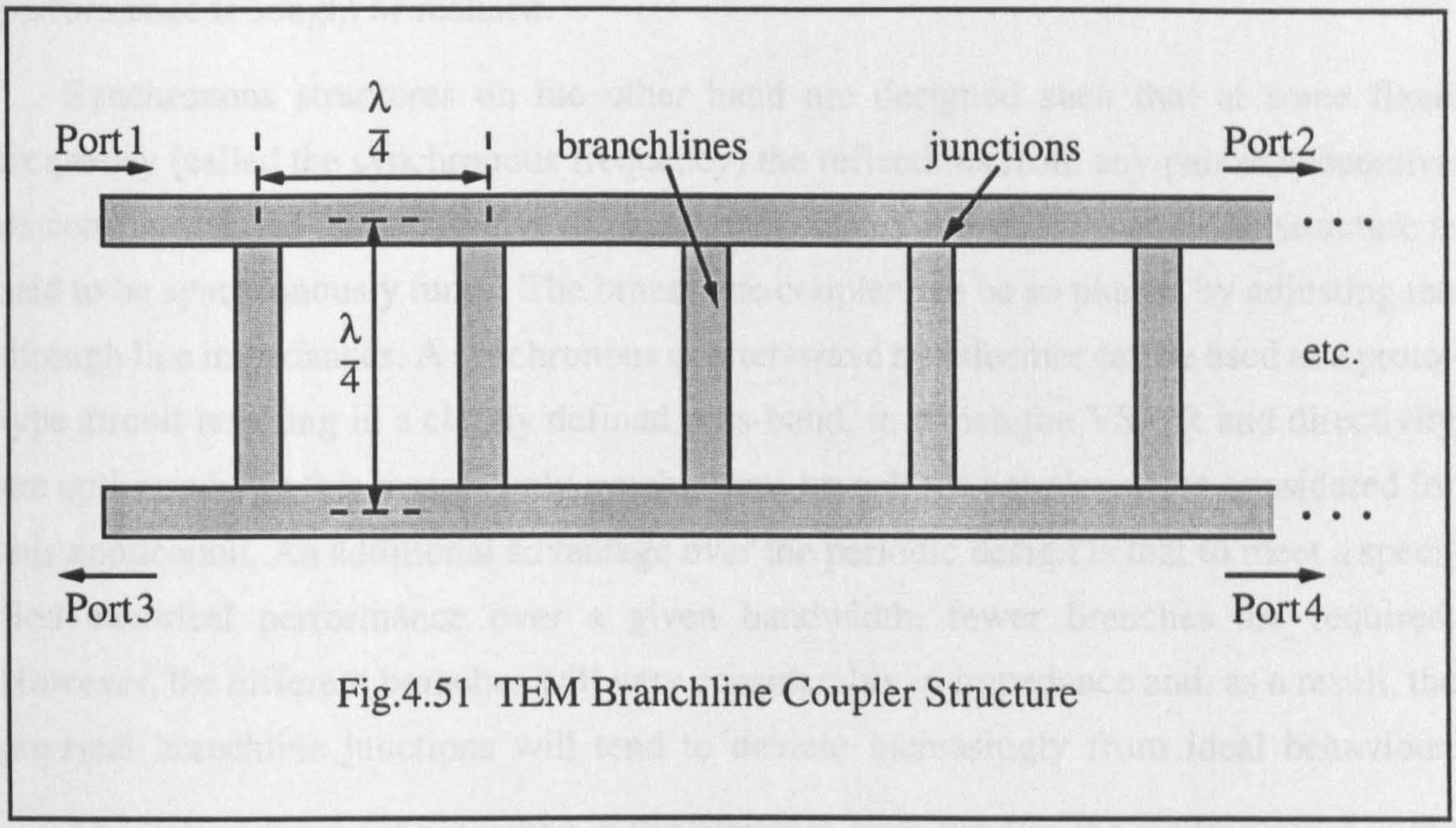

Fig.4.51 TEM Branchline Coupler Structure

Branchline couplers are directional couplers consisting of two parallel transmission lines coupled by a number of orthogonal branch lines. The lengths of the branch lines and their spacings are all one quarter-wavelength at the centre frequency. The characteristic impedances of the two parallel main lines may be changed from section to section and the branch impedances may also be adjusted, in order to define the electrical performance.

The branchline coupler is suitable for low PIM applications because the centre conductor can be made in a one-piece bar-line construction with no metal-metal junctions. This structure is also appealing as it exhibits forward coupling. i.e. if port 1 of Fig.4.51 is the input port, the coupled port will be port 4 and the isolated port will be port 3. This leads to more compact circuit layout and reduces cabling requirements.

Initially, it was also thought that the design of such couplers was relatively simple. However, it will be shown in this section that this is far from being the case.

Numerous literature has been published on the design of branchline couplers [140-151] and many tables have been produced for determining the correct line impedances to implement a wide range of generalized coupler responses.

There are essentially two main types of branchline coupler; the periodic coupler and the synchronous coupler. Transmission lines that are periodically loaded with identical obstacles are referred to as periodic structures. In the case of branchline couplers the obstacles are the branchline junctions. A periodic branchline coupler has uniform imped-

ance through-lines and all the interior branchlines are the same. Such couplers have some of the advantages and disadvantages of periodic structures; they are simpler to construct than less regular structures, but they have no clearly defined pass-band in which optimum performance is sought or realised.

Synchronous structures on the other hand are designed such that at some fixed frequency (called the synchronous frequency) the reflections from any pair of successive discontinuities, are phased to give the maximum cancellation. In this state the structure is said to be synchronously tuned. The branchline coupler can be so phased by adjusting the through line impedances. A synchronous quarter-wave transformer can be used as a prototype circuit resulting in a clearly defined pass-band, in which the VSWR and directivity are optimised. For this reason, only synchronous branchline couplers were considered for this application. An additional advantage over the periodic design is that to meet a specified electrical performance over a given bandwidth, fewer branches are required. However, the different branches will vary considerably in impedance and, as a result, the physical branchline junctions will tend to deviate increasingly from ideal behaviour.

The design formulas presented in the literature were used as the starting point in the design of an L-band coupler for use in the PIM system. The data presented in the literature is optimised for only a limited number of bandwidths and coupling factors. As such, a design based on this data is not necessarily optimised for a particular application.

In accordance with the system specification, the device should deliver 3 dB coupling over an effective bandwidth of 1.55 GHz to 1.65 GHz, centred on 1.6 GHz, or 6.25% of f_O. This covers the parent signals of the L-band measurement system and up to the 7th order PIM product. The return loss was specified to be better than 30 dB across the band. It was decided to fully optimise the coupler design to deliver the exact specification. This was carried out using the MDS microwave circuit simulator, described in Section 4.2.1.2.

As a first approximation, a coupler was designed using the data in the paper by Levy and Lind [142]. Table II in the paper indicates that the desired response could be met by a coupler with three branchlines. However, the minimum bandwidth that can be achieved using the given data is 20% of the centre frequency, f_O. This is clearly much more than required. The design was entered into the MDS program and the impedance values were adjusted to give a response which more closely matched the desired specification. The final impedance values and the simulated response are indicated in Fig.4.52.

The network simulation results from the program give precise results for idealized components only. This assumes that the junctions between transmission lines are perfect and that the only mis-match at these junctions is due to the different impedances of the

adjoining lines. However, it has been well documented that, far from exhibiting ideal behaviour, physical junctions in transmission lines are highly influenced by localised field distortion and can behave very different to the ideal case[152-168].

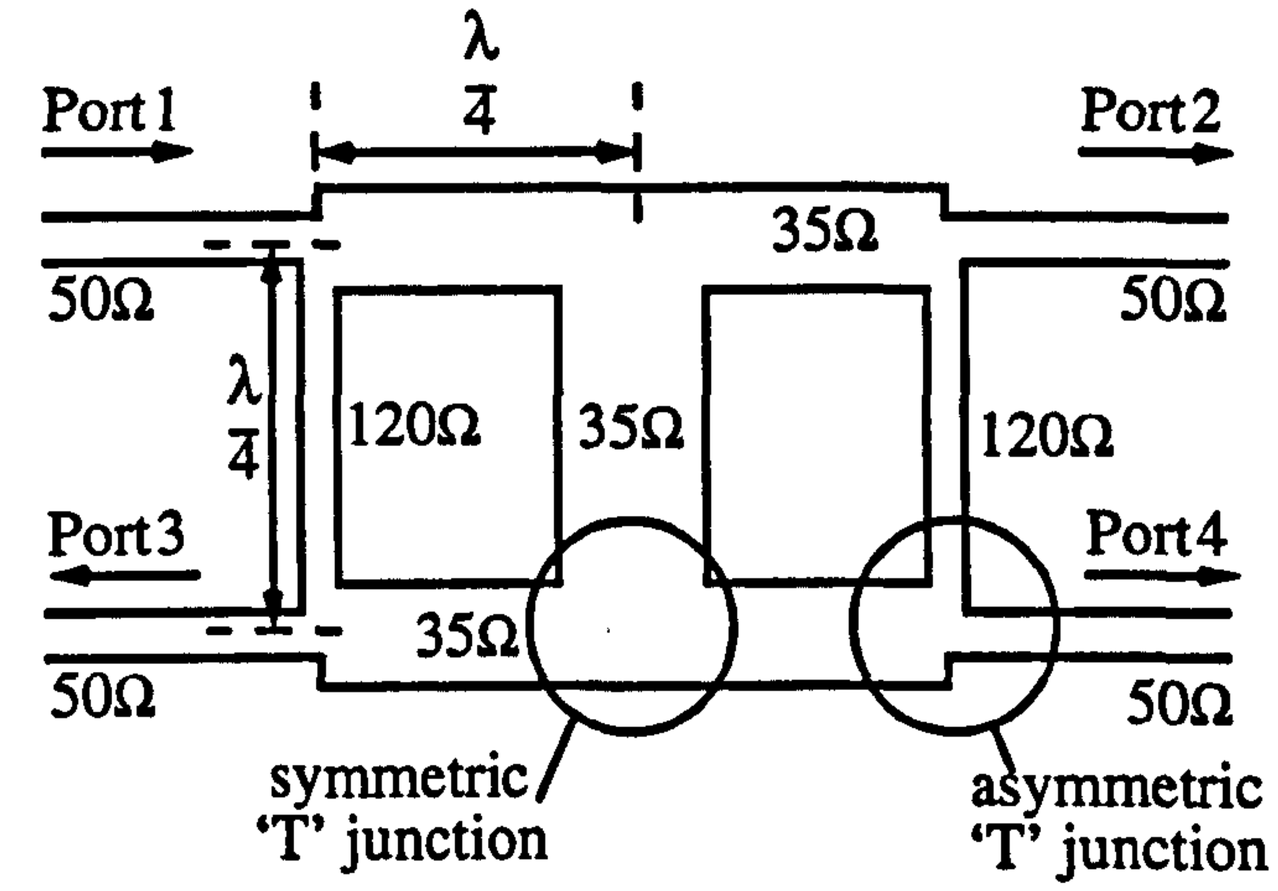

(a) Impedances

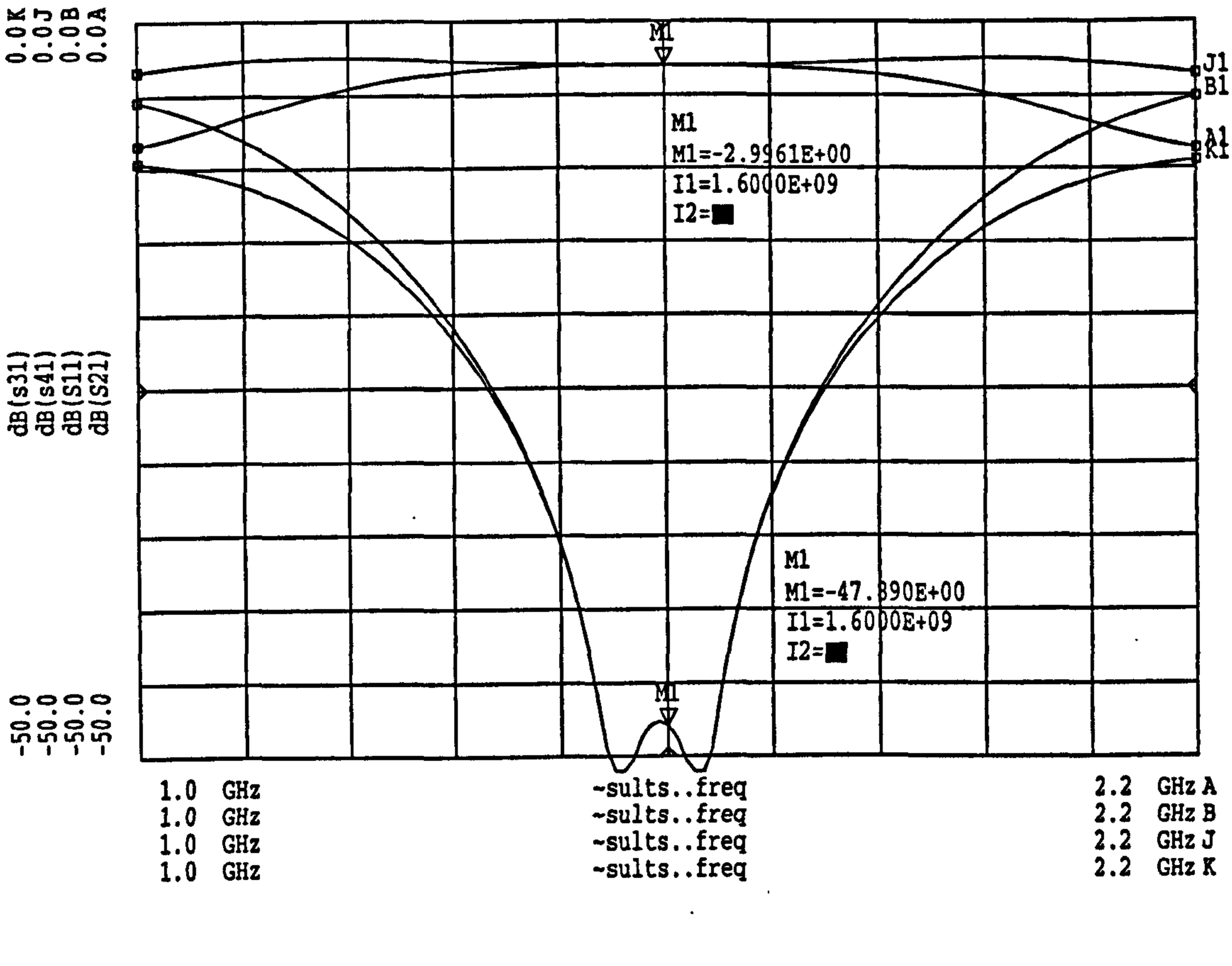

(b) Ideal Response

Fig.4.52 L-band Branchline Coupler Design

By the same reasoning that led Whinnery and Robbins to postulate the existence of higher-order modes at the discontinuities in coaxial lines (see Section 4.4.2 and refs. [114, 115]), it is accepted, that in the close vicinity of a transmission line "T" junction, there also exists field distortion which can be considered as a superposition of higher-order modes. The effect is particularly pronounced in bar-line structures where the significant centre conductor thicknesses readily lend themselves to the establishment of fringing fields at junctions as illustrated in Fig.4.53.

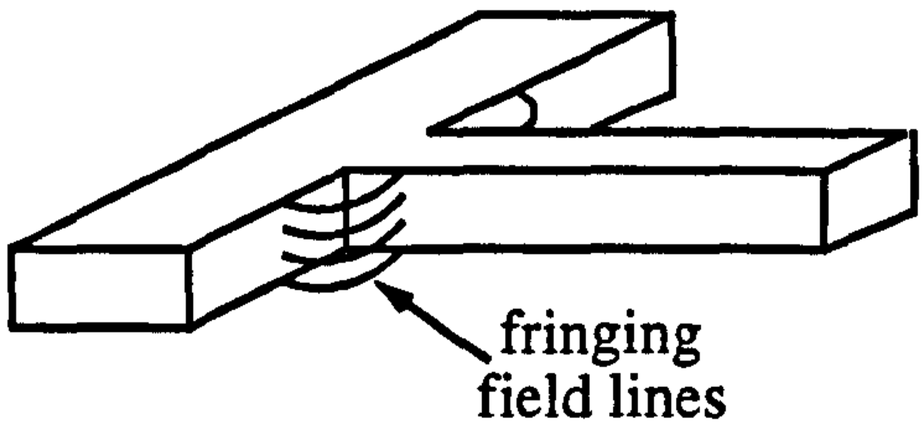

Fig.4.53 T-Junction Fringing Fields

Another factor in the design of practical junctions is the path length of a signal passing through the junction. Fig.4.54 indicates the position of the reference planes of an ideal junction from where ideal $\lambda/4$ joining lines are measured. It is obvious, however, that physical signals will not trace such a regular path but will tend to take a shorter route through the junction, as indicated. The physical reference panes are therefore seen to be displaced from the ideal planes by a small distance.

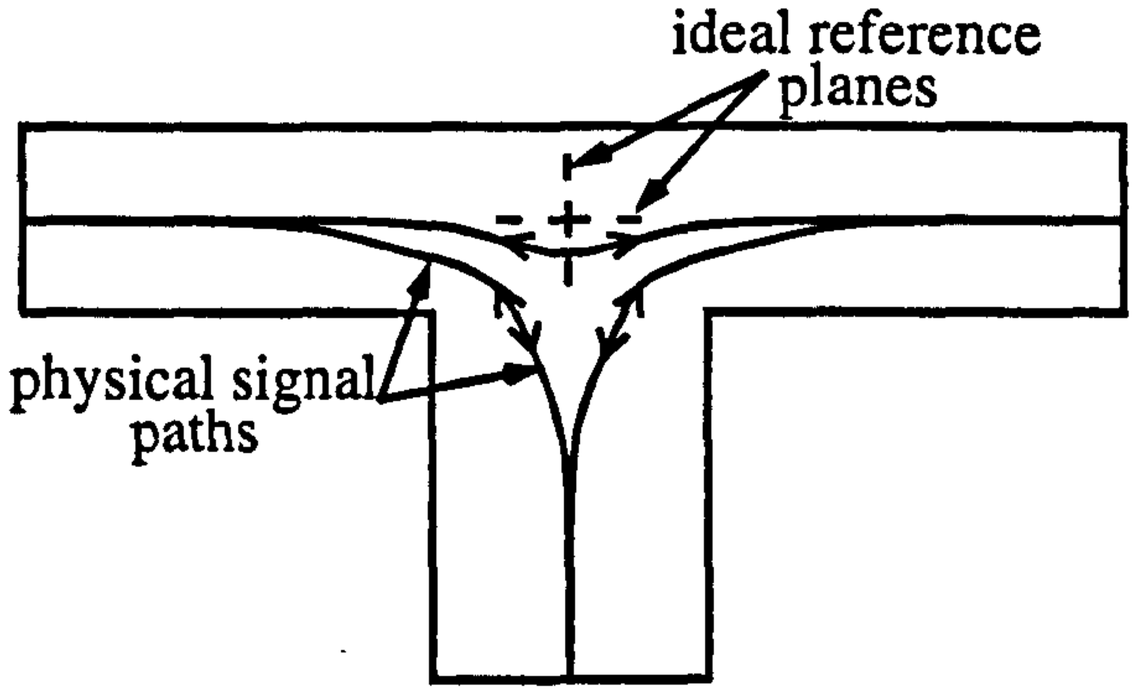

Fig.4.54 Reference Plane Location

These physical effects must be included in the design of any component or device having such junctions in order for the device to behave as desired. To this end, a great deal of material has been published on the modelling of these physical effects with the object of providing hard-data for use in improving design accuracy [152-168]. The results are, however, rather limited in their use. The vast majority of research has been conducted into

thin strip-line and microstrip structures where it is assumed that the centre conductor is thin enough to be of little or no significance. For these structures, junction dimensions at frequencies below 1 or 2GHz are generally very small compared to a wavelength and the discontinuity effects are negligible. Data also exists for waveguide junctions [169] where it is shown that if the if the waveguide heights are small compared with a wavelength then, again, junction effects are negligible. It has also been shown that in cases where stripline or waveguide discontinuities *are* significant then the published data can be used to predict the behaviour of the junction, therefore, components containing such junctions can be designed more accurately.

In bar-line, any impedance (within reason) may be implemented in an almost infinite number of ways depending upon line thickness, line width and ground plane spacing. Such versatility is a key feature of bar-line technology but makes the modelling problem much more complex. Since each impedance can be implemented in a large number of different physical configurations, it is evident that junctions in bar-line and their associated parameters can also take on a large number of different implementations. Bearing this in mind, it is not surprising to find that most of the work published on bar-line 'T' junctions deals with the techniques used to calculate discontinuity parameters rather than providing data on the actual parameters of particular junction implementations[160-168]. A large amount of the published work is theoretical and describes complex field analysis techniques which are outwith the scope of this project. It was therefore decided to look more closely at the modelling process and determine an alternative method of solving the problem.

4.9.3.1 'T' Junction Modelling

In general, the properties of a three-port network can be characterised by an impedance matrix of order 3x3 [170]. The nine complex numbers relate the amplitude and phase of the input and output signals of a given pair of ports. However, for reciprocal, lossless networks, $Z_{ij}=Z_{ji}$ and only six complex numbers are required to define a three-port network. Accordingly, in order to completely and accurately define a three-port 'T' junction at any given frequency, a model must contain six independent parameters. A standard model for a 'T' junction is illustrated in Fig.4.55 where the six variables are l_1, l_2, l_3, n_1, n_2 and C. The impedances Z_1, Z_2 and Z_3 are the same as the respective port impedances to which the 'T' is connected.

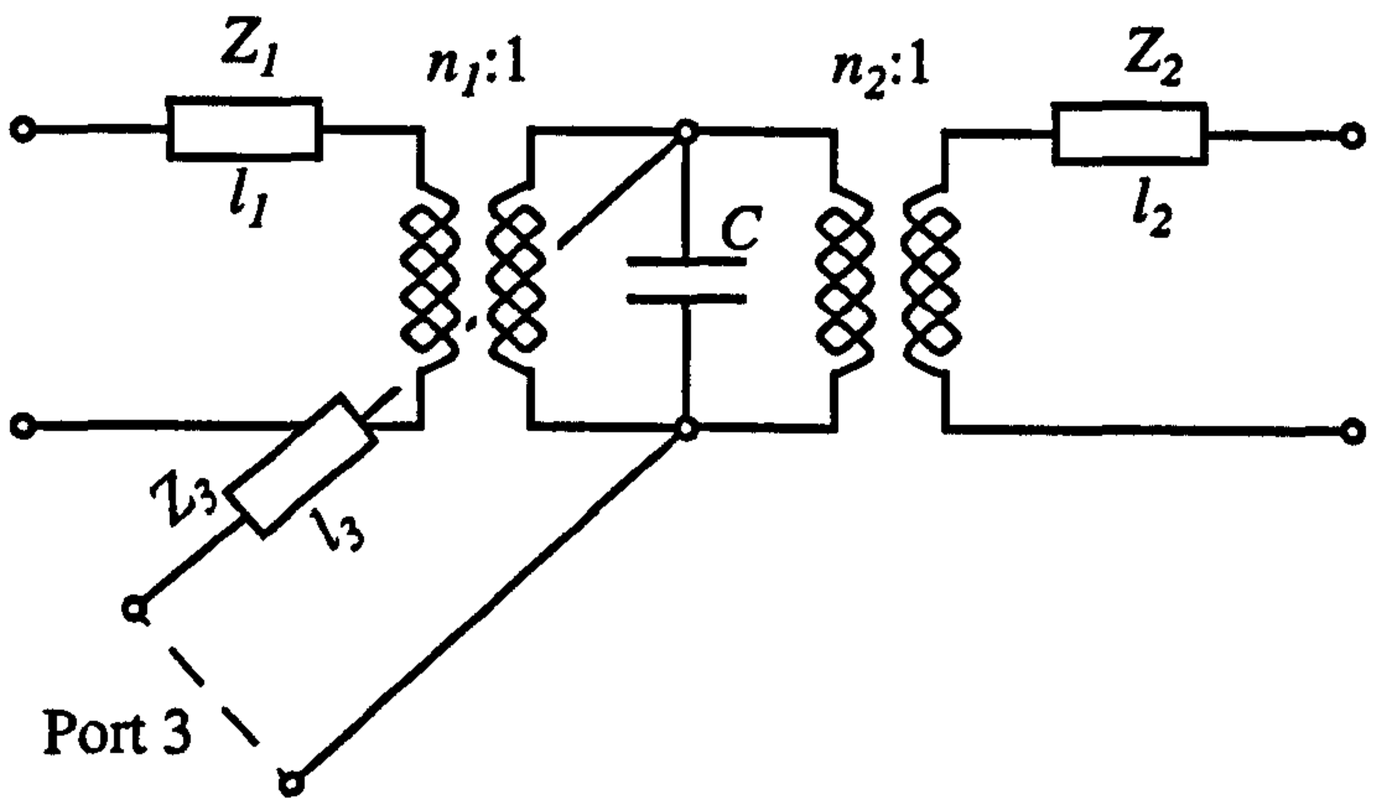

Fig.4.55 Ideal, six parameter, 'T' junction model

It is often the case that $Z_1=Z_2$. This allows the model of Fig.4.55 to be simplified to that of Fig.4.56. Such junctions are called symmetrical 'T' junctions for obvious reasons and require that only 5 parameters be defined. Where all of the arms of the 'T' have different impedances the junction is said to be asymmetric.

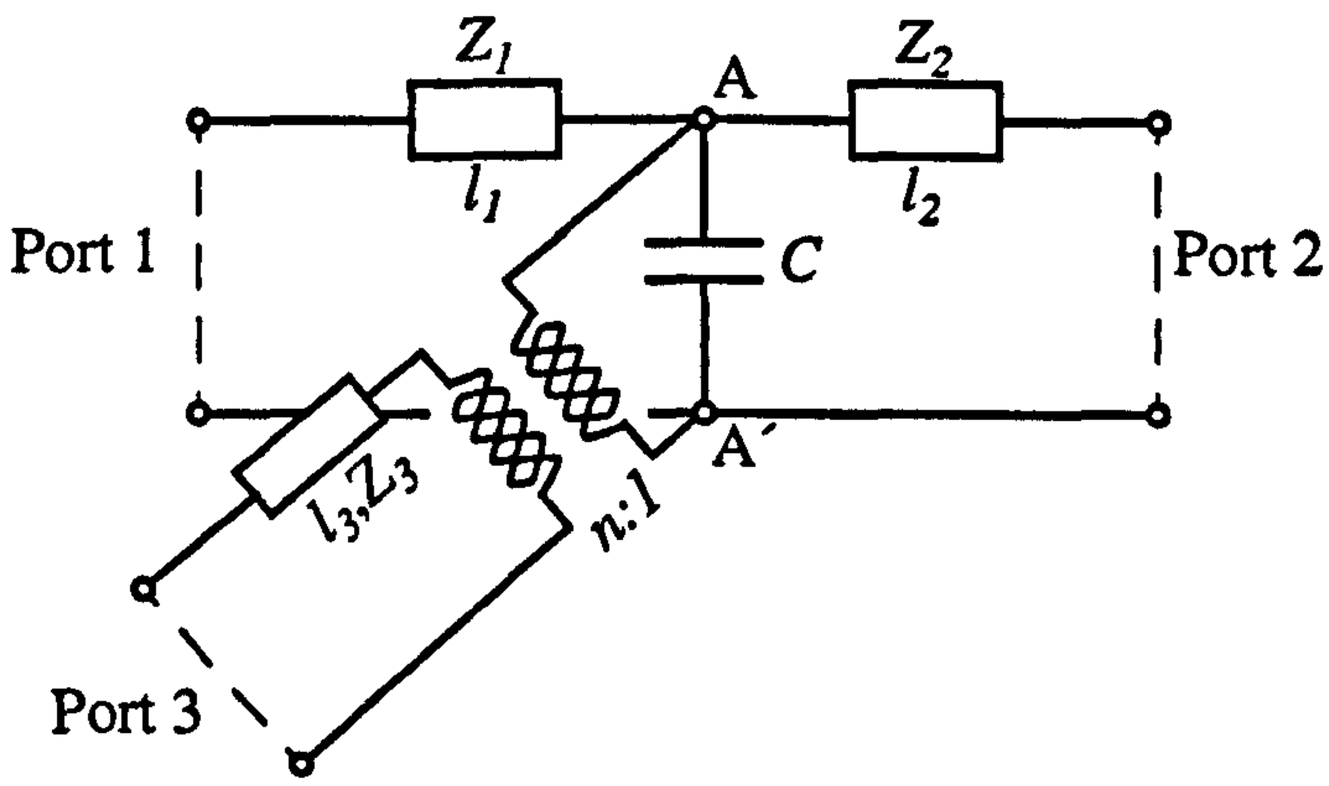

Fig.4.56 Five parameter, symmetrical 'T' junction model

The problem with branchline couplers is that there are potentially many different 'T'-junction configurations. In the three-branch synchronous coupler, there are two different junction configurations. Two identical symmetric junctions and four identical asymmetric junctions as indicated in Fig.4.52(a). In order for the coupler to function properly, there must be a degree of consistency in the electrical performance of the junctions, and their models.

For instance, consider the length l_3 in the models which represents the reference plane offset of the branchline. In a physical coupler it would be very difficult to make the lengths of the of the branches different from each other due to the mechanical constraints in machining the device. This suggests that the *physical* branchline lengths should be the same. Also, given that the electrical lengths of all lines in the coupler are $\lambda/4$ at the centre frequency, then the *electrical* length of the branch lines should also be the same. Hence, if there is a significant difference in l_3 between the two junction models, the response of the final coupler will be compromised.

In addition, consider the model of Fig.4.55. If this model were to be used for all of the junctions, then the turns ratios of the ideal transformers in the through lines would have to be consistent. If the transformer ratios for successive junctions were different, then each junction would 'see' a different value of impedance for the through lines. For the coupler to function properly, the impedance seen by each junction should be the same. Additionally, having a transformer in the 50Ω feed arms of the network would mean that the physical impedance of the feed lines would have to deviate from the nominal 50Ω in order for the junction and its transformer to 'see' 50Ω. This would require additional impedance transformers in all four feed lines to maintain compatibility with the rest of the system.

The discontinuity capacitances also have to be identical at each junction in order to give a perfect match. In the branchline coupler junctions are spaced a quarter wavelength apart electrically. Thus when the two capacitances are equal the resulting reflected signals will cancel each other out. Failing this, the capacitances should be made as small as possible so that their effects are minimised.

In order to promote consistency between the two different junctions, it was decided to model both junctions using the circuit of Fig.4.56. This model is accurate for the symmetric 'T' junction but not so for the asymmetric 'T' junction.

The transformer turns ratio in the branchline represents the high frequency effect of a load connected to the shunt branch arm. At very low frequencies any such load will appear directly connected across the through line, i.e. when $f \rightarrow 0$, $n \rightarrow 1$.

At microwave frequencies a load connected at some point along the shunt branch will appear transformed by the ration $1/n^2$. For an asymmetric 'T' junction the different through line impedances will not be related to the branchline impedance by the same ratio. However, in this particular case, the branchline impedance is very high, hence, its cross-sectional centre conductor dimensions are small compared with the mid-band wavelength. Consequently, it was thought that the field perturbation would be small and that the model would be a good approximation. However, some compromise in accuracy was expected.

The question now arises of how to determine the parameters of a specific junction in order that they may be optimised and taken into account in the final design. The two methods generally used to determine the junction parameters are by physical measurement of actual prototype junctions or by field analysis computation.

The physical measurement technique yields relatively accurate results because there are no approximations involved, although some degree of experimental error must be assumed. There are however some more serious drawbacks to the experimental approach.

a) The design process for establishing the correct junction configuration is iterative. After each test, the junctions will have to be compared with each other, modifications made and more tests carried out. The test procedure will have to be repeated many times until the combination of physical structure and model parameters yields a junction which delivers the desired performance. Each iteration will involve the manufacture of new tees and this can make the whole process time consuming and laborious.

b) The measurement procedure is not straight forward. Many measurements have to be made on each junction in order to characterize it completely. Use of the results is complicated further by the fact that the junctions involve transmission lines whose impedance can deviate significantly from 50Ω. Most measurement systems and equipment use a 50Ω impedance standard therefore the mismatch due to the different impedances must also be taken into account during calculations.

On the other hand, data on theoretical field analysis is sparse and the subject matter complex. The methods described in the literature have taken teams of researchers years to develop and could not be repeated within the time-scale of this project [160-168].

In the end it was decided to use the HFSS program described in Section 4.2.1.1. First the physical junction structures are drawn on HFSS which then performs a computationally intensive analysis of the structure and delivers the results in the form of S-parameters. These results can then be imported into a standard linear network simulator such as the MDS package mentioned in Section 4.2.1.2. Here, ideal lengths of line and ideal terminations may be added to the ports of the tee. Simulated experiments can then be performed, using the HFSS results, to determine the junction model parameters.

The experimental determination of the $\frac{N(N+1)}{2}$ network parameters, that characterise an N terminal junction, involves the placement of known impedances at N-1 "output" terminals and measurement of the resulting impedance at the remaining input terminal [170]. Input impedance measurements must be performed for $\frac{N(N+1)}{2}$ arbitrary but independent sets of output terminations. The determination of the network

parameters from these measurements can be considerably simplified by a judicious choice and placement of the output impedances. A variable length of short circuited line provides a convenient way of setting the output impedance.

For example, consider the equivalent circuit of Fig.4.56 which has been chosen to represent the 'T' junctions. The first step is to determine the reference plane offset length at each port. This is necessary so that these lengths may be taken into account when setting the length of the ideal short circuited lines to provide known terminating impedances. The lengths can easily be determined if we consider that the input impedance of a transmission line repeats itself every half-wavelength, therefore, the input impedance to a $\lambda/2$ shorted line is zero. If this is connected across a junction, the junction is shorted and no transmission will take place between the remaining lines. Therefore, if we place an ideal short on each port in turn, transmission between the other two ports will be observed to be a minimum when the line is electrically $\lambda/2$ long from the junction reference plane. The length of the short is varied until the minimum coincides with the centre frequency of the band of interest. Comparing this length with the physical length of a $\lambda/2$ line will give the reference plane offset for the port which is terminated in the short circuit.

The reference plane information can then be used to calculate the shunt capacitance. Short circuited lines are placed on two branches of the junction and set to be electrically $\lambda/4$ from the junction reference plane. The short circuits will then be transformed to open circuits at the plane of the junction and will be in parallel with the shunt suceptance at the junction. Hence, the remaining line only sees the shunt suceptance. If the remaining line is made $\lambda/2$ long (remembering to take the offset length into account) the shunt suceptance will be transformed to the input port and can simply be read off there.

All that remains is the calculation of n, the transformer turns ratio. This is obtained from a knowledge of the other parameter values and by using them to effect known impedances at the reference plane of the junction. Consider the 'T' model of Fig.4.56. The transformed impedance of the orthogonal branch-line, at the plane AA´ is determined by:

$$Z_{in} = \left(\frac{N_1}{N_2}\right)^2 \cdot Z_L \qquad \text{Eq.4.71}$$

Where N_1 and N_2 are the primary and secondary turns ratios respectively. In this case N_1=1 and N_2=n, hence:

$$Z_{in} = \frac{Z_L}{n^2} \qquad \text{or;} \qquad Y_{in} = n^2 \cdot Y_L \qquad \text{Eq.4.72}$$

Now, the input is nominated as being at one of the other ports, say port 1 for example. With known loads at plane AA′ (taking l_1, l_2, l_3 and C into account), we can readily obtain an expression for n as follows:

(i) First make the feed line from port 1 to the junction $\lambda/2$ long electrically, i.e. taking the offset l_1 into consideration. Due to impedance transformation, the input impedance registered at port 1 will be exactly the same as the impedance at the plane of the junction AA′.

(ii) To effect a "known" impedance at plane AA′ from port 2, a $3\lambda/8$ long (electrically), shorted transmission line of impedance Z_2 is added. Now the input impedance to a $3\lambda/8$ length of shorted line is given from Eq.4.1 as:

$$Z_{in} = jZ_{O2} \cdot tan\beta l \qquad \text{Eq.4.73}$$

Now, $\beta = \frac{2\pi}{\lambda}$ and $l = \frac{3\lambda}{8}$, therefore $\beta l = \frac{3\pi}{4}$ and:

$$Z_{in} = -jZ_{O2} \qquad \text{and} \qquad Y_{in} = jY_{O2} \qquad \text{Eq.4.74}$$

(iii) Similarly, if a $5\lambda/8$ long length of shorted line were attached to port 3 with an impedance of Z_{O3}, the input impedance would be:

$$\begin{aligned} Z_{in} &= \left(\frac{1}{n^2}\right) \cdot jZ_{O3} \cdot tan\beta l \\ &= j\frac{n^2}{Z_{O3}} \qquad \text{Eq.4.75} \\ \text{and } Y_{in} &= -jn^2 Y_{O3} \end{aligned}$$

(iv) Now if we remember to take the discontinuity capacitance into account we can write an equation for the now simple parallel network in terms of only one unknown variable, n:

$$Y_{in} = j(B_D + Y_{O2} - n^2 Y_{O3}) \qquad \text{Eq.4.76}$$

Hence we can establish all of the required junction parameters in order to be able model the physical 'Tee' junctions and design an optimised branch-line coupler.

4.9.3.2 Practical Branchline Coupler Design

The specification and ideal impedance levels for the 3 dB coupler were established in Section 4.9.3. The next step is to determine the physical dimensions of the coupler which will deliver the specification.

The coupler was cut from one piece of metal to form a bar-line structure. The first stage was to determine the cross section of the bar-line which would be used. The main problem with the design of tightly coupled synchronous couplers is the range of impedances which have to be realised. The outer branches are 120Ω whilst the inner branches are 35Ω. This means that for a given ground plate separation and conductor thickness, the width of the lines will be hugely different. The high impedance lines will be very narrow whilst the low impedance line will be very wide. A balance must be struck between making the low impedance line narrow enough to avoid over-moding and large discontinuities (which it may not be possible to compensate effectively), and making the high impedance line wide enough to be practically fabricated in a workshop environment.

One way around this problem is to have lines of different thickness. For a fixed impedance and ground plane spacing, the width of a bar-line will get narrower if the thickness is increased whilst the width will get larger if the thickness is reduced.

In this case, the centre conductor thickness for all but the high impedance lines was specified as being 6.35mm (1/4") thick as this size material is readily available from suppliers and minimises machining.

The ground plane spacing was then calculated to give practical widths for the low-impedance lines using data from the literature [116]. In this case a spacing of 14mm was chosen to give line widths of 6.84mm (50Ω), and 13.06mm (35Ω). The next step was to establish a width and thickness for the high impedance lines so that they could be easily fabricated. With the ground spacing maintained at 14mm the dimensions required for a 120Ω line were chosen to be a width of 2.0mm and a thickness of 2.0 mm. Obviously, these dimensions are still relatively small and great care is required during machining.

Having established the physical dimensions of the bar-line the next step was to model the tee junctions in HFSS. In the first instance, the tees were modelled as though they were ideal i.e. $l_1=l_2=l_3=C=0$, and $n=1$. On modelling the tees the junction parameters can be calculated using the methods of Section 4.9.3.1. These parameters can then be used to develop a new junction configuration which will better approximate the desired junction behaviour. This is an iterative process because each new tee model is based upon the junc-

tion parameters of the previous design and the parameters for the new junction will not be exactly the same. In practice however, the error becomes very small after only a few iterations.

The objective of this modelling stage is to establish the physical dimensions of the junctions and transmission lines in the branchline coupler design which will make the coupler perform as designed.

4.9.3.3 Simulation Results

Each 'T' junction was tested in numerous different configurations, each varying only slightly from previous tests. In this manner it was possible to determine the effects of the physical changes, on the different junction parameters. Each 'T' was subjected to minor adjustments until both sets of parameters began to satisfy the criteria laid out above and the parameters were consistent between junctions.

Once the individual 'T' junctions had begun to converge to the desired specification, a full branchline coupler was modelled on MDS using ideal transmission lines. Each 'T' junction was replaced by its lumped equivalent model, after Section 4.56. In this way it was possible to determine whether a satisfactory coupler could be configured using the junctions or whether it was necessary to carry out further modelling.

The initial and final junctions, and their parameters are illustrated in Fig.4.57. Comparing parameters it is observed that the final junctions are much more compatible and should therefore yield a better coupler.

The two finalised junctions were then used to model a full size branchline coupler using the HFSS program. Simulating the whole coupler on HFSS can take up to eight hours to complete, hence, this was simply used as a method of checking the results from MDS. It also gives a more accurate indication of how the final device will perform.

The offset reference plane lengths were used to calculate the correct lengths of all the adjoining lines and the final model was set up according to the dimensions of Fig.4.58.

The results from the HFSS simulation were excellent and are repeated in Fig.4.59. It can be seen that the design bandwidth, coupling, return loss and directivity are almost the same as those in the ideal design.

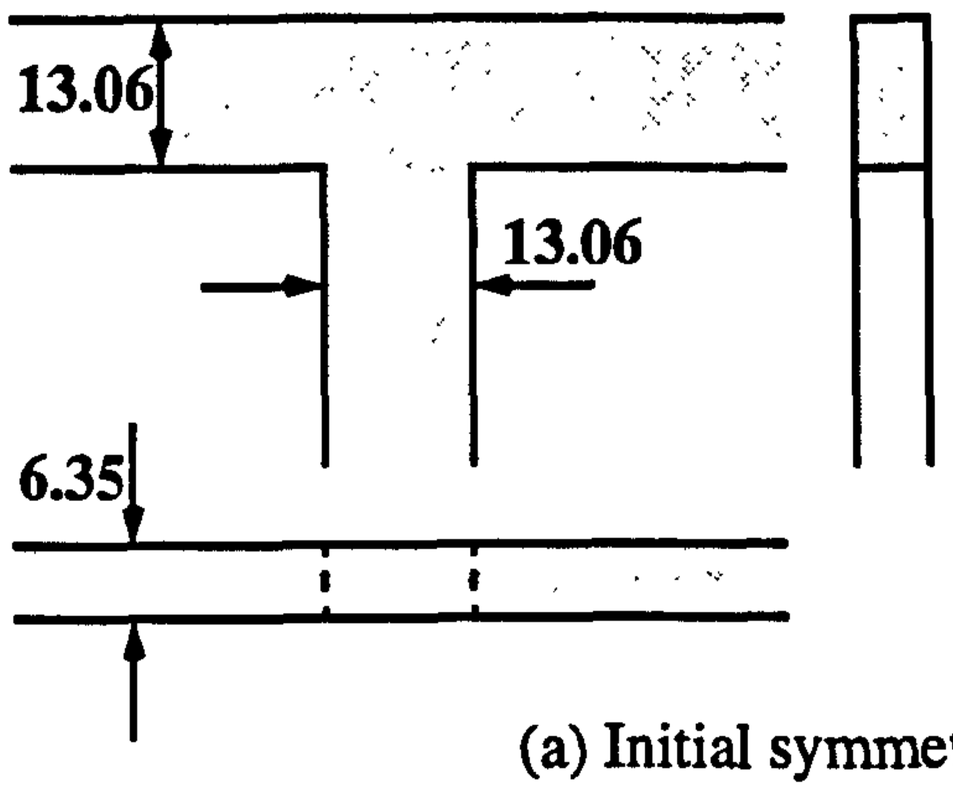

Parameter	Value
l_1	5.64mm
l_2	5.64mm
l_3	-0.81mm
C	-0.15Pf
n	1.02

(a) Initial symmetric junction

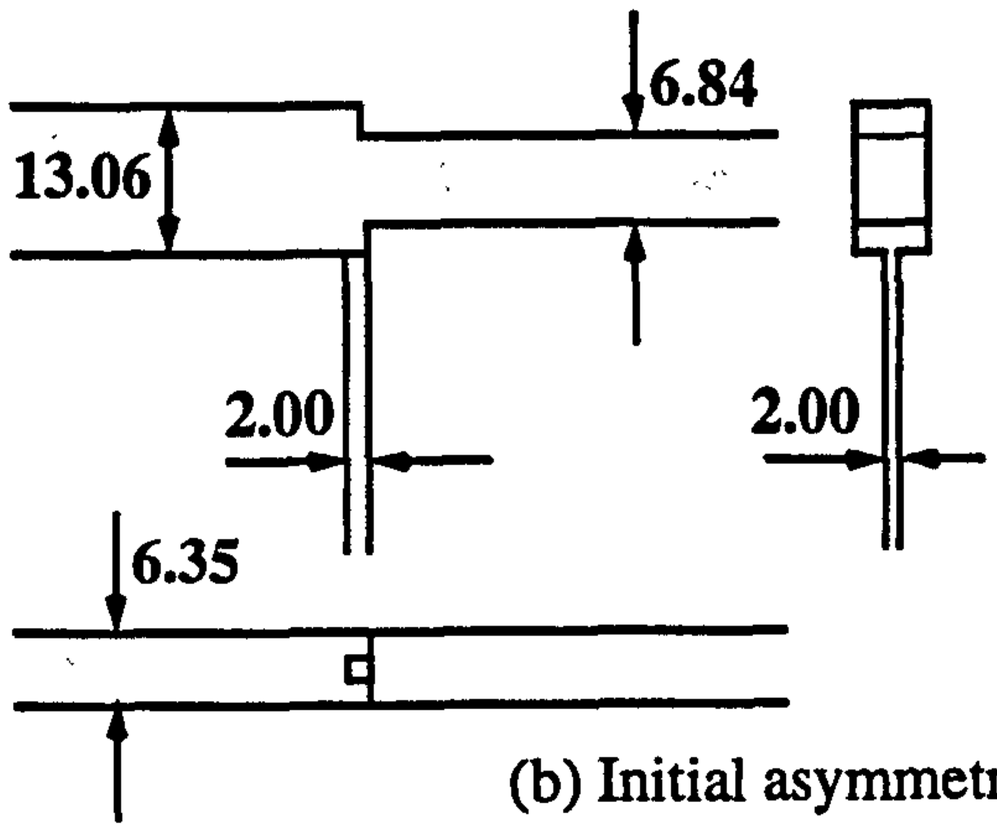

Parameter	Value
l_1	0.86mm
l_2	1.59mm
l_3	1.35mm
C	0.041Pf
n	0.99

(b) Initial asymmetric junction

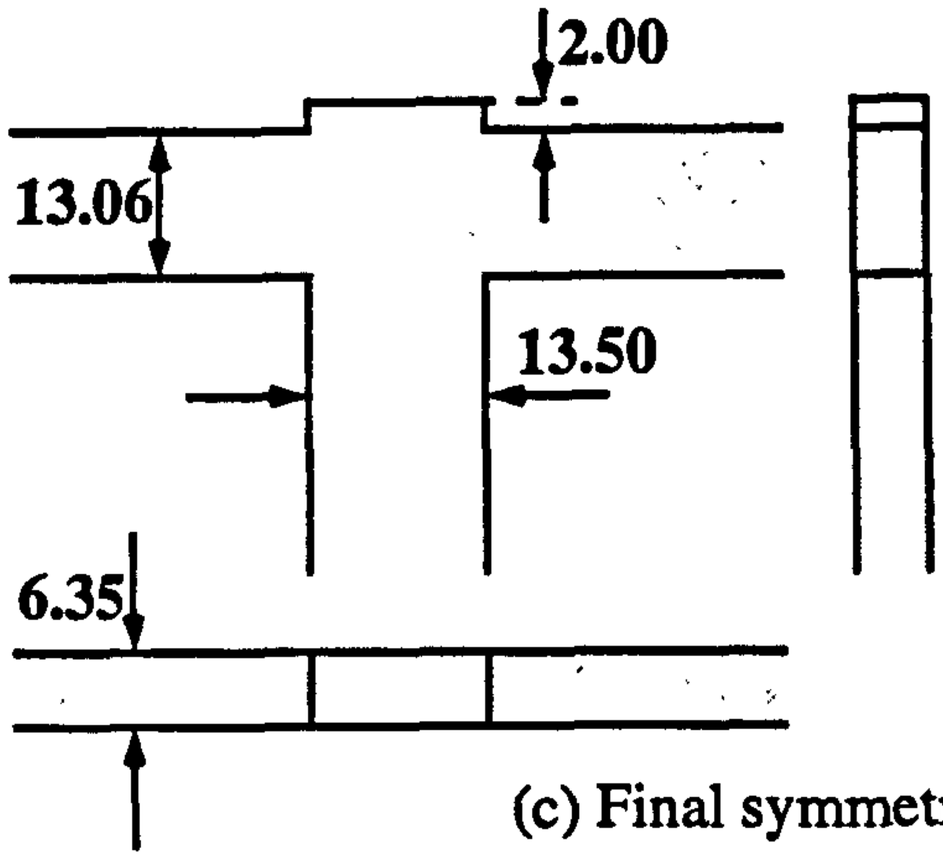

Parameter	Value
l_1	5.27mm
l_2	5.27mm
l_3	-0.03mm
C	0.039Pf
n	1.03

(c) Final symmetric junction

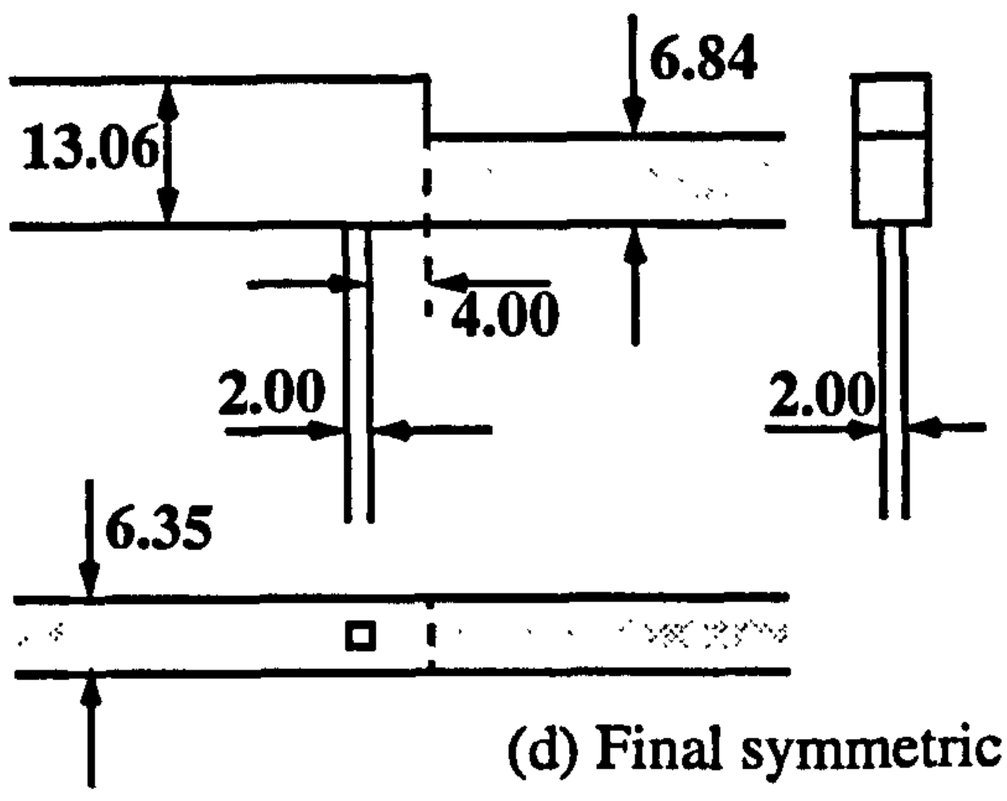

Parameter	Value
l_1	2.73mm
l_2	3.57mm
l_3	0.41mm
C	0.026Pf
n	1.02

(d) Final symmetric junction

Fig.4.57 Simulated 'T' junction parameters

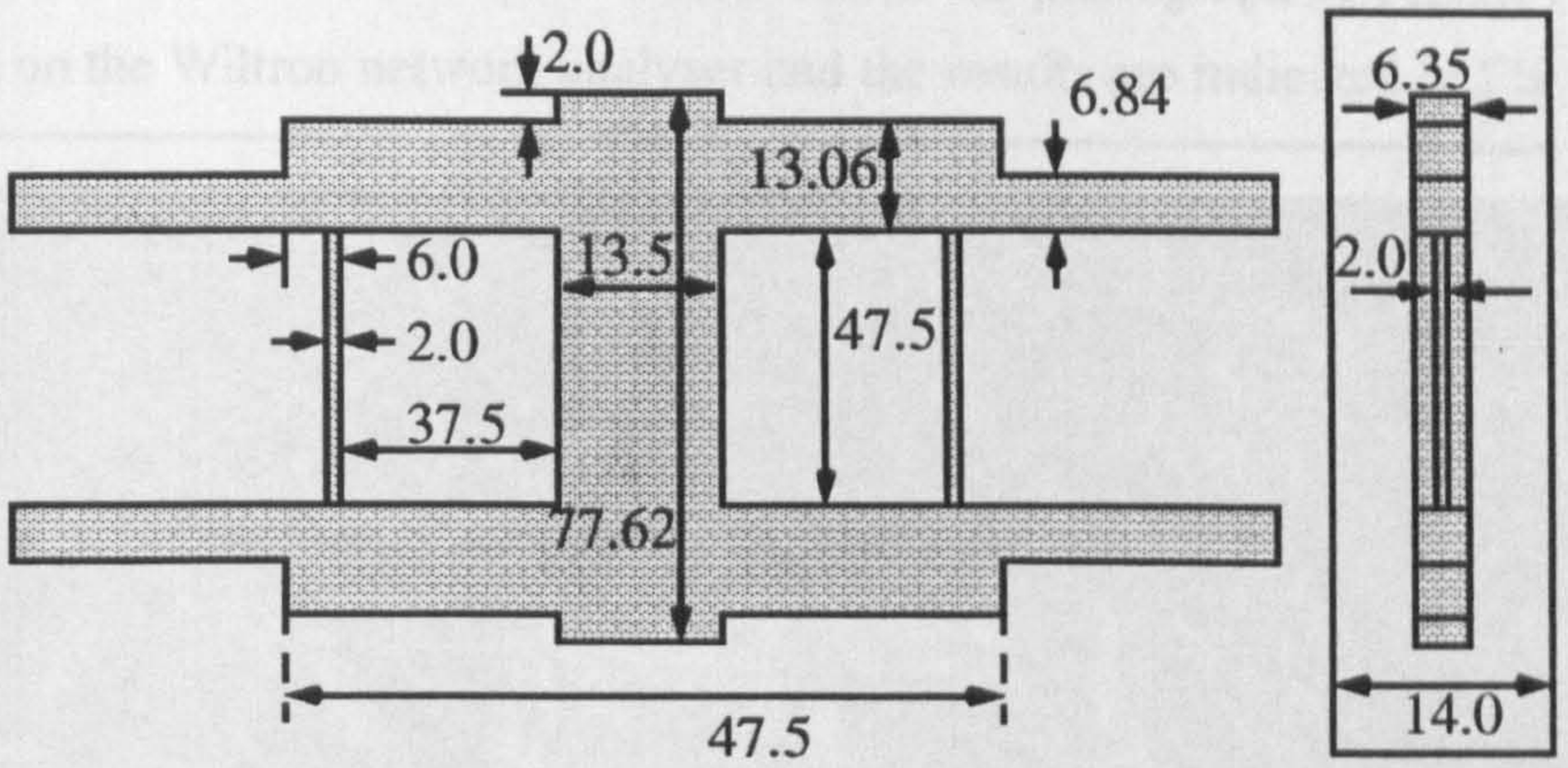

Fig.4.58 Final coupler dimensions

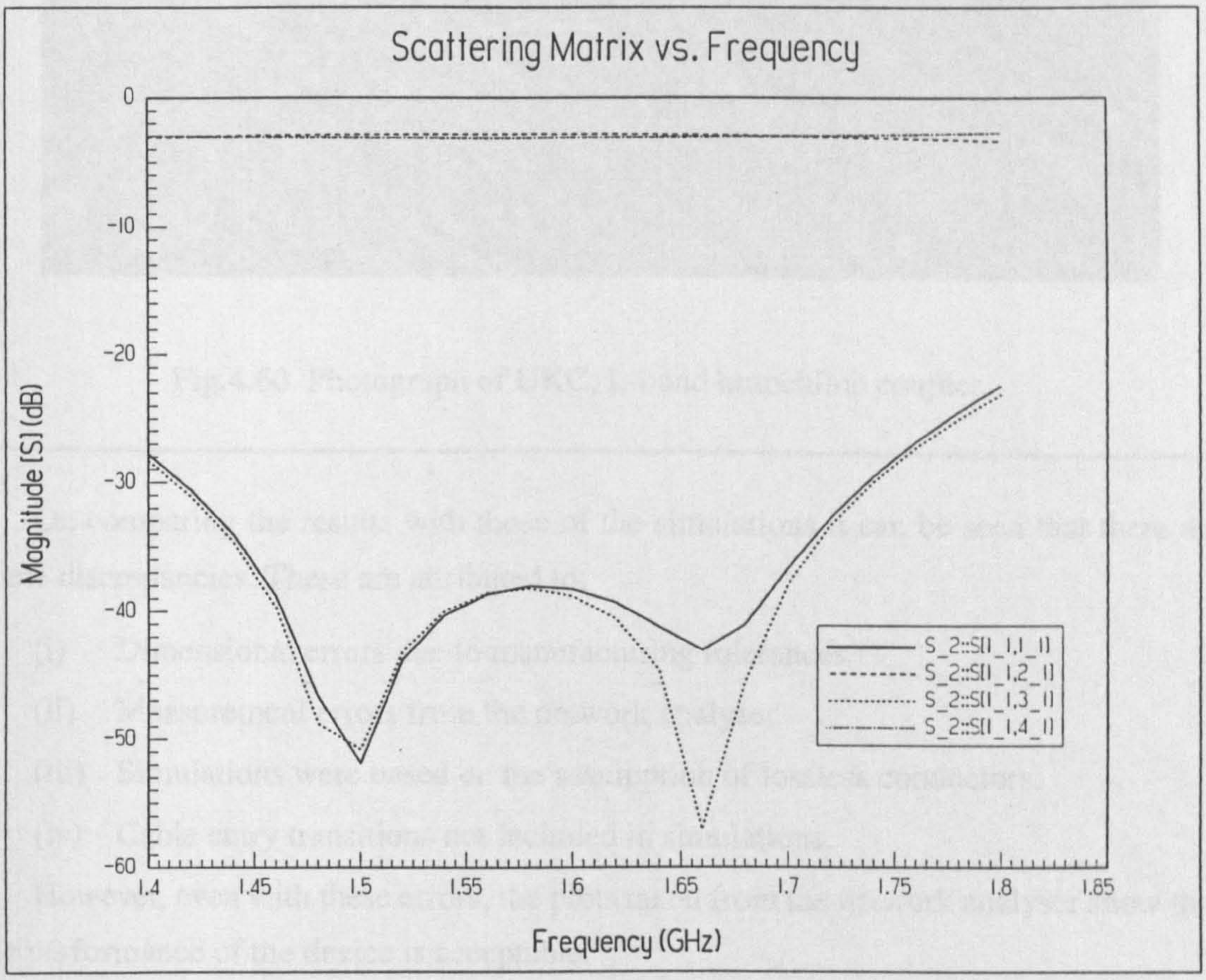

Fig.4.59 HFSS simulation results of whole coupler

4.9.3.4 Actual Performance

The final step was to have the coupler manufactured in the mechanical workshop to the dimensions which were established form the modelling process. The centre conductor of the coupler was machined in one-piece from ex-stock brass plate and the 50 ohm feed lines of the coupler were drilled to accommodate the contactless UT-250 probe.

The finished branchline coupler is indicated in the photograph of Fig.4.61. The unit was tested on the Wiltron network analyser and the results are indicated in Fig.4.60.

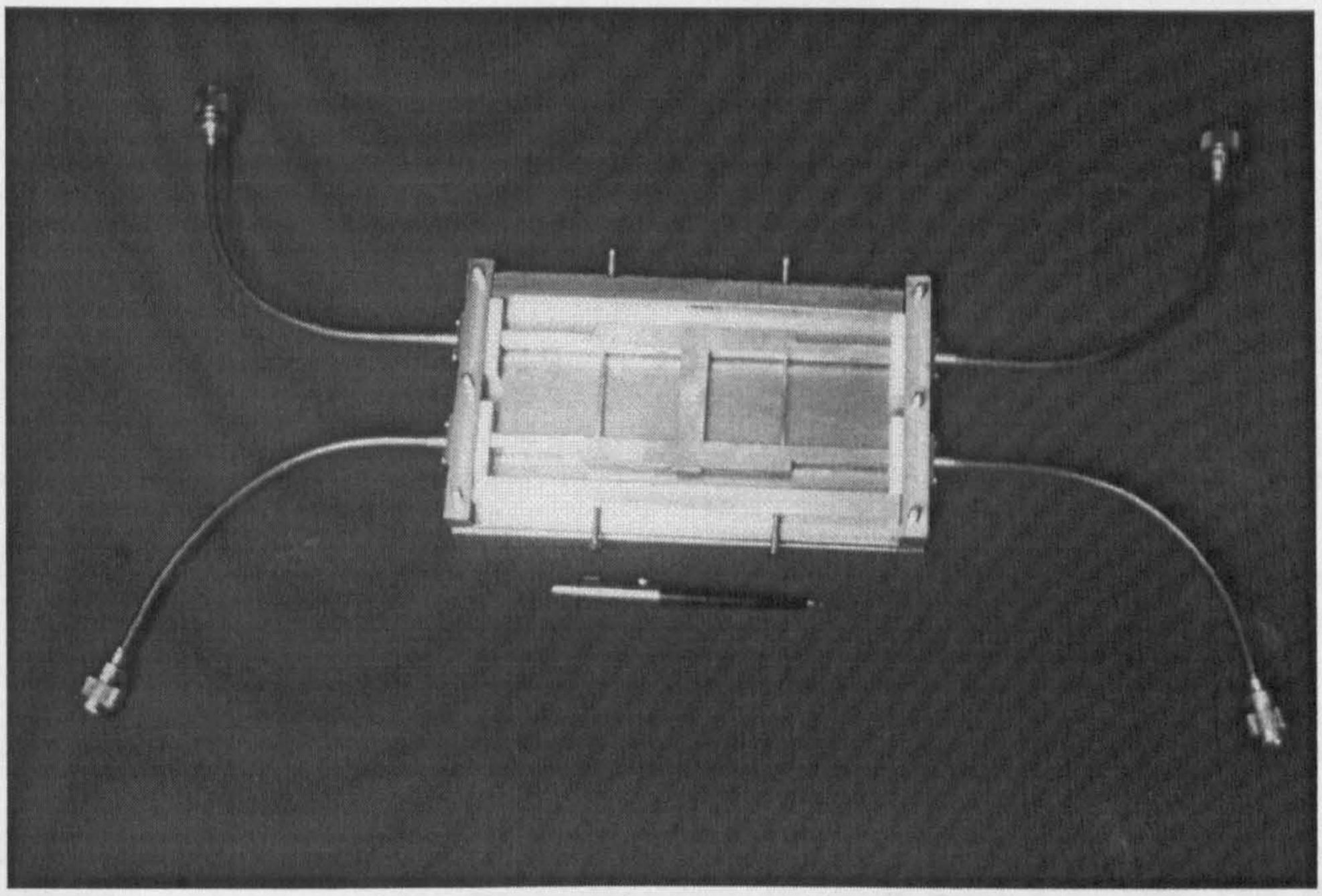

Fig.4.60 Photograph of UKC, L-band branchline coupler.

On comparing the results with those of the simulations it can be seen that there are some discrepancies. These are attributed to:

(i) Dimensional errors due to manufacturing tolerances.

(ii) Measurement errors from the network analyser.

(iii) Simulations were based on the assumption of lossless conductors.

(iv) Cable entry transitions not included in simulations.

However, even with these errors, the plots taken from the network analyser show that the performance of the device is acceptable.

The project to design a branchline coupler has proved successful. However, due to time constraints and the excellent performance of the re-entrant coupler, the branchline device was not tested in terms of its PIM performance. The coupler was tested electrically using only a simple test enclosure and was not packaged for low-PIM performance. However, it is not anticipated that the coupler would give any problems as couplers of this type have already been designed for use in aerospace applications [159, 160, 165-168] where they have had to conform to rigid PIM specifications. The dominant factor is likely to be the effectiveness of the low PIM enclosure.

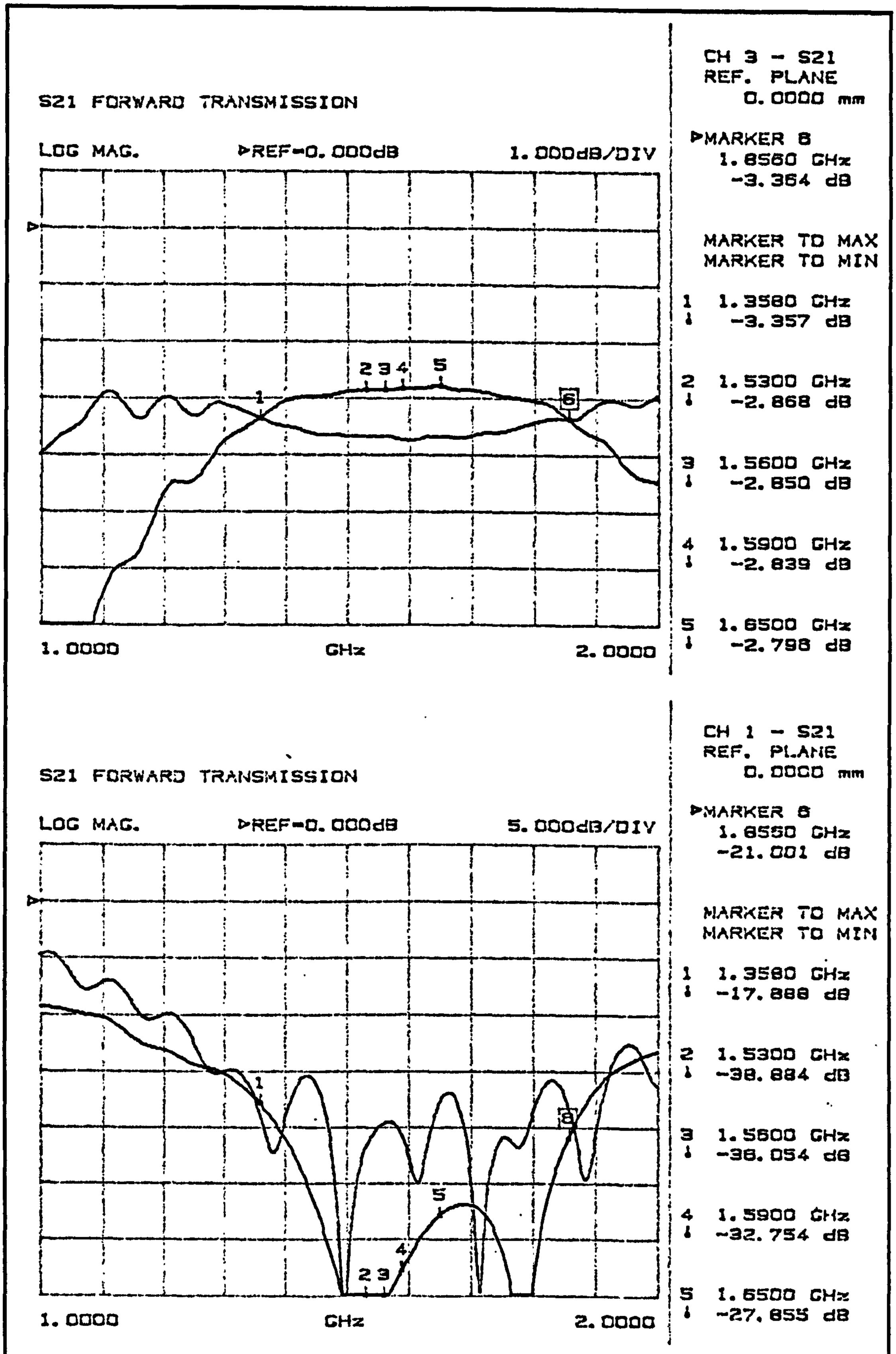

Fig.4.61 Frequency response of physical branchline coupler

4.10 Test Jigs

4.10.1 Introduction

In order to study the non-linearities of passive materials, test samples of a well defined nature need to be excited under controlled environmental conditions. If they cannot be directly connected into the laboratory measurement system, then some kind of test fixture is required. In this section, the main requirements of test fixture design are considered. There then follows a full description of several, novel, low-PIM test-jigs developed for this project.

4.10.2 Requirements

The principal requirement for a low-PIM test fixture (and for that matter a low-PIM test system) is a low and consistent level of non-linearity. If a test chamber is made using non-linear materials or has non-linear junctions at points of significant current density, the intermodulation signals that could be generated will mask the PIM signals produced by any test sample. This effectively reduces the useful dynamic range of the system and lowers the sensitivity of the system to effects from the sample under test. It is also extremely important that the chamber exhibits consistent and repeatable PIM behaviour. Many different samples have to be tested in order to provide enough data to be able to characterise PIM behaviour. Therefore, it is imperative that the test-jig shows consistently low PIM levels so that the measured data can confidently be attributed to the test samples and not some spurious response in the performance of the fixture. A consistently low level of residual PIM also means that the test results between different samples can be directly compared with the confidence that the results reflect the influence of the different test parameters.

In addition to good linearity, the test fixture must also allow for good impedance matching of the sample to the rest of the system. If the sample is not properly matched, the full potential of the system will not be realized because the maximum available power will not be conducted across the sample. The reflected power from a bad match could also damage the sensitive test equipment. Additionally, a poor impedance match will result in a significant VSWR (voltage standing wave ratio) which will increase the field strength and current density at other points of the system and could lead to the generation of higher levels of residual PIM.

The test fixture must also have a sufficient bandwidth to satisfactorily propagate the two parent signal frequencies plus any PIM frequencies which are being measured or once again the potential sensitivity of the system may be compromised.

Other important requirements are that the fixture should have the flexibility to incorporate a variety of test samples, it should allow for quick and easy access to the sample to promote a fast turnover of tests and the jig should be shielded to minimise external EMI

In practise it can be very difficult to design a single test fixture which satisfies all of these requirements and there will generally be a trade-off between them. In the UKC system for example a degree of flexibility in the variety of the test samples was sacrificed and two different jigs were made to test two different sample formats.

Several types of jig are described in the literature which have been used in conductive measurement systems to test chemical compounds [86], jointed-plate samples [25] ferromagnetic materials [38] and 1 m long structural components [7]. However, all of the jigs described use standard connectors to couple RF energy into the sample. The samples were soldered or even screwed in place. These characteristics are highly likely to increase the PIM levels of the jig itself and make it difficult to distinguish PIM signals due solely to the sample. Therefore, it was decided that for the UKC system, the contactless techniques which have been developed and exploited in the rest of the system, should be utilised in the design of low-PIM test enclosures. This should provide the desired low-PIM integrity and continuity in the sensitive areas of the system and should optimise PIM sensitivity and consistency.

4.10.3 Prototype Engineering Sample Jig

The first jig which was designed is shown in Fig.4.62. The jig was designed to take solid metal rod samples 9 mm in diameter and 166 mm long. The large diameter and circular cross section format of the samples was chosen in order that a range of standard engineering type finishes and coatings could easily be applied to the samples. It was considered that this would provide data which is directly indicative of practical situations and applicable to the engineering world.

The sample was made to be 50Ω inside a rectangular section outer conductor using the data of reference [119]. The cross sectional configuration is as shown in Fig.4.62. A rectangular outer conductor was selected as this would be easy to machine and would also lend itself to implementation using the low-PIM enclosure of Section 4.5. The cylindrical inner conductor meanwhile, was considered to be suitable for the implementation of the contactless principles of Section 4.3 and it would also allow for easier sample fabrication.

RF energy is coupled to and from the sample using quarter-wavelength series stubs as illustrated in Fig.4.62. The coupling sleeves are free to slide back over the feed lines to facilitate quick and easy changing of the sample. When assembled as shown, the sleeve

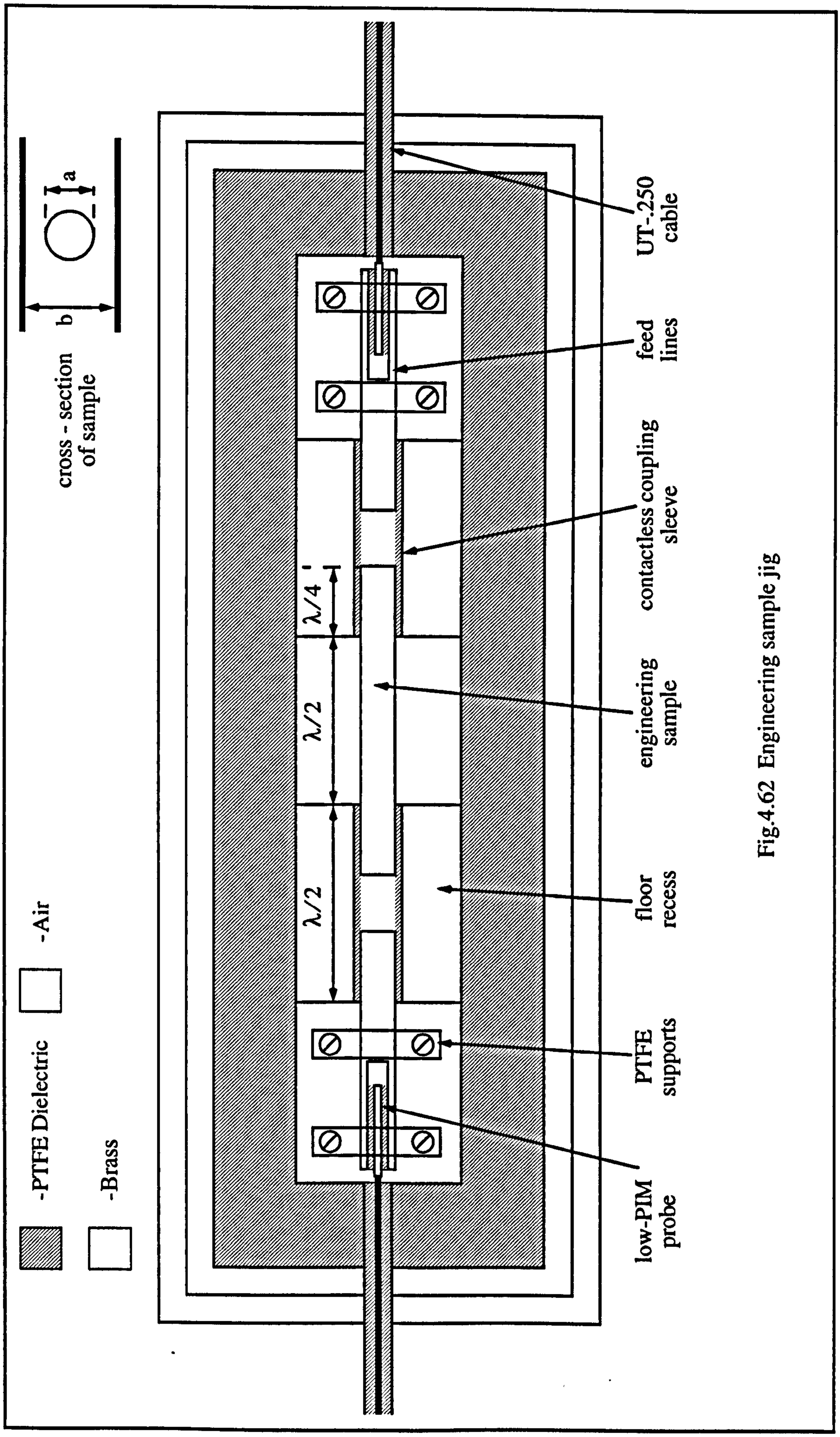
a
b
cross - section of sample
-Air
-PTFE Dielectric
-Brass
UT-.250 cable
feed lines
contactless coupling sleeve
engineering sample
Engineering sample jig
floor recess
PTFE supports
low-PIM probe
λ/4
λ/2
λ/2

Fig.4.62 E

also forms a section of 50Ω transmission line. This was achieved by machining extra depth into the base and lid to maintain the *b/a* ratio for 50Ω, thus allowing for the increased diameter. The sleeves were also made to be λ/2 long in air at the mid-band frequency in order to cancel any mismatch at the ends of the sleeve.

The feed lines are fitted with a quarter wavelength sheath of PTFE which is then inserted into the sleeve. The sample has a similar PTFE sheath and this is inserted from the other end. Owing to the higher dielectric constant of PTFE compared to air, a half wavelength in PTFE is shorter than that in air. This results in a gap between the end of the feed line and the sample of some 20mm, inside the brass sleeve. This is sufficient to effect an open circuit at the end of both lines which will be transformed to a short circuit at the ends of the sleeve thus providing a continuous flow of power over the sample.

The feed lines themselves are contactlessly coupled to the semi-rigid input lines at each end of the jig leaving the whole structure free of any metal junctions which are at points of significant current density. This in turn should mean reduced levels of residual PIM. However, the centre conductors, being contactless, must be supported and held firmly in place to maintain the correct dimensional relationships. In this way, compensation lengths at the transitions will not be liable to change and the characteristic impedance will remain stable. A clamping mechanism was formed using two short blocks of PTFE. These blocks were split through the middle in a similar fashion to those used to support the resonators of the 1st bandstop filter prototype (see Section 4.6.4.1). They were fitted around the centre conductor and then fixed to the floor of the jig using cross-linked polystyrene screws.

The outer enclosure of the jig was designed to be a low-PIM enclosure after Section 4.5. The bandstop filter of Section 4.7 indicated an overmoding problem with this type of enclosure, however the level of the next higher order mode was found to be around 30 dB down on the TEM mode inside the cavity and most of the energy remained in the dominant TEM mode. For the engineering sample jig, the width of the internal enclosure did not have to be as great as that used in the filter. Hence, it was expected that the level of overmoding would be less. However, even at 30 dB down on the TEM mode, any overmoding in this instance would be insignificant.

The engineering sample jig enclosure was machined from solid brass, the external dimensions of which are approximately 66 x 21 x 6 cm. The centre conductor is manufactured from brass in several sections. The contactless connection is realised by a brass sleeve which slides over the input/output line and each end of the sample rod. Quarter wavelength PTFE sleeves cover the ends of the input/output lines and the sample rod, thus avoiding any metal to metal contact but allowing RF transmission with minimum loss.

The electrical performance of the ESJ was found to be reasonable. Fig.4.63 indicates a return loss of better than -18 dB over the frequencies of interest and the insertion loss was measured at about 0.3 dB over the test band.

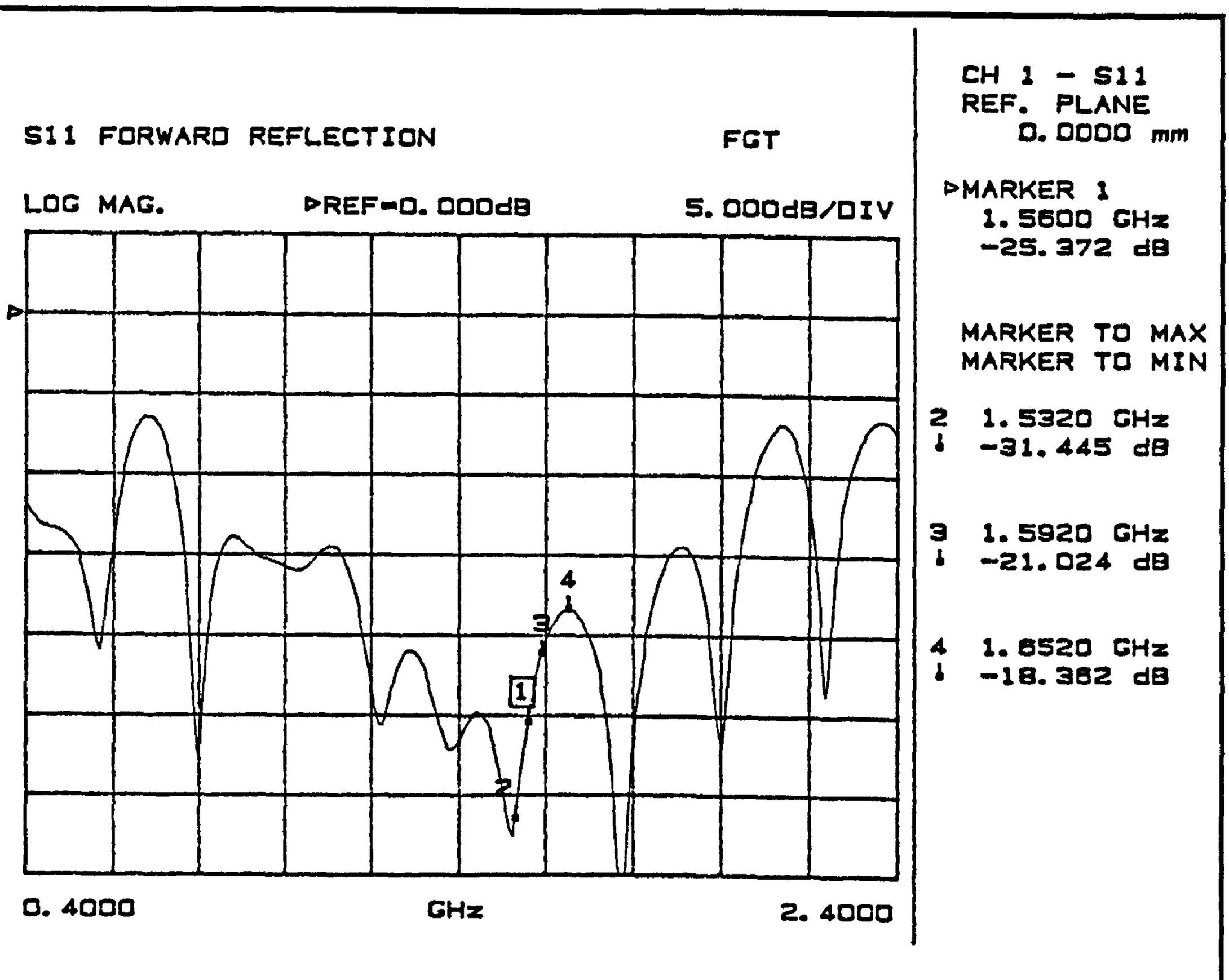

Fig.4.63 Engineering sample jig return loss

The one major difference between the sample jig and the prototype low-PIM box was in the lid fixing mechanism. On the prototype box, the lid was fixed in place by a number of M6 bolts which were screwed into the body of the box. For the Engineering sample jig, this was considered to be too cumbersome. The large size of the lid meant that a large number of bolts would have to be used to fix it in place. For each sample test, all of the bolts would have to be removed, the sample exchanged and the bolts replaced and tightened. The time taken to change a sample would then be far in excess of the time taken to perform PIM tests on the sample making the system very inefficient. It was therefore decided to look for an alternative solution.

The problem was how to provide sufficient clamping pressure between the lid and the enclosure body in order to keep the system residual consistently low yet allow the lid to be raised quickly in order to be able to change the sample. Another area for concern was the size and weight of the lid. It would require 2 people to safely and accurately lift the lid into position thus using valuable manpower.

In the end a complex gantry was developed which facilitated both manoeuvring of the lid and clamping it in place on top of the jig. The arrangement is shown in the photograph of Fig.4.63. The lid can be raised and lowered using a winch mechanism which has been fitted over the lid. The lid is attached to linear guide rails in order to ensure that it is located correctly when lowered onto the jig. Clamping of the lid is facilitated by eight toggle clamps which are attached to the steel surround. The surround is bolted to a steel plate which provides a rigid mounting against which the clamps can exert a considerable force. When fixed in position the clamps can provide a holding force of up to 250kg each.

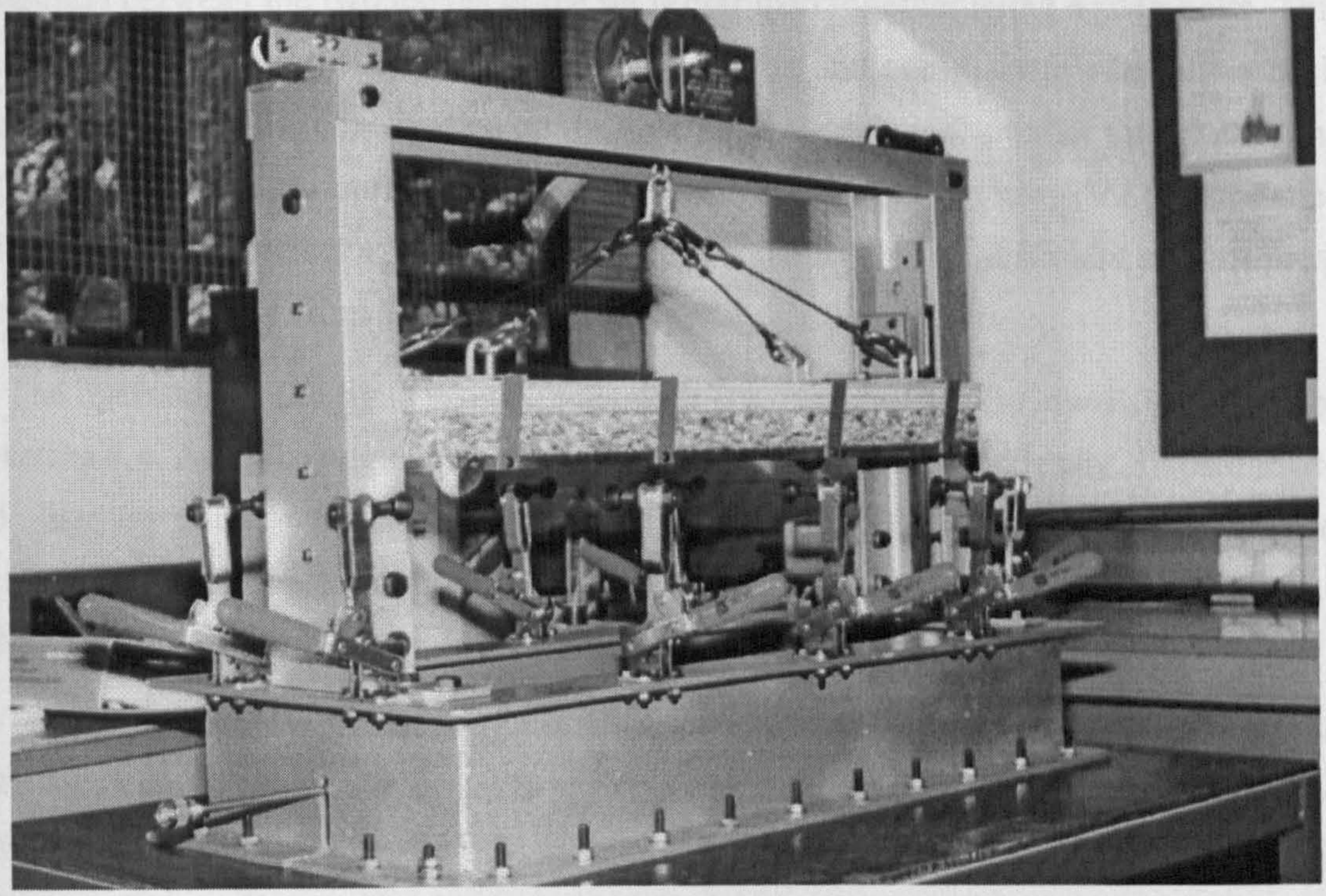

Fig.4.64 Engineering sample jig - lid mechanism

The jig was tested using a polished sample of beryllium copper. Beryllium copper has been cited as exhibiting some of the lowest PIM levels for any conductor [53]. The system PIM residual with ESJ in the system was initially found to be very variable at around -120 dBm, the level being notably dependant upon slight differences in lid clamping pressure. The residual was improved to about -136 dBm +/- 2 dB (7^{th} order PIM with 2 x 25 W carriers) by machining a new, thicker, lid with improved surface flatness resulting in an improved contact area. This allowed preliminary measurements to be made on the sample materials (see Chapter 5). However, the PIM level of the jig was still above the system residual (-154 dBm) and most of the samples caused no discernable change in this level. Hence, it was clear that an improved measurement jig was required.

4.10.3.1 Coaxial Sample Jig

In order to overcome the difficulties encountered in achieving a consistent level of residual PIM from the engineering sample jig, a coaxial sample jig (CSJ) was designed incorporating the principal of forced minimum current density points at all metal-metal junctions (as used in the UKC contactless connectors described in Section 4.3). The jig is illustrated in Section 4.65 and was designed to mount the same samples as were used in the engineering sample jig discussed above.

The body of the jig is made entirely from brass and has solid PTFE inserts. The connection between the two halves of the jig is clamped together using 4xM6 bolts. This was far less than used on the prototype low-PIM box and could always be increased if required. However, the contact area on the new jig is a great deal smaller than that of the prototype. Given the low current density at the joint, and the proven low-PIM performance of the contactless connector, the 4 bolts were expected to deliver sufficient contact pressure to minimise PIM from the jig itself.

The operation of the jig is synonymous with the operation of the low-PIM connector of Section 4.4. As in the engineering sample jig, the sample is contactlessly coupled to the feed lines by a close-fitting, low impedance, $\lambda/4$, PTFE sleeved section. However, inserting samples is less straightforward and requires careful alignment of the sample and feed line.

The frequency response of the jig is illustrated in and Fig.4.66. It is evident from the return loss plot that the optimum mid-band performance of the jig, just fails to coincide with the centre frequency of the PIM system at 1.59GHz. This is likely to be as a result of the cumulative effects of having so many $\lambda/4$ sections operating in close proximity and the errors involved in calculating the physical $\lambda/4$ lengths to the desired accuracy. However, it was decided that the performance of the jig was adequate for the intended tests.

On inserting the jig into the system and once again using a polished beryllium copper sample, it was found that this jig has an excellent PIM performance. No degradation in the overall system PIM residual of -151 dBm (7^{th} order) from 2 x 25 W carriers was observed.

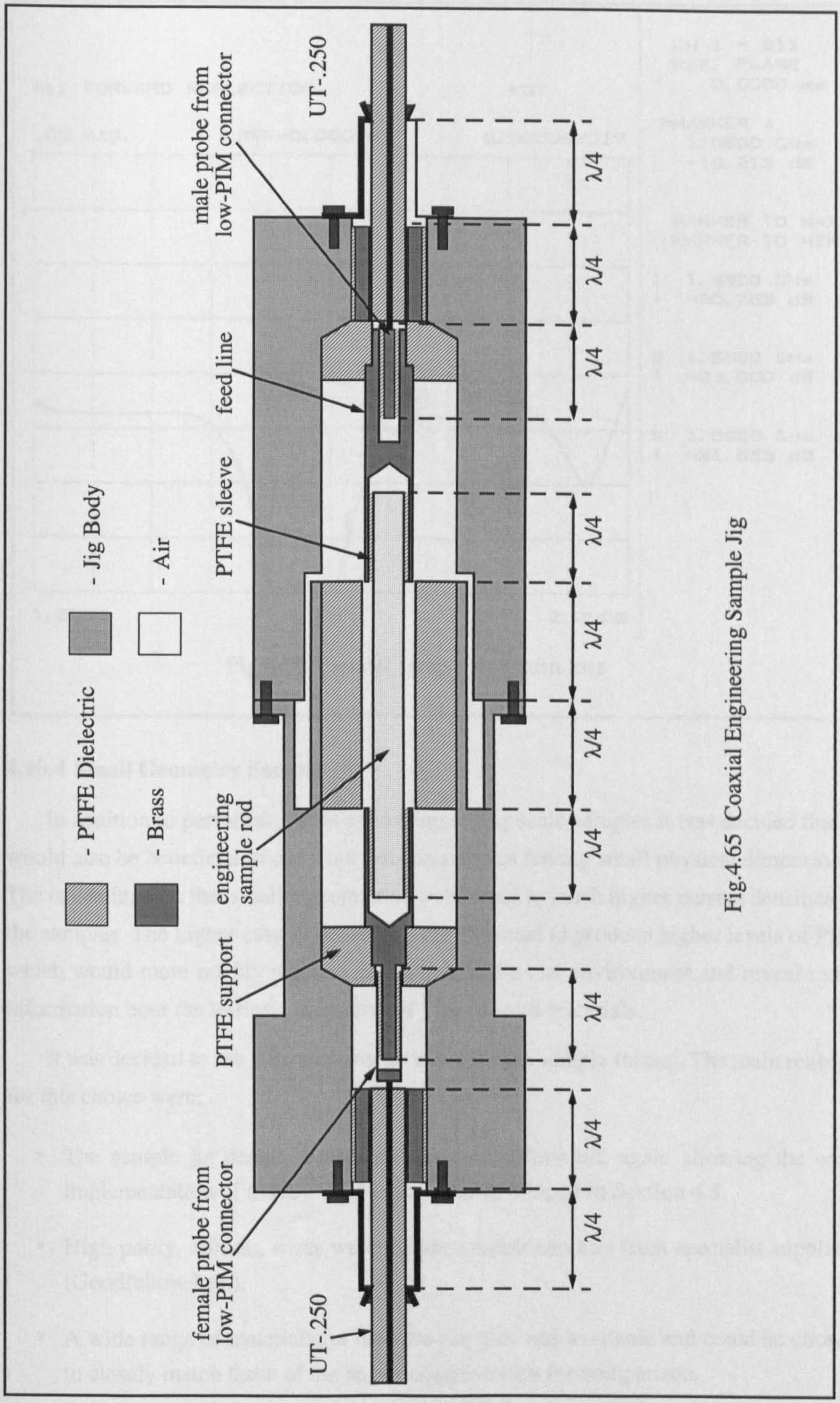

Fig.4.65 Coaxial Engineering Sample Jig

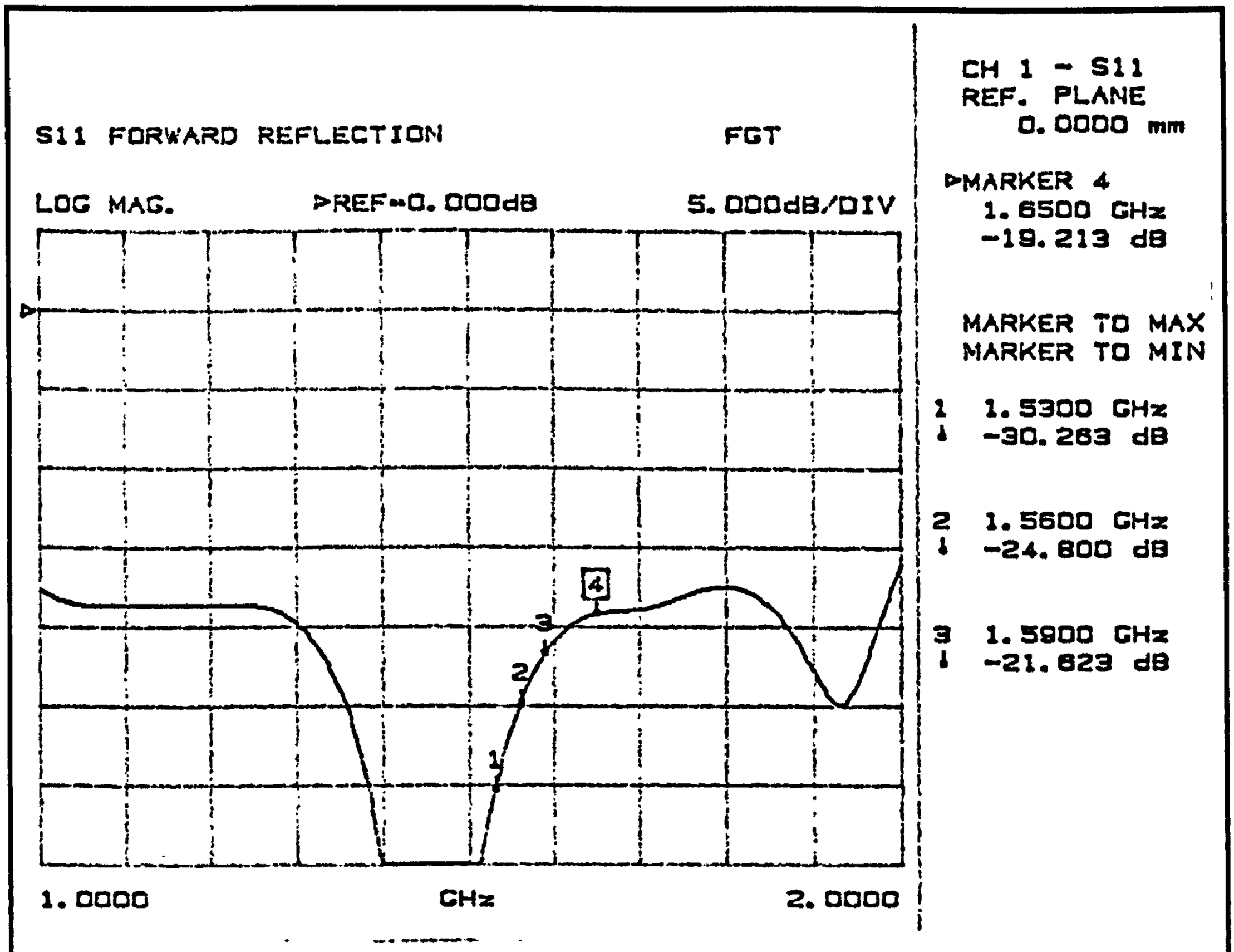

Fig.4.66 Coaxial sample jig return loss

4.10.4 Small Geometry Sample Jig

In addition to performing tests upon engineering scale samples it was decided that it would also be beneficial to carry out tests on samples having small physical dimensions. The reasoning was that smaller geometries would lead to much higher current densities in the samples. The higher current densities were expected to produce higher levels of PIM which would more readily respond to changes in the test environment and reveal more information bout the intrinsic properties of PIM in solid materials.

It was decided to use 1.0mm diameter wires for the sample format. The main reasons for this choice were:

- The sample jig design would be very straightforward, again allowing the easy implementation of the low-PIM techniques developed in Section 4.3.
- High purity, 1.0mm, wires were readily available to buy from specialist suppliers (Goodfellow Ltd.).
- A wide range of materials for the wire samples was available and could be chosen to closely match those of the engineering samples for comparison.

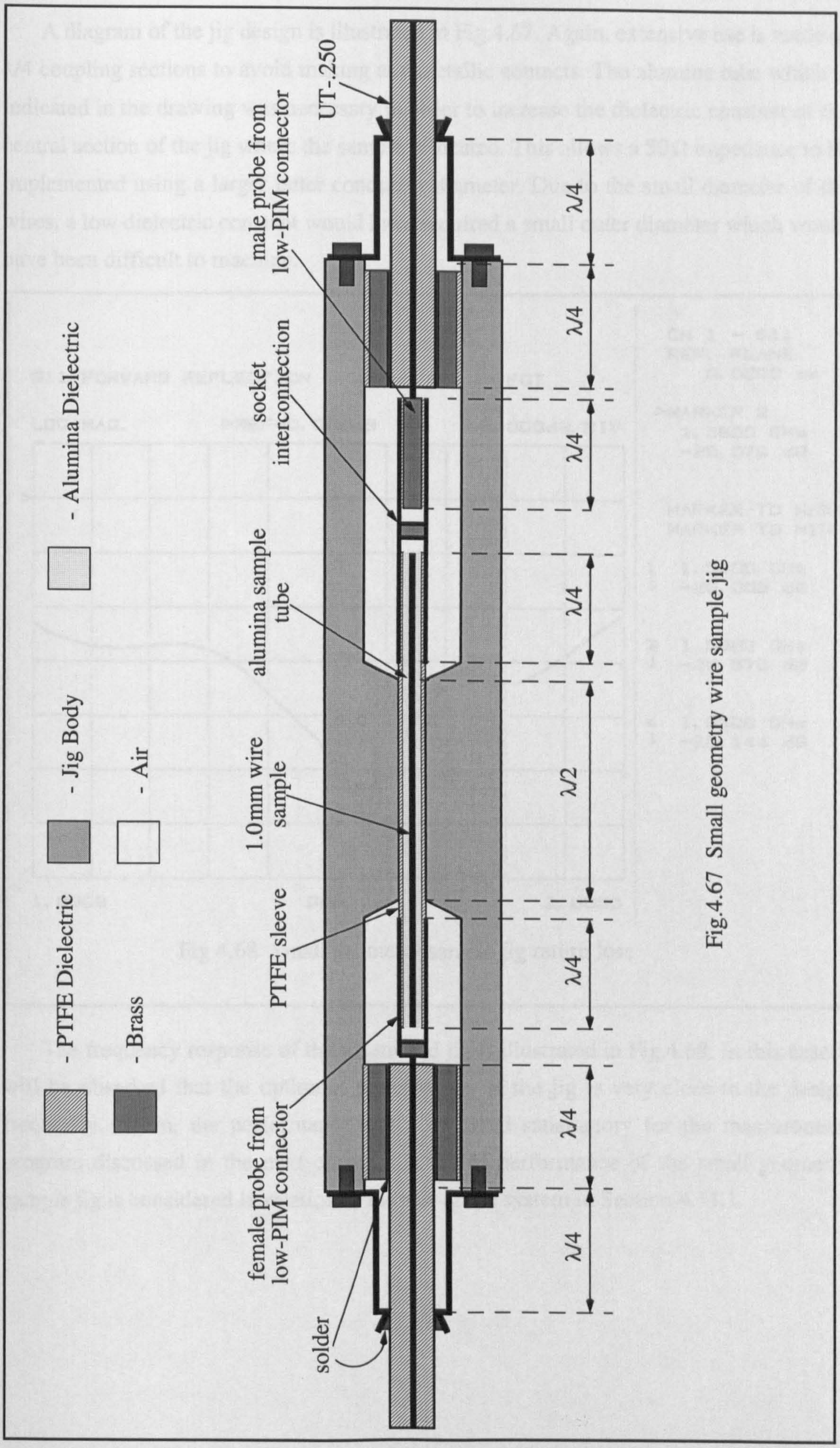

Fig.4.67 Small geometry wire sa

A diagram of the jig design is illustrated in Fig.4.67. Again, extensive use is made of λ/4 coupling sections to avoid making any metallic contacts. The alumina tube which is indicated in the drawing was necessary in order to increase the dielectric constant of the central section of the jig where the sample is located. This allows a 50Ω impedance to be implemented using a larger outer conductor diameter. Due to the small diameter of the wires, a low dielectric constant would have required a small outer diameter which would have been difficult to machine.

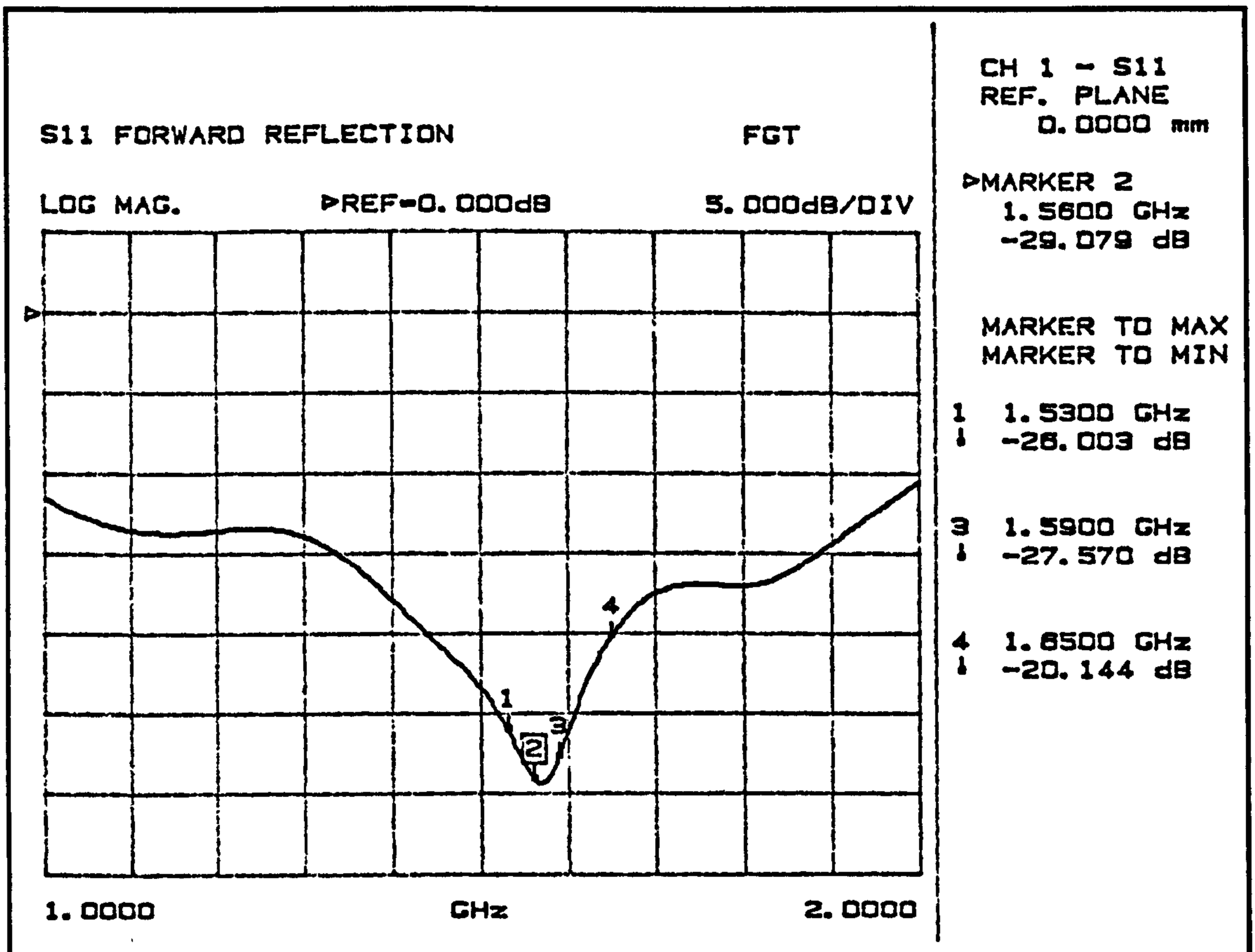

Fig.4.68 Small geometry sample jig return loss

The frequency response of the assembled jig is illustrated in Fig.4.68. In this case it will be observed that the optimum performance of the jig is very close to the design frequency. Again, the performance was considered satisfactory for the measurement program discussed in the next chapter. The PIM performance of the small geometry sample jig is considered in relation to the rest of the system in Section 4.11.1.

4.11 Reconfigured System Performance

The development of low-PIM components has been described in this chapter. The components were systematically inserted into the system and were observed to improve the residual PIM level in terms of achieving low-level, repeatable and stable performance. For the measurement programme the system was configured according to Fig.4.69.

After combining the parent signals using the directional filter set up of the original system, they are transmitted through a second directional filter assembly. The directional filter is comprises two low-PIM bandstop filters, tuned to the PIM frequency of interest, and two 3dB hybrids. The first hybrid is a commercial unit as discussed in Section 3.5.2.2. This device is not required to have an exceptional PIM performance since PIM generated before the bandstop filters will be reflected into a load. The first hybrid serves to split the power between the two filters which then heavily attenuate any PIM which has been generated in the earlier stages. The signals are then recombined by the second hybrid. The PIM performance of this coupler is important hence the re-entrant low-PIM hybrid as described in Section 4.9.2 was used. The combined excitation signals are then propagated through the test jig and directly into the high power load.

The generation of PIM is assumed to be an isotropic process after the discussion of Section 3.3.1 so that any generated signals will propagate equally in both directions from the source. In this case, the reverse transmitted PIM signals were measured. This simplifies the system a great deal because, for forward PIM detection, the PIM signal must be separated from the high power carrier signals and this would require another high-power, low-PIM directional filter. In the reverse direction this isolation is still necessary but the parent signals are much weaker (at least 25dB down on the forward travelling signals due to the return loss from the load connector).

Isolation of the PIM signal is achieved via the same bandstop directional filter as was used to clean the parent signals. The PIM signals travelling back from the DUT are reflected by the bandstop filters and recombined at the isolated port of the low-PIM hybrid. Signals at the parent frequencies however, are passed by the filters and combine at the isolated port of the first hybrid where they are dissipated.

The PIM signal is further isolated from any breakthrough of the carrier signals by additional filtering. This is performed by a low-PIM bandstop filter tuned to attenuate the parent frequencies and one of the original Trilithic® bandpass filters. The attenuation provided by the bandstop filter ensures that no significant PIM is generated in the Trilithic® filter. The Trilithic® filter has been included to ensure that there is no possibility of active intermodulation products being generated in the detection circuitry. The PIM signal itself is then amplified by the LNA and displayed on the spectrum analyser.

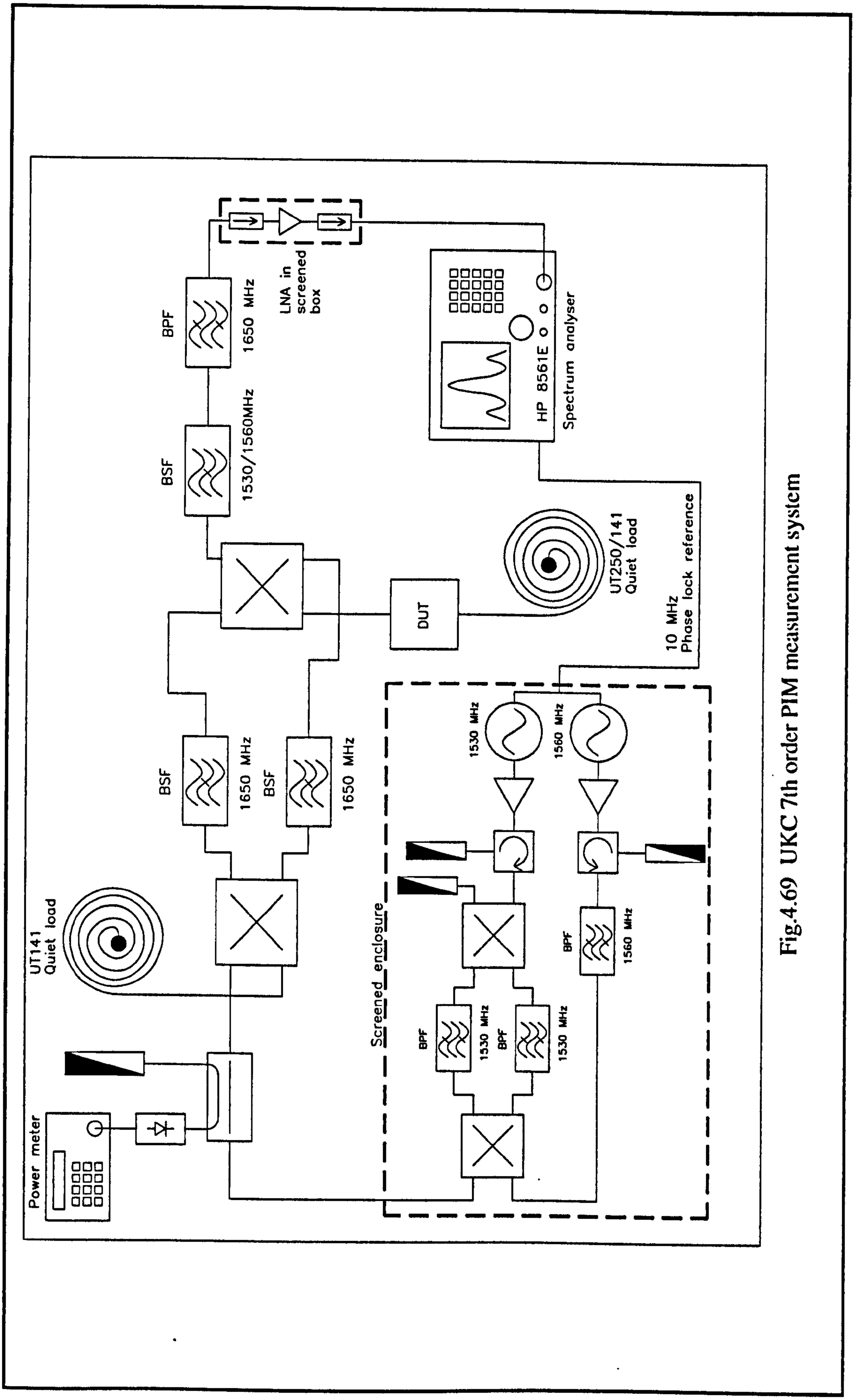

Fig.4.69 UKC 7th order PIM measurement system

4.11.1 Residual PIM Levels

The system was carefully cleaned and initially set up with no DUT or test jig in place. The low-PIM, semi-rigid load was connected directly to the output of the re-entrant coupler by means of the low-PIM connector described in Section 4.4. At an input power of 25Watts (or 44dBm) per carrier at the DUT position (i.e. at the low-PIM load connector), the 1650MHz, 7th order residual PIM level, at the same point, at was recorded as -154dBm or -195dBc. In comparison with Table 3.1, this represents a significant increase over previous coaxial PIM measurement systems. However, as well as the extremely low level of residual PIM, the signal was also very stable, and insensitive to physical agitation of the system. The level could also be repeated with a high degree of consistency, even after de-mounting and re-mounting some of the system components.

Even after the whole system had been transported to ESTEC in Holland and back to carry out the tests discussed in Chapter7, the residual PIM signal was within 1dB of its original level. This provided an excellent indication of the robustness of the system and of the new low-PIM components.

The low-PIM, load connector was then replaced by the coaxial sample jig. A sample of beryllium copper was used to determine the residual level of the jig. Beryllium copper has been suggested in the literature to have the one of the lowest intrinsic PIM levels of any conductor and this was confirmed in the experiments for the materials tested [53]. At 25Watts per channel the presence of the jig indicated no degradation in the level of system residual PIM of -154dBm. Once again the level was both stable and repeatable indicating the excellent performance of the jig and the low-PIM contact mechanism. This also proved the worth of the sample format and excitation method which was seen to deliver a hitherto unheard of level of consistency.

The residual levels with the small geometry sample jig (SGJ) were also measured. In this case a wire sample of beryllium copper was used to give an indication of the performance of the jig. The jig was tested at 25Watts per channel once again and PIM level of -142dBm was recorded. A second sample produced a PIM level of -144dBm. The indications were that the PIM level in the system was being limited by the performance of the jig or the wire samples. However, given the much higher current densities present in the wire samples it is not surprising to find that the PIM level increases accordingly. The PIM level was observed to be just as stable as that from the other residual tests, however, it was slightly less repeatable, with variations of as much as ±2dB observed between tests. This slight variability must be taken into account when comparing the results of the tests described in the next chapter.

The tests on the residual PIM in the system indicate that the first main objective has been achieved, namely that of developing a low-PIM measurement system with a very low, stable and repeatable level of residual PIM. This then provides an excellent starting point from which to begin a study of PIM generation in aerospace materials, knowing that the results can confidently be attributed to the sample under test.

CHAPTER 5

Measurement Programme

This chapter describes the experimental programme which was carried out in the investigation of passive intermodulation generation by commonly used aerospace materials. The experimental techniques are described followed by a detailed account of the measurements and observations made during the programme.

5.1 Introduction

This section of the project takes the form of an experimental study into PIM occurring in space qualified materials. The objectives of the study were set out as follows:

- To produce a set of PIM measurements which describe the characteristics of selected materials for Passive Intermodulation Product generation
- To propose a standard methodology to enable the PIM characteristics of materials to be measured and compared in a consistent manner
- To identify the dominant causative mechanisms of PIM behaviour.

This investigation has been principally research orientated although most of the measurement data presented will be of use to R.F. engineers.

The lack of reliable and consistent measurement data was highlighted in Chapter 2. It was also shown that the best approach to gaining a better understanding of PIM generation in practical engineering situations was to perform measurements on carefully selected engineering materials and junctions. From the results it is a matter of isolating those areas which exhibit interesting PIM behaviour and merit further investigation. This formed the basis of the UKC measurement program which is described in the following sections.

5.2 Measurement Technique

Measurements on different aerospace materials were carried out using the test jigs described in Section 4.10. The RF power is conducted through the sample in order to produce a detectable PIM signal from any non-linear mechanisms which are present.

For each experiment a sample must be placed in the jig and the jig assembled correctly. The sample is part of the jig and is essential for the jig and the measurement system to operate in the proper manner. Accordingly, the RF power must be turned off each time the sample is changed.

Initially, the high voltage supply to the power amplifiers has to be allowed to warm up for a few minutes. The RF power was monitored in the system using a Marconi power meter. The two carrier signals are set to equal powers by operating each one individually and adjusting the output to the desired level. Again, when each amplifier is operating at high RF power the output must be given time to settle.

Once the carrier powers have been set, both sources are turned on and the combined power and system match are checked. Provided that the LNA is on and functioning correctly, the PIM signal can then be observed on the spectrum analyser and recorded.

The two parent signal sources are locked to the 10MHz reference of the spectrum analyser to prevent the PIM signal from drifting in frequency allowing very low resolution bandwidth and span settings.

5.2.1 System Performance Considerations

Two basic configurations were used on the spectrum analyser whilst making measurements. One used the spectrum analyser with a 10 Hz resolution bandwidth employing video averaging to record the magnitude of stable PIM signals, reducing the variability introduced by noise signals of a similar order. The other configuration used zero frequency span (without video averaging) to monitor the dependence of the PIM signal in the time domain, whilst specific test parameters were adjusted. Table 5.1 summarises configuration differences at the analyser.:

Configuration 1:				Configuration 2:		
frequency span	-	500 Hz		frequency span	-	500 Hz
resolution bandwidth	-	10 Hz		resolution bandwidth	-	0 Hz
centre frequency	-	1650 MHz		centre frequency	-	1650 MHz
noise floor (with video averaging)	-	-130 dBm		noise floor (no video averaging)	-	-110 dBm max.

Table 5.1 System performance figures

It can be seen from the table that when a signal of interest approaches -100 dBm on the spectrum analyser, interference from system noise starts to become more noticeable.

The current system PIM residual for 2x25W carriers is about -154dBm and the gain of the receiver is 39dB in total, hence, a PIM signal level of -115dBm from the DUT would be displayed on the spectrum analyser. Without the use of video averaging this residual signal can fluctuate between -105.4dBm and $-\infty$ dBm. With video averaging the variation is reduced to approximately ±1.1 dB. The actual variation observed for a given measurement was of this order although the absolute magnitude of the system residual was seen to vary on occasions by about ±2dB. This was normally due either to extensive use of the system without occasional cleaning of un-mated connectors, or prolonged operation of the system causing high temperatures in the quiet load and consequent variability in its PIM performance.

The consequence of such variations means that PIM levels measured close to the system residual (i.e. within ±2dB of it) need to be viewed more cautiously when conclusions are being drawn. In most cases, conclusions can only be tentative when they are based on changes of a few dB's occurring within several dB's of the system residual. Consequently, behaviour displaying deviations of greater than 10dB have been highlighted as being noteworthy and, in many cases, have merited further investigation.

5.3 Engineering Sample Measurement Program

The interests of the collaborating body, ESA, have been continually borne in mind throughout this project and especially during the measurement campaign. The intention of this part of the investigation was to take specific materials which are typically used in space hardware and to quantify their performance in relation to PIM generation such that a qualitative list could be drawn up indicating their relative PIM behaviour. Such data is not readily available therefore, it was considered highly relevant information for the aerospace community and would also highlight materials requiring further investigation.

Table 5.2 lists the materials which have been selected for test and the relevant ESA standards which they meet. All of these items have been received with a detailed breakdown of chemical composition so that full information on the materials involved would be readily available if required.

Two test methods were proposed to measure the PIM performance of the samples. The initial intention was to establish the bulk properties of the various materials in relation to PIM generation.The second was to monitor the performance of a more limited number of materials in relation to their PIM performance when used in a junction format. The test samples were designed and manufactured with these methods in mind.

Material	Composition	Supplier
Aluminium	99.5%: A-1 in PSS-01-701	Goodfellow
Aluminium alloy	4.5% Cu, 1.5% Mg, 0.6% Mn, 0.5% Fe, 0.5% Si, 0.3% Zn, 0.2% Ti, 0.1% Cr, rem Al: AA 2024, A-2 in PSS-01-701	Aerospace Metals
Aluminium alloy	1% Mg, 0.7% Fe, 0.6% Si, 0.25% Cu, 0.25% Zn, 0.2% Cr, 0.15% Mn, 0.15% Ti, rem Al: AA 6061	Aerospace Metals
Aluminium alloy	5.6% Zn, 2.5% Mg, 1.6% Cu, 0.5% Fe, 0.4% Si, 0.3% Mn, 0.3% Cr, 0.2% Ti, rem Al: AA 7075, A-5 in PSS-01-701	Aerospace Metals
Copper (oxygen free)	99.95%: C-5 in PSS-01-701	Goodfellow
Beryllium copper	1.85% Be, 0.36% Co+Ni+Fe, rem Cu: B-1 in PSS-01-701	Aerospace Metals
Nickel	99.7% Ni	Aerospace Metals
Silver loaded epoxy	Eccobond solder 56 C: E-1 in PSS-01-701	RS Components
Solder	60% Sn, 40% Pb: S-12 in PSS-01-701	RS Components
Solder	62% Sn, 36% Pb, 2% Ag: S-14 in PSS-01-701	RS Components
Indium solder	50.6% In, 49.4% Pb	Indium Corporation
Stainless steel 303	17.2% Cr, 8.7% Ni, 1.8% Mn, 0.4% Mo, 0.4% Si, 0.3% S, 0.3% Cu, rem Fe: AISI 303	Aerospace Metals
Stainless steel A286	25% Ni, 14.7% Cr, 2.2% Ti, 1.1% Mn, 1.3% Mo, 0.4% Si, 0.3% At, 0.3% Cu, 0.2% V, rem Fe: A286, S-17 in PSS-01-701	Aerospace Metals
Stainless steel 15-5PH	15.1% Cr, 4.8% Ni,3.3% Cu, 0.4% Si, 0.4% Mn, 0.3% Mo, rem Fe: 15-5PH	Aerospace Metals

Table 5.2 Material selection for solid and jointed sample rods

5.3.1 Engineering Sample Rods

Two sample designs were produced for PIM testing the listed materials, with the purpose of comparing PIM characteristics in relation to both bulk surface and junction properties under engineering conditions. No attempt was made during these measurements to isolate specific mechanisms which may be operating. This is intended to be of direct use to the engineer in relation to low-PIM material selection during system and component design.

One of the main objectives of the project was to develop a standard methodology for the measurement and comparison of PIM generated by different materials under identical but variable environmental conditions. The sample design must reflect this objective. Only in this way can direct comparisons be confidently made between their respective results.

The basic sample design is depicted in Fig.5.1 and consists of a simple rod of circular cross section which is machined to a carefully controlled diameter, i.e. solid sample rods. The length of the rod is such that the central section is a half-wavelength in air and the ends are quarter wavelength long for a PTFE dielectric medium. PTFE sleeves slide over the ends enabling contactless connection with the contactless sockets in both sample jig designs (refer to Fig.5.1). All of the sample rods were machined to a surface finish of 0.1 microns and were then polished to have a good optically reflective surface. At least three rods were prepared for each material type to allow testing of consistency during reference measurements and for different surface treatments to be applied independently of one another. Each three identical rods constitute a specific material set. The PIM characteristics of the solid sample rods would be expected to be dominated by surface effects due to the skin effect. At high frequencies 98% of the current flow is limited to four skin depths from the surface of the material. At 1.6GHz, the skin depth of copper is only around 1.65μm, hence, most of the current is condensed into a surface layer ≈7μm thick.

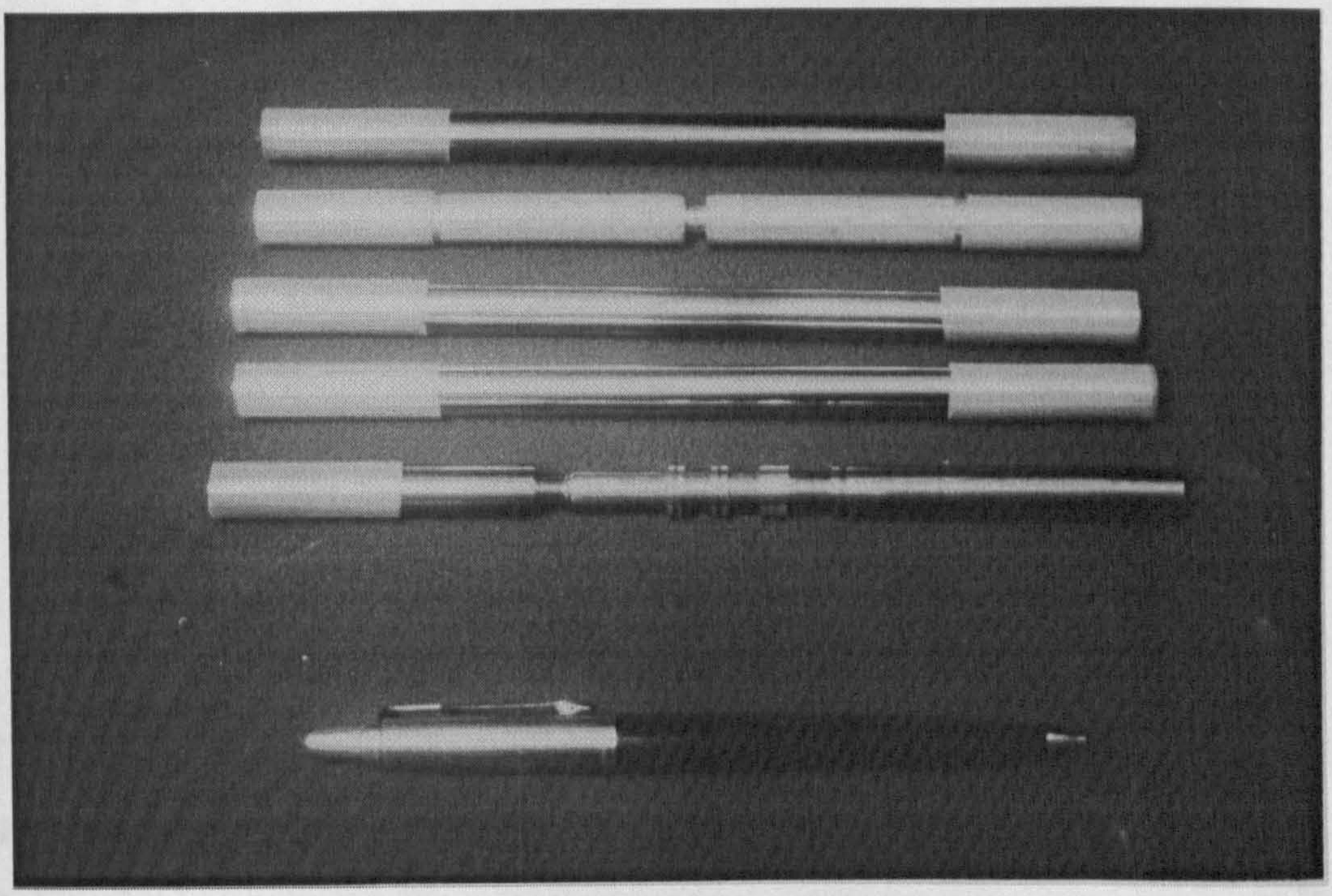

Fig.5.1 Engineering sample rods

The second design involved jointed sample rods. These were formed by mounting a specially fabricated range of 'washers' onto a mandrill. The mandrill consists of two sections of beryllium copper which screw together as indicated in Fig.5.2. The washers are mounted over the reduced diameter section and the two sections are tightened. Bolts were fixed into the ends of the rods to allow the complete assembly to be torqued up to a predetermined value. Beryllium copper was chosen as the base material of the mandrill because of its cited low-PIM performance [53]. The surface finish of the mandrill is the same polished finish as used for the solid sample rods. It was expected that the PIM characteristics of the jointed sample rods would be dominated by the junctions with a less significant contribution due to the surface properties. Three different sizes of washers were tested for each material in order to observe the effects of sample size, the number of junctions present and junction repeatability. A 50mm single sleeve of material gives a system of two junctions, one at each end between the sleeve and the beryllium copper mandrill. 10 x 5mm washers give 11 junctions whilst 51 junctions can be formed using 50 x 1mm washers. Improved consistency was anticipated in the measurements where a statistically larger number of junctions are present, i.e. when using the thinnest washers, as compared to using a single tube of material.

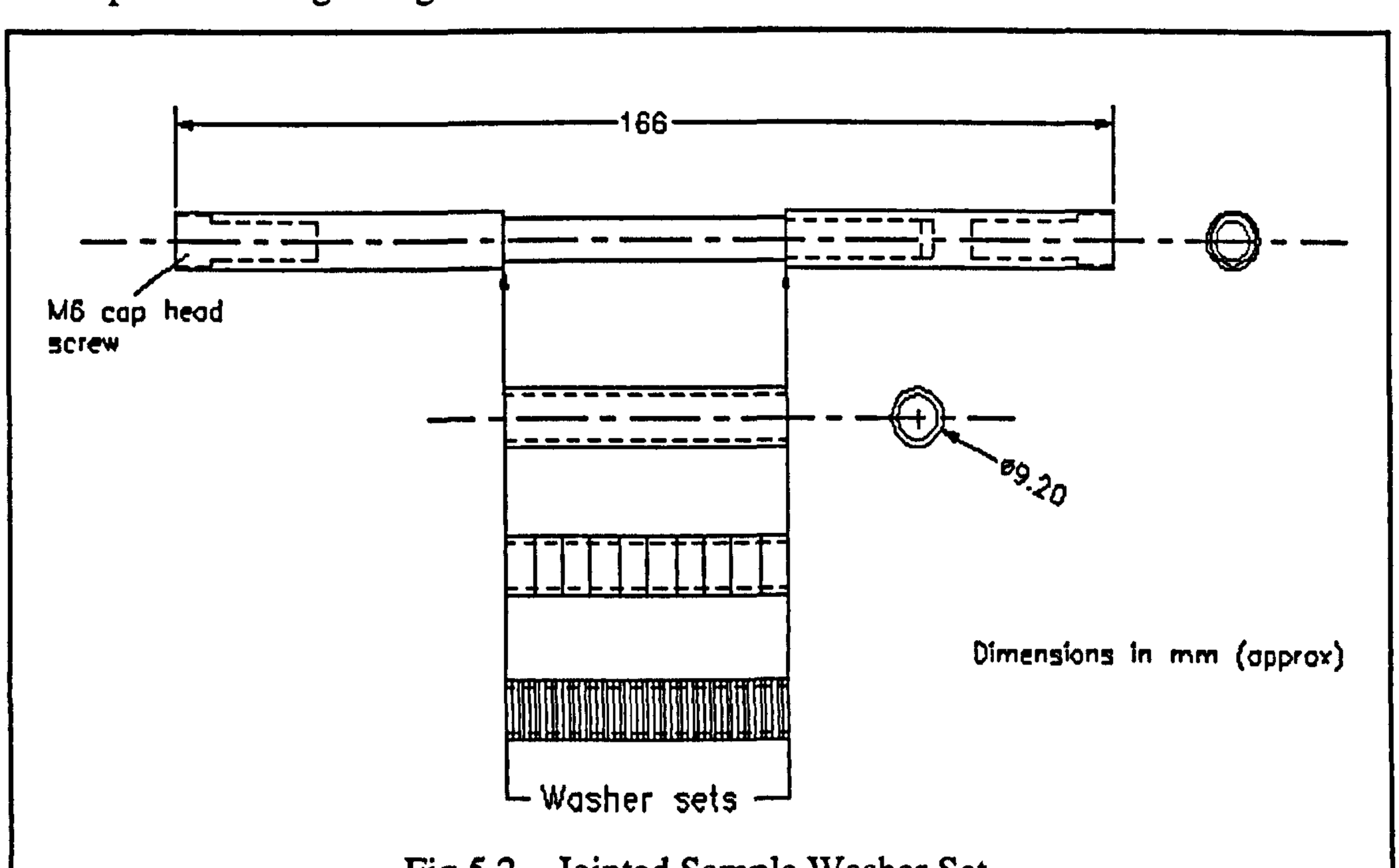

Fig.5.2 Jointed Sample Washer Set

5.4 Engineering Sample Measurements

All of the measurements were performed at ambient temperature and pressure to avoid introducing additional parameters into the evaluation of the PIM behaviour of the material in question.

5.4.1 Solid Sample Rods

Measurements were initially made on each test material sample in their 'as-machined' state, but polished and degreased, in order to obtain a series of reference levels for each sample set. Various surface treatments were then applied to selected material samples and PIM measurements repeated for the new conditions. The treatments are described as follows:

Oxidation: The sample was heated to +400°C for 30 minutes then allowed to cool naturally. It is known that the presence of oxides at junctions can cause significant non-linearities, however, no data exists on the effects of oxides on normal conducting surfaces.

Abrasion: Each sample was abraded circumferentially (i.e. transverse to the direction of current flow with graded abrasive paper (150-FF). This was carried out in order to gauge the effect of disrupting the current flow in the surface layer of the material. It was also thought that the small voids created by abrading may create microscopic metal junctions and alter the PIM signature of the sample. Abraded samples were tested 'clean' and 'dirty'. Samples were ultrasonically cleansed in an isopropyl alcohol bath after abrasion, tested, then dirtied with general grime from the workshop bench and re-tested. The was to assess the effects of surface contaminants

Thermal Stressing: The samples were heated to +400°C then plunged into cold water - the number of cycles is indicated in Table 5.3. In the space environment, materials will undergo extreme thermal cycling hence the relevance of this test. The test was designed to induce a degree of thermal stress in the samples and to examine its effects. It was thought that treatment of this sort would produce cracks and voids in the surface oxide layer and in the metal itself which could lead to microscopic metal-insulator-metal junctions at points of high current flow.

Magnetization: Samples were initially placed in the centre of a solenoid coil of DC field strength ≈240 Oersteds for 5 minutes. The magnetization was applied to the samples of steels and nickel before insertion in the test jig. The test was carried out to determine whether the residual magnetization or 'memory' effects of ferromagnetic materials had any bearing on PIM generation.

Alocrom 1200: Alocrom is a chromate/phosphate coating which is applied to aluminium surfaces to improve corrosion protection and to establish a base for paint primers [171]. It is also being increasingly used in high-power radar systems to suppress another anomalous effect called 'multipactor'[173], [174]. The coating is used extensively in the aerospace industry and to date there have been no measurements on its PIM performance, hence, its inclusion in these tests.

Silver Plating: Silver plating is applied to many materials in communications systems. Primarily this is because silver the least lossy conductive material which exists after gold and can be applied to cheaper and lighter base materials to improve their conductivity. In high power systems silver plating also helps to increase the multipactor threshold of components. Silver plating has always been considered as exhibiting low-PIM performance therfore it was included in these tests.

Surface treatments were applied to those materials where considered appropriate, i.e. oxidation was not applied to aluminium as it always has an oxide layer present. and magnetisation was applied only to the samples containing ferromagnetic materials.

The measured PIM levels of solid samples with the above surface treatments are indicated in Table 5.3. Note that these values have been obtained using the coaxial sample jig as this produced no measurable PIM signature above that of the system residual itself.

Observations:

Only three of the solid sample materials exhibited a PIM signature significantly above the system residual, two of which were found to clearly display magnetic properties (remnant magnetisation). It is relevant to note that both stainless steel A286 and 303 showed no measurable magnetization whilst within the activated solenoid, yet the steel 303 samples did display a high PIM signature. These materials may be hard ferromagnets and would not clearly display external magnetization effects until subjected to a very high field. The mechanism responsible for PIM generation in the steel 303 may still be a magnetic one due to the presence of internal magnetic domains.

Of the two materials which did clearly display ferromagnetism (steel 15-5PH and nickel), it could be casually assumed that the causative mechanism for their PIM signature is related to their magnetic properties, even though no change was observed in the PIM level after magnetising the samples. This effect was more clearly demonstrated by applying a stronger magnetic field whilst the sample was in the test jig, (refer to Section 5.4.1.1).

The reason for the lack of PIM signatures from the other samples is assumed to be due to insufficient current densities being present on the sample surfaces. The diameter of the sample rods is 9.2mm compared to a diameter of 1.63mm for the centre conductor of the UT250 semi-rigid cables. Consequently, there is a drop of surface current density in the samples in the ratio of approximately 5.6:1 relative to the semi-rigid cables (the ratio of the surface areas).

Material	No surface treatment			Oxidat -ion	Abrasion (S3)		Magnet -ization	Thermal stressing (S2)		Silver plating	Alocrom 1200 (BeCu ref. level = -150 dBm)		
	S1	S2	S3	S2	clean	dirty	S1	1 x	5 x	S4	S4	S5	S6
Aluminium 2024	-152	-152	-152	-	-152	-152	-	-152	-152	-151	-	-	-
Aluminium 6061	-152	-152	-153	-	-152	-152	-	-152	-152	-151	-	-	-
Aluminium 7075	-151	-153	-151	-	-152	-152	-	-152	-152	-	-149	-149	-148
Aluminium (99.5%)	-153	-151	-153	-	-152	-152	-	-152	-152	-	-149	-149	-150
Beryllium copper	-154	-151	-154	-152	-148	-151	-	-152	-152	-	-	-	-
Brass (CZ121)	-152	-152	-	-151	-	-	-	-	-	-	-	-	-
Copper	-152	-152	-153	-151	-152	-152	-	-	-	-	-	-	-
Stainless steel A286	-153	-151	-152	-	-	-	-148	-	-	-	-	-	-
Stainless steel 15-5PH	-143	-145	-147	-	-	-	-144 *	-	-	-	-	-	-
Stainless steel 303	-123	-121	-123	-	-	-	-122	-	-	-	-	-	-
Nickel	-123	-123	-122	-	-	-	-124 *	-	-	-153(S3)	-	-	-

Table 5.3 7th order PIM levels of solid samples in dBm (25 W per carrier)

* These samples showed remnant magnetization. No change in PIM level was observed with change in sample orientation in jig

The values S1, S2, etc. indicate the sample number of the material within a given material set.

5.4.1.1 Effect of Transverse D.C. Magnetic Field

As initial tests on the effect of magnetisation of sample rods was inconclusive, further investigations were made using a larger, variable, electromagnet. This time the electromagnet was arranged so that a field could be applied across the sample whilst the PIM was being measured. The brass sample jig, being non-magnetic, is transparent to the applied field. The field was applied across the sample at right angles to the flow of power. As well as the steels and nickel, a sample of copper was tested as a control. The results are summarised in Table 5.4, Table 5.5 and Table 5.6.

The magnitude of the magnetic field strength is given throughout this report in Oersteds (Oe) in order to allow direct comparison with other papers considering magnetic effects on materials. (In SI units $79.58\,Am^{-1} = 1\,Oe$).

In several experiments the direction of the magnetic field was reversed (by changing the direction of drive current) to determine whether this had any influence on the results. The direction of the field is indicated by a positive or negative sign before the field values.

5.4.1.2 Nickel

Transverse magnetic field (reversed)			Transverse magnetic field	
Field Strength (kOe)	PIM level (dBm) run 1	PIM level (dBm) run 3	Field Strength (kOe)	PIM level (dBm) run 2
0.05	-127.5	-128.5	-0.05	-128.5
-1.0	-126.7	-128.5	1.0	-128.5
-1.4	-121.0	-128.5	1.4	-128.5
-1.9	-122.2	-129.3	1.9	-128.8
-2.2	-123.7	-130.0	2.2	-129.5
-2.4	-124.0	-130.2	2.4	-130.0
-2.7	-124.0	-131.0	2.7	-130.3
-0.05	-128.5	-128.3	0.05	-128.3

Table 5.4 7th order PIM level variation of solid nickel sample rod (S2) with transverse magnetic field (25W per carrier)

Observations:

Three test runs were made as shown in the columns of the above table, their order being indicated by the run number. It can be seen that the levels of PIM observed for runs 2 and 3 are very similar to each other, whereas those in run 1 differ markedly both in magnitude and behaviour. Run 1 indicates a maximum PIM level achieved with about

-1.4 kOe. Runs 2 and 3 however, show a small drop in PIM signal to a minimum level when 2.7 kOe is applied. The difference between these runs is assumed to be due to the initial (unknown) magnetic state of the nickel rod. If, after run 1 the magnetic state of the rod has been moved to a well defined point on its hysteresis curve, the two following runs should then move the magnetic field strength of the rod along paths on the hysteresis curve which are also well defined and symmetrical about the axis thus manifesting as repeatable results with reversal of field.

5.4.1.3 Stainless Steel 303.

Transverse magnetic field			Transverse magnetic field (reversed)	
Field Strength (kOe)	PIM level (dBm) run 1	PIM level (dBm) run 3	Field Strength (kOe)	PIM level (dBm) run 2
0.05	-125.5	-130.0	0.05	-130.0
0.5	-130.3	-131.0	-0.5	-131.2
1.0	-131.5	-131.0	-1.0	-132.0
1.4	-132.0	-131.7	-1.4	-132.0
1.9	-133.0	-132.5	-1.9	-132.5
2.2	-133.5	-133.0	-2.2	-133.3
2.4	-134.0	-133.5	-2.4	-134.0
2.7	-134.3	-134.2	-2.7	-134.2
0.05	-130.0	-130.0	-0.05	-130.0

Table 5.5 7th order PIM level variation of solid stainless steel 303 sample rod (S2) with transverse magnetic field (25W per carrier)

Observations:

As with the nickel sample, the initial test run shows some differences in PIM level compared to the two following runs. This can again be explained in terms of the path followed on the hysteresis curve. Run 1 probably moves from the origin to a well defined point. Runs 2 and 3 move along paths which are symmetrical about the field strength axis, indicating that, as suspected, the material is ferromagnetic.

Similarly to the nickel, the PIM level reduced as the field was increased, once magnetisation of the material had been initially effected. This would suggest that the material was approaching magnetic saturation.

5.4.1.4 Stainless steel A286 (S2)

No change in PIM level was observed in material sample S2, with application of transverse magnetic field up to 2.7 kOe in either direction.

5.4.1.5 Stainless steel 15-5PH

No noticeable change in PIM level was observed in material sample S2, with application of transverse magnetic field up to 2.7 kOe. Very small changes appeared to occur when the field was changed, i.e. during field collapse.

5.4.1.6 Oxygen Free Copper

Field Strength (kOe)	Comments
0.05	PIM level -152 dBm ±3 dB
2.4	Average PIM level -156 dBm
0.05	As field turned off, PIM level rises to -140 dBm for 2 seconds then falls to -154 dBm. Above procedure was repeated but then no increase in PIM level was observed
0.05	Sample left in residual magnetic field overnight
0.05	Average PIM level -163 dBm.
2.7	Average PIM level -160 dBm for 2 minutes
0.05	PIM level fluctuates about -160 dBm average value to -140 dBm maximum.

Table 5.6 7th order PIM level variation of solid copper (OFHC) sample rod (S1) with transverse magnetic field (25W per carrier)

Observations:

A small reduction in PIM level was initially observed with applied magnetic field. This increased significantly however, when the sample was left in the residual magnetic field overnight. Further application of higher magnetic fields appeared to degrade this improvement. This phenomenon was studied more closely during the small geometry programme and is covered in Section 5.5.2.

5.4.2 Jointed Sample Rods

A range of materials was selected from those used as solid samples in order to produce washer sets for the jointed samples. A washer set consisted of one 50mm sleeve, ten 5mm thick washers and fifty 1mm thick washers (as in Fig.5.2). In the same manner as the solid samples were treated, a number of finishes were applied to the jointed samples. The materials used and the surface treatments are summarised in Table 5.7.

Surface treatment	Material	Comments
Abrasion	Aluminium (pure) Aluminium alloy 7075 Beryllium copper Brass (CZ121) Copper Nickel Stainless Steel 303	Samples first tested 'as-machined', then mating surfaces ground to reduce asperities and improve repeatability using fine abrasive paper (grade P600A). The samples were then re-tested
Oxidation	Brass (CZ121) Copper	Brass samples heated to +400° C then allowed to cool naturally. Copper heated to +250° C to avoid formation of brittle oxide layer
Magnetization	Nickel Stainless Steel 303	Samples placed in solenoid on jig former with D.C. field strength of 240 Oersteds for 5 minutes
Alocrom 1200	Aluminium (pure) Aluminium alloy 7075	Chromate conversion of surface conforming to Def. standard 03-18. Application by POETON (Cardiff) to spec. PP1 29
Silver plating	Aluminium (pure) Aluminium alloy 7075 Nickel	Space qualified finish without brighteners, 10 to 15 microns thick. Application by Johnson Matthey (Herts.), inspection level C
Solders	In-Pb (50/50) Sn-Pb (60/40) Sn-Pb-Ag (62/36/2)	Brass washers act as base metal After bonding washers together, surface of tube was skimmed to remove superficial solders/ adhesive, leaving only bonding agent between washer interfaces
Adhesive	Silver loaded epoxy	

Table 5.7 Materials for jointed samples and their surface treatments

In the case of the solders and adhesive, a set of washers consisted of one reference 50mm brass sleeve and fifty 1mm brass washers, which were bonded by the material under test. The purpose of these tests was to evaluate these bonding materials which are commonly used in space hardware and for which no clear data on PIM generation is available.

The effect of various levels of torque was also investigated as this was expected to have a strong bearing on the repeatability of measured PIM levels. The torque was applied using a standard torque wrench. A first order analysis of the contact pressure expected between the washers for an applied torque of 5Nm is given below: (refer to Fig.5.3)

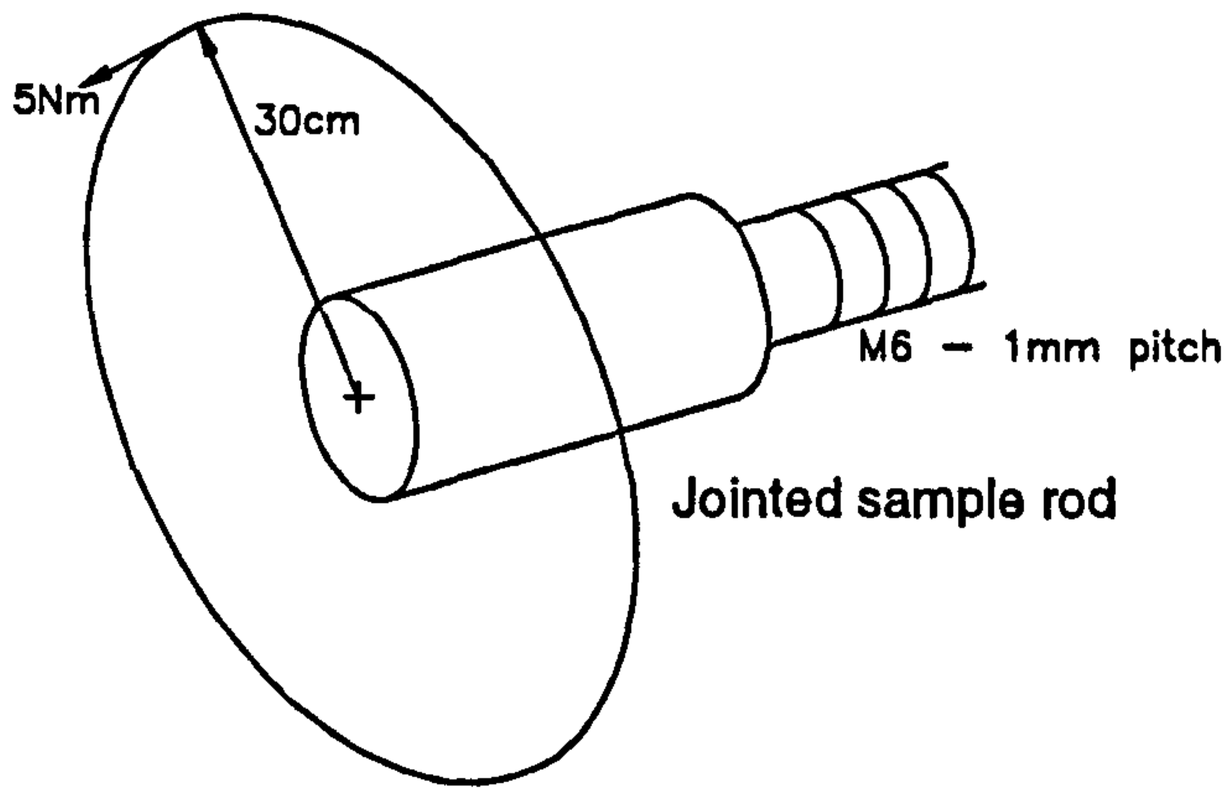

Fig.5.3 Application of torque to a jointed sample rod

- For a torque wrench length of 30 cm, one full turn equates to 1 mm of sample compression. Therefore, the mechanical advantage (ignoring friction) is 2π x 300:1 = 1885:1.

- The force which needs to be applied at a distance of 30 cm to produce a torque of 5 Nm = 16.7 N. This force is effectively magnified by the mechanical advantage at the washer interfaces.

- Therefore, force between washers (ignoring frictional losses) = 3.1×10^4 N.

- Surface area of washers = 28 mm^2. Therefore, pressure applied between washer surfaces = **1.1 GPa** (ignoring frictional losses).

If frictional losses are assumed to be as much as 90%, the pressure between the washers will then be of the order of **110 MPa.**

From the above simplified calculations it can be seen that a substantial pressure is present between the washer interfaces for an applied torque of 5 Nm. The magnitude is of the order normally required when producing high contact pressure joints in microwave components, i.e. greater than 60 MPa, (being dependant on the tensile properties of the material). It is not surprising therefore, to observe the PIM level reducing to a lower and more consistent level in the jointed samples when these pressures are achieved.

As with the solid samples, measurements were initially made on each washer set in their 'as-machined' state (de-burred and de-greased finish), in order to obtain a series of reference levels.

The results of the jointed sample measurement program are given in the following sections.

5.4.2.1 Surface Finish

The majority of the following measurements were made using the initial engineering sample jig and only those values of interest were revisited using the improved coaxial sample jig. A comparison can be made between the two sample jigs by comparing columns marked ESJ and CSJ in Table 5.8

		Unground faces					Ground faces	
		Finger-tight		5 Nm		7 Nm	5 Nm	5 Nm
Material		ESJ	CSJ	ESJ	CSJ	ESJ	ESJ	CSJ
Aluminium (43 unground) (47 ground)	( ) washers	-105	-119	-134	-151	-136	-	-151
	10 spacers	-126	-141	-138	-151	-134	-	-151
	Single tube	-131	-79	-134	-153	-133	-	-154
Beryllium copper (45 unground) (52 ground)	( ) washers	-118	-152	-138	-153	-	-	-156
	10 spacers	-138	-134	-138	-154	-	-	-154
	Single tube	-138	-123	-138	-152	-	-	-156
Brass (CZ121) (41 unground) (41 ground)	( ) washers	-	-145	-	-146	-	-	-150
	Single tube	-	-119	-	-155	-	-	- 155
Copper (39 unground) (39 ground)	( ) washers	-132	-131	-137	-151	-	-	-151
	10 spacers	-137	-148	-137	-151	-	-	-153
	Single tube	-135	-139	-135	-152	-	-	-153
Nickel (45 unground) (53 ground)	( ) washers	-108	-	-112	-	-109	-129	-142
	10 spacers	-118	-	-126	-	-127	-	-131
	Single tube	-113	-	-125	-	-125	-	-131
Stainless Steel 303 (42 unground) (46 ground)	( ) washers	-107	-	-112	-	-113	-115	-122
	10 spacers	-98	-	-120	-	-121	-120	-128
	Single tube	-111	-	-123	-	-123	-121	-130

Table 5.8 7th order PIM level (dBm) of untreated jointed samples with different applied torques (25 W per carrier)

Note that the effect of surface abrasion was tested in a different manner for the jointed samples. The sample washers were first measured in their 'as-machined' state, i.e. de-burred with unground mating faces. The mating faces of the relevant washers were then ground down to reduce surface asperities, using fine abrasive paper. Measurements were repeated to determine the effect of improving the interfacial contact area.

Observations:

Above a torque of 5 Nm, the PIM level in all tests was observed to be very consistent and independent of the order in which the washers were placed on the jig.

Comparison of the non-abraded and surface ground washers reveals a drop in PIM level as the surface contact was improved. Nickel showed a significant change. The reduction in PIM level for the steel 303 was less dramatic and only occurred for the 1 mm washers. (In both cases the number of 1 mm washers tested was larger after surface grinding due to a reduction in their width).

Comparison of the un-ground 1 mm nickel washers to the spacers and tube of the same set shows a significant reduction in PIM levels as the sample size increase, i.e. the number of junctions goes down. However, comparison of the surface ground nickel washer set with the solid material shows an unexpected *reduction* in the PIM level compared to the solid sample. This behaviour although highly unexpected, was found to produce very stable and repeatable results.

5.4.2.2 Surface Treatments

The surface treatments, as indicated in Table 5.7, were then applied to each material set and PIM measurements repeated for the new conditions. Table 5.9 indicates the measured PIM values obtained with the relevant surface treatments using the coaxial sample jig.

Note that the surface treatments were applied to the samples after they had been de-burred and ground from their 'as-machined' state using fine abrasive paper. Where relevant, the measurements for the ground samples are repeated in Table 5.9 so that they may be easily compared with the measurements on surface treatment.

Material		Ground surfaces	Oxidation	Magnetization	Silver plating	Alocrom 1200		Bonding			
						Set A	Set B	Sn/Pb	Sn/Pb/Ag	In/Pb	Loaded epoxy
Aluminium	47 washers	-151	-	-	-150 (52)	-65	-73	-	-	-	-
	10 spacers	-	-	-	-150	-100	-141	-	-	-	-
	Single tube	-	-	-	-149	-154	-151	-	-	-	-
Aluminium alloy 7075	52 washers	-	-	-	-154	-87	-91 (51)	-	-	-	-
	10 spacers	-	-	-	-153	-76	-85	-	-	-	-
	Single tube	-	-	-	-152	-149	-149	-	-	-	-
Brass (CZ121)	41 washers	-146	-147	-	-	-	-	-148 (46)	-148 (46)	-147 (47)	-150 (46)
Copper	39 washers	-151	-151	-	-	-	-	-	-	-	-
Nickel	53 washers	-142	-	-141 #	-154 (50)	-	-	-	-	-	-
	10 spacers	-131	-	-	-151	-	-	-	-	-	-
	Single tube	-131	-	-	-151	-	-	-	-	-	-
Stainless Steel 303	46 washers	-122	-	-122 #	-	-	-	-	-	-	-
	10 spacers	-128	-	-	-	-	-	-	-	-	-
	Single tube	-130	-	-	-	-	-	-	-	-	-

Table 5.9 7th order PIM levels of Jointed Samples in dBm (5 Nm, 25 W)

No change was observed in PIM level when replacing the washers in a different order on the jig.
( ) Numbers in brackets indicate number of 1 mm washers used for the related test

Observations:

Silver plating has clearly removed the deleterious effect of nickel, bringing its PIM level down to that of the system residual. The skin depth of silver at 1650 MHz is approximately 1.6 microns. The silver plating is approximately 13 microns thick which is 8 skin depths. For the power levels used here, it is clear that the field strength within the sample at 8 skin depths has decreased sufficiently not to cause any measurable stimulation of the nickel structure.

Alocrom 1200 revealed extremely high levels of PIM which varied in magnitude between different sets and decreased in magnitude with decreasing number of junctions. Further tests were performed on Alocrom to begin to determine the cause of the PIM, refer to Table 5.10.

As for the plain samples, no change was observed in the PIM level with either oxidation of the surfaces or with magnetization. The same reasons as stated earlier are also suspected as being operative here. Namely, that insufficient current densities are present in the case of oxidation and that the induced magnetic field is too weak or wrongly orientated in relation to the propagation field.

No obvious problems were observed with any of the solders or adhesives. Comparison of the reference level for brass washers alone shows no significant change when the interfaces consisted of solders or adhesive.

5.4.2.3 Dissimilar Metal Junctions

Alternating junctions of different metals were assembled on the jointed sample jig and measurements performed. The results are presented in Table 5.10. The numbers in brackets indicate the configuration of the washers used. The term alternated is used to define the way in which washers of different types were placed alternately, one-at-a-time, onto the sample rod.

Observations:

- The only dissimilar metal junction which had a detectable PIM signature was that of aluminium-Alocrom 1200. It is quite clear from the results that the PIM mechanism is related to junctions between the aluminium/aluminium oxide and Alocrom as Alocrom with any other metal does not produce high PIM levels. The single instance of a brief PIM signal for the silver plated aluminium-Alocrom is assumed to be due to surface contaminants of aluminium as a repeat test failed to reveal this anomaly. The results of further tests carried out on the aluminium-Alocrom junction can be found in the next section.

Washer arrangement (No. 1 mm washers)	PIM level & comments
Al (Cu + Al(alternated)(Al (2) (17 + 16) (8)	-150 dBm, stable
Al + Ag-plated Al (26 + 25) alternated	-149 dBm, stable
Al + Alocrom Al (set A) (25 + 24) alternated	-87 dBm with ±3 dB fluctuations, settling to -85 dBm after 2 minutes
BeCu + Alocrom Al (set A) (27 + 26) alternated	-151 dBm, stable
Ag-plated Al + Alocrom Al (set A) (29 + 28) alternated	-150 dBm, although brief jump to -74 dBm, level returning to -150 dBm
Ag-plated Al + Alocrom Al (set A) (29 + 28) alternated	(Check on above performance). PIM level remains around -154 dBm with no jumps in PIM level seen
Ag-plated Ni + Alocrom Al (set A) (27 + 26) alternated	-149 dBm, stable
Al + Alocrom Al (set A) (25 + 24) alternated	Begins at -82 dBm gradually falling to -84 dBm
Al + Alocrom Al(7075) (set A) (25 + 24) alternated	-82 dBm, stable

Table 5.10 7th order PIM levels of dissimilar junctions (25 W per carrier)

5.4.3 The Aluminium-Alocrom Junction

As extensive use is made of Alocrom or Alodine surface conversions in space hardware, it was considered judicious to make a more detailed investigation of the behaviour of possible junctions between this and other materials. The choice for this approach becomes even more important when the exceedingly high levels of PIM already observed with the aluminium-Alocrom junction are taken into account.

It can be imagined that the junction between aluminium and Alocrom treated aluminium will consist of asperities which penetrate the opposite surface, after the contact model of Section 2.4.2.1 on page 26. At the point of penetration there will be very thin layers of aluminium, aluminium oxide and Alocrom. The surface physical structure of these two materials (aluminium and Alocrom) thus leads one to suggest that semiconductor action and/or the tunnelling effect would be the most likely dominant non-linear mechanisms involved in any PIM generation between a junction of the two. Consequently, it was considered most appropriate to study this particular junction

5.4.3.1 Effect of Temperature on Multiple Aluminium-Alocrom Junctions

Thermal cycling of the sample was achieved by passing pressurised pre-cooled/ heated air through the internal volume of the coaxial measurement jig. The jig was modified by drilling two small holes through the outer wall at either end of the internal cavity. Two copper tubes were soldered into the holes so that flexible tubing could be attached allowing airflow through the jig. The holes are small enough such that no R.F. leakage will take place due to their being waveguide beyond cutoff. On testing, the modifications had no effect on the PIM performance of the jig.

Cooling was achieved by first drying the air (to remove water vapour which may affect the measurements) by passing it through a glass coil sat in liquid air. The air was then further cooled by passing it through a second stage copper coil also sat in liquid air. The air could be heated by replacing the second stage coolant by a heater jacket. The rate of cooling and heating was controlled by control of the air pressure.

Two thermal cycling runs were made prior to PIM testing the samples with no R.F. power present and a thermocouple attached to the surface of the sample. In this way, the rate of change of temperature of a sample placed inside the measurement jig, whilst subjected to the temperature controlled air flow could be calibrated. From these runs the approximate temperature of the sample could be estimated at a given time. The minimum temperature achieved was -80° C and the maximum +40° C.

Prior to testing the aluminium-Alocrom washer arrangement, a solid beryllium copper sample was mounted in the coaxial sample jig and this was run through a single temperature cycle. Some brief increases in PIM to a level of -134 dBm were observed with the nominal level remaining around -145 dBm. These variations are believed to have been due to heating effects in the quiet load which had no forced cooling aids at the time. A fan was later placed on the load to improve heat dissipation. As the level of any fluctuations in PIM were observed to be far below the PIM level generated by the aluminium-Alocrom junctions the test set-up was considered to be in a satisfactory state to proceed with further temperature cycling tests.

25 aluminium washers and 24 Alocrom (aluminium alloy 7075) washers were mounted alternately on the jointed sample jig, such that an aluminium washer was at either end (to reduce damage of the Alocrom coating due to rotational washer movement

during tightening).The sample jig was tightened to a torque of 5 Nm at 30 cm (equivalent to a maximum washer contact pressure of ≈1120 MPa). A constant 25 Watts per carrier was applied throughout the tests, the results of which are indicated in Table 5.11

Time (mins)	Estimated temp. (° C)	Comments
0	20	PIM level allowed to stabilise over 10 minute period. Starting level of -77 dBm
2	0	PIM level -75 dBm
4	-20	PIM level -73 dBm
5	-30	PIM level -72 dBm
7	-55	PIM level -72 dBm
12	-75	PIM level -72 dBm
20	-80	PIM level stable at -72 dBm
35	-80	2nd stage cooling stopped to begin heating cycle.
38	-60	PIM level -73 dBm
41	-40	PIM level -74 dBm
46	-20	PIM level -75 dBm
57	-10	PIM level -76 dBm
78	-5	PIM level -77 dBm
87	0	Heater jacket on 2nd stage coil, heating begun.
93	10	PIM level -80 dBm
98	10	1st stage air drying coil removed from liquid air
114	30	PIM level -80 dBm
124	40	PIM level -80 dBm
133	40	PIM level -81 dBm
136	40	Heating stopped, air flow continued to cool sample
164	20	PIM level -78 dBm

Table 5.11 Multiple aluminium-Alocrom washer interfaces under thermal cycling (25 W per carrier)

5.4.3.2 Effect of Transverse Magnetic Field

Following completion of the above test a transverse magnetic field was applied to the sample set. The field was increased from the residual level (≈ 40 Oersted) to 2.7 kOe but no significant change in the PIM level was observed.

5.4.3.3 Effect of Contact Pressure Between Interfaces.

Several tests of the PIM behaviour versus applied torque were made on an alternating set of aluminium (25) + Alocrom coated aluminium alloy 7075 (24) 1 mm washers. During the preliminary test no measure of the applied torque was made (due to lack of appropriate equipment). However, the torque was kept below that used for the majority of the jointed sample measurements (5 Nm).

Preliminary Measurements.

The spectrum analyser was set on zero frequency span during these tests to allow a more continuous observation of the PIM behaviour with time. With this set-up PIM levels close to the system residual showed a variation of about ±2 dB.

Applied torque (qualitative)	Comments
45° rotation of rod past finger-tight torque	PIM level begins at -78 dBm dropping to -80 dBm after 2 minutes, then to stable level of -81 dBm after further 1minute.
90° rotation of rod past finger-tight torque	PIM level begins at -59 dBm falling in 2 minutes to -69 dBm. Level falls to -80 dBm in next minute then gradually to -83 dBm over further 4 minutes.
135° rotation of rod past finger-tight torque (now 5 Nm)	PIM level begins at -74 dBm falling to stable level of -82 dBm in 1 minute.
	Before commencing the next set of measurements the washer arrangement was cleaned with high pressure air.
Finger tight	PIM level initially -64 dBm, fluctuating greatly until after 2 minutes it stabilises at -92 dBm. Power was turned off for 30 mins. then turned on again. PIM level starts at -99 dBm rising gradually to -93 dBm in 1 minute then to -91 dBm after further 3 minutes.
10° rotation of rod past finger-tight torque	PIM level starts at -64 dBm, oscillating between -83 dBm and -69 dBm for 10 seconds then gradually falls to -107 dBm over 3 minutes. Jump of level to -76 dBm and gradual fall to -85 dBm over 30 seconds. Level stabilises around -89 dBm.
20° rotation of rod past finger-tight torque	PIM level oscillates between -74 dBm and -82 dBm for 30 seconds then stabilises around -75 dBm.
30° rotation of rod past finger-tight torque	PIM level oscillates from -84 dBm to -81 dBm then gradually rises to -78 dBm over 1 minute. Level then gradually approaches and stabilises around -85 dBm.
Washers loosened, blown clean with high pressure air and re-tightened to 10° rotation of rod past finger-tight torque	PIM level begins at -67 dBm for 45 seconds the gradually falls to -82 dBm in 2 minutes. Level stabilises around -83 dBm.

Table 5.12 7th order PIM level with unmeasured low washer interface contact pressures (25 W per carrier)

Application of Low Contact Pressures.

In light of the qualitative results obtained for different contact pressures between washer faces, it was seen to be useful to progress one step further in being able to quantify the magnitude of contact pressure being used. In order to produce lower contact pressures between the washer faces as had been used previously, a simple jig was set-up allowing known masses to apply a calculable torque to the sample rod. The maximum contact pressure between washer faces was then determined in the same way as has been described in Section 5.4.2.1.

Mass (g)	Max. Pressure (MPa)	Comments
150	34	PIM level fluctuates between -84 dBm and -91 dBm for 2 minutes, approaching -89 dBm level. After further 1 minute, level drops to -95 dBm, gradually falling to stable level of -102 dBm in next 5 minutes. Washers were loosened off and high pressure air used to clean between them before next increase in contact pressure
300	67	PIM level initially -80 dBm falling gradually to -96 dBm in 1 minute. Stable for 30 seconds then falling gradually to -99 dBm over next 5 minutes
500	112	PIM level starts at -85 dBm falling quickly to -86 dBm then gradually to -83 dBm over 2 minutes. Stable at -83 dBm for 3 minutes, creeping up to -80 dBm in 1 minute (and remaining for 3 minutes) then falling back to -82 dBm
650	145	PIM level initially -89 dBm increasing gradually to -87 dBm in 1 minute. Stabilises at -86 dBm after further 2 minutes
1180	264	PIM level falls from -99 dBm to stable level of -103 dBm in 30 seconds
1898	425	PIM level falls from -89 dBm to -91 dBm in 20 seconds, rises briefly to -88 dBm then stabilises at -91 dBm
2370	531	PIM level fluctuates ±2 dB about -89 dBm for 1 minute, stabilising at -88 dBm
3048	683	PIM level starts at -89 dBm, fluctuating from -100 dBm to -80 dBm for 20 seconds. Level approaches -77 dBm for 2 minutes, stabilising at -79 dBm
3766	844	PIM level increases from -88 dBm to -81 dBm in 40 seconds, falling to -85 dBm in further 30 seconds. Falls to -89 dBm in further 30 seconds eventually stabilising at -91 dBm
	1120	Sample jig torqued up to normal value with torque wrench (5 Nm at 30 cm). Level increases from -86 dBm to -79 dBm in 20 seconds then fluctuates ±2 dB about -80 dBm for 30 seconds. Stabilises at -80 dBm

Table 5.13 7th order PIM level with low washer interface contact pressures (25 W per carrier)

Observations:

Inspection of the washer faces after testing showed damage to the Alocrom finish for those washers nearest the jig end piece which turned during tightening. The extent of the damage decreased further away from this end piece. Clearly, removal of the Alocrom occurred when the washer faces ground against each other during tightening. The amount of movement of washers (and thus damage) decreased along the length of the sample jig. The majority of the washers revealed damage to the middle section of the faces indicating that less contact was occurring at the inner and outer washer edges. To minimise this damage a single washer pair were assembled in the middle of the sample jig. Further details are given in the following sub-section.

Single Macroscopic Alocrom-Aluminium Junction.

In order to avoid removal of the Alocrom surface during increase in contact pressure a different arrangement of washers was used. This involved only one aluminium and one Alocrom washer surrounded by an appropriate number of beryllium copper washers. Three different pairs of aluminium-Alocrom washers were tested for statistical comparison. The results are given in the following tables:

Max. Pressure (MPa)	Comments
67	PIM level initially -84 dBm falling to -88 dBm in 1 minute. Level then decreases to -91 dBm in next minute, to -93 dBm in following minute, eventually stabilising at -95 dBm after a further minute.
264	PIM level starts at -110 dBm falling to -114 dBm in 2 seconds. After 20 seconds level then jumps to -86 dBm falling back to -107 dBm after 10 seconds. Level then falls to -111 dBm over 2 minutes. Level gradually stabilises at -117 dBm
1120	PIM level less than -143 dBm
	Inspection of the washer surfaces under 20x magnification showed no visible damage to the Alocrom surface

Table 5.14 PIM behaviour of aluminium-Alocrom junction - washer pair 1

Max. Pressure (MPa)	Comments
67	PIM fluctuates ±3 dB about -135 dBm level
264	PIM fluctuates wildly from -55 dBm to -90 dBm for 2 minutes. Settles to -97 dBm ±2 dB for 2 minutes then stabilises at -97 dBm
1120	PIM level initially -96 dBm rising to -92 dBm in 20 seconds then returning to -96 dBm. Fluctuations between -100 dBm to -90 dBm occur over next 2 minutes then stabilising at -86 dBm for 2 minutes. Slow decrease in level to -89 dBm followed by a drop to -93 dBm then gradual increase towards a stable level of -90 dBm
	Inspection of the washer surfaces under 20x magnification showed a very small area of damage to the Alocrom surface where aluminium showed through

Table 5.15 PIM behaviour of aluminium-Alocrom junction - washer pair 2

Mass (g)	Max. Pressure (MPa)	Comments
300	67	PIM level initially -54 dBm falling to -86 dBm in 20 seconds. Level decreases to -92 dBm in further 30 seconds then to -97 dBm in following minute. Level fluctuates about -99 dBm ±2 dB before stabilising at -101dBm
1180	264	PIM level falls from -97 dBm to stable level of -98 dBm in 1 minute Sample rod turned (Alocrom on i/p side): PIM level starts at -94 dBm for 10 seconds dropping to -106 dBm where it fluctuates for 20 seconds before returning to a stable level of -94 dBm Sample rod turned (Aluminium on i/p side): PIM level initially -98 dBm. Brief jump in level to -94 dBm then fluctuates from -99 dBm to -104 dBm for 20 seconds before stabilising at -98 dBm Sample rod turned (Alocrom on i/p side): PIM level stable at -94 dBm
	1120	PIM level increases from -119 dBm to -93 dBm in 30 seconds. After 30 seconds at -92 dBm PIM falls to stable level of -96 dBm over 1 minute.
		Inspection of the washer surfaces under 20x magnification showed no visible damage to the Alocrom surface

Table 5.16 PIM behaviour of aluminium-Alocrom junction - washer pair 3

Observations:

- In general the level of PIM decreases with increasing contact pressure. This has not been found to be entirely repeatable for all washer pairs. The cause of this is assumed to be due to the variable amount of surface damage occurring on tightening the washer arrangement. Damage could be occurring either by rotational movement of one surface against the other. However the variation in PIM may also be due to an increase in the number of asperities penetrating through the Alocrom layer thus forming more non-linear junctions.

- In the majority of cases the PIM signal began at a high level for up to 30 seconds falling towards a stable level after several minutes.

- In one instance very low stable levels of PIM were observed for a fixed contact pressure. If the nominally average PIM level were to be taken as -95 dBm, this level was more than 40 dB lower than this and only 10 dB to 15 dB above the system residual.

- On reversing the position of the interface materials (Alocrom & aluminium) relative to the signal carrier direction, a repeatable difference in the stable PIM level was observed, refer to Table 5.16.

Effect of Temperature on a Single Aluminium-Alocrom Washer Pair

A thermal cycle was carried out on a single aluminium-Alocrom washer pair to determine whether any clear conclusions could be drawn about the nature of the mechanism at work. A 5 mm aluminium washer and 5 mm Alocrom (Al 7075) washer were placed on the sample jig surrounded by beryllium copper washers. The jig was tightened to achieve a contact interface pressure of approximately 264 MPa. The results of this test are given in Table 5.17.

Observations:

- The PIM level was seen to increase with decreasing temperature. This was observed with both the multiple washer sample and the single washer pair. On returning to ambient temperature the sample did not regain its initial PIM level. It actually produced a lower level of PIM.

Time (mins)	Estimated temp. (° C)	Comments
0	20	PIM level allowed to stabilise over 10 minute period. Starting level of -79 dBm
1	10	PIM level -77 dBm
7	-55	PIM level -77 dBm
12	-75	PIM level -77 dBm
20	-80	PIM level stable at -77 dBm
40	-80	PIM level stable at -77 dBm
45	-80	Transverse magnetic field applied to sample junction. Field varied between residual level (40 Oe) to 2.5 kOe but no significant change in PIM level observed
55	-80	2nd stage cooling stopped to begin heating cycle.
60	-60	PIM level -78 dBm
70	-15	PIM level -81 dBm
78	-15	Heater jacket on 2nd stage coil, heater on
80	0	PIM level -83 dBm.
90	15	PIM level -84 dBm. 1st stage air drying coil removed from liquid air
100	25	PIM level -86 dBm
140	40	PIM level -89 dBm
145	40	Heating stopped, air flow continued to cool sample
170	20	PIM level stable at -87 dBm

Table 5.17 Single aluminium-Alocrom washer interface under thermal cycling (25 W per carrier)

5.4.4 High Density Multi-junction Samples

A commonly cited strategy proposed for identifying the effect of specific mechanisms is to produce a single ideal grown junction exhibiting the required mechanism and then to observe the PIM characteristics of this junction when subjected to two RF signals [23]. This approach is considered to have the following drawbacks:

- materials available to produce an ideal junction are limited and would not provide a reasonable comparison with the engineering materials already investigated

- an ideal junction may be quite different from those which occur in normal engineering practise

- it would be time consuming to produce a single ideal junction exhibiting the preferred mechanism satisfactorily

- consistency of PIM behaviour between a number of such junctions would be difficult to achieve

With the success of the jointed sample measurement jig, a different approach was proposed in order to tackle the problem of mechanism identification more logically. The proposition was to produce a more effective multi-junction sample in which engineering materials could easily be used, with the expectation that a large number of junctions would produce a greater and more consistent PIM level than has been observed with single, jointed, engineering samples. Having achieved consistent behaviour the emphasis would then lay in devising techniques to identify the dominant PIM mechanisms at work, e.g. by controlled variation of specific parameters such as temperature, electric/magnetic field, DC bias, etc. Consistency of performance is considered to be a key factor without which meaningful conclusions cannot be easily drawn.

A preliminary multi-junction sample was produced and tested. Fig.5.4 shows an outline of the sample construction. The sample material was placed in granulated form between the jointed sample jig former and a PTFE sleeve then the jig is torqued up to ensure good contact between the material granules. The following material types were tested:

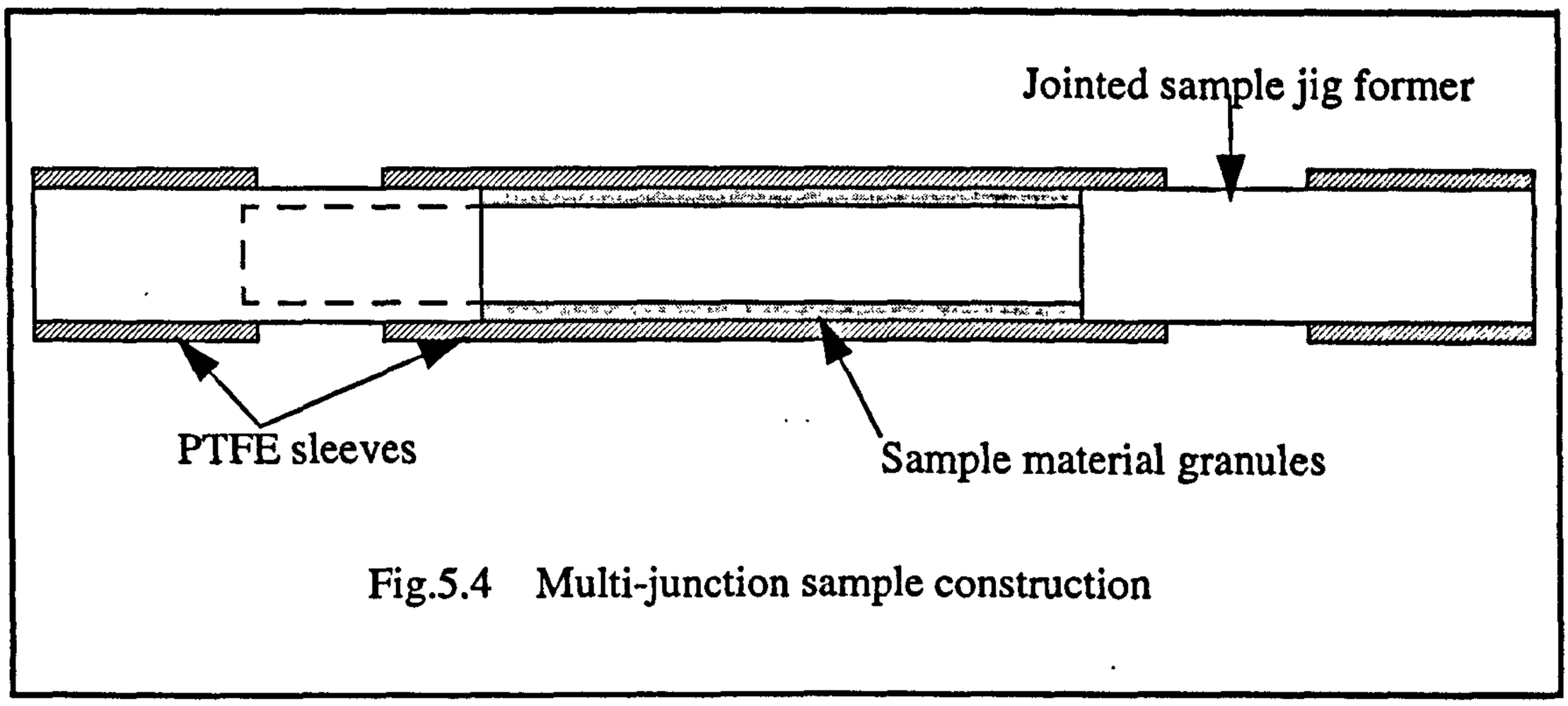

Fig.5.4 Multi-junction sample construction

- brass turnings:

  - return loss > 16 dB from 1530 MHz to 1650 MHz

  - PIM level -60 to -80 dBm (25 W per carrier), variable level observed

- aluminium alloy 6061 filings:
    - PIM level -80 to -110 dBm (25 W per carrier), stable periods of several minutes observed

Although the preliminary sample did not produce sufficiently consistent levels to allow meaningful measurements to be made it does show potential as one form of a multi-junction sample jig.

This is the point at which the engineering scale sample programme was brought to a conclusion. Due to time constraints it was decided to move on to the small geometry sample programme which is described in the next section.

5.5 Small Geometry Sample Programme

It can be seen from measurements performed on the engineering samples that higher current densities are required to resolve the PIM characteristics of certain material types over and above that of the system PIM residual. For this reason it was decided from the start of the programme to move progressively from large scale engineering type samples to smaller scale samples where higher current densities can be achieved. The adopted format of these smaller scale samples is 1 mm diameter wires, which are readily available in numerous materials. The wire format lends itself very satisfactorily to use in a simple coaxial test jig which is compatible with the rest of the PIM system and was described in Section 4.10.4. This is an important factor as it minimises system design considerations and enhances the potential for reliable, consistent measurements. A selection was made of material types in wire form which correspond in chemical composition, as closely as possible, to those tested in the large scale engineering format. These are given in Table 5.18.

Material	Composition
Aluminium (99.5%)	Cu < 500, Fe < 4000, Mn < 500, Si < 3000, Zn < 1000, rem Al
Aluminium alloy (6061)	Cr 2500, Cu 2500, Mg 1%, Si 6000, rem Al
Copper (99.95% OFHC)	Ag 100, Al 1, Bi 1, Ca 3, Cd 1, Fe 2, Mg 1, Pb 3, Si 2, Sn 2, rem Cu
Beryllium copper	Be 1.7 - 1.9%, Co+Ni 500-4000, total impurities 5000, rem Cu
Nickel (99.98%)	Co 8, Cr 8, Cu 10, Fe 10, Mg 10, Mn 10, Si 8, Ti 10, C 70, S 10, rem Ni
Stainless steel AISI 304	Cr 17 - 20%, Mn < 2%, Ni 8 - 11%, C < 800 rem Fe

Table 5.18 Wire sample material compositions (1 mm diameter)

Note: The elemental composition values in Table 5.18 are given in percentage where indicated and parts per million (ppm) elsewhere.

5.5.1 Wire Sample Tests

Initial preparation of the samples involved cutting the wires to a length of 127mm (±0.5mm), squaring off the ends and removing any burrs using fine abrasive paper (on wire ends only). The wire was then cleaned in isopropyl alcohol (IPA) before inserting it into a PTFE sleeve. The sleeve had been cleaned internally by running some IPA through it which was blown through thoroughly using clean high pressure air. After testing each sample in its untreated state various surface treatments were applied in order to follow up the work conducted on the engineering samples, (refer to Table 5.19). Measurements results for the different surface treatments are given in Table 5.20 and Table 5.21.

Surface treatment	Material	Comments
Abrasion	Aluminium (pure) Aluminium alloy 6061 Beryllium copper Copper Nickel Stainless steel 304	Transverse abrasion: samples abraded circumferentially with abrasive paper (grade 150-FF) then ultrasonically cleaned in IPA. Longitudinal abrasion: samples abraded along axial length with abrasive paper (grade 150-FF) then ultrasonically cleaned in IPA.
Oxidation	Beryllium copper Copper	Beryllium copper sample heated to +400° C then allowed to cool naturally. Copper heated to +250° C to avoid formation of brittle oxide layer
Thermal stressing	Aluminium (pure) Aluminium alloy 6061 Beryllium copper Copper Nickel Stainless steel 304	Sample dipped in liquid air for 20 seconds then into water at room temperature. Process was then repeated.
Alocrom 1200	Aluminium (pure) Aluminium alloy 6061	Chromate conversion of surface conforming to Def. standard 03-18. Application by POETON (Cardiff) to spec. PP1 29
Silver plating	Aluminium (pure) Aluminium alloy 6061 Nickel	Space qualified finish without brighteners, 10 to 15 microns thick. Application by Johnson Matthey (Herts.), inspection level C

Table 5.19 Materials for wire samples and their surface treatments

Material	Un-treated	Transverse abrasion		Longitudinal abrasion		Oxidation	Thermal stressing
		A	B	A	B		
Aluminium (99.5%)	-144	-136	-129	-140	-	-	-142
Aluminium alloy (6061)	-144	-135	-129	-136	-	-	-143
Copper (99.95% OFHC)	-144	-138	-122 *	-143	-	-143	-140
Beryllium copper	-144	-139	-131 *	-143	-	-144	-141
Nickel (99.98%)	-97	-93	-94	-95	-	-	-98
Stainless steel AISI 304	-105	-90	-83	-110	-100	-	-104
	-106	-	-	-104	-100	-	-

Table 5.20 7th order PIM levels of treated wire samples in dBm (25W per carrier)

* Both the beryllium copper and copper wire samples were oxidised following the abrasion process but no further change in PIM level was observed.

Columns A and B indicate two stages of abrasion applied to the same wire sample, stage B having received further abrasion.

Material finish	1	2	3	4
Silver plated Aluminium (99.5%)	-148	-146	-145	-147
Silver plated Aluminium alloy (6061)	-145	-146	-145	-146
Silver plated Nickel (99.98%)	-145	-146	-	-
Alocrom coated Aluminium (99.5%)	-141	-142	-141	-142
Alocrom coated Aluminium alloy (6061)	-142	-143	-142	-143

Table 5.21 7th order PIM levels of coated wire samples in dBm (25W per carrier)

Observations:

- Both nickel and stainless steel produce high PIM signatures which can be attributed to their magnetic properties. This was investigated further and is described in Section 5.5.2.

- Although only a qualitative assessment can be made, transverse abrasion of a material appeared to increase the PIM level more than longitudinal abrasion. This would appear to be a reasonable expectation as transverse abrasions introduce a greater number of irregularities across the direction of current flow thus increasing the non-linear properties of the material surface.

- As was seen with the engineering samples, silver plating the nickel wires reduced the PIM level down to that of the system residual.

- Alocrom 1200 showed no PIM signature whilst present only as a surface treatment. This is in agreement with the results shown in Table 5.3.

- Oxidation and thermal stressing showed no change in the PIM levels of the materials tested.

5.5.2 Magnetic Field Interaction

The affect of applying a D.C. magnetic field transverse to the direction of R.F. current flow in the sample (dominant propagation mode current) was investigated.

For the wire samples a maximum magnetic field strength of approximately 4.2kOe could be achieved at the surface of the wire. In the case of the Solid and Jointed samples a maximum magnetic field strength of only 2.7kOe could be attained due to the larger jig which required the poles of the electromagnet to be spaced further apart.

When the magnetic field was turned off a very small field was still present between the pole pieces due to the remnant magnetisation of the steel jig on which the field coils were mounted. This field was measured to be about 50Oe ±10Oe. When this value appears in the tables it indicates that the field had been turned off and that the sample remained between the magnetic pole pieces. Considering the results of the following measurements this very low field strength can be considered to be essentially zero. Several entries of 0Oe are to be found in the tables and these represent measurements made with the magnet moved away from the test sample and where the field strength measured in the vicinity of the sample is below 5Oe.

The accuracy in the magnitude of the measured fields is ±0.2kOe.

5.5.2.1 Transverse Magnetic Field Applied to Wire Samples.

In the first instance, tests were carried out on the wire samples by simply applying the full magnetic field available or no field at all. This was simply to give an initial indication of the behaviour of the samples. No tests of this kind have been carried out previously, hence the outcome was unknown and these initial tests would highlight those areas worthy of further investigation.

	Magnetic field strength				
Material	**≈ 50 Oe**	**2.7 kOe**	**≈ 50 Oe**	**-2.7 kOe**	**≈ 50 Oe**
Aluminium (99.5%)	-145	-154	-145		
Aluminium alloy (6061)	-143	-154	-143		
Copper (99.95% OFHC)	-143	-149	-142		
Beryllium copper	-144	-154	-144		
Nickel (99.98%)	-99	-93	-99	-93	-99
Stainless steel AISI 304	-105	-106.5	-106	-105.5	-105.5

Table 5.22 7th order PIM levels of wire samples in a transverse magnetic field (level in dBm, 25W per carrier)

Observations:

- All of the non-ferromagnetic materials demonstrated a measurable reduction in their PIM level when the magnetic field was applied.

More detailed tests were carried out on the two ferromagnetic materials, nickel and stainless steel 304, and also copper which displayed some anomalous behaviour whilst subjected to a transverse magnetic field. These are described in the following sections.

5.5.2.2 Effects of Magnetic Field on Nickel Wire

Transverse magnetic field		Transverse magnetic field (reversed)	
Field strength (kOe)	PIM level (dBm)	Field strength (kOe)	PIM level (dBm)
0.05	-99	-	-
1.0	-98	-1.0	-98
1.9	-97	-1.9	-97
2.7	-95	-2.7	-95
3.3	-92	-3.3	-92
3.6	-93	-3.6	-93
3.9	-95	-3.9	-95
4.1	-96	-4.1	-96
0.05	-99	-0.05	-99

Table 5.23 7th order PIM level variation of nickel wire sample with transverse magnetic field (25W per carrier)

Observations:

- The levels of PIM observed were the same for both directions of transverse magnetic field for a given magnetic field strength. As nickel magnetically saturates around 6kOe, the field strengths which have been applied will be driving the nickel very nearly into saturation. With the sample material in such a magnetic state hysteresis effects are likely to be very small indeed. Thus, PIM levels for both forward and reverse directed transverse magnetic fields will be essentially the same.

- A maximum in the PIM level is achieved with a transverse magnetic field of about 3.3kOe.

5.5.2.3 Effect of Magnetic Field on Stainless Steel (304) Wire

Transverse magnetic field		Transverse magnetic field (reversed)	
Field strength (kOe)	PIM level (dBm)	Field strength (kOe)	PIM level (dBm)
0.05	-108.7	-	-
1.0	-108.3	-1.0	-107.7
1.9	-108.3	-1.9	-107.5
2.7	-109.0	-2.7	-108.3
3.3	-110.0	-3.3	-109.8
3.6	-110.8	-3.6	-110.8
3.9	-111.5	-3.9	-111.5
4.1	-112.0	-4.1	-112.0
0.05	-108.8	-0.05	-108.8

Table 5.24 7th order PIM level variation of stainless steel 304 wire sample with transverse magnetic field (25W per carrier)

Observations:

- Due to the small change in PIM level observed with applied transverse magnetic field a higher resolution for the PIM signal has been recorded. This level of resolution allows the variation of PIM level with field to be more clearly apparent. The levels observed were seen to be extremely stable hence it is valid to quote the levels to such high resolution.

- The levels of PIM observed for both directions of transverse magnetic field were virtually the same for a given field strength. The slight differences noted for the lower field strengths may be due to hysteresis effects brought about by magnetic 'memory effects' due to the field applied in the first test run (identified by the positive field direction).

- A maximum in the PIM level is achieved with a transverse magnetic field of about 1.9kOe.

5.5.2.4 Effects of Magnetic Field on Copper Wire

Although copper wire initially behaved in a similar way to the other non-ferromagnetic materials when subjected to a transverse magnetic field, prolonged investigations revealed unexpected behaviour in the PIM signal.

Small variations in the PIM level were found to occur when moving electromagnet along the length of the wire sample jig (2dB to 3dB). However, during the investigation of this effect, the PIM level was seen to suddenly jump from the nominal suppressed level of ≈-150dBm (refer to Table 5.22) to about -110dBm. Fluctuations in the level occurred between -110dBm and -140dBm for about 1 minute. The magnetic field was turned off and the PIM level gradually steadied at -135dBm ±5dB. The following tables summarise the behaviour of different samples of copper wire with transverse magnetic field. All wire samples were cut from a single batch length.

PIM levels close to the system residual (-150dBm) typically displayed a variability of about ±3dB. Where levels were not constant (i.e. ±1dB), the variation is indicated in the tables. Due to the highly variable nature of the PIM signals observed, the results are presented in a different format than those of the other materials. Each change in behaviour was noted and is recorded, along with the observed PIM levels, in the tables.

It should be noted that before each test the jig, all its constituent parts and the sample itself were all thoroughly cleaned and de-greased. Gloved hands were used at all times during handling to avoid contamination from fingerprints.

Field strength (kOe)	Comments
2.7	Jump in PIM level from -150 dBm to -110 dBm. Level fluctuates about -110 dBm to -140 dBm
0.05	PIM level approaches -135 dBm ±5 dB
2.7	PIM level -105 dBm ±2 dB
0.05	PIM level falls to -137 dBm ±2 dB
2.7	PIM level initially -105 dBm falling to -150 dBm after several seconds
0.05	PIM level jumps from -150 dBm to -105 dBm as field removed then gradually falls to -140 dBm over 2 minutes
0.05	R.F. and field off for 20 minutes. R.F. on, PIM level initially -135 dBm dropping to -142 dBm after 20 seconds
2.7	PIM level initially -110 dBm then fluctuates between -140 dBm to -100 dBm, does not appear to approach a constant level
0.05	Field turned off when PIM level was -135 dBm, level jumps to -110 dBm then settles towards -140 dBm ±3 dB
Magnet below jig @ 2.7 kOe	PIM level -142 dBm ±3 dB, no change with field on or off
2.7	Magnet moved up around sample jig, PIM level increases from -142 dBm to -107 dBm then drops to -154 dBm remaining at this level with magnet at jig centre
0.05	As field removed, PIM level jumps to -110 dBm gradually dropping to -140 dBm. No further jumps in level observed

Table 5.25 7th order PIM level variation of copper wire sample 1 with transverse magnetic field (25W per carrier)

Observations:

- A transverse magnetic field was found to stimulate increases in the PIM signal of about 30dB above the level normally observed with copper. This level was not sustained but showed fluctuations which tended to be abrupt, step changes between the residual level and the maximum level.

- In several cases the maximum PIM level was stimulated briefly (for less than one second) when the magnetic field was turned off, i.e. during field collapse.

The magnetic field was clearly demonstrated to be responsible for stimulating the effect. When the magnetic field present inside the jig was reduced to a very low level (of the order of 5 Oe) the PIM level remained close to its residual value. Additionally, moving the magnet up from below the jig, closer to the wire sample, caused the PIM level to increase immediately in the manner described above.

In order to determine whether the anomalous effects were due to system fluctuations or were peculiar to copper, other material samples were tested in a similar manner:

Aluminium - Residual PIM level at -143 dBm. Level reduced to -149 dBm with application of magnetic field. No large increases in PIM level seen with application of magnetic field.

Aluminium alloy (6061) - Residual PIM level at -143 dBm. Level reduced to -149 dBm with application of magnetic field. No large increases in PIM level seen with application of magnetic field.

Beryllium copper - Residual PIM level at -144 dBm. Level reduced to -154 dBm with application of magnetic field. No large increases in PIM level seen with application of magnetic field.

Following the normal behaviour exhibited by the above materials a new copper wire sample (sample 2) was prepared and tested. A summary of results is given in Table 5.26 to Table 5.28.

Field strength (kOe)	Comments
0.05	PIM level -143 dBm
2.7	PIM level reduces to -158 dBm ±3 dB for 1 minute, then level jumps to -120 dBm and fluctuates about -120 dBm to -155 dBm. After 5 minutes level reduces to -158 dBm. No further jumps seen
0.05	PIM level returns to -143 dBm
2.7	PIM level to -158 dBm, large dips occasionally seen
0.05	PIM level to -146 dBm
2.7	PIM level to -158 dBm, dips occur
0.05	PIM level to -147 dBm
2.7	PIM level to -160 dBm, dips occur
0.05	PIM level to -147 dBm
0.05	R.F. off for 1 hour. PIM level -154 dBm
2.7	PIM level jumps briefly to -130 dBm then settles at -158 dBm
0.05	Level jumps briefly to -130 dBm as field turned off then approaches -152 dBm
2.7	PIM level fluctuates between -126 dBm and -150 dBm for 10 seconds then gradually falls. After 3 minutes sudden drop in level to -160 dBm
0.05	PIM level remains around -156 dBm
2.7	PIM level -156 dBm, no jumps for 10 minutes
0.05	No jumps in PIM level. R.F. off for 20 minutes
0.05	PIM level -157 dBm
2.7	Brief jump in level to -130 dBm, then remains at -160 dBm
0.05	Brief jump in PIM then level sits at -152 dBm
2.7	Brief jump in PIM level then level rises to -130 dBm ±2 dB for 10 minutes.
0.05	PIM level drops to -154 dBm
2.2	PIM level to -123 dBm for 10 seconds then drops to -160 dBm. Occasional jumps to -123 dBm
1.7	PIM level at -160 dBm. Field turned on and off several times. On some occasions very brief jumps in PIM observed to a maximum of -120 dBm (~ 20 msec duration)
1.5	PIM level -154 dBm. No further jumps in PIM level observed with switching field on and off

Table 5.26 7th order PIM level variation of copper wire sample 2 with transverse magnetic field *Test 1* (25W per carrier)

Observations:

- Sudden step changes of PIM level were clearly visible. The maximum and minimum step change levels were well defined. The existence of intermediate levels was unclear.

- The step changes were excited by the presence of the RF and magnetic field together.

- The step changes occurred fairly erratically. Their occurrence was not easily associated with any manipulation of the magnetic field.

- There was an apparent annulling of the system steady state residual at high magnetic field strength.

The measurements were then repeated using the same sample. This time the magnitude of the field strength was increased as high as 4.2 kOe. The results table is given overleaf.

Field strength (kOe)	Comments
0.05	PIM level -146 dBm
4.2	PIM level -125 dBm
0.05	PIM level initially -124 dBm, drops to -145 dBm after 3 minutes. Level jumps up suddenly, magnet lowered below jig and level drops. After several minutes PIM level jumps to -122 dBm for 2 minutes
0.05	Magnet raised to centre of jig. PIM level fluctuates between -125 dBm and -144 dBm
0.9	PIM level -130 dBm, fluctuates to -146 dBm
1.5	PIM initially falls from -146 dBm to -155 dBm for 2 minutes then fluctuates about -133 dBm ±4 dB
3.3	PIM drops to -160 dBm with jumps to -125 dBm
3.9	PIM fluctuates between -160 dBm and -125 dBm
4.1	PIM level fluctuates remaining for longer periods at -125 dBm. Immediate drop in level when field is turned off
1.0	PIM level jumps to -125 dBm and remains there
0.05	PIM level remains at -125 dBm. Magnet lowered below jig and keeper placed across poles, PIM remains at -125 dBm for 10 minutes
2.3	Magnet poles at jig centre, PIM shows some jumps in level. Field removed, PIM level rises to -125 dBm and stays there
-1.0	PIM drops from -125 dBm to -146 dBm
0.05	PIM level returns to -125 dBm
-1.0	PIM level -146 dBm
0.05	PIM level returns to -125 dBm
-1.0	Field applied for several minutes
0.05	PIM level to -130 dBm then drops to -146 dBm
-2.3	PIM level falls to -160 dBm
-4.2	PIM level remains at -160 dBm, large dips occurring at times, no jumps observed. R.F. off for 1 hour
0.05	PIM level -146 dBm. Very brief jump to -130 dBm then remains at -146 dBm for next 10 minutes

Table 5.27 7th order PIM level variation of copper wire sample 2 with transverse magnetic field *Test 2* (25 W per carrier)

Observations:

All of the characteristics observed with sample 1 were noted with sample 2 with the addition of:

- Once excited, the high PIM levels could persist for minutes when the magnetic field was removed.

- Where the high step levels persisted for zero magnetic field, these could be brought down to a low level by magnetic field reversal.

- The step behaviour tended to be reduced and eventually died away with the repeated application of reverse magnetic field.

A third test was carried out on sample 2 in order to further examine the effects of reversing the magnetic field

Field strength (kOe)	Comments
-2.7	Reverse magnetic field applied across sample for 25 minutes with no R.F. present
0	(Magnet below jig). PIM level -146 dBm. After 1 minute, level jumps to -115 dBm for 1 second. After further 1 minute, level jumps to -120 dBm for 1 second. Level remains at -146 dBm for next 5 minutes

Table 5.28 7th order PIM level variation of copper wire sample 2 with transverse magnetic field *Test 3* (25W per carrier)

Observations:

- Further application of reverse magnetic field did not appear to alter the PIM characteristics of the sample greatly. Short-lived bursts (less than one second) of PIM above the previously observed excited levels were recorded, although no persistent level changes were seen.

A third sample (sample 3) was tested. The following table indicates the results.

Field strength (kOe)	Comments
0.05	PIM level -146 dBm, remains here for 25 minutes
-2.7	No R.F. applied, reverse field on for 60 minutes
0	Magnet lowered below jig. R.F. on, PIM level -146 dBm. No jumps observed for 20 minutes.
2.7	No R.F. applied, field on for 60 minutes
0	Magnet lowered below jig. R.F. on, PIM level -145 dBm. No jumps observed for 20 minutes
0.05	Magnet poles at jig centre. PIM level -144 dBm
-1.0	Small, short-lived fluctuations of PIM level to -140 dBm
-1.9	PIM level fluctuates between -155 dBm and -137 dBm for first 30 seconds. Level then moves between -155 dBm to -146 dBm for next 2 minutes
-2.7	PIM level predominantly at -155 dBm. Large dips seen and maximum level -150 dBm
-3.3	PIM level predominantly at -160 dBm. Large dips seen and maximum level -155 dBm
-3.6	PIM level predominantly at -165 dBm. Large dips seen and maximum level -155 dBm
-3.9	PIM level predominantly at -165 dBm. Large dips seen and maximum level -155 dBm
-0.05	PIM level -149 dBm. R.F. off for 1 hour
-0.05	R.F. on, PIM level -149 dBm
1.0	PIM level -145 dBm
1.9	PIM level -145 dBm for 1 minute. Level then falls to -150 dBm with occasional fluctuations to -145 dBm over 2 minutes. PIM level fluctuates between -155 dBm to -140 dBm for next 2 minutes
2.7	PIM level -145 dBm with fluctuations down to -160 dBm over 4 minutes
3.3	PIM level predominantly at -160 dBm with brief increases to -140 dBm
3.6	PIM level predominantly at -165 dBm rising to -145 dBm occasionally
3.9	PIM level predominantly at -160 dBm rising to -145 dBm occasionally
0.05	PIM level -150 dBm ±3 dB. R.F. off for 90 minutes
0.05	PIM level -146 dBm
1.9	PIM level predominantly at -155 dBm rising to -147 dBm occasionally

Table 5.29 7th order PIM level variation of copper wire sample 3 with transverse magnetic field (25 W per carrier)

Field strength (kOe)	Comments
3.3	PIM level predominantly at -165 dBm rising to -142 dBm occasionally
0.05	PIM level -146 dBm
3.3	PIM level -165 dBm
4.1	PIM level predominantly at -165 dBm rising to -146 dBm occasionally
0.05	PIM level -150 dBm

Table 5.29 7th order PIM level variation of copper wire sample 3 with transverse magnetic field (25 W per carrier)

Observations:

- Sample 3 showed no unusually large jumps in PIM level with application of magnetic field, as had been observed with the two previous samples. The small fluctuations observed above the nominal PIM level for copper wire without magnetic field could be due to system variations such as heating effects in the quiet load. These increases are insignificant compared to those recorded for the first two copper wire samples (excitation of 20 dB to 30 dB).

- A significant, repeatable reduction in PIM level can still be observed with the application of transverse magnetic field. Generally, an increase in the field magnitude increases the reduction of PIM signal, although this could only be tested for fields up to a maximum of about 4 kOe.

- The reduction in PIM level is not wholly dependant on the continued presence of the magnetic field, the reduced PIM level has been observed when no field is available.

At this point it was decided to briefly re-test samples 1 and 2. The results are presented in Table 5.30 and Table 5.31.

Field strength (kOe)	Comments
0	Magnet below jig centre. PIM level initially at -142 dBm gradually falling to -160 dBm. Level fluctuates between -160 dBm and -145 dBm for several minutes. Level approaches -150 dBm
1.0	PIM level -150 dBm becoming more variable. After 4 minutes starts approaching -142 dBm
1.9 → 3.3	PIM level consistently -155 dBm ±5 dB
0.05	PIM level -155 dBm ±5 dB
-1.0	PIM level increases from -155 dBm to -146 dBm, fluctuating occasionally to -155 dBm
-1.9	PIM level -155 dBm ±5 dB
-2.7	PIM level -155 dBm ±5 dB
-0.05	PIM level -148 dBm
1 → 4.1	No jumps in PIM level seen for fields of 1 kOe to 4.1 kOe
0.05	PIM level -154 dBm

Table 5.30 7th order PIM level variation of copper wire sample 1 with transverse magnetic field *retest* (25W per carrier)

- **Observations:**

- Despite the application of high magnetic fields no large fluctuation in PIM level was observed during these tests. Note that earlier tests on the same sample had clearly revealed this excitation.

- A reduction in the PIM level with applied field was still observable. This was also observed at the beginning of the tests before the field had been applied, clearly indicating some form of magnetic memory or short term structural change.

Field strength (kOe)	Comments
0.05	PIM level -150 dBm, dips appearing
1.9	PIM level -160 dBm, dips more frequent
3.3	PIM level -165 dBm, dips deeper and more frequent
2.7	PIM level -163 dBm

Table 5.31 7th order PIM level variation of copper wire sample 2 with transverse magnetic field *retest* (25W per carrier)

Observations:

- No highly fluctuating levels of PIM were observed with this re-test as for the re-test of sample 1.

- A reduction in the PIM level with applied field was still observable.

As a final verification of the system performance, two samples which had been previously tested were rechecked.

Beryllium copper - This sample had been previously magnetised. The PIM level with no field applied was found to be -153 dBm (the same level as was previously measured with field applied). This level was reduced by several dB's with the application of a magnetic field.

Aluminium - This sample had been tested under thermal stressing. The PIM level was found to be stable at -146 dBm. The previous measured PIM level was -142 dBm.

5.5.3 Removal of Alumina Dielectric

The apparent change in behaviour of the copper samples gave cause for concern and it was decided to scrutinise the measurement procedure and set-up. It was decided to investigate the effect of the alumina which remained somewhat of an unknown quantity in terms of PIM.

A second, slightly modified, small geometry sample jig was made which could facilitate measurements on wire samples with and without the alumina dielectric. The central section of the jig employed a composite dielectric of a thin section of alumina and PTFE. The alumina could be replaced with PTFE to give a solid PTFE dielectric with no discernable change in electrical performance. Although the dielectric constant of alumina is considerably higher than PTFE, when the two are combined in the one structure (along with air gaps) the effect of a small section of alumina becomes negligible. This was not appreciated during the design of the first jig.

The new jig was designed to take samples of UT-250 inner conductor, diameter 1.6mm. UT-250 is in use throughout the system and is capable of very low-PIM levels as has been shown. The following results were obtained with and without the alumina present:

Field strength (kOe)	Comments
0	Residual PIM level -103 dBm
2.7	PIM level -108 dBm
0.05	PIM level -104 dBm
2.7	PIM level -108 dBm (parent signals slightly adjusted)
0.05	PIM level -105 dBm

Table 5.32 7th order PIM level variation of UT-250 inner conductor + alumina & PTFE dielectric sample with transverse magnetic field (25W per carrier)

Field strength (kOe)	Comments
0	Residual PIM level -110 dBm
2.7	PIM level -108 dBm
0.05	PIM level -109 dBm

Table 5.33 7th order PIM level variation of UT-250 inner conductor + PTFE dielectric only sample with transverse magnetic field (25W per carrier)

This obviously shows that not only does the alumina apparently generate a slightly higher residual level of PIM, but also, that it seems to be the alumina which responds to the applied magnetic field in the majority of cases.

Unfortunately, this discovery was made at the end of the experimental program and it was not possible to re-test all of the small geometry samples due to the available time. It was also the case that the alumina-free jig was designed around a larger sample size and would have to be redesigned to accommodate the 1 mm wire samples.

This point marked the conclusion of the experimental work. Although there are areas which would obviously benefit from further investigation, time constraints prevented further measurements from being made.

5.6 Summary of Experimental Programme

An experimental programme has been conducted into the generation of PIM in common aerospace metals. Two types of standard sample have been developed. A larger engineering scale sample was employed to provide useful practical data, whilst a smaller sample was used to excite higher current densities in materials, in order to gain an insight into the physical mechanisms of PIM generation.

5.6.1 Engineering Sample Measurements

The results of the experiments on the solid engineering samples indicate that magnetic effects dominate PIM levels for this type of sample at L-band frequencies. It was shown that by silver plating ferromagnetic material to a thickness greater than 8 skin depths the PIM level dropped and became indistinguishable from the system residual PIM. Other effects such as oxidation and surface abrasion were seen to have no effect.

In the multi junction samples it was observed that loose junctions were very erratic and unpredictable, but at high contact pressure, all PIM from non-magnetic samples was below the level of system residual PIM. Magnetic materials were once again observed to dominate.

In the case of Nickel, a strange phenomenon was observed in that the samples with a higher number of junctions actually produced lower levels of PIM. However by coating the material in silver plating the level was reduced to below that of the system.

Additionally, junctions involving aluminium and Alocrom coated aluminium were seen to produce very high levels of PIM on occasion. However junctions between either material and any of the others resulted in no visible effect.

All other treatments such as bonding, material finish, magnetisation and oxidation were observed to have little effect

5.6.2 Small Geometry Measurements

On testing the untreated small geometry samples, once again, only the ferromagnetic materials registered PIM levels above the system residual, and again, these levels could be reduced significantly by silver plating.

Again, thermal stressing and oxidation had little effect, however abrading the material surfaces was seen to generate higher levels of PIM, particularly when the abrasion was applied transverse to the direction of current flow.

The Alocrom coating and silver plating applied to the aluminium samples were also observed to generate no observable level of PIM.

For the small geometry samples effects were much more evident from tests using applied magnetic fields. The application of a transverse D.C. magnetic field brought about changes in the level of PIM generated by all of the samples currently tested. This is to be expected with a ferromagnetic material which already displays a high level of non-linearity due to its magnetic properties. However, for weakly magnetic materials the magnitude of change was not expected.

Two distinct types of behaviour were observed for the non-ferromagnetic materials:

- a magnetic field applied to the sample caused the PIM level to fall below that of the material with no magnetic field applied. In many cases this suppressed level was also below the system residual. This strongly suggests that the magnetic field stimulates a PIM signal which is out of phase and of a similar magnitude to the system residual.
- the PIM level can be excited 20 dB to 30 dB above the residual PIM level of the material (i.e. with no magnetic field). This was only observed with copper wire and not in a consistent manner for all samples.

For both of the above types of behaviour, the change in PIM level, once stimulated, did not always require the presence of the magnetic field to be sustained. The implication of this is that some form of structural change (physically or magnetically) occurs within the material allowing this behaviour to be observed without the stimulus field.

Additionally, however, it was discovered that the alumina dielectric in the small geometry sample jig was responsible for increased levels of residual PIM and for some if not all of the observed changes under magnetic field excitation.

The implications of this and of all the measurement data will be considered in the next chapter.

CHAPTER 6

Analysis Of Results

The object of this chapter is to present an analysis of the laboratory measurement results described in Chapter 5. Several aspects of the measurement data are discussed and where necessary, theory has been applied in order to provide possible explanations for the behaviour observed.

6.1 Introduction

One of the original aims of this project was to develop a better understanding of the mechanisms responsible for PIM generation in space qualified materials. The successful measurement programme, described in Chapter 5, was conducted in order provide results for the analysis of PIM mechanisms.

In Chapter 2, several mechanisms were discussed which have been frequently cited as being responsible for PIM generation. On closer examination however it is evident that it would be difficult to demonstrate the presence of such mechanisms in engineering scale samples. This is due to the degree of environmental control required and the amount of information which is needed about the test variables.

The aim of this chapter is to examine the results and observations of the measurement programme and to consider the physical processes which may be at work.

At no point is it intended to present irrefutable conclusions on the causes of PIM generation as it is felt that a great deal more measurement data is required.

6.2 Solid Samples

Both types of solid sample are considered in the following sections. The larger 'engineering' scale sample and the 'small geometry' sample. Both are compared in order to draw conclusions about the effects of higher current densities.

6.2.1 Non-magnetic Materials

This section deals with all the non-ferromagnetic materials tested i.e. excluding Nickel, Stainless steel 303, Stainless steel A286 and Stainless steel 15-5PH.

6.2.1.1 Untreated Samples

The first tests on the solid samples looked at the PIM generation in polished materials of beryllium copper, copper, aluminium and its alloys and brass. In the case of the engineering samples, all materials indicated no PIM above the residual level of the system. However, with the small geometry samples levels of PIM notably above the system residual were recorded. It is difficult to know whether the increased levels can be directly attributed to the smaller sample size. Indeed it was shown in Section 5.5.3 that the Alumina is responsible for a certain amount of the observed PIM level in the wire sample tests. However, given the careful design of the jig to minimise PIM it is assumed that the residual PIM from the rest of the jig is negligible. As the test jig cannot function without a sample of some sort, the levels observed can only be compared relative to each other.

Due to the skin effect, the reduction in sample size will lead to a large change in the surface current density on the smaller samples. It is assumed that all of the current in the sample is located in a surface layer, 4 skin depths thick. At 1.6 GHz, the skin depth, δ_s, for copper is 1.65 μm, hence all of the current will be within about the first 7 μm of the surface. Now the surface area is given approximately by:

$$A_s = 2\pi \cdot r \cdot 4\delta_s \qquad \text{Eq.6.1}$$

Provided that δ_s is extremely small. Given that the radius of the engineering samples is 9.3 mm and the small geometry samples is 1.0 mm, the current density is therefore increased in the small geometry samples by a factor of 9.3. To obtain the same increase in current density by raising the drive levels of the parent signals would require multiplication of the input power by a factor of 9.3^2 or 86.5, a rise of 19.37 dB.

For simple nonlinearities, as described in Section 2.2.3, the 7th order PIM signal will change at a rate of 7 dB per dB change in the parent signal. Assuming an implied increase in power of 19dB, the change in the PIM level due to the sample size reduction would be over 100 dB. In practice it is not likely to be as great as this but there will be a very large difference between the PIM levels displayed by the different sized samples. Given the levels obtained for the wire samples, this suggests that the PIM from the engineering samples is well below the level of system residual PIM and hence no useful analysis can be made on the measurements.

On the other hand, the PIM recorded for the small geometry samples would appear to emanate from the samples themselves. Several theories have been put forward by several researchers [30, 53] as to the mechanisms which may be responsible. These are briefly described in the following sections:

A) Deviation From Ohm's Law:

It is known that not all conductors are ohmic. An example of a non-ohmic conductor is thyrite [175] in which current is roughly proportional to the cube of voltage. For most applications, however, current flow in metallic conductors is assumed to be ohmic (i.e. their resistance is constant). Nevertheless, some evidence of weak deviation from Ohm's law for metals was mentioned in a few places [176, 177]. For most metals, ref. [176] indicates there is little change in resistance for current densities up to 10^5 A/cm^2. In the case of gold, there is no notable change in the resistivity for current densities as high as 10^5 A/cm^2 and a change of only a few percent at 10 times that amount.

However, [177] states that no deviation has ever been clearly demonstrated experimentally and according to one theoretical prediction, departures of the order of 1 percent might only be expected at a current density of 10^9 A/cm^2.

In the case of the small geometry samples the combined average input power is 50 Watts. With the characteristic impedance equal to 50 ohms the peak current is given by:

$$\begin{aligned} P_{av} &= I_{rms}^2 \cdot R \\ &= \frac{\hat{I}^2}{2} \cdot R \\ \therefore \hat{I} &= \sqrt{\frac{2P_{av}}{R}} \end{aligned} \qquad \text{Eq.6.2}$$

Which, in this case equals 1.41 Amps. Now from Eq.6.1 the surface area at 4 skin depths for copper is 2.07 x 10^{-8} m^2 or 2.07 x 10^{-4} cm^2. Therefore the maximum current density is ≈6812 A/cm^2. This suggests it is unlikely that deviation from ohms law is responsible for PIM generation in the small samples.

Lee in ref. [38] however, considers the theoretical third order PIM level in a 19 foot section of UT 141 semi-rigid cable (inner conductor diameter 0.91 mm) for a surface current density of J_m=8730 A/cm^2. Based upon ref. [175], he assumes a 3 percent change in resistivity at a current density of 10^7 A/cm^2. The non-linear electric field - current density relation was simplified to the first two terms in a power series expansion such that:

$$\begin{aligned} E &= \rho(J) \cdot J \\ &= (\rho_O + \rho_2 J^2) \cdot J \\ &= \rho_O\left(1 + \frac{\rho_2 J^2}{\rho_O}\right) \cdot J \end{aligned} \qquad \text{Eq.6.3}$$

For a 3 percent change in resistivity at a current density of 10^7 A/cm^2, we have:

$$\begin{aligned} \frac{\rho_2 J^2}{\rho_O} &= 0.03 \qquad \text{for} \quad J = 10^7 \text{A/cm}^2 \quad \text{or} \\ \frac{\rho_2}{\rho_O} &= 3 \times 10^{-16}\ \text{cm}^4/\text{A}^2 \end{aligned} \qquad \text{Eq.6.4}$$

Hence, for J_m=8730 A/cm^2, the ratio of the 3rd order PIM field to that of the dissipation loss at the fundamental frequency is given by:

$$\frac{\rho_2 J_m^2}{\rho_O} = 2.28 \times 10^{-8} \qquad \text{Eq.6.5}$$

Which equates to a power level 153dB down on the combined dissipated power.

Lee's cable has an insertion loss of 1dB which, for two 25 Watt carriers, results in a predicted third order PIM signal of -119 dBm.

The UKC L-band facility was set-up to measure seventh order PIM products and sample sizes were shorter than the section of UT 141 semi-rigid cable which Lee used. Hence, it is not entirely inconceivable that the levels around -141dBm which were observed were due to very small deviations in Ohm's law.

B) Resistive Heating

This effect has been discussed in several places [19, 30, 31]. Here, it is intended to provide a qualitative description of the relationship between resistive heating and PIM.

Resistivity in metals can be considered as the sum of a temperature independent component and a temperature dependent component (Matthiessen's rule) [178]. The former results from defects and strains in the lattice and from the presence of impurities such as alloying constituents. For good electrical conductors, at normal temperatures, it makes only a small contribution to the total resistivity. The latter, and major part of the resistivity, is caused by the scattering of electrons from thermal vibrations of the lattice. Typically, the resistivity increases as the third or fifth power of temperature. Above about -200°C to -100°C (depending on the metal), the predominant behaviour is a linear increase

in the resistivity with temperature. This dependence on temperature means that any heating caused by the passage of an alternating electric current may result in non-linear behaviour. The significance of this depends on whether it is overshadowed by direct non-linear behaviour and on the rapidity with which local temperatures can follow changes in current density.

Conductors carrying a continuous RF current will reach an equilibrium temperature at each point, this is determined by the time average of J^2 and the rate of heat loss (or gain) by conduction to other regions of the conductor as well as by radiation. For resistive heating to cause intermodulation, periodic fluctuations of the local temperature about its equilibrium must occur. The amplitude of these will depend on the thermal properties of the material and on geometrical considerations.

A number of authors have published analyses of intermodulation in various situations resulting from resistive heating in metallic conductors and have arrived at a range of answers. Rootsey et. al. concluded that the effect would be negligible in waveguide at X-band [19], whereas Wilcox and Molmud (coaxial cable at UHF) [31] and Stauss et. al. (X-band waveguide and high-Q structures at UHF) [30] predicted very significant levels of intermodulation in some cases, albeit at very high power densities (up to 4.5×10^3 W/m^2).

In the UKC set up, the thermal effects are considered to be negligible because the sample is thermally insulated from the rest of the system by way of the contactless connectors. The samples themselves also have a relatively small thermal mass and it is thought that once stable, the temperature will not tend to vary. However the effect cannot be completely discounted due to insufficient measurement control and data.

C) Magnetoresistive Generation

Magnetic fields applied to a conductor will have the effect of altering its resistivity [178], the effect is called magnetoresistance. The fields associated with currents in the material can, therefore, potentially create PIM signals. Two different coefficients of are normally defined. Longitudinal magnetoresistance describes the effect of a magnetic field parallel to the direction of current flow, while transverse magnetoresistance applies when the field is orthogonal to the current. Since an electric current creates an orthogonal electric field, it is the latter effect which is of most interest here. In non-ferromagnetic metals, the resistance generally increases by an amount proportional to the square of the transverse field. The resistance saturates at large fields in most metals, although in some it may continue to increase proportionally to the field or to the square of the field.

At the surface of the centre conductor in a coaxial line, the magnetic field, $\boldsymbol{B}$, is given by:

$$B = a_{\phi}\frac{\mu I}{2\pi r} \qquad \text{Eq.6.6}$$

Where a_{ϕ} is the unit vector in the direction of the field (tangential to the surface of the conductor) and r is the radius of the inner conductor. In this case $\mu = \mu_O$ because the conductor is non-ferromagnetic. In the UKC small geometry sample measurements, $I_{max} = 1.41\,\text{A}$ as before and $r = 0.5\,\text{mm}$, hence the magnetic field is $B = 450$ Tesla. In ref. [30], Stauss cites the transverse magnetoresistive coefficient of copper to be:

$$\frac{\rho - \rho_O}{\rho_O} = 3.98 \times 10^{-17} \cdot H^2 \qquad \text{Eq.6.7}$$

Where H is the magnetic field intensity given by $B = \mu_O H$. The left-hand side of Eq.6.7 is the fractional deviation of the resistivity from linearity. Hence, in the case of the small geometry samples resistance changes of one part in 10^{-12} are possible.

In his paper, Stauss considered magnetoresistance as a cause of third order PIM in copper and concluded that it was much less important compared with thermal effects in the two examples he gave. It was noted, however, that magnetoresistive generation differs from thermal PIM generation both in its dependence on carrier and intermodulation frequencies, and on the relevant material properties, so it is not clear that this comparison is generally applicable.

Conclusion

It has been demonstrated, possibly for the first time, that PIM is generated by the intrinsic properties of non-ferromagnetic metals. The theoretical mechanisms which have been proposed by other researchers have been considered and it is likely that one, if not all, of the mechanisms could be contributing to the overall level. However, it is apparent that stricter experimental controls and more experimental work is necessary to establish which, if any, of the effects is most dominant.

Nevertheless, the data is useful to engineers in the design of systems where extremely high current densities may be encountered. Situations where extensive use is made of small diameter coaxial cables operating at medium power levels are not uncommon, hence extreme care must be taken to ensure that no significant PIM is generated.

6.2.1.2 Surface Treated Samples

Several different treatments were applied to the surfaces of the non-ferromagnetic solid samples. In the case of the engineering samples, again, no PIM was registered above the system residual level. Coatings such as silver plating and Alochrom are used extensively in the aerospace industry and these were not expected to give any problems. However, in the case of oxide layers, abrasion, thermal stressing and contamination it was initially expected that some increase in the PIM signals would be observed. On considering the results from the small geometry samples, it was evident that the current densities in the engineering samples were likely to be too low to register any effects.

The results from the small geometry programme indicate that only by abrading the surface of the material can significant variation in PIM level be produced. Interestingly, applying surface abrasion transverse to the direction of current flow produces higher levels of PIM than longitudinal abrasion.

At microwave frequencies the skin effect results in all of the current flow occurring in the first few microns (μm) of the surface layer. This intensifies the effects of surface imperfections such as scratches, holes, contaminants, etc. creating anomalous skin current paths and possibly even small metal-to-metal contact junctions. The abrupt termination of the crystalline lattice during the formation of a new surface causes many structural imperfections on the newly formed surface.

In the case of inducing roughness on a metal sample, where the imperfections impede the flow of current, the resistivity of the sample will increase. In a paper by S.P.Morgan [179] it is stated that for abrasions applied transverse to the flow of current, an increase in resistivity of up to 100% is possible. In the same paper it is stated that longitudinal abrasion (parallel with current flow) will also increase resistivity but by a much smaller amount. Thus in the small geometry test samples, transverse abrasion will introduce a greater number of irregularities across the direction of current flow and a higher resistivity. The higher resistivity results in an increased dissipation of energy in the sample and will, therefore, serve to accentuate those effects discussed in Section 6.2.1.1.

In some cases the irregularities in the surface may give rise to microscopic metal junctions which exhibit non-linear behaviour and hence, produce increased PIM signal levels. In any case, it is difficult to say with any degree of accuracy what exactly is responsible for the increase in PIM. Again, however, the information is invaluable to engineers concerned with the design of low-PIM systems. All conducting surfaces should have a smooth finish where possible to minimise PIM and to reduce system losses.

6.2.2 Ferromagnetic Materials

6.2.2.1 Untreated Samples

The ferromagnetic materials make up the remainder of the materials which were tested and comprise the stainless steels plus nickel. Nickel is a well known ferromagnetic material and several studies have highlighted its propensity to generate PIM [30, 35, 36, 37, 39]. However, nickel is still used in the aerospace industry often as the plating on RF connectors. It has been included in this study to demonstrate the generation of PIM in the sample format and to continue to highlight its poor PIM performance. The remaining ferromagnetic materials, i.e. the stainless steels, are also used in aerospace applications as they offer excellent corrosion resistance. However, no data has previously existed as to the PIM performance of these materials, hence their inclusion in the study.

From the engineering sample data, it is evident that both nickel and stainless steel 303 exhibit high levels of intrinsic non-linearity. The stainless steel 15-5PH also exhibits non-linearity but at a much lower level. The remaining steel, A286, is indistinguishable from the system residual and on that basis performs very well. That this is so is not apparent from the composition of the steels. Stainless steel 303 has less nickel and chromium content than A286 and both of these elements are known to exhibit strong nonlinearity.

For the small geometry tests only nickel and stainless steel 304 (which is very similar to 303) could be procured. The smaller samples generate much higher levels of PIM and, as with the engineering scale samples, their levels are very similar. The increased levels are undoubtedly the result of much higher current densities on the sample.

The effect of residual magnetism seems to have little effect on the materials. Residual or remnant magnetism is present after a DC magnetic bias has been applied to the material and when it is removed the orientation of the magnetic domains is no longer random (as with an unmagnetised sample) but tend to favour a particular direction and exhibit an external magnetic force. Curiously though, the 303 stainless steel, which exhibited no residual magnetisation, produced a PIM level almost exactly that of nickel, which did. Also, the steel 15-5PH exhibited residual magnetisation stronger than that of the nickel yet generated PIM at a much lower level. This suggests that PIM generation from ferromagnetic materials is not a strong function of the "memory" of the material. It should also be noted that steel A286 showed no magnetic effects and was therefore considered to be a non-ferromagnetic conductor.

In the report by Stauss [30], he states that ferromagnetic materials experience the same effects as non-magnetic samples i.e. resistive heating and magnetoresistance as discussed in Section 6.2.1.1. However, the effects are generally greater. Ferromagnetic

materials have large coefficients of magnetoresistance whilst hysteresis losses result in much greater self heating than in metals where this is due only to resistivity. However, it is found that a much stronger candidate for the source of nonlinearity in ferromagnetic materials is the direct variation of the permeability with current.

Consider the classical hysteresis curve of Fig.6.1. It is evident that the permeability, μ (the slope of the curve), varies non-linearly with the magnetic field up to some field strength at which the process saturates. Since the passage of an alternating electric current produces a fluctuating magnetic field which, in turn, induces an alternating current, the non-linear behaviour of the permeability acts as a source of PIM.

The skin depth of a material is defined as follows:

$$\delta_s = \frac{1}{\sqrt{(\pi \cdot f \cdot \sigma \cdot \mu)}} \qquad \text{Eq.6.8}$$

Where σ is the conductivity and μ is the permeability. If the conductor is a non-ferrous metal, such as silver, a linear relationship exists between the resulting magnetic flux, **B**, and the magnetic field intensity, **H**, with current flow; i.e. $\mathbf{B} = \mu\mathbf{H}$ where μ is a constant, very close to that of free space ($\mu_o = 4\pi \times 10^{-7}$ Henries per meter). For this linear relationship, δ_s can be analytically determined. Silver for example, has a skin depth of $\approx 1.6 \times 10^{-6}$ m at 1.6 GHz.

On the other hand, if the current carrying conductor is ferromagnetic, μ is not constant, but varies with **H** in a very non-linear manner as indicated by Fig.6.2. **B** depends not only on **H** but also on previous values of **H**. The skin depth equation is therefore non-linear with "memory" and cannot be solved analytically. Of greater concern, however, is the variation of skin depth caused by permeability change; which is equivalent to a non-linear circuit impedance change - being a function of instantaneous current amplitude. This effect is evident in the following numerical approximations of skin depth for nickel plating, based upon data from [30]. The hysteresis loop of nickel at room temperature is shown in Fig.6.1, and the non-linear change in relative permeability, μ_r, as a function of field strength, **H**, is shown in Fig.6.2.

If we first assume an extremely small signal current amplitude, the initial permeability of nickel, $\mu_i = 4\pi \times 10^{-5}$ H/m, may be used. The conductivity of nickel, σ_{Ni}, is $\approx 1.3 \times 10^7$ mhos/m. This results in a skin depth, δ_i of $\approx 4.4 \times 10^{-7}$ m at 1 GHz, a value approximately 1/5 that of silver. As the signal current increases, the permeability of nickel increase, reaching μ_{max}, 10 to 100 times μ_i. This further decreases the skin depth by a factor of 3 to 10 times. Beyond some critical current, however, permeability decreases,

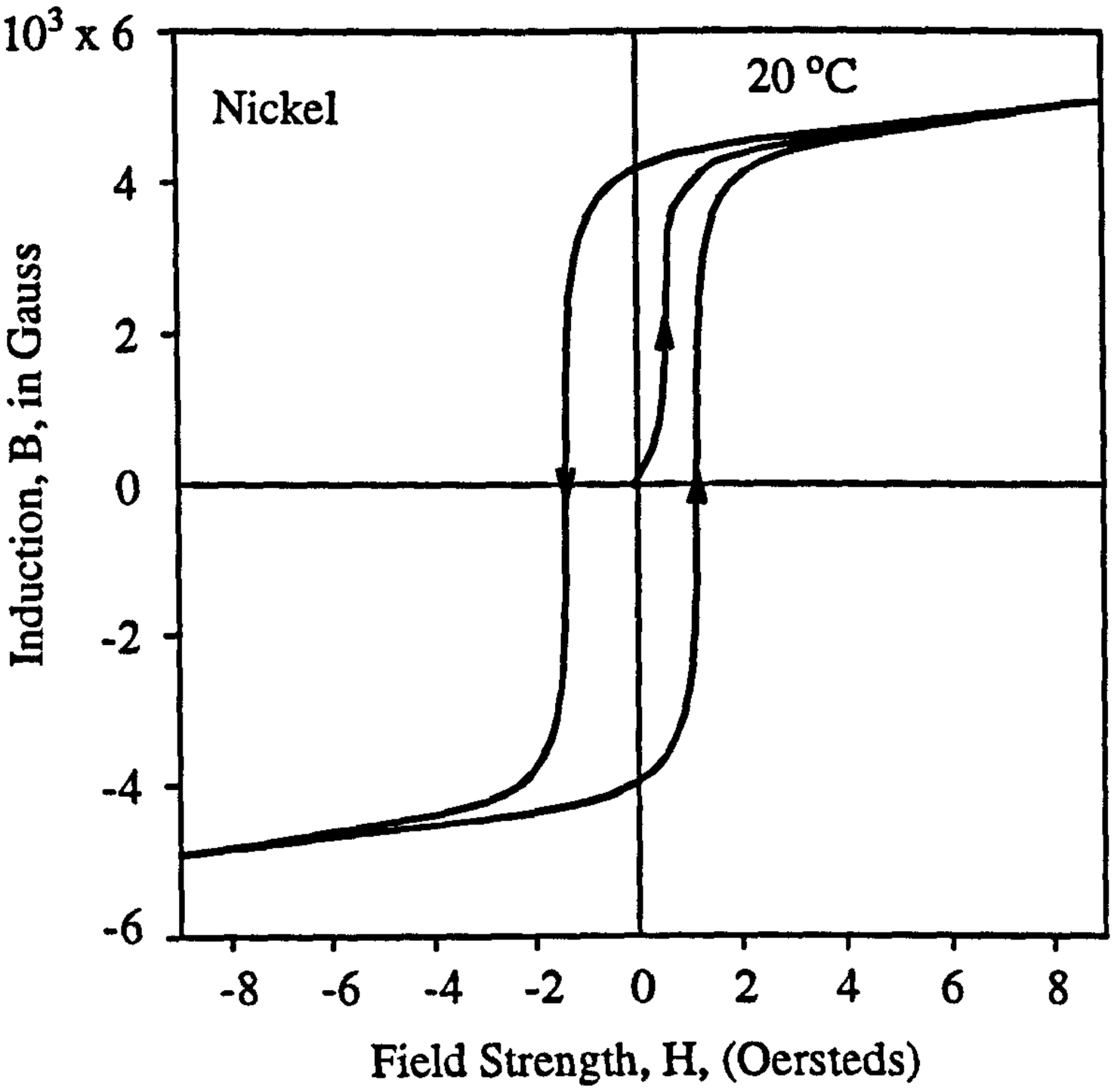

Fig.6.1 Hysteresis in Nickel

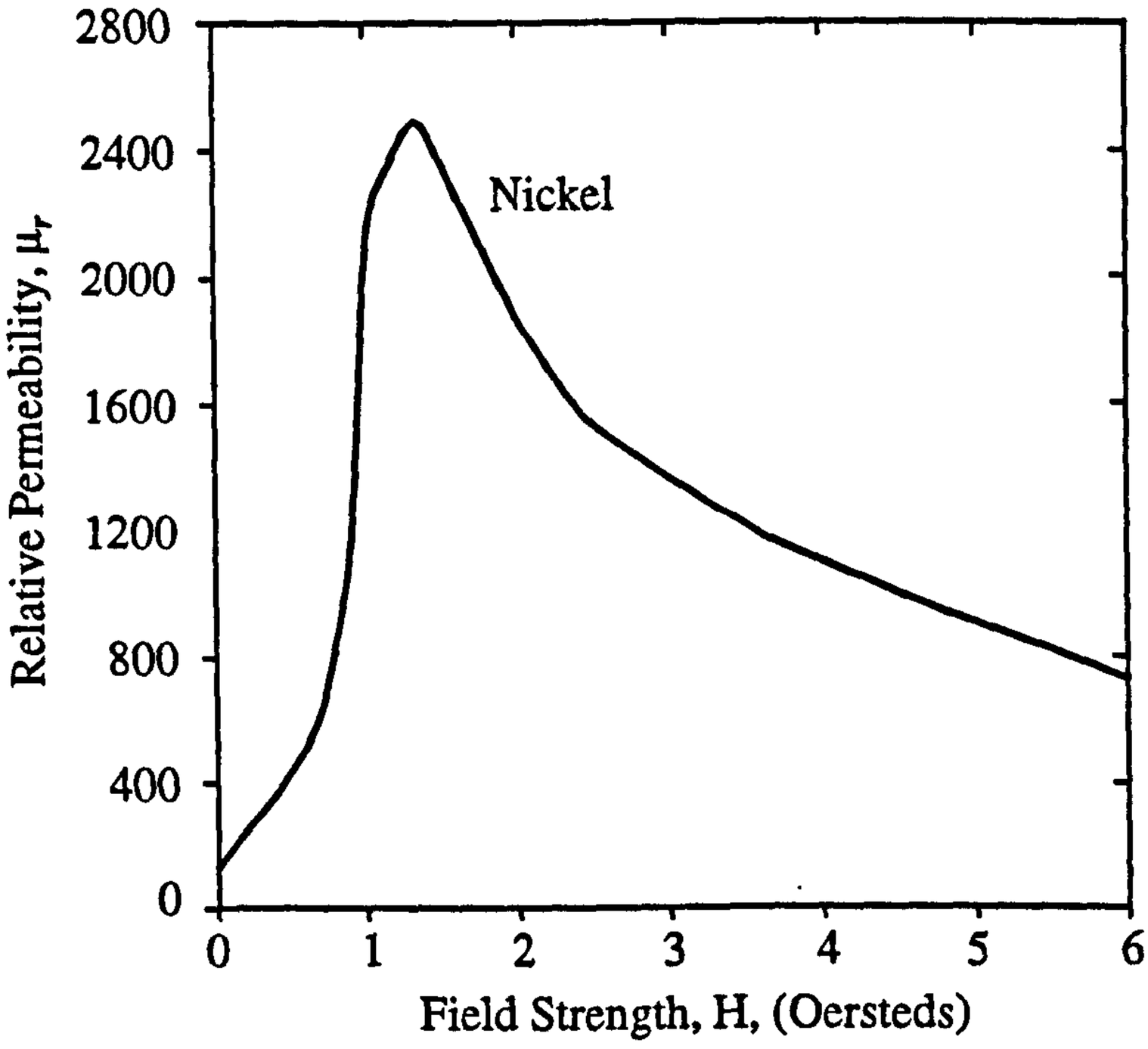

Fig.6.2 Non-linear permeability in Nickel

finally reaching saturation, $\mu_{sat} = \mu_o = 4\pi \times 10^{-7}$ H/m (free space); resulting in a maximum skin depth for nickel of approximately twice that for silver, due to the poorer conductivity of nickel. Thus, a very large non-linear change in skin depth by at least an order of magnitude, can be visualised as a function of current flow.

Bailey and Ehrlich [35] go further and consider the vibrating magnetic domain wall in ferromagnetic materials as a non-linear system. They conclude that this is a significant mechanism in terms of generated PIM levels and that the intermodulation signal should decrease monotonically with the magnetic domain-wall density in the sample.

Conclusions

It has been observed that PIM levels generated by ferromagnetic materials are very much higher than those of non-magnetic materials. Several mechanisms are likely to be operative in such materials but it is likely that the apparent "modulation" of the skin depth with current flow will be dominant. The effect of domain wall vibration is also thought to be significant but this will be considered later in the chapter in terms of the applied DC magnetic bias field.

In terms of engineering relevance, the results once again highlight the need to avoid ferromagnetic materials in the construction of RF equipment and systems. Even the presence of ferromagnetic materials in close proximity to RF systems (particularly if they are radiative) could cause problems. The results also highlight the need to carry out experimental work on a wider range of materials as it is evident that stainless steel, A286, contrary to initial expectations, performs quite well.

6.2.2.2 Silver Plating

Silver plating was only applied to the solid nickel samples. The results clearly indicate that silver plating has removed the deleterious effect of nickel, lowering its PIM level to that of the system residual. The skin depth of silver at 1.6 GHz is approximately 1.6 μm. The silver plating is approximately 13 μm thick which is 8 skin depths. For the power levels used here, it is clear that the field strength within the sample at 8 skin depths has decreased sufficiently not to cause any measurable stimulation of the nickel structure. However, it would not be recommended to resort to the silver plating of nickel in order to reduce PIM where the use of nickel can be avoided from the outset. Any surface damage to the silver plating could easily allow the intrinsically high level of PIM in nickel to be stimulated.

6.2.3 DC Magnetic Bias Field

Initial tests using the engineering samples of nickel, stainless steel 303 and copper seemed to indicate slight changes in the PIM level with the application of a transverse DC magnetic field. However, due to the size of the jig, the poles of the electromagnet were spaced some distance apart and the resultant magnetic field intensity was relatively low. Given the higher values of PIM observed and the smaller jig, it was felt that more meaningful results would be obtained from the small geometry samples.

For the small geometry samples, the application of a transverse D.C. magnetic field brought about changes in the level of PIM generated by all of the samples tested. This was expected of the ferromagnetic materials due to their magnetic properties and from previous research [35]. However, for weakly magnetic materials the magnitude of change was not expected. Two distinct types of behaviour were observed for the non-ferromagnetic materials:

- A magnetic field applied to the sample caused the PIM level to fall below that of the material with no magnetic field applied. In many cases this suppressed level was also below the system residual. This strongly suggests that the magnetic field stimulates a PIM signal which is out of phase and of a similar magnitude to the system residual.

- The PIM level can be excited 20 dB to 30 dB above the residual PIM level of the material (i.e. with no magnetic field). This was only observed with copper wire and not in a consistent manner for all samples.

For both of the above types of behaviour, the change in PIM level, once stimulated, did not always require the presence of the magnetic field to be sustained. The implication of this is that some form of structural change (physically or magnetically) occurs within the material allowing this behaviour to be observed without the stimulus field.

The next section aims to provide plausible explanations for the observed changes in PIM levels with applied DC field.

6.2.3.1 Ferromagnetic Materials

Similar effects concerning the cancellation of system residual by magnetically induced PIM have been reported for nickel in the presence of an applied D.C. magnetic field, [35]. The system PIM residual was found to be phased out by the PIM signal produced by nickel when subjected to a field of several thousand Oersteds. In the report,

Bailey and Ehrlich give explanations of two possible processes involved in magnetically related PIM signals. For completeness, a brief summary of the processes they describe are given here.

When a ferromagnetic material is subjected to a magnetic field there is a tendency for the domains to align with the applied field, the tendency being dependent upon the applied field strength. As the domains line up the domain walls disappear until the material is eventually magnetically saturated when no domain walls remain. Both explanations of the source of PIM in such structures is related to the dynamics of the domain walls (where these vibrate non-linearly due to the stimulus signals, producing PIM) and therefore, as the number of domains decrease with applied field, the level of PIM also decreases.

The first proposed mechanism is due to certain intra-domain-wall excitations which are most important for domain walls where the RF magnetic field is perpendicular to the magnetisations of the two domains separated by the domain wall, and to the wall itself. The second mechanism is the vibration of domain walls as a result of excitation by the two frequencies, f_1 & f_2. The intermodulation signals arise due to the absorption of the applied RF field energy by the oscillating wall and the subsequent re-emission of energy at the same frequencies and at the PIM frequencies.

Both processes are however, related to the presence and behaviour of magnetic domains within the sample and the existence of domains only ever appears to be related to ferromagnetic materials. However, the interpretation of the dependence of the observed signal on the applied DC magnetic field is rather complex for the following reason. In a wire, the relative orientations of the RF magnetic field and the applied DC magnetic field are not unambiguously defined. That is, with the DC field transverse to the wire, for example, there are regions in which the DC and RF fields are parallel, perpendicular and at all angles in between the two. For this reason, in their study, Bailey and Ehrlich measured flat plate samples to try and obtain a more explicit relationship between the two fields. However, in this study only round wire samples were tested.

The changes observed in the PIM levels of the ferromagnetic samples was consistent with the results obtained by Bailey and Ehrlich, however, the magnitude of the variation was not as great. This is attributed to two factors. The first is the use of wire samples rather than flat plates as described above. The second factor is that in this project, the samples were only magnetized along a portion of their length. This means that only a small section of the sample would be saturated, having fewer domains. The remainder of the sample would be relatively unaffected, hence, there would still be a significant number of domain walls where PIM could be generated. To observe a larger decrease in PIM it would be necessary to apply the field over a greater length of the sample.

6.2.3.2 Non-ferromagnetic Materials

If magnetic domains do not exist in non-ferromagnetic materials then a different explanation of the mechanism responsible for PIM generation in these materials is required.

It should be borne in mind however, that it was discovered after the tests, that the alumina dielectric used in the small geometry sample jig was responsible for a significant amount of variation in the PIM signal with the applied magnetic field. It is currently thought that this is due to contamination of the alumina (which is given as being 99% pure) possibly during some stage of the manufacturing process. However, this does not explain the highly erratic behaviour observed in only the copper wire samples.

The non-magnetic materials studied in this investigation were both paramagnetic and diamagnetic.

- Paramagnetic materials contain magnetic dipoles which are randomly orientated in the absence of an external magnetic field. When an external field is applied these dipoles begin to align themselves in the same direction as the field, losing this general alignment when the field is removed. Aluminium and its alloys are paramagnetic.

- Diamagnetic materials acquire a dipole moment opposed to the direction of an external magnetic field when it is applied. Again, this dipole moment disappears when the field is removed. Copper is a weakly diamagnetic material. However, all materials will have this property although it is normally masked by stronger effects such as paramagnetism.

As both of these forms of behaviour produce a magnetic field within the material, it is conceivable that this internal field may influence the R.F. currents in a (currently unknown) non-linear manner, producing intermodulation products. As both of the above magnetic forms of behaviour require the presence of an external magnetic field they do not seem to offer a satisfactory mechanism to fully explain the observed phenomenon, particularly in relation to the irregular behaviour of the copper samples in the absence of an applied field.

However, according to ref. [30], the use of PIM detection as a technique for indicating minute changes in magnetic behaviour is probably the most sensitive one currently available so it may well be that magnetic effects on a microscopic level are being revealed. Again, there is a great deal more work which could be carried out in this area.

6.3 Jointed Samples

6.3.1 Non-magnetic Materials

It is evident from the experimental results at low contact pressures that more junctions give a higher level of PIM. It was also observed that the level was more stable and repeatable. Using samples with a coarse, "as machined", finish resulted, not surprisingly, in slightly more erratic performance. The ground washers although more numerous (due to their smaller size after grinding) gave more stable results.

On the application of a 5 Nm torque to apply a high contact pressure (>100MPa), the PIM level in all cases was seen to drop below the system residual level. This was found to be very repeatable independent of material or surface finish. Such consistently low levels were not expected for multi junction samples. This result is very significant since it verifies the contact model of Section 2.4.2.1 and illustrates that PIM at junctions can be lowered substantially using high contact pressures.

Further experimentation could be carried out in order to establish a threshold contact pressure, or to relate contact pressure and mechanical properties (ductility, elasticity, hardness, etc.) with PIM levels. Information about the long term effects of maintaining high contact pressures would be useful for gauging the suitability of using high pressures in low-PIM design.

6.3.2 Ferromagnetic Materials

In the ferromagnetic materials which were tested (nickel and stainless steel 303) the same behaviour was observed as for the non-magnetic materials. The levels however were generally higher. Once again the PIM level could be reduced by applying a high contact pressure.

Nickel is a very hard material and in its "as machined" state had many burrs and the contact faces were very coarse, hence it is not surprising that the levels for the greater number of junctions are higher. What is surprising, however, is that once the washers had been ground flat and the mating surfaces were smooth, the jointed sample of nickel with the most junctions actually displayed a lower level than the other sample formats which have much fewer junctions. The experiment was performed several times, at even higher contact pressures, but the result was the same each time.

One possible explanation is that eddy currents within the nickel are responsible for PIM generation. The eddy currents will be excited by the time-varying RF magnetic flux in a direction orthogonal to the lines of flux as in Fig.6.3. Eddy currents are higher in

ferromagnetic materials and lead to increased losses. This translates to increased energy dissipation in the material and any nonlinearities which are present will generate higher PIM.

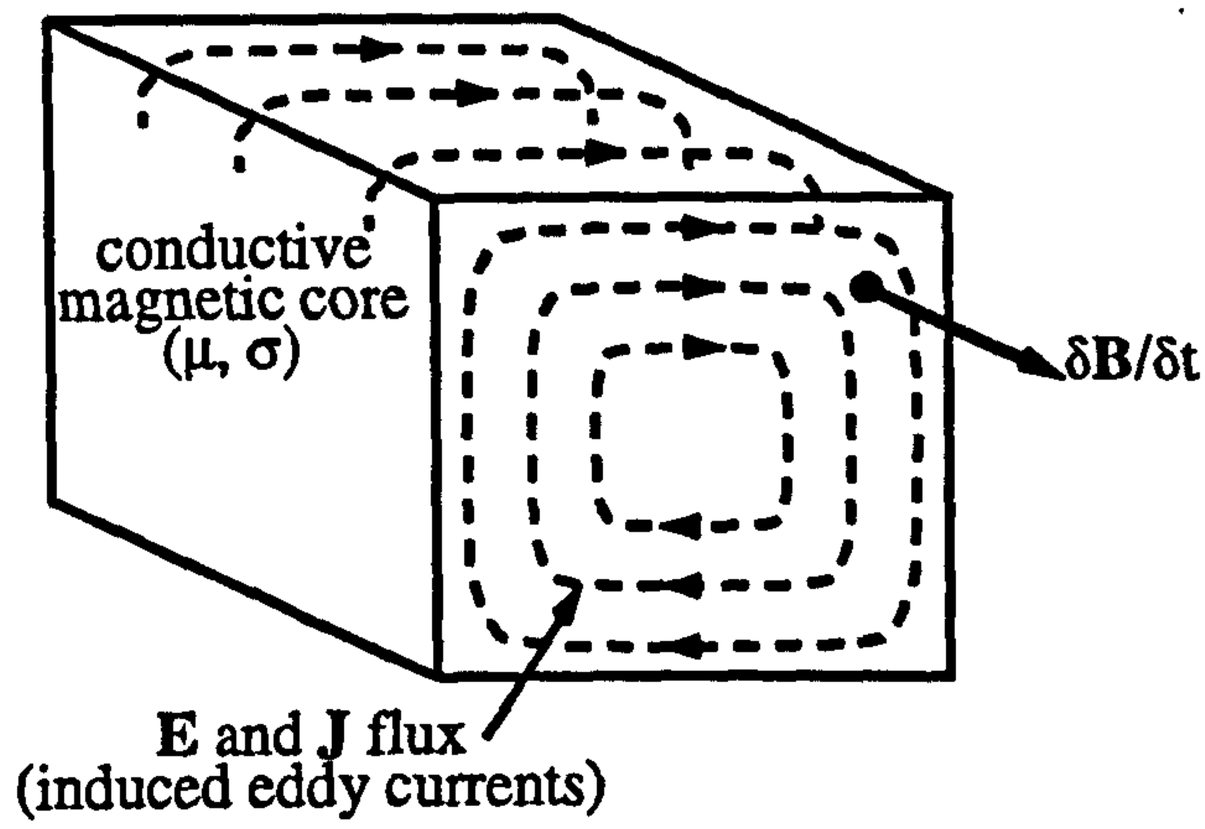

Fig.6.3 Eddy Currents in a Conductor Immersed in a Time-Varying B Field

By dividing the sample up, it is known from work in other fields (e.g. laminated transformer cores) that eddy currents are likely to be reduced. Hence if these currents are contributing to the PIM generation in the sample, the PIM level will be reduced.

Alternatively, the grinding of the washer faces may have resulted in changes to the microscopic structure of the nickel, altering its properties and reducing the PIM level.

In all cases, rearranging the washers on the former and reversing their orientation with respect to current flow made no difference to the PIM levels, indicating that remnant magnetisation is not a significant effect.

As in the case of the solid samples of nickel, silver plating the washer samples reduces the PIM levels in nickel to below the system residual level. This indicates that the PIM is more likely to be a bulk property of the material rather than a junction effect.

It is concluded that the higher levels are due solely to ferromagnetic effects and once again highlights the need to completely avoid such materials in RF system design.

6.3.2.1 Aluminium-Alochrom Junctions.

Some of the highest levels of PIM thus far observed with the system were during the tests on the aluminium-Alochrom junctions.

Each material, when tested individually, in both solid and jointed formats, gave levels of PIM much lower than those for the two materials in combination. Two papers were sourced relating to the Alochrom coating which is also known as Alodine in [171, 172].

In ref. [171], R.J. Sunderland presents a chemical analysis of the coating and concludes that the principal elements in the coating as they occur on aluminium surfaces are chromium, oxygen, flourine, zirconium and zinc. He also found small quantities of potassium, sodium and iron. The abundance of elements makes it much more difficult to determine the PIM mechanism(s) at work. Chromium and iron are both ferromagnetic, however there is little information as to whether they exist in their pure form or are compounded with other elements, or both.

The thickness of the coating was found to be around 500Å to 600Å thick (Å=Angstroms or atomic layers=1×10^{-10}m) and comprised mainly from the chromium oxide Cr_2O_3. This would tend to rule out tunnelling as a candidate mechanism since it only becomes operative for thicknesses less than about 20Å (see Section 2.4.2.2).

During the PIM tests, thermally cycling the aluminium-Alochrom junction through a relatively large temperature range resulted in an increase in PIM with a decrease in temperature. However, this has not revealed any clear indications as to the mechanism which might be operative. Both semiconductor action and tunnelling exhibit positive changes with increasing temperature, i.e. the PIM level would be expected to increase as temperature increases. Referring to Fig.2.9 on page 30, the rate of change of current associated with semiconductor action is significantly greater than that from tunnelling (for aluminium oxide-aluminium the currents are similar at -40° C). This was not apparent in the tests. The only explanation which can presently be given for the increase in PIM signal with decrease in temperature is that it is associated with changes of interface pressure. As the temperature decreases the contact pressure reduces. This moves the junctions apart from each other reducing the ohmic contact (which occurs at the centre of an asperity) forcing a higher current to flow through the aluminium/aluminium oxide-Alochrom junction. A higher current through the junction produces a higher PIM level. As the temperature is increased again the interface pressure increases producing a larger area of ohmic contact at a given junction due to the penetration of the asperity. Consequently the PIM level drops. As the increased contact pressure causes physical damage to the surface the PIM level remains low, even when the original temperature is reached. The effect of changing pressure may thus be masking the expected temperature dependence of the original mechanism. Clearly, this explanation is only based on supposition and remains to be explored, as does any other explanation which may be put forward.

6.4 Summary of Engineering Recommendations

In light of the experimental work described in Chapter 5 and the work carried out in developing the L-band measurement system, a list of recommendations is presented for minimising PIMI in vulnerable communications systems. A set of general recommendations was given in Section 2.4.3. the recommendations given here are based solely on the experience gained on this project.

1. In coaxial systems, semi-rigid cable should be used at all times where possible. Semi-rigid cable has been found to out-perform all types of flexible in terms of PIM generation (see Section 3.10.2).

2. Connections between metal surfaces should always be made, where possible, at a point of minimum current flow. Where such points are not obvious, a current minimum can be forced by using quarter wavelength transmission line sections (after Section 4.3)

3. If step 2. is not possible, all metal joints must be made at very high contact pressure (>60MPa). It was shown during the jointed sample measurements (Section 5.4.2) that this was an effective method of reducing PIM but only if the surfaces are uniform and flat.

4. In the design of microwave networks it should be noted that resonant structures which couple into high power signals will create vastly increased currents and fields within that structure. If more than one signal is present it is likely that high levels of PIM will be generated (Section 3.8.2). Such resonant structures should be avoided, or at the very least, thoroughly isolated from multiple frequency signals.

5. Provisions for tuning of resonant structures should only be made where it is possible to significantly reduce the current and field intensity impinging on any tuning elements. Tuning elements generally consist of metallic moving parts in loose contact with each other suggesting a greater propensity to generate high levels of PIM (see Chapter4).

6. The results of the experiments described in Chapter5, between the engineering scale and small geometry samples have been compared. It is evident that the dimensions of current carrying conductors should be made as large as possible to minimise current densities and therefore minimise PIM.

7. In Section 5.5.1 it was observed that the surface finish of the samples had a significant effect on the measured PIM level - the more abraded the surface, the higher the PIM. Consequently it is recommended that all current carrying surfaces be finished as finely as possible - polished if necessary - to avoid unnecessary PIM generation.

8. It was found that the high PIM level of nickel could be reduced to that of the system residual by silver plating it (see Section 5.4.1). However, resorting to such a method of PIM reduction for intrinsically non-linear materials would not be recommended where the use of such materials can be avoided at the outset. Any surface damage to the silver plating could easily allow the intrinsically high PIM levels of such materials to become apparent.

9. Bearing (8) in mind it is worth noting that alternative materials are available for low-PIM use. Contrary to expectations, in Section 5.4.1 stainless steel A286 was shown to have a PIM signature no higher than the system residual level - even on the application of a large DC bias field.

10. The behaviour of the aluminium-Alocrom 1200 junction is of great concern due to the extensive use of Alocrom as a method of surface protection and multipactor reduction in space RF hardware. Unexpectedly high and variable levels of PIM have been consistently observed during the measurement programme (Section 5.4.3). Based on the present findings, it would be strongly recommended to avoid the use of this form of chromate conversion coating in any PIM sensitive areas of a system.

11. Unusual PIM behaviour was observed in copper wire when subjected to a transverse DC magnetic field (Section 5.5.2). The behaviour was not consistent from test to test and could not easily be associated with any manipulation of the magnetic field. It was clear however that this was not an anomaly of the measurement system as repeated observations were made and other materials did not reproduce the behaviour when subjected to the same conditions. Given the widespread use of copper in communications systems it would be prudent to recommend that care be taken where large magnetic fields are in close proximity to RF current carrying conductors. This is borne out by the fact that all of the materials tested exhibited changes in PIM level in the joint presence of the magnetic field and RF.

CHAPTER 7

PIM Characterisation of Compact Payload Test Range

This chapter describes additional work carried out at the European Space Research and Technology Centre (ESTEC) in the Netherlands. The work involved using the UKC, L-band PIM measurement system to characterize the background PIM levels of ESTEC's Compact Payload Test Range (CPTR).

7.1 Introduction

It has been shown in Chapter 2 that PIMI poses a very real threat to the success of any satellite mission. Communications channels can be rendered totally useless due to interference from PIM. One of the main objectives of this project was to investigate the phenomena of PIM in order to better understand the mechanisms behind it. This knowledge can then be used to help engineers avoid materials and practices that can cause PIM and thus reduce the likelihood of PIM affecting the successful operation of future satellite missions.

In the meantime however, organisations like ESA continue to develop and produce ever more complex and sophisticated satellite programmes which increasingly lend themselves susceptible to the effects of PIM.

Where the frequency regime of the satellite is such that PIM could potentially cause interference, the components of the satellite which are exposed to high-power multi-frequency signals must be tested to make sure that they do not generate threatening levels of PIM. Even at the stage where components have been tested and have indicated no threat of PIM generation, there is always a chance that problems could arise during final integration with the complete payload assembly. It is therefore evident that the payload as a whole must also be tested prior to launch, and under operational conditions, to guarantee as far as possible that the satellite will operate free of interference from PIM.

The work described in this chapter looks at the PIM characterisation of a payload test chamber at ESTEC. This work has been published in ref. [12]. The test range is a potential site for evaluating the PIM performance of satellite payloads and it is essential to measure the background levels of PIM generated by the chamber itself to make sure that the levels are not high enough to interfere with payload testing.

7.2 The Compact Payload Test Range (CPTR)

The ESTEC CPTR is depicted in Fig.7.1. The range was designed and built in order to measure the behaviour of radiating satellite payloads under the electrical field conditions they would experience in orbit. Any radiating payload is operating in a region known as the "far field". In this region, the separation between the payload and the ground based transmission is sufficiently large that any signal arriving at an antenna has a uniform phase and amplitude distribution across the antenna aperture - this is called a plane wave

The far-field is generally defined as the distance R between source and receiver where:

$$R > \frac{2D^2}{\lambda}$$

D = Largest antenna aperature dimension
λ = Smallest wavelength of interest

Eq.7.1

Any payload test facility has to be large enough to satisfy this criterion. However, for large antennas operating at millimetre wave frequencies, the shortest far-field distance can easily exceed several kilometres. An indoor facility such as the CPTR, with a controlled environment suitable for satellite testing, must therefore find another way of forming a plane wave in a shorter distance.

In the CPTR, the curvature of the transmitted radio wave is removed by means of two reflectors which combine to give a large test zone with the required flat wave front. In order to minimise distortions in the resulting plane wave, the surface accuracy of the reflectors has to be extremely good. This is particularly important at higher frequencies where the wavelength of a signal begins to approach a few millimetres and any small surface blemishes could produce phase variations which will disrupt the uniformity of the field. Despite the size of the reflectors, both of which are about $80m^2$, the surfaces are accurate to within 50microns and can operate satisfactorily up to 40GHz.

In addition to the reflectors, several other elements are present within the chamber which are necessary for its correct operation. One of the most important parts of the test range is the radio absorbing material or RAM which is used to line the interior surfaces of the chamber. The RAM lining absorbs any incident signal power and dissipates the energy as heat. This prevents the reflection of test signals from the chamber walls and helps to

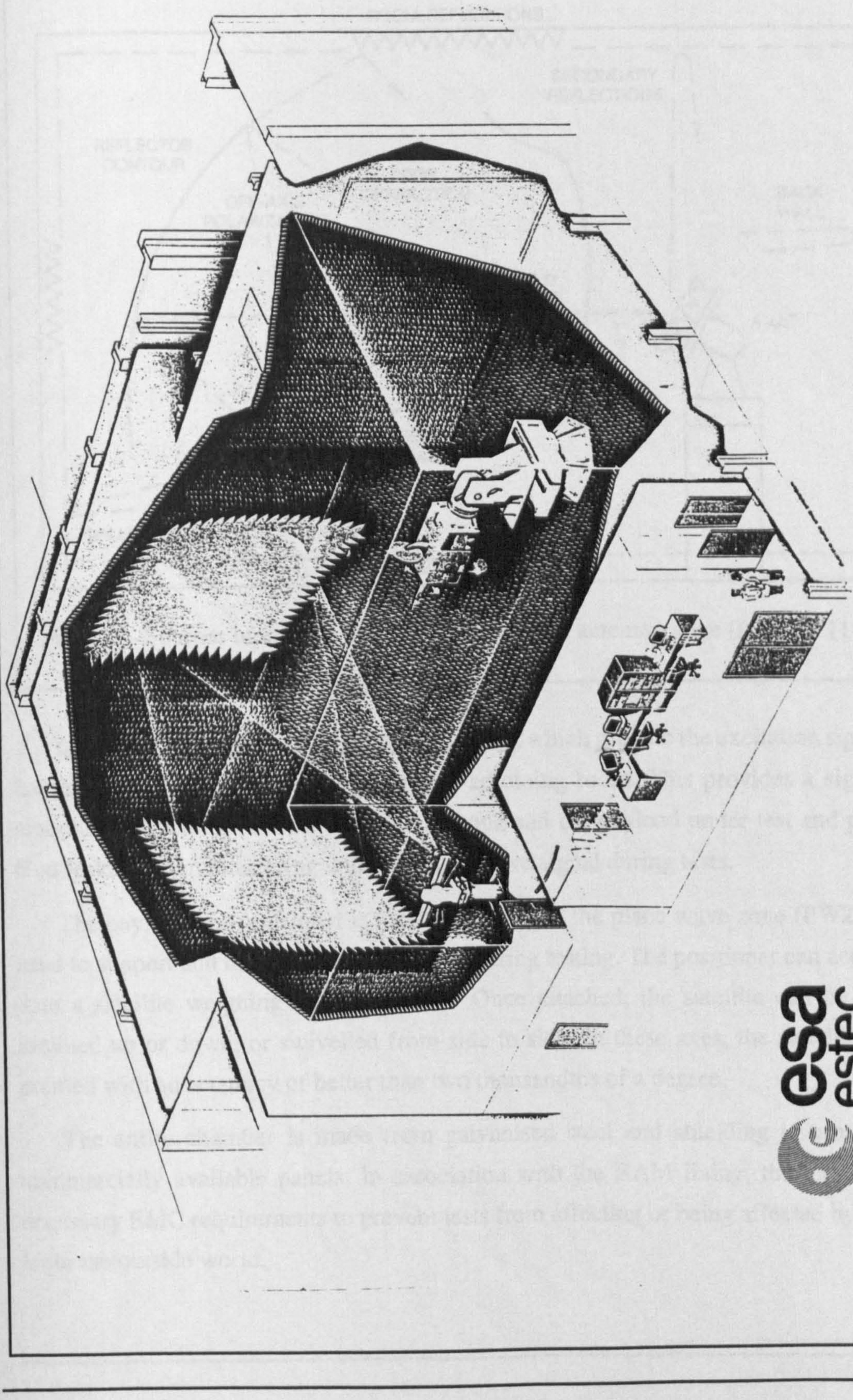

Fig.7.1 ESTEC Compact Payload Test Range.

stop the test signals from leaking and causing electromagnetic interference (EMI) in the external environment. If the reflected signals were to go unchecked, they would interfere with the desired test signals and distort the uniformity of the plane wave field, invalidating any measurements. Other sources of error signals are indicated in Fig.7.2.

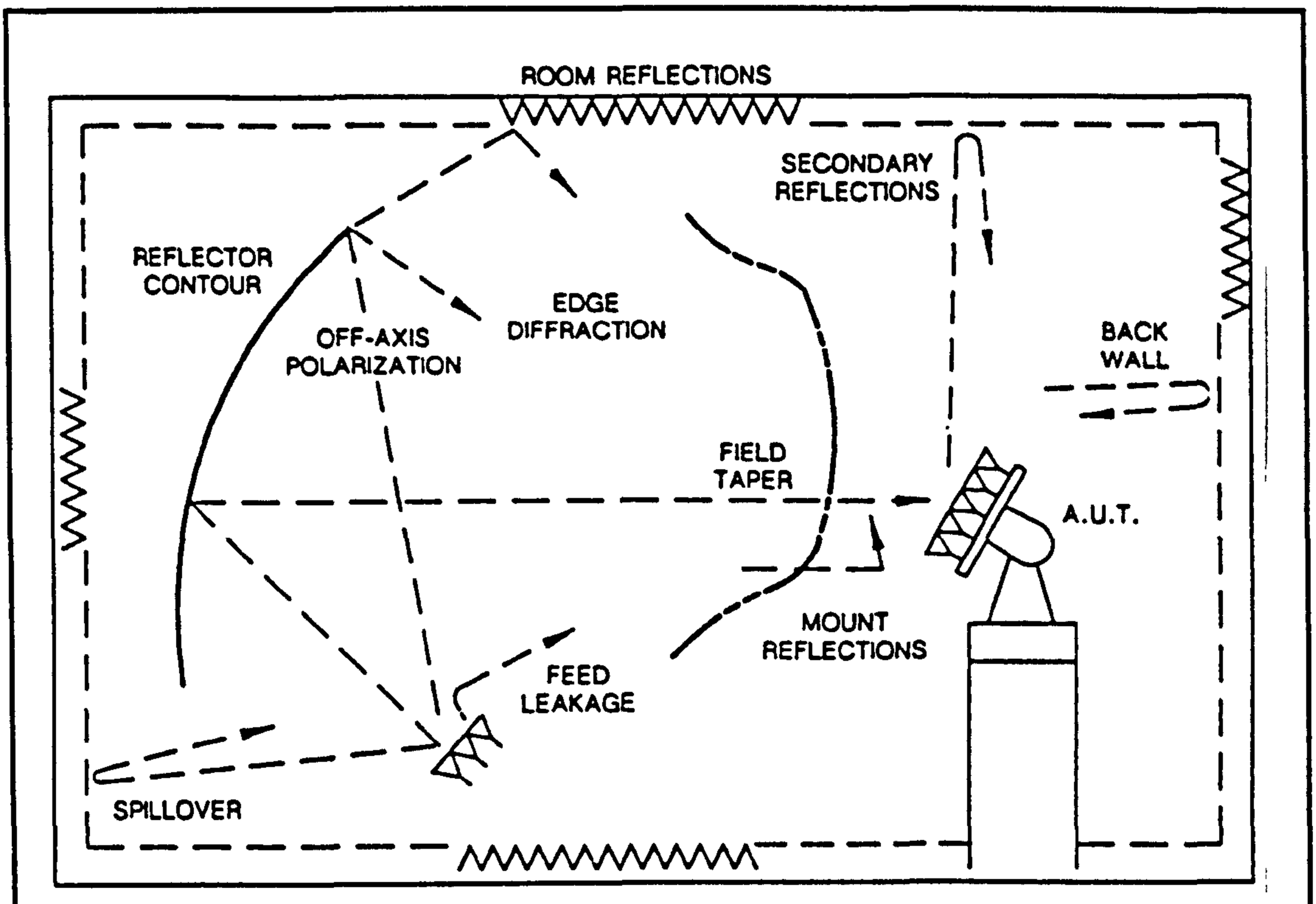

Fig.7.2 Sources of error in an offset-fed reflector antenna range (from ref.[180]).

In the CPTR, the feed antenna and positioner, which provide the excitation signals for the tests, are located in a small, recessed, adjoining room. This provides a significant amount of screening between the feed antenna and the payload under test and prevents feed leakage from interfering with the plane wave signal during tests.

The payload test positioner is located directly in the plane wave zone (PWZ) and is used to support and manipulate the payload during testing. The positioner can accommodate a satellite weighing up to 5 tonnes. Once attached, the satellite can be rotated, inclined up or down, or swivelled from side to side. In these axes, the satellite can be pointed with an accuracy of better than two thousandths of a degree.

The entire chamber is made from galvanised steel and shielding is provided by commercially available panels. In association with the RAM lining, this provides the necessary EMC requirements to prevent tests from affecting or being affected by, signals from the outside world.

At the time of its inception, it was not envisaged that the CPTR would be used for PIM testing. As such, no special measures were taken to minimise the possibility of PIM generation from the internal components and structure of the chamber. Recently, however, it was decided that ESA's latest communications satellite ARTEMIS, should be tested for PIM in its fully deployed configuration. The ARTEMIS payload has been described in Section 1.2 and Section 4.1.1 where it was shown to be susceptible to interference from 7th order PIM products. The threat from such low order products is extremely significant, hence the need for a rigorous test programme before launch.

In order to be able to test the ARTEMIS payload in the CPTR it is essential to measure the background levels of PIM generated by the range itself to make sure that the levels are not so high as to interfere with payload testing. Due to the expertise gained at L-band and the availability of the L-band measurement system, the Noise Measurements Group at UKC was commissioned by ESTEC to undertake PIM characterisation of the chamber, under conditions compatible with ARTEMIS requirements. The work presented in this chapter has been described in two reports to ESA [13,181].

The major implication of undertaking this project was that of reconfiguring the measurement system. The L-band system developed at UKC was configured to perform conducted measurements as described in previous chapters. For the CPTR tests, the system, quite clearly, had to be configured to radiate test signals around the chamber in order to be able to scan for sources of PIM. This required considerable modification to the existing system. However, in order to make sure that the reconfigured system delivered adequate performance, it was first necessary to establish the exact requirements of the program.

7.3 Test Requirements

For the ARTEMIS PIM measurement programme, the payload would be mounted on the positioner of the ESTEC CPTR. It is therefore necessary to determine the background PIM levels, generated by the CPTR reflectors, absorbers and other structures, under conditions identical to those of the actual payload tests. The specification of the ARTEMIS payload defines acceptable levels of PIM which the satellite can tolerate without threat to its correct operation. If the residual PIM levels of the CPTR are too high it will not be possible to determine whether the payload is within the desired specification. In essence, the levels from the chamber must be lower than the specification for the payload or test results would be meaningless. The maximum acceptable residual PIM levels from the chamber can be calculated from a knowledge of the payload and the CPTR.

7.3.1 Derivation of Test Specification

The parameters used to derive the test specification apply to the conditions of the ARTEMIS payload as it would experience when fully deployed in orbit around the earth. These parameters were obtained from ESTEC [182] and are summarised as follows:

Test Frequencies	f1, f2	1530 MHz & 1560 MHz
PIM Frequency	(4f2 - 3f1)	1650 MHz (7th order)
Wavelength PIM(1650MHz)	λ	0.18169m
ARTEMIS Antenna Gain	G_A	26 dBi (398 linear)
ARTEMIS Transmit Power	P_t	20(x2) W
Maximum allowable PIM Power at ARTEMIS Receive Antenna Feed	P_{Rx}	-155 dBm
Distance Payload to PIM Source (CPTR Main Reflector)	R	15 m

Table 7.1 ARTEMIS Payload Specification.

The radius of 15 metres to the CPTR main reflector was chosen for the reference as it was felt that as the reflectors form an integral part of the range, any PIM generated by them would create a major problem. The surface structure of the reflectors comprises a 1.5mm thick skin of carbon fibre reinforced plastic (CFRP) on top of an expanded aluminium alloy honeycomb mesh. The top layer is covered with a fine aluminium mesh and coated with an aluminium loaded resin. This composition suggests that a large number of metal to metal contacts and metal oxide deposits are present. Under the high fields to which the reflectors are exposed during the tests, the reflector construction could be a significant PIM source and this was one of the main concerns during the CPTR characterisation.

It should also be noted at this point that three rectangular waveguide, L-band, horn antennas were acquired for the tests. Two of the horns were used to transmit the individual excitation signals and each has a gain of 20dBi. The remaining 16dBi horn was used to detect any PIM signals generated in the chamber. The horns were purchased by ESTEC.

7.3.2 Power Density

In order to test ARTEMIS for PIM problems, the payload will have to be operated at full power and be allowed to radiate freely in the chamber, just as it would in space. Therefore, the first step was to establish the power density that the ARTEMIS payload will impart upon the CPTR. This had to be matched by the PIM test set-up in order to provide

meaningful results. It was observed in Section 2.2.3 that PIM variation with power level does not obey a simple relationship, therefore, extrapolation of PIM levels from any other data is certain to be misleading.

It was then necessary to work out how much C.W. transmit power is required of the test set in order to deliver the calculated power density. The figure is calculated by referring the ARTEMIS power density back to the input of the horns used in the test set up.

Referring to Table 7.1, the maximum PIM power allowed at the R_x (receive) antenna output of the ARTEMIS satellite, P_{Rx}, is governed by the sensitivity of the payload receiver circuitry. An additional 10dB has been added in order to give an extra margin for safety. The payload transmit power, also including a factor of safety, is for two 20 W carriers at 1530MHz and 1560MHz. Neglecting losses, this power level was assumed to be at the input port of the ARTEMIS transmit antenna feed horn. The 15m distance is based upon the CPTR reflector to positioner distance but other possible PIM generators such as the support structures, lights etc. were included in other calculations.

Note that in the following equations, the subscripts *(sat)* and *(sys)* refer to the ARTEMIS *sat*ellite payload and UKC measurement *sys*tem respectively.

The total power density, P_d, 15m from the ARTEMIS antenna, for two 20 W carriers, is given by [183]:

$$P_d = \frac{P_{Tx(sat)} \bullet G_{Tx(sat)}}{4\pi \bullet R^2} \quad \text{W/m}^2$$

$$= \frac{40 \bullet 398}{4 \bullet \pi \bullet 225} \qquad \text{Eq.7.2}$$

$$\underline{P_d = 5.63} \quad \text{W/m}^2$$

This equates to a power density requirement of 2.8 W/m^2 per carrier and determines the transmit (T_x) power which should be available at the inputs to the transmit horns of the PIM test setup. Given that the gain of each UKC, T_x horn is 20dBi (100 linear), and that the test radius, R, remains 15 metres, the transmit power can be determined by rearranging Eq.7.2:

$$P_{Tx(sys)} = \frac{P_d \bullet G_{Tx(sys)}}{4\pi \bullet R^2} \quad \text{Watts}$$

$$= \frac{2.8 \bullet 100}{4 \bullet \pi \bullet 225} \qquad \text{Eq.7.3}$$

$$\underline{P_{Tx(sys)} = 79.2} \quad \text{Watts}$$

Therefore around 80 Watts is required at the input of each horn i.e. per carrier.

7.3.3 Receiver Sensitivity

The next step is to determine the sensitivity that must be delivered by the test setup in order to meet the specified sensitivity of the ARTEMIS payload. This states that the maximum level of 7th order PIM signal at the output of the ARTEMIS receive (R_x) horn feed should be less than -155dBm, and includes a 10dB margin of safety. This level must be translated back to the CPTR reflector in order to determine the maximum allowable strength of any PIM source. The receiver circuit of the measurement system must be able to pick out signals at or below this level, in order to identify those sources which exceed the ARTEMIS specification and which would de-sensitise the ARTEMIS PIM tests in the CPTR.

Any PIM generated in the chamber is assumed to be isotropic, i.e. radiating equally well in all directions. This assumption allows us to model the behaviour of the PIM source which is essential in order to calculate the test parameters and to quantify the PIM generated by the CPTR. The assumption is justified because although it is unlikely that every PIM source radiates identically and isotropically, assuming that they do represents a worse case situation.

Assuming an isotropic PIM source 15m from the ARTEMIS antenna, the intensity of that source necessary to produce a level, P_{Rx}, of -155dBm at the output of the ARTEMIS feed horn is calculated from:

$$P_{Rx(sat)} = \frac{P_{PIM} \cdot A_{R(sat)}}{4\pi \cdot R^2} \qquad \text{Eq.7.4}$$

Where $A_{R(sat)}$ is the effective area of the ARTEMIS receive antenna and the denominator on the right hand side of Eq.7.4 is the equation for the surface area of a sphere, radius R. P_{Rx} is, therefore, that portion of the total PIM power intersected by the antenna at a distance R, and has a maximum value of -155dBm.

The effective ARTEMIS antenna area, $A_{R(sat)}$, is given by [183]:

$$A_{R(sat)} = \frac{G_{Rx(sat)} \cdot \lambda^2}{4\pi} \qquad \text{Eq.7.5}$$

Substituting Eq.7.4 into Eq.7.5 gives:

$$P_{PIM} = \frac{P_{Rx(sat)}}{G_{Rx(sat)}} \cdot \left(\frac{4\pi R}{\lambda}\right)^2 \qquad \text{Eq.7.6}$$

in decibel form:

$$\begin{aligned} P_{PIM}\,(\text{dBm}) &= P_{Rx(sat)}\,(\text{dBm}) - G_{Rx(sat)}\,(\text{dB}) + 20log\left(\frac{4\pi R}{\lambda}\right)^2 \\ &= \left(-155 - 26 + 20log\left(\frac{4\pi R}{\lambda}\right)^2\right) \\ &= \underline{-121\ \text{dBm}} \end{aligned} \qquad \text{Eq.7.7}$$

Now this means that an isotropic PIM radiator (G_{Tx}=1, linear) of -121dBm at the main reflector has to be, at least, the minimum signal detectable by the receiver. Given that the gain of the PIM measurement system receive horn is 16dBi, then the minimum sensitivity of the UKC system at the output of the R_x horn feed is given, from Eq.7.6, by:

$$\begin{aligned} P_{Rx(sys)} &= P_{PIM} \times G_{Tx(PIM)} \times G_{Rx(sys)}\left(\frac{\lambda}{4\pi R}\right)^2 \\ &= -121\ (\text{dBm}) + 0\ (\text{dB}) - 44\ (\text{dB}) \\ &= -165\ \text{dBm} \end{aligned} \qquad \text{Eq.7.8}$$

Which is also the maximum allowed PIM level at the output of the UKC receiver horn. Any signal recorded above this level could lead to inaccuracies during any ARTEMIS PIM tests.

Clearly, to be able to resolve such a low level signal the receiver needs to be extremely sensitive. The UKC test system used equipment with the following performance characteristics:

Spectrum analyser N.F. = 28 dB (10 MHz - 2.9 GHz)

L.N.A. gain = 42.4 dB N.F. = 1.8 dB

Rx chain losses = 2.9 dB (includes filters + cables)

By the method of Section 3.6.1, the above figures result in a receiver noise figure (N.F.) of 4.8 dB which gives a sensitivity of about -168 dBm/Hz at the *Rx* horn output. It can be seen that this is sufficient to be able to resolve the minimum PIM signal level of interest when the receiver is operated with a 1Hertz bandwidth.

A summary of the system parameters used during characterisation are tabulated below.

Test frequencies	-	1530 MHz & 1560 MHz
PIM frequency	-	1650 MHz (7th order)
Test power @ T_x horn input	-	80 W
Power density on CPTR reflector @ 15m from positioner	-	2.8 Wm^{-2} per carrier
Required *Rx* system sensitivity @ *Rx* horn output	-	< - 165 dBm
Rx system sensitivity @ *Rx* horn output (in 1 Hz res. b.w)	-	- 168 dBm
Rx system noise floor (1 Hz r.b.w)	-	- 168 dBm
Polarisation	-	Vertical and horizontal linear

Table 7.2 UKC Test System Parameters

7.4 Measurement System

The UKC L-band measurement system, described in Chapters 3 & 4, was used to conduct the PIM characterisation of the CPTR. However, in order to be able to carry out tests of this nature, the system had to be reconfigured to allow the test signals to be radiated around the CPTR, and to allow PIM signals which are radiated by the chamber to be picked up by the receiver circuit. Three horns were acquired for the task, one for each of the transmitted carrier signals and one to detect the resultant PIM signals. Using separate horns and hence separate feed chains, greatly reduces the likelihood of generating PIM in the transmitter path. It also dispenses with the need for frequency combiner circuitry therefore, the complexity of the system is decreased and due to the reduced number of components, the losses are kept to a minimum.

It is possible however, that PIM may be generated in the receive (R_x) chain due to test signals getting into the R_x path and combining at sites of non-linearity. This can happen due to the test signals being reflected from the CPTR structure or by cross coupling of the test signals between the transmit and receive horns. The risk of either situations causing a problem can, however, be minimised by careful system design and configuration.

7.4.1 Equipment Configuration

A single basic configuration of test equipment was used during the complete test programme with only a slight alteration made at the power amplifier output sections when the initial system performance was being verified. A general overview of the system operation follows (refer to Fig.7.3).

The test signals of 1530 MHz and 1560 MHz are generated by two oscillators which are phase locked to a 10 MHz reference from the spectrum analyser. This provides the necessary frequency stability for the use of the minimum resolution bandwidth available on the analyser (1 Hz), thus achieving maximum sensitivity. These two low level signals go through three stages of amplification, starting with a solid state stage, followed by two stages of valve amplifiers, the final stage being UKC designed and built. As this uses water cooled valves, power levels in excess of 130 W per carrier can readily be achieved. A UKC designed high power coupler is incorporated at the output of each final power amplifier in order to allow monitoring of the forward and reflected power - forward power being displayed on a power meter and the reflected power fed to a crystal detector and displayed on an oscilloscope.

The amplified test signals are fed via (5 m) low-loss Heliax® flexible cables through a band-pass filter (BPF) followed by a band-stop filter (BSF) and thence to the transmit horns. The BSF's (as described in Section 4.6) are UKC designed and include contactless cable assemblies. These have been described in Section 4.3 and have a very low PIM residual ensuring excellent PIM performance compared with standard connector types. Contactless connectors were used at all critical sites, except on the horn antennas which were ESA property.

A system configuration using two separate transmit paths was chosen to achieve very low PIM levels from the transmit section. The BPF's increase the degree of isolation between the two test signals, particularly with regard to cross-coupling between the horns due to their close proximity. Measurements made at UKC, with the three horns mounted on their support structure, gave maximum cross-coupling values of -85 dB between the transmit horns and -70 dB between the transmit and receive horns. Thus, with an additional 20 dB rejection from the BPF's, signal leakage is kept to a minimum and helps to prevent the generation of active intermodulation products in the amplifier output stages (as described in section Section 2.3). Additional protection is provided by the BSF's which reject any intermodulation generated in the amplifiers by a factor of >80 dB.

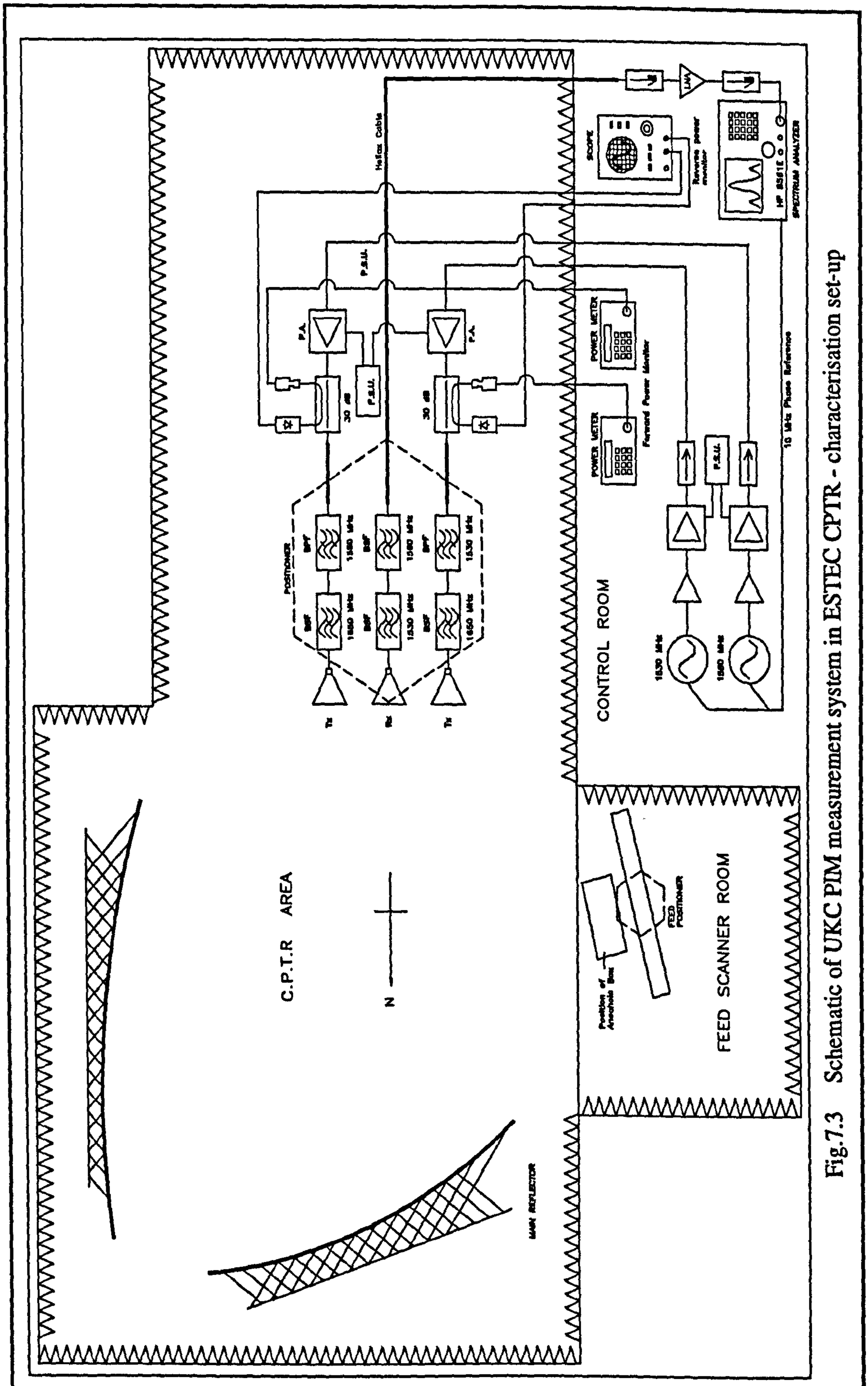

Fig.7.3 Schematic of UKC PIM measurement system in ESTEC CPTR - characterisation set-up

The T_x horns were manufactured according to specific UKC requirements designed to minimise internal PIM generation. Each horn consists of two pre-formed sections of aluminium welded along the centres of the H-plane walls. A waveguide to coaxial adaptor section is bolted to the horn. The coaxial interface is a silver-plated brass N-type connector. Each transmit horn and its associated PIM stop and band-pass filters were mounted in a custom made wooden support frame which allowed each horn to be individually adjusted in azimuth and elevation. The feed end of each horn is attached to its own support frame via a ball joint with the upper body of the horn being positionally located by four threaded studs contacting the sides of the horn (see Fig.7.4). Adjustment of the

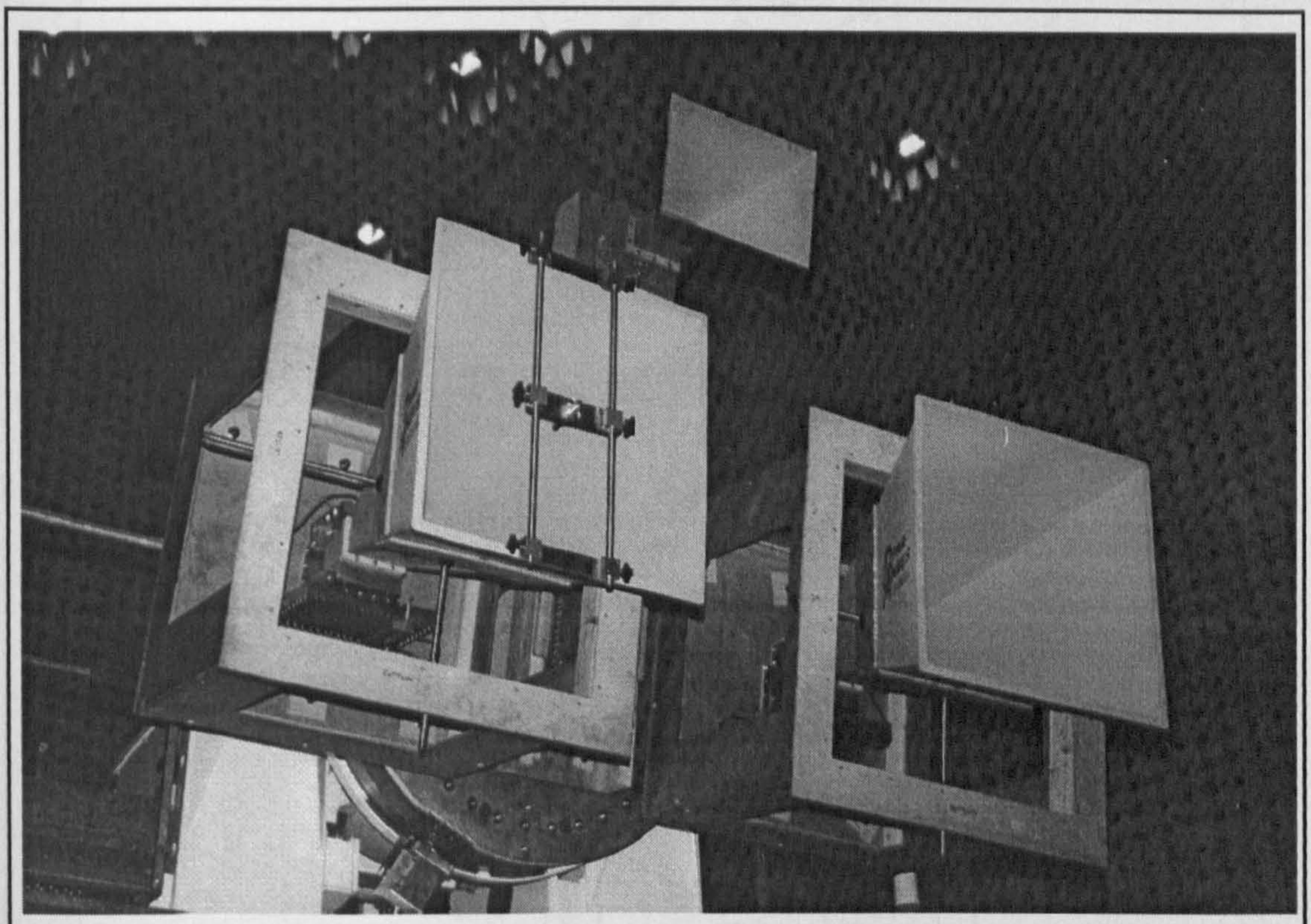

Fig.7.4 Horn mounting structure

studs can allow up to about 10° of movement of the horn from the normal to the frame.

All three horns and attendant frame structures were then fixed to the CPTR positioner via two cast iron girders as shown above. The positioner was then controlled from outside the chamber to direct the horns as desired. The definition of the angular coordinate axes of the positioner are shown in Fig.7.5. The positioner allows for complete 360° rotation in the azimuth plane and ranges from -100° to +100° in the elevation plane.

Reception of both parent test signals as well as any PIM generated is via a separate receive system. Signals intercepted by the R_x horn are filtered by two UKC designed BSF's. These reject the two test frequencies by a factor of > 80 dB each, ensuring that any

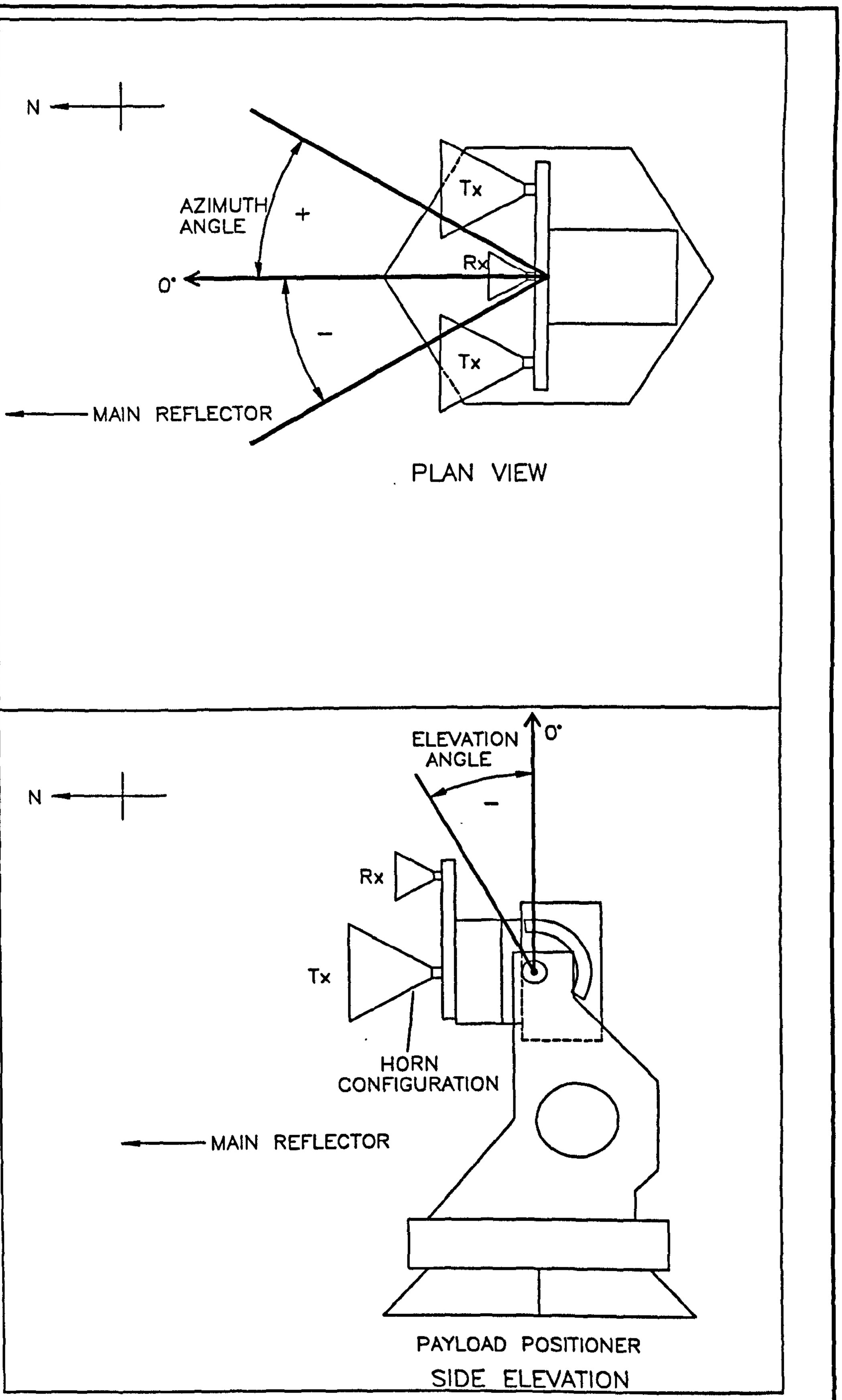

Fig.7.5 Definition of angular coordinate axes

IM generation occurring in the rest of the receiver system will be well below the required sensitivity level. The filters use UKC contactless connectors to minimise PIM generation. The standard N-type connector on the R_x horn could not be replaced since it is an ESA owned unit. After parent signal filtering, the PIM signal is fed to a low noise amplifier via a (20 m) length of Heliax® cable. The resultant amplified signal is displayed on a spectrum analyser.

7.4.2 System Performance Verification

Before PIM characterisation of the CPTR could take place it was necessary to demonstrate that the test system itself was free of PIM to a degree that allowed undistorted monitoring of PIM in the test range. As the test system was configured to have separate transmit paths this left the R_x section as the predominant area for PIM generation. The two situations which may result in PIM appearing in the receiver are considered:

- test signals reflected into R_x chain path combining non-linearly

- test signals leaking into R_x horn via cross-coupling then combining non-linearly in the R_x chain or leakage signals producing PIM on nearby structures (positioner/ support structures) which couple into the R_x chain

In the first situation, the worst case scenario to be expected is if the test signals were to be directly reflected off the CPTR reflector back into the R_x horn. Using Eq.7.8 we can determine the maximum test signal levels at the R_x horn output for this situation:

R = 2 x 15 m, λ = 0.196 m (1530 MHz)

then P_{rx} = 19.3 dBm (86 mW) per carrier

In order to test the system PIM residual for the above R_x levels, a plane reflector was used to illuminate the T_x/R_x structure with the same maximum power density which might be expected from reflected signals during characterisation (in this configuration a lower T_x power is used due to lower space losses). Thus, the PIM performance of the R_x chain and the T_x/R_x structure can be evaluated under the conditions of measurement. A simple plane reflector was chosen as this was assumed to be essentially PIM-free. The plane reflector was set-up in front of the T_x/R_x structure at a known distance and the test signals which would produce the above power levels in the receiver were transmitted directly at it. The required T_x level was determined using Eq.7.8:

with R = 2 x 4.7 m,

then P_{tx} = 7.85 W per carrier

In order to reflect the majority of the *Tx* power, the size of the plane reflector was arranged to have at least a -10 dB illumination taper at its periphery; i.e. at the edge of the reflector, the T_x signal is 10 dB down on its boresight strength. This is required in order to minimise problems from edge diffraction. The reflector consisted of two sheets of aluminium each of width 1.25 m and height 3.3 m - producing a total area of 2.5 m x 3.3 m. The sheets were joined electrically along the centre line using aluminium tape and the complete construction made rigid by a wooden backing structure. It can be shown using simple geometry together with standard horn radiation patterns that, when the T_x horns are at a distance of 4.7 m from the reflector, an edge taper of -10 dB is achieved on the reflector.

The plane reflector was suspended by polypropylene ropes from a ceiling crane in the CPTR, with its centre at the same height as that of the T_x/R_x structure. The reflector was prevented from twisting by rope stays attached between its lower edge and weights on the CPTR floor (see Fig.7.7).

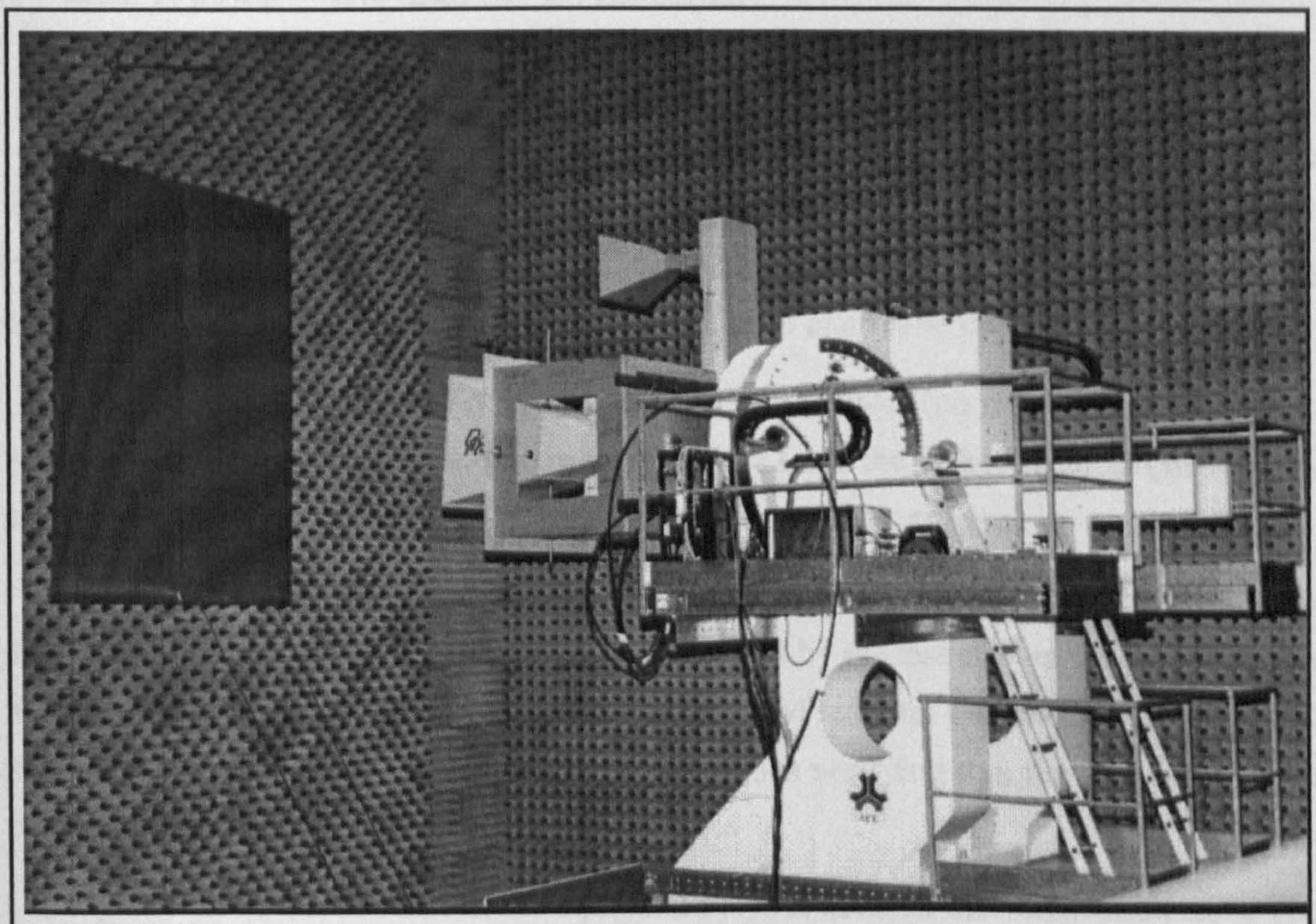

Fig.7.6 Plane reflector configuration

The positioner was adjusted to direct the T_x/R_x antennas towards the centre of the plane reflector. 10 W of power was applied to the inputs of each T_x horn and the level of 7^{th} order PIM noted on the spectrum analyser. The initial PIM residual level was variable around -90 dBm to -110 dBm at the R_x horn output. Changing the level of applied power

suggested that it was being caused by a single source since a drop of 20 dB in PIM level was observed for a 4 dB reduction in test signals. On scanning the positioner over a small azimuth angle the PIM level increased to a maximum of -102 dBm when at 2° off centre, then decreased until it was in the system noise at 15° off centre. As it was initially thought to be due to edge effects of the reflector, aluminium tape was attached to the edges to see if any change could be brought about. No changes were observed. Grounding the reflector to earth also had no effect on the PIM level. Finally, on checking the connector torques, tightening the output connector of the R_x horn brought the PIM residual down below the noise floor of the system at -168 dBm.

For the second situation, the maximum power expected to leak into the R_x horn can be calculated from measurements made on the cross-coupling factor as given in Section 7.4.1:

T_x-R_x cross-coupling = -70 dB

Max. T_x power = 49.0 dBm (80 W) per carrier

then max. signal level at R_x horn output = -21 dBm per carrier

It can be seen that this leakage is far below the maximum signal level expected due to direct reflection and would, therefore, not be expected to be readily observable. However, testing for the presence of PIM generated on nearby structures (which may couple into the R_x horn) remains relevant as this level cannot be predicted.

Therefore, the system was operated at the full test power (no reflector) to check that no significant PIM was generated due to spill-over from the T_x horns impinging on any nearby structures or due to cross-coupling effects into the R_x system.

The plane reflector was completely removed from the CPTR so that only a large area of RAM (Radio Absorbent Material) was illuminated by the test system. 80 W per carrier was applied to the inputs of the *Tx* horns and the PIM residual observed.This was found to be in the system noise at a level of -168 dBm, thus verifying that the system achieves the required sensitivity.

Fig.7.7 shows a schematic of the equipment layout used for the verification tests. The filter assemblies were attached to the support structures of the T_x and R_x horns whilst the final stage power amplifiers, with their associated power and cooling systems, were mounted on the upper working platform of the payload positioner (see Fig.7.7). Interconnection between the filters and relevant amplifiers was via Heliax cables. It should be noted that the only difference between this layout and that used for PIM characterisation

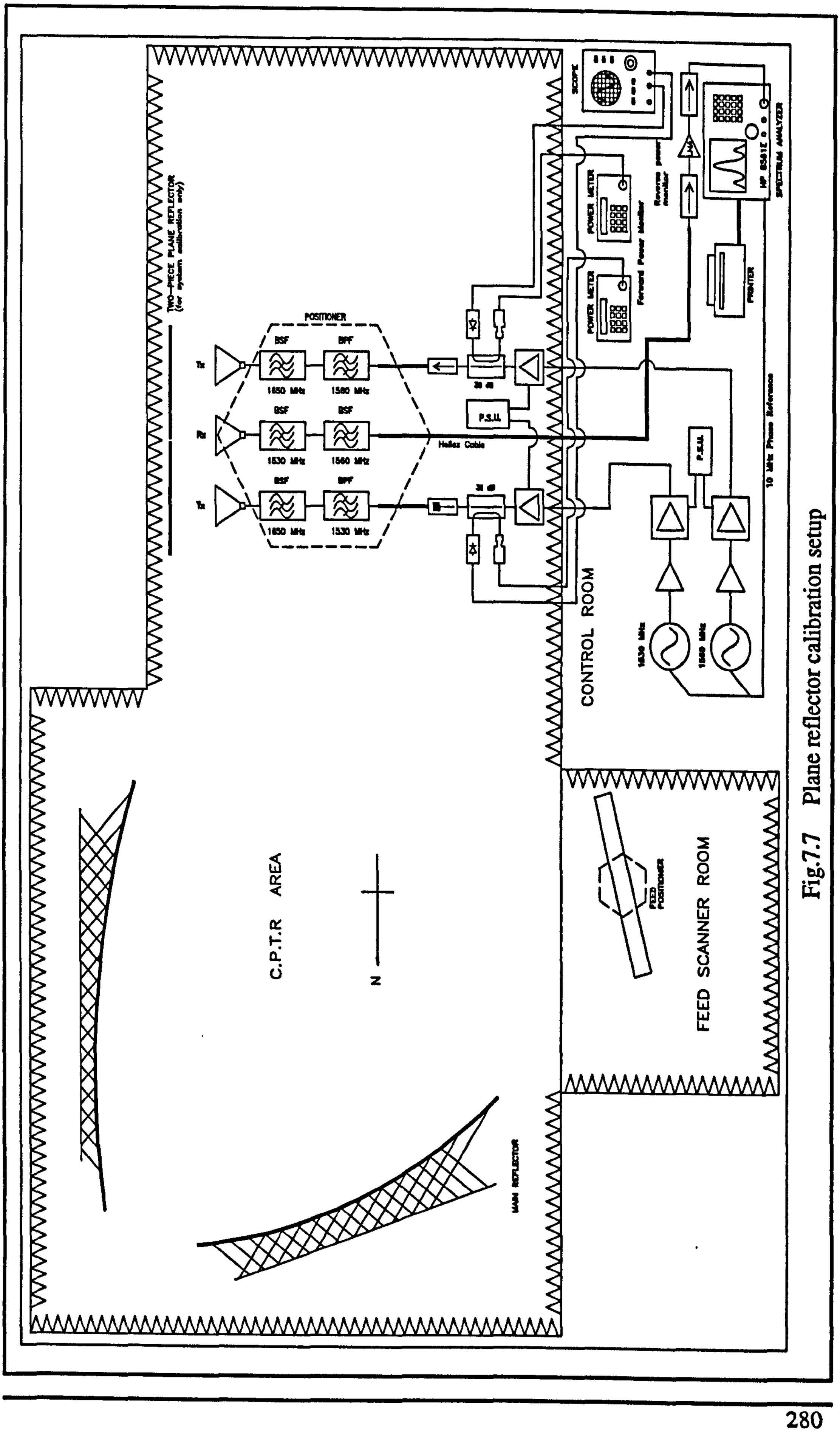

Fig.7.7 Plane reflector calibration setup

is in the position of the high power isolators. During the initial verification test they were placed on the outputs of the power amplifier couplers as an additional protection against any excessive power reflected back from the plane calibration reflector.

7.4.3 Horn Alignment

A laser pointing device was used to ensure that all three horns were accurately aligned. A mounting jig was designed to fix squarely on the horn aperture holding the laser device normal to the plane of the aperture (see Fig.7.4). The orthogonality of the laser was checked by rotating the mounting jig whilst observing the size of circle traced out by the laser spot on a distant target - the laser mounting was adjusted to reduce the circle to a spot, indicating true orthogonality. As the R_x horn was rigidly fixed to the support structure its mechanical boresight (indicated by the laser pointer) was used as the reference point towards which the T_x horns were aimed.

Initial alignment of the horns was made with the T_x/R_x structure on the floor, pointing toward the ceiling about 10 m above. This minimised the amount of adjustment later required when the T_x horns were mounted on the positioner. With the T_x/R_x structure mounted securely on the positioner the T_x horns could be more accurately aligned with the R_x horn using the CPTR main reflector as the target area. The laser pointer was first mounted on the R_x horn and the payload positioner set such that the laser spot impinged on a well defined point on the CPTR reflector - the point chosen was an optical target near to the centre of the main reflector. The positioner azimuth and elevation angles were recorded from the positioner controller and used as reference values for the R_x horn pointing angle. The laser pointer was then mounted on one of the T_x horns and the positioner adjusted such that the laser spot again highlighted the same optical target. The azimuth and elevation angles of the positioner at this point were used to determine the angular offset of the T_x horn boresight relative to that of the R_x horn and this, in turn, was used to calculate the amount of mechanical adjustment required to align the T_x horn with the R_x horn. On making this correction the pointing angle of the T_x horn was again checked against the reference. The same procedure was applied to the other T_x horn.

Table 3.3.1 details the positioner's four axis coordinate values during horn alignment on an optical target of the CPTR main reflector.

As can be seen from the table, the final mechanical boresights of the T_x horns relative to that of the R_x horn are within 0.5° at the plane of the main reflector.

	Positioner axis coordinates			
Laser pen mounting position	Azimuth (A1 - deg.)	Elevation (A3 - deg.)	Polarisation (A4 - deg.)	Position (A2 - mm)
R_x horn, reference pointing angle	-1.13	-91.78	+45.0	-225.4
T_x horn 1, initial pointing angle	-2.40	-87.50	+45.0	-225.4
T_x horn 1, final pointing angle	-1.19	-91.35	+45.0	-225.4
T_x horn 2, initial pointing angle	+0.65	-87.85	+45.0	-225.4
T_x horn 2, final pointing angle	-1.18	-91.58	+45.0	-225.4

Table 7.3 Positioner four axis coordinates during horn alignment

7.5 Measurement Programme

7.5.1 PIM Characterisation

Fig.7.3 shows a schematic of the system layout during characterisation. North direction has been defined on the figure as an aid to identifying the walls when reviewing the results. Fig.7.5 defines the positioner coordinate axes which are used in this report.

Two types of measurement were made during characterisation:

- **spot measurements** - the T_x/R_x system was kept stationery and the PIM level was recorded using maximum system sensitivity, i.e. minimum resolution bandwidth with video averaging

- **scan measurements** - the T_x/R_x system was scanned between spot measurement, during which time the PIM level was observed with the receiver set to zero frequency span, thus displaying the time variation of PIM signal with angular position. the indicated level was manually recorded at every 2.5°.

Spot measurements were made at the following angles:

azimuth: -90°, -60°, -30°, 0°, 30°, 60°, 90°,

all at elevation angles of:-100°, -90°, -75°, -60°, -45°, -30°, -15°

Thus, a total of 49 spot measurements were made for each polarization (horizontal and vertical). Additional spot measurements were made where an increase in the PIM level or some constructional feature prompted the need for increased detail.

When areas were located with high PIM levels, where possible, measures were taken to verify a source and determine whether it could be significantly reduced, e.g. covering the source with RAM.

The change in polarization was made by rotating the complete T_x/R_x structure on the positioner by 90° (rotation about the normal to the positioner platen).

7.6 Results

Table 7.5 and Table 7.6 summarise the spot measurement PIM levels recorded for vertical and horizontal polarizations respectively.

The following abbreviations are used in the tables:

P_{sp}	-	level of PIM (dBm) as recorded on spectrum analyser
P_{rx}	-	level of PIM (dBm) at R_x horn output
P_d	-	power density of measured PIM signal ($dBmWm^{-2}$) at plane of R_x horn aperture.

Table 7.4

The correction factor between R_x horn output and spectrum analyser input was + 39.5 dB which includes the filter and cable losses together with L.N.A. gain.

Table 7.5 Vertical Polarisation

Azimuth	-90°			-60°			-30°			0°			30°			60°			90°		
Elevation	P_{sp}	P_{rx}	P_d	P_{sp}	P_{rx}	P_d	P_{sp}	P_{rx}	P_d	P_{sp}	P_{rx}	P_d	P_{sp}	P_{rx}	P_d	P_{sp}	P_{rx}	P_d	P_{sp}	P_{rx}	P_d
-100°	-124	-163	-153	-131	-170	-160	-117	-156	-146	-77	-116	-106	-115	-154	-144	-132	-171	-161	-130	-169	-159
-90°	-125	-164	-154	-120	-159	-149	-121	-160	-150	-107	-146	-136	-118	-157	-147	-118	-157	-147	-126	-165	-155
-75°	-127	-166	-156	-130	-169	-159	-118	-157	-147	-79	-118	-108	-110	-149	-139	-126	-165	-155	-126	-165	-155
-60°	-100	-139	-129	-127	-166	-156	-80	-119	-109	-120	-159	-149	-79	-118	-108	-130	-169	-159	-125	-164	-154
-45°	-82	-121	-111	-122	-161	-151	-119	-158	-148	-109	-148	-138	-86	-125	-115	-121	-160	-150	-125	-164	-154
-30°	-73	-112	-102	-86	-125	-115	-118	-157	-147	-92	-131	-121	-118	-157	-147	-112	-151	-141	-127	-166	-156
-15°	-117	-156	-146	-115	-154	-144	-125	-164	-154	-118	-157	-147	-122	-161	-151	-117	-156	-146	-117	-156	-146
0°	-130	-169	-159																		

Table 7.6 Horizontal Polarisation

Azimuth	-90°			-60°			-30°			0°			30°			60°			90°		
Elevation	P_{sp}	P_{rx}	P_d	P_{sp}	P_{rx}	P_d	P_{sp}	P_{rx}	P_d	P_{sp}	P_{rx}	P_d	P_{sp}	P_{rx}	P_d	P_{sp}	P_{rx}	P_d	P_{sp}	P_{rx}	P_d
-100°	-130	-169	-159	-130	-169	-159	-126	-165	-155	-126	-165	-155	-109	-148	-138	-130	-169	-159	-125	-164	-154
-90°	-130	-169	-159	-128	-167	-157	-130	-169	-159	-130	-169	-159	-113	-152	-142	-113	-152	-142	-127	-166	-156
-75°	-130	-169	-159	-106	-145	-135	-124	-163	-153	-92	-131	-121	-123	-162	-152	-86	-125	-115	-130	-169	-159
-60°	-130	-169	-159	-108	-147	-137	-61	-100	-90	-69	-108	-98	-82	-121	-111	-130	-169	-159	-130	-169	-159
-45°	-105	-144	-134	-130	-169	-159	-101	-140	-130	-103	-142	-132	-101	-140	-130	-130	-169	-159	-81	-120	-110
-30°	-130	-169	-159	-105	-144	-134	-112	-151	-141	-109	-148	-138	-83	-122	-112	-94	-133	-123	-54	-83	-73
-15°	-130	-169	-159	-125	-164	-154	-130	-169	-159	-127	-166	-156	-130	-169	-159	-121	-160	-150	-112	-151	-141
0°																			-114	-153	-143

The PIM power densities at the R_x horn aperture, given in Table 7.5 and Table 7.6, are presented graphically in figures 7.8 and 7.9 for each polarisation. The angular positions at which spot measurements were made are clearly visible as elliptical zones on the plots. Interpolation between the spot measurements was carried out at 2.5° intervals.

This form of presentation has also been used to map out the PIM levels at the CPTR walls on the assumption that the PIM sources are all isotropic in nature. This approach has been adopted in order to simplify the location of PIM sources in the CPTR. Plots 7.11, 7.14, 7.16 and 7.18 show contour representation of PIM at the CPTR walls for vertical polarisation and plots 7.12, 7.15, 7.17 and 7.19 for horizontal polarisation. In all plots, the origin of the coordinate system is at the centre of rotation of the positioner. Distances to the chamber walls (used in calculating the space loss factor) have been derived from scale plans of the CPTR layout and standard trigonometrical techniques used to determine the slant lengths for positioner elevation angles. It will also be noted that the areas mapped out for the various walls are different in size to the actual wall size. This is a consequence of the mapping process between what is essentially a spherical polar surface transformed to a number of planar surfaces. Both spot and scan measurement values have been used to produce these plots and consequently the azimuth cuts do not have such a coarse appearance as those displaying the PIM power densities where only spot measurements have been used (plots 7.8 and 7.9).

7.6.1 Location of PIM Sources in CPTR

At the start of characterisation, azimuth cuts were made at elevation angles of -100° and -90° (vertical polarisation) with no RAM covering the CPTR feed scanner, the results of which are given in the first two rows of Table 7.5. It was apparent from these results that the feed scanner was contributing significantly to the PIM level observed due to both direct illumination and radiation reflected off the CPTR reflectors. To minimise the effect of this, RAM was used to cover the feed scanner positioner (see Fig.7.10). All of the subsequent measurements were made with this RAM in place.

An assessment of figures 7.11 to 7.20 is now made in order to identify various PIM sources present in the CPTR. Each wall is considered in turn (for both polarizations) and where relevant reference is made to additional printed results. The approximate tracks of each azimuth cut have been indicated on the plots in order to clarify the mapping process a general observation for all of the plots is that a large proportion of the PIM sources are polarisation sensitive.

The PIM location coordinate axes (x,y,z) correspond to the chamber width, length and height axes, respectively.

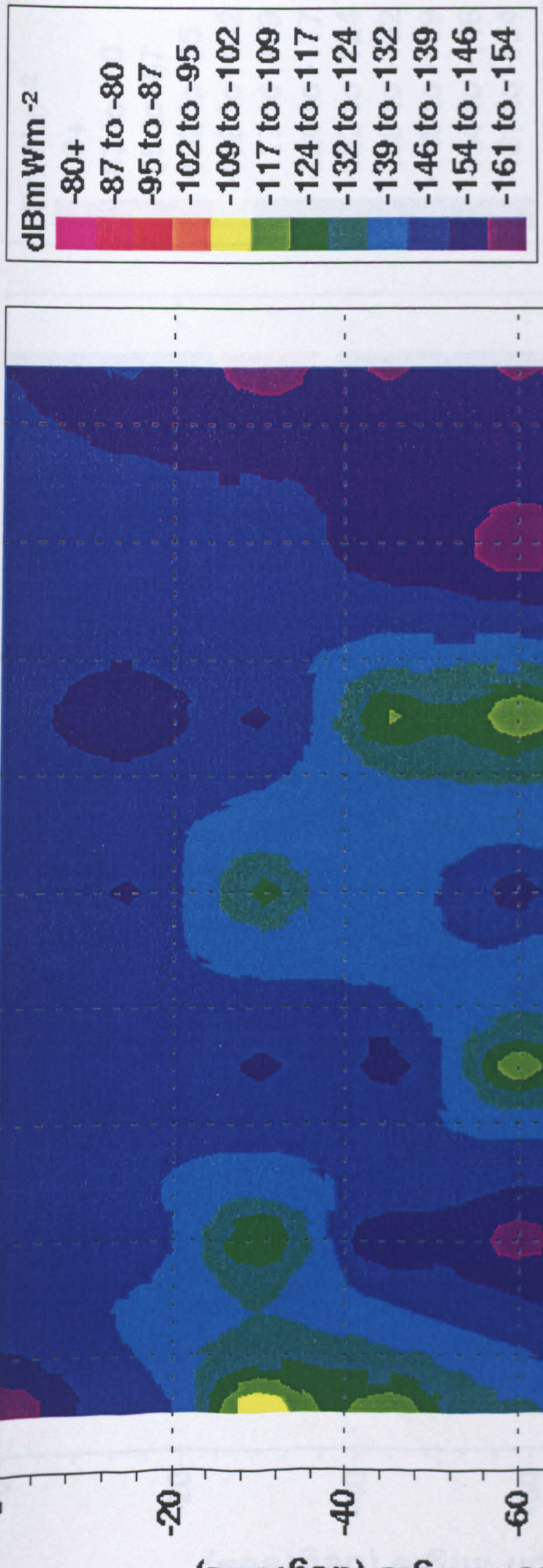

Fig.7.8 PIM Power Density at Receive Horn Aperture - Vertical Polarization.

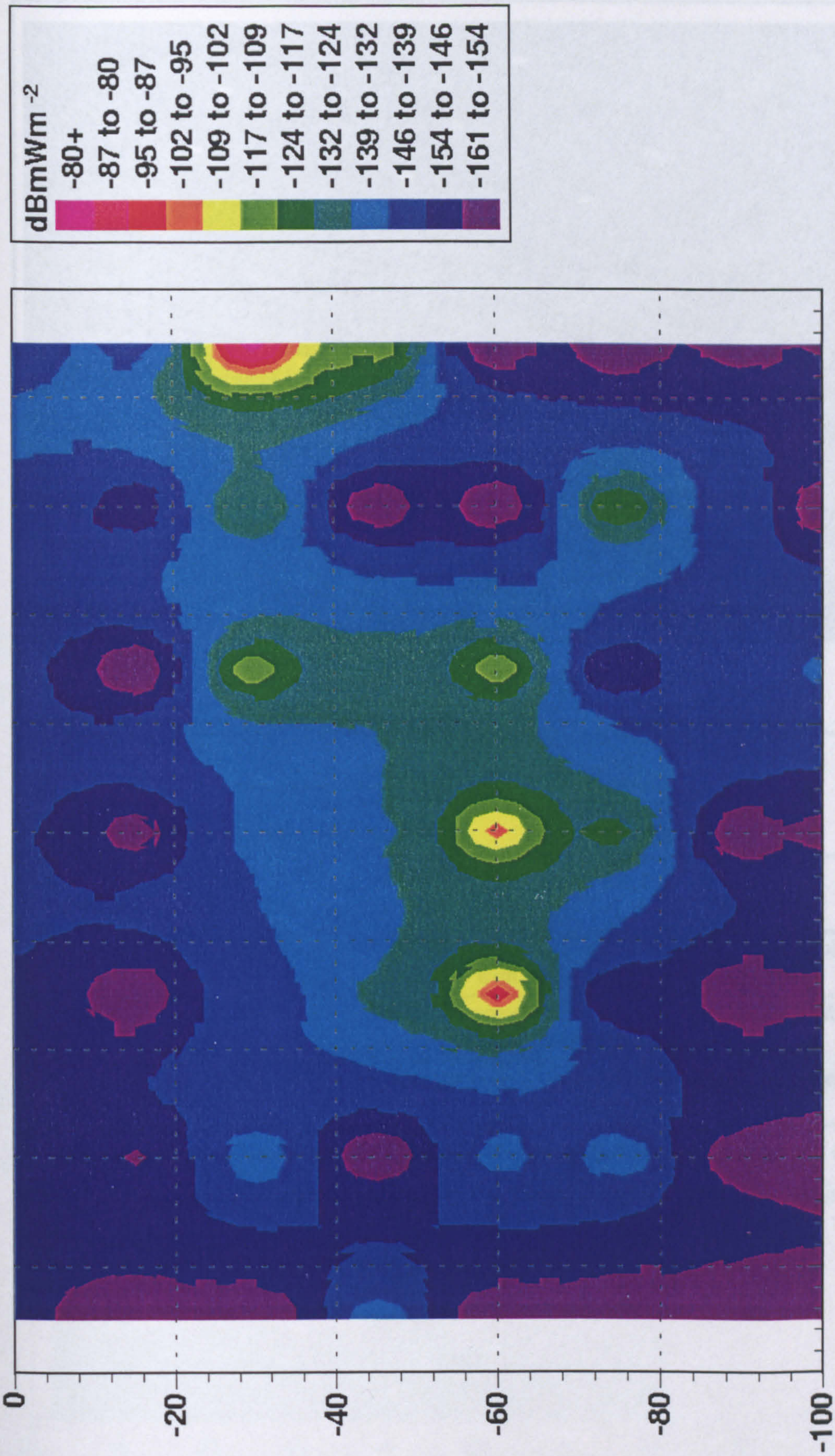

Fig.7.9 PIM Power Density at Receive Horn Aperture - Horizontal Polarization.

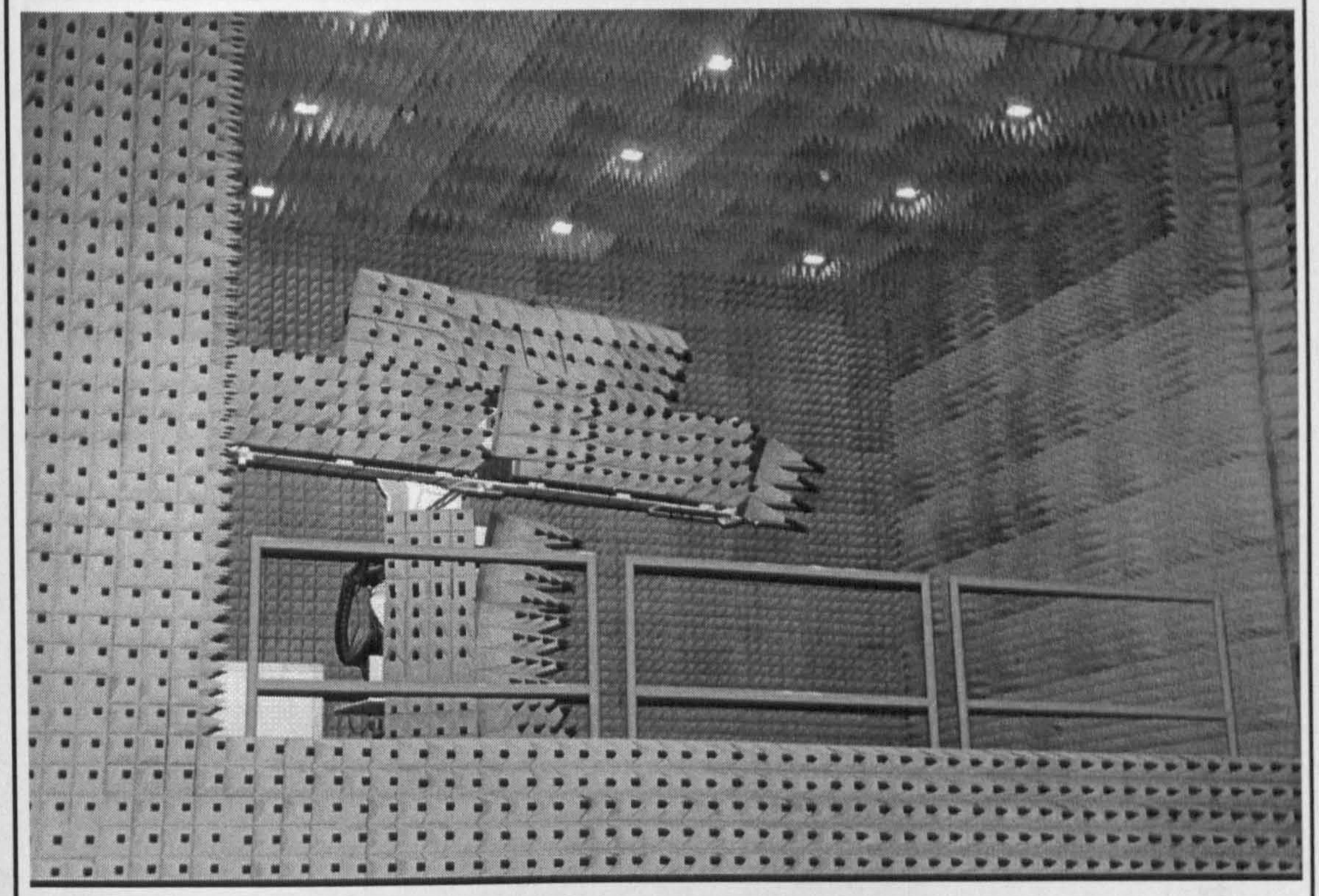

Fig.7.10 RAM covering of feed scanner positioner

West wall (plots 7.11 and 7.12):

PIM location [y, z (m)]	Azimuth cut (°)	Observations
16, -3	-100	Both polarizations show moderate PIM level - coincides with iron post near main reflector
3, 2	-75	Horizontal polarisation only shows moderate PIM level - coincides with flame detector
5, 4.5	-60	Corresponds to PIM source on ceiling, see **Ceiling** assessment

The feed scanner room showed a moderately low level of PIM once the feed positioner itself had been covered in RAM, the level being slightly higher for vertical polarisation.

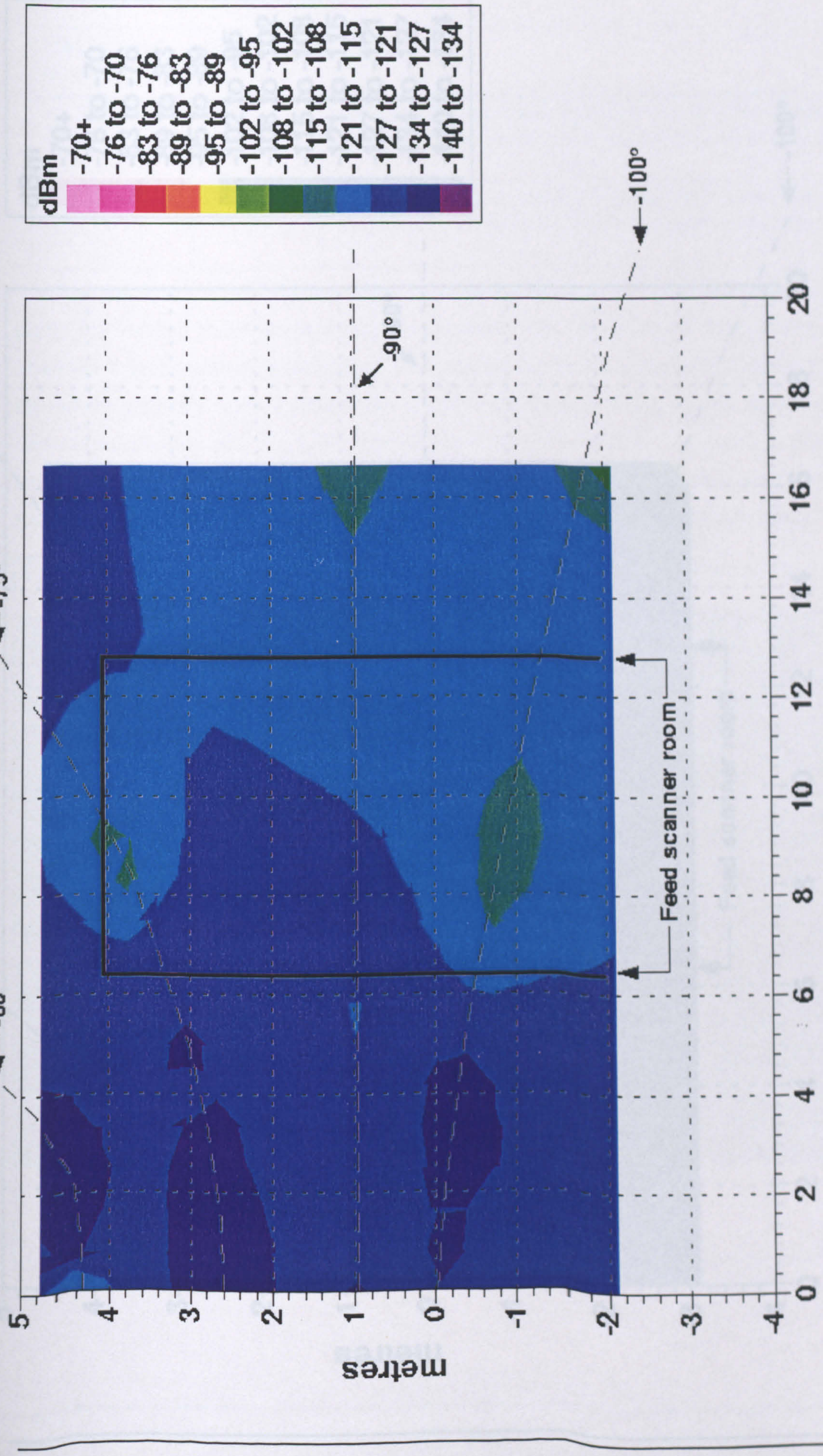

Fig.7.11 PIM on West Wall (dBm) - Vertical Polarization.

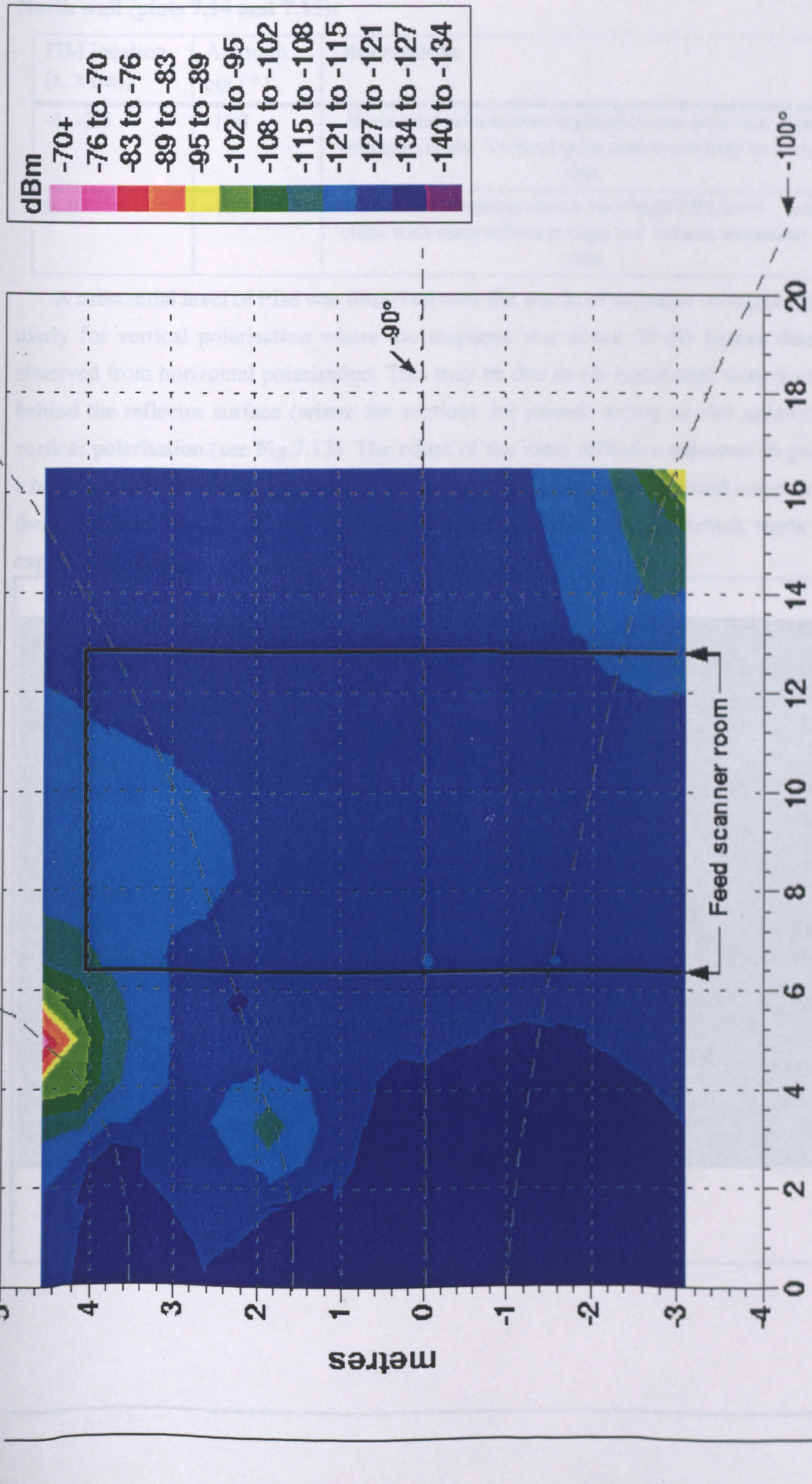

Fig.7.12 PIM on West Wall (dBm) - Horizontal Polarization.

North wall (plots 7.14 and 7.15):

PIM location [x, z (m)]	Azimuth cut (°)	Observations
-4, -2.5	-100	Horizontal polarisation highlights iron post near main reflector, again. Vertical polarisation too high to reveal this
6, 0	-100	Vertical polarisation shows very high PIM level - coincides with main reflector edge and camera mounting at side

A substantial level of PIM was observed over the whole of the main reflector - particularly for vertical polarisation where the response was about 20 dB higher than that observed from horizontal polarisation. This may be due to the horizontal slots occurring behind the reflector surface (where the sections are joined) acting as slot antennas for vertical polarisation (see Fig.7.13). The edges of the main reflector appeared to produce a higher PIM level than the centre which is due most likely to the serrated edges around the reflector. This may be due to the backing honeycomb structure which tends to be exposed to radiation at these positions.

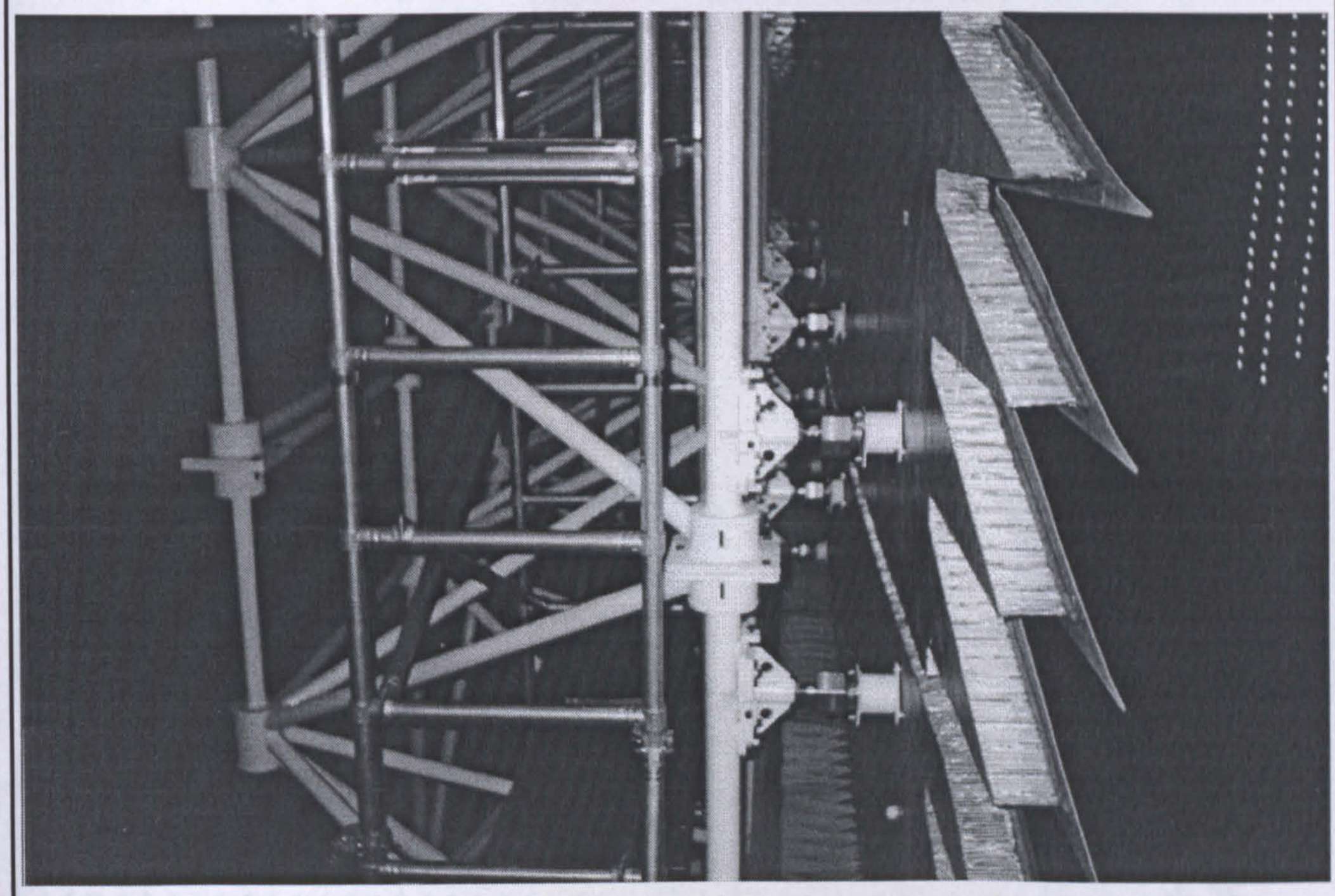

Fig.7.13 Reflector backing structure

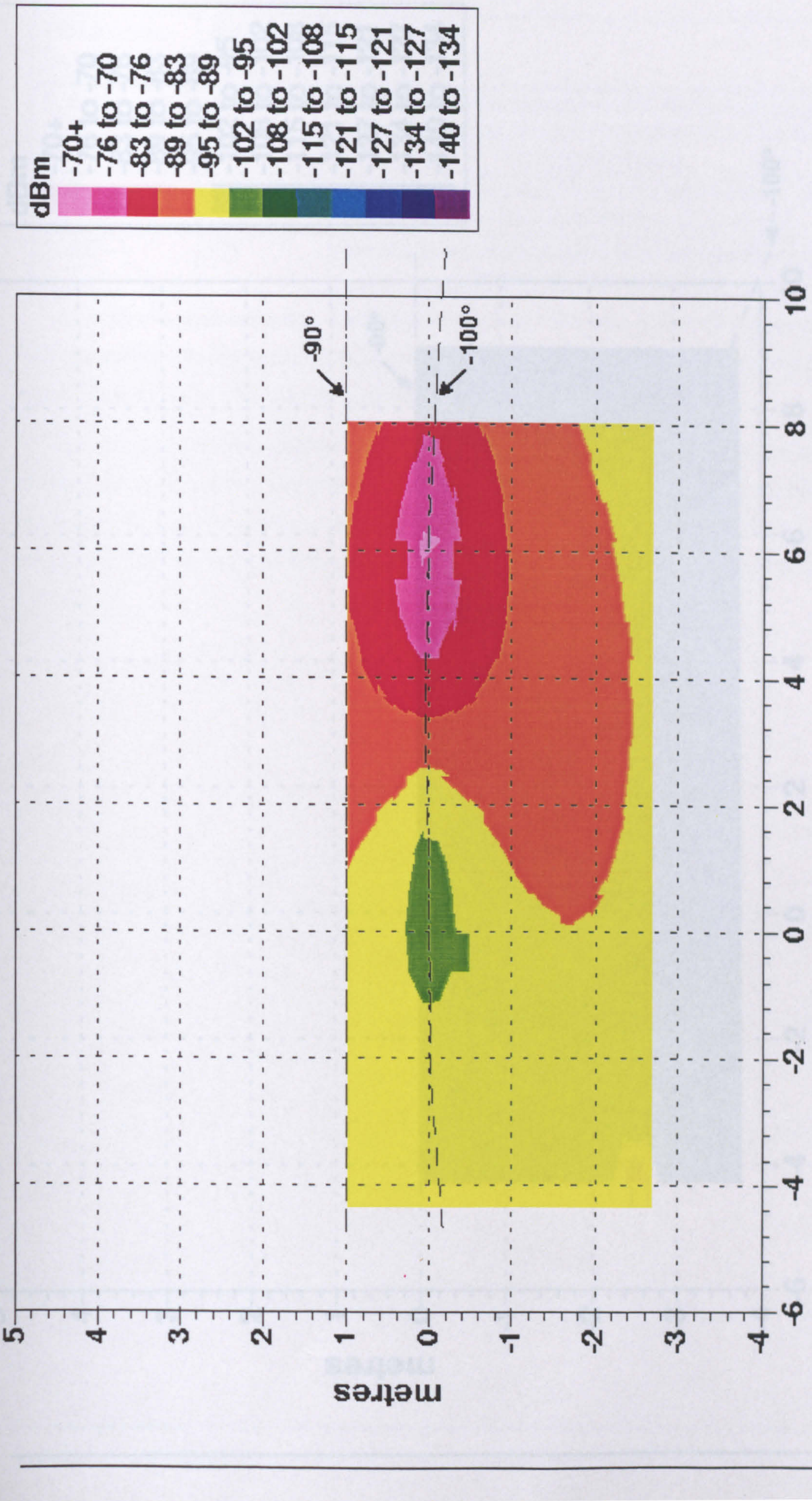

Fig.7.14 PIM on North Wall (dBm) - Vertical Polarization.

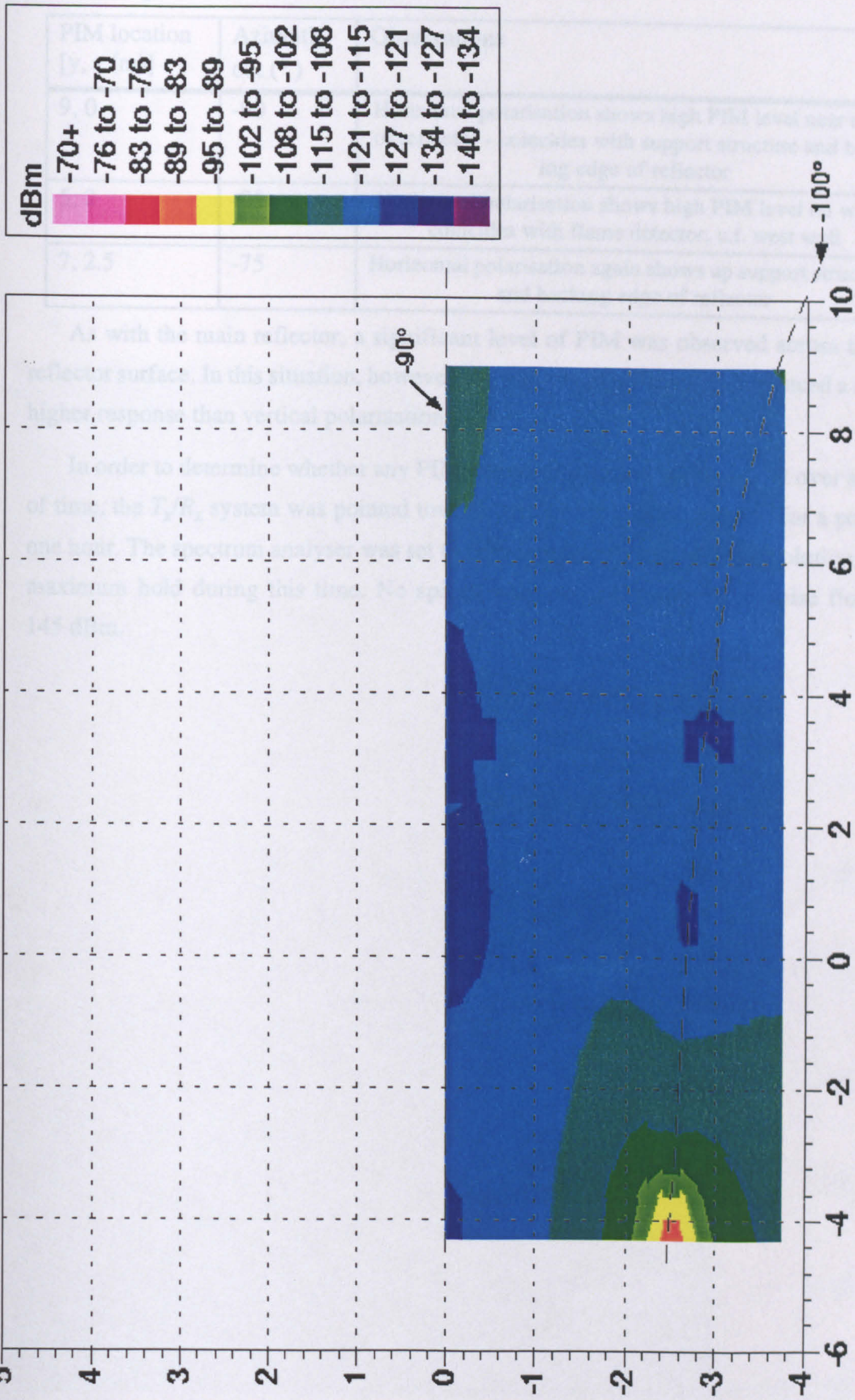

Fig.7.15 PIM on North Wall (dBm) - Horizontal Polarization.

East wall (plots 7.16 and 7.17):

PIM location [y, z (m)]	Azimuth cut (°)	Observations
9, 0	-90	Horizontal polarisation shows high PIM level near edge of reflector - coincides with support structure and backing edge of reflector
5, 2	-75	Horizontal polarisation shows high PIM level on wall - coincides with flame detector, c.f. west wall
7, 2.5	-75	Horizontal polarisation again shows up support structure and backing edge of reflector

As with the main reflector, a significant level of PIM was observed across the sub-reflector surface. In this situation, however, the horizontal polarisation produced a slightly higher response than vertical polarisation.

In order to determine whether any PIM impulse responses were present over a period of time, the T_x/R_x system was pointed toward the east wall and irradiated for a period of one hour. The spectrum analyser was set to zero frequency span, 30 Hz resolution and on maximum hold during this time. No spikes were observed above the noise floor of -145 dBm.

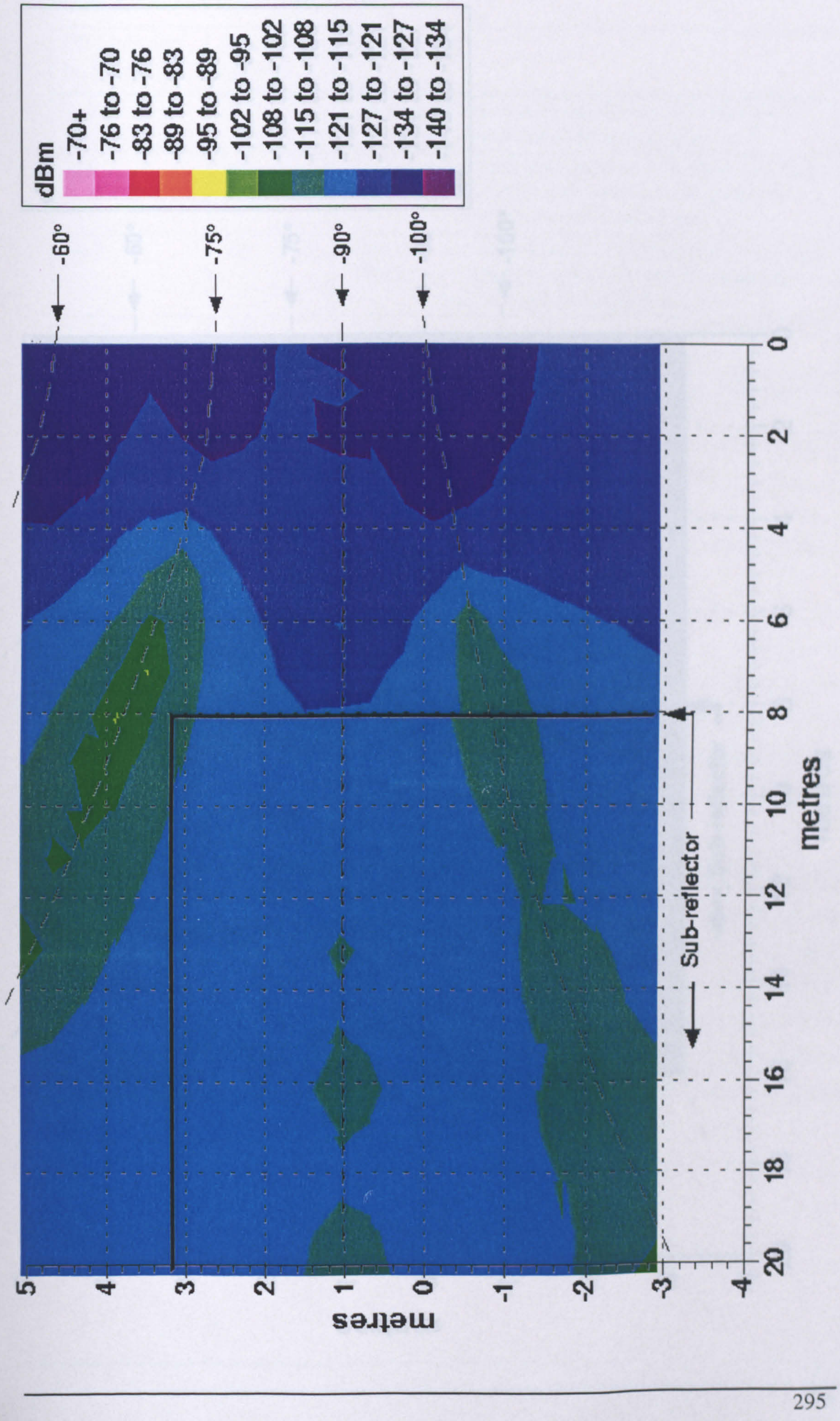

Fig.7.16 PIM on East Wall (dBm) - Vertical Polarization.

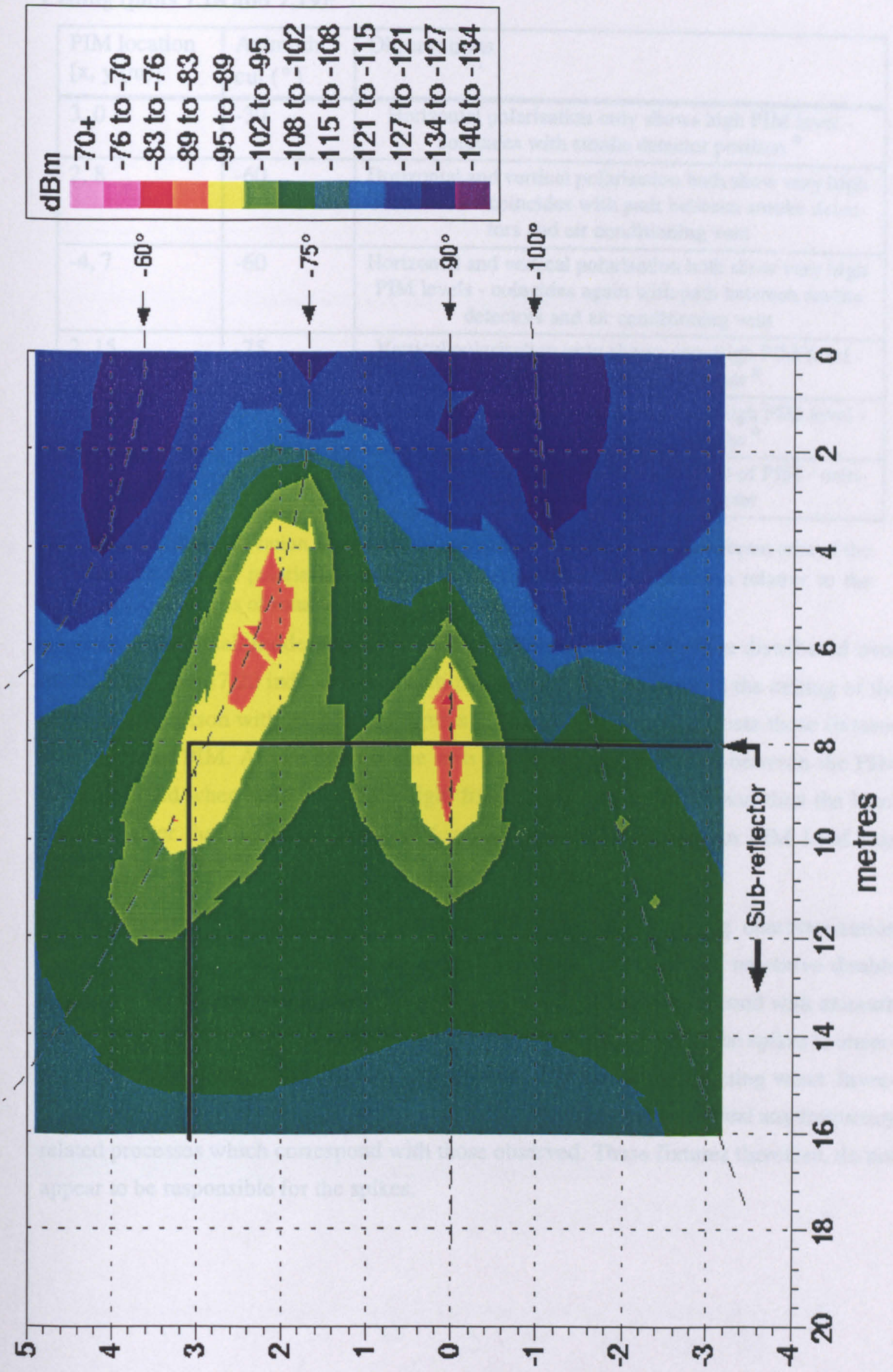

Fig.7.17 PIM on East Wall (dBm) - Horizontal Polarization.

Ceiling (plots 7.18 and 7.19):

PIM location [x, y (m)]	Azimuth cut (°)	Observations
3, 0	-30	Horizontal polarisation only shows high PIM level - coincides with smoke detector position #
2, 8	-60	Horizontal and vertical polarisation both show very high PIM levels - coincides with path between smoke detectors and air conditioning vent
-4, 7	-60	Horizontal and vertical polarisation both show very high PIM levels - coincides again with path between smoke detectors and air conditioning vent
2, 15	-75	Vertical polarisation only shows very high PIM level - coincides with smoke detector #
-3, 15	-75	Vertical polarisation again shows very high PIM level - coincides with smoke detector #
0, 19	-75	Horizontal polarisation shows high level of PIM - coincides with top of main reflector

at these high elevation angles the R_x horn points to a substantially different area of the ceiling for each polarisation due to the offset position of the R_x horn relative to the polarisation axis of rotation.

Some additional, moderately high PIM signatures can also be seen distributed over the ceiling. Figure7.20 indicates the positioning of the light fixtures on the ceiling of the CPTR. Comparison with the plots of figures 7.18 and 7.19 clearly indicate these fixtures as a source of PIM. At one point in the tests a comparison was made between the PIM level observed when illuminating the light fixtures with the lights on and then the level obtained after the lights had been off for one hour. No difference in PIM level was observed.

An unusual PIM signature which appeared several times during characterisation consisted of a large step change in PIM level (~ 20 dB) together with repetitive double spikes appearing on top of the received signal. This was seen to correspond with azimuth cuts over the smoke detectors and air conditioning vents. The origin of the spikes is uncertain although it is suspected that they may be related to the air conditioning vents. Investigation into the operation of the smoke and flame detectors does not reveal any frequency related processes which correspond with those observed. These fixtures therefore, do not appear to be responsible for the spikes.

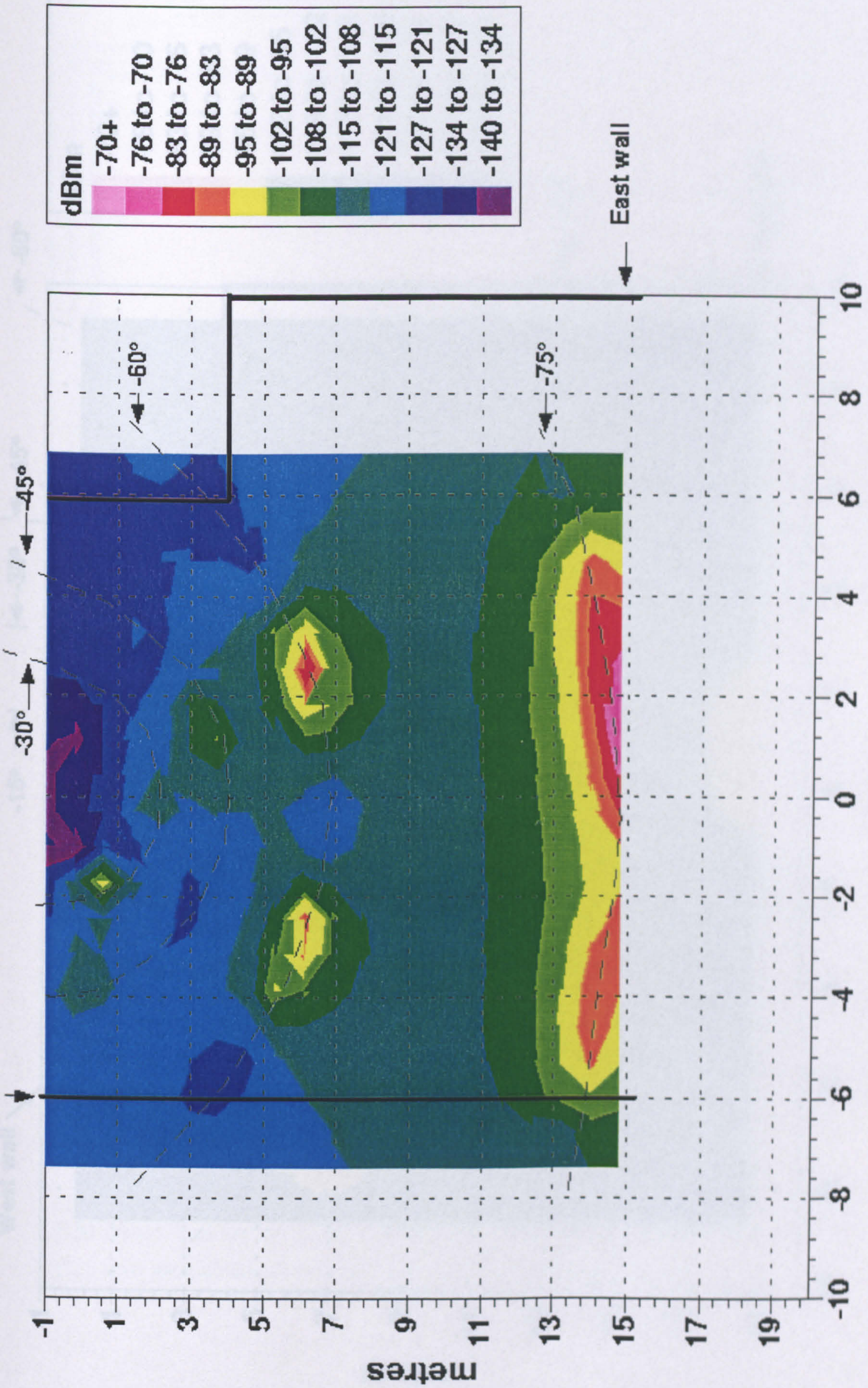

Fig.7.18 PIM on Ceiling (dBm) - Vertical Polarization.

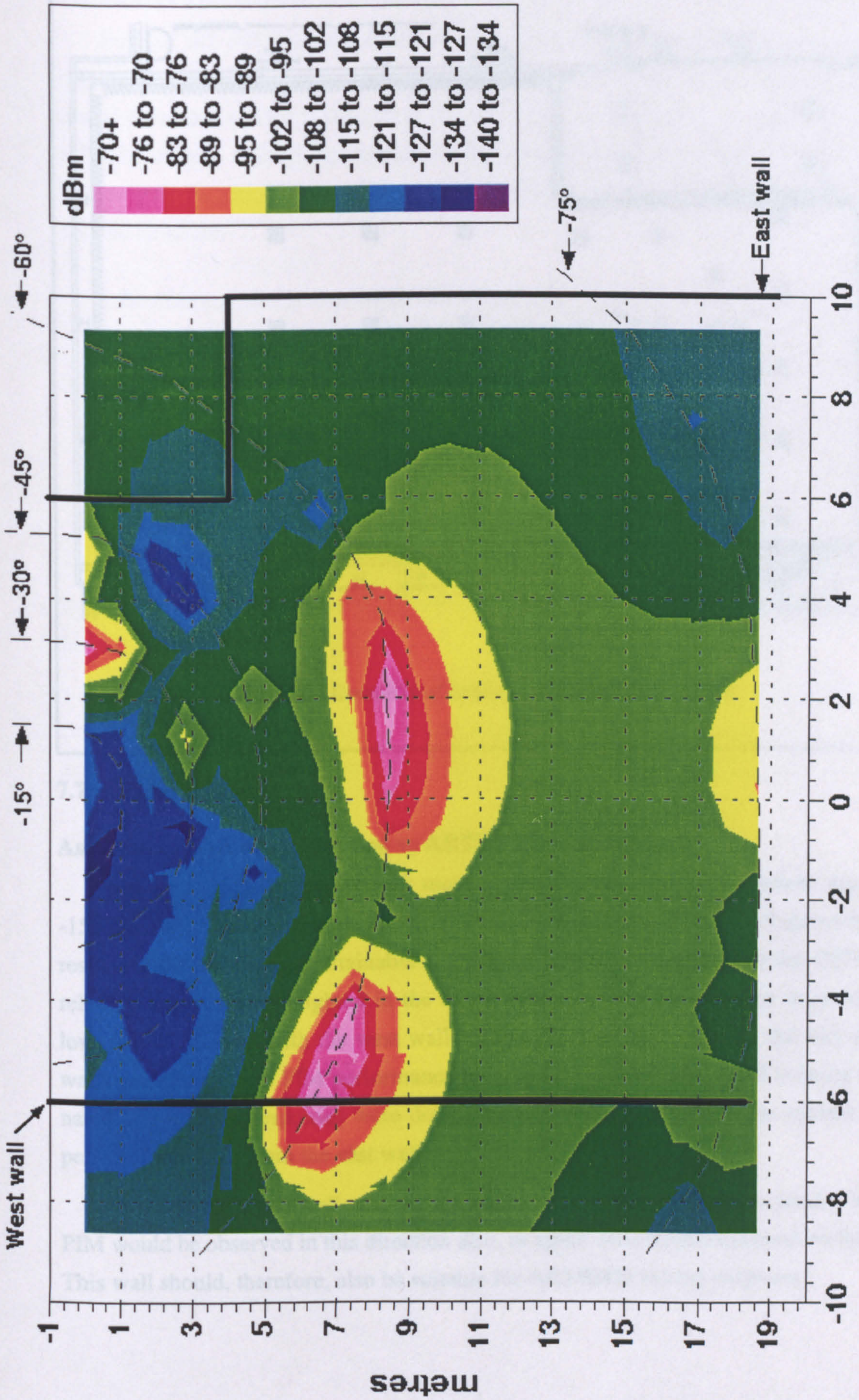

Fig.7.19 PIM on Ceiling (dBm) - Horizontal Polarization.

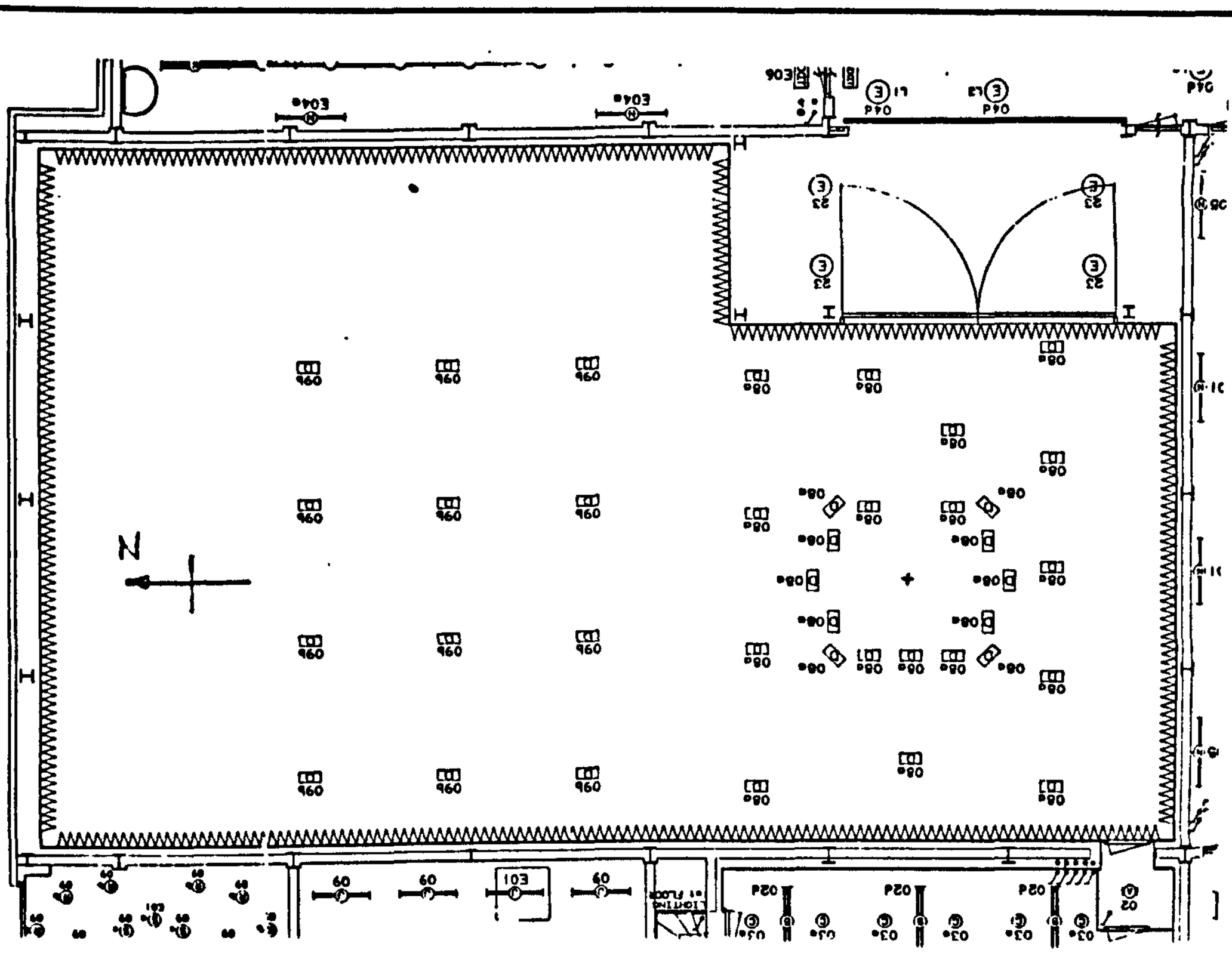

Fig.7.20 Location of ceiling light fixtures in CPTR.

7.7 Conclusions

Assessment of results in relation to ARTEMIS requirements:

In order to meet the ARTEMIS requirement of a maximum PIM power density of -155 dBmWm^{-2} (at the receiver aperture), inspection of figures 7.8 and 7.9 shows that this residual PIM level is only attainable at a limited number of locations in the CPTR - the relevant angles are highlighted in the tables. The east wall can be seen to provide the lowest PIM residual with the west wall being only marginally worse - the fact that the walls provide the best PIM performance is to be expected as only RAM is being illuminated. No impulse responses were detected above the noise floor of the system over a period of one hour from the east wall.

Although the south wall was not characterised, it is assumed that a similar level of PIM would be observed in this direction also, as again, only RAM is present on this wall. This wall should, therefore, also be suitable for ARTEMIS testing purposes.

Location of PIM sources in CPTR:

Both of the reflectors produced a moderately high PIM level, being polarisation dependant - the vertical polarisation showing a response 20 dB higher than that of horizontal polarisation. This is thought to be due to the horizontal slots occurring behind the reflector surface (where the sections are joined) acting as resonant slot antennas for vertical polarisation. The overall level of PIM from the reflectors is most likely due to the surface structure:

- the core material is aluminium alloy flexcore
- this core is covered by a 1.5 mm thick skin of CFRP
- the CFRP skin is itself coated with a gel loaded with aluminium powder and a fine aluminium mesh

A number of fixtures have been identified as PIM generators manifesting a differing degree of intensity. Smoke and flame detectors have generally shown the highest PIM levels with light fittings being relatively less significant and showing no variation in PIM level when either on or off.

Unusual repetitive spikes were observed on several occasions. These do not appear to originate with either the smoke or flame detectors but may be related to the air conditioning vents. The actual source of this phenomenon is currently uncertain.

CHAPTER 8

Conclusions and Recommendations

This chapter concludes the study of passive intermodulation interference due to non-linearities in aerospace RF hardware. The work which was carried out and the main features of the findings are discussed. The chapter closes with a series of recommendations for further work in the area of PIM research.

8.1 Conclusions

The objectives of this project were defined at the start as follows:

- Investigate the characteristics of passive intermodulation generation in space qualified materials.
- Design and build a highly sensitive and consistent PIM measurement system at L-band.
- Develop standardised methods enabling the PIM characteristics of the materials to be compared in a reliable and consistent manner.
- Provide the aerospace industry with hitherto unavailable data on the PIM behaviour of commonly used materials and engineering processes.
- Analyse the data to determine the possible mechanisms behind PIM generation.
- An additional objective was the PIM characterisation of a satellite payload testrange in the Netherlands using the L-band system.

Initially, a detailed overview of topics related to PIM was conducted. The principles of intermodulation generation in communications systems were presented regarding product generation and power level relationships. This was followed by discussions of both active and passive intermodulation, their causes, expected levels and resultant effects. Some of the physical mechanisms previously cited as being responsible for PIM generation were identified and the implications for future communications systems were highlighted. Traditional PIM avoidance techniques were covered next followed by a review of previous studies on passive intermodulation in communications systems. It was concluded from this initial work that the current body of knowledge of passive intermodulation was lacking in many respects. A lot of the information was found to be contradictory and inconsistent particularly with regard to experimental work.

The next body of work, covered in Chapter 3, dealt with the principles of designing passive intermodulation measurement systems. The difficulties in designing such systems were highlighted, especially given that the system itself will produce PIM signals obscuring those which we desire to measure. Next, the many different system design considerations were discussed. These were then applied to the design of an initial L-band coaxial system for use in this study. The specification of the initial system was presented in full, including detailed descriptions of the individual constituent components. The performance of the system was presented next in terms of the theoretical, thermal-noise limited sensitivity followed by a discussion on the PIM levels generated in the system. This indicated that whilst many of the individual components were adequate electrically, their PIM performance left a lot to be desired. It was concluded that, as expected, it is not possible to assemble a PIM measurement system, using commercial components, to deliver the state-of-the-art performance demanded by modern communications systems.

In Chapter 4, low-PIM techniques were introduced. Series branchline stubs have been thoroughly analysed and developed to the point where they have been incorporated in all of the custom built low-PIM components. A low-PIM connector and test enclosure were built and were very successful in verifying the theory. The techniques were then taken further and applied to the design of couplers and bandstop filters. The use of low-PIM bandstop filters further enhances the system performance. By using bandstop filters, high field intensities from the parent signals are avoided. The structure is almost totally contactless therefore PIM generation is minimal. The filters are complemented by a low-PIM re-entrant coupler design which is also virtually contactless. A novel approach to the design of branchline couplers was also developed, again, with great success.

A great deal of effort was required in order to develop all of the custom made components to the point where they could be confidently inserted into the system without risk of problems from their electrical performance or from PIM generation. The effort was rewarded when the final system displayed extremely low levels of residual intermodulation which were inherently stable and repeatable. The residual PIM level for the system was recorded as -151dBm for two 25Watt carrier signals. These figures are at the DUT position in the system. The variation of the residual PIM signal, with no DUT present, was less than ± 1 dBm. Such stability and consistency were considered to be crucial to the success of the measurement programme. The main outcome of this part of the project was the significance of moving points of metal-metal contact to points of minimum current density. This was seen to be the most effective method of reducing the residual PIM.

The next stage involved designing a set of measurements which could be performed upon commonly used aerospace materials. Accordingly, two test jigs were designed around two different, standard, sample formats. The jigs were designed using the same low-PIM techniques which had been exploited in the rest of the system and exhibited very low levels of intrinsic PIM. The engineering scale format was designed to be representative of the kind of dimensions and finishes that one would expect to encounter in a typical application. Engineering samples consist of a 9.3 mm diameter rod which is 120 mm long and are contactlessly inserted into the system so avoiding interference from junction non-linearity. The small geometry samples were designed to excite higher current densities in the materials and expose non-linearities which operate at lower levels. They consisted of a length of 1 mm diameter wire and resulted in a surface current density over nine times that of the engineering samples. By comparing the results it was sought to gain an insight into the mechanisms of PIM generation which dominate in practical situations.

Using the laboratory measurement system, the relationships between PIM levels and combined input power levels, types of metals, finishes, coatings and junction pressures were all studied. Numerous experiments were performed on the two types of test sample. It became apparent that the test power of 25 Watts per carrier was enough to excite non-linear mechanisms in the small geometry samples but was too low to excite PIM in all but the most non-linear engineering scale samples.

From the laboratory results it was discovered that non-magnetic conductors do generate PIM albeit at very low levels and at high current densities. This is thought to be the first instance where non-linearities in "ohmic" conductors have been measured using this method. This has strong implications for the RF industry in that every conductor will generate PIM products at some level. However, if current densities are kept low, in most cases the levels produced by such materials will be negligible. Nevertheless, it is not diffi-

cult to envisage future communications networks in which this could be a problem. Particularly in deep space communications where the dynamic range requirements of systems will become greater.

Of the materials tested, those plated with silver displayed the lowest levels of PIM. This confirms that silver and silver plating are particularly useful in systems where PIM is expected to be a problem. It was also found that ferromagnetic materials generate some of the strongest intermodulation signals, but if silver plated, then the plated layer will conduct most of the RF currents and the ferromagnetic non-linearities will become insignificant.

Unusual PIM behaviour was observed in copper wire when subjected to a transverse DC magnetic field. The PIM level exhibited sporadic step change behaviour when the copper was excited by the RF signals in the presence of the magnetic field. This excitation process was not consistent from test to test and could not easily be associated with any manipulation of the magnetic field. It was clear however that this was not an anomaly of the measurement system as repeated observations were made and other materials did not reproduce the behaviour when subjected to the same conditions. This remains therefore as another form of behaviour deserving further investigation.

The consistent reduction in PIM level of all materials tested when subjected to a transverse DC magnetic field appears to be a potentially useful one. Not only was the residual PIM level of each material seen to reduce with magnetic field, but the system residual was in fact annulled by the production of a PIM signal stimulated by the magnetic field. This was clearly demonstrated by the typical thermal noise behaviour of the detected signal when the above technique was employed.

A range of multi-junction samples were also tested in the system. These took the form of washer samples placed onto a beryllium copper mandrill. In all of the junction samples tested, the PIM was seen to be reduced significantly by the application of a high contact pressure. This is significant as it clearly shows the importance of maintaining high contact pressures at metal junctions at all times, particularly where they exist in a strong current path. Just one loose connection could compromise the performance of a whole system.

The multi-junction nickel samples exhibited curious behaviour in that where more junctions were present, the level of PIM was actually less. This is contradictory to the results from all of the other materials which suggested that the PIM level would go up with the number of junctions. It was proposed that eddy currents were the cause.

Although the semiconductor, electron tunnelling, micro-discharge and contact mechanisms have been assumed or suspected to be responsible for the non-linear effect at metallic contacts, so far, only the contact mechanism discussed in Section 2.4.1 provides a more satisfactory explanation. It suggests that the non-linear effect is current dependent and the product level is proportional to the current densities at contacts. This may be used for explaining the non-linear effects at contacts, but further work is needed to provide a more rigorous model.

The behaviour of the aluminium-Alocrom 1200 junction is of great concern due to the extensive use of Alocrom as a method of surface protection and multipactor reduction in space RF hardware. Unexpectedly high and variable levels of PIM have been consistently observed during the measurement programme. Based on the present findings, it would be strongly recommended to avoid the use of this form of chromate conversion in any PIM sensitive areas of a system. The behaviour which has been observed may be related to the specific process used by the plating company responsible and it would therefore be prudent to investigate this subject matter more thoroughly. Such an investigation would clarify whether there is a fundamentally high PIM signature associated with the aluminium-Alocrom interface.

Finally, the L-band measurement system was reconfigured to perform radiative measurements. This was required in order to characterise the PIM generated in the Compact Payload Test Range at ESTEC in the Netherlands. On setting the system up, it was found that there were no problems due to residual PIM generation and a measurement sensitivity of some -160 dBm was achieved. The exercise highlighted the robustness of the system and the value of the low-PIM connections. Tests performed on the test range highlighted several sources of PIM in the chamber many of which were not a functional part of the chamber operation. Initial worries over the large reflectors in the chamber were overshadowed by high PIM levels from light fittings, structural components and smoke detectors.

To conclude, it is felt that the project has been very successful. The objectives have largely been met although, as with most research, there is considerable scope for further work.

8.2 Recommendations for Future Work

On the basis of the findings of this study, it is recommended that the following areas of work merit further investigation:

8.2.1 System Improvements

A) More PIM orders

In order to obtain more information on PIM mechanisms for use in modelling, it is apparent from Section 2.2.3 that measurements will have to be made at more than one PIM order. Ideally, it should be possible to measure the levels of several orders simultaneously. At present however, the bandstop filters in the system would have to be re-tuned to measure different frequencies and many of the components are narrowband, limiting the number of additional orders that can be measured.

One method of measuring more orders could be to implement a number of directional filters, each tuned to a separate PIM order as in Fig.8.1 where the sampler would be a directional filter. The DUT may be placed at either end of the chain to monitor either forward or reverse PIM signals. Obviously, the type of directional filter used thus far (see Section 3.5.2.3) would be bulky and expensive, however, there are other types which would be worthy of investigation [124, 184-186].

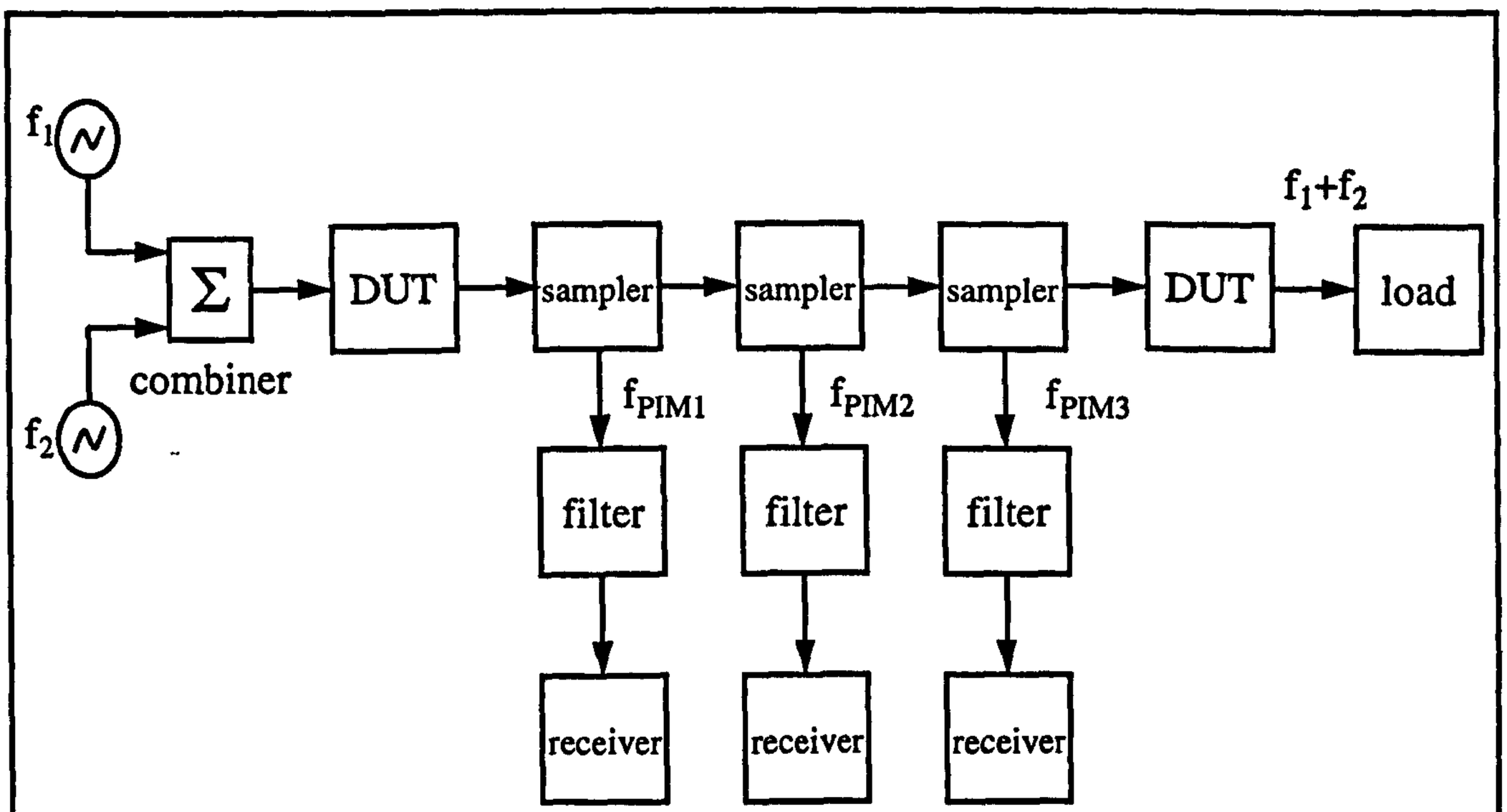

Fig.8.1 Multiple order PIM detection system

It may also be useful to space the parent frequencies further apart. At, present the very narrowband setup places great demands on component performance.

B) Increased Excitation Energy

From the results of the measurement program it is evident that intrinsic PIM mechanisms only become visible at very high current densities. It would therefore be useful to be able to excite high current densities only in the sample(s) whilst maintaining lower

current densities in the remainder of the system. This should raise observed PIM levels above the thermal noise floor and above the residual level. Measurement data would then be clearer and more reliable whilst the PIM performance of the rest of the system would be slightly less critical.

Methods of achieving this are, however, not so clear. Increasing drive power levels increases current densities throughout the system. However, by increasing the dimensions of the conductors in the system with respect to the sample, the relative current density in the sample will go up. In the L-band system, measures are currently under way to replace the UT-.250 semi-rigid cable with a larger diameter cable, having significantly larger conductor dimensions. This should also help to lower the residual PIM level which is thought to be limited, in part, by the small diameter core of the UT-.250 cable used at present.

C) Improving Residual PIM

Although the development of the low-PIM techniques in Chapter 4 have greatly reduced the level and variability of the residual PIM signal, there could still be room for improvement. For example, the branchline coupler and bar-line bandstop filter designs could be easily combined, as in Fig.8.2,to produce a monolithic directional filter with no metal-metal contacts between the components whatsoever. Obviously, the packaging of the device would present problems but the idea is appealing.

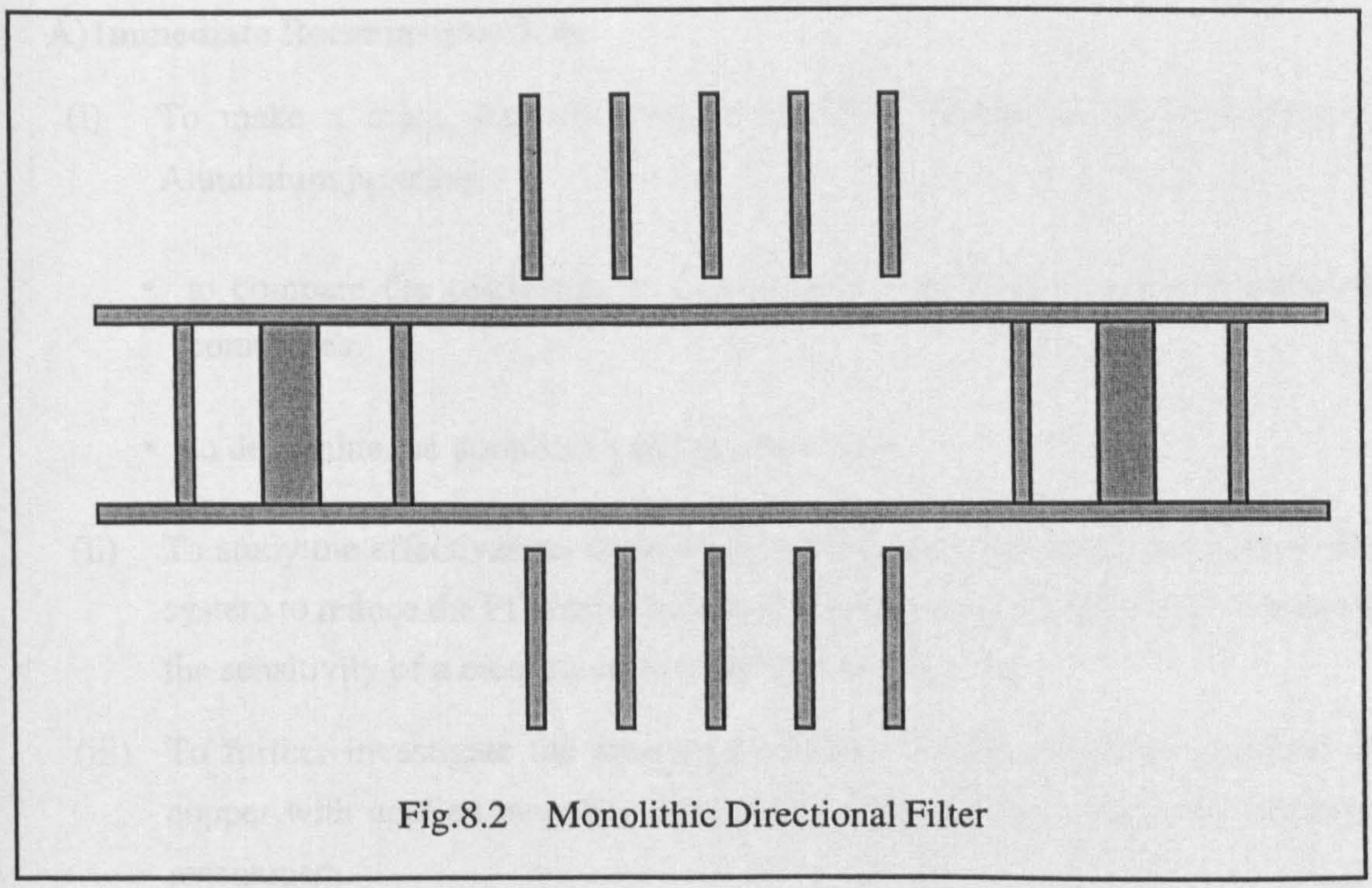

Fig.8.2 Monolithic Directional Filter

The development of a high performance, low-PIM directional filter could also be useful in minimising PIM from dummy loads. Prior to absorption, the parent signals could be separated, then dissipated in separate loads, thus minimising the risk of PIM generation in the loads.

Finally, as an alternative to the quarter-wavelength, low-PIM techniques described in this thesis, it may be possible to provide contactless connections using a large lumped capacitance to couple signals between conductors, similar to the method used by Lin [187]. Using this method, much larger bandwidths may be obtained which could be vital in measurements of multiple PIM orders. The connectors could also be made to be very compact and could possibly be tailored to suit aerospace applications. This method is extensively used in the design of coaxial DC blocks which are available from most suppliers, hence the technology is available at present.

8.2.2 Measurements

As regards future experimentation, there is a great amount of work which can be carried out. Some immediate recommendations can be made as a result of the experimental work carried out during this project and some can be made with more long term aims.The outcome of this work will obviously lead to even more avenues of exploration since the work described in this thesis forms a good foundation for investigations into intrinsic PIM mechanisms.

A) Immediate Recommendations

(i) To make a more detailed study of the PIM behaviour of the Alocrom-Aluminium junction:

- to compare the performance of coatings produced by a range of selected companies.

- to determine the dominant mechanism at work.

(ii) To study the effectiveness of applying a transverse D.C. magnetic field to the system to reduce the PIM residual below the thermal noise floor, thus extending the sensitivity of a measurement system to its maximum.

(iii) To further investigate the anomalous effects of PIM excitation observed in copper with applied magnetic field and to determine the dominant causative mechanism.

(iv) To further investigate the dielectric, alumina, and determine its significance in relation to PIM.

B) Long Term Aims

(i) Expansion of standardised PIM data to include a wider range of materials (including dielectrics) and associated structures. This will aid in the analysis of PIM in materials since there will be more data to compare.

(ii) Provide for greater environmental controls during experimentation e.g. vacuum, electrical bias. This will help to narrow down and isolate specific PIM mechanisms.

(iii) Make a more comprehensive experimental study of the PIM characteristics of selected mechanisms in order to produce sufficient data allowing preliminary models to be produced.

8.2.3 Analysis

Much more information is required in order to successfully analyse and model PIM behaviour hence only generalised recommendations can be made at this point.

(i) A thorough theoretical study will have to be made of nonlinear modelling techniques. This will help to determine the kind of information required from the experimental work and the amount required to produce accurate models.

(ii) Experimental data would be used to produce both empirical models and to aid in the understanding of the actual processes involved. The models would then be used to test predictions of PIM behaviour in other structures with the chosen mechanism.

References

[1] Foord, A. P., Rawlins, A. D.: 'A Study Of Passive Intermodulation Interference In Space RF Hardware', Final Report, ESTEC Contract 111036, May 1992.

[2] Hoeber, C.F., Pollard, D.L., Nicholas, R.R.: 'Passive Intermodulation Product Generation in High Power Communications Satellites', Proc. 11th Conference on Communication Satellite Systems, 1986, Ch. 89, pp. 361-374

[3] Lui, P.L. and Rawlins, A.D.: 'Radio Towers, Antenna and Mounting Components as Sources of Intermodulation Interference', International Symposium on Electromagnetic Compatibility, Japan, 1989.

[4] Lui, P.L. and Rawlins, A.D.: 'Passive Non-Linearities in Antenna Systems', IEE Colloquium on Passive Intermodulation Products in Antennas and related Structures, 1989, pp. 6/1 - 6/7.

[5] Lui, P.L. and Rawlins, A.D.: 'The Field Measurement of Passive Intermodulation Products', 5th IEE International conference on Mobile Radio and Personal Communications', UK, 1989, pp. 199-203.

[6] Lui, P.L. and Rawlins, A.D.: 'Measurement of Intermodulation Products Generated by Structural Components', electronics Letters, 24, 1988, pp. 1005-1007.

[7] Lui, P.L.: 'Passive Intermodulation Interference in Communication Systems', Electronics and Communications Engineering Journal, June 1990, pp. 109-118.

[8] Petit, J., Rosello, J. and Ampuero, A.: 'HISPASAT PIM Measurement Program', Proc. ESA Workshop on Multipaction and Passive Intermodulation Products Problems in Spacecraft Antennas, Dec. 1990.

[9] Strijk, S.: 'PIMP Measurements Performed on MBB Unfurlable Antenna', (XRM), XRM/356.89/SS/bg ESTEC, Aug. 1989.

[10] Ebbendorf, N.: 'PIMP Measurements on a Sample of ERS-1 Solar Array', (XRI), XRI/203.88/NE/bg ESTEC, DEC. 1988.

[11] Newport, C.: 'Flexible Waveguide Intermodulation Tests', (XRC), XRC/220.88/CN/bg ESTEC, Apr. 1988.

[12] Petit, J.S. and Mitchell, S.D.: 'PIM Characterisation of the ESTEC CPTR at L-band', Proc. Working Meeting on Multipactor and Passive Intermodulation in Space RF Hardware, ESTEC, The Netherlands, Mar. 1996, Session 5, 7.6.

[13] Petit, J.S., Rawlins, A.D., Mitchell, S.D.: 'PIM Characterisation of ESTEC CPTR for ARTEMIS PIM Testing', Final Report, UKC ref. JSP/ESTEC/03/96, Electronics Labs, University of Kent, Mar. 1996.

[14] Turner, C.: 'Intermodulation Interference in Radio Systems', Communication (USA), Vol. 20, No. 4, Ar. 1983, pp. 32-42.

[15] Keiser, B.: 'Principles of Electromagnetic Compatibility', 3rd Edition, Artech House Inc., Norwood, Mass., 1987.

[16] Gardiner, J. G. and Fudge, R. E.: 'Chapter 4 - Aerials and Base Station Design', Land Mobile Radio Systems, Edited by Holbeche, R.J., Published by IEE, 1985, pp. 53-59.

[17] Babcock, W.C.: 'Intermodulation Interference in Radio Systems', Bell System Technical Journal, Jan. 1953, pp. 63-73.

[18] Badr, A. H., Benson, F. A., Cudd, P. A. and Sitch, J. E.: 'Coupling Between a Pair of Coaxial Cables in a Multicable System', IEE Proc., Vol. 128, Part A, No. 8, Nov. 1981, pp. 547-551

[19] Rootsey, J. V., Gradisar, A. A. and Bordenave, J. R. P.: 'USACA HT-MT Terminals Program-Intermodulation Study Final Test Report', WDL-TR5243, Philco-Ford Corp., Palo Alto, USA, Aug. 1973.

[20] Pyeé, M., Ubersfeld, J.,Auvray, J. and Gastaud, C.: 'Experimental Microwave Study of Metal-to-Metal Point-Contact Diodes', Proc. IEEE, Vol. 62, No. 4, Apr. 1974, pp. 526-529

[21] Green, S.I., Coleman, P.D. and Baird, J.R.: 'The MOM Electric Tunnelling Detector', Symp. Submillimetre Waves, Polytech. Inst. Brooklyn, New york, 1970, pp. 369-389.

[22] Higa, W. H.: 'Spurious Signals Generated by Electron Tunnelling on Large Reflector Antennas', Proc. of IEEE, Vol. 63, No. 2, Feb. 1975, pp. 306-313.

[23] Bond, C. D., Guezener, C. S. and Carosella, C. A.: 'Intermodulation Generation by Electron Tunnelling Through Aluminium-Oxide Films', Proc. of IEEE, Vol. 67, No. 12, Dec. 1979, pp. 1643-1652.

[24] Guezener, C. S.: 'Comments on "Spurious Signals Generated by Electron Tunnelling on Large Reflector Antennas"', Proc. of IEEE, Vol. 64, Feb. 1976, pp. 283.

[25] Shands, T. G. and Woody, J. A.: 'Metal-Insulator-Metal Junctions as Surface Sources of Intermodulation', Georgia Institute of Technology, USA, Report No. RADC-TR-83-31, Feb. 1983.

[26] Henisch, H.K.: 'Semiconductor Contacts', Clarendon Press, Oxford, 1984.

[27] Kao, K.C., and Hwang, W.: 'Electrical Transport in Solids', Pergamon Press, Oxford, 1981.

[28] Lamb, D.R.: 'Electrical Conduction Mechanisms in Thin Insulating Films', Methuen, London, 1967.

[29] Anderson, J.C., Leaver, K.D., Rawlings, R.D. and Alexander, J.M.: 'Materials Science', Van Nostrand Reinhold, Wokingham, 1985.

[30] Stauss, G. H., Bailey, G.C., Bond, C.D., Carosella, C.A., Ehrlich, A.C., Guezener, C. S., Kamn, G.N. and Young, C.E.: 'Studies on the Reduction of Intermodulation Generation in Communication Systems', NRL Memorandum Report 4233, 1980.

[31] Wilcox, J.Z. and Molmud, P.: 'Thermal Heating Contributions to Intermodulation Fields in Coaxial Waveguides', IEEE Transactions on Communications, 24, 1976, pp.238-243

[32] Von Hippel, A.R.: 'Dielectrics and waves', The M.I.T. Press, Cambridge, Massachusetts, 1954.

[33] Landau, L.D., Lifshitz, E.M. and Pitaevskii, L.P.: 'Electrodynamics of Continuous Media', Pergamon Press, Oxford, 1984.

[34] Kumar, A.: 'Passive IM Products Threaten High-Power Satcom Systems', Microwaves & RF, Dec. 1987, pp. 98-102.

[35] Bailey, G.C. and Ehrlich, A.C.: 'A Study of RF Nonlinearities in Nickel', Journal of Applied Physics, 50, 1979, pp. 453-461

[36] Young, C.E.: 'An Update on Intermodulation Generation by RF Connector Hardware Containing Ferromagnetic Materials', Proc. of the Ninth Annual connector Symposium, Cherry Hill, New Jersey, 1976, pp. 266-283.

[37] Young, C.E.: 'Connector design Techniques to Avoid RFI', Proc. of the Eleventh Annual connector Symposium, Cherry Hill, New Jersey, 1978, pp. 174-184

[38] Lee, J.C., 'Intermodulation Measurement in the UHF Band and an Analysis of Some Basic Conducting Materials', Massachusetts Institute of Technology, Lincoln Laboratory, Technical Note, 1979-70, Nov. 1979.

[39] Arazm, F. and Benson, F.A.: 'Nonlinearities in Metal Contacts at Microwave Frequencies', IEEE Trans. on Electromagnetic Compatibility, Vol. EMC-22, No. 3, Aug. 1980, pp. 142-149.

[40] Landau, L.D., Lifshitz, E.M. and Pitaevskii, L.P.: 'Electrodynamics of Continuous Media', Pergamon Press, Oxford, 1984.

[41] Burfoot, J.C. and Taylor, G.W.: 'Polar Dielectrics and Their Applications', Macmillan Press, London, 1979.

[42] Böttcher, C.J.F.: 'Theory of Electric Polarisation', Elsevier, Amsterdam, 1973.

[43] Johnk, C.T.A.: 'Engineering Electromagnetic Fields and Waves', John Wiley and Sons Ltd., New York, 1988.

[44] Khattab, T., Rawlins, A.D.: 'Non-linear Behaviour In Commonly Used Non-polar Dielectrics at Microwave Frequencies', Rome, Sept. 1996.

[45] Foster, D.E.: 'A New Form of Interference - External Cross Modulation', RCA Review, 1, 1937, pp. 18-25.

[46] Cox, R.D.: 'Measurements of Waveguide Components and Joint Mixing Products in 6-GHz Frequency Diversity Systems', IEEE Trans. on Communication Technology, Vol. Com-18, No. 1, Feb. 1970, pp. 33-37.

[47] Chapman, R.C., Rootsey, J.V. and Polidi, I.: 'Hidden Threat: Multicarrier Passive Component IM Generation', AIAA/CASI 6th Communication Satellite Systems Conference, Montreal, canada, Apr. 1976, pp. 357-372.

[48] Nuding, E.: 'Non-linearities of Flange Connections in transmission Lines Carrying High RF Power', 4th European Microwave Conference, 1974, pp. 613-618.

[49] Matos, F.: 'A Brief Survey of Intermodulation Due to Microwave Transmission Components', IEEE Trans. on Electromagnetic Compatibility, Feb. 1977, pp. 33-34.

[50] .Bayrak, M and Benson, F.A.: 'Intermodulation Products From Nonlinearities in transmission Lines and Connectors at Microwave Frequencies', IEE Proc., Vol. 122, No. 4, Apr. 1975, pp. 361-367.

[51] Kellar, B.S.: 'Measurement of Intermodulation Products Generated by Corroded or Loose Connections in CATV Systems', Technical Paper Annual NCTA Convention, 1984, pp. 23-28

[52] Ghione, G. and Orefice, M.: 'Intermodulation Products Generation From Carbon Fibre Reflector Antennas', IEEE International Symposium on Antennas and Propagation, 1985, pp. 153-156.

[53] Lee, J.C.: 'Intermodulation Measurement and Analysis of Some Conducting Materials Commonly Used in Aerospace', IEEE International Conference on Communications, Vol. 2, June 1980, pp. 25.6.1-25.6.6

[54] Elsner, R.F., Smulkstys, L.S.: 'Linear Dummy Loads', IEEE Trans. on Electromagnetic Compatibility, Vol. EMC-10, No. 3, Sept. 1968, pp. 320 - 324.

[55] Elsner, R.F.: 'Comments on "Coaxial Cables as Sources of Intermodulation Interference at Microwave Frequencies"', IEEE Trans. on Electromagnetic Compatibility, Vol. EMC-21, No. 1, Feb. 1979, pp. 66.

[56] Elsner, R.F., Frazier, M.J. and Morissette, S.: 'Engineering Study For Electrical Hull Interaction', Report No. IITRI E6013, IIT Research Institute, Illinois, USA, Jan. 1965, pp.239-258.

[57] Elsner, R.F.,Frazier, M.J., Smulkstys, L.S. and Wilson, E.: 'Environmental Interference Study Aboard a Naval Vessel', IEEE Electromagnetic Compatibility Symposium, 1968, pp. 330-338.

[58] Sanli, H.: 'Nonlinear Effects in Contacts and Coaxial Cables at Microwave Frequencies', M Eng. Thesis, University of Sheffield, 1975.

[59] Sanli, H.: 'Nonlinear Effects at Contacts at Microwave Frequencies', PhD Thesis, University of Sheffield, 1982.

[60] Amin, M.B. and Benson, F.A.: 'Nonlinear Effects in Coaxial Cables at Microwave Frequencies', Electronics Letters, Vol. 13, No. 25, Dec. 1977, pp. 768-770.

[61] Amin, M.B. and Benson, F.A.: 'Coaxial Cables as Sources of Intermodulation Interference at Microwave Frequencies', IEEE Trans. on Electromagnetic Compatibility, Vol., EMC-20, No. 3, Aug. 1978, pp. 376-384.

[62] Martin, R.H.: 'Intermodulation Product Generation studies on Materials, Connectors and Structures', IERE International Conference on Electromagnetic Compatibility, Apr. 1978, pp. 243-250.

[63] Von Heinz Neubauer,: 'Connector Intermodulation Phenomena', Nachrichtentech (German), Vol. 23, pt. 5, May 1970, pp. 266-267.

[64] Woody, J. A. and Shands, T.G.: 'Investigation of Intermodulation Products Generated in Coaxial Cables and Connectors', Report No. RADC-TR-82-240, Georgia Institute of Technology, USA, Sept. 1982.

[65] Shands, T.G., Denny, H.W. and Woody, J. A.: 'Intermodulation Interference Generated in Coaxial Cables and Connectors', IEEE National Symposium on Electromagnetic Compatibility, 1984, pp. 293-297.

[66] Gardiner, J.G., Howson, D.P. and Baghai, A.A.: 'Origins and Minimisation of Intermodulation Outputs From Mobile Radio Base Station Multicouplers', IERE International Conference on Electromagnetic Compatibility, 1984, pp. 211-216.

[67] King, J.: 'Intermodulation in Coaxial Connectors', RF Design, Vol. 19, No. 9, Sept. 1996, pp. 68-71.

[68] Blake, K.W.: 'External Cross-Modulation in the 100 Mc/s Band', Journal of IEE, Vol. 94, Part III-A, Mar.-Apr. 1947, pp. 659-662.

[69] Mason, H.P.: 'An Investigation into the Magnitude of Spurious Responses Produced From a Multiple Transmitting System Operating From a Common Aerial Aboard Ship', IEE Convention on HF Communication, ED 4, 1963, pp. 407-416

[70] Salisbury, G.C.: 'Topside Interference Aboard USS Mount Whitney, USS Blue Ridge and USS Iwo Jima', Naval Electronic Lab., USA, Report No. NELDC-7D-206, Dec. 1972.

[71] Betts, J.A. and Ebenezer, D.R.: 'Generation of Intermodulation Interference Due to Nonlinear Effects in the Near-Field region of Multiple Transmission Communications Systems', Proc. of the AGARD Conference on Aerospace Telecommunication Systems, May 1972, pp. 25.1-25.12.

[72] Betts, J.A. and Ebenezer, D.R.: 'Intermodulation Interference in Mobile Multiple-Transmission Communications Systems Operating at High Frequencies 93-30 MHz', Proc. of IEE, Vol. 120, No.11, Nov. 1973, pp. 1337-1344.

[73] Watson, A.W.D.: 'The Measurement, Detection, Location and Suppression Of External Non-linearities Which Affect Radio Systems', IERE conference on Electromagnetic Compatibility, 1980, pp. 1-10.

[74] Watson, A.W.D.: 'Improvements in the Suppression of External Non-linearities ("Rusty Bolt" Effects) Which Affect Naval Radio Systems', International Symposium on Electromagnetic Compatibility, 1983, pp. 157-160

[75] Brock, G.L.: An Overview of Aircraft Electromagnetic Compatibility', Proc. Of IEEE Region 5 Conference and Exposition, Emerging Technology - A Bridge to the Twenty-First Century, USA, May, 1982, pp. 67-71.

[76] Allen, J. L.: 'Investigation of Low Level Aircraft Nonavionic Nonlinear Interference', University of South Florida, USA, Report No. RADC-TR-81-26, Feb. 1983.

[77] Frazier, M.J. And Morissette, S.: 'Study Concerning Nonlinear Mixing of RF Signals in Steel Structures', Report No. IITRI 6047-7, IIT Research Laboratory, Illinois, USA, Oct. 1965.

[78] Gourlay, I. G.: 'Interference Problems at VHF & UHF Base Station Sites', SERT Journal, Vol. 5, Part 3, May 1971, pp. 58-64.

[79] Panell, W. M.: 'Frequency engineering in Mobile Radio Bands', Published by Granta Technical Editions, 1979, pp. 34-37.

[80] Turner, C.: 'Intermodulation Interference in VHF/UHF Land Mobile Radio', Global Communication (USA), Mar. 1983, pp.32 -36.

[81] Mawjoud, S.A. and Gardiner, J.G.: 'Some Origins of Radiated Noise From Communal Transmitting Sites', IEE Civil Land Mobile Conference, 1975, pp. 15-22.

[82] Sturton, C.H., Campbell, G.J. and Harnett, B.T.: 'Investigation of Intermodulation Interference in the 100-108 Mc/s Mobile Radio-Telephone Service', Radio Report no. 50, New Zealand Post Office, Mar. 1953.

[83] Shepherd, N.H.: 'A report on Interference Caused by Intermodulation Products Generated In or Near Land Mobile Transmitters', Internal Report, General Electric Co., Lynchburg, Virginia, USA, pp. 16-19.

[84] Betts, J. A.: 'The significance of the Rusty-Bolt Effect in Mobile Radio Communication Systems', IEE Colloquium on Intermodulation Affecting Junction, Oct. 1976, pp. 1/1 - 1/3.

[85] Betts, J.A. and Debney, C.W.: 'Intermodulation Measurements on Land Mobile Radio Sites', IEE Conference on Radio Transmitter, 1980, pp. 52-57.

[86] Bevan, H.L., Frampton, L.G., Ho, P., Tseung, A.C.C. and Wilkinson, W. S.: 'Suppression of Intermodulation Product Generation in Materials and Structures Used in Radio Communications', IERE International Conference on Electromagnetic Compatibility, 1986, pp. 103-110.

[87] Buley, P., Tomlinson, P.M. and Watts, D.W.: 'Investigation of Intermodulation Products Generated by Antenna Towers at Radio Sites Utilised for Land Mobile Radio Services', IERE International Conference on Electromagnetic Compatibility, 1986, pp. 111-119.

[88] Fudge, R.E.: 'The Re-Engineering of VHF Mobile Radio Services in the United Kingdom', PhD Thesis, City University, 1984.

[89] Mishra, S.R., Charron, P., Arbour, C.: 'Measurement of Passive Intermodulation (PIM) Levels in Communication Satellite Components', International Conference and Workshop on Electromagnetic Compatability (INCEMIC), Bangalore, India, Sept. 12-16, 1989.

[90] Tang, W.C. and Kudsia, C. M.: 'Multipactor Breakdown and Passive Intermodulation in Microwave Equipment For Satellite Applications', MILCOM '90, A New Era: Military Communications Conference, IEEE, 1990, Vol. 1, pp.181-187.

[91] McMillan, R.S.: 'Non-linear Junction Characterization', Technical Note 79-7, Defence Research Department, Ottawa 1979.

[92] Heiter, G.L.: 'A Microwave Linearity Test Set', IEEE International Microwave Symposium Digest, San Diego, 1977, pp. 107-109.

[93] Mantovani, J.C. and Denny, H.W.: 'Technique for Locating Passive Intermodulation Sources', IEEE National Symposium on Electromagnetic Compatibility, San Antonio, 1984, pp. 311-315.

[94] Ho, P.O., Wilkinson, W.S. and Tseung, A.C. 'The Suppression of Intermodulation Product Generation in Materials and Structures Used in Radio Communications', IEE Colloquium on Passive Intermodulation Products in Antennas and Related Structures', London, 1989, pp. 5/1 - 5/5.

[95] Bahr, A.J.: 'Microwave detection of Third Order Non-linearities in Fatigue Cracks', Electronics Letters, 16, 1980, pp. 150-152

[96] Siegenthaler, J. and Stager, C.: 'The Measurement of Microwave Intermodulation Effects on Passive Components and System Parts', Proceedings of Microwaves and Optoelectronics, Wiesbaden, 1988, paper 1A-5.

[97] Mizzoni, R., De Gennaro, F. and Rosati, G.: 'Survey on Selenia Spazio's Activities on High Power Aspects in Radar and Communications Antennas', ESTEC Workshop on Multipaction and Passive Intermodulation Products Problems in Spacecraft Antennas, Noordwijk, 1990.

[98] Hamer, G., Kazeminejad, S. and Howson, D.P.: 'Test Set for the Measurement of IMDs at 900 MHz', IEE Colloquium on Passive Intermodulation Products in Antennas and Related Structures', London, 1989, pp. 8/1 - 8/3.

[99] Engelson, M.: 'Measuring IMD by Properly Using the Spectrum Analyser', Microwaves and RF, Vol. 27, prt. 2, Feb. 1988, pp. 85-90

[100] 'Fundamentals of Spectrum Analysis Using Spectrum Analyser FSA', Rhode & Schwarz application note.

[101] 'Spectrum Analyser Basics' Application Note 150, Hewlett Packard, Nov. 1989.

[102] '6910 RF Power Sensor Instruction Manual', H6190, Marconi Instruments Ltd. Nov. 1987

[103] Jacobi, J, H.: 'IMD: Still Unclear after 20 Years', Microwaves and RF, Vol. 25, pt. 12, Nov. 1986, pp. 119-126.

[104] 'Spectrum Analysis... Noise Measurements' Application Note 150-4, Hewlett Packard, Apr. 1974.

[105] 'HP8561E Spectrum Analyser: Installation and Verification Manual', HP Part No. 5961-6712, Hewlett Packard, Jan. 1993.

[106] Foord, A.P., Mitchell, S.D. and Rawlins, A.D.: 'A Study of the PIM Characteristics of Space RF Applications Materials at L-Band', Final Report, Noise Measurements Group, University of Kent, Apr. 1993.

[107] 'Semi Rigid Coaxial Cable', (Catalogue), Micro-Coax Components Inc. page 59.

[108] Chang, W.: 'Accurate Analysis Method for Rectangular-Coaxial Line Components', Frequenz Journal, Vol. 43, No. 10, 1989, pp. 271-276.

[109] Mok, C.K. and Martin, A.: 'Lightweight Compact Feed Network at 6/4 GHz for BrasilSat Antenna', Satellite Communications Conference, Ottawa, 1983, pp. 29.4.1-29.4.4.

[110] Ragan, G.L.: 'Microwave Transmission Circuits', M.I.T. Radiation Lab. Series, McGraw-Hill Inc., New York, 1948, Vol.9, pp. 540-565.

[111] Ramo, S., Whinnery, J.R. and Van Duzer, T.: 'Fields and Waves in Communication Electronics', 3rd Edition., John Wiley and Sons Inc., New York, 1994.

[112] Rizzi, P.A.: 'Microwave Engineering: Passive Circuits', Prentice-Hall Inc., New Jersey, 1988.

[113] King, H.E.: 'Broad-Band Coaxial Choked Coupling Design', IRE Transactions on Microwave Theory and Techniques, Vol. MTT-8, Mar. 1960, pp. 132-135.

[114] Whinnery, J.R. and Jamieson H.W.: 'Equivalent Circuits for Discontinuities in Transmission Lines', Proceedings of the I.R.E., Feb. 1944, Vol. 32, pp. 98-115.

[115] Whinnery, J.R., Jamieson H.W. and Robbins, T.E.: 'Coaxial Line Discontinuities', Proceedings of the I.R.E., Nov. 1944, Vol. 32, pp. 695-709.

[116] Bates, R. H. T.: 'The Characteristic Impedance of the Shielded Slab Line', IRE Transactions on Microwave Theory and Techniques, Vol. MTT-4, Jan. 1956, pp. 28-33.

[117] Packard, K.S.: 'Optimum Impedance and Dimensions for Strip Transmission Line', IRE Transactions on Microwave Theory and Techniques, Vol. MTT-5, Oct. 1957, pp. 244-247.

[118] Cruzan, O.R. and Garver, R.V.: 'Characteristic Impedance of Rectangular Coaxial Transmission Lines', IEEE Transactions on Microwave Theory and Techniques, Sept. 1964, pp. 488-495.

[119] Howe, Jr., H.: 'Stripline Circuit Design', Artech House Inc. Dedham, MA., 1974.

[120] Costamanga, E. and Fanni, A.: 'Analysis of Rectangular Coaxial Structures by Numerical Inversion of the Schwarz-Christoffel Transformation', IEEE Transactions on Magnetics, Vol. 28, No. 2, Mar. 1992, pp. 1454-1457.

[121] Wood, P.J.: 'TEM Line Technology for Satellite Antenna Feed Applications', Satellite Communications Conference, Ottawa, 1983, pp. 29.6.1-29.6.4.

[122] Mok, C.K. and Martin, A.: 'Lightweight Compact Feed Network at 6/4GHz for Brasilsat Antenna', Satellite Communications Conference, Ottawa, 1983, pp. 29.4.1-29.4.4.

[123] Schiffman, B. M. and Matthaei, G. L.: 'Exact Design of Band-Stop Microwave Filters', IEEE Transactions on Microwave Theory and Techniques, Vol. MTT-12, Jan. 1964, pp. 6-15.

[124] Matthaei, G., Young, L. and Jones, E.M.T.: 'Microwave Filters, Impedance-Matching Networks and Coupling Structures', Artech House Books Inc., Norwood, Mass., 1980.

[125] Schiffman, B. M.: 'A Harmonic Rejection Filter Designed By an Exact Method', IEEE Transactions on Microwave Theory and Techniques, Vol. MTT-12, Jan. 1964, pp. 58-60.

[126] Schiffman, B. M.: 'A Multi-Harmonic Rejection Filter Designed By an Exact Method', IEEE Transactions on Microwave Theory and Techniques, Vol. MTT-12, Sep. 1964, pp. 512-516.

[127] Schiffman, B. M.: 'Capacitively Coupled Stub Filter', IEEE Transactions on Microwave Theory and Techniques (Corr.), Vol. MTT-12, Mar. 1964, pp. 253-254.

[128] Cristal, E.G.: 'Addendum to "Exact Method for Synthesis of Microwave Band-Stop Filters", IEEE Transactions on Microwave Theory and Techniques, Vol. MTT-12, May 1964, pp. 369-382.

[129] Young, L., Matthaei, G.L. and Jones, E.M.T.: 'Microwave Band-Stop Filters with Narrow Stop Bands', IEEE Transactions on Microwave Theory and Techniques, Vol. MTT-10, Nov. 1962, pp.416-427.

[130] Torgow, E.N.: 'Band-Stop Filters for High-Power Applications', IEEE Transactions on Microwave Theory and Techniques, Vol. MTT-13, Sep. 1965, pp. 508-513.

[131] Taub, J.J. and Sleven, R.L.: 'Design of Band-Stop Filters in the Presence of Dissipation', IEEE Transactions on Microwave Theory and Techniques, Vol. MTT-13, Sep. 1965, pp. 589-616

[132] Matsumoto, A. (Ed.): 'Microwave Filters and Circuits - Contributions from Japan', Academic Press, 1970, pp.105-109.

[133] Standley, R.D. and Todd, A.C.: 'A Note on Strip-Line Band-Stop Filters with Narrow Stop Bands', IEEE Transactions on Microwave Theory and Techniques (Correspondence), Vol. MTT-11, Nov. 1963, pp. 548-549.

[134] Hect, S., Kurpis, G.P., Taub, J.J.: 'A Microstrip Diplexer Using Bandstop Filters', Proc. IEEE Microelectronics Symposium, Microwave Microelectronics, 1969, A-4, pp. 1-3.

[135] Cohn, S.B.: 'Thickness Corrections for Capacitive Obstacles and Strip Conductors', IRE Transactions on Microwave Theory and Techniques, Vol. MTT-8, Nov. 1960, pp. 638-644.

[136] Van Valkenburg, M.E.: 'Analog Filter Design', CBS College Publishing Inc., New York, 1982, Chapter 9, pp. 261-275.

[137] Moschytz, G.S. and Horn, P.: 'Active Filter Design Handbook', John Wiley & Sons Ltd., London, 1981, Chapter 3

[138] Cohn, S.B.: 'The Re-Entrant Cross Section and Wide-Band 3-dB Hybrid Couplers', IEEE Transactions on Microwave Theory and Techniques, Vol. MTT-11, No.7, Jul. 1963, pp. 254-258.

[139] Jones, E.M.T and Bolljahn, J.T.: 'Coupled-Strip-Transmission-Line Filters and Directional Couplers', IRE Transactions on Microwave Theory and Techniques, Vol. MTT-4, Apr. 1956, pp. 75-81.

[140] Reed, J. and Wheeler, J.: 'A Method of Analysis of Symmetrical Four-Port Networks', IRE Transactions on Microwave Theory and Techniques, Vol. MTT-4, Oct. 1956, pp. 246-252.

[141] Young, L.: 'Synchronous Branch Guide Couplers for Low and High Power Applications', IRE Transactions on Microwave Theory and Techniques, Vol. MTT-10, Nov. 1962, pp. 459-475.

[142] Levy, R. and Lind, L.F.: 'Synthesis of Symmetrical Branch-Guide Directional Couplers', IEEE Transactions on Microwave Theory and Techniques, Vol. MTT-16, No.2, Feb. 1968, pp. 80-89

[143] Lind, L.F.: 'Synthesis of Asymmetrical Branch-Guide Directional Coupler-Impedance Transformers', IEEE Transactions on Microwave Theory and Techniques, Vol. MTT-17, No.1, Jan. 1969, pp. 45-48.

[144] Riblet, H.J.: 'Comment on "Synthesis of Asymmetrical Branch-Guide Directional Coupler-Impedance Transformers", IEEE Transactions on Microwave Theory and Techniques, Vol. MTT-18, No.1, Jan. 1970, pp. 47-48.

[145] Levy, R.: 'Analysis of Practical Branch-Guide Directional Couplers', IEEE Transactions on Microwave Theory and Techniques, Vol. MTT-17, No.5, May. 1969, pp. 289-290.

[146] Levy, R.: 'Zolotarev Branch-Guide Couplers', IEEE Transactions on Microwave Theory and Techniques, Vol. MTT-21, No.2, Feb. 1973, pp. 95-99.

[147] Hammerstad, E.: 'Computer-Aided Design of Microstrip Couplers with Accurate Discontinuity Models', IEEE MTT Symposium Digest 1981, pp. 54-56.

[148] Celliers, A.F. and Malherbe, J.A.G.: 'Design Curves for -3dB Branchline Couplers', IEEE Transactions on Microwave Theory and Techniques, Vol. MTT-33, No.11, Nov. 1985, pp. 1226-1228.

[149] Anada, T. and Jui-Pang, H.: 'Analysis of Balanced Stripline Branch-Line 3-dB Hybrid Circuit Based on Planar Circuit Model', Electronics and Communications in Japan, Vol. 71, Part 1, No. 12, 1988, pp. 78-89.

[150] Anada, T. and Jui-Pang, H.: 'Synthesis of Balanced Stripline Branch-Line 3-dB Hybrid Circuit Based on Planar Circuit Model', Electronics and Communications in Japan, Vol. 71, Part 1, No. 12, 1988, pp. 90-98.

[151] Knöchel, R.: 'Broadband Branchline Power Combining/Dividing Structures for Power Amplifiers', ESA Study Report, ESTEC P.O. No. 103 452, Dec. 1991.

[152] Vogel, R.W.: 'Effects of the T-Junction Discontinuity on the Design of Microstrip Directional Couplers', IEEE Transactions on Microwave Theory and Techniques, Vol. MTT-21, No.3, Mar. 1973, pp. 145-146.

[153] Leighton, W.H. and Milnes, A.G.: 'Junction Reactance and Dimensional Tolerance Effects on X-band 3-dB Directional Couplers', IEEE Transactions on Microwave Theory and Techniques, Vol. MTT-19, No.10, Oct. 1971, pp. 818-824.

[154] Cohn, S.B. et al.: 'Design Criteria for Microwave Filters and Coupling Structures', Stanford Research Inst., Melno Park, California, SRI Project 2326, Tech. Rept. 3, Aug. 1958, pp. 23-29.

[155] Hammerstad, E.: 'Equations for Microstrip Circuit Design', Proceedings of the 5th European Microwave Conference, Sep. 1975, pp. 268-272.

[156] Altschuler, H.M. and Oliner, A.A.: 'Discontinuities in the Centre Conductor of Symmetric Strip Transmission Line', IRE Transactions on Microwave Theory and Techniques, Vol. MTT-8, May. 1960, pp. 328-339.

[157] Easter, B.: 'The Equivalent Circuit of Some Microstrip Discontinuities', IEEE Transactions on Microwave Theory and Techniques, Vol. MTT-23, No.8, Aug. 1975, pp. 655-660.

[158] Franco, A.G. and Oliner, A.A.: 'Symmetric Strip Transmission Line Tee Junction', IRE Transactions on Microwave Theory and Techniques, Vol. MTT-10, Mar. 1962, pp. 118-124.

[159] Arndt, F., Ellerman, D., Häusler, H.W., Strube, J.: 'Field Theory Analysis and Numerical Synthesis of Symmetrical Multiple-Branch Waveguide Couplers, Frequenz Journal, Vol. 36, No. 10, 1982, pp. 262-266.

[160] Chang, W.: 'Accurate Analysis Method for Rectangular-Coaxial Line Components', Frequenz Journal, Vol. 43, No. 10, Oct. 1989, pp. 271-276.

[161] Sorrentino, R. and Itoh, T.: 'Transverse Resonance Analysis of Finline Discontinuities', IEEE Transactions on Microwave Theory and Techniques, Vol. MTT-32, No.12, Dec. 1984, pp. 1633-1638.

[162] Alessandri, F., Bartolucci, G. and Sorrentino, R.: 'Admittance Matrix Formulation of Waveguide Discontinuity Problems: Computer-Aided Design of Branch Guide Couplers', IEEE Transactions on Microwave Theory and Techniques, Vol. MTT-36, No.2, Feb. 1988, pp. 394-403.

[163] Alessandri, F. and Sorrentino, R.: 'Analysis of T-Junction in Square Coaxial Cable', 18th European Microwave Conference Proceedings, Sep., 1988, pp. 162-167.

[164] Alessandri, F., Capece, P. and Sorrentino, R.: 'Theory and Experiment on Rectangular Line Discontinuities and Junctions', IEEE International Microwave Symposium Digest, 1990, Vol. 1., pp. 259-262.

[165] Sorrentino, R., Mezzanotte, P., Roselli, L., Mongiardo, M. and Alessandri, F.: 'Process-Oriented CAD of Rectangular Coaxial Line Components for Beam Forming Networks', 23rd European Microwave Conference Proceedings, Sep. 1993, Vol. 1., pp. 640-641.

[166] Alessandri, F. Mongiardo, M. and Sorrentino, R.: 'Computer-Aided-Design of Beam Forming Networks for Modern Satellite Antennas', IEEE Transactions on Microwave Theory and Techniques, Vol. MTT-40, No. 6, Jun. 1992, pp. 1117-1127.

[167] Navarro, E.A., Such, V., Gimeno, B. and Cruz, J.L.: 'T-Junctions in Square Coaxial Waveguide: A FD-TD Approach', IEEE Transactions on Microwave Theory and Techniques, Vol. MTT-42, No. 2, Feb. 1994, pp. 347-50.

[168] Xu, S., Wu, X., Guo, W. and Li, Z.: 'Scattering Characteristics of Rectangular Coaxial Line Discontinuities', IEE Proc. Microwaves Antennas and Propagation, Vol. 142, No. 3, Mar 1995, pp. 257-264.

[169] Marcuvitz, N.: 'Waveguide Handbook', McGraw-Hill Book Co. Ltd., New York, 1951.

[170] Montgomery, C.G., Dickie, R.H. and Purcell, E.M.: 'Principles of Microwave Circuits', Dover Publications Inc., New York, 1965.

[171] Sunderland, R.J.: 'Analysis of Chromate Conversion Coatings on Aluminium', Proceedings of the 6th International Vacuum Conference, Japan, 1974, Applied Physics Supplement 2, Part 1, pp. 347-350.

[172] Scott, P.S.G.: 'An Investigation of Alodine Surface Finish on Three Aluminium Alloys', ESTEC Internal Working Paper No. 1435, Oct. 1985.

[173] Hatch, A.J. and Bartel-Williams, H.: 'The Secondary Electron Resonance Mechanism of Low-Pressure, High-Frequency, Gas Breakdown', Journal of Applied Physics, April 1954, Vol.25, No.4.

[174] Clancy, P.F.: 'Multipactor Control in Microwave Space Systems', Microwave Journal, March 1978.

[175] Harnwell, G.P.: 'Principles of Electricity and Electromagnetism', McGraw-Hill, New York, 1949, pp. 93 & 148.

[176] Duffin, W.J.: 'Electricity and Magnetism', McGraw-Hill, London, 1990, pp. 133.

[177] Purcell, E.M.: 'Electricity and Magnetism', McGraw-Hill, New York,1965, pp. 126.

[178] Meaden, G.T.: 'Electrical Resistance of Metals', Plenum Press, New York, 1965.

[179] Morgan, S.P.: 'Effect of Surface Roughness on Eddy Current Losses at Microwave Frequencies', Journal of Applied Physics, Apr. 1949, Vol. 20, pp. 352-362.

[180] Evans, G.E.: 'Antenna Measurement Techniques', Artech House Publishing Ltd., 1990, Ch. 5, pp. 121-135.

[181] Mitchell, S.D. and Rawlins, A.D.: 'Passive Intermodulation Characterisation of ESTEC Compact Payload Test Range', Final report, ESTEC purchase order no. 135030, Electronics Labs., University of Kent, Mar. 1994.

[182] Kroone, W.: 'PIM Characterisation of ESTEC CPTR', ESA Request For Quotation AOP/WK/328832, Sept. 1994.

[183] Blake, L.V.: 'Antennas', John Wiley & Sons, New York, 1966.

[184] Coale, F.S.: 'A Travelling Wave Directional Filter', IRE Transactions on Microwave Theory and Techniques, Vol. MTT-4, Oct. 1956, pp. 256-260.

[185] Wanselow, R.D. and Tuttle, Jr.,L.P.: 'Practical Design of Strip-Transmission-Line Half-Wavelength Resonator Directional Filters', IRE Transactions on Microwave Theory and Techniques, Vol. MTT-7, Apr. 1959, pp. 168-173.

[186] Weir, W.B. and Adams, D.K.: 'Wideband Mutiplexers Using Directional Filters', Microwaves, May 1969, pp. 44-50.

[187] Lin, C.M.: 'A Broad-Band Microwave Coaxial Connector with Capacitive RF Coupling and Isolated DC Returns', IRE Transactions on Microwave Theory and Techniques, Vol. MTT-6, Apr. 1958, Corr. pp. 454-455.

[188] Deats, B. and Hartman, R.: 'Measuring the Passive-IM Performance of RF Cable Assemblies', Microwaves and RF, March 1997, pp. 108-114.